Technische Universität München
TUM School of Natural Sciences

TUM

Functional (Co)Polymers from
Group-Transfer and Ring-Opening Polymerization –
Monomers, Catalysis, Applications

Moritz Kränzlein

Vollständiger Abdruck der von der TUM School of Natural Sciences der Technischen

Universität München zur Erlangung eines

Doktors der Naturwissenschaften (Dr. rer. nat.)

genehmigten Dissertation.

Vorsitz: Prof. Dr. Angela Casini

Prüfer*innen der Dissertation:

1.   Prof. Dr. Dr. h. c. Bernhard Rieger
2.   Prof. Dr. Klaus Köhler
3.   Prof. Dr. Michael Buchmeiser

Die Dissertation wurde am   07.11.2022 bei der Technischen Universität München eingereicht

und durch die TUM School of Natural Sciences am 07.12.2022 angenommen.

"The secret of genius is to carry the spirit of the child into old age,
which means never losing your enthusiasm."

- Aldous Huxley

"The secret to success is not get discouraged."

- Ernest Hemingway

Für meinen Vater

Danksagung

_____

Table of Contents

_____

List of abbreviations

Table 1: General abbreviations.

Abbreviation	Signification
AMM	activated monomer mechanism
BCF	tris(pentafluorophenyl)borane
BenzPyOTBDMS	4-(((4'-(tert-butyl-dimethylsilyl)oxy)methyl)phenyl)-2,6-dimethylpyridine
BID	β-diiminato ligand
BIH	1,3-dimethyl-2-phenyl-2,3-dihydro-1H-benzo[d]imidazole
CIM	coordination-insertion mechanism
CLP	classical *Lewis* pair
Cp	cyclopentadienyl ligand
Cp*	1,2,3,4,5-pentamethyl cyclopentadienyl ligand
Cp'	1,2,3,4-tetramethylcyclopentadienyl ligand
Cp^{TMS}	trimethylsilyl cyclopentadienyl ligand
CTA	chain-transfer agent
dcm	dichloromethane
dmb	4,4'-dimethyl-2,2'-bipyridine
EBI	ethylene bis(indenyl) ligand
Et	ethyl-
FLP	frustrated *Lewis* pair
GTP	group-transfer polymerization
I	Integral
ILP	interacting *Lewis* pair
iROP	immortal ring-opening polymerization
LA	*Lewis* acid
LB	*Lewis* base
LCST	lower critical solution temperature
LED	light-emitting diode
Ln	lanthanide
L$_n$	ligand with n chelating positions
LPP	*Lewis* pair polymerization
*m*CPBA	*meta*-chloroperbenzoic acid
Me	methyl-
MeCN	acetonitrile
M^{n+}	metal cation with n+ positive charges

Abbreviation	Signification
Mon	monomer
NHC	*N*-heterocyclic carbene
NHI	*N*-heterocyclic imine
NHO	*N*-heterocyclic olefin
^{n}Bu	*n*-butyl
Oct	2-ethylhexanoate / *n*-octyl – as indicated
OERS	one-electron-reduced species
(ONOO)^{tBu}	6,6'-(((2-methoxyethyl)azane-diyl)-bis(methylene)-bis(2,4-di-*tert*-butylphenolate)) ligand
Ph	Phenyl-
Pol	Polymer
REM-GTP	rare-earth metal-mediated group-transfer polymerization
ROP	ring-opening polymerization
SKA	silyl ketene acetal
sym-col	1,3,5-trimethylpyridine
^{t}Bu	*tert*-butyl-
TEOA	triethanolamine
THF	tetrahydrofuran as solvent molecule
thf	tetrahydrofuran as coordinating molecule
TMPy	2,3,5,6-tetramethylpyrazine
TMS	trimethylsilyl-
UCST	upper critical solution temperature

_____

Table 2: Abbreviations for formula signs.

Sign	Signification [Unit]
$Đ$	Polydispersity index [-]
dn/dc	ref*ract*ive index increment [mL/g]
I.E.	initiation efficiency [%]
k_i	rate constant of initiation [M/s; 1/s; 1/(M·s); 1/(M^n·s)]
k_{Pr}	rate constant of propagation [M/s; 1/s; 1/(M·s); 1/(M^n·s)]
k_{Tr}	rate constant of transfer reaction [M/s; 1/s; 1/(M·s); 1/(M^n·s)]
M_n	number average molecular weight [kg/mol]
M_w	weight average molecular weight [kg/mol]
$M_{n,abs}$	absolute molecular weight [kg/mol]
$M_{n,rel}$	relative molecular weight [kg/mol]
R_f	Retention factor [-]
T	temperature [°C]
T_g	glass transition temperature [°C]
T_m	melting temperature [°C]
TOF	turnover frequency [s^{-1}]
TON	turnover number [-]

Table 3: Abbreviations for methods.

Abbreviation	Signification
AFM	atomic force microscopy
ATR-IR	attenuated total reflection infrared spectroscopy
CA	contact angle
DLS	dynamic light scattering
DSC	differential scanning calorimetry
EA	elemental analysis
ESI-MS	electron spray-ionization mass spectrometry
GPC	gel-permeation chromatography
MALDI-MS	matrix-assisted laser-desorption ionization mass spectrometry
NMR	nuclear magnetic resonance spectroscopy
SCXRD	single-crystal X-ray diffraction
SEC	size-exclusion chromatography
TGA	thermogravimetric analysis
TLC	Thin layer chromatography
pXRD	powder X-ray diffraction

Table 4: Abbreviations for monomers.

Abbreviation	Signification
Acrylates	
dcPA	dicyclopentadienyl acrylate
EtA	ethyl acrylate
MA	methyl acrylate
^{n}BuA	*n*-butyl acrylate
^{t}BuA	*t*-butyl acrylate
Methacrylates	
AMA	allyl methacrylate
EGDM	ethylenglycol dimethacrylate
EtMA	ethyl methacrylate
FMA	furfuryl methacrylate
MMA	methyl methacrylate
^{n}BuMA	*n*-butyl methacrylate
^{t}BuMA	*t*-butyl methacrylate
VBM	vinyl benzyl methacrylate
Acrylamides	
APY	acryloyl pyrrolidine
APP	acryloyl piperidine
DAlAA	diallyl acrylamide
DIPA	di-*iso*-propyl acrylamide
DMAA	dimethyl acrylamide
DMMA	dimethyl methacrylamide
DPAA	diphenyl acrylamide
MPAA	methyl phenyl acrylamide
Alkyl vinylphosphonates	
DAlVP	diallyl vinylphosphonate
DEVP	diethyl vinylphosphonate
DMVP	dimethyl vinylphosphonate
DPVP	di-*n*-propyl vinylphosphonate
DTPVP	(1-phenylethoxy)piperidin-4-yl) vinylphosphonate
Vinylpyridines & others	
2VP	2-vinylpyridine
4VP	4-vinylpyridine
4VQ	4-vinylquinoline
DMVP	2,6-dimetyl vinylpyridine

_____

Abbreviation	Signification
VBpy	4-viny-4'-methyl-2,2'-bipyridine
IPOx	*iso*-propenyl-2-oxazoline
Lactones	
αCarL	α-Carenelactone
εCarL	ε-Carenelactone
3CarDiol	3-carene diol
BBL / PHB	β-butyrolactone / poly(3-hydroxybutyrate)
βPL	β-propriolactone
CL	ε-caprolactone
δVL	δ-valerolactone
GA	glycolide
LA	lactide
M	(-)-menthide

The corresponding polymers to each monomer are denoted with capital letter P prior to the monomer abbreviation unless indicated otherwise.

_____

List of Publications

1. Kränzlein, M., Pehl, T.M., Adams, F. and Rieger, B., Uniting Group-Transfer and Ring-Opening Polymerization – Block Copolymers from Functional Michael-Type Monomers and Lactones, *Macromolecules*, **2021**, 54, 23, 10860-10869.

2. Kränzlein, M.[*], Pongratz, S.[*], Bruckmoser, J., Bratić, B., Breitsameter, J.M. and Rieger, B., Polyester synthesis based on 3-carene as renewable feedstock, *Polymer Chemistry*, **2022**, 13, 3726-3732. [*] *These authors contributed equally.*

3. Maier, A.[*], Thomas, C.[*], Kränzlein, M.[*], Pehl, T.M. and Rieger, B., Macromolecular Rhenium-Ruthenium Complexes for the Photocatalytical CO_2 Conversion – from catalytic *Lewis*-Pair Polymerization to well-defined Poly(vinyl bipyridine)-Metal Complexes, *Macromolecules*, **2022**, 55, 16, 7039-7048. [*] *These authors contributed equally.*

4. Pehl, T.M.[*], Kränzlein, M.[*], Adams, F.[*], Schaffer, A. and Rieger, B., C-H Bond Activation of Silyl-Substituted Pyridines with Bis(phenolate) Yttrium Catalysts as Facile Tool towards Hydroxyl-Terminated Michael-Type Monomers, *Catalysts*, **2020**, 10, 4, 448.[*] *These authors contributed equally.*

Publications beyond the scope of this thesis:

5. Schaffer, A., Kränzlein, M. and Rieger, B., Precise Synthesis of Poly(dimethylsiloxane) Copolymers through C-H bond-activated Macroinitiators via Yttrium-Mediated Group Transfer Polymerization and Ring-Opening Polymerization, *Macromolecules*, **2020**, 53, 19, 8382-8392.

6. Schaffer, A., Kränzlein, M. and Rieger, B., Synthesis and Application of Functional Group-Bearing Pyridyl-Based Initiators in Rare Earth Metal-Mediated Group-Transfer Polymerization, *Macromolecules*, **2020**, 53, 11, 4345-4354.

7. Adams, F., Pehl, T.M., Kränzlein, M., Kernbichl, S.A., Kang, J.-J., Papadakis, C.M. and Rieger, B., (Co)polymerization of (-)-menthide and β-butyrolactone with yttrium-bis(phenolates): tuning material properties of sustainable polyesters, *Polymer Chemistry*, **2020**, 11, 27, 4426-4437.

8. Pehl, T.M., Adams, F., Kränzlein, M. and Rieger, B., Expanding the Scope of Organic Radical Polymers to Polyvinylphosphonates Synthesized via Rare-Earth Metal-Mediated Group-Transfer Polymerization, *Macromolecules*, **2021**, 54, 9, 4089-4100.

9. Denk, A., Kernbichl, S.A., Schaffer, A., Kränzlein, M., Pehl, T.M. and Rieger, B., Heteronuclear, Monomer-Selective Zn/Y Catalysts Combines Copolymerization of Epoxides and CO_2 with Group-Transfer Polymerization of Michael-Type Monomers, *ACS Macro Letters*, **2020**, 9, 4, 571-575.

10. Watson, I.C., Zhou, Y., Ferguson, M.J., Kränzlein, M., Rieger, B. and Rivard, E., Trialkylaluminum N-Heterocyclic Olefin (NHO) Adducts as Catalysts for the Polymerization of Michael-type Monomers, *Zeitschrift für anorganische und allgemeine Chemie*, **2020**, 646, 13, 547-551.

11. Späth, F., Donau, C., Bergmann, A.M., Kränzlein, M., Synatschke, C.V., Rieger, B. and Boekhoven, J., Molecular Design of Chemically Fueled Peptide-Polyelectrolyte Coavervate-Based Assemblies, *Journal of the American Chemical Society.*, **2021**, 143, 12, 4782-4789.

Abstract

With the change from using polymer purely as commodity mass ware to utilizing polymers in high-tech applications, precisely tuning and modifying these materials is a main requirement to make them suitable for the desired use cases. Herein, several methods for modifying polymers in the context of group-transfer and ring-opening polymerization are investigated. The first modification point that will be addressed is the introduction of functional end-groups to group-transfer polymerization-based polymers by means of C-H bond activation. Utilizing this method, functionalized α-methylpyridines can be introduced to yttrium catalysts as initiators, which are linked covalently to the polymer chain upon initiation. To make these molecules applicable as initiators, functional groups are introduced and protected to facilitate controlled C-H bond activation of yttrium bis(phenolate) and cyclopentadienyl catalysts. Broadening the scope of introducible end-groups, different 2,6-dimethylpyridines are prepared, bearing silyl-protected hydroxyls, a catechols, alkynes or an unprotected azide. These novel initiators are used to prepare functionalized poly(diethyl vinylphosphonate). With regards to sidechain functionalization, a vinyl bipyridyl-based *Michael*-acceptor monomer is polymerized using catalytic *Lewis* pair polymerization, providing well-defined poly(vinyl bipyridines) with narrow polydispersity. To these polymers, rhenium and ruthenium complexes are introduced as pendent side groups, giving access to highly stable polymeric photocatalysts for CO_2 reduction. Another tuning point for polymers in this context is the introduction of innovative monomers based on biogenic feedstocks. To gain access to biobased polyesters, 3-carene is chemically converted into different monomers and successfully polymerized *via* polycondensation and ring-opening polymerization. Dependent on their structure, these polyesters were either amorphous or semi-crystalline. The last and maybe most versatile modification point addressed herein is the copolymerization of *Michael*-type monomers and lactones by sequential, catalytic copolymerization using yttrium bis(phenolate) catalysts. Different AB- and BAB- di- and triblock copolymers from 2-vinylpyridine and ε-caprolactone or (-)-menthide are prepared and investigated regarding polymerization catalysis and material properties. Those copolymers exhibit microphase separation and pH-dependent micellization in aqueous media. The kinetic investigation revealed a living-type polymerization for both group-transfer and subsequent ring-opening polymerization and provided a deeper understanding of the underlying copolymerization mechanism.

Zusammenfassung

Seit Polymere nicht mehr nur als Gebrauchswaren genutzt werden, sondern zunehmend auch in verschiedenen High-Tech Anwendungen zu finden sind, ist eine gezielte Einstellung und Modifikation dieser Strukturen notwendig, um die geforderten Anforderungsprofile erfüllen zu können. Im Rahmen dieser Arbeit werden verschiedene Methoden zur Modifikation von Polymeren im Kontext der Gruppentransfer- und Ringöffnungspolymerisation untersucht. Mit Blick auf den ersten Modifikationspunkt wird die gezielte Einführung funktioneller Endgruppen mittels C-H Bindungsaktivierung an Gruppentransferpolymerisations-basierten Polymeren untersucht. Mithilfe dieser Methode können funktionalisierte α-Methylpyridine als Initiatoren in Yttrium-Katalysatoren eingeführt werden, die während der Initiation kovalent an die Polymerkette gebunden werden. Um passende Moleküle als Initiatoren zu generieren, werden funktionelle Gruppen eingeführt und geschützt, um eine selektive C-H Bindungsaktivierung am Yttrium-Bis(phenolat)- und Yttrium-Cyclopentadienyl-Katalysatoren gewährleisten zu können. Um die Gruppe an funktionellen Initiatormotiven zu erweitern, werden 2,6-Dimethylpyridine mit silylgeschützen Alkoholen, Catecholen und Alkynen und einem ungeschützten Azid synthetisiert. Mithilfe dieser Initiatoren werden funktionalisierte Poly(diethylvinylphosphonate) hergestellt. Im Rahmen von Seitenkettenmodifikationen wird ein Vinylbipyridin-basiertes *Michael*-Monomer mittels katalytischer *Lewis*paar-Polymerisation kontrolliert polymerisiert. An dieses Polymer werden Rhenium- und Rutheniumkomplexe als Seitenketten eingeführt, um hochstabile, polymere Photokatalysatoren für die CO_2-Reduktion zu erhalten. Ein weiterer Modifikationspunkt ist zudem die Synthese neuartiger Monomere aus biobasierten Rohstoffquellen. Um biobasierte Polyester zu erhalten, wird 3-Caren chemisch in verschiedene Monomere umgewandelt und mittels Polykondensation und Ringöffnungs-polymerisation polymerisiert. Die so erhaltenen Polyester weisen entweder amorphe oder semikristalline Eigenschaften auf. Als letzter Modifikationspunkt wird die Copolymerisation von Michael-Monomeren und Lactonen mittels sequenzieller, katalytischer Copolymerisation mit Yttrium-Bis(phenolat)-Katalysatoren untersucht. Es werden verschiedene AB- und BAB- Di- und Triblockcopolymere aus 2-Vinylpyridine und ε-Caprolacton oder (-)-Menthid hergestellt und hinsichtlich Polymerisationskatalyse und Materialeigenschaften untersucht. Diese Copolymere weisen eine Mikrophasenseparation auf und können in wässigen Medien pH-abhängig mizellieren. Die kinetischen Untersuchungen zeigen eine lebende Polymerisation für die Gruppentransfer- und die nachfolgende Ringöffungspolymerisation und geben ein tieferes Verständnis für den zugrundeliegenden Copolymerisationsmechanismus.

1. Introduction – polymers in the 21st century

Since the introduction of the concept of macromolecules being many equal monomer units covalently linked to each other by Hermann Staudinger in 1920, more than a century has passed.[1,2] Within the last 100 years, the way we view and use polymer materials has undergone a drastic change. Still the majority of polymers we encounter on a daily base is made up from commodity polymers like polyolefins, polyesters, vinyl polymers or styrenics and acrylics. However, by now, polymers can also be found in highly sophisticated areas of applications, including heat insulation, fibers, apparel, mobility, construction materials, microelectronics, green energy generation, soil fertility, food packaging, regenerative medicine, drug-delivery, advanced manufacturing techniques, lightweight composite materials, e-mobility, membrane technologies and many others.[3]

In a recent commentary article from the editors and advisory board of *Macromolecular Chemistry and Physics* on the upcoming century of polymer chemistry, the authors identify three different branches defining and influencing modern polymer chemistry. These branches are (**1**) new properties and applications, (**2**) new synthesis methods and (**3**) sustainability, impacting the way research is performed. Further the authors argue, that there is a "[…] tension in research between developing fundamentally new methods without knowing what useful materials they might give access to and creating new materials with specific functions by applying the available toolbox".[3] Building on a strong foundation of research, we now have a broad understanding on how to perform and control polymerization reactions and post-synthetically modify the obtained polymers in a way that we gain access to materials with the desired property profiles. This allows modern day polymer chemists to choose from a variety of different methods and tools for the synthesis of tailor-made polymer materials. Throughout this thesis, different approaches towards introducing advanced functionalities are explored, utilizing a more "retrosynthetic" approach. Starting from different requirements and application scopes, known techniques and tools are used to address certain modification points of synthetic polymers, tuning, and adapting them towards their supposed application.

Different modification points in the context of group-transfer and ring-opening polymerization as new tools towards the generation of highly functional (co)polymers will be discussed within the context of this thesis.

2. Polymerization techniques for functional materials

2.1. Group-transfer polymerization

2.1.1. General remarks and monomer scope

In search for new polymerization techniques for methyl methacrylate (MMA), Webster *et al.* discovered the controlled polymerization of this monomer with a tandem system of dimethyl ketene methyl trimethylsilyl acetal with bifluoride sources in 1983. Assuming a mechanism where the trimethylsilyl group (TMS) is transferred onto the next monomer unit, they introduced the term of "group-transfer polymerization" (GTP). While nowadays this reversible addition of the TMS group has been refuted, the term GTP prevails, describing the repeated conjugate-addition polymerization of 1,4-unsaturated *Michael* acceptor monomers, also referred to as poly-1,4-addition, with various different catalysts (Scheme 1).[4–9]
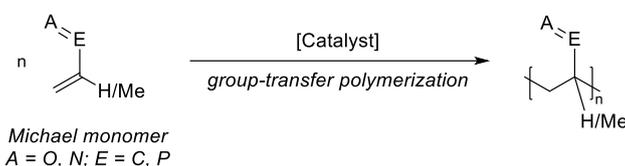
Scheme 1: Generalized polymerization of a *Michael*-acceptor monomer (A = O, N; E = C, P) *via* catalytic group-transfer polymerization.

Today, four different methods of polymerizing such monomers can be differentiated. By using silyl ketene acetals with different nucleophilic sources, *Michael*-type monomers can be polymerized in the so-called silyl ketene acetal group-transfer polymerization (SKA), this polymerization method is also the first reported one for these systems.[4,5,7,10] A major milestone in GTP marks the year 1992, when both Yasuda *et al.* and Collins and Ward introduced different metal catalysts for the polymerization of MMA. Yasuda *et al.* presented the neutral samarocene catalyst $[Cp*_2SmH]_2$ (Cp* = pentamethyl cyclopentadienyl), marking the starting point for rare-earth metal-mediated group-transfer polymerization (REM-GTP).[11] Collins and Ward found a group IV based, cationic zirconocene system $Cp_2ZrMe_2/[Cp_2ZrMe(thf)]^+[BPh_4]^-$ (Cp = cyclopentadienyl), introducing the group IV based GTP catalysts.[12] As a latest method, polymerizations using various *Lewis* pair systems can be performed as introduced by Chen *et al.* in 2010.[13] While initially, Frustrated *Lewis* pairs were used, nowadays a broad variety of different *Lewis* Pairs are applied, generally referred to as *Lewis* Pair polymerization (LPP).[13–15]

While all these different polymerization methods use very different catalyst systems, all of them exclusively follow the conjugate-addition polymerization of *Michael*-type acceptor systems. These *Michael* monomers consist of a vinyl group in conjugation to an acceptor atom-carbon double bond, forming an α,β-unsaturated carbonyl system with nitrogen or oxygen as acceptor

atoms (Scheme 2A). The resonance structure exhibited by such systems allow coordination and bonding to the catalyst systems in their respective keto- or enolate form, later on responsible for the polymerization propagation. In the α-position of the carbonyl, either protons or methyl groups can be found, severely influencing the polymerization behavior of different monomer classes. This is caused by an interaction of steric influence of the side-group functionalities and the α-position substituent. For sterically less demanding esters, little steric repulsion allows for a good p-orbital overlap of the carbon-carbon bond between the ester and the vinyl group, making both methyl acrylate (MA) and MMA polymerizable *via* GTP. Contrary, for dimethyl acrylamide (DMAA) and dimethyl methacrylamide (DMMA), steric repulsion between the amide substituents and the α-position either allow or distort the p-orbital overlap. DMAA with a proton in α-position shows good overlap and is thus polymerizable *via* GTP, while in DMMA with a methyl group in α-position the steric repulsion induces torsion around the C–C bond between the vinyl group and the amide, decreasing the orbital overlap and making it non-polymerizable *via* GTP (Scheme 2B). Additionally, protons in α-positions to carbonyls possess relatively high C–H bond acidity, allowing additional side reactions. In the β-position of the carbonyl usually protons are present, however recently β-substituted monomers have been introduced as well.[6,7,10,16–21]
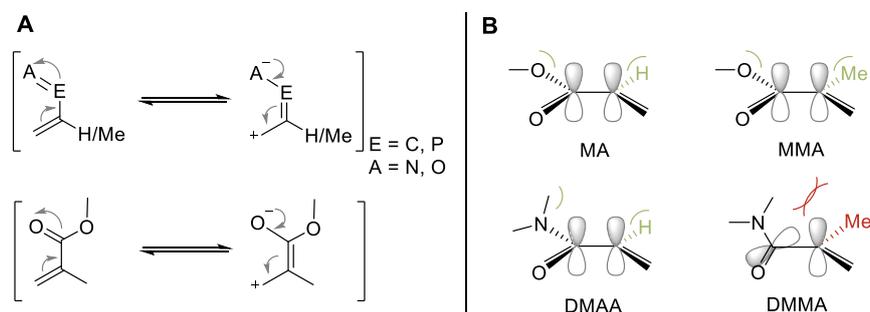
Scheme 2: General resonance structure of α,β-unsaturated *Michael* monomers with acceptor atom A = nitrogen, oxygen and E = carbon, phosphorus (top), exemplary resonance structure of MMA (**A**) and schematic representation of the p-orbital overlap in differently α-substituted monomers MA, MMA, DMAA and DMMA (**B**).[6,7,20]

Initially, GTP research was heavily focusing on alkyl substituted methacrylates and acrylates such as MMA or MA, as classical anionic or radical polymerization methods showed some severe limitations for such systems. However, within the last 30 years, a plethora of different monomers emerged, forming different classes of *Michael* monomers. Some common classes of these monomers are methacrylates, acrylates, acrylamides, vinylpyridines and vinylphosphonates, however also various other monomers have been reported. In recent years also the topic of biobased monomer has been tackled successfully in the context of GTP with the introduction of monomers based on crotonates, cinnamates or methylene butyrolactones. An overview of this classification with different simple and advanced examples is given in

Figure 1. Generally, due to the conjugation character of the vinyl bond to the acceptor function resulting from p-orbital overlap, acrylamides, vinylpyridines and vinylphosphonates are limited to protons in α-position. Due to the lower steric demand of the esters, both acrylates and methacrylates can be polymerized *via* GTP. [7,10,13,15,17–20,22–41]
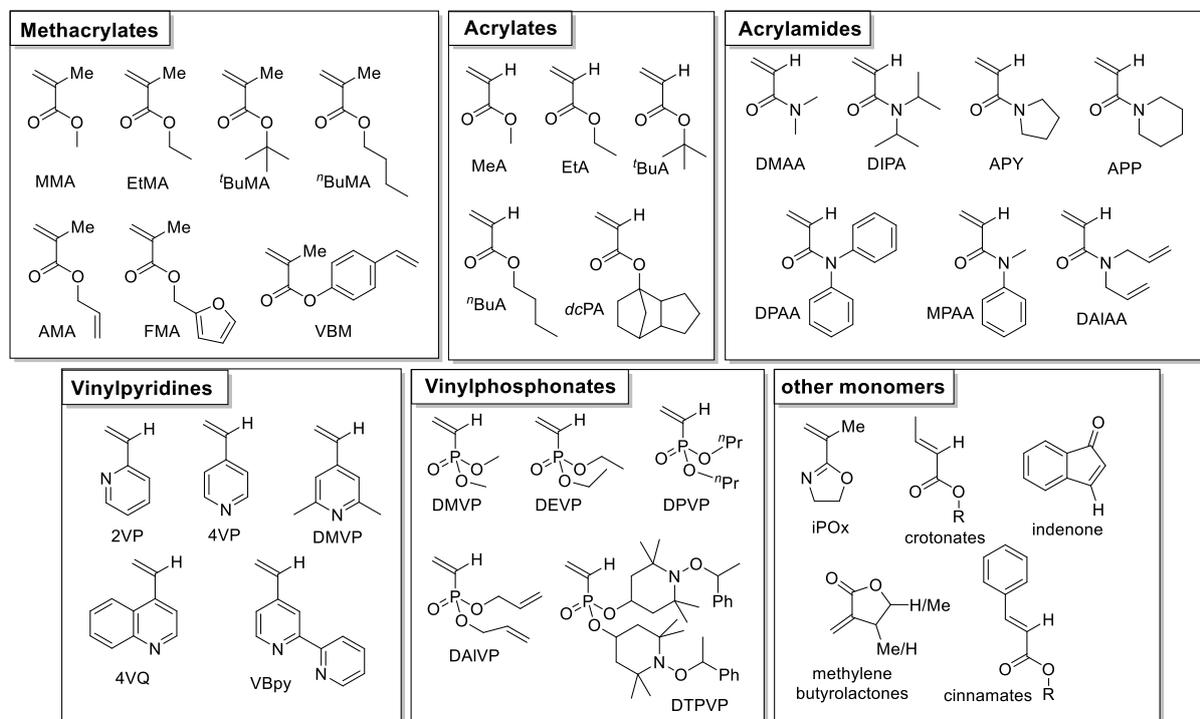
Figure 1: Overview on the different classes of *Michael*-type monomers applied in group-transfer polymerization with common and advanced examples for each class.[7,10,13,15,17–20,22–41]

Generally, GTP monomers can be considered a class of highly functional monomers based on their chemical structure. For the acrylates, methacrylates, and acrylamides a multitude of ester/amide substituents are known, introducing different types of functionalities to the polymers obtained. Two polymer types from *Michael*-type monomers with special functionality worth mentioning are the poly(vinylpyridines) and the poly(dialkyl vinylphosphonates). Due to the pyridine function, poly(vinylpyridines) possess a pH-responsive character based on reversible protonation of the nitrogen and are capable of interacting with metal ions/complexes by metal-pyridine complexation. The poly(dialkyl vinylphosphonates), a class of partially water-soluble polymers, exhibit a tunable lower critical solution temperature (LCST) with reversible phase-transition in water due to temperature changes in the region of 30 – 50 °C. Another way of exploiting the distinct 1,4-*Michael* acceptor character of such monomers is the incorporation of vinyl substituents as side chains like in allyl methacrylate (AMA), vinyl benzyl methacrylate (VBM), diallyl acrylamide (DAIAA), 2,5-divinylpyridine or diallyl vinylphosphonate (DAIVP). As GTP, unlike e.g. radical polymerization, is highly chemoselective towards conjugate addition, those vinyl functions remain intact, providing a starting point for polymer functionalization.[7,10,13,15,17–20,22–40,42–49]

2.1.2. Catalysts for group-transfer polymerization

2.1.2.1. Overview on different catalyst classes

Based on the four different methods capable of polymerizing the described *Michael*-type monomers, different catalyst classes emerged. Within the last 40 years, a plethora of catalysts has been reported, ranging from various rare-earth metals to group IV titanocenes or zirconocenes to main group metal complexes, different *Lewis* pairs or organocatalysts. In Figure 2, a short overview of the different catalyst classes with historic and recent examples is shown, subdividing the different catalysts in classes based on their composition and reaction mechanism.[7,10]
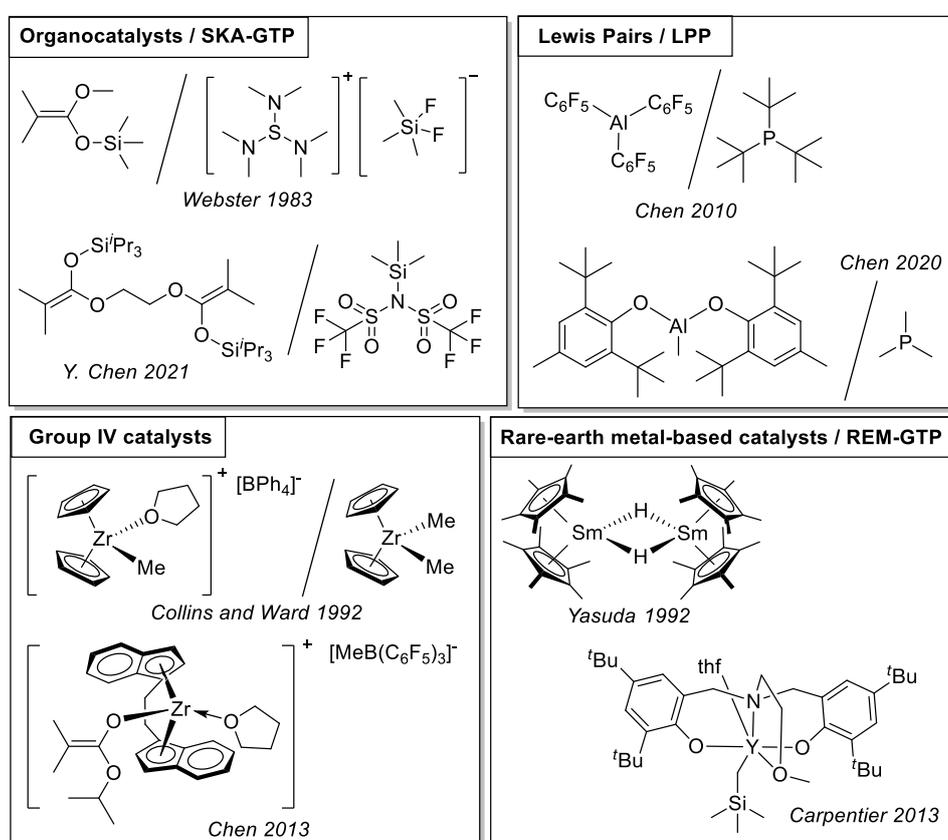
Figure 2: Different historic and recent examples for catalysts subdivided into the four different GTP catalysis methods of silyl-based organocatalysis (top left), *Lewis* Pair mediated polymerizations (top right), group IV metal complexes (bottom left) and rare-earth metal-based catalysts (bottom right).[4,11–13,27,39,50–52]

The first class of catalysts for GTP are two-component systems using silyl ketene acetals (SKA) as initiators in combination with nucleophilic anions like $SiMe_3F_2^-$, HF_2^-, F^-, CN^-, N_3^- or oxyanions with sterically bulky cations like tetraalkylammonium or tris(dialkylamino)sulfonium. In recent years, SKAs in combination with activating agents like (*Lewis*) acids, *Lewis* bases or carbocations instead of the more classic nucleophiles have been reported, complemented by the Tandem SKA with alkyl silanes and *Lewis* acids. A plethora of different combinations has

been investigated since, summarized nowadays under the term of organocatalytic GTP. While these systems remain of high interest, they are beyond the scope of this thesis.[4,5,28,53,54]

A versatile class of catalysts can be found in the *Lewis* Pair catalysts, consisting of a *Lewis* acid (LA) and a *Lewis* base (LB) featuring distinct side-group design to facilitate targeted reactivity. Dependent on their interaction strength, different kinds of *Lewis* Pairs can be distinguished. As first class, so-called classic *Lewis* pairs (CLP) are defined, in which the LA as electron-deficient species and the LB with an electron lone-pair share this electron pair by interaction, severely altering the individual reactivity of both reaction partners forming a stable *Lewis* adduct. CLPs like BMe_3/PMe_3 with close contact of LA and LB are usually considered dormant for polymerizations. This concept was extended with the discovery of so-called Frustrated *Lewis* Pairs (FLP) as introduced by Stephan in 2006, in which no interaction of LA and LB can be exhibited due to strong sterical hinderance between both, as it is the case for $B(C_6F_5)_3$ and $(C_6H_2Me_3)_2PH$. While initially there was a discrete change between CLP and FLP assumed, an intermediate state has been discovered for combinations like $B(C_6F_5)_3$ and 2,6-dimethyl pyridine, which behaves more like a CLP at low temperatures and exhibits FLP-like reactivity in solution, coining the term interacting *Lewis* Pair (ILP). Both FLPs and ILPs have successfully been used in polymerizations of various *Michael*-monomers, summed up under the term of *Lewis* Pair polymerization LPP. An overview on different *Lewis* acids and bases applied in the LPP of *Michael*-type monomers is given in Figure 3. The *Lewis* acids employed are usually electron-deficient, electrophilic compounds with a single coordination side, capable of stabilizing the active species and activating the next monomer unit. Commonly applied are group 13 elements like aluminum or boron, but also rare-earth metal complexes or salts with cations like Zn^{2+}, Mg^{2+}, Hg^{2+} or Y^{3+} exhibit suiting reactivity. The *Lewis* base is usually a neutral, strong base which can also act as nucleophile. Here, a broad range of phosphines, SKAs, phosphazene bases, but also more advanced structures like *N*-heterocyclic carbenes (NHC), *N*-heterocyclic olefins (NHO), *N*-heterocyclic imines (NHI) or ylides has been reported. Also bridged of covalently connected LA/LB combinations have been used for LPP.[13–15,30,31,38,45,50,55–62]
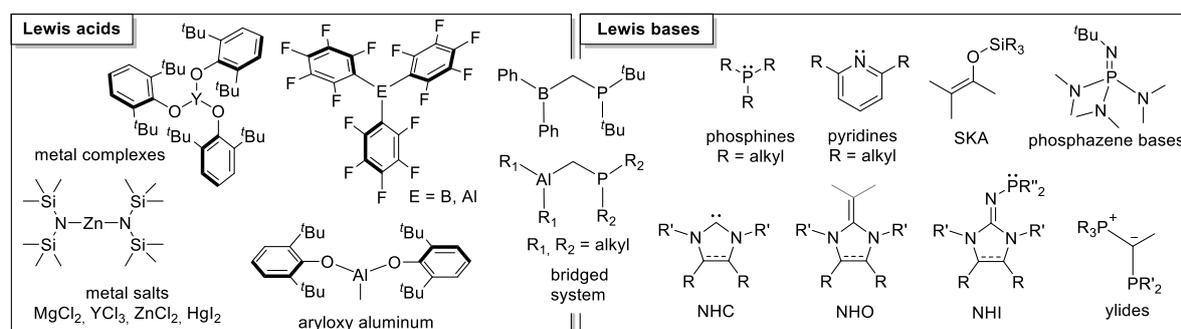
Figure 3: Overview on different *Lewis* acids and *Lewis* bases used in the *Lewis* Pair mediated group-transfer polymerization.[13–15,31,50,57–62]

Apart from those catalysts used in SKA-GTP and LPP, distinct single-site group IV metal complexes for the polymerization of *Michael*-type monomers, with primary focus on acrylates, methacrylates and acrylamides have been reported. Initially designed by Collins and Ward as two-component systems as well, also monometallic catalyst structures have been prepared based on titanium, zirconium, or hafnium. Today, these metallocenes and half-metallocenes with various initiators and symmetries as one- or two-component systems are used for the polymerization of different monomers. To induce fast polymerization initiation, bulky *Lewis* bases are used as cocatalysts (Figure 4).[10,12,39,63–66]
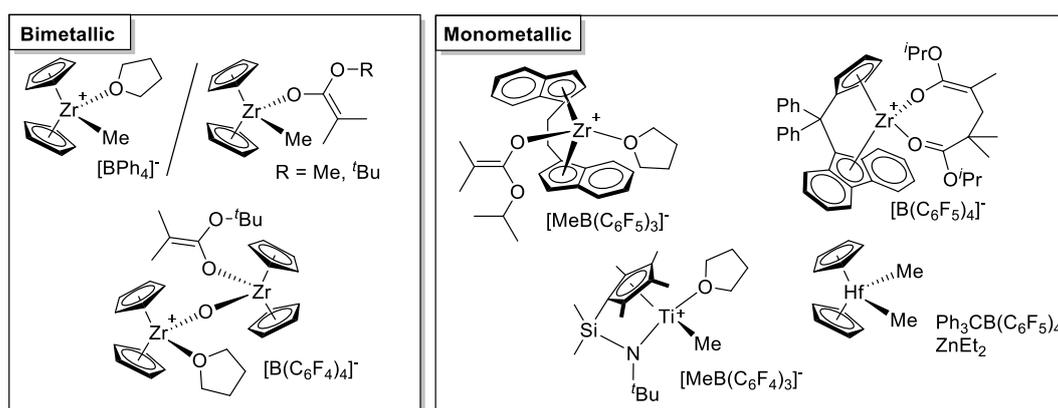
Figure 4: Selected examples of group IV based cationic bi- and monometallic complexes for the polymerization of *Michael*-type monomers.[10,39,63–66]

As a last catalyst class, complexes based on rare-earth metals with various ligand spheres can be distinguished. While the initial metallocene systems introduced by Yasuda *et al.* were designed for the polymerization of MA and MMA, this class of catalysts has gained remarkable attention focusing on the polymerization of vinylphosphonates, vinylpyridines and other functional systems. Within the last 40 years, multiple different catalyst systems for the REM-GTP of *Michael* monomers have emerged, which can be subdivided into metallocene catalysts, half-metallocenes and non-metallocenes (Figure 5).[7,10,11]
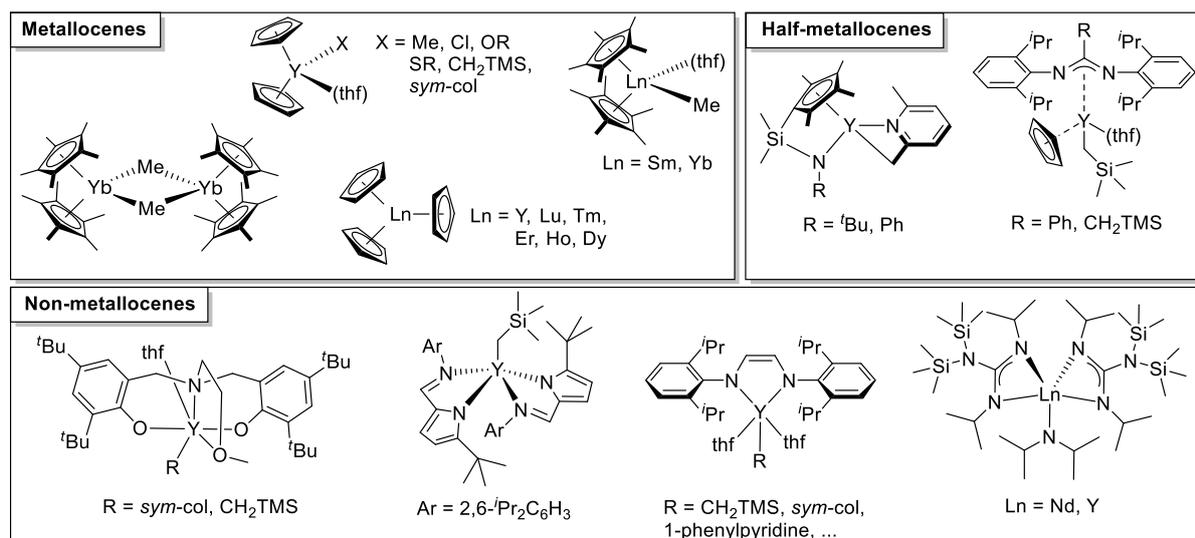
Figure 5: Different REM-GTP catalysts subdivided into the three groups of metallocenes, half-metallocenes and non-metallocenes.[6,10,22,24,29,51,67–73]

The metallocene-based catalysts form the largest group of REM-GTP catalysts, including the first reported catalyst system [Cp*$_2$SmH]$_2$, and are generally very well investigated and understood.[10,22,68] Apart from the classic metallocenes, a sub-class of half-metallocenes emerged, which only possess one Cp ligand and additional substituents as for example found in the so-called constrained-geometry catalysts (CGCs), in which the geometry of the half-metallocene is distorted by using a certain type of substituted Cp ligand.[24,69] REM-GTP catalysts, however, are by no means limited to Cp-ligated complexes. A variety of different complexes exist incorporating ligands like ene-diamido structures, bis(phenolates), pyrolldiminates or guadinates, each exhibiting distinct reactivity towards different *Michael* monomers.[10,29,51,52,70–74]

2.1.2.2. CH-bond activation

Within the group of rare-earth metal-based catalysts, a special type of reactivity can be exploited to give access to even better adapted catalyst species (*vide infra*). Based on the electronic configuration of most Ln^{3+} systems with a d^{0}f^n orbital occupation, no oxidative addition/reductive elimination reactions can take place. First observed by Watson 1983, d^{0}f^n lanthanide metal complexes can undergo σ-bond metathesis, leading to ligand exchanges, metal-element bond formation/cleavage or element-element bond formation/cleavage.[75–79] One major transformation exploited in the context of catalyst synthesis is the CH-bond activation of certain carbon-hydrogen bonds, introducing metal-alkyl moieties.[75–77,80] This CH-bond activation can mechanistically be described as σ-bond metathesis *via* [2σ+2σ]-cycloaddition. The reaction proceeds *via* a concerted reaction of a 4-membered ring metalacyclic intermediate in a kite-like transition state (Scheme 3A).[75,81] While CH-bond

activation is an interesting method for the activation of small molecules in general, in the context of GTP, this reaction is mostly used for the attachment of alkynes or substituted (bi)pyridines as functional initiator moieties of the catalyst as introduced by Mashima *et al.* By reacting the precursor alkylyttrium ene-diamido complex **1** with different substituted alkynes or pyridines, various CH-bond activated metal complexes **2-4** were obtained (Scheme 3B).[7,29,82]
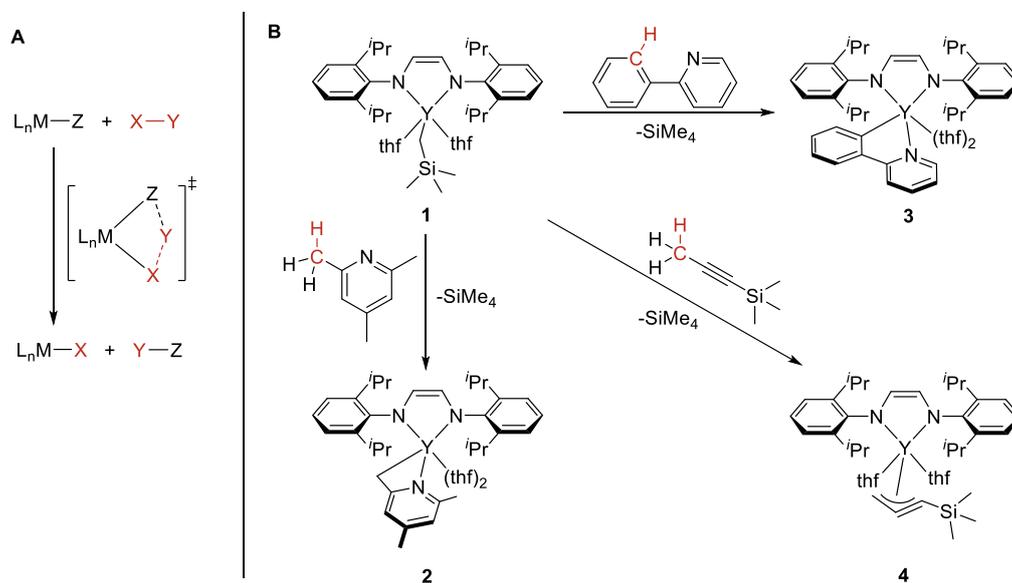
Scheme 3: Generalized reaction scheme and kite-like transition state of the σ-bond metathesis of d[0]f[n] lanthanide metal complexes (**A**) and CH-bond activation of an alkylyttrium ene-diamido complex **1** with different substrates to complexes **2-4** as introduced by Mashima *et al.* (**B**).[29,75]

The CH-bond activation of 2,4,6-trimethylpyridine (*sym*-col) on different lanthanocenes and lanthanide bis(phenolate) catalysts by Rieger *et al.* led to the discovery of different tailor-made catalysts with highly beneficial properties for the GTP of different *Michael*-type monomers.[68,70] Both Mashima *et al.* and Rieger *et al.* further successfully used 2,3,5,6-tetramethylpyrazine (TMPy) for the synthesis of bimetallic catalysts (Figure 6A, **5-7**).[29,44] As derived from single crystal X-Ray diffraction (SCXRD) of complexes **6** and **7**, the binding motif of the pyridine can best be described as η^3-(C,C,N)-aza-allylic coordination, an intermediate of the η^2-allylic-amine and the η^1-amido-olefinic coordination reported by Teuben *et al.*[44,70,83,84] For complex **6**, the Y-N bond is shorter than the Y-C$_\alpha$, indicating a primary coordination by the nitrogen moiety. All carbon-carbon bonds within the aromatic ring exhibit bond-length between those of single and double bonds as expected for aromatic systems. Based on the binding motif, the activated methyl group and the respective carbon-carbon bond C$_6$-C$_7$ has a reduced bond length with predominant double bond character and conjugation to the aromatic ring. The other two, non-activated methyl groups with the carbon-carbon bonds C$_2$-C$_8$ and C$_4$-C$_9$ exhibit bond lengths in the normal single bond region with no conjugation to the aromatic system (Figure 6B). The

same η^3-(C,C,N)-aza-allylic coordination can be found for bimetallic catalyst **7**, in which the two adjacent methyl groups are activated.[44]
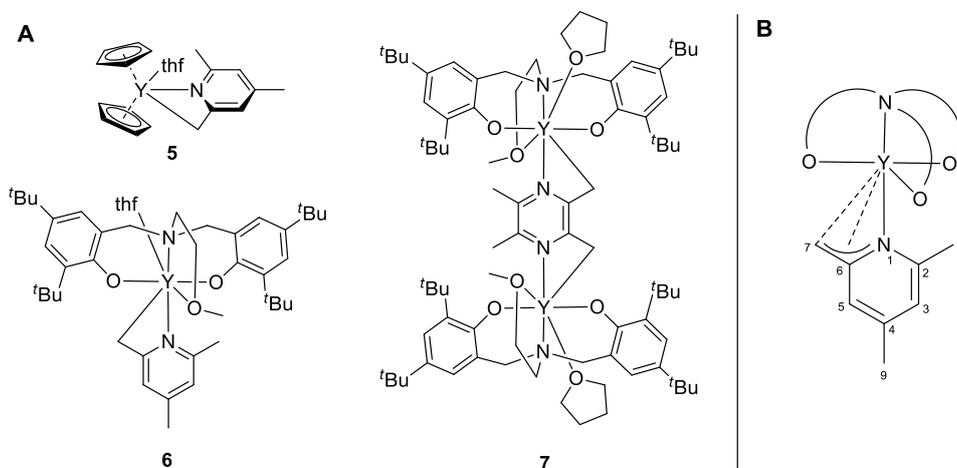
Figure 6: CH-bond activated bis(cyclopentadienyl) yttrium complex **5** and bis(phenolate) yttrium catalysts **6**-**7** (**A**) and close-up of the binding motif of complex **6** (**B**).[44,68,70]

Both the CH-bond activated bis(cyclopentadienyl) yttrium complex **5** and the yttrium bis(phenolate) complex **6** are prepared *via* the same activation of their respective CH$_2$TMS alkylyttrium precursor with *sym*-collidine. In terms of reactivity, the CH-bond activation of yttrium metallocene compounds usually proceeds within 2-3 hours at room temperature with little to no side reactions. Based on this behavior, an *in-situ* approach has been developed, in which the CH-bond activation is performed prior to polymerization and the monomer is just added to the catalyst without catalyst isolation.[7,68,85–88] Contrary, for the yttrium bis(phenolate) catalyst **6**, the activation has to be performed at elevated temperatures with prolonged reaction times. This leads to some decomposition side reactions and makes catalyst purification necessary.[32,44,70] While the *in-situ* approach is much faster to perform and requires no complex catalyst purification, yttrium bis(phenolate) catalysts show higher versatility in terms of monomer scope or stereo control. Yet, both ways additionally offer the possibility of introducing functional groups to the polymers as well.[43,44,70,74,85–89]

2.1.3. Mechanistic aspects

2.1.3.1. Rare-earth metal-mediated group-transfer polymerization

One main mechanistic step in the polymerization of *Michael*-type monomers like vinylphosphonates with rare-earth metal-based catalysts is the initiation reaction, in which the catalyst-coordinated initiator moiety reacts with the first monomer unit to form an active chain-end. In the REM-GTP of trivalent lanthanides, this initiation reaction can occur *via* different pathways, depending on the catalysts' structure and initiator motif.[90,91] While the initiation reaction is best investigated for bis(cyclopentadienyl) lanthanides, initiation behavior and reaction pathways are generally quite similar for non-metallocene catalysts as well.[7,10,51,70,92] Depending on the initiator of the catalyst and whether pre-coordination with tetrahydrofuran as loosely bound ligand is present (Scheme 4A), the initiation starts with either dissociation of bimetallic catalysts or displacement of the THF moiety by coordination of the first monomer unit. This step can severely influence the polymerization performance of the catalyst. If the coordination strength of the monomer is not sufficient to intercalate between the two catalyst moieties, no polymerization takes place, whereas a slow cleavage can lead to an initiation delay and broadened polymer dispersity.[32,70,90,92] Moreover, different initiating groups undergo different reactions to initiate the polymerization. The most common initiation is the nucleophilic transfer of the initiator *via* a 6-electron process (Scheme 4B) in which initiators like *tert*-butyl thiolate or $N(SiMe_2H)_2$ act as nucleophiles and are transferred onto the first monomer unit, forming the active enolate-catalyst species responsible for propagation.[90] For certain initiators with a C=C double bond conjugation such as *sym*-collidine or Cp, this nucleophilic transfer can also proceed as 8-electron process (Scheme 4C).[68,93,94] Both pathways have in common that the initiator is irreversible transferred onto the first monomer unit and is present in the polymer chain after polymerization, with some being stable and other such as S^tBu being prone to elimination.[32,68,88,90] Strongly basic alkyl initiators like methyl or CH_2TMS can additionally initiate polymerizations of non-α-substituted monomers *via* deprotonation of the acidic α-H leading to an allenylic intermediate (Scheme 4D), however this type of initiation is usually disfavored as it leads to low initiation efficiencies and long initiation delays, possibly broadening the polydispersity. Yet, these initiators are not limited to this type of reactivity and can also undergo nucleophilic transfers.[51,70,90] Aside from these three major pathways, some additional reactivities have to be considered for Cp_2LnX (X = Cl, OR) or Cp_3Ln systems. In tris(cyclopentadienyl) catalysts, two Cp-ligands are coordinated in a η^5-fashion and the third unit is, depending on the central metals' ionic radius, switching its hapticity between a η^5- and a η^1-coordination. The η^1-coordinated ligand is then acting as nucleophile and attacks either *via* the 6-electron or the 8-electron nucleophilic transfer.[21,67,94] For the chlorido and alkoxylate complexes, the interactions between the Cl/OR ligand and the metal center is too strong to

directly initiate a polymerization *via* nucleophilic transfer/deprotonation. Instead, a reversible ligand transfer takes place, forming $CpLnX_2$ and Cp_3Ln both coordinating monomer units and the reaction is again initiated by one Cp-unit of Cp_3Ln.[21,90] For the rare case of divalent lanthanocenes like Cp_2Sm, a radical initiation is proposed.[90,95]

Generally, control of the initiation pathway is crucial for obtaining defined polymers. Usually, very short initiation phases with high initiator efficiencies are desired, where only one initiation pathway is possible. Deprotonation is not desired and catalyst design has focused on optimizing the catalysts' properties to facilitate controlled initiation of different monomers. One very striking example is the introduction of α-methyl pyridine moieties to this class of catalysts as a very suiting initiator group for a variety of monomers by mimicking the transition state of the polymerization during initiation.[7,10,21,70,90,93]
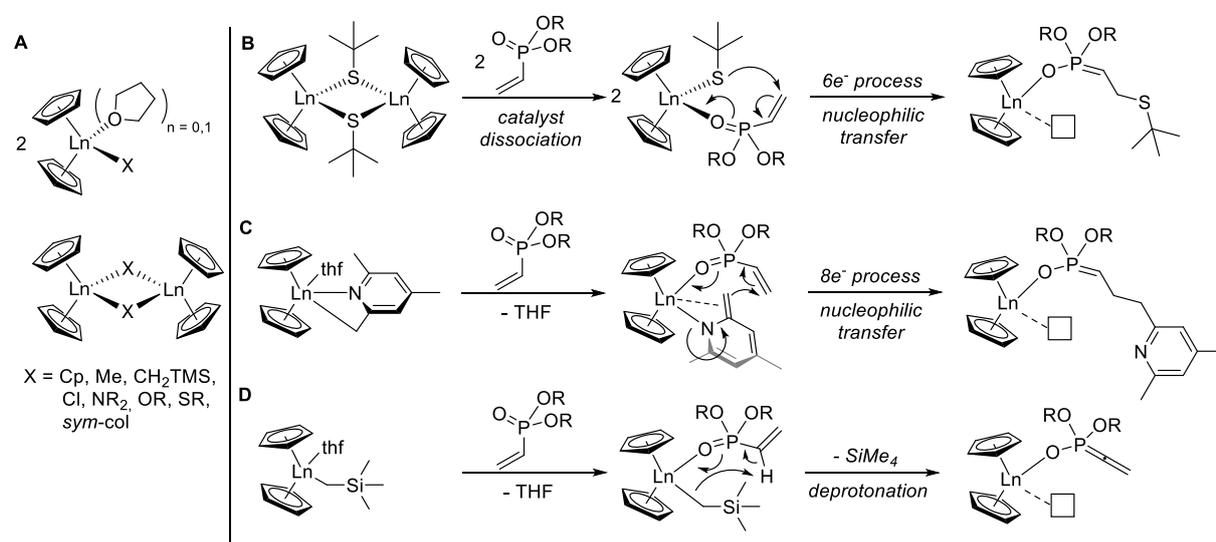
Scheme 4: Initiation pathways of different bis(cyclopentadienyl) lanthanoid catalysts Cp_2LnX (X = Cp, Me, CH_2TMS, Cl, NR_2, OR, SR, *sym*-col) (**A**) *via* 6-electron nucleophilic transfer of the initiator (**B**), 8-electron nucleophilic transfer of the initiator (**C**) or deprotonation by highly nucleophilic initiators (**D**).[6,21,68,90,94]

After initiation, the first monomer unit is covalently bound to the catalyst in its enolate form with a free coordination side on the metal center, where the next monomer is coordinating *via* its keto form. With the monomer being activated by this coordination, the enolate is acting as a nucleophile and attacks the monomer in an 8-membered ring transition state (Scheme 5, state **I**). This 1,4-conjugate addition or *Michael*-addition catalyzed by the metal center is also referred to as monometallic *Yasuda*-type mechanism and can be observed for the polymerization of different monomers *via* REM-GTP.[10,11,22,51,96,97] After this nucleophilic attack, a metallacycle is formed, in which the last attacked monomer unit is covalently attached to the metal center in its enolate form, and the previous unit is coordinated in its keto form. This keto-enolate structure is the resting state of the polymerization, in which the polymerization remains

upon full consumption of the monomer, being responsible for the highly living character of REM-GTP (Scheme 5, state **II**). This stable intermediate has been confirmed by Yasuda *et al.* *via* X-Ray structure elucidation of Cp*$_2$Sm(MMA)$_2$ formed by addition of two equivalents of MMA (*per* Sm center) to the catalyst [Cp*$_2$SmH]$_2$ (Scheme 5, right).[10,11,21,22,93,96] The rate-determining step in the propagation of vinylphosphonates is the S_N2-type displacement of the keto-coordinating polymer chain by the next monomer in a pentacoordinate intermediate (Scheme 5, state **III**).[21] In the context of REM-GTP, the catalyst molecule serves as initiator and catalyst responsible for stabilizing the polymerization propagation.[10]
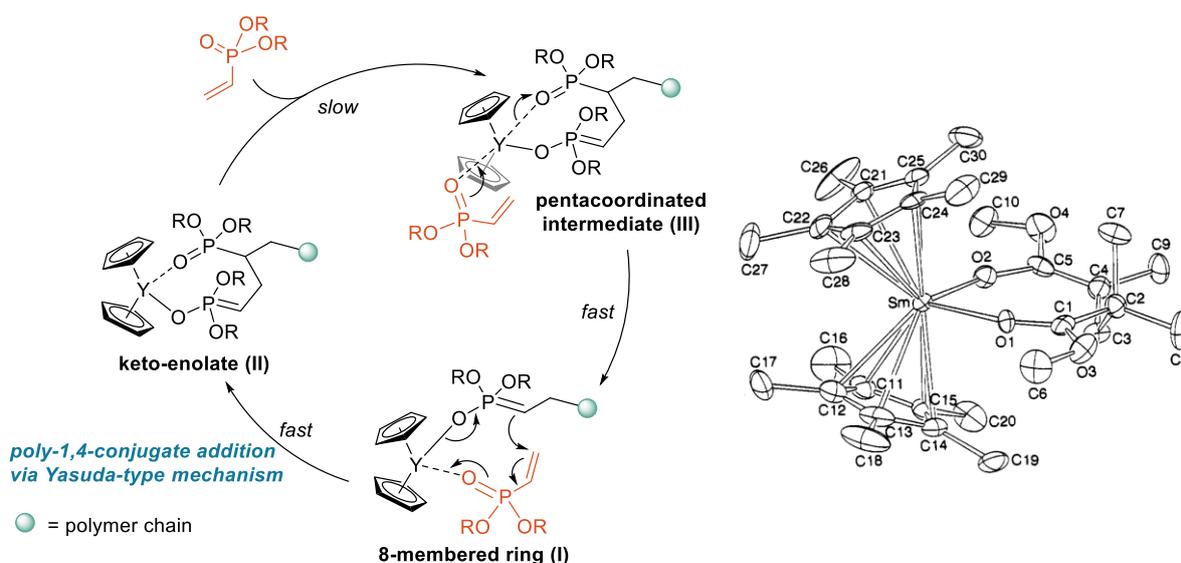
Scheme 5: Monometallic *Yasuda*-type propagation in the rare-earth metal-mediated group-transfer polymerization of *Michael* monomers, adapted from Rieger *et al.* (left) and crystal structure of Cp*$_2$Sm(MMA)$_2$ determined by Yasuda *et al.* (right).[11,21,22]

While the propagation is mechanistically indifferent for various types of monomers, the metal center has a tremendous influence on the catalyst activity. The two best-studied systems in this context are dialkyl vinylphosphonates and methyl methacrylate. As determined by Yasuda *et al.*, the activity of structural identical complexes with different central metal atoms in the polymerization of MMA with Cp*$_2$LnMe (Ln = Sm, Y, Yb, Lu) increases with increasing ionic radius of the metal in the order Sm (1.11 Å) > Y (1.04 Å) > Yb (1.01 Å) > Lu (1.00 Å).[22] Contrary, Rieger *et al.* found an inverse dependency for the polymerization of diethyl vinylphosphonate (DEVP) with Cp$_2$LnCl (Ln = Tb, Y, Tm, Lu), where the activity is enhanced by decreasing ionic radii of the metal centers from Tb (1.06 Å) < Y (1.04 Å) < Tm (1.02 Å) < Lu (1.00 Å).[21] Investigations in the cause of this behavior revealed an activity independency on enthalpic effects in DAVP polymerization, where the Ln–(O=P) bond strength based on *Lewis* acidity and metallacycle ring strain does not influence reaction rates. They deduced the change in activity from a change of the activation barrier resulting from an entropic change of the metallacycle transition state. Based on further investigations on monomer size influence and

results from Ziegler *et al.* and Chen *et al.,* they were able to draw a set of conclusions for the REM-GTP of *Michael*-type monomers like DEVP. Firstly, the steric demand of the incoming monomer is of minor influence for the propagation of the polymerization, as the metal–(C=O) bond of the monomer is much longer than for the polymer in the transition state **III**, leading to a low steric demand of the next monomer. Secondly, smaller metal centers in structurally identical complexes destabilize the propagation state due to higher steric constraint of the eight-membered metallacycle state **II**. This destabilization results from entropic effects rather than enthalpic effects due to the high steric demand of the metallacycle compared to the ligands. At last, in terms of monomer size versus metal size, increasing steric demand of the polymer chain destabilizes the metallacycle transition state **II** due to entropic and enthalpic effects, whereas the steric demand of the monomer is of minor influence for both alkyl vinylphosphonates and alkyl methacrylates. While the behavior of lanthanocene catalysts is well-investigated in the context of vinylphosphonates and in part for methacrylates, it remains of major interest for understanding REM-GTP.[10,21,22,33,39,90,98]

As for the metal center, the ligand type does not influence the propagation type of the REM-GTP, yet, it has an influence of the propagation rate and entropic and enthalpic behavior of the polymerization. For lanthanocenes, the polymerization activity decreases with steric increase of the ligand sphere, as observed for MMA polymerization by Yasuda *et al.* with Cp^*_2Ln systems being considerably slower than Cp_2Ln catalysts. Rieger *et al.* observed the same trend for the catalysts $Cp_3Y > Cp^{TMS}_3Y$ ($Cp^{TMS} = C_5H_4TMS$) > Cp'Y (Cp' = C_5Me_4H).[22,94] While lanthanocenes have been investigated thoroughly, they exhibit a major limitation of showing poor performance for the polymerization of nitrogen-containing monomers like 2VP or 2-*iso*-propenyl-2-oxazoline (IPOx).[17] This lead later on to the emergence of non-metallocenes with different ligand types like ene-diamido or bis(phenolates) for REM-GTP catalysts as a new, versatile catalyst class.[29,51]
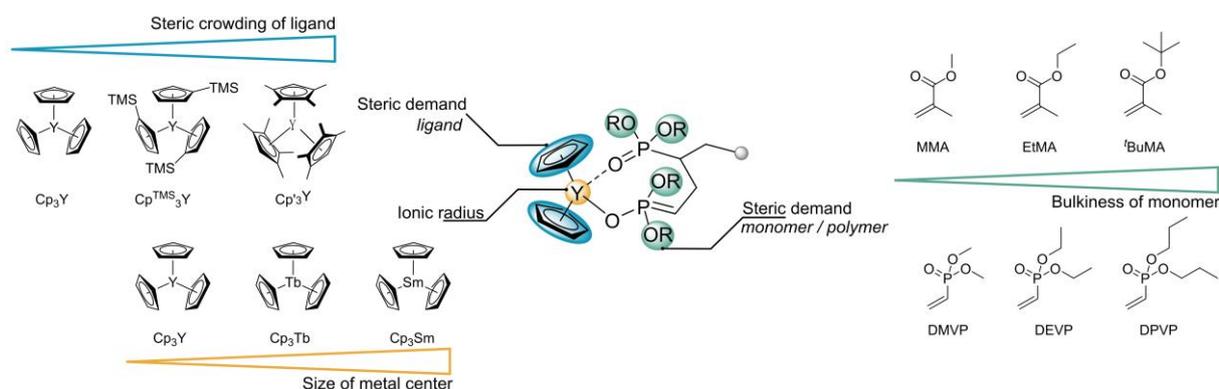

Figure 7: Influencing parameters on the polymerization activity of different lanthanocenes complexes.[22,33,94]

Applying metal catalysts for the polymerization of *Michael*-type monomers offers a broad range of unique advantages. Not only do they feature high activities while maintaining narrow polydispersity ($Đ < 1.05$), but also the initiation pathway can be adjusted to the monomer systems, allowing precise molecular weight control based on the used catalyst:monomer ratios (M_n up to 500 kg/mol). Tailoring such properties appropriately to the monomer system enables precise and adjustable polymer synthesis for a broad range of different functional polymers.[6,7,10,16,22,90,99] Other advantages are the high chemoselectivity of the polymerization, leaving functional groups like allylic sidechains intact or the broad temperature range over which the polymerization remains controlled.[22,26,34,46] Additionally, like most metal-catalyzed polymerizations, REM-GTP is also suited for the introduction of different types of stereoregularity to most of the polymers synthesized. This can, dependent on the combination of monomer and catalyst, occur either *via* chain-end or enantiomorphic site control.[22,69–72,74,92]

Furthermore, due to stabilization of the active chain-end, REM-GTP exhibits a highly living character of the polymerization even after full consumption of the monomer. This living character usually can also be observed by a linear increase of the molecular weight with monomer conversion. While this is inherently already an advantage of metal catalysis, also the synthesis of (multi-)block copolymers is possible by means of (REM-)GTP. By using sequential addition, different types of *Michael*-monomers can be copolymerized to block copolymers, however, there is one major aspect one must consider. As during propagation of REM-GTP the next monomer unit has to displace the polymer chain coordinating to the catalyst, its coordination must be stronger than the coordination of the polymer carbonyl unit. While this is the case within one class of monomers, e.g., alkyl vinylphosphonates, this does not hold true for different classes of monomers. *Via* copolymerization screenings, the following relative coordination strength series (with respect to the same central metal) has been determined: DEVP > DMAA > MMA > IPOx > 2VP (Scheme 6). Accordingly, differently substituted monomers from the same monomer class can be copolymerized statistically, while combinations of different monomer classes are strictly limited to block structures. This is for example the case for the differently substituted vinylphosphonates with ethyl (DEVP), methyl (DMVP) or *n*-propyl (DPVP) side chains. If monomers from two different classes are added to the catalyst at the same time, only the stronger coordinating one is polymerized.[7,8,20,33,100,101]
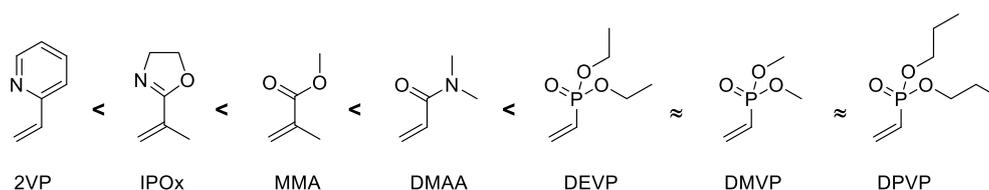
Scheme 6: Relative coordination strength of different classes of *Michael*-type monomers to the same metal center.[7,8,20,33,100]

2.1.3.2. Group IV metallocene catalysis

In terms of catalytic behavior, many similarities can be drawn between trivalent, neutral lanthanide catalysts and cationic group IV transition metal catalysts. Herein, generally two different mechanisms can be distinguished, exhibiting either mono- or bimetallic polymerization propagation. In terms of initiation, mono- and bimetallic systems behave very similar to each other while both exhibit a distinct difference compared to the REM-GTP catalysts.[7,10] The main class of monomers for this class of catalysts are methacrylates and acrylamides.[7,10,12,63,66]

As initially reported by Collins and Ward, MMA is readily polymerized with the bimetallic catalyst system [$Cp_2ZrMe(thf)$]$^+$[BPh_4]$^-$/Cp_2ZrMe_2.[12] Again, first an initiation step has to take place before the polymerization itself can be performed. As in the case of REM-GTP, a ligand exchange from THF to a coordinated MMA unit takes place at the cationic [$Cp_2ZrMe(thf)$]$^+$ center. Subsequently, the methyl group attacks the β-carbon of the coordinated MMA in a 6-electron nucleophilic transfer similar to the initiation in REM-GTP (Scheme 7, left initiation pathway).[10,102] However, the initiation by methyl groups is very slow, influencing the polymerization negatively.[63,66,102,103] Addressing this issue, a new class of initiators has been developed using ester enolates covalently attached to the metallocene, severely increasing the initiator efficiency.[64,102,104,105] *Chen et al.* further developed this principle presenting zirconocene ester and amide enolate complexes like [*rac*-(EBI)ZrMe(OC(O^{i}Pr)=CMe$_2$)] or [*rac*-(EBI)ZrMe(OC(NMe$_2$)=CMe$_2$)] (EBI = ethylenebis(indenyl)) exhibiting remarkable stability upon activation.[66,97,103] These neutral *ansa*-zirconocenes were not able to initiate the polymerization of MMA or DMAA themselves due to a strong Zr–Me interaction. Activation with bulky aluminum or boron *Lewis* acids like $B(C_6F_5)_3$ (BCF) generates a cationic zirconium active center with a very loosely coordinating anions, allowing the first monomer unit to be coordinated. Subsequently, the initiating ester/amide enolate moiety acts as nucleophile and undergoes an 8-electron nucleophilic transfer similar to the REM-GTP initiation, starting the polymerization (Scheme 7, right initiation pathway).[10,63,66,97] This gave access to catalysts with nearly quantitative initiation efficiencies, severely improving this class of catalysts. As reason for this behavior, the structural similarity of the initiator and hence the similarity of the initiation step to the propagation step is assumed.[10,63,103]

When looking at the propagation of this class of metal catalysts, again a difference has to be made between the monometallic and the bimetallic systems. The initial two-component system reported by Collins and Ward follows a bimetallic propagation pathway, in which one metallocene is responsible for coordinating and activating the monomer, while the other complex stabilizes the active enolate chain-end. Then an intermolecular 1,4-*Michael* addition between the two species takes place, leading to chain elongation and recapture of another monomer unit (Scheme 7, left propagation cycle). In this case, the propagation *Michael-*

addition is the rate-determining step.[10,12,102,105] Contrary, kinetic investigations on the *ansa*-metallocenes introduced by Chen *et al.* revealed a first-order dependency on the catalyst concentration, indicating a monometallic propagation of the polymerization. In fact, in these systems the propagation again follows a *Yasuda*-type mechanism with an 8-membered ring metalacyclic intermediate, which is also the resting state of this polymerization (Scheme 7, right propagation cycle).[63,66,97] Using these catalysts, narrow polydispersities have been achieved while retaining a highly living character. Block copolymers of methacrylates and acrylamides are accessible, however with the same addition sequence limitation as in REM-GTP. Additionally, high degrees of tacticity could be induced to methacrylates and acrylamides, based on enantiomorphic site control by the catalysts employed.[10,63–65,97,106]
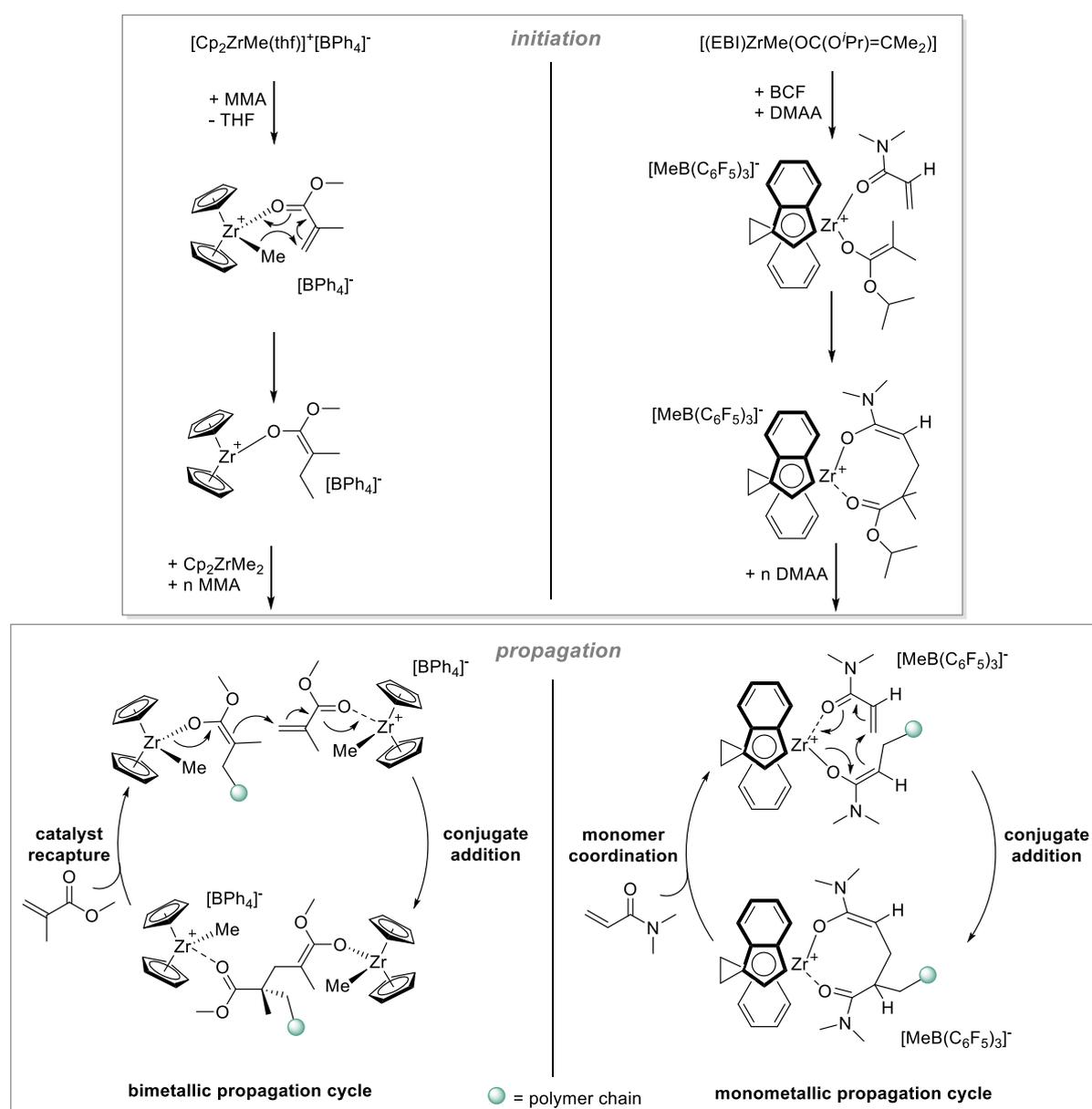
Scheme 7: Initiation and propagation of MMA polymerization by two-component zirconocene catalyst systems as introduced by Collins and Ward (left) and initiation and *Yasuda*-type propagation of DMAA polymerization by monometallic *ansa*-zirconocenes as proposed by Chen *et al.* (right).[7,10,12,63,66,97,98,102]

2.1.3.3. *Lewis* Pair mediated group-transfer polymerization

To use *Lewis* Pairs for the polymerization of *Michael* monomers, the amphiphilic character of the monomers is exploited. The carbonyl function itself is a *Lewis* basic site and has the ability to form adducts with *Lewis* acids, activating the carbonyl function and thus the monomer. The conjugated vinyl function is *Lewis* acidic and can react with *Lewis* bases to form adducts (Scheme 8). By exploiting this reactivity, the (co)polymerization of various *Michael* monomers like different (meth) acrylates and acrylamides has been successfully addressed. Additionally, also vinylphosphonates or N-acceptor containing monomers like IPOx or 2VP, the extended 1,6-acceptor system 4-vinylpyridine, as well as cyclic monomers like methylene butyrolactones or indenone could be polymerized by appropriate catalyst choice.[13,15,30,38,45,50,57,59]
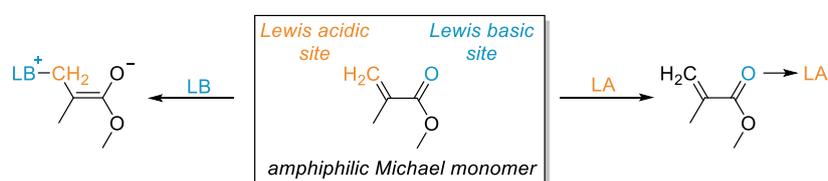
Scheme 8: Amphiphilic character of *Michael*-type monomers like MMA and reactivity towards *Lewis* acids and *Lewis* bases to form the respective LA/LB adducts.[14]

By exploiting this reactivity, the monomer can be activated by the LA, increasing its reactivity and susceptibitliy towards nucleophilic attacks. Then the LB attacks the first monomer in a conjugate addition, forming the active chain-end stabilized by the LA with the LB covalently bound to the monomer (**Scheme 9**, top pathway). For the case of monomers substituted with protons in α-positions like DEVP or MA, an additional initiation pathway is accessible, in which the LB deprotonates the α -position, forming an allylenic monomer unit stabilized by the LA (Scheme 9, bottom pathway). In the case of the conjugate addition, the polymer is terminated by the LB, while for the deprotonation, olefinic chain-ends are generated.[14,15,45,57]
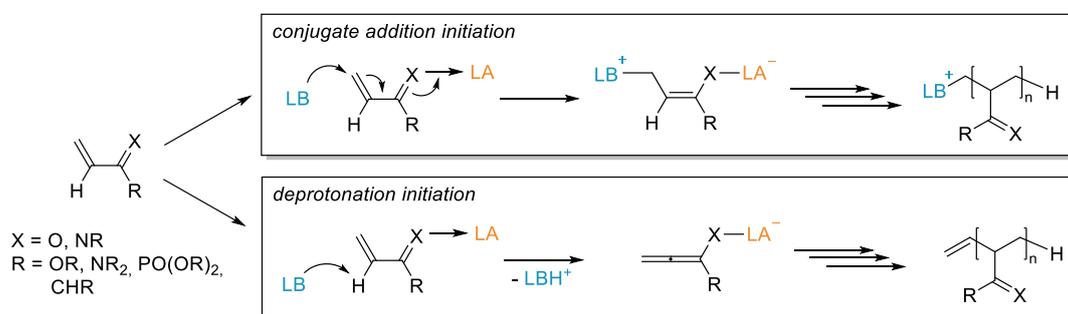
Scheme 9: Initiation of the *Lewis* Pair mediated GTP of different α-H-substituted *Michael*-type monomers (X = O, NR; R = OR, NR$_2$, PO(OR)$_2$, CHR) *via* conjugate addition pathway (top) or deprotonation pathway (bottom).[14,15,38,59]

Usually, *Lewis* Pair polymerizations are performed with one equivalent of LB and two equivalents of LA, which is originating from the dual functionality of the LA. It is capable of stabilizing the reactive enolate chain-end and is simultaneously responsible for activating the monomer (**Scheme 10**, **I**), which is inactive on itself. With respect to this reactivity, the applied LA are usually electrophilic compounds with a single coordination site, which becomes saturated upon stabilization of the chain-end anion. Based on this behavior, one LA molecule is responsible for stabilizing the polymer chain while the other LA molecule activates a monomer simultaneously. The propagation proceeds then *via* a bimolecular reaction of the polymer chain with the activated monomer (**Scheme 10**, **II**), in which the LA-stabilized enolate attacks the LA-activated monomer nucleophilic in a conjugate addition (**Scheme 10**, **III**). This reaction is the rate-determining step (r.d.s.) of the LPP, leading to the same stabilized enolate-chain end and the second LA coordinating to the carbonyl function of the polymer chain (Scheme 10, **IV**). In a last step, the active chain releases the coordinating LA, which coordinates the next monomer unit, repeating the propagation cycle.[14,38,57]
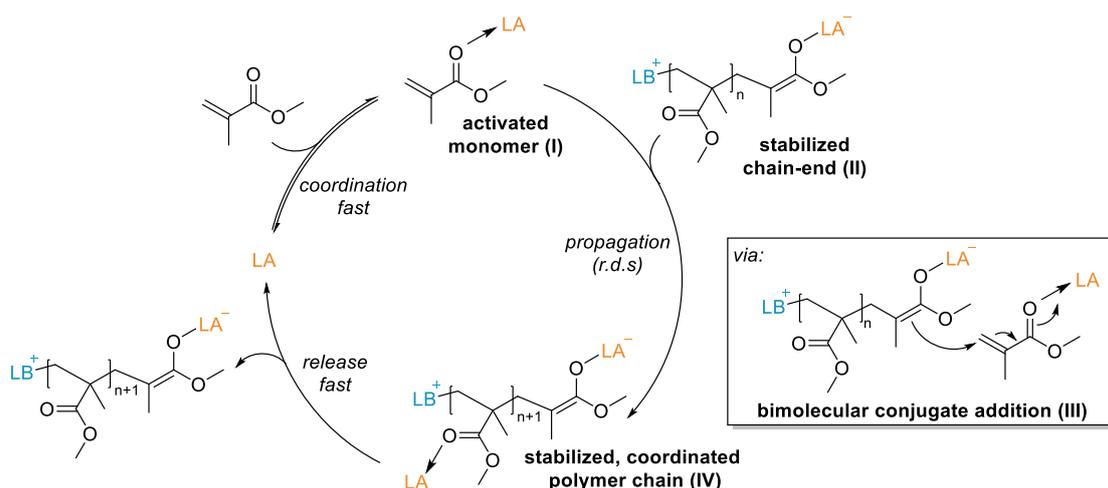
Scheme 10: Catalytic propagation of a *Lewis* Pair Polymerization of *Michael*-type monomers catalyzed by *Lewis* acids and initiated by *Lewis* bases.[14,38,50]

Kinetically, the LPP of *Michael* monomers usually is zero-order in the monomer and first-order in the LA, leading to a linear conversion over time profile. This behavior is caused by the inability of non-activated monomers to react with the chain end, respectively by the inability of the stabilized chain-end to attack any other carbonyl function than the activated one. Generally, LPP can be considered a highly tunable polymerization technique capable of polymerizing *Michael* monomers with high control and precision with respect to polymer parameters like chain-length, macrostructure, dispersity, reactivity, or monomer selectivity. Based on the tremendous number of reports on this technique, a broad library of (commercially) available *Lewis* acids and *Lewis* bases can be used for tailoring suited LPP systems for various (functional) monomers.[14,50,57]

2.2.   Ring-opening polymerization

2.2.1.   General remarks and monomer scope

For ring-opening polymerization (ROP) in general terms, a plethora of different monomer classes can be employed, involving different mechanisms ranging from radical and ionic polymerizations to catalytic methods like metathesis or coordinative-anionic mechanisms. The scope of available monomers comprises many different monomer classes, with all of them being cyclic as the name of ROP implies. This includes olefins, (thio) ethers, disulfides, silicones, phosphoesters, phosphazenes, carbonates, anhydrides, carboxyanhydrides, morpholines, amides, lactames or esters (lactones) and diesters (glycolides) as well as their sulfur derivatives.[107,108] Generally, three different pathways for the synthesis of polyesters are possible, involving polycondensation of diacids and diols, ring-opening copolymerization of cyclic anhydrides and epoxides or ring-opening polymerization of lactones.[109]
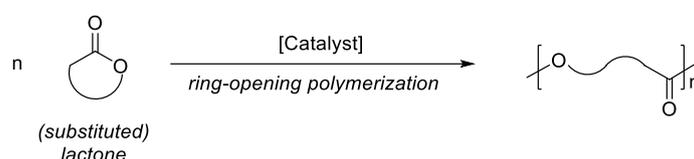
Scheme 11: Generalized reaction scheme for the ring-opening polymerization of lactones.

In terms of monomer scope and synthesis, application profile and advanced properties like degradability or feedstock sourcing, (aliphatic) polyesters from (substituted) lactones and glycolides remain one of the most interesting and well-researched classes of ROP monomers, on which also this work will focus. In Figure 8 different examples for lactones available for ROP are shown.[107,109–112]
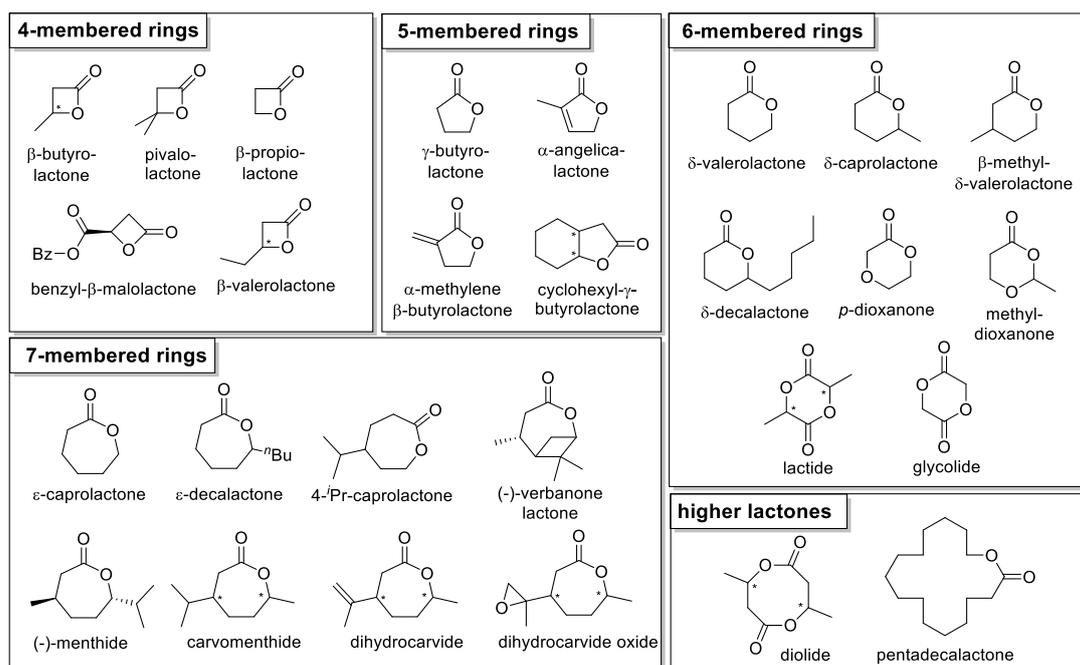

Figure 8: Examples for lactones available for polyester synthesis, grouped by ring size.[110,112–117]

2.2.2. Terpenes in polyester synthesis

While a broad range of different lactones are known for the synthesis of polyesters, within recent years aspects like degradability and sourcing of monomer feedstocks have gained increasing attention. Especially with depletion of fossil fuels, the main source of monomer feedstocks, the search for replacement feedstocks based on renewable materials has intensified. Bio-based polymers can be produced from a variety of different sources, involving natural acids, sugars, terpenes, terpenoids, lignin-based structures or other sources.[114,118–124] When looking for new, biobased feedstocks to produce polymer materials, several aspects have to be considered. Two major points which need to be addressed are the pricing of the product, making it necessary to use feedstocks with high abundance and easy/cheap isolation and work-up, and the competition with crop space.[120,122,125–129] One class of feedstock materials capable of addressing these issues are the terpenes/terpenoids, as some of them show high natural abundance and are sometimes even byproducts from large-scale industrial applications. The major feedstocks interesting for the production of polymeric materials in this context are limonene, with menthol and carvone as derived terpenoids, and turpentine oil, mostly consisting of α-pinene, β-pinene and 3-carene.[110,114,130,131] These molecules can be transformed into polymers by a variety of different routes, e.g. by direct cationic or radical polymerization to polyhydrocarbons[132–135], epoxidation and ring-opening polymerization to polyethers[136] or epoxidation and copolymerization with CO_2 to polycarbonates.[137,138]

With respect to polyester synthesis, four different pathways can be used, transformation into diols/diacids for AA/BB-type polycondensation with suiting comonomers[124,139], transformation into difunctional carboxylic acid alcohols for AB-type polycondensation[140], ring-opening copolymerization of epoxides and anhydrides[141,142] or oxidation and ring-extension *via Baeyer-Villiger* oxidation to lactones for subsequent ROP.[110,143] For the last approach, various synthesis pathways to the respective lactones based on (-)-menthol, (-)-carvone, α-pinene or β-pinene have been introduced.[128,130,139,143–145] The terpenoids menthol and carvone used as starting material are biosynthetically produced from limonene as terpene intermediate and can be isolated from mint or caraway seed, while the terpenes α-pinene and β-pinene are commonly abundant in turpentine oil as the two major compounds, obtained as byproduct from pulp production.[114,126,127,131,139,143] The transformation of these terpenes and terpenoids usually involves reactions such as oxidations, hydrogenations and/or rearrangements prior to the synthetic key step, the ring expansion by oxidative *Baeyer-Villiger* oxidation (Scheme 12).[128,130,139,143–145]
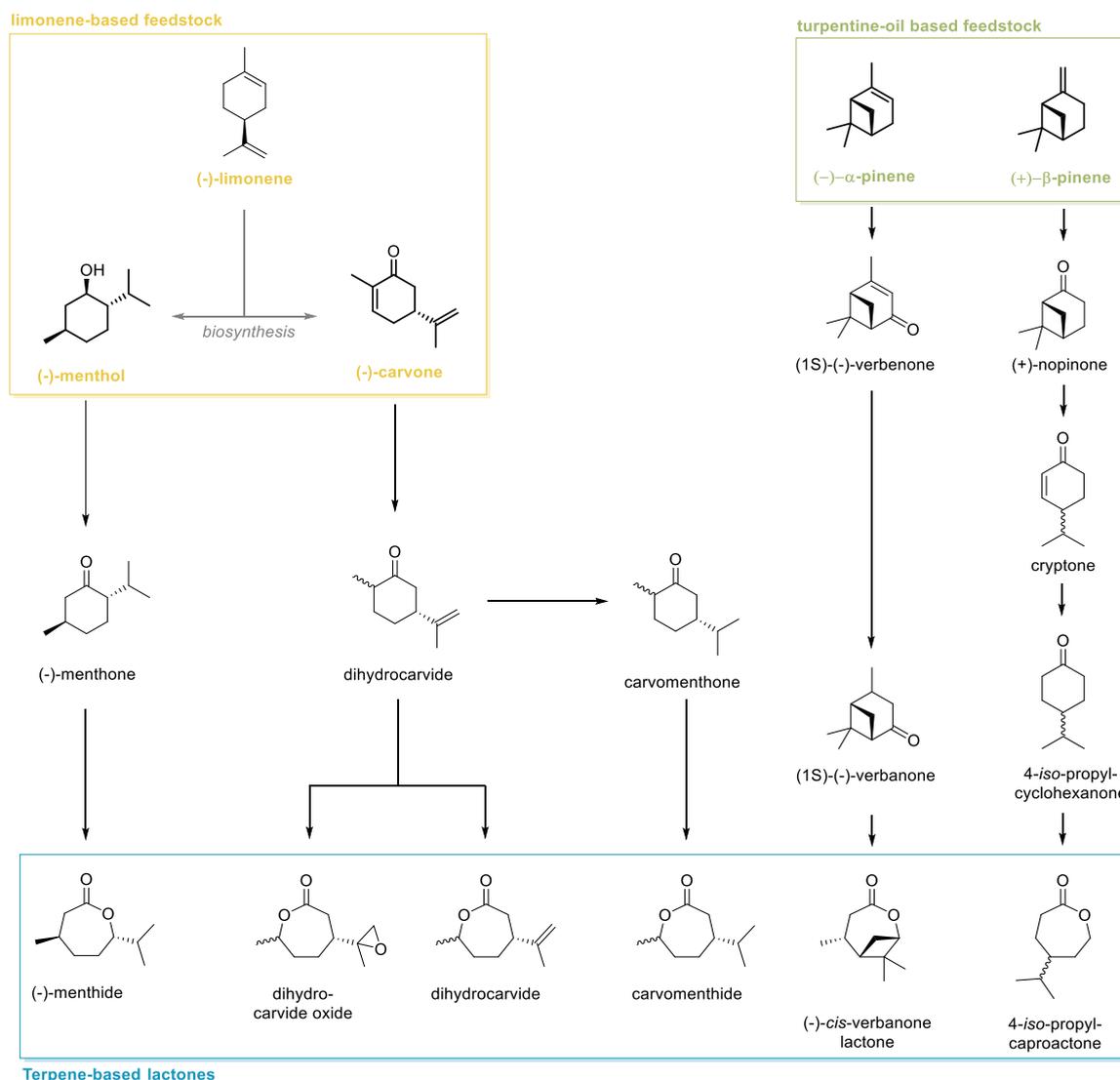
Scheme 12: Lactones obtained from chemical transformation of limonene-based terpenoids (-)-menthol or (-)-carvone and turpentine oil-based terpenes α-pinene and β-pinene.[110,114,130,139,143–147]

The key step for those transformations is the ring-extension of cyclic terpene-based ketones *via Baeyer-Villiger* oxidation, yielding the desired lactones by an insertion of an additional oxygen atom into the bond between carbonyl carbon and the adjacent carbon atom. In 1899 Baeyer and Villiger reported the conversion of ketones to esters with Caro's acid, introducing a nowadays widely used synthetic tool.[148,149] Overall, the *Baeyer-Villiger* oxidation is a versatile reaction capable of transforming ketones into esters, cyclic ketones into lactones, benzaldehydes into phenols or carboxylic acids into anhydrides while simultaneously showing high chemoselectivity.[150] The reaction proceeds *via* a peroxydester intermediate, the Criegee intermediate (**I**), formed by nucleophilic attack of the peracid onto the carbonyl unit, followed by a concerted migration step (Scheme 13A).[151,152] Within this concerted rearrangement (**II**), the migrating group R^M is in an antiperiplanar position to the peroxide O–O leaving group (primary stereoelectronic effect) while simultaneously also standing antiperiplanar to the

hydroxyl group lone pair (secondary stereoelectronic effect). This rearrangement is usually the rate-determining step of the *Baeyer-Villiger* oxidation and plays a crucial role as for what isomers are formed during the reaction.[149,150] For most systems, the migration aptitude of the migrating rest R^M can be predicted as following: tertiary alkyls > cyclohexyl > secondary alkyls > benzyl > phenyl > primary alkyls > methyl (Scheme 13B).[150,153]

A) Baeyer-Villiger mechanism
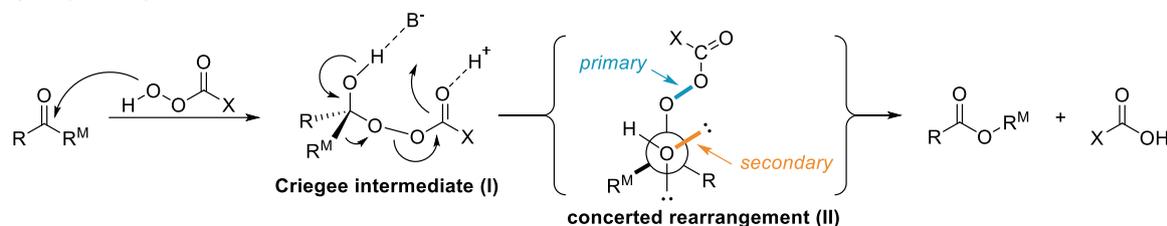
B) Migration aptitude
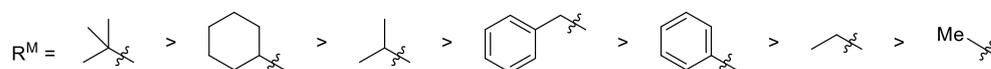
Scheme 13: Mechanism of the *Baeyer-Villiger* oxidation of ketones to esters *via* Criegee intermediate (**I**) and concerted migration (**II**) involving primary and secondary stereoelectronic effects (**A**) and migration aptitude of the migrating rest in decreasing order (**B**).

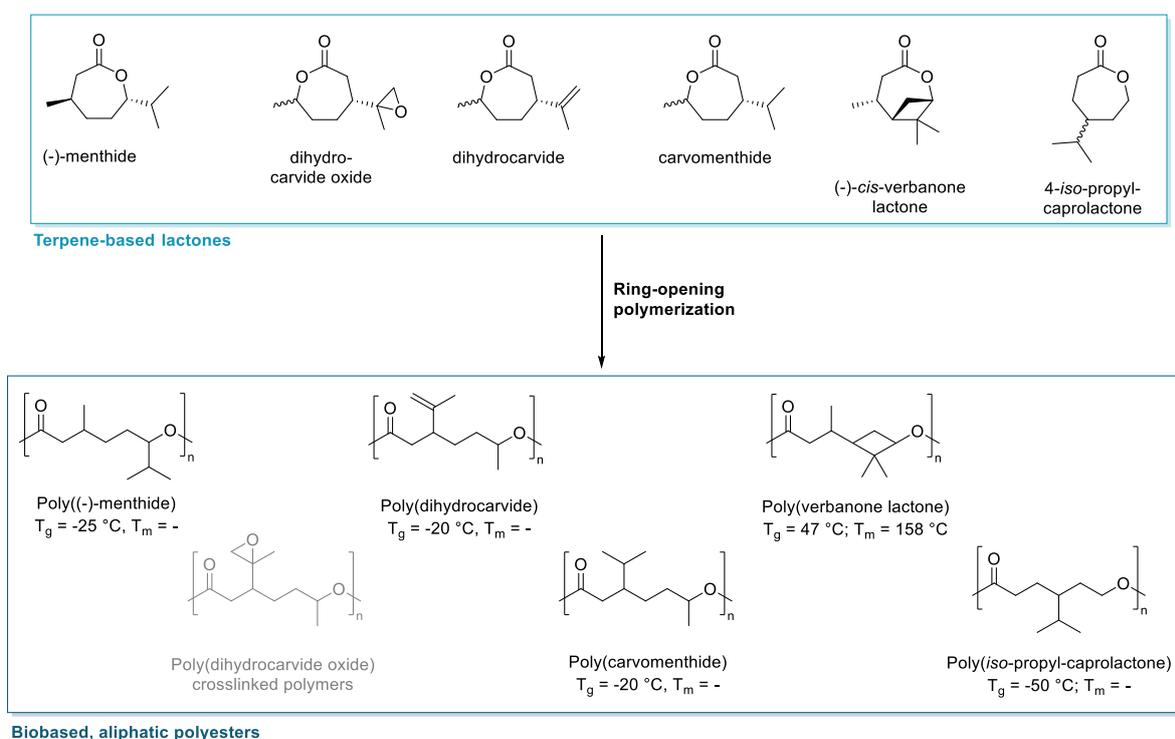This highly controlled behavior makes the *Baeyer-Villiger* oxidation an interesting method for the synthesis of lactones from cyclic ketones as new monomers, especially in a context of biobased feedstocks. For this transformation, a broad variety of oxidants is reported. Commonly used systems are for example *meta*-chloro perbenzoic acid (*m*CPBA), perfluoro acetic acid, performic acid, monopermaleic acid, monoperphtalic acid, *tert*-butyl hydroperoxide or hydrogen peroxide.[150,153] Aside from those, recent research also focuses on more sustainable approaches, involving e.g. Oxones[154], enzymatic approaches[155,156], catalytic systems with hydrogen peroxide (derivatives)[157] or even heterogeneous catalyst systems like Sn-β/H$_2$O$_2$[158] or Sn-MCM-41/H$_2$O$_2$.[159,160] Overall, this reaction is a powerful tool for the synthesis of new monomers from biogenic resources with potentially green, sustainable synthesis routes.

For the limonene-derived and turpentine oil-based feedstocks, a variety of different lactones have successfully been synthesized and polymerized within the last years. The most well-known example is (-)-menthide derived from *Baeyer-Villiger* oxidation of (-)-menthol with *m*CPBA, introduced by Hillmyer *et al.* in 2005. Catalytic ROP of (-)-menthide yields an aliphatic polyester with an *iso*-propyl and a methyl sidechain with molecular weights of up to 91 kg/mol (*Đ* = 1.1), ultimately leading to an amorphous material with low glass transition temperatures of about -25 °C.[143] Additionally, degradable poly((-)-menthide) has been investigated in much more detail as comonomer for block copolymerizations targeting advanced polymeric materials

like nucleation agents, elastomers, polyurethanes or thermoplastic elastomers.[89,145,161–165] Anionic ROP of regioisomeric carvomenthide yields structurally very similar polyesters with molecular weights of up to 62 kg/mol ($Đ$ = 1.16) and again low glass transition points of -20 °C. Contrary, if the double bond of the *iso*-propenyl function from the (-)-carvone feedstock is preserved during the synthesis by omitting the intermediate hydrogenation step, the ROP of the derived lactone dihydrocarvide yields lower molecular weights with broader dispersity under the same conditions, exhibiting the same glass transition of about -20 °C.[144,162] Yet, poly(dihydrocarvide) features a reactive *iso*-propenyl sidechain available for post-polymerization functionalization, making it an interesting candidate for advanced polymer materials like hydrogels.[110,166] In a contrary approach, the already epoxidized dihydrocarvide oxide monomer can be used for statistical ring opening copolymerization with CL to yield cross-linked polyesters directly from the polymerization.[147] Switching to turpentine oil-based feedstocks, Jones *et al.* introduced a multi-step synthesis pathway to transform β-pinene to 4-*iso*-propylcaprolactone, ultimately producing an aliphatic polyester with moderate molecular weight (M_n up to 23 kg/mol with $Đ$ = 1.34) and a very low glass transition temperature of -50 °C.[130] Utilizing α-pinene, Syrén *et al.* introduced a transformation yielding (-)-*cis*-verbanone lactone, which upon ROP gives a semicrystalline polymer material with a glass transition temperature of 47 °C and a melting point at 158 °C even at low molecular weights (M_n = 7.3 kg/mol, $Đ$ = 1.1), showcasing the high potential of biobased monomers in aliphatic polyester synthesis (Scheme 14).[110,128,139]

Terpene-based lactones

(-)-menthide   dihydro-carvide oxide   dihydrocarvide   carvomenthide   (-)-*cis*-verbanone lactone   4-*iso*-propyl-caprolactone

Ring-opening polymerization

Poly((-)-menthide) T_g = -25 °C, T_m = -

Poly(dihydrocarvide) T_g = -20 °C, T_m = -

Poly(verbanone lactone) T_g = 47 °C; T_m = 158 °C

Poly(dihydrocarvide oxide) crosslinked polymers

Poly(carvomenthide) T_g = -20 °C, T_m = -

Poly(*iso*-propyl-caprolactone) T_g = -50 °C; T_m = -

**Biobased, aliphatic polyesters**

Scheme 14: Polymerization of terpene-based lactones to aliphatic polyesters with their respective glass transition temperatures T_g and melting points T_m.[110,114,130,139,143–147]

2.2.3.   Catalysts for ring-opening polymerization

While there are many different methods of polymerizing lactones, including cationic or anionic pathways, they mostly suffer from uncontrolled side reactions (*vide infra*), broadening the polymers polydispersity and hindering efficient, steerable polyester synthesis. This led to the emergence of a variety of different (organo)catalysts for the ring-opening polymerization of lactones, offering unique advantages like narrow polydispersity, molecular mass control, introduction of stereoregularity, suppression of side reaction, fast reaction kinetics, targeted synthesis of various polymer architectures or synthesis of (multi)block copolymers by exploiting the living-type polymerization propagation.[108,111,116,167–170]

In the field of metal-catalyzed ROP, pioneering work by Teyssié *et al.* achieving living-type anionic coordination-insertion polymerization of ε-caprolactone (CL), β-propiolactone (βPL) and δ-valerolactone (δVL) with soluble, bimetallic Al_2/Zn(II) and Al_2/Co(II) μ-oxo alkoxides, being one of the first examples of catalytic ROP (Scheme 15). For this system, high reaction rates with suppression of side reactions like termination or transfer could be observed, featuring a linear dependency of molecular weight with conversion due to a living character.[171]
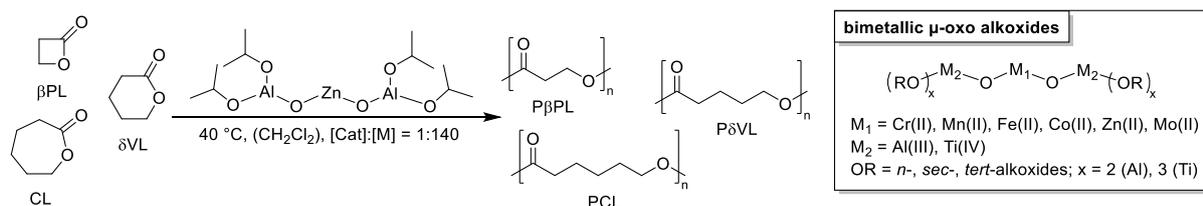
Scheme 15: Ring-opening polymerization of different lactones with bimetallic μ-oxo alkoxides as reported by Teyssié *et al.* in 1977.[171]

Since then, a multitude of different metal catalysts have been introduced. As for the GTP of *Michael*-type monomers, an important class of catalyst involving rare-earth metals has been developed, featuring various different elements like yttrium, lutetium, samarium, neodymium, cerium, and many others. Different types of rare-earth metal-based catalysts have emerged, varying from alkoxide-clusters to metallocenes or complexes with multidentate ligands like bis(phenolate)s or salenes. In the 1990s, work by McLain and Drysdale, Hubert-Pfalzgraf *et al.* or Feijen *et al.* expanded the scope of catalysts with the use of lanthanide *iso*-propoxide oxo-alkoxide clusters like $Ln_5(\mu$-O)(O^{i}Pr)$_3$ (Ln = Y, Er, La, Sm, Yb, Dm, Dy).[96,172–176] Those systems have been extended to the use of more simple lanthanide systems, obtained by reacting precursor complexes like $Ln(N(SiMe_3)_2)_3$ (Ln = Y, Nd) or lanthanide tris(2,6-di-*tert*-butylphenolate)s (Ln = Y, La) *in-situ* with alcohols.[96,177–180] Switching to metallocene complexes, both di- and trivalent complexes of various rare-earth metals can be used for the ROP of a variety of lactones. Herein, various complexes based on samarium and yttrium reported by Yasuda *et al.* like Cp*$_2$SmMe(thf), [Cp*$_2$SmH]$_2$, Cp*SmOEt(OEt$_2$), [Cp*YOMe]$_2$ or

Cp*$_2$YOMe(thf) were used for the polymerization of lactones like CL, δVL or βPL.[22,181,182] Another important class of ROP catalysts make up the bis(phenolate) complexes as introduced by Carpentier *et al.* in 2007. Those catalysts show high activities, allow for immortal ring-opening polymerization (*vide infra*) and are capable of introducing stereoinformation to demanding monomers like lactide or β-butyrolactone (BBL).[183–185] While those complexes mentioned certainly play an important role in the ROP of different lactones, the rare-earth metal complex are by no means limited to the ligands presented. Within the last 30 years, a multitude of different systems have been introduced, including different ligands like salenes, salans, guanidinates, oxazolylphenolates, diamine-diamines and many other, even including supported systems. An overview of different rare-earth metal based ROP catalysts is shown in Figure 9.[111,167,186–194]
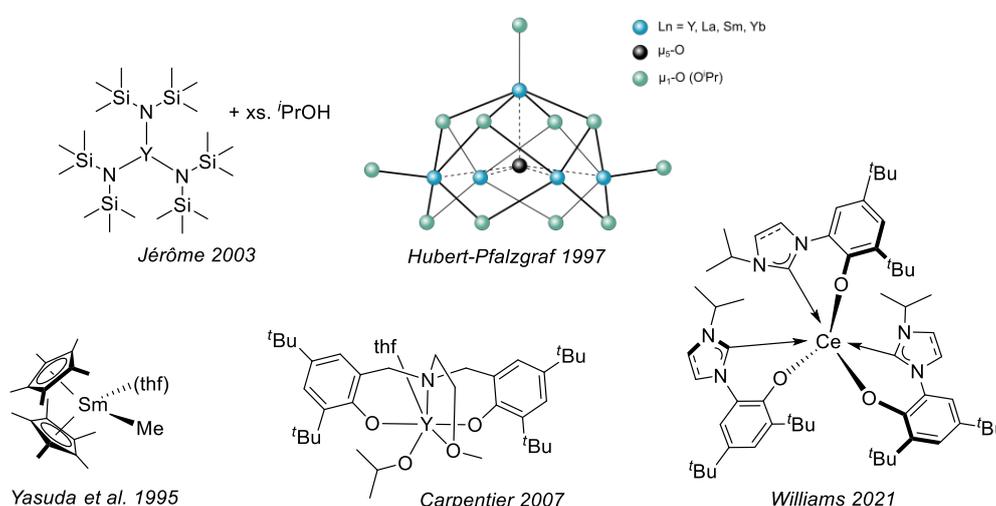

Figure 9: Overview of different rare-earth metal compounds active as ring-opening polymerization catalysts.[96,172–176,182,183,194]

Changing the central metal type from rare-earth elements to transition elements, especially complexes with chromium, zirconium or zinc have shown interesting properties for ROP catalysts. While there are some reports on complexes based on chromium, like the Cr(III) salophen complex introduced by Rieger *et al.* in 2008,[195,196] zirconium based systems like [Cp$_2$ZrMe]$^+$[B(C$_6$F$_5$)$_4$]$^-$ (Mukaiyama *et al.*)[197] or (*ansa*)-metallocene bis(ester enolate)s (Chen *et al.*)[198] and many other active metals[199], the most commonly found transition metal in ROP catalysis is certainly zinc. Here, the pioneering work on zinc β-diiminates (BID) catalysts by Coates *et al.* starting in 1999 followed by various complexes from Hillmyer, Tolman and coworkers make up one of the most important classes of catalysts for the synthesis of aliphatic polyesters. Those show unprecedented activity in the ROP of various lactones such as lactide, BBL, CL or β-valerolactone. Some of these catalysts are exemplarily shown in Figure 10.[200–205]
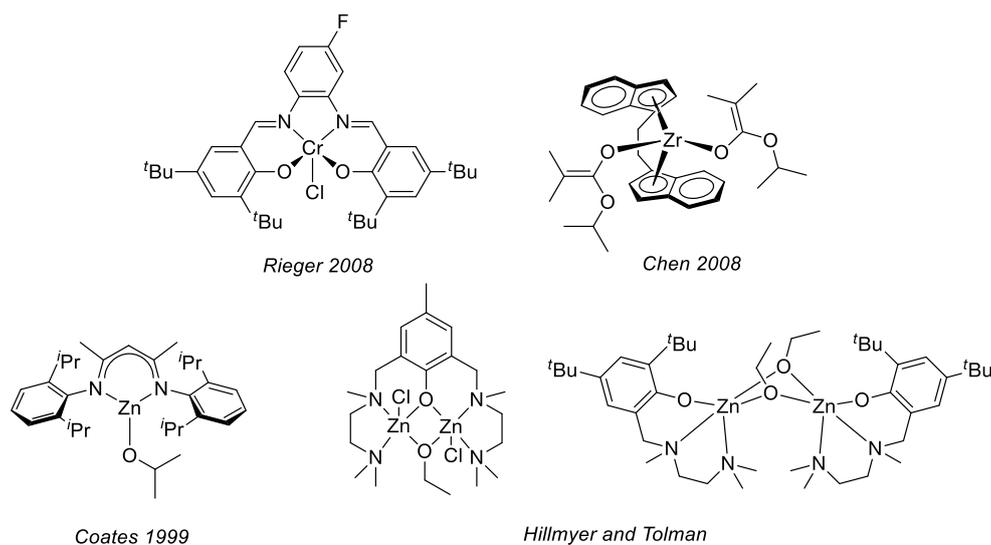
Rieger 2008

Chen 2008

Coates 1999

Hillmyer and Tolman

Figure 10: Various transition metal-based ring-opening polymerization catalysts.[195,197,198,200–204]

Besides rare-earth elements and transition metals, various different main group element complexes have successfully been introduced to ROP, mainly focusing on elements like indium, aluminum, or tin. The most archetype catalysts in this context are aluminum based alkoxide systems Al(OR)$_3$ or the widely applied tin(II) 2-ethylhexanoate catalyst SnOct$_2$, which are still used, even on industrial scale.[111,168,206] Yet also more well-defined metal catalysts are applied, with a strong focus on aluminum and indium based complexes with a variety of different ligands.[207–211] A broad range of different aluminum based salen catalysts have been reported for example by Spassky, Gibson or Feijen, starting in the early 2000s. Salen and salan-type ligands are amine- or imine-bridged phenolates, sharing a tetradentate ONNO coordination motif. Those offer a broad range of substitution points, with different substituents being introduced into the *ortho*- and *para*-position of the phenolates, the use of various different bridging backbones, and, for the case of salans, additional substituents on the nitrogen atoms. This makes this class of catalyst high adaptable, leading to the design of very well-adjusted catalysts.[208,212–218] Yet, various different ligands with varying bonding motifs have been explored, involving for example bidentate phenoxyimines, tridentate *Schiff*-bases, tetradentate bis(pyrrolidine) and many others.[208,210,211,219] Within recent years, also the use of indium as catalytically active metal has gained increased attention, as it is considered more active and functional-group tolerant than aluminum catalysts. An entry point to these complexes marks the work by Mehrkhodavandi *et al.*, reporting the highly active and controlled polymerization of lactide and BBL catalyzed by dinuclear indium complexes.[116,220–222] A selection of different main-group metal based catalysts is exemplarily given in Figure 11.
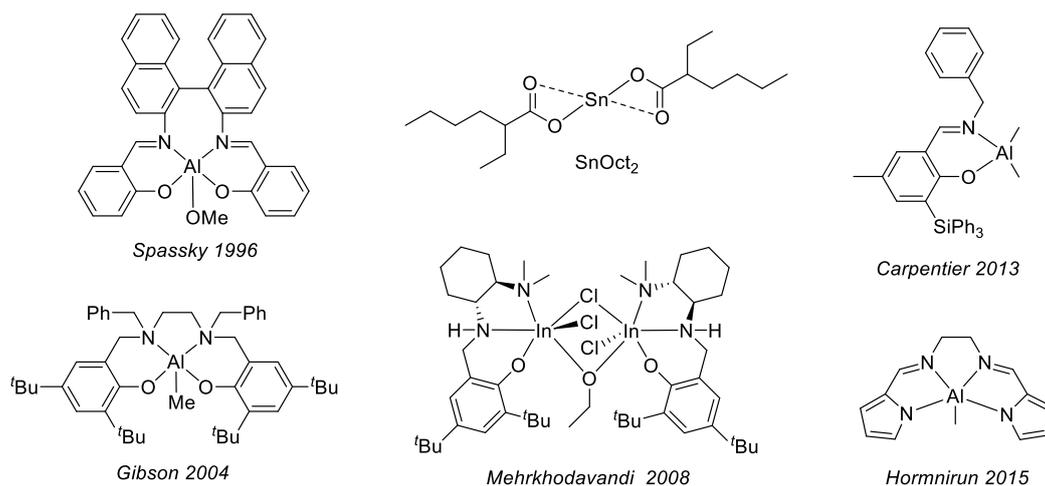
Figure 11: Selected examples for main-group element based ring-opening polymerization catalysts.[111,168,208,211–213,216,219,221,223]

While these complexes shown certainly mark important examples for ROP, there is almost no limitation in the scope of these catalysts. Aside from organometallic complexes comprising a broad variety of different active metals, also organo-catalyzed ROP, for example with urea derivatives, has gained increasing attention. Generally, when ROP of lactones is performed using (organometallic) catalysts, several different advantages can be exploited. Most importantly, these catalysts are capable of introducing stereocontrol to the polymerization and exhibit a living-type character with suppression of most side reactions like transesterification or chain termination. This allows the synthesis of polyesters with steerable molecular weights and narrow distributions. Additionally, those catalysts possess a high degree of tunability, making them adjustable to the monomer by means of ligand, central metal, and initiator choice. Dependent on the systems used, there exist some mechanistical differences.[91,169,199,224–234]

2.2.4. Mechanistic aspects

Generally, two different experimental approaches for lactone ROP can be employed dependent on the catalyst system used. The classic ROP observed for a multitude of different metal complexes uses catalysts which act as both initiator of the polymerization and stabilizing agent of the propagating chain. The main requirement for such metal complexes is that they carry a nucleophilic group capable of acting as initiator. For this mechanism, the ratio of catalyst/initiator to monomer determines the number of chains started and thus the chain length (Scheme 16A). This type of polymerization is to be performed under exclusion of protic impurities or nucleophiles, as they quench the reactivity of the catalyst or the active chain, which is the main drawback of this method. The second approach, the so-called immortal ring-opening polymerization (iROP) as introduced by Inoue *et al.*, utilizes the addition of an excess of external nucleophiles with respect to the metal, acting as chain-transfer agents (CTA). These react with the catalyst to form the active species, acting as initiators of the reaction, while the catalyst molecule is only responsible for stabilizing the propagating species, exhibiting true catalytic activity. The number of chains started is thus independent from the number of catalyst molecules but is determined by the ratio of monomer to CTA (Scheme 16B).[91,169,224–230]
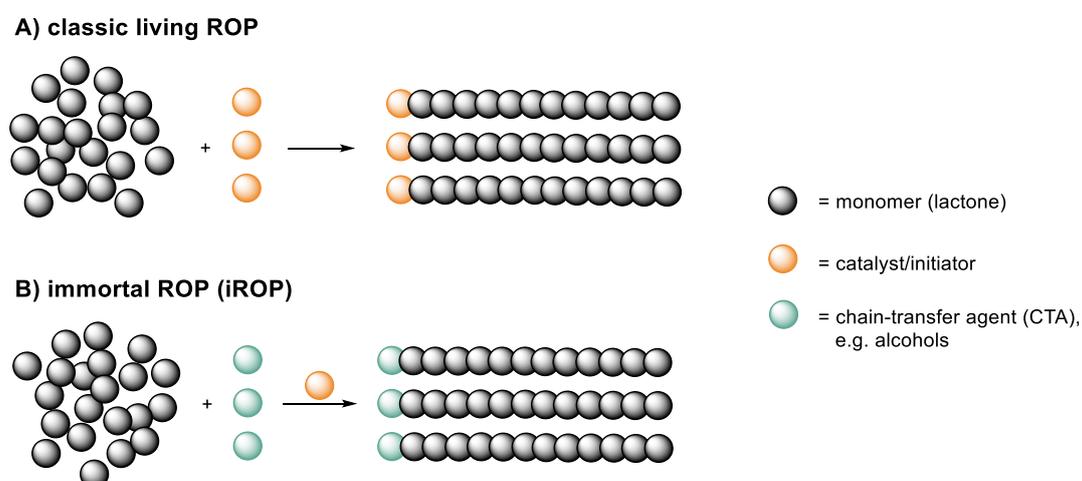
Scheme 16: Differentiation between classic living ROP of lactones with a bifunctional catalyst/initiator molecule (**A**) and catalytic immortal ROP with catalyst/chain-transfer agent systems (**B**), adapted from Carpentier *et al.*[224]

The iROP of lactones with alcohols as nucleophiles exhibits a certain kinetic behavior as underlying reason for the catalytic activity of the metal complexes. For the classic ROP, the catalyst-bound nucleophile initiates the polymerization by nucleophilic attack of the first monomer unit. Contrary, for iROP a pre-activation is performed, where the catalyst is reacted with an excess of nucleophile, e.g. alcohol, to form the active metal alcoholate (Scheme 17, reaction **I**). As for ROP, in iROP the polymerization is initiated by nucleophilic attack on the

first monomer, yet this time the alcoholate starts the reaction. Afterwards, the lactone is opened and forms a new alcoholate coordinated to the catalyst, propagating the polymerization. For both ROP and iROP, the rate constant of initiation k_i should exceed the rate constant of the propagation k_{pr} in order to maintain a narrow polydispersity and to avoid initiation delays (Scheme 17, reaction **II**). Exclusively for iROP, an exchange reaction of the active site can occur, in which the stabilized chain end alcoholate exchanges with either another CTA or a hydroxyl terminated polymer chain. Herein, the active chain becomes the dormant, α-hydroxyl-ω-carboxylate terminated species while either the CTA starts a new chain or a formerly dormant chain switches back into the active state (Scheme 17, reaction **III**). In terms of kinetics, the rate constant of the transfer k_{tr} must exceed the reaction rate of the propagation k_{pr} in order to maintain control over the polymerization process. This exchange or transfer reaction is responsible for the behavior observed for the CTA and the catalyst.[224,225,235,236]
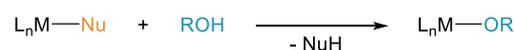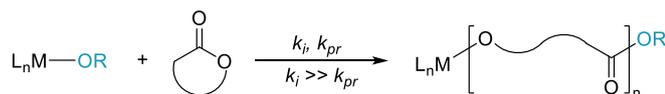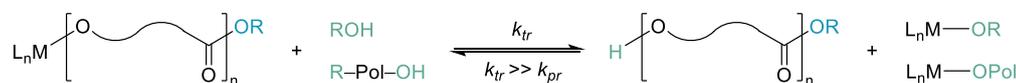

Scheme 17: Kinetics of the immortal ring-opening polymerization of lactones with metal catalysts (L_nM–Nu) and alcohols as chain-transfer agents.[224,236]

Mechanistically, the propagation of ROP and iROP of lactones behave very similarly. Usually, this type of catalysis proceeds *via* the coordination-insertion mechanism (CIM) of electrophilic, *Lewis* acidic metal complexes bearing σ-bonded, nucleophilic ligand groups capable of acting as initiators, like alkoxides. The propagation cycle starts with a coordination of the catalyst to the carbonyl moiety of the monomer to the *Lewis* acid metal center. Then the monomer inserts into the metal-alkoxy bond by nucleophilic attack of the alkoxide on the carbonyl carbon atom, followed by ring opening of the monomer by acyl-oxygen cleavage (*vide infra*). This cleavage leads to an ester-terminated metal alkoxide complex, reforming the active, nucleophilic species and allowing propagation to the next monomer unit (Scheme 18A). When comparing ROP and iROP, no difference in the propagation step itself can be seen, but in the initiation. In classic ROP, the first monomer unit has to insert into the metal-nucleophile bond of the σ-bonded initiator, while for iROP, *in-situ* metal alkoxides are formed with the CTAs added. Also, in classic ROP, the resting state metal-polymer-alkoxide species cannot interchange with other

chains, while in iROP, rapid chain-exchange reactions take place (*vide supra*).[224,229,237] A special case can be observed for *Lewis* acidic metal salt catalyzed iROP reactions, like for example triflate salt alcohol systems $M^{n+}(F_3CSO_3^-)_n$/ROH. Herein, the activated monomer mechanism (AMM) takes place, in which the metal salt activates the monomer by coordination of the carbonyl moiety, making it more susceptible to nucleophilic attacks. Now the alcohol as external nucleophile attacks the carbonyl carbon, leading to ring-opening of the lactone and formation of a new α-hydroxy-ω-carboxyl species, which can again act as nucleophile for subsequent propagation. This species is still coordinated with the *Lewis* acid, which upon reaction with another monomer unit is transferred onto the monomer, activating the next unit (Scheme 18B). The main difference between AMM and CIM is, that in AMM the catalyst/initiator system is a true two-component system, while for CIM, the catalyst acts as one-component catalyst-initiator tandem system.[175,224,238,239]
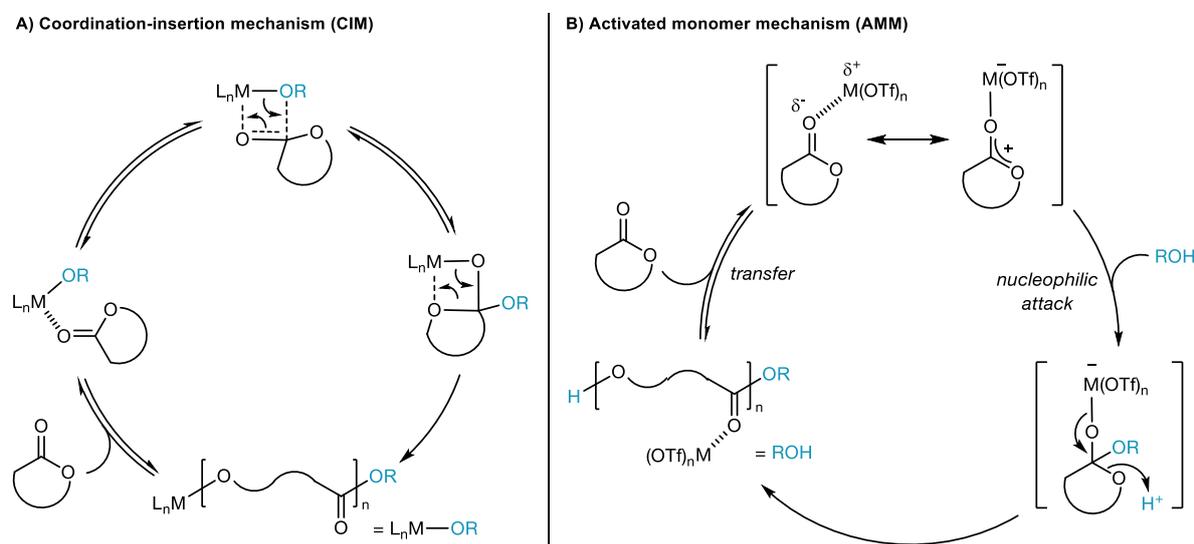
Scheme 18: Propagation cycle of lactone ROP for the coordination-insertion mechanism (**A**) or the activated monomer mechanism (**B**).[111,170,224,238]

Generally, in anionic and coordinative-anionic polymerization of lactones, and especially for β-substituted lactones like the widely investigated β-butyrolactone, two different ring-opening mechanism exist. For strong nucleophiles, an acyl-oxygen cleavage between the carbonyl carbon and the ring oxygen takes place, accompanied by a retention of stereoconformation, generating alcoholate chain-ends (**Scheme 19**, pathway **I**). Contrary, weak nucleophiles open the lactones *via* alkyl-oxygen cleavage of the β-carbon atom and the ring oxygen, leading to stereoconformation inversion and carboxylate chain-ends (Scheme 19, pathway **II**). This behavior is an important influencing factor when considering stereocontrol of the polymers prepared, often addressed by introducing elaborate metal complexes for ROP catalysis.[167,168,224]
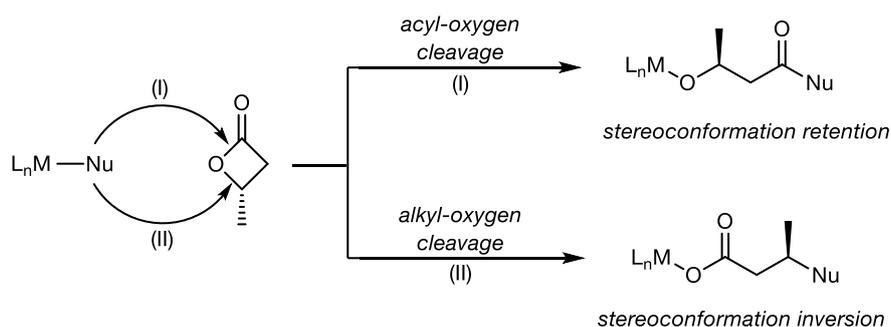
Scheme 19: Ring-opening of β-substituted lactones *via* nucleophilic attack and acyl-oxygen cleavage to a metal-alcoholate with stereoconformation retention (**I**) or alkyl-oxygen cleavage to a metal-carboxylate with stereoconformation inversion (**II**).[167]

Due to coordination and stabilization of the chain-ends by the metal catalyst, side reactions in catalyzed ROP are largely suppressed. The main side-reaction type observed in ROP is transesterification, as the active chain is not only capable of attacking the next lactone but can also react with every other ester unit present in the polymer chain. This can happen either between chains (intermolecular backbiting), or within the active chain (intramolecular backbiting or end-to-end cyclization), leading to a broadening of the polydispersity and/or cyclization of the polymer (Scheme 20). For β-lactones, also hydrogen transfer reactions or transfer of the active chain onto the monomer are known as side reactions.[167,168,240]
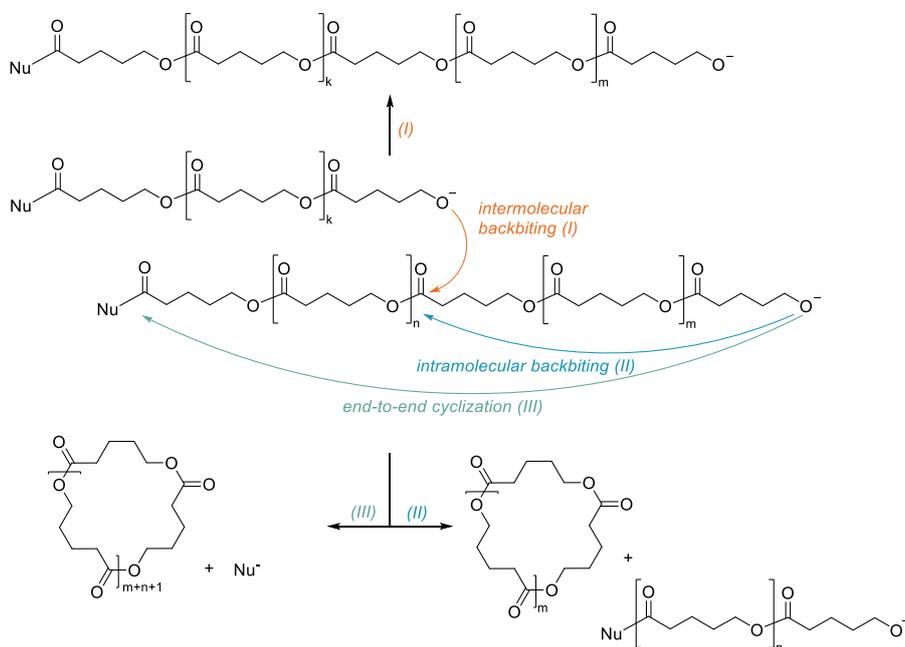
Scheme 20: Transesterification side reactions *via* intermolecular backbiting (**I**), intramolecular backbiting (**II**) or end-to-end cyclization (**III**), Nu = nucleophilic initiator.[240]

2.2.5 Copolymerization of GTP and ROP

To gain access to more functional polymer materials, the (block) copolymerization of monomers from different monomer classes with distinct chemical characteristics remains an interesting method. In the context of group-transfer and ring-opening polymerization, this combination remains a highly challenging task. So far, the scope of *Michael*-type monomers comprises only MMA (derivatives) in combination with some lactones like CL, βPL, δVL or lactide.[22,241] While there are some examples involving combinations of ROP and radical methods like atom-transfer radical polymerization (ATRP) or reversible-addition-fragmentation chain-transfer polymerization (RAFT) using polymer postfunctionalization steps or bifunctional initiators (Figure 12), there are only few examples of true catalytic, one-pot approaches.[242–249]
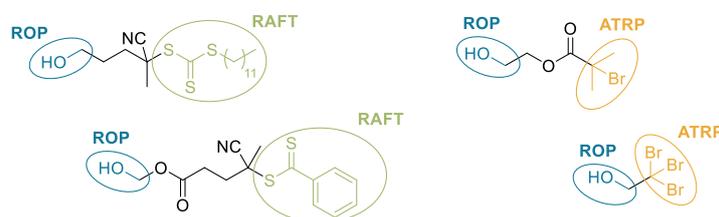

Figure 12: Different examples for bifunctional initiators used in ROP/RAFT and ROP/ATRP approaches towards block copolymers from *Michael*-type monomers and lactones.[243,245,246,248,249]

The first reported example of a catalytic copolymerization of GTP and ROP has been reported by Yasuda *et al.* in 1995, copolymerizing MMA with βPL, δVL, or CL sequentially, using Cp*$_2$LnMe(thf) as catalyst. The copolymers prepared exhibited molecular weights in the range of 23 – 42 kg/mol with narrow polydispersity of 1.11 – 1.32 , matching in their observed molecular composition with the used feed ratio of MMA:lactone = 50:50 (Scheme 21).[26]
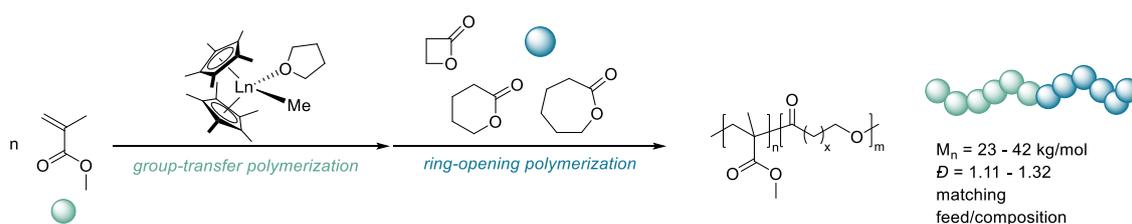
Scheme 21: Copolymerization of MMA and βPL, δVL or CL with Cp*$_2$LnMe(thf) as reported by Yasuda *et al.* in 1995.[22]

They found that block copolymerization is only possible when the *Michael*-type monomer is added first, followed by the lactone, as no MMA polymerization was observed for reversed-order addition of the monomers. This indicates that the coordination strength of the monomers, similar as for pure GTP block copolymers (*vide supra*) plays a role for this copolymerization as well. However, little characterization of the obtained materials has been performed.[26] Similar polymers were prepared by Chiellini, Solaro and Cantoni in 1995 – 1997, who reported the

copolymerization of MMA with CL, δVL, γVL, and BBL with bis(diethyl aluminum) sulfate (DEAS) or tri-*iso*-butyl-aluminum (TIBA) as catalysts, obtaining semi-degradable thermoplastic block copolymers and mixtures of two homopolymers. Yet, the presented systems showed severe limitations in terms of monomer conversion (X = 4-79%), adjustability of composition by feedstock and polydispersity of the obtained materials ($Đ$ = 1.5-12.9), showcasing the challenges faced for this type of monomer class combination (Scheme 22).[250,251]
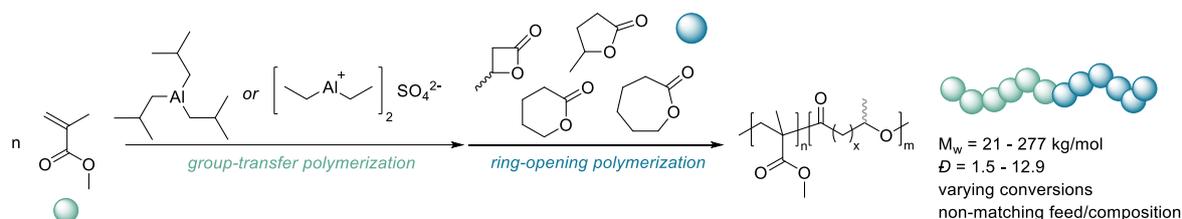
Scheme 22: Copolymerization of MMA with BBL, γVL, δVL or CL using TIBA, or DEAS as reported by Chiellini, Solaro and Cantoni in 1995 – 1997.[250,251]

Another attempt has been made by Hadjichristidis *et al.* in 2007, copolymerizing MMA with CL or δVL using $Cp_2ZrMe_2/B(C_6F_5)_3$ as catalyst system (Scheme 23).[252] In their experiments, they obtained the block copolymers of MMA with CL and δVL with high molecular weights (M_w = 280 – 300 kg/mol) and narrow polydispersity ($Đ$ = 1.21 – 1.29), yet again the feed ratio of MMA:lactone of 1:1 differed from the obtained molecular composition of the copolymers, which were in the range of 4.2 – 4.7:1. In accordance with the experiments by Yasuda *et al.*, it was found that the addition sequence again plays a crucial role in whether MMA is polymerized or not. For the first time, they proposed a mechanism of the active MMA chain acting as ester enolate, initiating the ROP by ring-opening of the first lactone unit in a mono- or bimetallic mechanism. Additionally, thermal analysis of the polymers showed a depression of the melting point of the polyester block with little to no influence on the glass transition point of PMMA, proofing successful block copolymerization and indicating microphase separation of the block copolymers.[22,252]
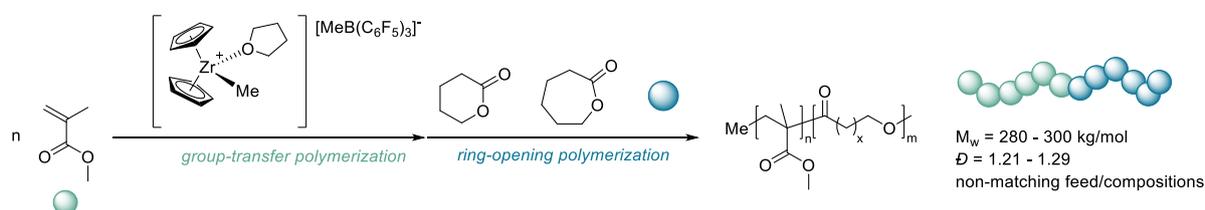
Scheme 23: Copolymerization of MMA and δVL or CL using $Cp_2ZrMe_2/B(C_6F_5)_3$ as reported by Hadjichristidis *et al.* in 2007.[252]

A similar approach was utilized by Li *et al.* in 2022, copolymerizing MMA and lactide using the organocatalytic system benzyl alcohol with the phosphazene base $^tBuP_4$ and di-*iso*-propyl thiourea (Scheme 24). Rapid consumption of both monomers (usually within an hour) with high

conversions (X = 74 – 99%) was observed, yielding block copolymers with narrow polydispersity ($Đ$ < 1.66) and molecular weights in the range of 15 – 35 kg/mol. In terms of monomer addition sequence, they again observed no conversion of MMA for sequential polymerization of lactone followed by MMA and full polymerization of both monomers for the reversed addition order MMA-lactone and their polymers behaved similar in terms of thermal transitions.[253]
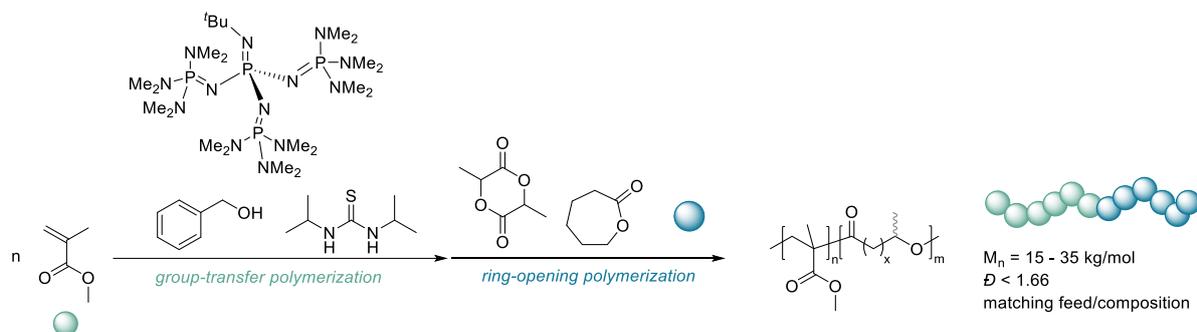
Scheme 24: Copolymerization of MMA with *rac*-lactide or CL using the organocatalytic system benzyl alcohol, *t*BuP₄, di-*iso*-propyl thiourea as reported by Li *et al.* in 2022.[253]

The last remarkable study on the copolymerization of *Michael*-type monomers and lactones has been published by Mehrkhodavani *et al.* in 2020, who introduced a neutral indium complex capable of sequentially copolymerizing MMA with either CL or *rac*-lactide regardless of monomer addition order (Scheme 25). Their copolymers from MMA and *rac*-lactide exhibited molecular weights from 110 – 140 kg/mol with narrow dispersity ($Đ$ = 1.46 – 1.95) and their copolymers from MMA with CL showed molecular weights of about 60 kg/mol ($Đ$ = 1.50 – 1.60), regardless of addition order, with the conversion of MMA ranging between 53 – 87% and high conversion of the lactone (X > 95%). Dependent on addition order, they proposed two transfer mechanisms of the active MMA chain for subsequent ROP and of the active PLA chain with subsequent GTP *vice versa*, following a coordination-insertion mechanism in the lactone ROP and a Michael addition polymerization in the GTP polymerization with no further specification on the exact mechanistic details.[241]
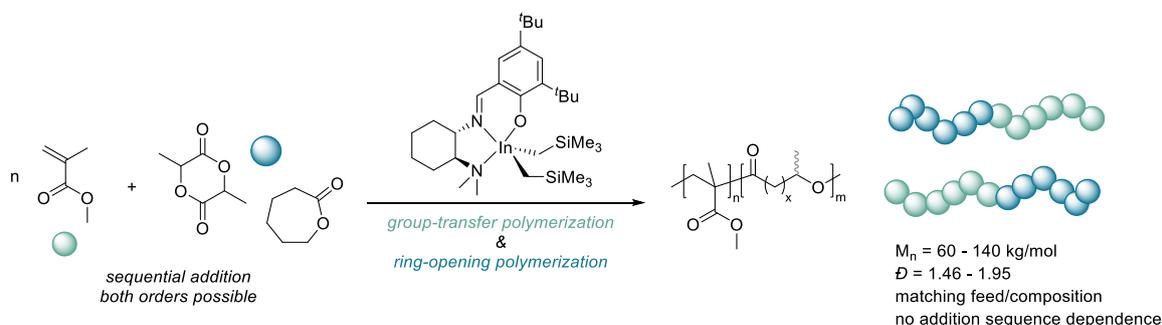
Scheme 25: Copolymerization of MMA with *rac*-lactide or CL using a neutral indium complex in a one-pot approach allowing both addition orders as reported by Mehrkhodavandi *et al.* in 2020.[241]

All those examples highlight the interest in obtaining block copolymers comprising a block of *Michael*-type monomers linked to aliphatic polyester chains. Yet so far, only little is known regarding variation of the *Michael*-type monomer, or the material properties of the block copolymers obtained. Yet, this combination of different monomer class would offer access to a variety of different, functional materials. Polyesters based on ROP could be incorporated in such systems utilizing their main chain cleavability and biocompatibility, while polymers from *Michael*-type monomers show a high degree of tunability in terms of their functional sidechains and inherently possess interesting properties such as pH- or temperature responsiveness. Combining these polymer types into (multi-) block copolymers might generate a highly versatile class of polymer materials comprising the unique properties of the respective homopolymers. Such materials could for example be used in different biomedical applications like drug-delivery, exploiting their responsive behavior to external stimuli. The overall scope of applicable monomers for both the GTP- as well as the ROP block is much broader than currently covered in literature, including interesting monomer (classes) like (substituted) vinylphosphonates or vinylpyridines, biobased lactones and many more. In the following chapter, some of the polymer response behaviors are explained in more detail to highlight the functionality of such polymers and their potential scope of applications.

2.3.   Functional precision polymers in applications

2.3.1.   Responsive polymers

With advanced monomers being introduced to polymer science, so-called "smart" polymers, possessing responsiveness to external stimuli like pH, temperature, specific molecules, irradiation, ionic strength, light, electric or magnetic field or heat compose a new class of highly interesting materials. This responsiveness allows for dynamic modulation of the polymer behavior based on its surrounding, making them interesting materials for use in application fields like drug delivery, cell culture technologies, separation, sensors or actuators. Such polymers can be responsive to one stimulus or multiple stimuli, or different monomers with various responses can be connected in (block) copolymers.[42,44,254,255]

One such response is the change of behavior towards heat/cold by temperature-responsive polymers as exhibited by poly(*N-iso*-propylacrylamide). Such polymers can be described best using the terms lower critical solution temperature (LCST) and upper critical solution temperature (UCST) based on their phase behavior. When mixing the polymer with a suitable solvent, mostly water, intermolecular interactions between hydrophilic parts of the polymer with the solvent molecules like hydrogen bonding allow for the formation of a homogeneous, single-phase system, in which the polymer is dissolved as random coil. Upon heating, the solvent molecules show increasing mobility, exposing the hydrophobic parts of the polymer, leading to an increase in intramolecular hydrophobic interactions. If the LCST is surpassed, those hydrophobic interactions lead to a collapse of the random coils to globule and agglomeration and thus, demixing into a two-phase system of non-dissolved polymer and the solvent (Figure 13).[33,254,256,257]
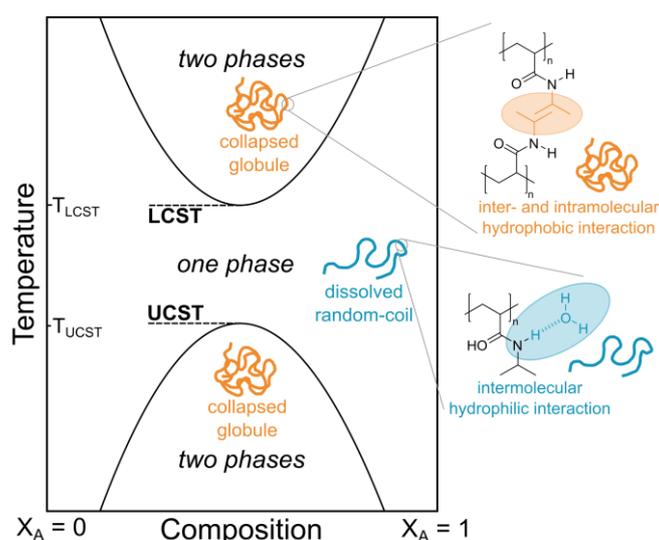

Figure 13: Phase diagram of a polymer-solvent mixture with $T_{LCST} > T_{UCST}$ and schematic representation of the hydrophobic interactions within the collapsed globule in the two-phase regime and the hydrophilic interactions of the random coils with solvent molecules in the one-phase regime.[254,257]

The reverse effect is exhibited when the UCST is surpassed upon further heating. Important characteristics of the LCST effect are reversibility, with or without resolution hysteresis, and the entropic nature of the effect. For the determination and characterization of this effect, cloud point determination by turbidity measurements as well as dynamic scanning calorimetry can be used.[33,254,256] While there is a wide variety of thermoresponsive polymers, especially those with a response within a physiological range make interesting candidates for advanced polymer applications in a biomedical context. Some common examples of thermoresponsive polymers are for example poly((vinyl methyl ether), poly((vinyl methyl ether)-*co*-(vinyl acetate)), poly(*N*-vinyl caprolactam), poly(ethylene oxide), poly(2-oxazoline), poly(propylene oxide) or poly(2-dimethylamino)ethyl methacrylate).[254,256]

From the class of GTP polymers, the dialkyl vinylphosphonates possess a LCST within a physiological range. Based on the length of the alkyl chain attached to the side-group of the poly(vinylphosphonate), the hydrophobicity of the respective polymer is altered. Rieger *et al.* performed a detailed characterization of the LCST behavior of these polymers in dependency on the copolymer composition. For the pure PDEVP homopolymer with only ethyl sidechains in water with a concentration of 1.0 wt%, an LCST of 42 °C without any precipitation/dissolution hysteresis is measured *via* cloud point determination. By statistical copolymerization of DEVP with the shorter-chain and thus more hydrophilic methyl derivative DMVP, the cloud point could successfully be increased to a range of 56 °C – 92 °C, while incorporation of the more hydrophobic, longer-chain *n*-propyl derivative DPVP resulted in an LCST depression down to a range of 5 °C – 34 °C, depending on composition (Figure 14). This high tunability of the LCST in a physiological relevant range makes the GTP-based poly(vinylphosphonates) interesting polymers for biomedical applications.[33,42,44]
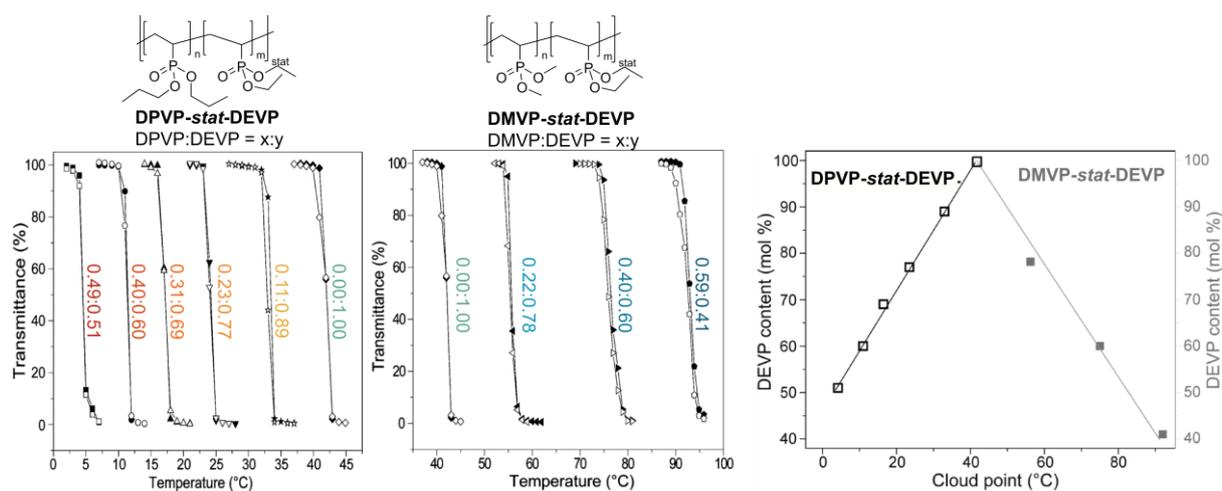

Figure 14: LCST determination *via* turbidity measurements of statistical copolymers of DPVP-*stat*-DEVP (left) and DMVP-*stat*-DEVP (middle) and cloud point dependency on the percentage of DEVP content (right), adapted from Rieger *et al.*[33]

The second stimulus with broad application range is the responsiveness towards changes in the pH value. Polymers are considered pH-responsive, if their solubility, hydrodynamic volume, configuration, or conformation can be altered by means of changing the external pH-value of the media.[258] pH-responsive polymers are considered polyelectrolytes which contain weak acidic or basic groups within their main chain or sidechains, which are capable of reversibly accepting or releasing protons depending on the pH of the medium. Based on the ionization of these groups, the polymer reacts with changes of the formerly stated parameters. Different functional groups like carboxylates, pyridines, sulfonic acids, phosphates, or amines are commonly applied to synthesize polymers with variable pK_a values over the range of $1 - 14$. Depending on their chemical structure, pH-responsive polymers can be divided into the two sub-classes of acidic or basic polymers (Scheme 26).[259,260]
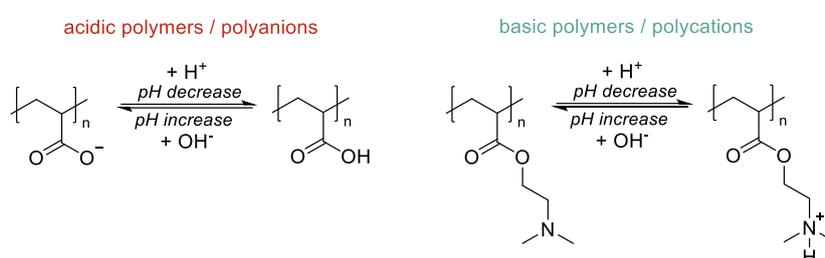
Scheme 26: Responsiveness of acidic and basic polyelectrolytes to a change in pH by reversible protonation/deprotonation.[261]

The first sub-class are polymers with acidic pendent groups, forming so-called polyacids or polyanions. These polymers are capable of accepting H^+ at low pH values (high H^+ concentrations), forming neutral polymers and accordingly release H^+ at neutral or high pH (low H^+ concentration), resulting in a negatively charged polymer. Some common polymers studied in this context are poly(acrylic acid) or poly(methacrylic acid), poly(vinylphosphonic acid), poly(4-styrenesulfonic acid) or poly(aspartic acid) and a multitude of their structural derivatives (Figure 15, top).[259,262] Contrary to those polymers, the second sub-class of pH-responsive polymers comprises polybases or polycationic polymers which accept H^+ at low pH-values and release them again under basic conditions. Such polymers use amines, morpholine units, pyrrolidines, piperazines, pyridines or imidazoles as reactive groups for their responsiveness. In this context, polymers like poly((2-dimethylamino)ethylmethacrylate), poly(acryloyl-morpholine), (branched) poly(ethyleneimine), poly(N-vinylimidazole) or poly(2-vinylpyridine) (P2VP) and poly(4-vinylpyridine) (P4VP) have been reported (Figure 15, bottom).[259,262]
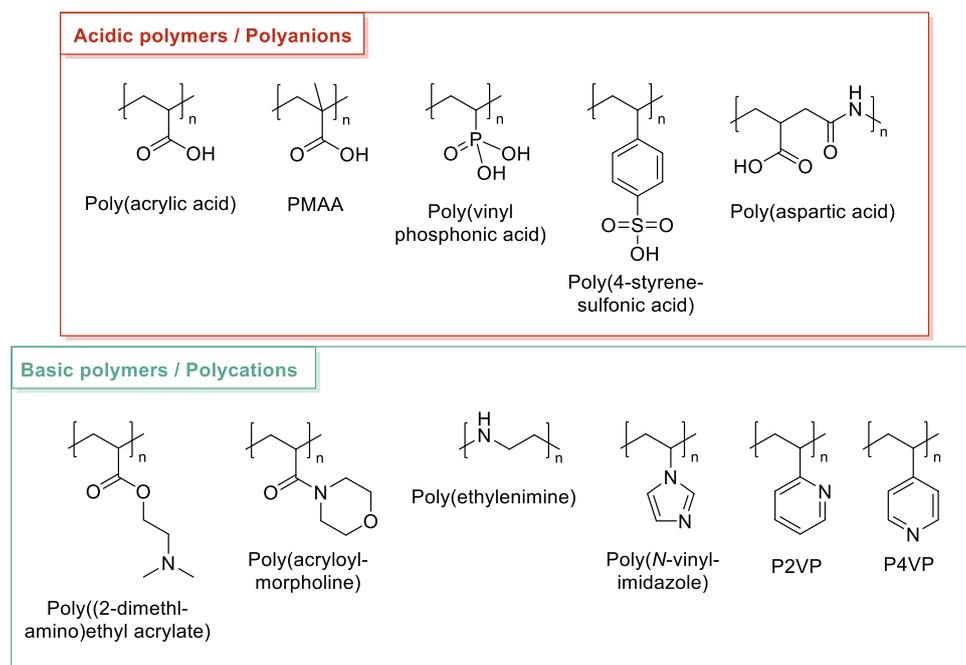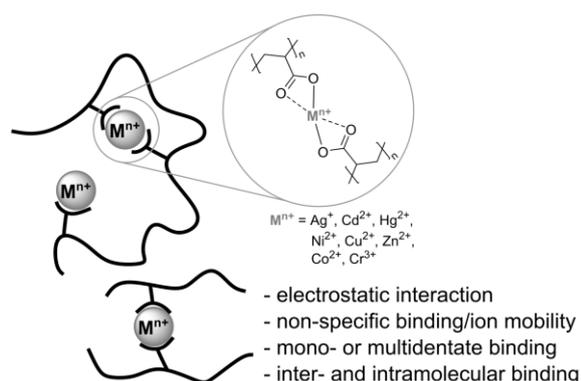
Figure 15: Examples of acidic pH-responsive polymers (top) and basic pH-responsive polymers (bottom).[259]

Based on their high degree of tunability in terms of polymer structure, (block) copolymerization, polymer morphology or pK_a value, pH-responsive polymers are widely used with a focus on a biomedical context, compromising material uses involving dendrimers, polymerosomes, micelles, polymer-drug conjugates or hydrogels with adjustable properties.[262,263] Some of those polymers can be prepared by means of precision polymerization techniques like GTP as more elaborate synthesis method compared to other polymerization techniques, leading to precisely defined polymers with tunable molecular weights, morphologies and compositions.[15,22,67]

Very similar in terms of polymer responsiveness is the interaction of such polymers with metal ions or metal complexes. Instead of protons, the pendent sidechains interact with the metal ions or complexes in a specific way to form polymeric metal complexes or ionomers, again resulting in a response of the polymer regarding its properties. Interactions between metal ions or complexes and polymers result mainly from electrostatic forces or formation of coordinative bonds, accompanied by weak interactions such as trapping. Those interactions are usually described using coordination theories, yet there are some small differences when considering macromolecules as ligands like total saturation of the metal ions ligand sphere, resulting in high chemical and thermal stability of the polymer metal chelates. There can either occur interactions of the metal ions with a single polymer chain – mono- or multidentate, or by intramolecular interaction of the ions with multiple polymer chains. A further distinction is made between polyelectrolytes and polychelatogenes. Polyelectrolytes, like the pH-responsive polymers, possess charged groups along their chain which are ionizable, binding to their respective counterions by electrostatic interaction, involving territorial binding, site binding and

hydrophobic binding, leading to a non-specific bonding of the metal to the polymer chain. Such interactions are of particular interest in applications like electrolyte membranes, ionomers, shape-memory materials, or metal ion sensing. Contrary, polychelatogenes carry functional groups along the polymer capable of forming coordinative bonds to the ions or complexes, which can be found in a variety of applications like homogeneous catalysts, light-emitting devices, sensors, or conductive polymers (Figure 16). Such interactions often lead to increasing thermal and chemical stability.[264–273]

A) Polyelectrolyte - metal interactions

B) Polychelatogene - metal interactions

$M^{n+} = Ag^+, Cd^{2+}, Hg^{2+},$
$Ni^{2+}, Cu^{2+}, Zn^{2+},$
Co^{2+}, Cr^{3+}

- electrostatic interaction
- non-specific binding/ion mobility
- mono- or multidentate binding
- inter- and intramolecular binding

- coordinative bonding
- specifically bonded metal complex
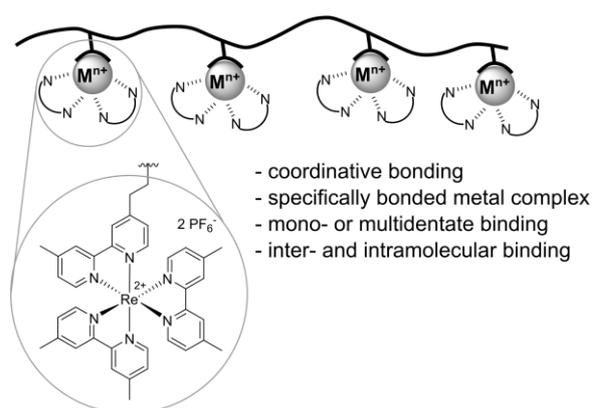- mono- or multidentate binding
- inter- and intramolecular binding

Figure 16: Interactions between polyelectrolytes and metal ions *via* electrostatic interactions (**A**) and interaction of polychelatogenes with metal complexes *via* coordinative bonding (**B**).[264,267,274]

Especially the polychelatogenes have attracted increasing attention within the last years, as they combine the processability of the polymeric ligand with the reactivity of the interacting, coordinatively bound complex. There is a variety of different ways of incorporating suitable structures into polymer materials (Figure 17). The different approaches include attachment of (multifunctional) end-groups (**I**), synthesis of (co)polymers with suiting sidechains (**II**), incorporation of the ligand motif into the main chain (**III**) or formation of polymer chains by ligand-metal interactions (**IV**). Additionally, the binding can again occur in a monodentate or multidentate way, involving only one polymer chain or intramolecular interaction between different polymer chains, dependent on the valency of the metal ions/complexes and the ligands involved. By means of polymer synthesis, a broad variety of tuning points can be addressed, allowing for targeted macroligand design. The preparation of such compound materials can be performed *via* two different synthesis approaches. In the first approach, polymers are synthesized *via* various methods carrying appropriate ligand motifs, for example by initiation with suiting molecules or by polymerizing monomers with pending ligand structures. After polymerization, these macroligands reacted with precursor complexes in a polymer-analogous reaction to form the polymeric metal complexes. In the second approach, initiators or monomers are prepared, to which the metal complexes are already linked coordinatively prior to the polymerization. One class of materials of particular interest are bipyridine and

terpyridine derived polymer metal complexes, which have been addressed in various publications and reviews.[268,269,274–282]
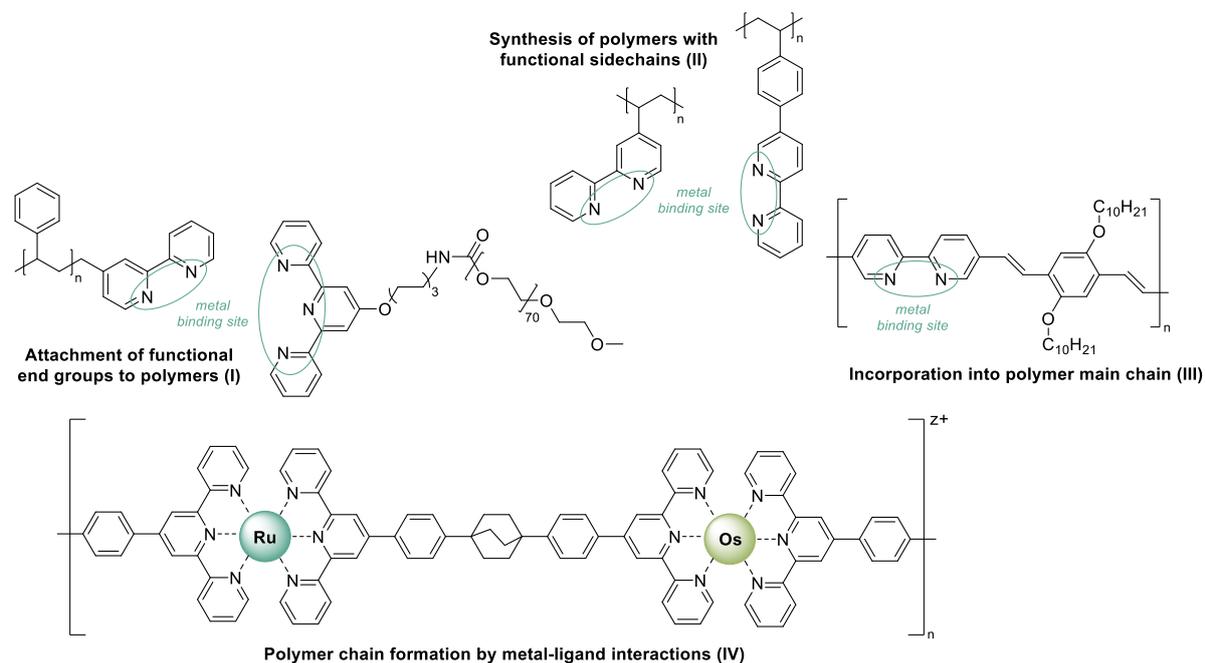

Figure 17: Approaches for the synthesis of polymer-metal complexes *via* attachment of functional end-groups (**I**), synthesis of polymers with functional sidechains (**II**), incorporation of functional units into polymer main chains (**III**) or formation of polymer chains *via* metal-ligand interactions (**IV**).[268,269,276–279]

Again, especially with focus on P2VP, P4VP, PDEVP and its derivatives, group-transfer polymerization can provide a useful tool for the synthesis of (multi)responsive polymers, combining the advantages of catalytic precision polymerization with targeted polymer design for certain applications. Overall, group-transfer polymerization has shown to be an interesting tool in this context.[15,29,33,42,44,48,82]

2.3.2. Drug-delivery systems

By using (multi)responsive materials, polymers can be designed with specific reactivities towards certain environmental parameters, allowing them to address certain tasks. One such application is the use of (co)polymers for drug-delivery systems, targeting specific parts of the body for drug administration. According to Kankane *et al.* controlled drug release can have a variety of benefits. By means of drug-delivery, the concentration of the active substance can be held constant over a longer period of time, avoiding fluctuation and thus side-effects, waste, and frequent dosing. Overall, the release of the drug is more predictable and reproducible, leading to an optimized therapy and better patient compliance. Additionally, the active compound is protected by the polymers, overcoming problems like short half-life or drug stability. Generally, there are five different release profiles desired in drug-delivery, which are shown in Figure 18.[168,283]
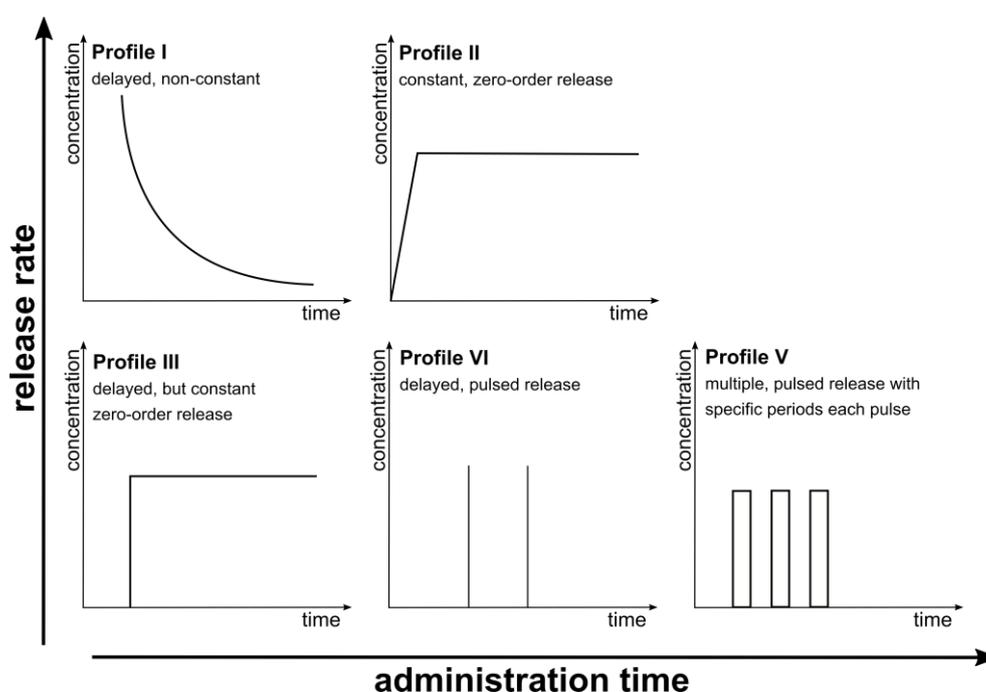

Figure 18: Five different controlled drug-release profiles **I-V** according to Kankane *et al.*[283]

The most commonly encountered drug-delivery profiles are **I** and **II**, showing either conventional, non-constant release after a specific delay (**I**) or constant release (**II**). Profile **III** shows the same constant compound concentration as profile **II**, but with a specific delay between drug administration and drug release. Contrary, in profile **IV**, the drug is released as very tight pulse, again with a specific delay. Similarly, for profile **V**, multiple pulses with specific periods between pulses is desired.[283] According to Khare *et al.*, those specific release profiles can be achieved by diffusion-controlled systems, with either reservoirs or matrices, by chemically-controlled systems based on degradation or pendent sidechains, by solvent-activated systems (osmosis or swelling) or by modulated release.[283,284] There is a variety of

different polymeric systems, which can be used for drug-delivery applications, including hydrogels, polymerosomes, polymer-drug conjugates, nanocapsules, nanoparticles dendrimers or micelles, opening up a very broad application field for specifically designed (co)polymers. There is a broad variety of different review articles regarding structure-property relationships, response mechanisms or influencing parameters for polymer-based drug-delivery applications.[262,285–290]

With respect to group-transfer polymerization-based polymers for drug delivery, the work by Rieger *et al.* has successfully shown the huge potential of this technique for the synthesis of multiresponsive drug carrier systems. By sequential copolymerization of 2-vinylpyridine with diethyl vinylphosphonates and its methyl and propyl derivates using the monometallic yttrium bis(phenolate) catalyst **6** and the bimetallic yttrium bis(phenolate) catalyst **7**, they were able to synthesize amphiphilic AB-, ABB'- and BAB-type block copolymers with hydrophobic P2VP block covalently linked to hydrophilic poly(vinylphosphonates) blocks. Those precisely defined copolymers are pH- and temperature responsive with a tunable LCST and a hydrodynamic diameter D_h of the micelles under aqueous conditions of < 100 nm, being in a physiologically relevant size (Scheme 27).[42,44,168]
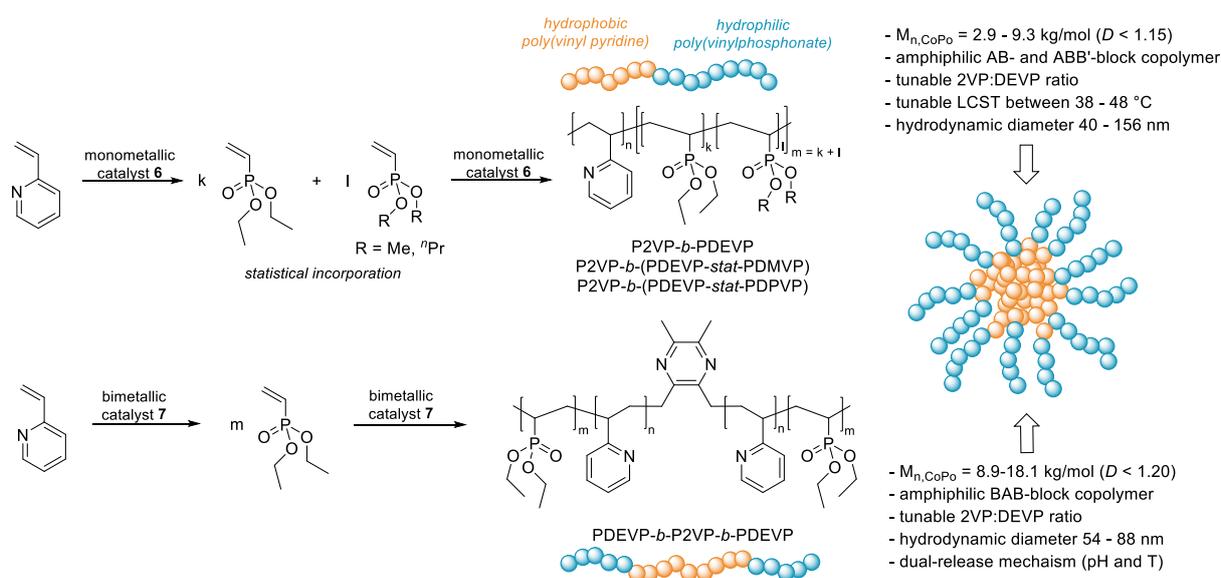
Scheme 27: Synthesis of amphiphilic, micelle-forming AB- and ABB'-type block copolymers by sequential copolymerization of hydrophobic 2VP with hydrophilic dialkyl vinylphosphonates by monometallic yttrium catalyst **6** and synthesis of a BAB-type copolymer from 2VP and DEVP with bimetallic yttrium catalyst **7** .[42,44]

Based on the response mechanism of the P2VP block towards pH and the temperature-response of the PDEVP block, such copolymers are promising candidates for targeted drug delivery. The pH-responsiveness can either be used for drug-delivery into cells, utilizing the pH-gradient observed between the extracellular fluid (pH = 7.35 – 7.45), endosomes

(pH = 5.5 – 6.0) and lysosomal compartments (pH = 4.5 – 5.0), with P2VP showing a response in the corresponding region, or targeting cancer cells with their slightly lower overall pH value of 5.7 – 6.8. Additionally, the temperature-responsiveness of the PDEVP blocks can be exploited as well for a sustained drug release. The synthesized BAB-type block copolymers PDEVP-*b*-P2VP-*b*-PDEVP have been investigated thoroughly regarding their fluoresceine release behavior upon changes of pH and temperature, critical micellization concentration and particle size *via* transmission-electron microscopy and dynamic light scattering (Figure 19).[44,291–293]
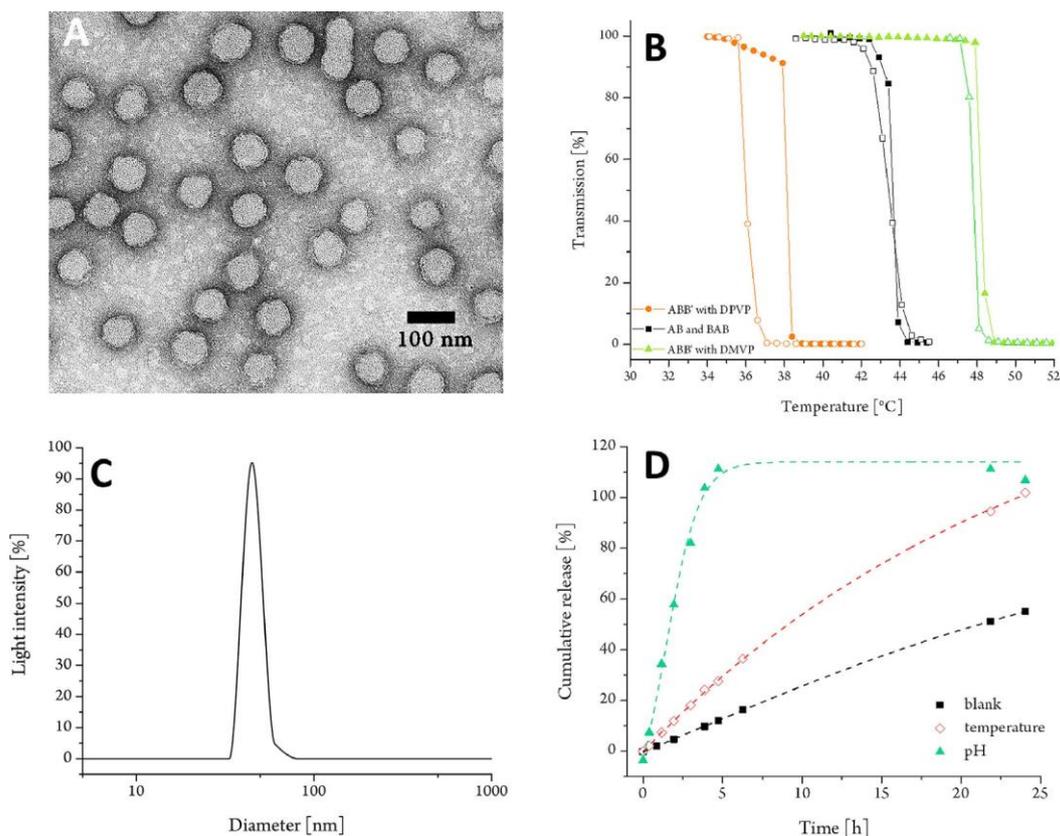

Figure 19: TEM image of a BAB micelle with D_h = 54 nm (**A**), cloud point determination by turbidity measurements of AB- and ABB'-diblock copolymers (**B**), micelle size determination *via* dynamic light scattering (D_h = 46 nm) (**C**) and fluoresceine release experiments of loaded BAB micelles (Dh = 88 nm) towards pH 4.5 and a temperature of 44 °C (**D**). (Reprinted with permission from ref. [7]. Copyright 2017 John Wiley and Son)

Cytotoxicity assays of the micelles revealed a high biocompatibility and low toxicity of the polymer material. Loading with the anticancer drug doxorubicin and its release into HeLa cells has been investigated, revealing a prolonged release and good apoptosis induction activity, making the presented polymers interesting candidates for targeted drug delivery.[44] Since then, PDEVP based, functionalized (co)polymers have been used for different biomedical applications involving polymer-drug conjugates, micelle-based drug-delivery or nanoparticles.[34,42,44,46,70,86,88,283,294,295]

While examples of GTP-based polymers remain sparsely throughout literature, aliphatic polyesters from ROP have been used extensively in medical applications and drug-delivery. One major advantage of these materials is their susceptibility towards degradation *via* random hydrolytic scission along the polymer backbone by cleavage of the labile ester bonds. Some of the most commonly applied polymers remain poly(lactic acid) (PLA), poly(glycolic acid) (PGA), PCL, PHB as well as their copolymers and many other polyester (co)polymers.[168,296,297] This degradation behavior makes aliphatic polyesters interesting candidates for drug-delivery systems based on a compound release upon degradation of the polyester matrix. One major advantage of this material class is their adjustability of their physical properties and biodegradability by changing structure and composition of the repeating unit in terms of chain flexibility, presence of polar groups, adjustment of molecular mass, crystallinity or orientation and by tuning (co)polymer composition or architecture during polymer synthesis.[168,297,298] Due to this versatility, various approaches have been reported, utilizing polyesters and their copolymers as micellar systems, polymer-drug conjugates, microcapsules or hydrogels for drug-delivery systems.[285,296–305]

As ROP catalysis offers a variety of different advantages like controllable molecular weight and microstructure, precisely defined polymers, or access to a variety of different polymer architectures, it remains a tool of high interest for the synthesis of functional polyesters for drug-delivery applications. In an example presented by Cheng *et al.*, the authors exploited the characteristics of the immortal ring-opening polymerization (*vide supra*). They used the mitotic inhibitor paclitaxel with three free hydroxyl groups within its structure as chain-transfer agent in combination with the zinc catalyst (BDI-X)ZnN(TMS)$_2$ for the ring-opening polymerization of *rac*-lactide, preparing linear polymer-drug conjugates while maintaining excellent molecular weight control (M_n = 7.8 – 31.4 kg/mol, $Đ$ = 1.03 – 1.30) and achieving a living polymerization, allowing copolymerization with other lactones like δVL or CL (Scheme 28).[302]
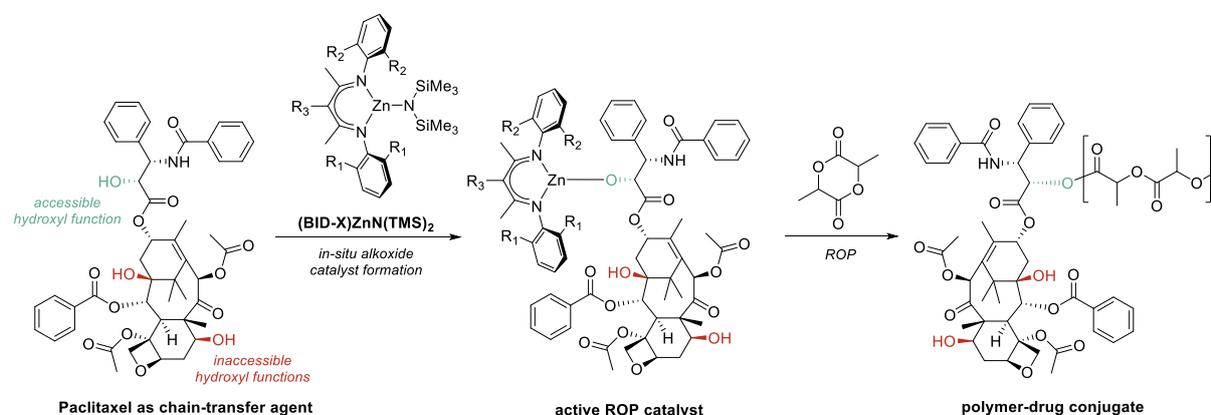
Scheme 28: Immortal ring-opening polymerization of *rac*-lactide with a (BID-X)ZnN(TMS)$_2$ catalyst and the bioactive compound paclitaxel as chain-transfer agent for the synthesis of well-defined polymer-drug conjugates.[302]

2.3.3. Polymers on surfaces

Another important aspect of modern biomedicine is the use of medical devices inside the body, like artificial joints or implants, stents, catheters, or replacements for blood vessels. Such devices can be produced from a variety of different materials including polymers like poly(tetrafluoroethylene), silicones, various polyesters, glass, or steel. As they come into contact with the surrounding body fluids, these materials have certain requirements regarding mechanical strength, surface friction, corrosion, or cell-adhesion. One way of modulation of these properties is by coating the surfaces of these materials with polymers.[168,306–308]

Generally, there are two different approaches conceivable when surfaces are to be coated with polymer materials. In the graft-to method, the surface of the substrate is functionalized molecules with distinct reactivity and a preformed polymer with a suiting functional group corresponding to the surface molecules is immobilized to the surface (**Figure 20**A). Contrary, in the graft-from method, the substrate is covered with molecules capable of inducing a polymerization reaction, allowing the polymer to grow from the surface (Figure 20B).[309,310]
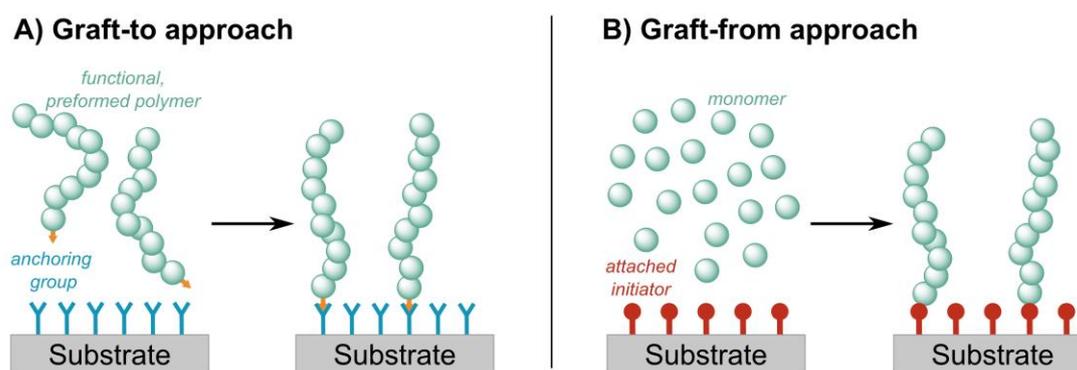

Figure 20: Methods for anchoring polymer materials to surface subtrates *via* graft-to of a preformed, functionalized polymer to an anchoring group on the surface (**A**) or graft-from by polymerization using surface-attached initiators (**B**).[311]

For graft-to approaches, a chemical reaction between reactive groups of polymer chains and corresponding functionalities attached to surfaces is performed, creating a covalent bond between the surface-anchored molecules and the polymer. Main advantages are a simpler experimental procedure in terms of functionalization and preparation as well as analytics. However, graft-to approaches are considered to be insuitable for the preparation of dense surface coverings.[310] To ensure high surface coverage, usually highly efficient conjugation reactions are applied like thiol-ene reactions, hetero Diels-Alder reactions, azide-alkyne cycloaddition reactions, or esterifications.[312,313] Darcos *et al.* used this graft-to approach for the synthesis of silica nanoparticles functionalized with well-defined polyesters. By immortal ring-opening polymerization of D,L-lactide with $Sn(Oct)_2$/benzyl alcohol they prepared hydroxyl-terminated polymers with defined chain-length and narrow polydispersity ($Đ < 1.16$).

Subsequently, they converted the hydroxy-terminus to a carboxylic acid before transforming it into a *N*-hydroxy succinimide (NHS) active ester. In parallel they prepared silica nanoparticles by a modified Stöber process followed by amino-functionalization with (3-aminopropyl)triethoxysilane. In a final step, they performed the graft-to of the PLA chains onto the silica nanoparticles by esterification of the NHS-active ester polymer chain with the pendent amino-functions on the nanoparticles (Scheme 29). The functionalized nanoparticles were investigated thoroughly by means of TEM, TGA, IR and solid-state ^{29}Si-NMR, ultimately aiming for applications in biomedical scaffold materials.[314]
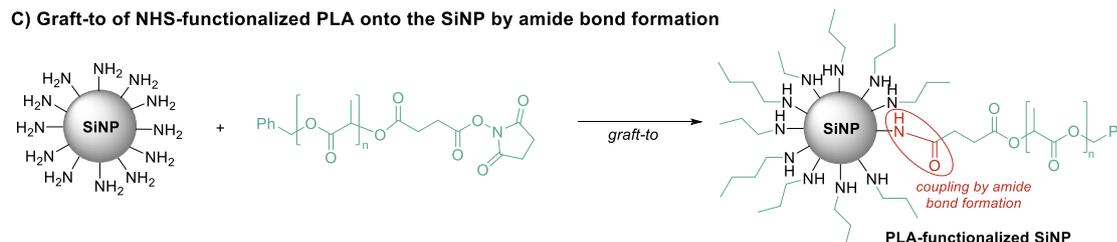
A) Synthesis of NHS-functionalized PLA
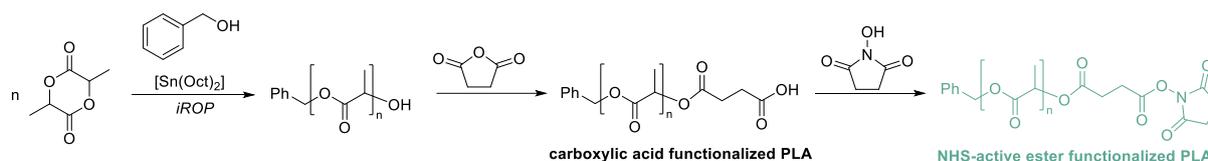
B) Synthesis of NH$_2$-functionalized SiNP
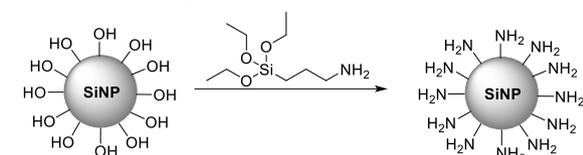
**C) Graft-to of NHS-functionalized PLA onto the SiNP by amide bond formation**

Scheme 29: Synthesis of an NHS-ester functionalized PLA *via* ROP and subsequent functionalization steps (**A**), preparation of amine-functionalized silicon nanoparticles (SiNP) (**B**) and graft-to of the functionalized PLA onto the SiNP surface *via* amide bond formation (**C**).[314]

For graft-from approaches, the polymer is grown on the surface rather than attaching a preformed polymer, induced by molecules anchored to the substrate. Herein, different approaches of surface-induced polymerizations have been presented, including various radical, ring-opening, or ring-opening metathesis polymerization techniques.[311,315,316] While graft-from approaches can achieve higher graft densities, they suffer from disadvantages like tedious synthetic procedures, low initiator efficiencies, broadening of the molecular weight distribution or monomer diffusion problems.[310] One example for a graft-from approach in the context of group-transfer polymerization has been presented by Rieger *et al.* They functionalized H-terminated silicon substrates with a poly(ethylene glycol dimethacrylate) (PEGDM) precoating by photoinduced hydrosilylation and photo-polymerization, providing dangling methacrylate moieties. By addition of Cp$_2$YbMe as catalyst and dialkyl vinylphosphonates (DEVP, DMVP and DPVP), they achieved a surface-initiated group-transfer

_____

polymerization, successfully grafting PDEVP and its derivatives from the silicon surface. Analysis by means of time-resolved atomic force microscopy (AFM) revealed a rapid growth of the polymer chains from the surface within a timescale of minutes (**Figure 21**A). Attachment of these poly(vinylphosphonates) to the surface allowed for a modulation of the surface contact angle (CA) to water depending on the hydrophilicity of the vinylphosphonates sidechain, with PDVMP showing the lowest CA of 17 ° and PDPVP showing the highest CA of 76 °C. Additionally, they were able to show that the polymers retained their LCST on the surface, with PDEVP exhibiting a CA of 46 ° at 25 °C and a CA of 66 ° at 50 °C (Figure 21B).[317]
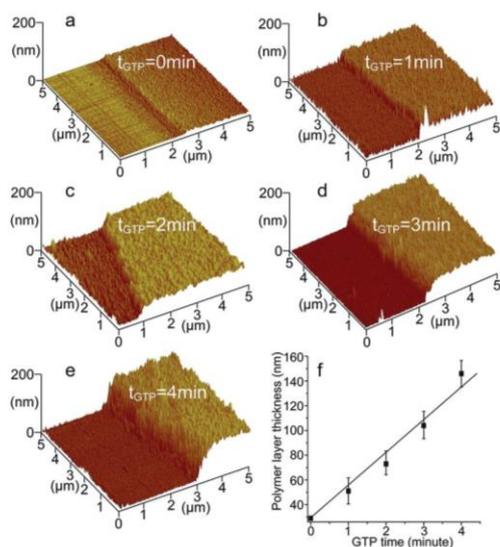
A) Time-resolved AFM   **B) CA measurements of coated surface**
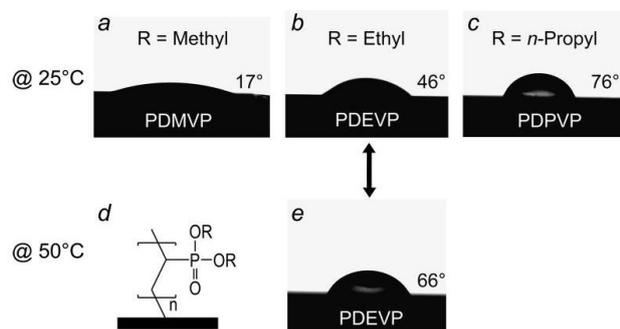

Figure 21: Time-resolved AFM measurements of a surface-initiated GTP of DEVP on a PEGDM-functionalized silicon wafer (**A**) and CA measurements of water on silicon wafer surfaces functionalized with PDMVP, PDEVP or PDPVP and temperature-response of the contact angle (**B**). (Reprinted with permission from ref. [317]. Copyright 2012 American Chemical Society.)

3. Aim – functionalizing polymers

Throughout this thesis, group-transfer and ring-opening polymerization as precision polymerization methods are to be used as tools to introduce functionality in different forms to the polymers synthesized, targeting certain application profiles. With regards to the different modification points conceivable for such catalytic polymerization techniques, different approaches will be tested to obtain new, smart polymeric materials. To fine-tune the properties of these polymers, the following points are addressed:

➤ End-group modification (**1**)

➤ Sidechain functionalization (**2**)

➤ Monomer variation (**3**)

➤ Copolymerization (**4**)

Both end-group and sidechain functionalization allow bringing polymeric materials into different applications, for example by introducing anchoring moieties for surface coatings or coupling metal complexes to the polymers. In a more retro-synthetic approach, structural variation of the monomers used can help achieving desired properties and understand structure-property relationships. The last modification point, the copolymerization of different monomers into a variety of different polymer architectures allows for the synthesis of advanced materials like responsive micelles. Overall, the high tuneability of these modification points offers a broad toolbox for the synthesis of advanced polymer structures, which will be explored in more detail throughout this thesis (Figure 22).
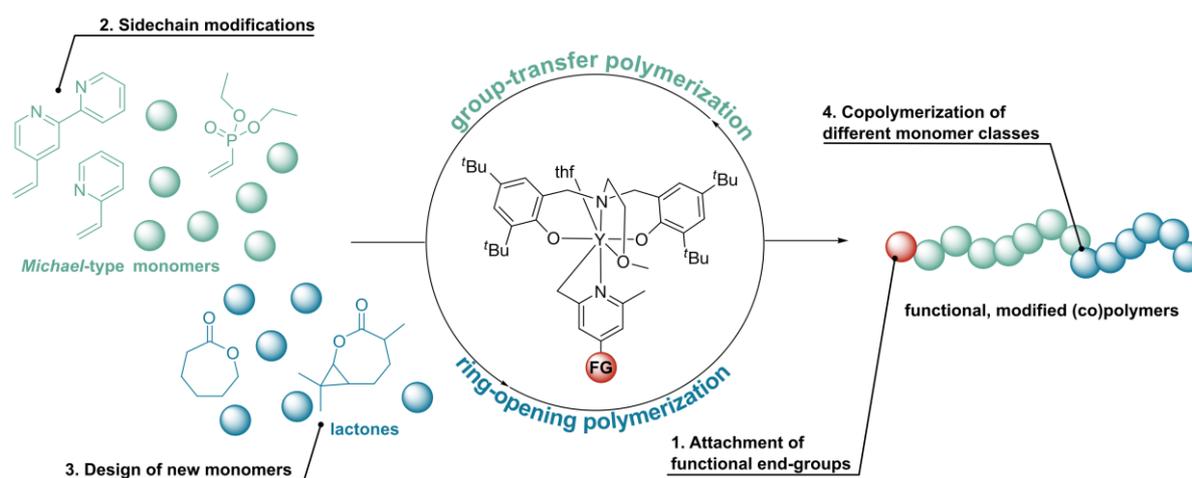

Figure 22: Possible modification points in the context of group-transfer- and ring-opening polymerization investigated throughout this thesis.

3.1.   Attachment of functional initiators

With focus on the attachment of functional initiators as end-groups of the polymers, different approaches are possible for GTP and ROP. In GTP, the CH-bond activation of yttrium catalysts can be utilized to introduce α-methylpyridines with (masked) functional groups as initiators, which are transferred onto the polymers upon initiation.[29,32,44,68,70,82,85–88,318] Herein, two different approaches have been established, either the *in-situ* activation of the cyclopentadienyl yttrium pre-catalyst Cp$_2$Y(CH$_2$TMS)(thf) at ambient temperature without catalyst isolation or the synthesis and isolation of the corresponding C-H bond activated yttrium bis(phenolate) catalysts,[68,88] derived from activation of the pre-catalyst [(ONOO)^{tBu}Y(CH$_2$TMS)(thf)].[32,44,70,82] To gain access to new functionalities, α-methylpyridines with various functional groups are synthesized and introduced to the catalysts, ultimately leading to incorporation of those into the polymers (Figure 23).
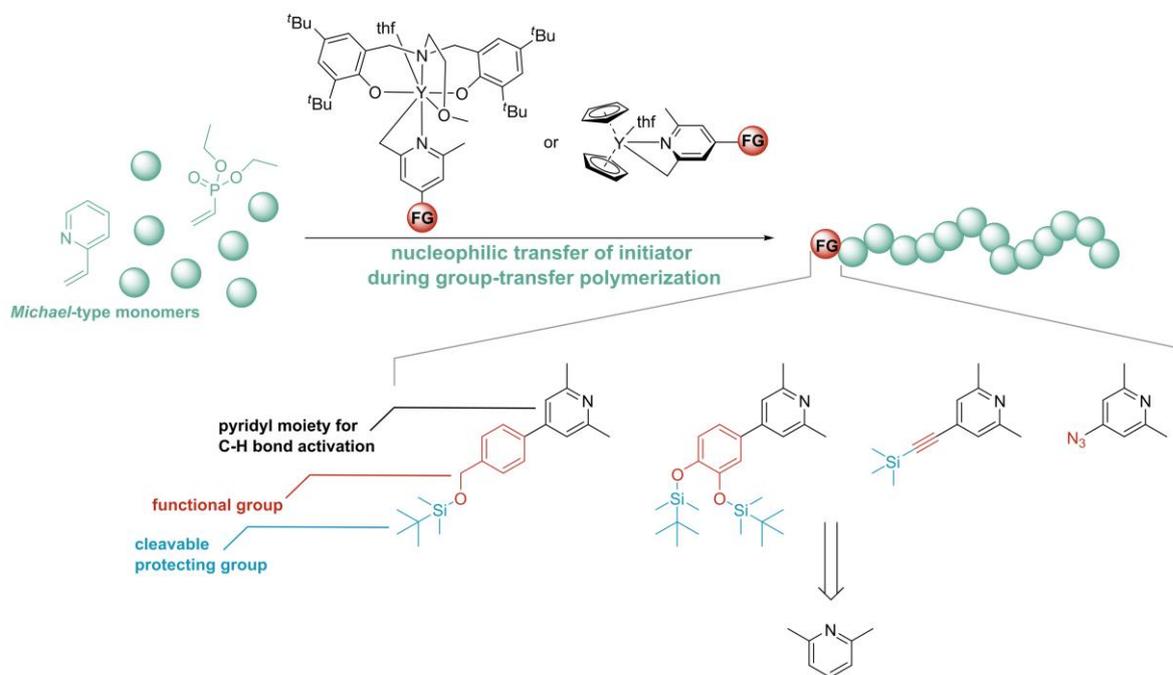

Figure 23: Introduction of functional groups to GTP-based polymers by C-H bond activation of yttrium catalysts with functionalized α-methylpyridines.

3.2. Sidechain modifications

With regards to sidechain modifications, especially polymers from *Michael*-type monomers show a broad platform of applicable pendent groups with distinct functionalities. In the context of this work, the class of poly(vinylpyridines) have been selected as functional polymer building blocks due to their responsiveness to changes in the pH as well as their capability of interacting with metal complexes. While the pyridiyl moiety of P2VP or P4VP itself introduces a certain degree of functionality to the polymers and is capable of interacting with metal ions as polyelectrolyte, modulation of the sidechain structure from a monodentate to a bidentate ligand motif allows for targeted use as macroligand for different metal complexes. Using bipyridines as pendent sidechains for metal complexation is a method widely used for the synthesis of polymer-metal complex compound materials and has been explored in great detail regarding a variety of different metal complexes for numerous applications.[274–279] By using the readily accessible 4,4'-dimethyl-2,2'-bipyridine as starting material, it is possible to introduce a vinyl bond in 4-position of the ring-nitrogen in a two-step synthesis, ultimately creating the conjugate 1,6-*Michael* acceptor system and 4VP derivate 4-vinyl-4'-methyl-2,2'-bipyridine (VBpy).[279] While there are various polymerization methods for this monomer, involving free radical polymerization,[319,320] ATRP,[278] or electropolymerization,[275,321,322] no catalytic polymerization method has been reported so far, despite offering unique advantages like tunable molecular weight with narrow dispersity. Herein, the LPP of 4VP with aluminum-based *Lewis* acids and phosphine-based *Lewis* bases as reported by Rieger *et al.* is used as template to synthesize precisely defined PVBpy.[15] This polymer will be used as macroligand for rhenium and ruthenium complexes to gain access to a highly active and stable macromolecular photocatalysts for CO_2 reduction by forcing these metal complexes into spatial proximity (Figure 24).
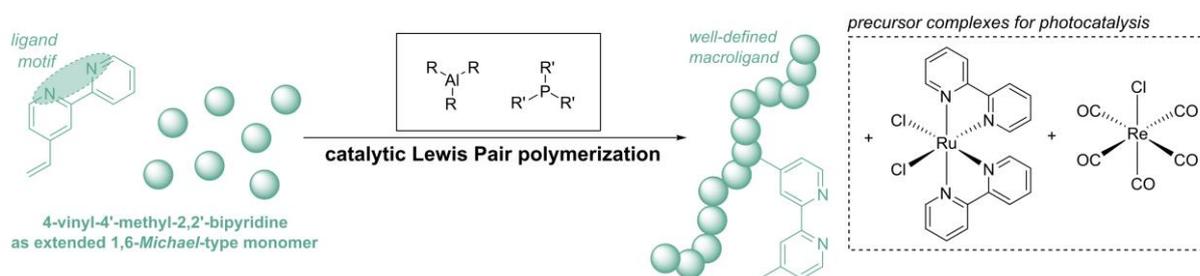

Figure 24: Catalytic *Lewis* pair polymerization of 4-vinyl-4'-methyl-2,2'-bipyridine towards well-defined polymer ligands for photocatalytically active complexes.

3.3.   Introducing new monomers

While the two modification points discussed priorly are mainly focusing on introducing functionality to known polymer systems, the introduction of new monomers offers the opportunity of generating completely new polymers directly targeting issues like monomer sourcing or polymer material properties. Especially in the context of polyesters, a major task remains converting abundant bio-based feedstocks into suitable monomers, as the resulting polymers would not only incorporate structures from biogenic resources but might offer advantages such as main chain degradability *via* hydrolysis or tuning of the thermal properties. One such feedstock is the cheap and abundant turpentine oil, a wood-based terpene source with high annual production volume and barely any value-added post-processing, making it an ideal candidate for polymer synthesis.[3,120,122] Turpentine oil contains a variety of different terpene structures with α-pinene, β-pinene or 3-carene being the most abundant ones. These terpenes feature interesting bicyclic structures, whose incorporation into the polymer backbone might modulate the polyesters properties in a beneficial way. This behavior has been observed by Syrén *et al.*, who presented an α-pinene based lactone, allowing incorporation of the 4-membered ring into the main chain upon ROP, obtaining a semi-crystalline, fully aliphatic polyester with a melting point at 158 °C.[139] Herein, synthesis pathways towards monomers and polymers from β-pinene and 3-carene are explored, ultimately aiming at polyesters utilizing the skeletal structure of these terpenes (Figure 25).
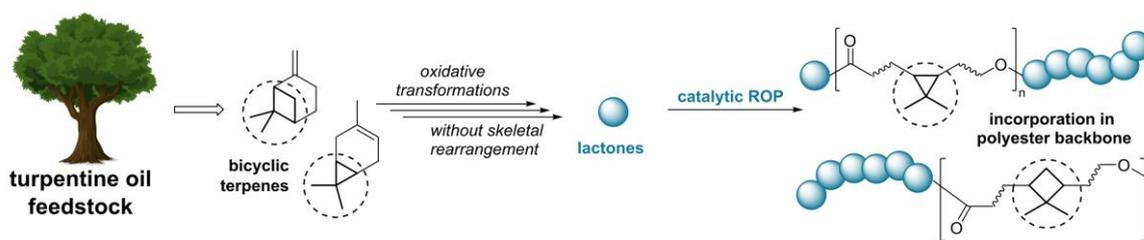

Figure 25: Utilization of turpentine oil-based β-pinene and 3-carene for polyester synthesis.

3.4. Copolymerization of *Michael*-type monomers and lactones

Overall, the last modification point, the copolymerization of different monomers or monomer classes, is a very versatile method of obtaining new, highly functional, and smart polymers by utilizing the distinct reactivity and structure of each block in one material. For GTP, various functional copolymer materials have been reported so far.[10,16,35,42,44,82] However, this technique suffers from the major drawback of being strictly limited to block copolymerization when dealing with different monomer classes (*vide supra*).[10,22,26,33] Contrary, ROP is far more versatile in terms of copolymerization, giving access to different architectures such as gradient copolymers, statistic copolymers or (multi)block copolymers, based on the monomers used and the synthesis procedure.[111,116] While there is a multitude of reports on new copolymers, one way of accessing new functional materials, however, is notably overlooked with only few examples of copolymerization of *Michael*-type monomers and lactones. While there are some examples of combining ROP with *Michael*-type monomers, those usually involve radical techniques such as ATRP or RAFT polymerization. Those often require reactions on polymeric intermediates, multi-functional initiators, or difficult purification steps.[242–249,323–326] Sparsely reported however is the utilization of catalytic methods for the synthesis of such copolymers, as it could offer different advantages such as better polymerization control, functionalization, or a broader monomer scope in general. Within the last 30 years, there have been some examples reported by Yasuda,[22] Hadjichristidis,[252] Chiellini,[251] Li[253] or Mehrkhodavandi,[241] yet those are limited to the catalytic copolymerization of different (meth)acrylates with few lactones (*vide supra*). However, for both polymerization types, GTP and ROP, the scope of available monomers is much broader, offering a wide range of applicable monomers. Herein, catalytical pathways to block copolymers from GTP and ROP are explored in more detail, addressing this gap of knowledge (Figure 26).
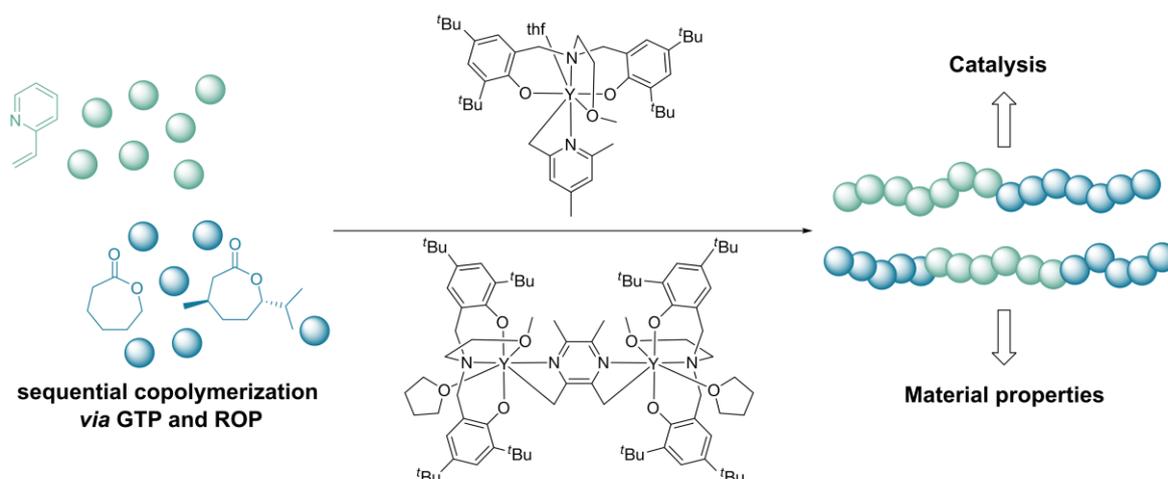

Figure 26: Sequential copolymerization of *Michael*-type monomers and lactones *via* GTP and subsequent ROP.

4. End-group modifications

"C-H Bond Activation of Silyl-substituted Pyridines with Bis(phenolate)-yttrium Catalysts as a facile Tool towards Hydroxyl-terminated *Michael*-type Polymers"

4.1. Bibliographic data

Title: "C-H Bond Activation of Silyl-substituted Pyridines with Bis(phenolate)-yttrium Catalysts as a facile Tool towards Hydroxyl-terminated *Michael*-type Polymers"

Status: Article, Publication Date: 22.04.2020

Journal: Catalysts

Publisher: MDPI

DOI: 10.3390/catal10040448

Authors: Thomas M. Pehl, Moritz Kränzlein, Friederike Adams, Andreas Schaffer and Bernhard Rieger[‡]

4.2. Content

As explained in detail in the previous chapter 2.3, polymers especially from group-transfer polymerization offer a high degree of functionality due to their responsiveness towards different stimuli like temperature or pH. To further increase the amount of functionality of these polymers, the selective attachment of end-groups can provide reactive groups, which can ultimately be used for advanced functionalizations like the formation of polymer-biomolecule conjugates[86,88] or can help modulating the polymer architecture by the use of multifunctional initiators.[85] In this context, the concept of C-H bond activation of yttrium pre-catalysts like $Cp_2Y(CH_2TMS)(thf)$ or $[(ONOO)^{tBu}Y(CH_2TMS)(thf)]$ with α-methylpyridines like *sym*-collidine for the generation of highly active GTP catalysts can be utilized.[68,70] During this C-H bond activation, the pyridine is covalently attached to the catalysts metal center and transferred irreversibly during the initiation of the group-transfer polymerization as explained in chapter 2.1.3.1. Dependent on the pre-catalyst used, the activation itself can either be performed *in-situ* (as for the $Cp_2Y(CH_2TMS)(thf)$ system) without catalyst isolation or requires work-up of the prepared catalyst (as for the $[(ONOO)^{tBu}Y(CH_2TMS)(thf)]$ pre-catalyst). If now a functional group is attached to the pyridine prior to C-H bond activation, it is transferred onto the polymer and remains covalently bound to the chain as an end-group, allowing quantitative chain functionalization. When designing suited molecules for the C-H bond activation, low-reactive functional groups like double-bonds or bipyridines can be used directly, while functional groups capable of interacting with the pre-catalyst must be protected to ensure a side-reaction free catalyst synthesis.[82,86] In these cases, post-polymerization reactions are required for end-group deprotection and retention of the original functional group. In order to broaden the versatility of this concept, a silyl-protected alcohol pyridine is designed, which has been applied in the C-H bond activation with both $Cp_2Y(CH_2TMS)(thf)$[88] as well as with the pre-catalyst $[(ONOO)^{tBu}Y(CH_2TMS)(thf)]$ as presented herein. Additionally, the scope of applicable pyridines is broadened by introduction of pyridines functionalized with a (protected) catechol, a (protected) alkyne or an azide, which were successfully introduced to PDEVP as end-groups. These molecules have been prepared in order to ultimately facilitate surface immobilization of GTP-based polymers, which has to be tested in the future.

4.3.   Manuscript

catalysts

MDPI

Article

C–H Bond Activation of Silyl-Substituted Pyridines with Bis(Phenolate)Yttrium Catalysts as a Facile Tool towards Hydroxyl-Terminated Michael-Type Polymers

Thomas M. Pehl [†], Moritz Kränzlein [†], Friederike Adams [†], Andreas Schaffer and Bernhard Rieger *

WACKER-Chair of Macromolecular Chemistry, Catalysis Research Center, Department of Chemistry, Technical University of Munich, Lichtenbergstr. 4, 85748 Garching near Munich, Germany; thomas.pehl@makro.ch.tum.de (T.M.P.); moritz.kraenzlein@makro.ch.tum.de (M.K.); rike.adams@makro.ch.tum.de (F.A.); andreas.schaffer@makro.ch.tum.de (A.S.)
* Correspondence: rieger@tum.de; Tel.: +49-89-289-13570
† These authors contributed equally to this work.

check for updates

Abstract: Herein, silicon-protected, *ortho*-methylated hydroxy-pyridines were reported as initiators in 2-aminoalkoxy-bis(phenolate)yttrium complexes for rare earth metal-mediated group-transfer polymerization (REM-GTP) of Michael-type monomers. To introduce these initiators, C–H bond activation was performed by reacting $[(ONOO)^{tBu}Y(X)(thf)]$ ($X = CH_2TMS$, thf = tetrahydrofuran) with *tert*-butyl-dimethyl-silyl-functionalized α-methylpyridine to obtain the complex $[(ONOO^{tBu}Y(X)(thf)]$ (X = 4-(4′-(((*tert*-butyldimethylsilyl)oxy)methyl)phenyl)-2,6-di-methylpyridine). These initiators served as functional end-groups in polymers produced via REM-GTP. In this contribution, homopolymers of 2-vinylpyridine (2VP) and diethyl vinyl phosphonate (DEVP) were produced. Activity studies and end-group analysis via mass spectrometry, size-exclusion chromatography (SEC) and NMR spectroscopy were performed to reveal the initiator efficiency, the catalyst activity towards both monomers as well as the initiation mechanism of this initiator in contrast to commonly used alkyl initiators. In addition, 2D NMR studies were used to further confirm the end-group integrity of the polymers. For all polymers, different deprotection routes were evaluated to obtain hydroxyl-terminated poly(2-vinylpyridine) (P2VP) and poly(diethyl vinyl phosphonate) (PDEVP). Such hydroxyl groups bear the potential to act as anchoring points for small bioactive molecules, for post-polymerization functionalization or as macroinitiators for further polymerizations.

Keywords: rare earth metal-mediated group-transfer polymerization; homogeneous catalysis; C–H bond activation; end-group functionalization; poly(diethyl vinyl phosphonate); poly(2-vinylpyridine); non-metallocenes

1. Introduction

Since the initial discovery of group-transfer polymerization (GTP) of methyl methacrylate (MMA) using silyl ketene acetals by Webster et al. in 1983 [1], this polymerization type has been continuously refined. The application of a neutral samarocene-based complex for the polymerization of MMA by Yasuda et al. in 1992 [2] introduced the field of rare earth metal-based group-transfer polymerization (REM-GTP). Mechanism elucidation on this reaction revealed a repeated 1,4-conjugate addition (Michael-addition) during propagation with a keto-enolate 8-membered cyclic intermediate [1–8]. Since the first polymerization attempts, various organocatalysts, metallocenes and non-metallocenes

were established for the synthesis of highly precise, tailor-made and functional polymers [3,5,7–14]. The scope of available 1,4-Michael-type monomers ranges from differently substituted acrylates, methacrylates, acrylamides or nitrogen bearing monomers (e.g., 2-vinyl pyridine (2VP)) to vinyl lactone systems and phosphorous containing monomers, i.e., dialkyl vinyl phosphonates (DAVP) [5,7,15,16].

The broad variety of monomers comes along with individual challenges for each monomer type, such as low activities or initiator efficiencies of the catalysts that have to be solved by the development of catalysts with enhanced performance. These catalysts were able to overcome the obstacles and produced high molecular weight polymers with very narrow molecular weight distributions and were in addition able to induce stereoinformation [10,15,17–21]. This enhanced performance was achieved by e.g., introducing highly sterically demanding ligands to non-metallocenes for stereoregular polymerization of MMA or 2VP [9,10,21], by controlled polymerization of vinyl phosphonates using non-metallocenes, frustrated Lewis pairs or trivalent metallocenes [12,14,15,17,22–24] or by utilizing C–H bond activation to obtain catalysts with higher initiator efficiencies [18]. Further to this, the synthesis of block copolymers was facilitated due to the living character of this polymerization type by simple sequential addition of different monomers with respect to their coordination strength to the metal center [7,25,26]. Additionally, C–H bond activation gave access to post-polymerization functionalization and facilitated the synthesis of new block copolymer structures and polymer architectures [7,18,27–34].

Lanthanide complexes can undergo σ-bond metathesis in a [2σ + 2σ] cycloaddition which is a very effective method for cleaving C–H bonds in metalorganic chemistry. Trivalent lanthanide and transition metal complexes with a d^0-configuration do not possess the ability to undergo oxidative addition or reductive elimination, making σ-bond metathesis via C–H bond activation the only possibility of introducing new molecules to this kind of complexes [35–38]. This principle of C–H bond activation was introduced in 1983 by Watson et al. [39,40], showing the activity of Cp*$_2$LuX (X = H, CH$_3$) complexes (Cp* = pentamethylcyclopentadienyl) towards [2σ + 2σ] cycloaddition with pyridine, benzene or a phosphorylidene. They further discovered the activation of methane in a C–H bond activation reaction with Cp*$_2$LuCH$_3$ by ^{13}C isotope labelling. This is the first example of activating the very inert sp^3-hybridized carbon–hydrogen bonds in methane, which are known to be reluctant to undergo any kind of activation [38–40].

The first example of polymerization catalysts obtained by C–H bond activation was developed by Mashima et al. in 2011 using an yttrium ene-diamido complex for enhancing the initiator efficiencies, but was also used for end-group functionalization of GTP-based polymers as the initiators serve as the end-groups of the polymers (Scheme 1) [18,27,28].
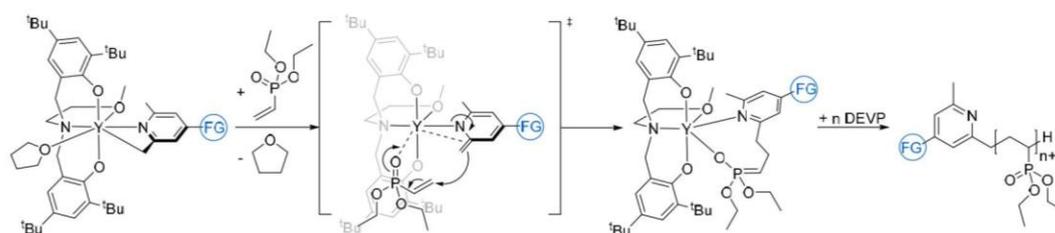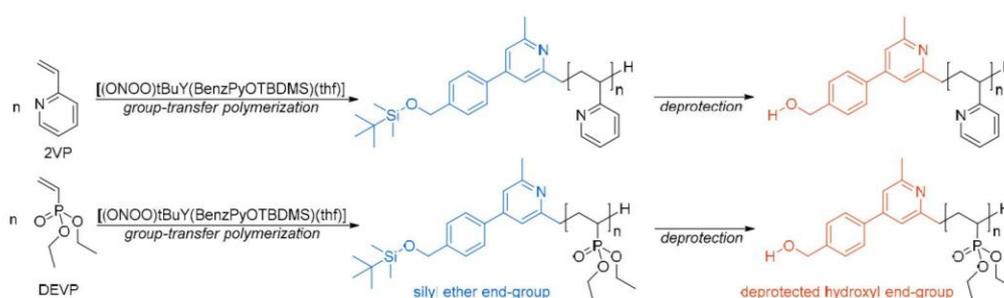

Scheme 1. Synthesis of an end-group functionalized poly(diethyl vinyl phosphonate) (PDEVP) via nucleophilic attack of an α-methylated pyridine initiator of a bis(phenolate)yttrium complex to the first monomer molecule during initiation [9,18,28].

The accessibility to phosphorus- and nitrogen-containing polymers in REM-GTP, especially, poly(diethyl vinyl phosphonate) (PDEVP) with its thermoresponsive behavior and poly(2-vinylpyridine) (P2VP) with its pH-dependent solubility, highlights the potential of this polymerization type to generate smart polymers. After developing capable catalysts using C–H bond activation or catalyst immobilization, differently constituted polymers from vinyl phosphonates and/or 2VP, e.g., block copolymers as drug carriers [29,33], polymer-metal complex conjugates [30],

polymer-biomolecule conjugates [31,32,41] or responsive polymer surfaces were synthesized as smart polymers so far [7,42].

Within this paper, a pathway towards hydroxy-functionalized P2VP and PDEVP is established, since commonly used initiators (e.g., alkyl initiators, cyclopentadienyl) led to solely hydrocarbon-containing end-groups. In this contribution, C–H bond activation is applied as a facile tool towards introduction of hydroxy-groups to Michael-type polymers. Since free hydroxyl groups cannot be introduced to rare earth metals directly due to their high acidity, protection group chemistry was utilized. The complex [(ONOO)^{tBu}Y(CH$_2$TMS)(thf)] was functionalized with 4-(((4'-(*tert*-butyl-dimethylsilyl)oxy)methyl)phenyl)-2,6-dimethylpyridine (BenzPyOTBDMS) in a C–H bond activation reaction to yield the desired catalyst ((ONOO)^{tBu}Y(BenzPyOTBDMS)(thf)). This catalyst gave access to P2VP and PDEVP with a silyl ether end-group, which was transformed into a hydroxyl end-group via a deprotection reaction (Scheme 2). Different deprotection reactions of the end-groups were carried out.


Scheme 2. Synthesis of P2VP (top) and PDEVP (bottom) with hydroxyl end-groups via REM-GTP using the functionalized yttrium catalyst [(ONOO)^{tBu}Y(BenzPyOTBDMS)(thf)] and subsequent deprotection.

The hydroxyl end-group was chosen as it could not only be used as a functional group for post-polymerization functionalization (e.g., coupling to biomolecules, fluorescent markers or dyes), but can also act as an anchoring point on surfaces, as a macroinitiator or chain transfer agent for subsequent copolymerization e.g., using immortal ring-opening polymerization [43] enabling the coupling of polyesters with Michael-type polymers. In addition, a commonly used strategy is the application of hydroxy-terminated polymers as precursors for macroinitiators for living-radical polymerizations (ATRP, SET-LRP) facilitating the coupling with non-polar vinyl monomers [44,45].

2. Results and Discussion

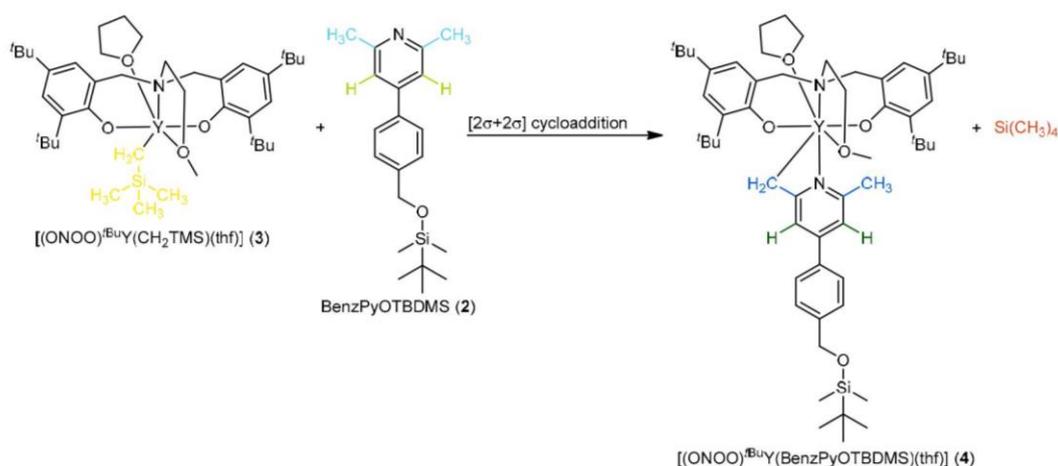### 2.1. Synthesis of the Functionalized Pyridine 2

By using purchased 2,6-dimethylpyridine as starting material, 4-chloro-2,6-dimethylpyridine was synthesized according to the literature [32]. Afterwards, Suzuki-coupling was used to react 4-chloro-2,6-dimethylpyridine with 4-hydroxymethyl benzyl boronic acid resulting in the coupling product **1**. To enable C–H bond activation with rare earth metals, acidic protons were masked by protection group chemistry. The hydroxy-group of **1** was converted to a *tert*-butyl-dimethylsilyl protection group (TBDMS) by reaction of **1** with TBDMS-Cl, yielding the protected α-methylated pyridine **2** (Scheme 3). The formation of a trimethyl silyl (TMS) ether instead was not applicable, because hydrogen chloride formed in this reaction cannot be fully quenched, resulting in a pyridinium salt. Using an alkaline work-up, this salt-formation is reversible when using the TBDMS-group instead of the TMS group due to its stability in an aqueous, basic medium [41].
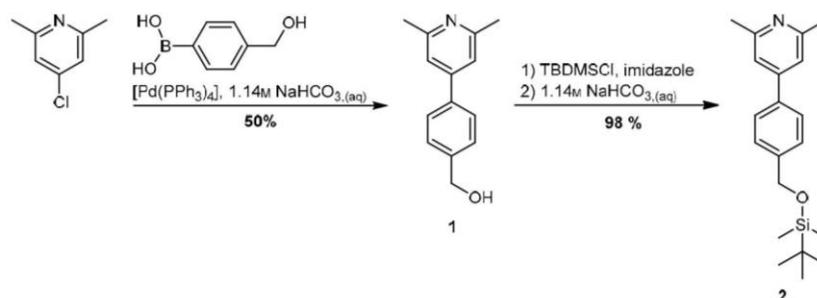
Scheme 3. Synthesis of silyl-protected pyridine **2** starting from 4-chloro-2,6-dimethylpyridine, Suzuki-coupling and subsequent protection.

2.2. C–H Bond Activation of 2 Using 2-Methoxyethylamino-Bis(Phenolate)Yttrium Complex 3

To reveal the general activity of **2** towards C–H bond activation using 2-methoxyethylamino-bis(phenolate)yttrium complex **3** [(ONOO)^{tBu}Y(CH$_2$TMS)(thf)], the reaction was first monitored in an ^{1}H-NMR kinetic experiment. **3** can undergo fast and selective C–H bond activation (Scheme 4) with a variety of different methylated pyridines via [2σ + 2σ] cycloaddition as previously reported [28,30,33].

Scheme 4. σ-Bond metathesis of silyl ether functionalized pyridine **2** and complex **3** to obtain catalyst [(ONOO)^{tBu}Y(BenzPyOTBDMS)(thf)] (**4**).

For the ^{1}H-NMR kinetic investigation on the C–H bond activation, complex **3** and the silyl-protected pyridine **2** were dissolved in deuterated benzene, the mixture was heated to 60 °C and an ^{1}H-NMR was performed at regular time intervals (Figure 1). As the reaction progresses, the signals of the trimethylsilyl group (δ = 0.49 ppm) and the CH$_2$-group (δ = −0.40 ppm) (Figure 1, yellow) of the CH$_2$TMS-initiator binding to the yttrium center decrease, and simultaneously, a new signal emerged at δ = 0.00 ppm, which corresponded to tetramethyl silane (Figure 1, orange). The signal of the methyl groups in α-position (δ = 2.51 ppm) (Figure 1, light blue) to the nitrogen atom of **2** decreased over time, while two new signals at δ = 2.22 ppm and δ = 2.67 ppm with an integral ratio of 3:2 were measured (Figure 1, dark blue). [2σ + 2σ]-cycloaddition of one of the methyl groups in α-position of the pyridine with the CH$_2$TMS group of **3** takes place, resulting in the successful attachment of **2** to the yttrium center. Furthermore, the signal of the two protons adjacent to the methyl groups of **2** (δ = 6.97 ppm, Figure 1, light green) split into two new signals with a ratio of 1:1 at δ = 6.25 ppm and δ = 7.07 ppm (Figure 1, dark green) over the course of the reaction due to an asymmetry caused by coordination to the yttrium-complex. Additionally, the ^{1}H-NMR kinetic indicates a selective C–H bond activation without the formation of side products.
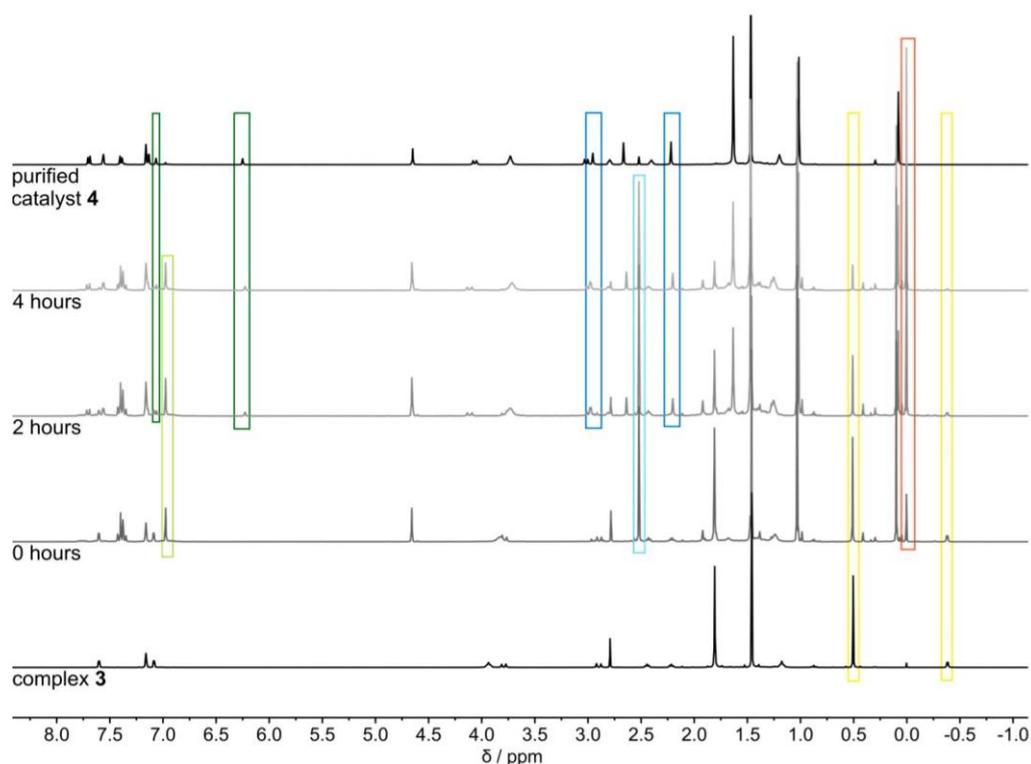
Figure 1. ^{1}H-NMR kinetic reaction of the σ-bond metathesis of complex **3** with the protected pyridine **2** to obtain silyl-protected catalyst **4** in benzene-d$_6$.

As the activation of compound **2** with yttrium-complex **3** on NMR scale was feasible, the catalyst synthesis was scaled up using toluene as the solvent and stirring of the mixture at 60 °C for 17 h to ensure full conversion. After purification by washing with pentane several times, catalyst **4** could be isolated in 72% yield. The complex was characterized by ^{1}H-/^{13}C-NMR spectroscopy (Figures S1 and S2) and elemental analysis. All methods indicated that despite the highly sterically demanding initiator, tetrahydrofuran is still present in catalyst **4**.

2.3. Investigation on Catalytic Activity of Catalyst **4**

Initially, the catalytic activity of catalyst **4** towards DEVP and 2VP polymerization was investigated. Therefore, the turnover frequency TOF [h^{-1}], initiator efficiency and normalized turnover frequency TOF* [h^{-1}] were determined (Table 1). For determination of the turnover frequency of catalyst **4** towards DEVP, conversions over time were measured via aliquots of a polymerization of DEVP in a catalyst-to-monomer ratio of 1/600 in toluene. Conversions were calculated from ^{31}P-NMR spectra (Figure 2, left) by integration of polymer (δ = 30–31 ppm) against monomer (δ = 15 ppm) signals. After plotting the conversion vs. time, the highest slope of this plot was used for calculating the turnover frequency. For the DEVP polymerization, the turnover frequency is 4320 h^{-1}. Regarding the incomplete initiation shown by an initiator efficiency below 100%, a normalized turnover frequency (TOF*) of 6350 h^{-1} was determined with regards to an initiator efficiency of 68%. Molar masses at the respective conversions were used to reveal the living character of the polymerizations. The living character of the polymerization is confirmed by a linear growth of the molecular weight with increasing conversion of the monomer and narrow polydispersities throughout the whole polymerization (Figure 2, right).

Table 1. Results from kinetic measurements of DEVP and 2VP polymerization with catalyst **4**.

Entry	M	[M]/[4] [a]	Conv. [b] (%)	$M_{n,calc}$ [c] (kg mol^{-1})	$M_{n,abs}$ [d] (kg mol^{-1})	Đ [d] (-)	I* [e] (%)	TOF (h^{-1})	TOF* [f] (h^{-1})
1	DEVP	600/1	86	83.1	139	1.29	68	4320	6350
2	2VP	400/1	99	40.8	55.7	1.02	67	500	750

[a] Monomer-to-catalyst ratio, $c_{Cat,0}$ = 2.3 mmol/mL, toluene, 25 °C; [b] Conversion calculated via aliquot method; ^{1}H-NMR (2VP) or ^{31}P-NMR (DEVP) spectra, [c] $M_{n,calc}$ from $M_{n,calc}$ = M × (([M]/[Cat]) × conversion) [d] Determined via SEC (P2VP: DMF+LiBr, 30 °C, dn/dc = 0.149 mL g^{-1} with triple detection SEC; PDEVP: THF:H_2O = 1:1, 40 °C, dn/dc = 0.0922 mL g^{-1}, SEC-MALS), polydispersity calculated from $M_{w,abs}/M_{n,abs}$ [e] Initiator efficiency I* at the highest slope in time-conversion plot via I* = $M_{n,calc}/M_{n,abs}$; [f] normalized TOF using I*; TOF* = TOF/I*.
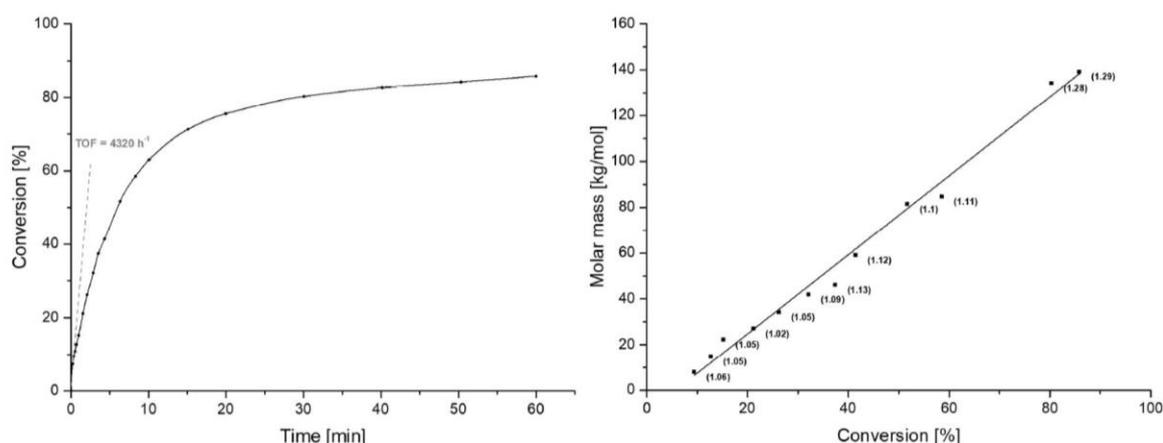
Figure 2. Time–conversion plot (left) and conversion–molar mass plot (right) of the DEVP polymerization with catalyst **4**.

The turnover frequency of catalyst **4** for 2VP polymerization was determined by performing a polymerization with a monomer-to-catalyst ratio of 400/1 in toluene at room temperature. Aliquots were taken from the reaction mixture at regular time intervals and conversions were calculated from ^{1}H-NMR via conversion = ($I_{Pol+Mon}$ (δ = 7.9–8.6 ppm) − I_{Mon} (δ = 5.4 ppm))/$I_{Pol+Mon}$ (δ = 7.9–8.6 ppm) (Figure 3, left). A turnover frequency of 500 h^{-1} and a normalized turn over frequency of 750 h^{-1} were calculated. For 2VP polymerization, the living character was confirmed with the conversion–molar mass plot (Figure 3, right).
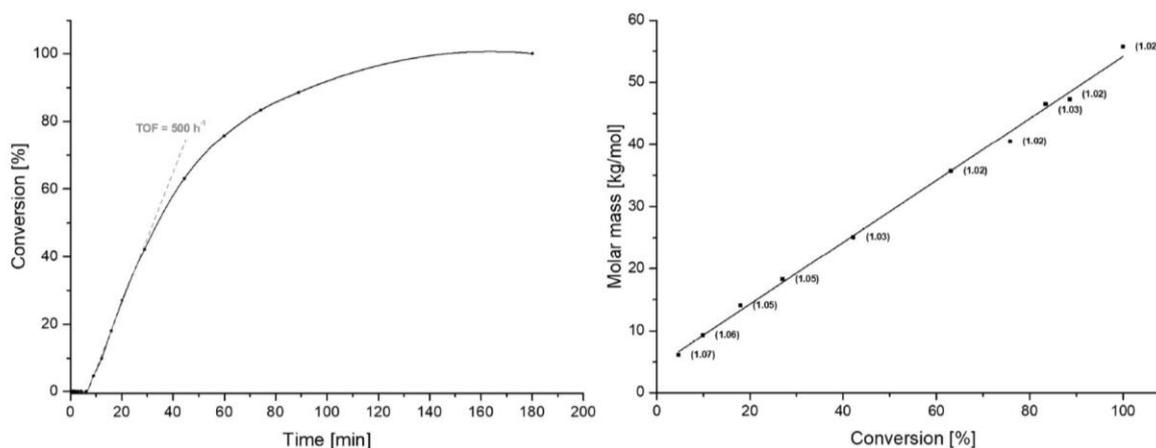
Figure 3. Time–conversion plot (left) and conversion–molar mass plot (right) of 2VP polymerization with catalyst **4** (Table 1, entry 2).

Because the initiator is not involved in the propagation step, the initiator has no influence on the catalyst activity, which is only determined by the metal center and the steric hinderance of the ligand. Catalyst **4** should therefore have a similar normalized turn over frequency as bis(phenolate)yttrium catalysts bearing the same ligand system such as complex **3** or a structure analogue bis(phenolate)yttrium complex such as [(ONOO)^{tBu}Y(*sym*-col)(thf)] (*sym*-col = 2,4,6-trimethylpyridine), which only differs in the initiator [9,28].

For DEVP, the polymerization proceeds without an initiation delay in the expected fashion, however, the turnover frequency of 4320 h^{-1} is about one magnitude higher than reported in the literature for complex **3**, indicating a different polymerization mechanism [19]. For 2VP, the normalized turnover frequency of 750 h^{-1} is in the same range as reported in the literature for complexes with the same ligand system [19,28,30], but in the time–conversion plot, an initiation delay of about 5 min was observed. This is in contradiction to the behavior of the other C–H bond activated catalysts reported in literature, which do not show initiation periods [28]. We suggest that catalyst **4** may not be present in the assumed monometallic state, but rather in a bimetallic state, since bimetallic complexes showed initiation periods in 2VP polymerization [9]. The dimerization might cause a detachment of the aminomethoxy handle from the metal center and the silyl ether group could be coordinating the yttrium instead. Due to a different chemical structure of the ligand after dissociation into a monomolecular species, the turnover frequency for DEVP could be higher than those reported [19]. As the coordination strength of 2VP is weaker than the one of DEVP [7,28], the dissociation period might be longer for 2VP resulting in an initiation delay. Despite this behavior, catalyst **4** polymerized DEVP and 2VP in a highly controlled way under mild conditions with very low polydispersities. In comparison, 2VP polymerization seems to be more controlled than DEVP polymerization, because the polydispersity of PDEVP increased over the course of the reaction, most likely due to undesired side reactions.

2.4. Polymerization Results

2.4.1. End-Group Analysis of PDEVP and P2VP Produced with Catalyst **4**

For obtaining highly defined, hydroxyl-terminated Michael-type polymers, a quantitative attachment of initiator **2** as an end-group is the main prerequisite. Therefore, a detailed end-group analysis of PDEVP and P2VP was performed via NMR spectroscopy, mass spectrometry and SEC to validate the attachment of initiator 2 to the polymer chains.

An ESI-MS of oligomeric DEVP (Figure 4) was recorded after reacting catalyst **4** with DEVP in a 1:6 ratio in toluene, quenching the polymerization with ethanol after 5 min and by immediate measurement of the reaction mixture in acetonitrile. The initiating pyridine **2** attached to the oligomer was observed in the ESI-MS spectrum by a mass shift of 327 m/z (mass of initiator **2** minus one proton) of the DEVP oligomers (m/z = ((M_{Ini} − H) + n × M_{DEVP} + H + H)$^+$, n = 2–5), while unreacted pyridine **2** (m/z = 328.5) and ligand (m/z = 512.9) were observed as well. Since the initiating groups were clearly visible in the ESI-MS, a nucleophilic transfer reaction of the initiator via a monomer insertion into an yttrium carbon bond during the initiation is evident, leading to the desired end-group (Scheme 1). Due to the exclusive presence of signals corresponding to nucleophilic transfer reaction, an initiation via deprotonation is excluded [15,19,30].
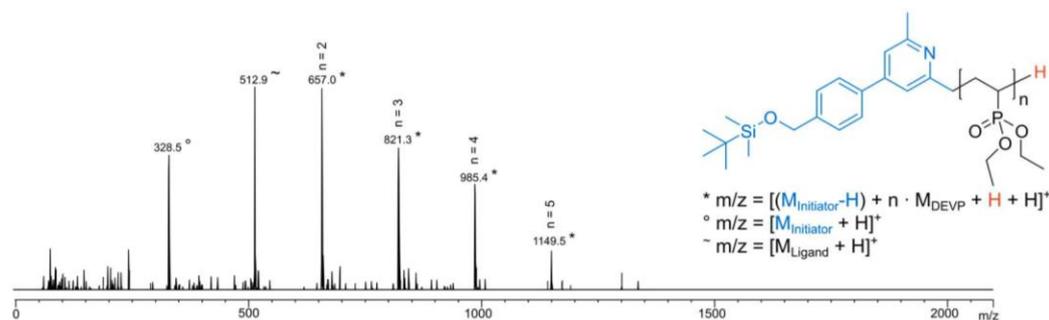
Figure 4. End-group analysis via ESI-MS of oligomeric DEVP (n = 2–5) produced with catalyst **4** ([4]/[DEVP] = 1:6, 25 °C, 10 min, toluene) in acetonitrile.

For P2VP, a MALDI-MS spectrum was recorded of purified 2VP oligomers from a reaction of catalyst **4** with 24 equivalents of 2VP in toluene (Figure 5). In this spectrum, a series of signals corresponding to m/z = $[(M_{Ini} - H) + n \times M_{2VP} + H + H]^+$ with n = 7–37 were observed, representing the 2VP oligomers functionalized with the protected initiator **2**. This not only underlines a covalently bonded initiator to the polymer chain, but also further substantiates the assumed initiation mechanism of a nucleophilic attack of the methyl pyridine **2** to the first monomer unit [19,30].
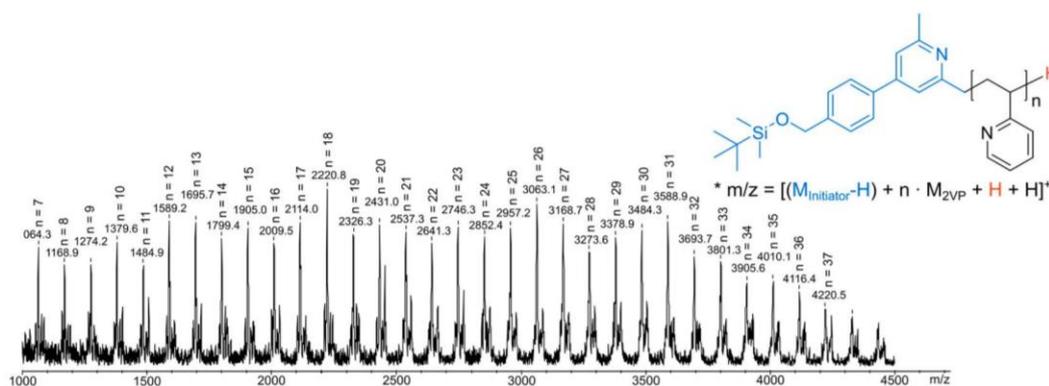

Figure 5. End-group analysis of oligomeric 2VP (n = 7–37) produced with catalyst **4** ([4]/[2VP] = 1:24, 25 °C, 3 h, toluene) via MALDI-MS in a dithranol matrix and sodium trifluoroacetate as matrix additive.

As free initiator or unfunctionalized polymers would disturb a successful post-polymerization functionalization, diffusion ordered spectroscopy (DOSY) was applied. To check whether the unbonded initiator is still present in the purified polymers, a DOSY of PDEVP with a number-average molecular weight of about 45 kg mol^{-1} was recorded (Figure S3). In this spectrum, the signals assigned to the methyl groups (δ = 0.10 ppm) and the *tert*-butyl group (δ = 0.94 ppm) of the silyl protection group of the initiator can be observed at the same diffusion coefficient as the polymer signals, indicating that no free initiator **2** is present in the PDEVP polymer. Analogously, a DOSY spectrum of purified P2VP with a number-average molecular weight of about 35 kg mol^{-1} (Figure S4) is recorded to check for the free initiator in the polymer sample. The silyl signals of the TBDMS-group at δ = 0.11 ppm (methyl silyl) and δ = 0.95 ppm (*tert*-butyl silyl) appear at the same diffusion coefficient as the polymer. Combining the results from mass spectrometry and DOSY-NMR measurement, a functionalization of the polymers with initiator **2,** without free initiator remaining in the polymer samples, can be confirmed.

2.4.2. Polymerization of DEVP and 2VP with Catalyst **4**

Catalyst **4** was further studied in homopolymerizations of DEVP and 2VP to evaluate the influence of the solvent and the monomer-to-catalyst ratio on the molar masses and polydispersities of the obtained polymers and the initiator efficiency of **4**, as these are critical parameters for obtaining highly defined

polymers with a high end-group integrity. As similar heteroaromatic bis(phenolate)yttrium catalysts are well-known to polymerize 2VP and DEVP rapidly at room temperature, higher temperatures were not used in this study [28]. In Table 2, the homopolymerization results of DEVP are summarized.

Table 2. Results of the REM-GTP of DEVP with catalyst **4**.

Entry	[DEVP]/[4] [a]	Solvent [b]	Conv. [c] (%)	$M_{n,calc}$ [d] (kg mol^{-1})	$M_{n,abs}$ [e] (kg mol^{-1})	$M_{n,NMR}$ [f] (kg mol^{-1})	$Đ$ [e] (-)	I [g] (%)
1	200/1	toluene	99	31.8	34.6	42.3	1.07	92
2	200/1	thf	99	32.8	38.0	48.3	1.13	86
3	200/1	dcm	44	14.8	25.0	34.0	1.29	59
4	100/1	toluene	99	15.8	16.6	22.5	1.04	95
5	400/1	toluene	96	61.8	104	122.3	1.33	58

[a] Monomer-to-catalyst ratio, n_{Cat} = 13.5 mmol; [b] Reaction time 60 min at 25 °C, 2 mL of solvent; [c] Calculated from ^{31}P-NMR spectrum of aliquots at the end of the reaction via ratio of signals of the polymer (δ = 30–31 ppm) and the monomer (δ = 15 ppm); [d] $M_{n,calc}$ from $M_{n,calc}$ = M ×(([M]/[Cat]) × conversion); [e] Determined via SEC-MALS in 50:50 THF/H$_2$O = 1:1, 40 °C, dn/dc = 0.0922 mL g^{-1}, polydispersity calculated from $M_{w,abs}/M_{n,abs}$, [f] calculated from ^{1}H-NMR $M_{n,NMR}$ = (I_{Et}/4)·M_{DEVP} + M_{Ini}; [g] I = $M_{n,calc}/M_{n,abs}$ at the end of the reaction.

As the kinetic measurement of DEVP with catalyst **4** has shown, the initiator efficiency was reduced when using a high monomer-to-catalyst ratio. Therefore, lower monomer-to-catalyst ratios of 100/1 to 400/1 were used in batch reactions, as these polymerizations proceeded too fast for kinetic measurements. Different solvents were chosen to study their influence of different solvents on the initiator efficiency and activity of **4**. For both toluene and tetrahydrofuran, full conversion was reached within the reaction time of 60 min. These polymers had a very narrow molecular weight distribution and initiator efficiencies were high (86–92%) when using a monomer-to-catalyst ratio of 100/1 or 200/1. The polymerization in dichloromethane proceeded much slower, with only 44% conversion after 60 min, broader polydispersity of the polymers and lower initiator efficiency of **4**. When the monomer-to-catalyst ratio for the polymerization in toluene as the most suiting solvent is increased, the polydispersity increased while the initiator efficiency decreased. The decreased initiator efficiency was most likely attributed to impurities, deactivating the catalyst species when the monomer loading was too high. Comparing the initiator efficiencies of catalyst **4** (86–92%) for 1/200 catalyst–monomer ratios to the initiator efficiency of the non-C–H bond activated complex **3** (36%) [28], I is significantly increased. This is due to a suppression of deprotonation as the initiation pathway for DEVP by C–H bond activation on such bis(phenolate)yttrium catalysts. The initiator efficiency of [(ONOO)^{tBu}Y(*sym*-col)(thf)] of I = 73% [28] is also slightly lower than those of catalyst **4** despite the high steric demand of **4**. The polydispersities of PDEVP prepared with catalyst **4** were in the same range as those reported in the literature ($Đ$ = 1.02–1.10) [18,28].

Additionally, the incorporation of the TBDMS-functionalized pyridine **2** in the polymers facilitates a reliable calculation of the number-average molecular weight from ^{1}H-NMR spectroscopy via the silyl ether end-group, and allowed a comparison with the number-average molecular weight obtained from absolute size-exclusion chromatography (SEC). For PDEVP, the molecular weights from ^{1}H-NMR spectra (Figure S5) were calculated by normalization of the silyl methyl signals (δ = 0.10 ppm, $I_{Me(TBDMS)}$ = 6) of the TBDMS-group to 6 and calculation of the molar mass with using the integral of the methylene unit in the ethyl groups on the PDEVP side chain (δ = 4.11 ppm, I_{Et}, 4 protons per repeating unit). The signals corresponding to the methyl groups of the PDEVP side chains and to the *tert*-butyl group in the initiator have shown to be unsuited due to overlapping with other signals in some polymer samples. The molecular weight was then calculated as $M_{n,NMR}$ = (I_{Et}/4) M_{DEVP} + M_{Ini}, assuming a quantitative incorporation of the initiator as proved by ESI-MS and DOSY measurements. The absolute molar mass is determined using SEC-MALS (Figure S7). The low deviation between the number-average molar masses obtained from SEC and calculated from ^{1}H-NMR (1%–24%) underline again a quantitative incorporation of the initiator. The deviations all show the same trend of overestimating the molecular weights from ^{1}H-NMR compared to those determined via SEC-MALS.

The polymerization behavior of catalyst **4** towards 2VP was investigated with regard to the same parameters as tested for DEVP polymerization (Table 3).

Table 3. Results of the REM-GTP of 2VP with catalyst **4**.

Entry	[2VP]/[4] [a]	Solvent [b]	Conv. [c] (%)	$M_{n,calc}$ [d] (kg mol^{-1})	$M_{n,abs}$ [e] (kg mol^{-1})	$M_{n,NMR}$ [f] (kg mol^{-1})	$Đ$ [e] (-)	I [g] (%)
1	200/1	toluene	99	22.1	25.0	27.2	1.04	89
2	200/1	thf	22	5.3	21.5	21.5	1.31	25
3	200/1	dcm	99	19.0	22.6	26.9	1.06	84
4	100/1	toluene	99	10.5	12.8	11.1	1.09	82
5	400/1	toluene	98	42.2	58.4	58.8	1.01	72

[a] Monomer-to-catalyst ratio, n_{Cat} = 13.5 mmol; [b] Reaction time 60 min at 25 °C, 2 mL of solvent; [c] Calculated from ^{1}H-NMR of aliquots via conversion = ($I_{Pol+Mon}$ (δ = 7.9–8.6 ppm) − I_{Mon} (δ = 5.4 ppm))/$I_{Pol+Mon}$ (δ = 7.9–8.6 ppm), [d] $M_{n,calc}$ from $M_{n,calc}$ = M × (([M]/[Cat]) × conversion) [e] Determined via SEC in DMF+LiBr (30 °C, dn/dc = 0.149 mL g^{-1}) with triple detection, polydispersity calculated from $M_{w,abs}/M_{n,abs}$; [f] calculated from ^{1}H-NMR as $M_{n,NMR} = I_{Ar} \times M_{2VP} + M_{Ini}$; [g] I = $M_{n,calc}/M_{n,abs}$ at the end of the reaction.

Toluene and dichloromethane were appropriate solvents for the synthesis of P2VP, as polymerizations in both solvents reached full conversion within 60 min while maintaining narrow polydispersities and high initiator efficiencies (I = 72–89%) at all monomer-to-catalyst ratios. The polymerization of 2VP in tetrahydrofuran proceeds much slower, with only 22% conversion after 60 min, while leading to broader polydispersities of the polymers. In addition, catalyst **4** only showed a low initiator efficiency (25%). This behavior is attributed to the weak coordination strength [6,28] of 2VP to the yttrium center and a competitive coordination of 2VP and tetrahydrofuran leads to an initiation delay, broadening of the polydispersity, lowering of the initiator efficiency and enhancing potential side reactions. Since DEVP is known to have a higher coordination strength to rare earth metal complexes, this phenomenon was not observed during DEVP polymerization. In general, tetrahydrofuran can be considered a well-suited solvent for REM-GTP as long as the coordination strength of the monomer to the metal center is stronger in comparison to the coordination strength of THF. Additionally, the tacticity of the P2VP was determined using ^{13}C-NMR according to the literature (Figure S9). As expected for this metal center and ligand, atactic P2VP was obtained, since the initiator did not influence the tacticity [9]. Comparing the initiator efficiencies of 72–89% of complex **4** to those reported in the literature (complex **3**: I = 99% [9,28]; [(ONOO)^{tBu}Y(*sym*-col)(thf)]: I = 42% [28]), the initiator efficiency of complex **4** is slightly decreased compared to **3** but is considerably higher than those reported for the C−H bonded analogue. This decrease in I of **4** compared to **3** for 2VP can be attributed to an electronic overload on the yttrium center, however, the initiator efficiency using the new initiator **2** is still increased compared to *sym*-collidine as initiator [30]. As for PDEVP, the polydispersities of P2VP synthesized with catalyst **4** matched with values reported in the literature [9,28,30].

Regarding the molecular weight calculation using ^{1}H-NMR spectroscopy, the calculation was performed using the integral of the protons in α-position of the nitrogen atom in the aromatic ring (δ = 8.0–8.6 ppm, I_{Ar}, one proton per repeating unit) (Figure S8), giving $M_{n,NMR} = I_{Ar} \times M_{2VP} + M_{Ini}$, which was compared to the absolute number-average molecular weight determined from SEC using triple detection (Figure S10). The signals of the *tert*-butyl group as well as other aromatic signals from P2VP have shown to be unsuited for calculation due to signal overlapping issues. Molecular weights determined via ^{1}H-NMR and SEC deviate only by 0–16% and are in quite good agreement, again indicating full end-group functionalization.

Overall, highly defined PDEVP and P2VP with tunable molecular weights and narrow polydispersities under mild conditions were synthesized using catalyst **4**. For different catalyst-monomer ratios in suiting solvents, a high end-group integrity was achieved. The combination of NMR analytics, mass spectroscopy, DOSY and SEC confirmed a quantitative end-group functionalization.

2.5. Deprotection of PDEVP and P2VP

To recover the free hydroxyl group from the silyl ether protected polymer, different deprotection strategies (A/B/C) were tested for PDEVP and P2VP (Scheme 5) [46–49]. ^{1}H-NMR spectra of the polymers were used to evaluate the degree of the silyl group removal upon deprotection. With regards to possible side reactions at the pendant groups or chain cleavage, SEC and NMR spectroscopy were used to check the structural integrity of the polymer after the deprotection reaction.

Scheme 5. Removal of the TBDMS protection group of PDEVP and P2VP using different reaction conditions (A/B/C).

As a first approach (A), deprotection using tetra-n-butyl ammonium fluoride (TBAF) as an anhydrous fluorine source in dry tetrahydrofuran was tested. An excess of 50 equiv. TBAF was used for the deprotection of PDEVP and P2VP. The reaction was stirred under ambient conditions overnight and purified with an aqueous work-up. While this reaction ensured a quantitative cleavage of the TBDMS ether for PDEVP with no side reactions or chain-breakage, it was not applicable for P2VP, because polymer deprotection was incomplete and side reactions were detected by ^{1}H-NMR spectroscopy. In a second approach, deprotection strategy B, an acid-based deprotection with HCl$_{(aq)}$ in ethanol under ambient conditions, was performed, which gave fully deprotected P2VP after a basic work-up. No alteration of the P2VP chain itself was verified using NMR spectroscopy and SEC (Figure S11 and S12). However, this reaction leads to the formation of side products for PDEVP, which were insoluble in dioxane, indicating side-reactions such as saponification to the free phosphonic acid or crosslinking between polymer chains. To obtain a method suitable for both polymers, and able to also deprotect block copolymers consisting of both subunits, strategy C was tested. This method involved the treatment of the polymers with glacial acetic acid in a tetrahydrofuran-water mixture under ambient conditions. Both polymer types, PDEVP (Figures S13 and S14) and P2VP, were deprotected completely within 24 h without the occurrence of side reactions or polymer degradation. Using this reaction, hydroxyl-terminated PDEVP and P2VP were synthesized. All polymers were analyzed using ^{1}H-NMR and SEC (Table 4).

Table 4. Results from SEC before and after deprotection of PDEVP and P2VP with the different reactions A/B/C.

Entry	Polymer	Deprotection Procedure	Before Deprotection		After Deprotection	
			$M_{n,abs}$ ^{a} (kg mol^{-1})	$Đ$ ^{a} (-)	$M_{n,abs}$ ^{a} (kg mol^{-1})	$Đ$ ^{a} (-)
1	PDEVP	A	43.4	1.11	40.6	1.18
2	P2VP	B	25.2	1.05	29.0	1.05
3	PDEVP	C	38.0	1.13	34.3	1.11
4	P2VP	C	25.8	1.09	28.7	1.10

^{a} Determined via SEC-MALS (PDEVP) or SEC using triple detection (P2VP).

3. Materials and Methods

3.1. Materials

All air and moisture sensitive compounds were prepared using Standard Schlenk techniques in dried glass flasks, using argon as inert gas or handled in an argon-filled glove box. Chemicals were purchased from Sigma-Aldrich (St. Louis, MI, USA), ABCR (Karlsruhe, Baden-Wuerttemberg,

Germany) or TCI Chemicals (Tokyo, Japan) and were used without further purification unless stated otherwise. Diethyl vinyl phosphonate and 2-vinylpyridine were stirred at room temperature over CaH_2 and distilled prior to use. Dry solvents were obtained from a MBraun MB-SPS-800 (Garching-Hochbrück, Bavaria, Germany) solvent purification system by drying over activated alumina, and were stored on 3 Å molecular sieve. DEVP, the $(ONOO)^{tBu}$-ligand, 2,6-dimethylpyridine-*N*-oxide, 4-chloro-2,6-di-methylpyridine, $LiCH_2TMS$, $Y(CH_2TMS)(thf)_2$ and $[(ONOO)^{tBu}Y(CH_2TMS)(thf)]$ were synthesized according to the literature [19,32,50–52].

3.2. Instrumentalization

Nuclear magnetic resonance spectroscopy (NMR) was performed at room temperature on either a Bruker Ascend spectrometer (Billerica, MA, USA) or a Bruker AV500C cryo-NMR spectrometer (Billerica, MA, USA) as indicated (^{1}H-NMR: 400 MHz/500 MHz; ^{13}C-NMR: 125 MHz; ^{29}Si-NMR: 80 MHz; ^{31}P-NMR: 162 MHz). All ^{1}H-NMR spectra were referenced to the residual proton signal of the deuterated solvent, ^{13}C-NMR spectra were referenced to the carbon signal of the deuterated solvent, background correction and phase correction were performed using MestreNova. Diffusion-ordered spectroscopy (DOSY) was measured on a Bruker AV-HD400 (Billerica, MA, USA) with 16 scans at room temperature and was transformed using the Bayesian method with a resolution factor of 5 using MestreNova. Signal multiplicities were abbreviated as following: s—singlet, d—duplet, t—triplet, m—multiplet.

Average absolute molecular weights and polydispersities of the polymers were determined via size-exclusion chromatography (SEC) with a sample concentration of 2 mg mL^{-1}. Measurements of PDEVP were performed using size-exclusion chromatography coupled with multi-angle light scattering (SEC-MALS), with THF:H_2O = 1:1 (with 9 g/L *tetra*-butyl-ammonium bromide and 272 mg L^{-1} 2,6-di-*tert*-butyl-4-methylphenol) as eluent at 40 °C, equipped with two Agilent PolarGel M columns (Santa Clara, CA, USA). For detection, a Wyatt Dawn Heleos II MALS light scattering unit (Santa Barbara, CA, USA) and a Wyatt Optilab rEX 536 RI unit (Santa Barbara, CA, USA) were used, the absolute molecular weight was determined using an experimentally measured dn/dc = 0.0922 mL g^{-1}. Measurements of P2VP were performed on an Agilent PL-GPC 50 (Santa Clara, CA, USA) with an integrated RI unit, two light scattering detectors (15° and 90°) and a differential pressure viscosimeter with two Agilent PolarGel M columns. As eluent *N*,*N*-dimethylformamide (with 2.096 g/L lithium bromide added) at 30 °C was used, absolute molecular weights were determined using dn/dc = 0.149 mL g^{-1} from the literature [30].

Electron-spray ionization mass spectrometry (ESI-MS) measurements of DEVP oligomer samples (catalyst-to-monomer ratio = 1:6, reaction time 5 min in toluene, quenched with ethanol) were performed on a Varian 500-MS (Palo Alto, CA, USA) with MeCN as the solvent in positive ionization mode (70 eV). Recorded mass spectra were analyzed using MS Data Review.

Matrix-assisted laser desorption ionization mass spectrometry (MALDI-MS) was performed on a Bruker Daltonics ultraflex TOF/TOF (Billerica, MA, USA). Oligomer samples of 2VP with a concentration of 2 mg mL^{-1} in THF were prepared and 3 μL of this solution was mixed with 1 μL of matrix solution (saturated dithranol in H_2O (+ 0.1 vol % TFA):MeCN = 2:1) and 1 μL of 5 mg mL^{-1} sodium trifluoroacetate in H_2O(+ 0.1 vol % TFA):MeCN = 2:1. The mass spectra were recorded in linear positive mode without deflection and gating. Spectra interpretation was performed using Bruker FlexAnalysis.

Lyophilization was performed on a VaCo 5-II-D from Zirbus technology GmbH (Bad Grund, Lower Saxony, Germany), with a pressure of 2 mbar and a condenser temperature of −90 °C. PDEVP was dissolved in either water or 1,4-dioxane, P2VP is dissolved in either benzene or 1,4-dioxane prior to freezing in liquid nitrogen.

Elemental analysis was performed by the Laboratory for Microanalytics at the Institute of Inorganic Chemistry at the Technical University of Munich, Department of Chemistry, Catalysis Research Center.

*3.3. Synthesis of Catalyst **4** [(ONOO)^{tBu}Y(BenzPyOTBDMS)(thf)]*

In total, 2.77 g (3.33 mmol, 1.0 equiv.) of complex **3** (ONOO^{tBu})Y(CH$_2$TMS)(thf) were dissolved in 30 mL dry toluene and 1.09 g (3.66 mmol, 1.1 equiv.) of the protected pyridine **2** dissolved in 6 mL dry toluene were added. The reaction mixture was stirred at 60 °C for 17 h before the solvent was removed in vacuo leaving a red, oily solid. Upon addition of 2 × 20 mL dry pentane and subsequent removal of the solvent in vacuo, a yellow precipitate was formed, which is subsequently washed with 2 × 25 mL dry pentane before drying under vacuum. Catalyst **4** [(ONOO)^{tBu}Y(BenzPyOTBDMS)(thf)] is obtained as yellow solid (2.57 g, 2.63 mmol, 72%).

^{1}H-NMR (400 MHz, C$_6$D$_6$, 300 K): δ (ppm) = 0.08 (s, 6H, Si(CH$_3$)$_2$), 1.02 (s, 9H, SiC(CH$_3$)$_3$), 1.16–1.22 (m, 4H, CH$_{2,thf}$), 1.47 (s, 18H, ^{t}Bu$_{ligand}$), 1.63 (s, 18H, ^{t}Bu$_{ligand}$), 2.21 (s, 3H, CH$_{3,pyridine}$), 2.41 (t, $^3J_{H,H}$ = 4.8 Hz, 2H, NCH_2CH$_2$OMe), 2.66 (s, 3H, OCH$_3$), 2.80 (t, $^3J_{H,H}$ = 4.8 Hz, 2H, NCH$_2$CH_2OMe), 2.96 (s, 2H, YCH$_{2,pyridine}$), 3.01 (d, $^2J_{H,H}$ = 12.5 Hz, 2H, ArCH$_{2,ligand}$), 3.73–3.77 (m, 4H, OCH$_{2,thf}$), 4.07 (d, $^2J_{H,H}$ = 12.5 Hz, 2H, ArCH$_{2,ligand}$), 4.65 (s, 2H, CH$_2$OSiR$_3$), 6.24 (s, 1H, H$_{Ar,pyridine}$), 7.06 (s, 1H, H$_{Ar,pyridine}$), 7.13 (d, $^4J_{H,H}$ = 2.6 Hz, 2H, H$_{Ar,ligand}$), 7.39 (d, $^3J_{H,H}$ = 8.0 Hz, 2H, H$_{Ar,benzyl}$), 7.56 (d, $^4J_{H,H}$ = 2.6 Hz, 2H, H$_{Ar,ligand}$), 7.70 (d, $^3J_{H,H}$ = 8.2 Hz, 2H, H$_{Ar,benzyl}$).

^{13}C-NMR (125 MHz, C$_6$D$_6$, 300 K): δ (ppm) = 5.1, 18.6, 23.7, 25.2, 26.2, 30.3, 32.3, 34.3, 49.5, 54.5, 59.7, 65.1, 65.2, 70.9, 72.9, 105.8, 113.9, 124.2, 124.5, 125.8, 126.8, 127.0, 136.6, 136.8, 139.6, 141.7, 147.3, 156.8, 161.7 (d, $^1J_{Y,C}$ = 2.5 Hz), 167.4.

^{29}Si-NMR (80 MHz, C$_6$D$_6$, 300 K): δ (ppm) = 19.7.

EA: Calc: C 68.65, H 8.79, N 2.81, O 8.02, Si 2.82, Y 8.91. Found: C 68.53, H 9.12, N 2.81.

For the ^{1}H-NMR kinetic experiment, 10 mg (0.013 mmol, 1 equiv.) of complex **3** were dissolved in 0.4 mL deuterated benzene and 6.88 mg (0.021 mmol, 1.6 equiv.) protected pyridine **2** were dissolved in 0.1 mL deuterated benzene. Both solutions were mixed inside a Young NMR tube and the reaction mixture was heated to 60 °C. Every 30 min, a proton-NMR spectrum was measured to evaluate the reaction progress.

3.4. Polymerization Procedure

For the polymerization of DEVP or 2VP, 13.5 mg (13.5 µmol, 1.0 equiv.) of catalyst **4** were weighed into a dried screw cap vial and dissolved in 2 mL dry solvent (toluene, thf or dichloromethane). Under vigorous stirring the calculated amount of monomer (50 equiv., 100 equiv., 200 equiv., 400 equiv. or 600 equiv.) was added in one portion and the reaction was stirred at 25 °C for 60 min. An aliquot of 0.1 mL of the reaction mixture was taken and quenched in wet CDCl$_3$ (PDEVP) or MeOD (P2VP) before stopping the reaction with 0.5 mL methanol. The polymers were precipitated in 50 mL pentane, centrifuged, and the solution was decanted off and the residue was freeze-dried. All polymer samples were analyzed using NMR and SEC.

3.5. Activity Measurements

For measuring the activity of catalyst **4** towards 2VP and DEVP polymerization, 22.5 mg (22.5 µmol, 1.0 equiv.) of **4** were weighed into a screw cap vial and were dissolved in 10 mL dry toluene. Under vigorous stirring, the monomer (2VP: 400 equiv., DEVP: 600 equiv.) was added in one portion. At certain time intervals, 0.2 mL aliquots of the reaction mixture were taken out and quenched by addition of 0.4 mL wet methanol-d$_4$. The conversion of 2VP was determined from ^{1}H-NMR, while for DEVP, conversion was calculated from ^{31}P-NMR. The aliquot NMRs were precipitated in 12 mL pentane, decanted off and dried in vacuo. The number-average molecular weight and polydispersity were determined using SEC (P2VP) or SEC-MALS (PDEVP). The turnover frequency was determined from the highest slope in the time–conversion plot and the normalized turnover frequency from an average initiator efficiency of these points. The living-type character of the polymerizations are determined from a linear increase of molecular weight in a conversion–molar mass plot.

3.6. Polymer Deprotection

(**A**) TBAF-deprotection: 150 mg PDEVP were dissolved in 10 mL dry tetrahydrofuran and 0.1 mmol of a 1 M TBAF solution in tetrahydrofuran was added. The reaction mixture was stirred for 24 h under ambient conditions. The solvent was removed in vacuo and the residue was subjected to dialysis in water (Spectra/Por 1 dialysis tubing, regenerated cellulose, molar-mass cut-off 5 kg mol^{-1}, 2 L water, five-fold solvent exchange). The residual polymer solution was dried and freeze-dried twice from high purity water.

(**B**) HCl-deprotection: 170 mg P2VP was dissolved in 6 mL ethanol and 0.6 mL concentrated HCl$_{(aq)}$ were added. The reaction mixture was stirred for 24 h under ambient conditions and afterwards the solvent was removed in vacuo. The residue was dissolved in dichloromethane and an excess of concentrated sodium hydrogen carbonate solution was added to deprotonate the pyridine side chain protonation of the P2VP polymer. After phase separation, the aqueous phase was extracted with dichloromethane twice. The organic phases were combined, and the solvent was removed in vacuo prior to freeze-drying from 1,4-dioxane.

(**C**) AcOH-deprotection: The polymer (140 mg P2VP/250 mg PDEVP) was dissolved in 5 mL of a mixture of glacial acetic acid-tetrahydrofuran-water in a ratio of 3:1:1, and the mixture was stirred for 24 h. For P2VP, the work-up from reaction (B) was applied, while PDEVP was dissolved in dichloromethane after solvent removal and purified via precipitation in excess of pentane and followed by freeze-drying from 1,4-dioxane.

4. Conclusions

A novel silicon protected hydroxy-pyridine initiator was synthesized and used for functionalization of [(ONOO^{tBu})Y(CH$_2$TMS)(thf)] via C–H bond activation to obtain a novel [(ONOO^{tBu})Y(X)(thf)] (X = 4-(4'-(((*tert*-butyldimethylsilyl)oxy)methyl)phenyl)-2,6-di-methylpyri-dine) complex in high purity and yield. Activity measurements of this complex showed a high initiator efficiency in the REM-GTP of DEVP and 2VP and the living character of the polymerization was proven. A series of well-defined polymers with different molecular weights and small polydispersities were obtained. End-group characterization via mass spectrometry and 2D-NMR studies revealed a covalent attachment of the silicon protected initiator to the obtained polymers. A good agreement between the absolute number average molecular weights obtained via SEC and those calculated via NMR-spectra using the silyl end-group also proof a quantitative attachment. Different deprotection routes for the silyl-protection group were evaluated for all polymers and with the use of glacial acetic acid full deprotection was facilitated obtaining hydroxyl-terminated PDEVP and P2VP while maintaining full structural integrity of the polymers.

deprotected blue); Figure S13: Representative comparison of ^{1}H-NMRs of protected (bottom) and unprotected (top) PDEVP (Table 4, entry 1) with close-up of the silyl region (TBDMS signals marked blue); Figure S14: Overlay of SEC-MALS RI traces of PDEVP (Table 4, entry 1) protected and deprotected (protected black, deprotected blue, Synthesis procedures of **1** and **2**.

Conflicts of Interest: The authors declare no conflict of interest.

References

1. Webster, O.W.; Hertler, W.R.; Sogah, D.Y.; Farnham, W.B.; RajanBabu, T.V. Group-transfer polymerization. 1. A new concept for addition polymerization with organosilicon initiators. *J. Am. Chem. Soc.* **1983**, *105*, 5706–5708. [CrossRef]
2. Yasuda, H.; Yamamoto, H.; Yokota, K.; Miyake, S.; Nakamura, A. Synthesis of monodispersed high molecular weight polymers and isolation of an organolanthanide(III) intermediate coordinated by a penultimate poly(MMA) unit. *J. Am. Chem. Soc.* **1992**, *114*, 4908–4910. [CrossRef]
3. Yasuda, H.; Ihara, E. Rare earth metal initiated polymerizations of polar and nonpolar monomers to give high molecular weight polymers with extremely narrow molecular weight distribution. *Macromol. Chem. Phys.* **1995**, *196*, 2417–2441. [CrossRef]
4. Yasuda, H.; Ihara, E.; Nitto, Y.; Kakehi, T.; Morimoto, M.; Nodono, M. Organo Rare Earth Metal Initiated Living Polymerizations of Polar and Nonpolar Monomers. In *Functional Polymers*; Patil, A.O., Schulz, D.N., Novak, B.M., Eds.; American Chemical Society: Washington, DC, USA, 1998; Volume 704, pp. 149–162.
5. Chen, E.Y.-X. Coordination polymerization of polar vinyl monomers by single-site metal catalysts. *Chem. Rev.* **2009**, *109*, 5157–5214. [CrossRef]
6. Salzinger, S.; Rieger, B. Rare Earth metal-mediated group transfer polymerization of vinylphosphonates. *Macromol. Rapid Commun.* **2012**, *33*, 1327–1345. [CrossRef] [PubMed]
7. Adams, F.; Pahl, P.; Rieger, B. Metal-Catalyzed Group-Transfer Polymerization: A Versatile Tool for Tailor-Made Functional (Co)Polymers. *Chem. Eur. J.* **2018**, *24*, 509–518. [CrossRef] [PubMed]
8. Collins, S.; Ward, D.G. Group-transfer polymerization using cationic zirconocene compounds. *J. Am. Chem. Soc.* **1992**, *114*, 5460–5462. [CrossRef]
9. Altenbuchner, P.T.; Adams, F.; Kronast, A.; Herdtweck, E.; Pöthig, A.; Rieger, B. Stereospecific catalytic precision polymerization of 2-vinylpyridine via rare earth metal-mediated group transfer polymerization with 2-methoxyethylamino-bis(phenolate)-yttrium complexes. *Polym. Chem.* **2015**, *6*, 6796–6801. [CrossRef]
10. Xu, T.-Q.; Yang, G.-W.; Lu, X.-B. Highly Isotactic and High-Molecular-Weight Poly(2-vinylpyridine) by Coordination Polymerization with Yttrium Bis(phenolate) Ether Catalysts. *ACS Catal.* **2016**, *6*, 4907–4913. [CrossRef]
11. Fuchise, K.; Chen, Y.; Satoh, T.; Kakuchi, T. Recent progress in organocatalytic group transfer polymerization. *Polym. Chem.* **2013**, *4*, 4278. [CrossRef]
12. Knaus, M.G.M.; Giuman, M.M.; Pöthig, A.; Rieger, B. End of Frustration: Catalytic Precision Polymerization with Highly Interacting Lewis Pairs. *J. Am. Chem. Soc.* **2016**, *138*, 7776–7781. [CrossRef]
13. Zhang, Y.; Miyake, G.M.; Chen, E.Y.-X. Alane-based classical and frustrated Lewis pairs in polymer synthesis: Rapid polymerization of MMA and naturally renewable methylene butyrolactones into high-molecular-weight polymers. *Angew. Chem. Int. Ed.* **2010**, *49*, 10158–10162. [CrossRef]

14. Salzinger, S.; Seemann, U.B.; Plikhta, A.; Rieger, B. Poly(vinylphosphonate)s Synthesized by Trivalent Cyclopentadienyl Lanthanide-Induced Group Transfer Polymerization. *Macromolecules* **2011**, *44*, 5920–5927. [CrossRef]

15. Soller, B.S.; Salzinger, S.; Rieger, B. Rare Earth Metal-Mediated Precision Polymerization of Vinylphosphonates and Conjugated Nitrogen-Containing Vinyl Monomers. *Chem. Rev.* **2016**, *116*, 1993–2022. [CrossRef]

16. Chen, X.; Caporaso, L.; Cavallo, L.; Chen, E.Y.-X. Stereoselectivity in metallocene-catalyzed coordination polymerization of renewable methylene butyrolactones: From stereo-random to stereo-perfect polymers. *J. Am. Chem. Soc.* **2012**, *134*, 7278–7281. [CrossRef]

17. Salzinger, S.; Soller, B.S.; Plikhta, A.; Seemann, U.B.; Herdtweck, E.; Rieger, B. Mechanistic studies on initiation and propagation of rare earth metal-mediated group-transfer polymerization of vinylphosphonates. *J. Am. Chem. Soc.* **2013**, *35*, 13030–13040. [CrossRef]

18. Soller, B.S.; Salzinger, S.; Jandl, C.; Pöthig, A.; Rieger, B. C–H Bond Activation by σ-Bond Metathesis as a Versatile Route toward Highly Efficient Initiators for the Catalytic Precision Polymerization of Polar Monomers. *Organometallics* **2014**, *34*, 2703–2706. [CrossRef]

19. Altenbuchner, P.T.; Soller, B.S.; Kissling, S.; Bachmann, T.; Kronast, A.; Vagin, S.I.; Rieger, B. Versatile 2-Methoxyethylaminobis(phenolate)yttrium Catalysts: Catalytic Precision Polymerization of Polar Monomers via Rare Earth Metal-Mediated Group Transfer Polymerization. *Macromolecules* **2014**, *47*, 7742–7749. [CrossRef]

20. Mariott, W.R.; Chen, E.Y.-X. Stereospecific, Coordination Polymerization of Acrylamides by Chiral ansa -Metallocenium Alkyl and Ester Enolate Cations. *Macromolecules* **2004**, *37*, 4741–4743. [CrossRef]

21. Rodriguez-Delgado, A.; Mariott, W.R.; Chen, E.Y.-X. Living and Syndioselective Polymerization of Methacrylates by Constrained Geometry Titanium Alkyl and Enolate Complexes. *Macromolecules* **2004**, *37*, 3092–3100. [CrossRef]

22. Weger, M.; Grötsch, R.K.; Knaus, M.G.; Giuman, M.M.; Mayer, D.C.; Altmann, P.J.; Mossou, E.; Dittrich, B.; Pöthig, A.; Rieger, B. Non-Innocent Methylene Linker in Bridged Lewis Pair Initiators. *Angew. Chem. Int. Ed.* **2019**, *58*, 9797–9801. [CrossRef] [PubMed]

23. Weger, M.; Giuman, M.M.; Knaus, M.G.; Ackermann, M.; Drees, M.; Hornung, J.; Altmann, P.J.; Fischer, R.A.; Rieger, B. Single-Site, Organometallic Aluminum Catalysts for the Precise Group Transfer Polymerization of Michael-Type Monomers. *Chem. Eur. J.* **2018**, *24*, 14950–14957. [CrossRef] [PubMed]

24. Weger, M.; Pahl, P.; Schmidt, F.; Soller, B.S.; Altmann, P.J.; Pöthig, A.; Gemmecker, G.; Eisenreich, W.; Rieger, B. Isospecific Group-Transfer Polymerization of Diethyl Vinylphosphonate and Multidimensional NMR Analysis of the Polymer Microstructure. *Macromolecules* **2019**, *52*, 7073–7080. [CrossRef]

25. Zhang, N.; Salzinger, S.; Soller, B.S.; Rieger, B. Rare earth metal-mediated group-transfer polymerization: From defined polymer microstructures to high-precision nano-scaled objects. *J. Am. Chem. Soc.* **2013**, *135*, 8810–8813. [CrossRef]

26. Miyake, G.M.; Chen, E.Y.-X. Metallocene-Mediated Asymmetric Coordination Polymerization of Polar Vinyl Monomers to Optically Active, Stereoregular Polymers. *Macromolecules* **2008**, *41*, 3405–3416. [CrossRef]

27. Kaneko, H.; Nagae, H.; Tsurugi, H.; Mashima, K. End-functionalized polymerization of 2-vinylpyridine through initial C–H bond activation of N-heteroaromatics and internal alkynes by yttrium ene-diamido complexes. *J. Am. Chem. Soc.* **2011**, *133*, 19626–19629. [CrossRef]

28. Adams, F.; Machat, M.R.; Altenbuchner, P.T.; Ehrmaier, J.; Pöthig, A.; Karsili, T.N.V.; Rieger, B. Toolbox of Nonmetallocene Lanthanides: Multifunctional Catalysts in Group-Transfer Polymerization. *Inorg. Chem.* **2017**, *56*, 9754–9764. [CrossRef]

29. Adams, F.; Altenbuchner, P.T.; Werz, P.D.L.; Rieger, B. Multiresponsive micellar block copolymers from 2-vinylpyridine and dialkylvinylphosphonates with a tunable lower critical solution temperature. *RSC Adv.* **2016**, *6*, 78750–78754. [CrossRef]

30. Adams, F.; Pschenitza, M.; Rieger, B. Yttrium-Catalyzed Synthesis of Bipyridine-Functionalized AB-Block Copolymers: Micellar Support for Photocatalytic Active Rhenium-Complexes. *ChemCatChem* **2018**, *10*, 4309–4316. [CrossRef]

31. Schwarzenböck, C.; Schaffer, A.; Nößner, E.; Nelson, P.J.; Huss, R.; Rieger, B. Fluorescent Polyvinylphosphonate Bioconjugates for Selective Cellular Delivery. *Chem. Eur. J.* **2018**, *24*, 2584–2587. [CrossRef]

32. Schwarzenböck, C.; Schaffer, A.; Pahl, P.; Nelson, P.J.; Huss, R.; Rieger, B. Precise synthesis of thermoresponsive polyvinylphosphonate-biomolecule conjugates via thiol–ene click chemistry. *Polym. Chem.* **2018**, *9*, 284–290. [CrossRef]

33. Altenbuchner, P.T.; Werz, P.D.L.; Schöppner, P.; Adams, F.; Kronast, A.; Schwarzenböck, C.; Pöthig, A.; Jandl, C.; Haslbeck, M.; Rieger, B. Next Generation Multiresponsive Nanocarriers for Targeted Drug Delivery to Cancer Cells. *Chem. Eur. J.* **2016**, *22*, 14576–14584. [CrossRef] [PubMed]

34. Pahl, P.; Schwarzenböck, C.; Herz, F.A.D.; Soller, B.S.; Jandl, C.; Rieger, B. Core-First Synthesis of Three-Armed Star-Shaped Polymers by Rare Earth Metal-Mediated Group Transfer Polymerization. *Macromolecules* **2017**, *50*, 6569–6576. [CrossRef]

35. Arndtsen, B.A.; Bergman, R.G.; Mobley, T.A.; Peterson, T.H. Selective Intermolecular Carbon-Hydrogen Bond Activation by Synthetic Metal Complexes in Homogeneous Solution. *Acc. Chem. Res.* **2002**, *28*, 154–162. [CrossRef]

36. Labinger, J.A.; Bercaw, J.E. Understanding and exploiting C–H bond activation. *Nature* **2002**, *417*, 507–514. [CrossRef]

37. Goldberg, K.I.; Goldman, A.S. (Eds.) *Activation and Functionalization of C—H Bonds*; American Chemical Society: Washington, DC, USA, 2004.

38. Adams, F.; Rieger, B. From Michael-Type Systems to Biobased Lactones: Designing Novel Polymer Microstructures with Modified Bis(phenolate)lanthanides. Ph.D. Thesis, Technical University Munich, Munich, Germany, 2019. Available online: http://nbn-resolving.de/urn/resolver.pl?urn:nbn:de:bvb:91-diss-20190123-1464556-1-9 (accessed on 1 April 2020).

39. Watson, P.L. Facile C–H activation by lutetium–methyl and lutetium–hydride complexes. *J. Chem. Soc. Chem. Commun.* **1983**, 276–277. [CrossRef]

40. Watson, P.L. Methane exchange reactions of lanthanide and early-transition-metal methyl complexes. *J. Am. Chem. Soc.* **1983**, *105*, 6491–6493. [CrossRef]

41. Schaffer, A.; Kränzlein, M.; Rieger, B. Synthesis and Application of Functional Group-Bearing Pyridyl-based Initiators to Rare-Earth Metal-Mediated Group-Transfer Polymerization. *Macromolecules.* under review.

42. Zhang, N.; Salzinger, S.; Deubel, F.; Jordan, R.; Rieger, B. Surface-initiated group transfer polymerization mediated by rare earth metal catalysts. *J. Am. Chem. Soc.* **2012**, *134*, 7333–7336. [CrossRef]

43. Ajellal, N.; Carpentier, J.-F.; Guillaume, C.; Guillaume, S.M.; Helou, M.; Poirier, V.; Sarazin, Y.; Trifonov, A.A. Bridging the gap in catalysis via multidisciplinary approaches. *Dalton Trans.* **2010**, *39*, 8354.

44. Anastasaki, A.; Nikolaou, V.; Nurumbetov, G.; Wilson, P.; Kempe, K.; Quinn, J.F.; Davis, T.P.; Whittaker, M.R.; Haddleton, D.M. Cu(0)-Mediated Living Radical Polymerization: A Versatile Tool for Materials Synthesis. *Chem. Rev.* **2016**, *116*, 835–877. [CrossRef]

45. Matyjaszewski, K. Advanced Materials by Atom Transfer Radical Polymerization. *Adv. Mater.* **2018**, *30*, e1706441. [CrossRef] [PubMed]

46. Bonnet, M.; Hong, C.R.; Wong, W.W.; Liew, L.P.; Shome, A.; Wang, J.; Gu, Y.; Stevenson, R.J.; Qi, W.; Anderson, R.F.; et al. Next-Generation Hypoxic Cell Radiosensitizers: Nitroimidazole Alkylsulfonamides. *J. Med. Chem.* **2018**, *61*, 1241–1254. [CrossRef] [PubMed]

47. Doundoulakis, T.; Xiang, A.X.; Lira, R.; Agrios, K.A.; Webber, S.E.; Sisson, W.; Aust, R.M.; Shah, A.M.; Showalter, R.E.; Appleman, J.R.; et al. Myxopyronin B analogs as inhibitors of RNA polymerase, synthesis and biological evaluation. *Bioorg. Med. Chem. Lett.* **2004**, *14*, 5667–5672. [CrossRef] [PubMed]

48. Greene, T.W.; Wuts, P.G.M. *Protective Groups in Organic Synthesis*, 3rd ed.; Wiley-Interscience: Hoboken, NJ, USA, 2002; pp. 201–270.

49. Nelson, T.D.; Crouch, R.D. Selective Deprotection of Silyl Ethers. *Synthesis* **1996**, *1996*, 1031–1069. [CrossRef]

50. Seemann, U.B. Polyvinylphosphonate und Deren Copolymere Durch Seltenerdmetall Initiierte Gruppen-Transfer-Polymerisation. Ph.D. Thesis, Technical University Munich, Munich, Germany, 2010. Available online: http://nbn-resolving.de/urn/resolver.pl?urn:nbn:de:bvb:91-diss-20101013-992998-1-7 (accessed on 1 April 2020).

51. Tshuva, E.Y.; Groysman, S.; Goldberg, I.; Kol, M.; Goldschmidt, Z. [ONXO]-Type Amine Bis(phenolate) Zirconium and Hafnium Complexes as Extremely Active 1-Hexene Polymerization Catalysts. *Organometallics* **2002**, *21*, 662–670. [CrossRef]

52. Hultzsch, K.C.; Voth, P.; Beckerle, K.; Spaniol, T.P.; Okuda, J. Single-Component Polymerization Catalysts for Ethylene and Styrene: Synthesis, Characterization, and Reactivity of Alkyl and Hydrido Yttrium Complexes Containing a Linked Amido–Cyclopentadienyl Ligand. *Organometallics* **2000**, *19*, 228–243. [CrossRef]

4.4. Addendum – additional initiators

To further broaden the scope of available end-groups, several substituted α-methyl pyridines were synthesized. With a special focus on grafting GTP-based polymers onto surfaces, two different approaches have been identified. For a direct grafting-to of the polymers, the catechol moiety has been chosen as novel initiator motif, as it has a high affinity towards almost all kinds of surfaces (Scheme 30A).[307,327] Utilizing the same surface covering affinity of catechol, a modal approach has been designed as well, where the surface coupling shall be achieved by an azide-alkyne cycloaddition between the functionalized polymer and suiting surface groups, like for example a dopamine-based azide (Scheme 30B). Therefore, polymers bearing either an azide or an alkyne chain end are required, which are introduced to α-methyl pyridines as well.
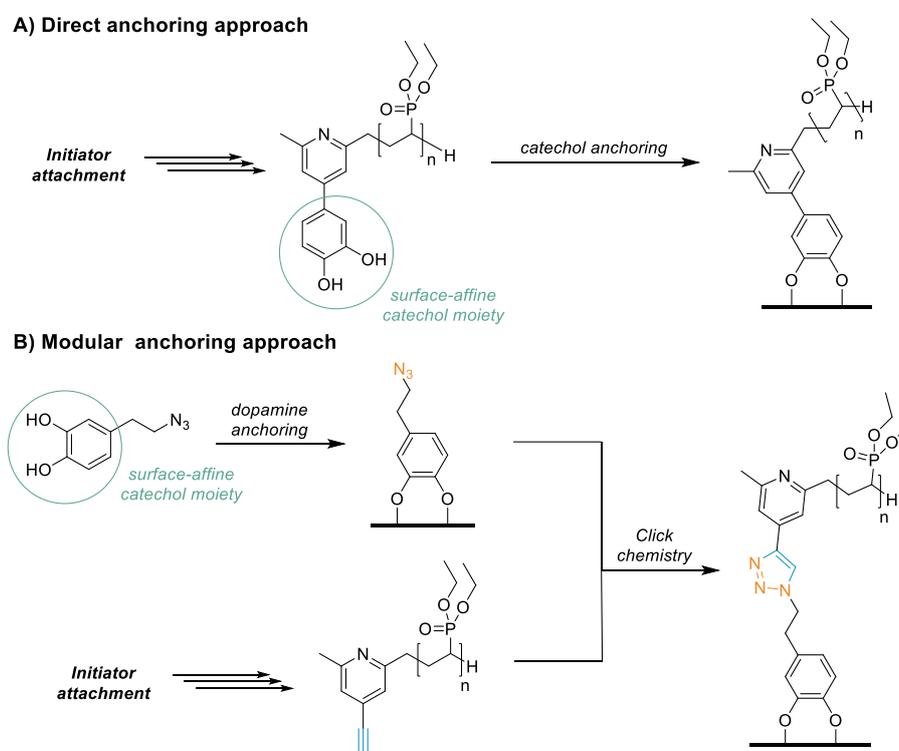
Scheme 30: Possible graft-to approaches towards anchoring GTP-based polymers *via* direct anchoring of an attached catechol moiety (**A**) or modular anchoring by azide-alkyne cycloaddition of an alkyne-modified polymer with an azide-functionalized dopamine on the surface (**B**).

4.4.1. Synthesis of functionalized pyridines

All syntheses routs towards the functionalized α-methylpyridines start from 4-chloro-2,6-dimethylpyridine (**1**), which is prepared from 2,6-dimethylpyridine *via* an established synthesis route.[86] For the preparation of the catechol-functionalized pyridine, a *Suzuki*-coupling of 4-chloro-2,6-dimethylpyridine (**1**) with the methoxy-protected 2,3-dimethoxyphenyl boronic acid (**2**) is performed, yielding 7.81 g (32.1 mmol, 91 %) of the desired 4-(3,4-dimethoxy-phenyl)-2,6-dimethylpyridine (**3**) in good purity with high yields after recrystallization from diethyl ether. The subsequent deprotection of the methoxy groups with BBr$_3$ as deprotection agent failed, most likely due to methylation of the pyridyl unit by the *in-situ* formed side-product methyl bromide. Deprotection by stirring with an excess of 40 % HBr under reflux for two days resulted in complete cleavage of the methoxy groups, yielding 1.73 g (8.03 mmol, 65 %) pure 4-(3,4-dihydroxyphenyl)-2,6-dimethylpyridine (**4**). To be able to perform a selective C-H bond activation, the hydroxyl units are reprotected with a *tert*-butyl-dimethyl-silyl protecting group. After column chromatography, 440 mg (1.00 mmol, 44 %) of pure 4-(3,4-di(*tert*-butyl-dimethylsilyl)oxy)-phenyl)-2,6-dimethylpyridine (**5**) were isolated (Scheme 31).
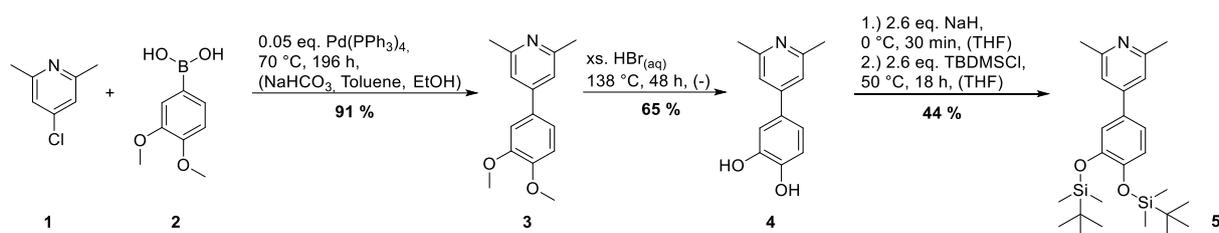
Scheme 31: Synthesis of the *tert*-butyl-dimethylsilyl protected catechol-pyridine (**5**) *via Suzuki* coupling, deprotection and reprotection.

For introduction of the last functional group, the alkyne, 4-chloro-2,6-dimethylpyridine (**4**) is converted to 4-iodo-2,6-dimethylpyridine (**6**) by a nucleophilic aromatic substitution *via* a modified, literature-known synthesis procedure.[86] By performing a copper-catalyzed *Sonogashira* coupling with 1-trimethylsilyl acetylene, 270 mg (1.32 mmol, 62 %) of the pure, already protected 4-trimethylsilylacetylene-2,6-dimethylpyridine (**7**) could be isolated after column chromatography in moderate yield (Scheme 32).[328]
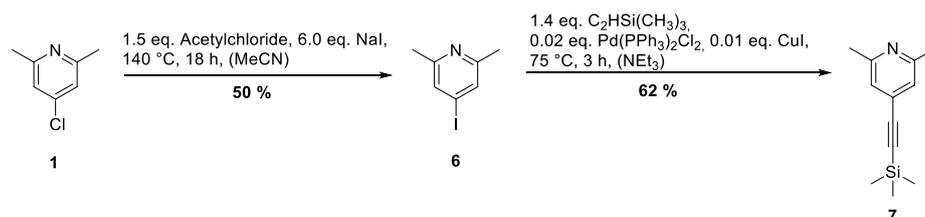
Scheme 32: Synthesis of the alkyne-pyridine (**7**) *via* nucleophilic aromatic substitution and *Sonogashira* coupling.

The synthesis of 4-azido-2,6-dimethylpyridine has successfully been realized by reacting 4-chloro-2,6-dimethylpyridine (**4**) with hydrazine-hydrate to 4-hydrazinethyl-2,6-dimethyl-pyridine (**8**) and subsequent diazotisation with sodium nitrite and 5 % hydrochloric acid.[329] The synthesis yielded 376 mg (2.54 mmol, 18%) of pure 4-azido-2,6-dimethylpyridine (**9**) with low yield (Scheme 33). The prepared azido-pyridine is directly used for C-H bond activation without prior introduction of a protecting group.
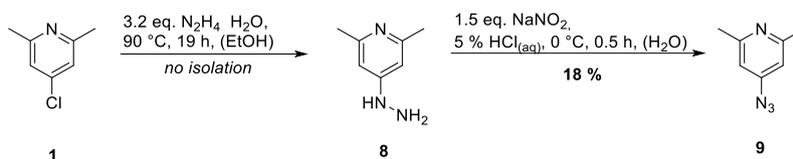
Scheme 33: Synthesis of the azido-pyridine (**9**) *via* nucleophilic aromatic substitution and diazotisation.

The three newly synthesized α-methylpyridines are next investigated regarding their reactivity towards C-H bond activation for the generation of catalysts, which transfer the functionalized pyridyl moieties to the polymers.

4.4.2.   C-H bond activation

Contrary to the previously described C-H bond activation using the yttrium bis(phenolate) precursor catalyst [(ONOO)^{tBu}Y(CH$_2$TMS)(thf)], the prepared functionalized pyridines are activated using Cp$_2$Y(CH$_2$TMS)(thf) to allow a fast assessment of their activation and subsequent initiation behavior. To investigate whether the *in-situ* C-H bond activation with the yttrium precursor proceeds without side-reactions, kinetic monitoring of the activation using ^{1}H-NMR spectroscopy has been performed. The monitoring of the C-H bond activation is performed as described in chapter 4.3 using the methyl signals and aromatic ring proton signals of the pyridyl unit as well as the CH$_2$TMS signal and the corresponding evolution of a tetramethylsilane signal. The C-H bond activation of the alkyne-pyridine (**7**) and the catechol-pyridine (**5**) proceeded without observable side-reactions within 2 hours at room temperature, facilitating an *in-situ* activation prior to polymerization without catalyst isolation and work-up. When reacting azide-pyridine (**9**) with the pre-catalyst Cp$_2$Y(CH$_2$TMS)(thf), no clean activation but catalyst decomposition can be observed as indicated by precipitation of a black solid and vanishing of defined signals in the ^{1}H-NMR. A similar activation protocol with [(ONOO)^{tBu}Y(CH$_2$TMS)(thf)] lead to catalyst decomposition at room temperature and elevated temperatures as well. The azide group seems to be too reactive to undergo controlled C-H bond activation with yttrium catalysts. In order to facilitate attachment of azide-groups nevertheless, the activation of **9** with the lutetium precursor Cp$_2$Lu(CH$_2$TMS)(thf) has been tested, as lutetium usually reacts much slower in C-H bond activation reactions.[70] This

approach allowed for a more controlled C-H bond activation of **9** within 24 hours at room temperature, yet appearance of some additional signals indicate minor side-reactions taking place. For all subsequent polymerizations, the respective C-H bond activated catalysts are generated *in-situ* by reacting 1.1 equivalents of the functionalized pyridine with 1.0 equivalents of with the respective pre-catalyst Cp$_2$Ln(CH2TMS)(thf) (Ln = Y, Lu) catalyst at room temperature as indicated.

4.4.3.   Polymerization of diethyl vinylphosphonate

For all polymerization reactions, DEVP is chosen as model monomer, as the obtained polymers remain water-soluble with an LCST at 42 °C, making them interesting candidates for surface modifications. Additionally, the molecular weight of the PDEVPs obtained can be determined absolutely *via* SEC-MALS, allowing accurate assessment of the initiation efficiency I.E. of the prepared pyridines. In a first step, the catechol-pyridine based catalyst **10** is formed *in-situ* and DEVP is added to generate catechol-functionalized polymers (Scheme 34). The polymerization results are summarized in Table 5.
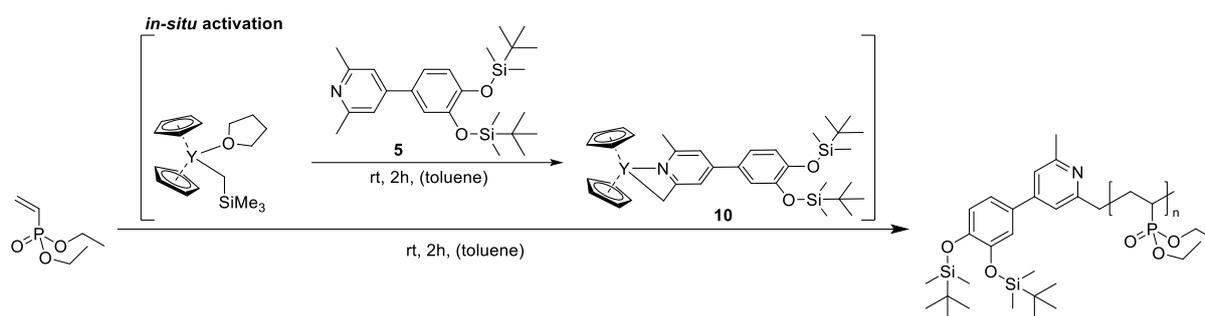
Scheme 34: Polymerization of DEVP with catalyst **10** generated *in-situ* from reacting the pre-catalyst Cp$_2$Y(CH$_2$TMS)(thf) with catechol-pyridine **5**.

Table 5: Results from DEVP polymerization with catalyst **10** generated *in-situ* from catechol-pyridine **5** with Cp$_2$Y(CH$_2$TMS)(thf).

Entry	[DEVP]/[Y] [a]	X [%] [b]	$M_{n,theo}$ [c] [kg/mol]	$M_{n,abs}$ [d] [kg/mol]	Đ [d] [-]	I.E. [e] [%]
1	100/1	99	16.2	19.0	1.13	85
2 [f]	175/1	99	29.7	48.7	1.02	62
3	200/1	99	35.2	47.9	1.03	73

[a] 13.5 µmol catalyst, 2 mL toluene, rt, 2 h; [b] conversion determined *via* integration of ^{31}P-NMR, [c] theoretical molecular weight determined as $M_{n,theo}$ = X·M_{DEVP}·[DEVP]/[Y]+M_{ini}; [d] absolute molecular weight and polydispersity determined *via* SEC-MALS in THF:H$_2$O with added TBAF, 40 °C, dn/dc = 0.0922 mL/g; [e] initiator efficiency determined *via* I.E. = $M_{n,theo}$/$M_{n,abs}$·100%; [f] double scale.

For the tested monomer/catalyst ratios of 100/1 and 200/1, the catalyst rapidly polymerized DEVP with full conversion as determined *via* ^{31}P-NMR spectroscopy, obtaining polymers with narrow polydispersity, indicating a very controlled polymerization. The initiation efficiency at 100/1 is with 85 % very high, slightly decreasing to 62 – 73 % for increased monomer amounts. Based on the high initiation efficiency, the determined absolute molecular weights are in good agreement with the theoretically calculated molecular weights at full initiation efficiency. To check if the attachment of the catechol-pyridine has been successful, ^{1}H-NMRs (**Figure 27**A) and DOSY-NMRs (**Figure 27**B**)** of the prepared polymers are measured. As the signals from the initiating group and especially from the protecting groups appear at the same diffusion coefficient as the polymer signals, attachment of the pyridyl unit is confirmed. By applying the same deprotection protocols as described in chapter 4.3, full removal of the silyl protecting groups of the catechol moiety was achieved as observed in ^{1}H-NMR (Figure 27C**)**. Overall, the established protocol for *in-situ* C-H bond activation, polymerization and subsequent deprotection allows the attachment of the desired catechol moiety to PDEVP polymers.
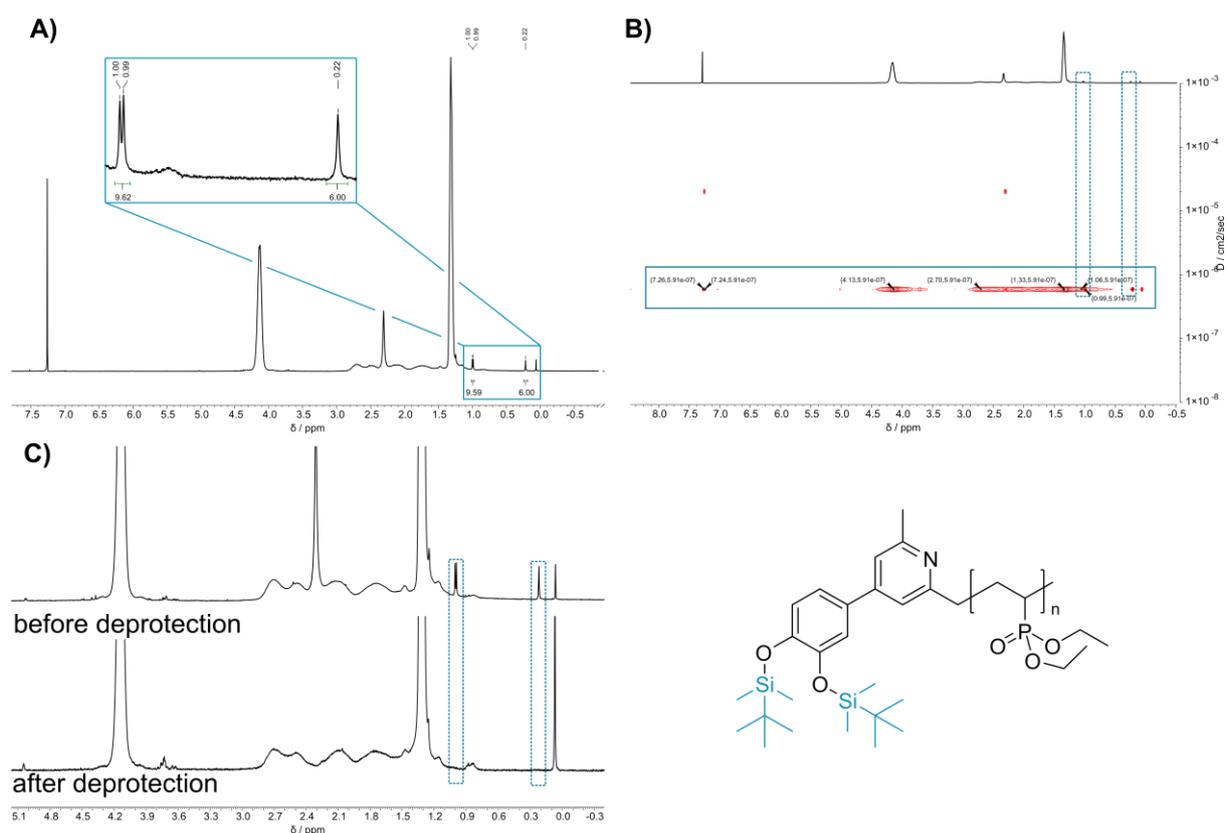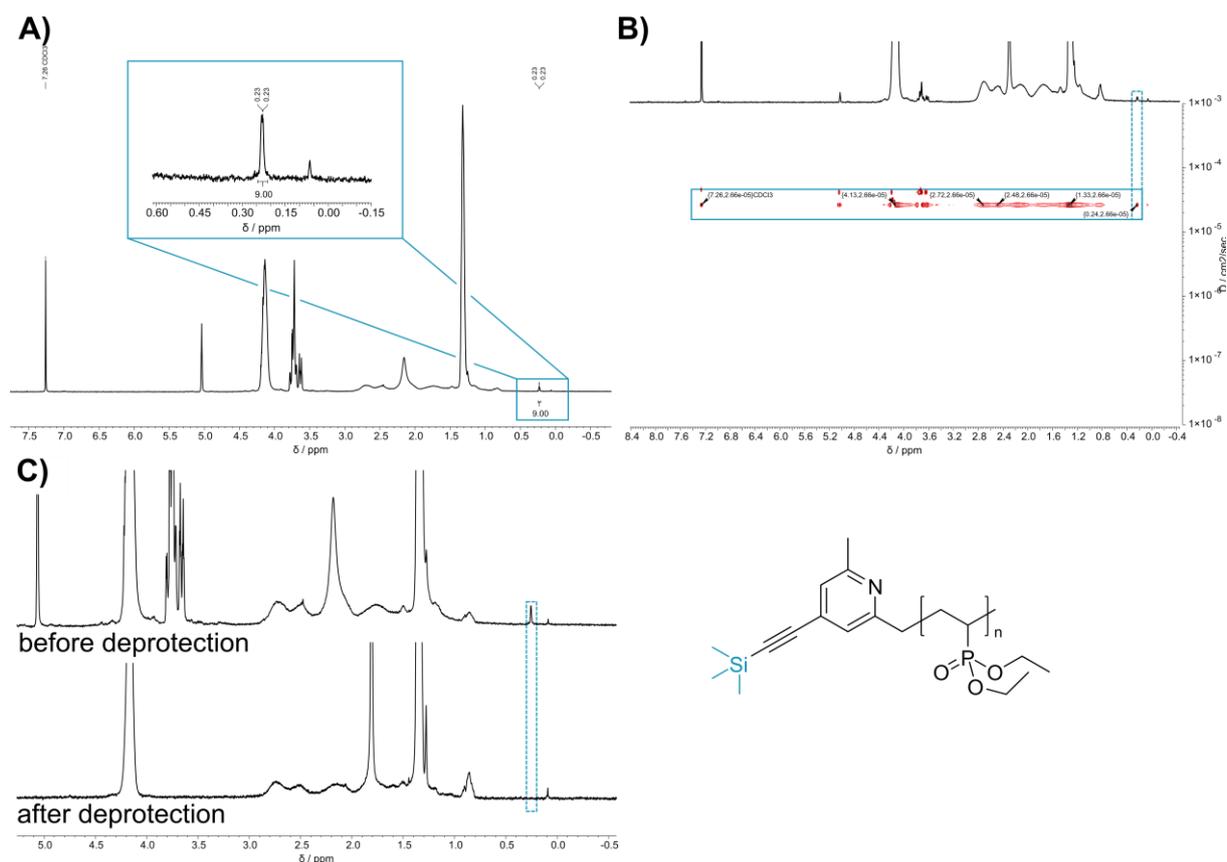

Figure 27: ^{1}H-NMR spectrum of PDEVP prepared with catalyst **10** with close-up of silyl region (**A**), DOSY-NMR of the same PDEVP sample, showing only one diffusion coefficient (**B**) and stacked ^{1}H-NMRs of catechol-functionalized PDEVP before and after deprotection (**C**).

Now, the alkyne-pyridine based catalyst **11** is tested towards DEVP polymerization. Again, the catalyst is formed *in-situ* from reaction of $Cp_2Y(CH_2TMS)(thf)$ with pyridine **7** prior to monomer addition (Scheme 35). The polymerization results are summarized in Table 6.
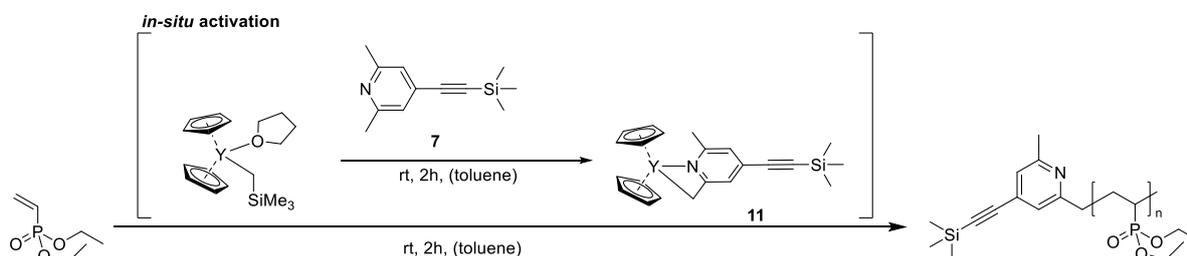
Scheme 35: Polymerization of DEVP with catalyst **11** generated *in-situ* from reacting the pre-catalyst $Cp_2Y(CH_2TMS)(thf)$ with alkyne-pyridine **7**.

Table 6: Results from DEVP polymerization with catalyst **11** generated *in-situ* from alkyne-pyridine **7** with $Cp_2Y(CH_2TMS)(thf)$.

Entry	[DEVP]/[Y] [a]	X [%] [b]	$M_{n,theo}$ [c] [kg/mol]	$M_{n,abs}$ [d] [kg/mol]	Đ [d] [-]	I.E. [e] [%]
1	50/1	99	8.7	19.6	1.09	44
2	100/1	99	16.7	31.5	1.09	53
3	200/1	99	33.3	66.1	1.05	50

[a] 13.5 µmol catalyst, 2 mL toluene, rt, 2 h; [b] conversion determined *via* integration of ^{31}P-NMR, [c] theoretical molecular weight determined as $M_{n,theo} = X \cdot M_{DEVP} \cdot [DEVP]/[Y] + M_{ini}$; [d] absolute molecular weight and polydispersity determined *via* SEC-MALS in THF:H_2O with added TBAF, 40 °C, dn/dc = 0.0922 mL/g; [e] initiator efficiency determined *via* I.E. = $M_{n,theo}/M_{n,abs} \cdot 100\%$; [f] double scale.

Similar to catalyst **10**, catalyst **11** is capable of fully polymerizing DEVP at room temperature within two hours. For all tested catalyst loadings from 50/1 to 200/1, the polymers obtained showed narrow polydispersity, indicating a very controlled polymerization reaction. For all tested ratios, the initiation efficiency is between 44 – 53 % and therefore about 20 – 30 % lower than the initiation efficiency of catalyst **10**. Nevertheless, PDEVPs with tunable molecular weights and narrow polydispersity can be prepared with catalyst **11** as well. Analogous to the catechol derivative, the initiator attachment is verified by ^{1}H-NMRs and DOSY-NMRs of the polymers, revealing the desired attachment of the TMS-protected alkyne (Figure 28A and B). To regain the reactivity of the alkyne, the TMS group is removed by stirring the polymer with potassium carbonate in methanol for two to three days at room temperature, fully cleaving of the protecting group as indicated by ^{1}H-NMR (Figure 28C**)**. Summarizing, the attachment and deprotection of alkynes-bearing initiator groups to PDEVP by the presented approach has been successful.

Figure 28: ^{1}H-NMR spectrum of PDEVP prepared with catalyst **11** with close-up of silyl region (**A**), DOSY-NMR of the same PDEVP sample, showing only one diffusion coefficient (**B**) and stacked ^{1}H-NMRs of alkyne-functionalized PDEVP before and after deprotection (**C**).

Lastly, the azide-pyridine based lutetium catalyst **12** is tested towards DEVP polymerization (Scheme 36), the corresponding polymerization results are summarized in Table 7.
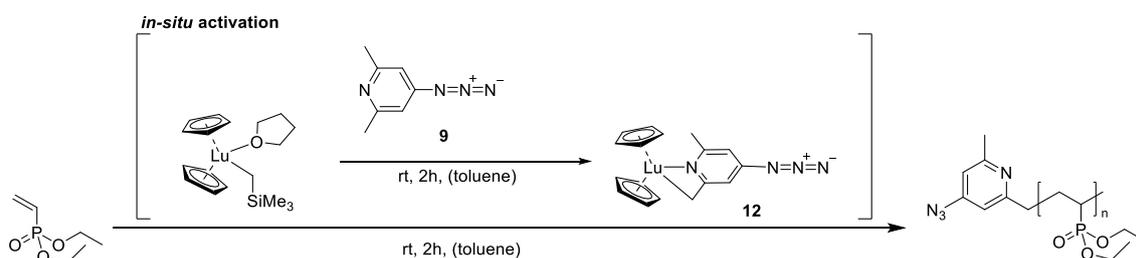
Scheme 36: Polymerization of DEVP with catalyst **12** generated *in-situ* from reacting the pre-catalyst Cp2Lu(CH2TMS)(thf) with azide-pyridine **9**.

Table 7: Results from DEVP polymerization with catalyst **12** generated in-situ from azide-pyridine **9** with Cp$_2$Lu(CH$_2$TMS)(thf).

Entry	[DEVP]/[Y] [a]	X [%] [b]	M$_{n,theo}$ [c] [kg/mol]	M$_{n,abs}$ [d] [kg/mol]	Đ [d] [-]	I.E. [e] [%]
1	25:1	99	4.3	40.1	1.21	10.7
2	50:1	99	8.4	69.6	1.15	12.1
3	100:1	99	16.6	219	1.19	7.6
4	200:1	99	33.0	391	1.16	8.4

[a] 13.5 µmol catalyst, 2 mL toluene, rt, 2 h; [b] conversion determined *via* integration of ^{31}P-NMR, [c] theoretical molecular weight determined as $M_{n,theo} = X \cdot M_{DEVP} \cdot [DEVP]/[Y] + M_{ini}$; [d] absolute molecular weight and polydispersity determined *via* SEC-MALS in THF:H$_2$O with added TBAF, 40 °C, dn/dc = 0.0922 mL/g; [e] initiator efficiency determined *via* I.E. = $M_{n,theo}/M_{n,abs} \cdot 100\%$; [f] double scale.

Like catalysts **10** and **11**, catalyst **12** is capable of polymerizing DEVP with full conversion within 2 hours at room temperature. However, the polydispersity of the polymers obtained is considerably higher than for catalyst **10**, indicating a less controlled polymerization. This is underlined by the much lower initiation efficiency between 8.4 – 12.1 %, leading to a drastically increased measured molecular weight compared to the theoretically calculated molecular masses. As the C-H bond activation with yttrium as central metal failed and led to catalyst decomposition, a similar behavior might cause the deviating behavior observed for the DEVP polymerization. As the activation kinetics already hinted, there are some minor side-reactions occurring during the C-H bond activation, leading to an overall decreased amount of active polymerization catalyst, explaining the lower initiation efficiency. Overall, the initiator efficiency is about half of the reported value for the structural analogue *sym*-collidine derivative Cp$_2$Lu(*sym*-col)(thf) of 21 %.[68] The increased polydispersity might be caused by the overall faster polymerization of DEVP by the lutetium catalyst compared to the yttrium catalyst in combination with a less precise initiation reaction.[68] At low monomer/catalyst loadings of 25/1 and 50/1, the ultrafast polymerization of DEVP with lutetium in combination with the low initiation efficiency leads to a broadening of the dispersity, while this effect is less pronounced at higher monomer loadings. Yet catalyst **12** is capable of producing defined PDEVPs with steerable molecular weights and moderate polydispersities. Again, to verify the attachment of the initiator, DOSY-NMRs of the polymers prepared are measured. However, as the molecular weight is considerably higher than for the polymers prepared with catalysts **10** or **11** and as the initiator is both considerably smaller with overall less detectable proton signals and no silyl protecting groups, verification of the attachment *via* NMR failed. Additionally, structural integrity of the azide group cannot be confirmed using ^{1}H-NMR, as decomposition of the azide moiety during C-H bond activation cannot be neglected. Therefore, oligomeric DEVP is prepared with catalyst **12** and an ESI-MS is measured (Figure 29), revealing covalent attachment of an intact azide moiety (black series) as well as partial recombination to the dimeric azo-species (blue

series). Yet overall, the attachment of an azide to PDEVP by using the *in-situ* approach seems to be successful as well.
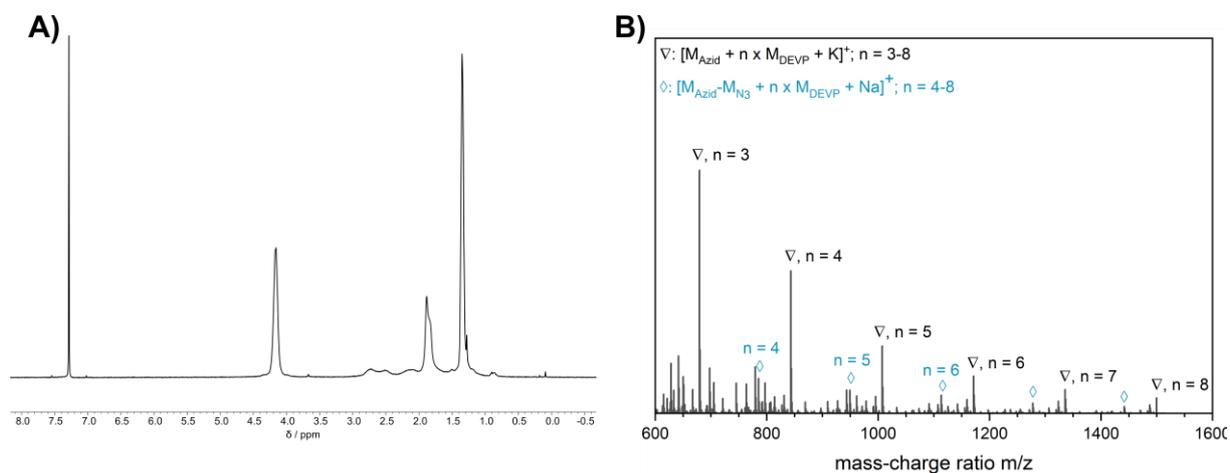

Figure 29: ^{1}H-NMR of PDEVP prepared with catalyst **12**, without signals from the initiator (**A**) and ESI-MS spectrum of PDEVP oligomers prepared with catalyst **12** showing to series, one with an intact azide attached and one with an initiator with decomposed azide (**B**).

4.4.4.   Utilization of the functionalized polymers

With the prepared functionalized polymers, different functionalization approaches will be tested. The catechol-functionalized polymer will be tested towards direct surface coating of different substrates due to the anchoring affinity of the catechol-function, while the azide-functionalized PDEVP is intended for a direct functionalization of carbon nanotubes. The alkyne as the most versatile end-group will be tested in the previously described modular azide-alkyne cycloaddition coating approach with dopamine-azide as functional group on the surface. Overall, these functional initiators serve as anchoring moieties for polymers prepared *via* group-transfer polymerization, possibly providing a versatile tool which can be used to immobilize a variety of different, functional, and responsive polymers on a variety of surfaces.

5.   Synthesis and characterization of polymeric photocatalysts

Macromolecular Rhenium–Ruthenium Complexes for Photocatalytic CO_2 Conversion: From Catalytic *Lewis* Pair Polymerization to Well-Defined Poly(vinyl bipyridine)–Metal Complexes

5.1.   Bibliographic data

5.2.   Abstract graphic (TOC)

Figure 30: Table of Content graphic for the manuscript titled "Macromolecular Rhenium–Ruthenium Complexes for Photocatalytic CO_2 Conversion: From Catalytic *Lewis* Pair Polymerization to Well-Defined Poly(vinyl bipyridine)–Metal Complexes".

5.3. Content

With respect to sidechain modifications, the monomer 4-vinyl-4'-methyl-2,2'-bipyridine (VBpy) as extended 1,6-*Michael* acceptor monomer is chosen to act as modifiable moiety for the synthesis of highly stable photocatalysts. The concept of using PVBpy as macromolecular ligand is widely known and used for a variety of different applications, yet no catalytic polymerization of VBpy is known so far. The pioneering work by Rieger *et al.* on the catalytic polymerization of 4-vinylpyridine using interacting aluminum/phosphine-based *Lewis* pairs for a controlled LPP[15] is used as a blueprint to find suitable *Lewis* acid/base pair combinations capable of polymerizing VBpy in a controlled, catalytic way. Various combinations of aluminum acids and phosphine bases are screened towards VBpy polymerization, and the obtained polymers are characterized regarding their absolute molecular weight and polydispersity. By using tri-*iso*-butyl aluminum and trimethyl phosphine as *Lewis* pair, PVBpy with narrow polydispersity could be obtained, while an end-group analysis revealed the presence of two different initiation pathways, conjugate addition and deprotonation. The main purpose of PVBpy is to act as a macromolecular ligand, forcing rhenium and ruthenium complexes into spatial proximity. This is done in order to increase the stability of photocatalytically active rhenium complexes by the photosensitizing effect of rhenium moieties. With these well-defined polymers, polymer-metal complexes are synthesized in a two-step loading with the pre-cursor complexes $Re(CO)_5Cl$ and $Ru(dmb)_2Cl_2$ (dmb = dimethyl bipyridine) and thoroughly characterized using UV-Vis, photoluminescence, and IR spectroscopy as well as ICP-MS to determine the metal loading. This characterization revealed an incomplete loading of the polymer with metal complexes with the herein presented synthesis pathways, achieving total metal loadings between 14 – 41 %. Nevertheless, the polymeric photocatalysts showed high activity and stability towards photocatalytic CO_2 reduction, with turnover numbers (TON) of up to 5650 and turnover frequencies (TOF) of 66 h^{-1}, while maintaining activity up to 30 days. This successfully shows that the use of PVBpy as macromolecular ligand influences the stability of this tandem system of a rhenium photocatalyst with a ruthenium photosensitizer beneficially. By means of LPP a catalytical polymerization of VBpy is now possible, allowing the synthesis of precisely defined polymers to be used as macroligands.

5.4. Manuscript

Macromolecules

Article

Macromolecular Rhenium–Ruthenium Complexes for Photocatalytic CO$_2$ Conversion: From Catalytic Lewis Pair Polymerization to Well-Defined Poly(vinyl bipyridine)–Metal Complexes

Anton S. Maier,[†] Christopher Thomas,[†] Moritz Kränzlein,[†] Thomas M. Pehl, and Bernhard Rieger*

Cite This: *Macromolecules* 2022, 55, 7039–7048

Read Online

ACCESS | Metrics & More | Article Recommendations | Supporting Information

ABSTRACT: Herein, the first catalytical polymerization of 4-vinyl-4′-methyl-2,2′-bipyridine (VBpy) via Lewis pair-mediated group-transfer polymerization using different combinations of Lewis acidic trialkyl aluminum compounds and Lewis basic phosphines is reported. In this context, a broad screening of different Lewis pairs is conducted, demonstrating the necessity of an adjustment of the steric and electronic properties of the Lewis pair to the demands of the monomer. Further, end-group analysis of short-chain oligomers via electrospray ionization mass spectrometry (ESI-MS) for the experimentally determined optimum combination Al(i-Bu)$_3$/PMe$_3$ (Đ = 1.31–1.36, I.E. = 45–51%) reveals the presence of two initiation pathways via conjugate addition and deprotonation. The well-defined polymers are subsequently loaded in a two-step synthesis protocol with different ratios of Re(CO)$_5$Cl and Ru(dmb)$_2$Cl$_2$, forming a photocatalytically active rhenium–ruthenium polymer complex with poly(vinyl bipyridine) as the macroligand. Catalyst loadings are characterized thoroughly by means of Ultraviolet–visible (UV–vis), photoluminescence (PL), and IR spectroscopy as well as inductively coupled plasma (ICP)-MS. Finally, a comparison of the photocatalytic CO$_2$ reduction performance of the polymeric catalysts in irradiation experiments is presented, revealing particularly high photostabilities and activities for **PVBpy**$^{5/95}$ (TON = 5650, TOF = 66 h^{-1}). This is due to an efficient electron transfer of the Ru(II)-one-electron-reduced species (OERS) to the rhenium centers facilitated by the spatial proximity of both metals attached to the macromolecular ligand PVBpy.
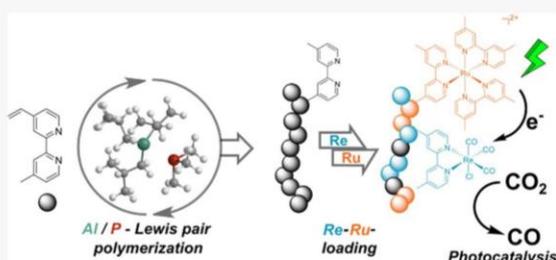
INTRODUCTION

Mononuclear rhenium complexes of the type [Re(dmb)(CO)$_3$X] (X = Cl$^-$, Br$^-$) with 4,4′-dimethyl-2,2′-bipyridine (dmb) ligands were established as catalysts for the photocatalytic reduction of CO$_2$ to CO due to their high activity and excellent product selectivity, favoring the formation of CO over other reduction products. In this context, the Re(I) centers were shown to act as photosensitizers, as well as the photocatalytic units, in the CO$_2$ conversion.[1,2] However, those photocatalysts suffer from premature catalyst deactivation due to the insufficient photostability of the Re(I)-OERS.[3] An increase in the photostability of Re(I)-based catalyst systems was achieved upon covalent linkage of rhenium centers, resulting in a binuclear mechanism that combines an effective two-electron transfer caused by the spatial proximity of the metal centers with the smooth generation of a free coordination site.[4] Further enhancement of the photocatalytic performance of multinuclear rhenium complexes is possible upon integration of ruthenium moieties as photosensitizing units for light capture.[5,6] The incorporation of Ru(II) into the rhenium-based photocatalytic systems allows for the utilization of lower energy light and thus helps suppress light-induced deactivation reactions.[7] Among those multinuclear systems for photocatalytic CO$_2$ reduction, particularly catalysts with [Ru(dmb)$_3$]$^{2+}$ moieties as photosensitizers covalently linked to [Re(dmb)(CO)$_3$Cl] derivatives, as the catalytic centers are very well studied.[8–10] Upon light absorption, the exclusive population of the ^{3}MLCT (metal-to-ligand charge-transfer) state of the ruthenium complexes was observed, which was transformed into the Ru(II)-OERS by reductive quenching with a suitable electron donor. Subsequent intramolecular electron transfer to the covalently bound Re(I) unit leads to the generation of the Re(I)-OERS capable of entering the catalytic cycle for the reduction of CO$_2$. In this context, the rate of the intramolecular electron transfer is of secondary importance, as the reduction of CO$_2$ at the Re(I) center was identified as the rate-limiting step of the overall process.[7] Nevertheless, studies revealed that supramolecular rhenium–ruthenium complexes with short, saturated linkers between the
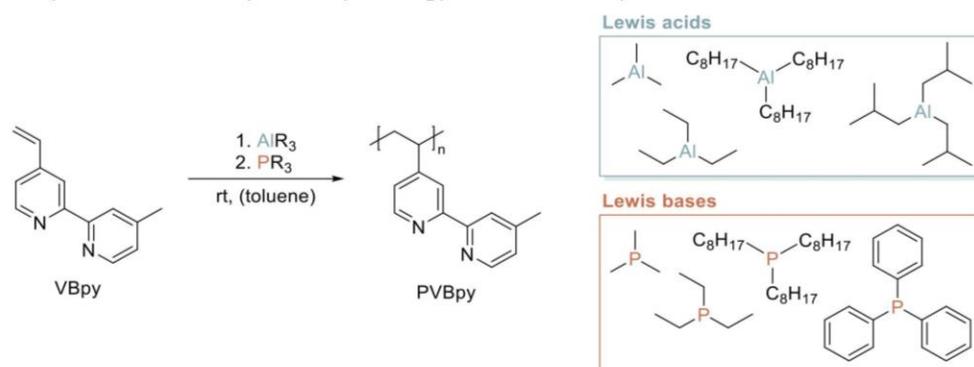
ACS Publications

7039

Scheme 1. Polymerization of 4-Vinyl-4′-methyl-2,2′-bipyridine Mediated by Different Lewis Pairs

metal centers exhibited the highest photocatalytic activities and stabilities.[11,12] This was attributed to π-conjugation significantly lowering the reduction potential of the Re(I)-OERS, therefore worsening the photocatalytic abilities of complexes with conjugated bridging ligands.[13] A concept for a trinuclear photocatalyst bearing two rhenium and one ruthenium moiety was introduced by Ishitani et al., revealing high photostability and high catalytic activities due to an efficient intramolecular electron transfer.[14] This fast and quantitative electron transfer is the main reason for a substantial stability increase, as light-induced deactivation reactions of the Ru(II)-OERS are generally considered the main route for catalyst degradation.[3,15] One main advantage regarding the photocatalytic performance of multinuclear rhenium–ruthenium complexes is their lower concentration dependency compared to a combination of mononuclear systems of Ru(II) and Re(I).[7] This is again due to the efficient electron transfer from photosensitizer to catalyst unit because of the covalent linkage of both key components of the photocatalytic system, enabling the electron and energy transfer also at very low concentrations.[7,16] To facilitate more spatial proximity for the photocatalytically active units, covalent linkages of multiple bipyridine units to a macromolecular ligand might be beneficial for the catalysts' stability.[17] Such polymers acting as macroligands for metal complexes have been long-known, and application of this principle to the photocatalytic reduction of CO_2 can eventually facilitate the formation of highly stable photocatalysts combining photocatalysis with properties inherent to polymers.[17–19] Usually, vinyl bipyridines can be applied in this context, being polymerized using free-radical polymerization,[20,21] atom-transfer radical polymerization (ATRP),[22] or electropolymerization,[17,23,24] yet accessing well-defined, controllable polymers with narrow dispersities remains a major challenge. One approach might comprise Lewis pair-mediated polymerization as a facile tool toward defined poly(vinyl bipyridines) as metal complex anchoring sites. In contrast to classical Lewis acid–base adducts,[25] Stephan et al. introduced the notion of frustrated Lewis pairs (FLPs) as a new concept for the description of combinations of sterically hindered Lewis acids and equally hindered Lewis bases.[26] Due to the steric repulsion of Lewis acid and base, the formation of a Lewis pair based upon donor–acceptor interactions is suppressed, resulting in an unusual and synthetically appealing reactivity of those frustrated Lewis pairs.[26] The first application of FLPs in polymerization catalysis allowed for the polymerization of methyl methacrylate

(MMA) and two methylene butyrolactones utilizing highly Lewis acidic $Al(C_6F_5)_3$ in combination with appropriate phosphines and N-heterocyclic carbenes as Lewis bases.[27] In analogy to the rare-earth metal-mediated group-transfer polymerization, monomers for Lewis pair-mediated polymerizations comprise α,β-unsaturated molecules (1,4-Michael acceptors) with a double bond conjugated to a heteroatom moiety allowing coordination to a catalytically active center. Besides MMA and a series of lactones, also polymers from the polar vinyl monomers 2-isoprenyl-2-oxazoline (iPOx) and 2-vinylpyridine (2VP), bearing a C=C–C=N functionality, were accessible applying a combination of $Al(C_6F_5)_3$ and N-heterocyclic carbenes as polymerization catalysts.[28] In 2016, the scope of available monomers was broadened by Rieger et al., reporting the controlled polymerizations of diethyl vinylphosphonate (DEVP), dimethyl acrylamide (DMAA), as well as the extended 1,6-Michael system 4-vinylpyridine (4VP) with several combinations of highly interacting Lewis pairs (HIPs) compromising organoaluminum compounds with less steric demand and small phosphines.[29] For these experiments, an adjustment of the steric and electronic parameters of the Lewis pairs to the steric and electronic properties of the respective monomers was necessary to achieve living type polymerizations while maintaining narrow polydispersities. In addition to that, the initiation mechanism of the polymerization was investigated by means of electrospray ionization mass spectrometry (ESI-MS) analyses of short-chain oligomers, revealing a terminal phosphine group and hence, strongly suggesting a conjugate addition pathway.[29] These examples demonstrate the broad applicability of Lewis pair catalysis for the polymerization of polar monomers that might not be accessible by other polymerization types. Transferring this concept to new monomers, the first catalytic polymerization of 4-vinyl-4′-methyl-2,2′-bipyridine using different Lewis pairs is reported. Using these well-defined polymers, rhenium–ruthenium-loaded polymeric metal complexes are prepared using a two-step synthesis protocol, and their photocatalytic activity in CO_2 reduction is investigated.

■ LEWIS PAIR POLYMERIZATION SCREENING

While polymeric forms of 4-vinyl-4′-methyl-2,2′-bipyridine are well known as macroligands for photocatalytically active complexes, no catalytically controlled polymerization procedure for this monomer is known so far, as most examples involve less defined electropolymerization or radical mechanisms.[17,18,20–24] In 2016, Rieger et al. published the first

- 89 -

Table 1. Polymerization of 4-Vinyl-4′-methyl-2,2′-bipyridine Using Different Lewis Pairs; LA = Lewis Acid, LB = Lewis Base

entry	Lewis acid	Lewis base	[VBpy]/[LA]/[LB][a] [equiv.]/[equiv.]/[equiv.]	t_R^b [h]	X_{VBpy}^c [%]	$M_{n,theo}^d$ [kg/mol]	$M_{n,abs}^e$ [kg/mol]	$Đ^e$ [-]	I.E.[f] [%]
1	AlMe₃	PMe₃	200/2/1	15	38	14.9	209	2.34	7.1
2	AlEt₃	PMe₃	100/2/1	7	87	17.4	151	2.08	12
3	AlEt₃	PMe₃	200/2/1	23	94	36.9	173	1.34	21
4	AlEt₃	PMe₃	400/2/1	68	35	27.5	90.8	1.41	30
5	AlEt₃	PEt₃	200/2/1	21	80	31.3	89.7	1.74	35
6	AlOct₃	PMe₃	200/2/1	43	59	23.1	91.0	1.66	25
7	AlOct₃	PEt₃	200/2/1	21	39	15.4	52.4	1.35	29
8	Al(i-Bu)₃	PMe₃	200/2/1	41	38	15.0	29.6	1.36	51
9	Al(i-Bu)₃	PMe₃	100/2/1	24	79	15.6	35.0	1.31	45
10	Al(i-Bu)₃	POct₃	100/2/1	65	89	17.6	36.9	1.35	48
11	Al(i-Bu)₃	PPh₃	100/2/1	9	61	12.0	40.8	1.35	29

[a]Desired reactant ratio. [b]1.02 mmol VBpy in 2 mL of toluene, room temperature, Lewis acid and monomer were premixed, and the polymerization was started by addition of Lewis base. [c]Determination of conversion via aliquot-¹H NMR; for a detailed calculation, see the Supporting information, Figure S2. [d]Theoretical molecular weight determined via $M_{n,theo} = X_{VBpy} \times M_{VBpy} \times [VBpy]/[LB]$, assuming full initiator efficiency. [e]Absolute molecular weight and polydispersity determined using SEC with triple detection in DMF with added LiBr (25 mmol/L) at 30 °C using the experimentally determined dn/dc = 0.190 mL g⁻¹ (Supporting information, Figure S5). [f]Initiator efficiency I.E. = $M_{n,theo}/M_{n,abs} \times 100\%$.

Scheme 2. Initiation Pathways of Lewis Pair-Mediated Polymerization of VBpy with the Lewis Pair Al(I-Bu)₃/PMe₃ via Conjugate Addition (Upper Pathway, Red) or Deprotonation (Lower Pathway, Green) Either Leading to Phosphine or Olefin-Terminated Polymer Chains[29]
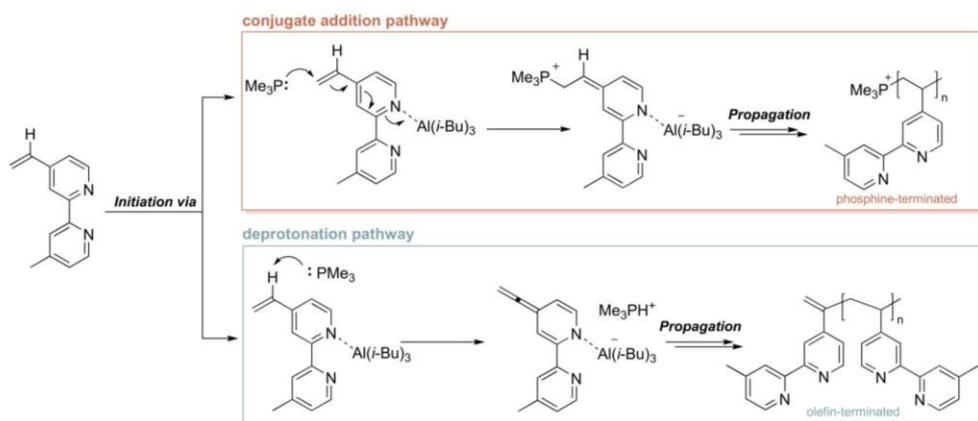
controlled polymerization of the extended Michael-type system 4-vinylpyridine, which is related to VBpy.[29] This concept is transferred onto the polymerization of VBpy for the synthesis of defined macroligands, as shown in Scheme 1.

For the polymerization of VBpy, different Lewis pairs with varying steric demands and, thus, different interactions were tested; the results are shown in Table 1. All polymerizations were performed in toluene at room temperature, and the obtained polymers were characterized for their chemical structure using ¹H NMR and ¹³C NMR. The absolute molecular weight distribution was determined via size-exclusion chromatography (SEC), and in terms of their thermal properties by differential scanning calorimetry (DSC) and thermogravimetric analysis (TGA).

Initial experiments with the two least sterically hindered acids and bases AlMe₃ and PMe₃ (Table 1, entry 1) yielded a conversion of 38% with a broad, bimodal dispersity (Đ = 2.34) and low initiation efficiency (I.E. < 10%). For the combination AlEt₃/PMe₃ (Table 1, entries 2−4), high conversions (X > 85%) with low to moderate polydispersities (Đ = 1.34−2.08) were obtained, only limited in conversion by higher monomer

loadings (Table 1, entry 4) while maintaining initiator efficiencies in the range of 12−30%. This limitation might be caused by monomer overload at the catalytic center or an overall increase of side reactions, or the reaction mixture's viscosity due to a higher monomer concentration. However, all combinations using small, sterically less demanding Lewis acids produced polymers with more or less pronounced bimodal character, as observed in the corresponding SEC traces (see the Supporting information, Figures S6−S10). This bimodality is most likely attributed to the presence of two initiation pathways, namely, conjugate addition of the phosphine and a deprotonation route, which differ in their reaction rates.[29] Switching to the sterically highly demanding AlOct₃ with small Lewis bases PMe₃ (Table 1, entry 6) and PEt₃ (Table 1, entry 7), VBpy conversion decreases with increasing steric demand of the Lewis base (59% for PMe₃ vs 39% for PEt₃). However, the polydispersity decreased from 1.66 to 1.35, while initiation efficiencies between 25 and 29% were observed for both systems. To facilitate higher conversion, the sterically less demanding Lewis acid Al(i-Bu)₃ is selected in combination with PMe₃ (Table 1, entries 8−9). Despite showing a severe

Scheme 3. Synthesis of Macromolecular Photocatalysts in a Two-Step Synthesis by Subsequent Loading of PVBpy1−3 with Re(CO)₅Cl and Ru(dmb)₂Cl₂
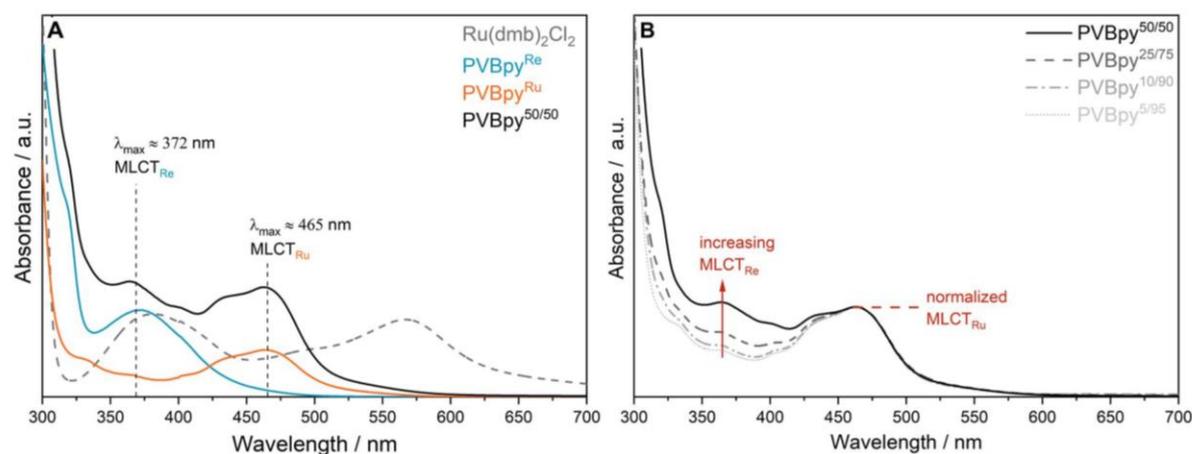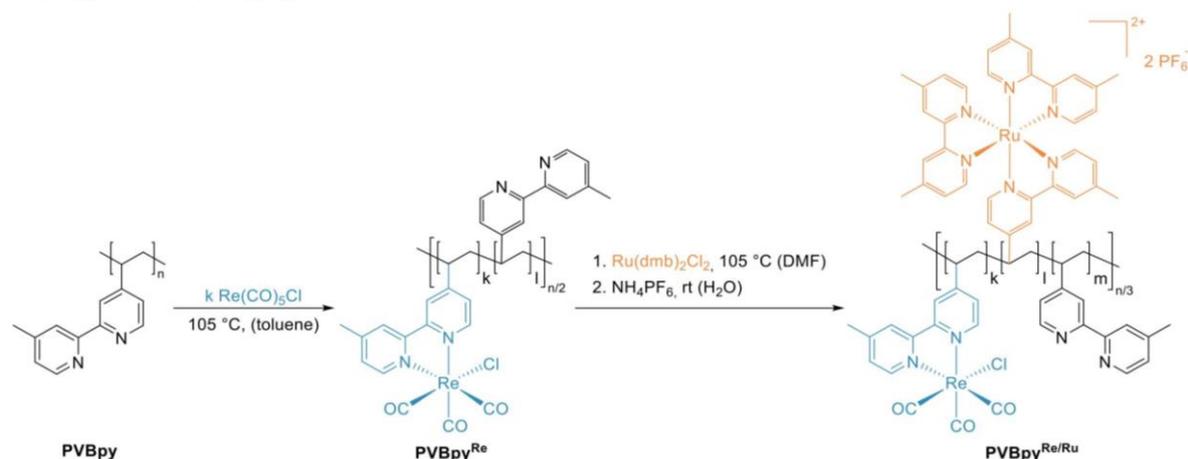
Figure 1. UV−vis spectroscopy for (A) photophysical investigation of the electronic ground state of different metal-loaded PVBpy samples with characteristic absorption maxima of Ru(dmb)₂Cl₂ (gray, dashed), Re-loaded PVBpy^{Re} (blue), Ru-loaded PVBpy^{Ru} (orange), and photocatalyst **PVBpy$^{50/50}$** (black) and (B) qualitative comparison of rhenium loading in different polymer samples via normalization of the respective MLCT$_{Ru}$.

decrease of the conversion with increasing monomer-to-Lewis pair ratio (100/2/1 with X = 79% vs 200/2/1 with X = 38%), this combination shows narrow dispersities ($Đ$ ≤ 1.36) as well as the highest initiator efficiencies (I.E. = 45−51%) among all tested Lewis pairs. Increasing the steric demand of the Lewis base using P(n-Oct)₃ (Table 1, entry 10) or PPh₃ (Table 1, entry 11) improved the overall conversion (89 and 61%) while maintaining narrow polydispersities ($Đ$ ≤ 1.35) and high initiation efficiencies (I.E. = 48 and 29%). Comparing the sterically more demanding Lewis pairs to the small Lewis pairs in terms of polymer dispersity, monomodal polymers were obtained, surpassing the limitation of less demanding Lewis pairs suffering from a less controlled initiation (Supporting information, Figures S11−S16). ESI-MS end-group analysis of PVBpy oligomers prepared with the Lewis pair Al(i-Bu)₃/PMe₃ (Supporting information, Figure S20), however, revealed the presence of species terminated by a phosphine or an olefin (Scheme 2). This indicates the presence of both initiation pathways, conjugate addition and deprotonation, in systems

with sterically more demanding Lewis acids as well. These results are in accordance with previous observations reported by Rieger et. al.[29] Nevertheless, monomodal polymers with narrow polydispersities were obtained, most likely due to conjugate addition and deprotonation, exhibiting similar reaction rates during initiation. Therefore, the Lewis pair Al(i-Bu)₃/PMe₃ emerged as the most appropriate combination among the investigated systems for the polymerization of VBpy as an extended Michael-type monomer.

Overall, tuning of the Lewis pair interaction allowed the first catalytically controlled polymerization of VBpy, giving access to defined and thoroughly characterized polymers as macro-ligands for metal complex loading. As a model system for further experiments, the combination Al(i-Bu)₃/PMe₃ with a ratio of 100/2/1 (Table 1, entry 9) was chosen, as it exhibited the smallest dispersity and yielded only monomodal polymers while maintaining high initiation efficiencies and reaching a conversion of 79% within the tested reaction times. Different polymers PVBpy1−3 for metal loading experiments were

Table 2. Catalyst Compositions of PVBpy$^{5/95}$, PVBp$^{10/90}$, PVBpy$^{25/75}$, and PVBpy$^{50/50}$ and Photocatalyst-to-Photosensitizer Ratio R$_{Re/Ru}$

sample	theoretical loading Re/Ru [%/%]	theoretical Re/Ru ratio $R_{Re/Ru,theo}$ [-]	calculated Re/Ru ratio $R_{Re/Ru,calc}$[a] [-]	Re-loaded VBpy-units[b] [%]	Ru-loaded VBpy-units[b] [%]	unoccupied VBpy-units[b] [%]	total metal loading of PVBpy [%]
PVBpy$^{5/95}$	5/95	0.05	0.25	2.70	11.1	86.2	13.8
PVBpy$^{10/90}$	10/90	0.11	0.80	6.60	8.20	85.2	14.8
PVBpy$^{25/75}$	25/75	0.33	1.70	19.9	11.6	68.5	31.5
PVBpy$^{50/50}$	50/50	1.00	4.70	34.1	7.30	58.6	41.4

[a]Calculated from the rhenium and ruthenium loadings [μmol/mg$_{polymer}$] determined via ICP-MS (see the Supporting information, Table S2 and eqs 1−3). [b]Calculated from the rhenium and ruthenium masses found via ICP-MS of the microwave-digested samples (see the Supporting information, Table S2 and eqs 4−11).

prepared using the same procedure; the results can be found in the Supporting information, Table S1, and Figures S17−S19. The obtained polymers are amorphous powders with a glass-transition temperature of 142 °C and a thermal decomposition onset temperature of 368 °C (for DSC and TGA, see the Supporting information, Figures S21 and S22).

■ SYNTHESIS OF MACROMOLECULAR METAL COMPLEXES

Metal loading onto the polymers was done in a two-step synthesis (Scheme 3). As the initial step, polymers 1–3 were reacted with Re(CO)$_5$Cl, followed by subsequent complexation with an excess of the ruthenium precursor complex Ru(dmb)$_2$Cl$_2$. The introduction of Re units into the polymers was accomplished by dissolution of the polymers in toluene and reaction with Re(CO)$_5$Cl at elevated temperatures. As the polymers exhibited a high solubility in methanol after loading with the ruthenium precursor, removal of Ru(dmb)$_2$Cl by washing with MeOH was not possible. However, the macromolecular rhenium−ruthenium complexes were successfully isolated by salt metathesis upon dissolution in methanol, followed by precipitation in an aqueous NH$_4$PF$_6$ solution. Subsequently, the Ru(dmb)$_2$Cl$_2$ precursor could be removed by washing with methanol, whereas the loaded polymers with the PF$_6^-$ counterions remained insoluble.

This approach enabled the synthesis of various macromolecular photocatalysts with different amounts of Re and Ru units. Successful incorporation of the metal centers was confirmed via Ultraviolet−visible (UV−vis) spectroscopy for all macromolecular complexes (Figure 1A). Moreover, the characteristic absorption maxima of Re and Ru, respectively, allowed for a qualitative determination of the Re(I)/Ru(II) ratio (Figure 1B). Spectroscopic investigation of the Ru precursor complex Ru(dmb)$_2$Cl$_2$ in N,N-dimethylformamide showed absorption maxima at 568 and 382 nm, which are in good agreement with the literature.[16] Compared to that, a polymer exclusively loaded with Ru centers exhibited a significant blue shift of the absorption maximum to lower wavelengths. This hypsochromic shift results from the substitution of the electron-withdrawing chloride ligands at the ruthenium center by the bipyridine ligands of the polymer chain. As a result of that, the stabilization of the π^* orbitals of the bipyridine ligands at the ruthenium is lost. Therefore, the formerly red-shifted, characteristic MLCT transition ($d\pi \rightarrow \pi^*$) occurs at a lower wavelength of 465 nm.[7] As opposed to that, a Re-loaded polymer shows the characteristic MLCT transition of bipyridine-substituted Re(I) complexes at a wavelength of 372 nm.[16] The appearance of both mentioned transitions in the UV−vis spectrum of **PVBpy$^{50/50}$** therefore

demonstrates the successful incorporation of Re and Ru centers into the PVBpy polymer, and the missing band at 568 nm confirms the complete removal of Ru(dmb)$_2$Cl$_2$ (Figure 1A).

UV−vis measurements were further employed for the qualitative comparison of the Re(I)/Ru(II) ratios of the photocatalysts (Figure 1B). Normalization of the UV−vis spectra to the MLCT transition of the Ru moieties allows the evaluation of the respective Re loading in each sample. Figure 1B clearly demonstrates a correlation of the intensity of the MLCT (Re) transition (λ_{max} = 372 nm) with the rhenium amount incorporated into the respective PVBpy sample, validating the synthetic approach toward different Re(I)/Ru(II) ratios. Besides UV−vis spectroscopy, also photoluminescence as well as IR spectra further confirmed the successful incorporation of Re and Ru centers into the polymers (for photoluminescence (PL) and IR spectra, see the Supporting information, Figures S23 and S24). IR spectra of the polymeric metal complexes after loading with Re-(CO)$_5$Cl revealed the characteristic Re-CO signals (in phase a′(1) (ν = 2015 cm^{-1}), antisymmetric a″ (ν = 1908 cm^{-1}), and out-of-phase symmetric a″(2) (ν = 1873 cm^{-1})). Further, attachment of ruthenium units was confirmed via IR spectroscopy by the relative decrease of the carbonyl stretches compared to the stretching of the bipyridine ligands observable at ν = 1616 cm^{-1} (I_{CO}/I_{Bpy} (PVBpy^{Re}) = 3.4 vs I_{CO}/I_{Bpy} (PVBpy$^{Re/Ru}$) = 3.0) (Figure S23).[30,31] Photoluminescence spectra of the macromolecular metal complexes upon irradiation at 365 nm are dominated by a strong emission at a wavelength of 639 nm caused by the ruthenium centers (Figure S24).[30] Emission of the Re units at 614 nm is negligibly small due to a low quantum yield of rhenium bipyridine complexes.[16] Additionally, the emission of the rhenium center is further reduced by the intramolecular energy transfer of the Re(I) centers to the Ru(II) centers. Excitation of the samples at 365 nm leads to an excited state of the Re complexes, which is energetically higher than the ^{3}MLCT (Ru) state, therefore enabling an energy transfer from Re to Ru, effectively decreasing the rhenium-centered emission and increasing the emission of the ruthenium moieties.[14] Overall, the results of the photoluminescence measurements demonstrate that the lowest energy level which is responsible for the observed luminescence is located at the ruthenium moieties of the polymers.

Quantification of the metal loadings of the polymers via ICP-MS analysis revealed a nonquantitative attachment of the Re and Ru centers in the desired ratios (Table 2; for calculations, see the Supporting information, eqs 1−11).

As indicated by the ICP-MS results presented in Table 2, total loadings of PVBpy between 13.8 and 41.4% were
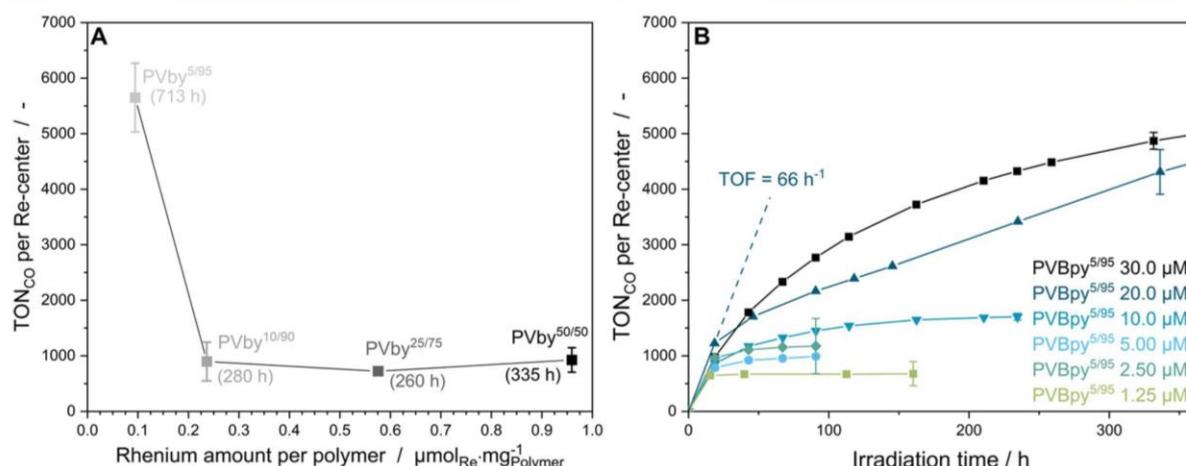
Figure 2. Photocatalytic experiments for (A) different macromolecular photocatalysts with varying rhenium loadings at a rhenium concentration of 20 μM (irradiation times corresponding to the reported TONs are denoted in brackets) and (B) **PVBpy$^{5/95}$** with different catalyst concentrations. The catalyst-containing, CO_2-saturated (15 min) DMF solution with BIH ([BIH]/[Re] = 10 000) and TEOA (1.72 M) was irradiated at λ = 520 nm.

generated applying the two-step approach introduced in this work. Samples with lower theoretical rhenium loadings (**PVBpy$^{5/95}$** and **PVBpy$^{10/90}$**) exhibit an overall metal content below 15% referred to the number of VBpy repetition units available for metal complexation. However, increasing the amount of Re(CO)$_5$Cl applied in the first step of the synthesis resulted in an increase of the total metal loading after the subsequent ruthenium loading with the respective calculated amounts of Ru(dmb)$_2$Cl$_2$. In this context, photocatalyst **PVBpy$^{50/50}$** revealed a total metal loading of 41%, significantly exceeding the metal contents of **PVBpy$^{5/95}$** and **PVBpy$^{10/90}$**. Whereas complexation of the Re-precursor Re(CO)$_5$Cl occurs to a large extent considering the targeted values, the values for ruthenium fall below the expected loading. This can be attributed to the steric demand of Ru(dmb)$_2$Cl$_2$ leading to a high steric crowding on the polymer chains on the one hand, and in case of highly rhenium-loaded polymers, a repulsion from polymer-bound Re units on the other hand. Additionally, electrostatic repulsion due to the cationic charges of the [Ru(dmb)$_3$]$^{2+}$ moieties could hinder the complexation of further ruthenium centers. Besides the mentioned metal−metal interactions, also the polymer secondary structure, i.e., coiling of the polymer chains, could interfere with the loading process of the polymers. Despite the application of a slight excess of the ruthenium precursor complex Ru(dmb)$_2$Cl$_2$, similar ruthenium loadings (7−12%) were found for all photocatalysts, hence suggesting that the ruthenium complexation step is limiting regarding the overall metal loading of PVBpy. Generally, however, the ICP-MS results demonstrate a slightly higher total ruthenium loading in polymers with low rhenium loadings, which represents the expected trend as more empty coordination sites are available for Ru complexation in polymers with low initial Re loading. The similar amounts of ruthenium centers despite varying rhenium loadings are reflected in the different Re(I)/Ru(II) ratios significantly increasing from **PVBpy$^{5/95}$** to **PVBpy$^{50/50}$**. These ratios become particularly important in photocatalytic experiments as the Re(I)/Ru(II) ratio displays the ratio of the photocatalyst to the photosensitizer, which are the two main components affecting the photostability and efficiency of the catalytic

system. In summary, all macromolecular photocatalysts are considered to be statistical copolymers composed of empty bipyridine units, Re moieties, and Ru sites. As opposed to conventional, rather tedious electropolymerization,[32,33] the presented polymerization procedure with subsequent two-step metal loading toward multinuclear metal complexes combines the simple synthesis of the catalysts with the facile adjustment of the Re(I)/Ru(II) ratio.

■ PHOTOCATALYTIC CO$_2$-CONVERSION

First, the rhenium−ruthenium-loaded polymers **PVBpy$^{5/95}$**, **PVBpy$^{10/90}$**, **PVBpy$^{25/75}$**, and **PVBpy$^{50/50}$** were tested for the reduction of CO$_2$ in photocatalytic experiments upon irradiation at 520 nm to evaluate the effect of different catalyst loadings. The irradiation setup consisted of eight green light-emitting diodes (LEDs) of the type LXZ1-PM01 from *Lumileds*, supplied by roughly 23 V and 60 mA with a radiometric power of 100 mW per LED. The reaction flasks containing pressurized, CO$_2$-saturated solutions of the photo-catalytically active substances in *N,N*-dimethylformamide were placed at a distance of 10 cm to the light source. Triethanolamine (TEOA) was added as a base and 1,3-dimethyl-2-phenyl-2,3-dihydro-1*H*-benzo[*d*]imidazole (BIH) ([BIH]/[Re] = 10 000) was applied as sacrificial electron donor due to its strong reduction potential and the inertness of the formed oxidation products.[34,35] In the irradiation experiments, all photocatalysts showed catalytic activity toward the conversion of CO$_2$ to CO (Figure 2A). Control experiments confirmed that CO evolution originates from the reported reaction cycle for photocatalytic reduction of CO$_2$ (Supporting information, Figure S26 and Table S4).[8] Gas chromatographic measurements during irradiation of the polymeric photo-catalysts using a thermal conductivity detector revealed the exclusive formation of CO without the detection of side products. Furthermore, NMR spectroscopic investigations of the reaction mixture did not indicate the formation of soluble side products during CO$_2$ reduction. A more detailed analysis of the gas-phase composition during the initial period of irradiation using a gas chromatograph equipped with a

reduction gas detector revealed the formation of traces of hydrogen. However, this detection technique could not be applied during routine gas chromatographic measurements due to the risk of destruction of the detector by the high amounts of CO formed. Compared to the supramolecular photocatalysts with a fixed stoichiometry defined by their molecular structure introduced by Rieger et al.[16] and Ishitani et al.,[7,36] the loaded polymers contain a much higher number of metal centers per molecule. Besides that, the herein established approach allows for a facile modification of the Re(I)/Ru(II) ratio upon catalyst synthesis. The rhenium catalyst concentration was adjusted to 20.0 μM based on the ICP-MS results shown in the Supporting information, Table S2, to facilitate a comparison of the effects of inter- and intramolecular Re(I)−Re(I) interactions, as those are known to be beneficial for the photocatalytic performance.[4]

The results presented in Figure 2A reveal increased photostabilities at low rhenium loadings with the turnover number of PVBpy$^{5/95}$ (TON = 5650) competing with the TON per rhenium center values of literature-known benchmark catalysts (TON = 6038).[36] In this context, common turnover numbers for the photocatalytic reduction of CO_2 with supramolecular rhenium−ruthenium catalysts and BIH as the sacrificial electron donor range from values between 100 and the mid-1000s.[9,37] Despite the apparent contradiction to the previously stated beneficial effect of Re(I)−Re(I) interactions,[4] the trend of PVBpy$^{5/95}$ exhibiting the highest turnover numbers can be most likely attributed to the stabilizing effect of Ru(II) photosensitizing units in the catalyst system.[38] In this respect, high concentrations of ruthenium moieties in photocatalytic systems protect the catalytic sites as well as other Ru(II) centers from deactivation of the OERS by overexcitation, as will be discussed in more detail later.[3,38,39] Additionally, PVBpy$^{5/95}$ exhibits the highest Ru(II)/Re(I) ratio (see Table 2), which increases the probability of a close proximity between a catalytic reduction site and photosensitizers. All catalysts have long lifetimes of over seven days, and in the case of PVBpy$^{5/95}$, the catalyst showed activity even after 30 days of irradiation (see the Supporting information, Figure S25). This catalyst lifetime is most likely due to the high amount of ruthenium photosensitizer in this macromolecular complex. In this context, losses of the photosensitizer due to light-induced deactivation reactions of the Ru(II)-OERS, which are generally considered the main route for catalyst degradation, are compensated by the high number of ruthenium centers in such systems.[3,15] Another contribution to the increased photostability of polymers with a high Ru(II)/Re(I) ratio, such as PVBpy$^{5/95}$, is the aforementioned elevated probability of spatial proximity between a photocatalytically active rhenium center and photosensitizing ruthenium units. This potential neighborhood enables an efficient electron transfer from the Ru(II)-OERS to the Re(I)-complexes, which is reflected in the high photostability (TON = 5650) and the long lifetime (30 days) of the catalyst. In photocatalysts with high Ru(II)/Re(I) ratios, excitation and reductive quenching by the electron donor accompanied by the formation of the Ru(II)-OERS occurs in large quantities. As a result of the subsequent electron transfer, also the Re(I)-OERS capable of entering the catalytic cycle of CO_2 reduction is formed in high amounts. As this becomes the main route of the overall process, the occurrence of side reactions, such as radical deactivation and overexcitation of the Re(I)-OERS, is significantly reduced.[3] In general, a good correlation between

the photostability, expressed as the turnover number, and the catalytic activity, expressed as the initial turnover frequency, was received (see the Supporting information, Table S3). Fast initial CO_2 conversion was observed in systems with high Ru(II)/Re(I) ratios, such as PVBpy$^{5/95}$ ($R_{Ru(II)/Re(I)}$ = 4.07, TOF = 66 h^{-1}), as excitation of the ruthenium photosensitizers occurs to a large extent and thus, the formed Ru(II)-OERS are able to provide the rhenium centers with electrons in high quantities. In comparison, PVBPy$^{50/50}$, exhibiting a significantly lower Ru(II)/Re(I) ratio ($R_{Ru(II)/Re(I)}$ = 0.21), showed a decreased turnover frequency of 4.2 h^{-1}. Besides intramolecular interactions of the ruthenium and rhenium units due to covalent linkage, also an intermolecular contribution of the electron transfer from Ru(II)-OERS to rhenium centers is expectable. To elucidate the role of intermolecular interactions, the best performing system PVBpy$^{5/95}$ was tested for the photocatalytic reduction of CO_2 in different concentrations (Figure 2B). In this context, catalyst solutions with concentrations ranging from 30.0 μM to 1.25 μM (see the Supporting information, Table S3 for concentrations) were irradiated, and the calculated turnover numbers were plotted against the reaction time (Figure 2B). Good photostabilities were obtained at high concentrations of the macromolecular complex (c_{Re} = 20.0 μM and c_{Re} = 30.0 μM). However, no significant increase of the turnover number upon further increase of the catalyst concentration was observable. On the one hand, this could be explained by the CO_2 reduction as the rate-limiting step of the overall process.[40] On the other hand, this well-known phenomenon can be assigned to the primary inner filter effect. In highly concentrated solutions and at low irradiation intensity, incident light is absorbed to a large extent by the part of the sample facing the light source.[41] In the context of photocatalysis, this inner filter effect leads to consistent photocatalytic results without further improvement above a certain catalyst concentration,[4] as only a partial excitation of all metal centers in the solution takes place.[42] In other words, this causes a limitation of the number of excited Ru(II) centers regardless of their overall concentration, and as a consequence of the electron transfer from Ru(II)-OERS to the rhenium catalyst units, a threshold of the CO_2 reduction is reached. In the low-concentration regime (c_{Re} <20.0 μM), the TONs significantly dropped to values below 1000. First, this can be attributed to a more pronounced degradation of the catalytic sites as well as the photosensitizers, which both are present in lower amounts due to overexcitation and other side reactions by excess irradiation.[3,15] Second, this could be a hint toward a decreasing contribution of intermolecular interactions involved in the two-electron reduction upon dilution. Despite the high amount of potential interaction partners of the metal centers along the polymer chain, intermolecular electron transfer between the polymer chains could likely assume a role for the photocatalytic reduction. To evaluate the impact of intermolecular interactions, initial turnover frequencies for all investigated catalyst concentrations of PVBPy$^{5/95}$ are considered, as catalyst decomposition should be less pronounced within the first hours of irradiation. All five concentrations of PVBPy$^{5/95}$ (c_{Re} = 30.0−1.25 μM) exhibit similar initial turnover frequencies (Figure 2B). This might be attributed to a comparably efficient, intramolecular electron transfer between the covalently linked ruthenium and rhenium centers because of the fixed catalyst composition, as the comparison of the various tested catalysts (Figure 2A) indicated a strong correlation between the Ru(II)/Re(I) ratio and the TOF. The

comparable initial TOFs among the investigated concentrations indicate a secondary role of the intermolecular interactions regardless of the applied catalyst amount. At elevated reaction times, a decrease of the turnover frequency was observed for all concentrations; however, this trend is more pronounced for the low polymer concentrations. In these cases, the total ruthenium content in solution is smaller, leading to lower total absorption, a weaker inner filter effect, and, therefore, exposing the ruthenium units to more light.[4] As a consequence, the ruthenium moieties are more prone to side reactions, such as overexcitation,[3] effectively decreasing their amount, which cannot be compensated as well in dilute systems due to the low initial ruthenium concentration.

CONCLUSIONS

Herein, the first catalytic polymerization of the extended Michael-type monomer 4′-vinyl-4-methyl-2,2′-bipyridine facilitated by different aluminum−phosphorus Lewis pairs is presented. A broad screening of the Lewis acids and bases used for the polymerization regarding achievable conversion, polydispersity, and initiator efficiency was performed, revealing the combination of tri-iso-butyl aluminum and trimethyl phosphine to show the best results with conversions of up to 80% while exhibiting high initiator efficiencies of 45−51% and maintaining narrow polydispersities below 1.36. End-group analysis revealed the presence of two initiation pathways, conjugate addition and deprotonation, yet precise control of the initiation rates gave access to polymers with monomodal, narrow weight distributions. These well-defined poly(vinyl bipyridine) polymers are amorphous with a thermal decomposition onset of 368 °C and a glass transition at 142 °C. Overall, this catalytic approach toward defined polymers allows the synthesis of tailor-made poly(vinyl bipyridines). This features advantages such as adjustable properties or block copolymerization with other Michael-type monomers like dialkyl vinyl phosphonates. The prepared poly(vinyl bipyridines), acting as macroligands due to the incorporated bipyridine motif, were subsequently loaded with rhenium and ruthenium centers. In this context, the facile two-step synthesis protocol using the precursor complexes $Re(CO)_5Cl$ and $Ru(dmb)_2Cl_2$ allows for an effortless variation of the Re(I)/Ru(II) ratio. UV−vis-, photoluminescence-, and IR spectroscopy were applied to qualitatively evaluate the metal loading on the polymer ligand, whereas quantification of the metal loading via ICP-MS revealed nonquantitative attachment to the metal centers, most likely due to steric reasons and the secondary structural motifs of the polymers. However, the expected trends in metal loading experiments were observable, and higher total polymer loadings upon optimization of the synthetic approach is a topic of current research. By means of the presented experimental procedure, a statistical copolymer composed of empty bipyridine side groups, rhenium, and ruthenium-loaded sites with a well-characterized Re(I)/Ru(II) ratio was accessible, exhibiting a highly defined structure in terms of polymer chain length and polydispersity. Four different polymeric complexes (**PVBpy**[5/95], **PVBpy**[10/90], **PVBpy**[25/75], and **PVBpy**[50/50]) with varying rhenium to ruthenium loading were prepared, thoroughly characterized, and investigated regarding their activity and stability in the photocatalytic reduction of CO_2 to CO. In this context, **PVBpy**[5/95] revealed particularly high photostabilities and activities (TON = 5650, TOF = 66 h^{-1}), competing with the respective values of literature-known benchmark catalysts.

This was attributed to the high probability of a spatial proximity between a photocatalytically active rhenium center and ruthenium photosensitizers, enabling an efficient electron transfer and decreasing the extent of side reactions. Among the tested catalysts, a correlation of the TON and the TOF according to the Ru(II)/Re(I) ratio of the respective catalyst was observed. Similar initial turnover frequencies of **PVBpy**[5/95] in a concentration study were assigned to the fixed catalyst composition; comparison with the TOFs found for the other catalysts, however, indicated a secondary role of intermolecular contributions to the electron transfer from ruthenium to rhenium. Whereas the positive effect on the photostability at higher concentrations was assigned to the protection of Re(I) centers due to an attenuation of the excitation beam by the increased number of photosensitizing Ru(II) units, the accelerated catalyst decomposition in the low-concentration regime was attributed to the absence of this effect.

In conclusion, aluminum−phosphorus Lewis pair-mediated polymerization has clearly proved to be a promising tool for the synthesis of well-defined poly(vinyl bipyridines). The polymers were successfully used as macromolecular ligands for the synthesis of multinuclear rhenium−ruthenium complexes, yielding well-characterized, polymeric photocatalysts. These catalysts revealed high activities and stabilities in the photocatalytic reduction of CO_2 to CO.

ASSOCIATED CONTENT

Ⓢ Supporting Information

The Supporting Information is available free of charge at https://pubs.acs.org/doi/10.1021/acs.macromol.2c00440.

> General experimental and synthesis/polymerization details, dn/dc-determination, SEC-data, thermal polymer characterization and end-group analysis, photocatalyst synthesis and characterization, as well as photocatalysis and control experiment results (PDF)

AUTHOR INFORMATION

Corresponding Author

Bernhard Rieger − WACKER-Chair of Macromolecular Chemistry, Department of Chemistry, Technical University of Munich, 85748 Garching, Germany; ⓘ orcid.org/0000-0002-0023-884X; Email: rieger@tum.de

Authors

Anton S. Maier − WACKER-Chair of Macromolecular Chemistry, Department of Chemistry, Technical University of Munich, 85748 Garching, Germany

Christopher Thomas − WACKER-Chair of Macromolecular Chemistry, Department of Chemistry, Technical University of Munich, 85748 Garching, Germany

Moritz Kränzlein − WACKER-Chair of Macromolecular Chemistry, Department of Chemistry, Technical University of Munich, 85748 Garching, Germany; ⓘ orcid.org/0000-0001-9851-0735

Thomas M. Pehl − WACKER-Chair of Macromolecular Chemistry, Department of Chemistry, Technical University of Munich, 85748 Garching, Germany

Complete contact information is available at:
https://pubs.acs.org/10.1021/acs.macromol.2c00440

■ ABBREVIATIONS

VBpy, 4-vinyl-4′-methyl-2,2′-bipyridine; PVBpy, poly(4-vinyl-4′-methyl-2,2′-bipyridine); FLP, frustrated Lewis pair; LA, Lewis acid; LB, Lewis base; AlOct$_3$, tri-n-octylaluminum; POct$_3$, tri-n-octylphosphine; SEC, size-exclusion chromatography; DSC, differential scanning calorimetry; TGA, thermogravimetric analysis; BIH, 1,3-dimethyl-2-phenyl-2,3-dihydro-1H-benzo[d]imidazole; TEOA, triethanolamine; OERS, one-electron-reduced species; MLCT, metal-to-ligand charge-transfer; TON, turnover number; TOF, turnover frequency; I.E., initiator efficiency; ESI-MS, electrospray ionization mass spectrometry; ICP-MS, inductively coupled plasma mass spectrometry; dmb, 4,4′-dimethyl-2,2′-bipyridine; LED, light-emitting diode

■ REFERENCES

(1) Hawecker, J.; Lehn, J.-M.; Ziessel, R. Efficient photochemical reduction of CO$_2$ to CO by visible light irradiation of systems containing Re(bipy)(CO)$_3$X or Ru(bipy)$_3$$^{2+}$ −Co^{2+} combinations as homogeneous catalysts. *J. Chem. Soc., Chem. Commun.* **1983**, 536−538.

(2) Lehn, J. M.; Ziessel, R. Photochemical generation of carbon monoxide and hydrogen by reduction of carbon dioxide and water under visible light irradiation. *Proc. Natl. Acad. Sci. U.S.A.* **1982**, 79, 701−704.

(3) Meister, S.; Reithmeier, R. O.; Tschurl, M.; Heiz, U.; Rieger, B. Unraveling Side Reactions in the Photocatalytic Reduction of CO$_2$: Evidence for Light-Induced Deactivation Processes in Homogeneous Photocatalysis. *ChemCatChem* **2015**, 7, 690−697.

(4) Bruckmeier, C.; Lehenmeier, M. W.; Reithmeier, R.; Rieger, B.; Herranz, J.; Kavakli, C. Binuclear rhenium(I) complexes for the photocatalytic reduction of CO2. *Dalton Trans.* **2012**, 41, 5026−5037.

(5) Balzani, V.; Bergamini, G.; Marchioni, F.; Ceroni, P. Ru(II)-bipyridine complexes in supramolecular systems, devices and machines. *Coord. Chem. Rev.* **2006**, 250, 1254−1266.

(6) Juris, A.; Balzani, V.; Barigelletti, F.; Campagna, S.; Belser, P.; Zelewsky, A. von. Ru(II) polypyridine complexes: photophysics, photochemistry, eletrochemistry, and chemiluminescence. *Coord. Chem. Rev.* **1988**, 84, 85−277.

(7) Gholamkhass, B.; Mametsuka, H.; Koike, K.; Tanabe, T.; Furue, M.; Ishitani, O. Architecture of supramolecular metal complexes for photocatalytic CO$_2$ reduction: ruthenium-rhenium bi- and tetranuclear complexes. *Inorg. Chem.* **2005**, 44, 2326−2336.

(8) Kamogawa, K.; Shimoda, Y.; Miyata, K.; Onda, K.; Yamazaki, Y.; Tamaki, Y.; Ishitani, O. Mechanistic study of photocatalytic CO$_2$ reduction using a Ru(ii)-Re(i) supramolecular photocatalyst. *Chem. Sci.* **2021**, 12, 9682−9693.

(9) Tamaki, Y.; Ishitani, O. Supramolecular Photocatalysts for the Reduction of CO$_2$. *ACS Catal.* **2017**, 7, 3394−3409.

(10) Furue, M.; Naiki, M.; Kanematsu, Y.; Kushida, T.; Kamachi, M. Intramolecular energy transfer in covalently linked polypyridine rhenium(I)/ruthenium(II) complexes. *Coord. Chem. Rev.* **1991**, 111, 221−226.

(11) Bian, Z.-Y.; Chi, S.-M.; Li, L.; Fu, W. Conjugation effect of the bridging ligand on the CO$_2$ reduction properties in difunctional photocatalysts. *Dalton Trans.* **2010**, 39, 7884−7887.

(12) Koike, K.; Naito, S.; Sato, S.; Tamaki, Y.; Ishitani, O. Architecture of supramolecular metal complexes for photocatalytic CO$_2$ reduction. *J. Photochem. and Photobiol.* **2009**, 207, 109−114.

(13) Takeda, H.; Ishitani, O. Development of efficient photocatalytic systems for CO$_2$ reduction using mononuclear and multinuclear metal complexes based on mechanistic studies. *Coord. Chem. Rev.* **2010**, 254, 346−354.

(14) Bian, Z.-Y.; Sumi, K.; Furue, M.; Sato, S.; Koike, K.; Ishitani, O. Synthesis and properties of a novel tripodal bipyridyl ligand tb-carbinol and its Ru(II)-Re(I) trimetallic complexes: investigation of multimetallic artificial systems for photocatalytic CO$_2$ reduction. *Dalton Trans.* **2009**, 983−993.

(15) Umemoto, A.; Yamazaki, Y.; Saito, D.; Tamaki, Y.; Ishitani, O. Synthesis of a Novel Re(I)-Ru(II)-Re(I) Trinuclear Complex as an Effective Photocatalyst for CO$_2$ Reduction. *BCSJ* **2020**, 93, 127−137.

(16) Meister, S.; Reithmeier, R. O.; Ogrodnik, A.; Rieger, B. Bridging Efficiency within Multinuclear Homogeneous Catalysts in the Photocatalytic Reduction of Carbon Dioxide. *ChemCatChem* **2015**, 7, 3562−3569.

(17) Kamata, R.; Kumagai, H.; Yamazaki, Y.; Sahara, G.; Ishitani, O. Photoelectrochemical CO2 Reduction Using a Ru(II)-Re(I) Supramolecular Photocatalyst Connected to a Vinyl Polymer on a NiO Electrode. *ACS Appl. Mater. Interfaces* **2019**, 11, 5632−5641.

(18) Schubert, U. S.; Eschbaumer, C. Macromolecules Containing Bipyridine and Terpyridine Metal Complexes: Towards Metallosupramolecular Polymers. *Angew. Chem., Int. Ed.* **2002**, 41, 2892−2926.

(19) Adams, F.; Pschenitza, M.; Rieger, B. Yttrium-Catalyzed Synthesis of Bipyridine-Functionalized AB-Block Copolymers: Micellar Support for Photocatalytic Active Rhenium-Complexes. *ChemCatChem* **2018**, 10, 4309−4316.

(20) Pitt, C. G.; Bao, Y.; Seltzman, H. H. The synthesis of polymers containing the 2,2′-bipyridine ligand. *J. Polym. Sci., Part C: Polym. Lett.* **1986**, 24, 13−16.

(21) Sumi, K.; Furue, M.; Nozakura, S.-I. Preparation and luminescence properties of tris(bipyridine) ruthenium(II)-containing vinyl polymers: Ru(bpy)$_2$ (poly-6-vinyl-2,2′-bipyridine)Cl$_2$ and Ru-(bpy)$_2$(poly-4-methyl-4′-vinyl-,2,2′-bipyridine)Cl$_2$. *J. Polym. Sci. Polym. Chem. Ed.* **1984**, 22, 3779−3788.

(22) Pefkianakis, E. K.; Tzanetos, N. P.; Kallitsis, J. K. Synthesis and Characterization of a Novel Vinyl-2,2′-bipyridine Monomer and Its Homopolymeric/Copolymeric Metal Complexes. *Chem. Mater.* **2008**, 20, 6254−6262.

(23) Gould, S.; Strouse, G. F.; Meyer, T. J.; Sullivan, B. P. Formation of thin polymeric films by electropolymerization. Reduction of metal complexes containing bromomethyl-substituted derivatives of 2,2′-bipyridine. *Inorg. Chem.* **1991**, 30, 2942−2949.

(24) Elliott, C. M.; Baldy, C. J.; Nuwaysir, L. M.; Wilkins, C. L. Electrochemical polymerization of 4-methyl-4′-vinyl-2,2′-bipyridine-containing metal complexes: polymer structure and mechanism of formation. *Inorg. Chem.* **1990**, 29, 389−392.

(25) Lowry, T. M. Valence and the structure of atoms and molecules. By Prof. G. N. Lewis. Pp. 172. American Chemical Monograph Series. New York: The Chemical Catalog Co., Inc., 1923. Price $3. *J. Chem. Technol. Biotechnol.* **1924**, *43*, 17.

(26) McCahill, J. S. J.; Welch, G. C.; Stephan, D. W. Reactivity of "Frustrated Lewis Pairs": Three-Component Reactions of Phosphines, a Borane, and Olefins. *Angew. Chem.* **2007**, *119*, 5056−5059.

(27) Zhang, Y.; Miyake, G. M.; Chen, E. Y.-X. Alane-Based Classical and Frustrated Lewis Pairs in Polymer Synthesis: Rapid Polymerization of MMA and Naturally Renewable Methylene Butyrolactones into High-Molecular-Weight Polymers. *Angew. Chem.* **2010**, *122*, 10356−10360.

(28) He, J.; Zhang, Y.; Chen, E. Synthesis of Pyridine- and 2-Oxazoline-Functionalized Vinyl Polymers by Alane-Based Frustrated Lewis Pairs. *Synlett* **2014**, *25*, 1534−1538.

(29) Knaus, M. G. M.; Giuman, M. M.; Pöthig, A.; Rieger, B. End of Frustration: Catalytic Precision Polymerization with Highly Interacting Lewis Pairs. *J. Am. Chem. Soc.* **2016**, *138*, 7776−7781.

(30) Bian, Z.-Y.; Wang, H.; Fu, W.-F.; Li, L.; Ding, A.-Z. Two bifunctional RuII/ReI photocatalysts for CO_2 reduction: A spectroscopic, photocatalytic, and computational study. *Polyhedron* **2012**, *32*, 78−85.

(31) Castellucci, E.; Angeloni, L.; Neto, N.; Sbrana, G. IR and Raman spectra of A 2,2′-bipyridine single crystal: internal modes. *Chem. Phys.* **1979**, *43*, 365−373.

(32) Portenkirchner, E.; Gasiorowski, J.; Oppelt, K.; Schlager, S.; Schwarzinger, C.; Neugebauer, H.; Knör, G.; Sariciftci, N. S. Electrocatalytic Reduction of Carbon Dioxide to Carbon Monoxide by a Polymerized Film of an Alkynyl-Substituted Rhenium(I) Complex. *ChemCatChem* **2013**, *5*, 1790−1796.

(33) Orchanian, N. M.; Hong, L. E.; Skrainka, J. A.; Esterhuizen, J. A.; Popov, D. A.; Marinescu, S. C. Surface-Immobilized Conjugated Polymers Incorporating Rhenium Bipyridine Motifs for Electrocatalytic and Photocatalytic CO_2 Reduction. *ACS Appl. Energy Mater.* **2019**, *2*, 110−123.

(34) Tamaki, Y.; Koike, K.; Ishitani, O. Highly efficient, selective, and durable photocatalytic system for CO_2 reduction to formic acid. *Chem. Sci.* **2015**, *6*, 7213−7221. Published Online: Sep. 29, 2015.

(35) Tamaki, Y.; Koike, K.; Morimoto, T.; Ishitani, O. Substantial improvement in the efficiency and durability of a photocatalyst for carbon dioxide reduction using a benzoimidazole derivative as an electron donor. *J. Catal.* **2013**, *304*, 22−28.

(36) Cancelliere, A. M.; Puntoriero, F.; Serroni, S.; Campagna, S.; Tamaki, Y.; Saito, D.; Ishitani, O. Efficient trinuclear Ru(ii)-Re(i) supramolecular photocatalysts for CO_2 reduction based on a new trischelating bridging ligand built around a central aromatic ring. *Chem. Sci.* **2020**, *11*, 1556−1563.

(37) Kuramochi, Y.; Ishitani, O.; Ishida, H. Reaction mechanisms of catalytic photochemical CO2 reduction using Re(I) and Ru(II) complexes. *Coord. Chem. Rev.* **2018**, *373*, 333−356.

(38) Stanley, P. M.; Thomas, C.; Thyrhaug, E.; Urstoeger, A.; Schuster, M.; Hauer, J.; Rieger, B.; Warnan, J.; Fischer, R. A. Entrapped Molecular Photocatalyst and Photosensitizer in Metal−Organic Framework Nanoreactors for Enhanced Solar CO_2 Reduction. *ACS Catal.* **2021**, *11*, 871−882.

(39) Ghosh, A. C.; Legrand, A.; Rajapaksha, R.; Craig, G. A.; Sassoye, C.; Balázs, G.; Farrusseng, D.; Furukawa, S.; Canivet, J.; Wisser, F. M. Rhodium-Based Metal-Organic Polyhedra Assemblies for Selective CO2 Photoreduction. *J. Am. Chem. Soc.* **2022**, *144*, 3626−3636.

(40) Yamazaki, Y.; Ohkubo, K.; Saito, D.; Yatsu, T.; Tamaki, Y.; Tanaka, S.'I.; Koike, K.; Onda, K.; Ishitani, O. Kinetics and Mechanism of Intramolecular Electron Transfer in Ru(II)-Re(I) Supramolecular CO2-Reduction Photocatalysts: Effects of Bridging Ligands. *Inorg. Chem.* **2019**, *58*, 11480−11492.

(41) Kubista, M.; Sjöback, R.; Eriksson, S.; Albinsson, B. Experimental correction for the inner-filter effect in fluorescence spectra. *Analyst* **1994**, *119*, 417−419.

(42) Kumar Panigrahi, S.; Kumar Mishra, A. Inner filter effect in fluorescence spectroscopy: As a problem and as a solution. *J. Photochem. Photobiol., C* **2019**, *41*, No. 100318.

6. Biobased monomers for polyester synthesis

Polyester synthesis based on 3-carene as renewable feedstock

6.1. Bibliographic data

Title: "Polyester synthesis based on 3-carene as renewable feedstock"

Status: Paper, Publication Date: 03.06.2022

Journal: Polymer Chemistry

Publisher: Royal Society of Chemistry (RSC)

DOI: 10.1039/d2py00409g

Authors: Moritz Kränzlein, Stefanie Pongratz, Jonas Bruckmoser, Brigita Bratić, Jonas Martin Breitsameter and Bernhard Rieger [‡]

6.2. Abstract graphic (TOC)
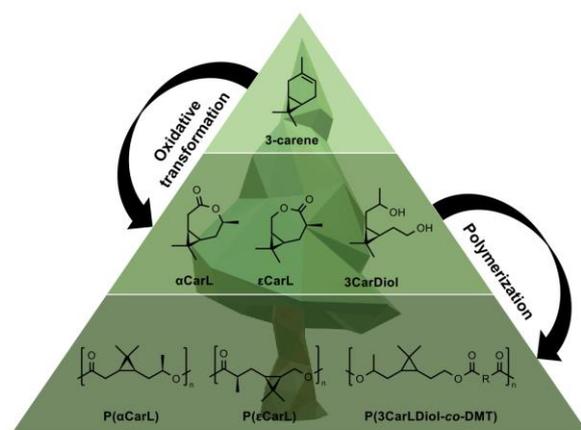
Figure 31: Table of content graphic for the manuscript titled "Polyester synthesis based on 3-carene as renewable feedstock".

6.3. Content

With the continuous depletion of fossil fuels, the search for feedstock substitution remains a major challenge for modern polymer chemistry. By introducing new monomers, polymer materials with certain application profiles can be synthesized, making it a suiting method to satisfy the requirements such polymers meet. In theory, a plethora of different feedstocks exist, yet there are certain requirements concerning the material properties. Especially with focus on sustainability as major requirement for modern-day polymer materials, polyesters offer the possibility to not only be prepared from biogenic resources but at the same time being (bio-)degradable. One class of feedstocks heavily investigated are the terpenes, as they offer high abundance paired with cheap pricing and not competing with crop-space. There are several approaches to utilize different terpenes and terpene-based molecules as new monomers for polyester synthesis. Yet, most polyesters prepared from terpenes as biobased feedstocks remain amorphous materials with low glass transition temperatures (*vide supra*), making them inappropriate for certain applications like packaging. In a recent report by Syrén *et al.* a polyester based on α-pinene was presented, in which the 4-membered ring from the terpenes basic carbon skeleton was incorporated into the polymer main chain, giving access to a semi-crystalline polyester with a melting point at 158 °C.[139] A similar approach is tested for 3-carene as terpene from turpentine oil, in which the 3-membered ring of the carbon skeleton is preserved throughout the chemical transformations towards suiting monomers. By means of reductive ozonolysis, a diol for an AA/BB polycondensation is prepared. Using different oxidative transformations and a *Baeyer-Villiger* oxidation as key step, 3-carene is converted to two regioisomeric lactones. All of these monomers still bear the 3-membered ring from the 3-carene framework. The diol is used in a polycondensation with dimethyl terephthalate as comonomer, while the two lactones were successfully homo- and copolymerized *via* catalytic ring-opening polymerization. From the four different polyesters prepared, three are amorphous with glass transitions between -12 – 45 °C and one is semi-crystalline with a melting point at 160 °C. Overall, the incorporation of cyclic systems into the main chains of the polymers seems to be a promising tool to generate semi-crystalline polyesters.[330]

6.4.   Manuscript
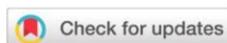
PAPER

Check for updates

Polyester synthesis based on 3-carene as renewable feedstock†

Moritz Kränzlein, [ID] ‡ Stefanie Pongratz, [ID] ‡ Jonas Bruckmoser, Brigita Bratić, [ID] Jonas Martin Breitsameter [ID] and Bernhard Rieger [ID] *

Utilizing renewable feedstocks for the synthesis of biobased and preferrable biodegradable polyesters as substitute for fossil-based polymers remains one of the major challenges towards a sustainable polymer economy. One such feedstock is turpentine oil, a byproduct from pulp industry which is additionally not competing to crop space. While two of the three main turpentine components found in wood, α-pinene and β-pinene could already be transformed to polyesters, 3-carene as third main component remains so far unexamined. Using a multi-step oxidative transformation involving hydroboration, oxidation and Baeyer–Villiger oxidation for obtaining 3-carene based lactones, two different regioisomers, α-carenelactone (αCarL) and ε-carenelactone (εCarL), could successfully be isolated. Both monomers and a mixture thereof were successfully polymerized using different metalorganic catalysts, yielding two amorphous and one semi-crystalline polyester. Additionally, 3-carene is subject to reductive ozonolysis, providing 3-carene diol (3CarDiol) which could be copolymerized with dimethyl terephthalate to obtain a polyester as well. All polyesters were examined using thermogravimetric analysis and differential scanning calorimetry, revealing glass transition temperatures between −15 to 50 °C and a melting point of up to 170 °C, making these polymers highly promising candidates for further research.

Introduction

As we observe continuous depletion of fossil fuels, the main monomer source focus is shifting towards polymers based on biogenic resources, coupled with an ever-increasing demand for commodity plastics.[1–3] While a plethora of different feedstocks for the synthesis of monomers is available in nature, exploiting this kind of sources remains difficult to some extent.[3–11] Not only do we have certain demands regarding material properties, we also are looking for abundant and easy to transform resources which offer sustainability in both generation of the polymers as well as their degradation.[8,12,13] In general, bio-based polymers can be produced from various sources such as acids, sugars or different terpenes and terpenoids.[3–7,11,14–16] However, pricing of those products usually remains a main hinderance for such materials to become substitutes for commodity polymers.[3,10,17] Another evident disadvantage one has to consider when looking for bio-based monomer sources is the use of crop space for culti-

vation of biomass being transformed to materials rather than food.[18–21]

One feedstock overcoming those problems might be turpentine oil, as it is a waste product mainly from pulp production with an annual production volume of about 300–350 kt/a. With a roughly estimated 3-carene fraction of between 12 to 56 kt/a, its availability is in the same range as other terpenes commonly used for polymer synthesis such as limonene or menthol.[10,19–25] This makes turpentine oil and 3-carene a comparably cheap and abundant source of compounds which could be exploited as monomer feedstock, if suiting transformations can be found.[3,21,22,25] Generally, α-pinene is the most abundant terpene found in turpentine oil with varying contents of 40–87 wt%. The content of β-pinene and 3-carene as second and third most compounds however vary strongly depending on the source of the turpentine oil with β-pinene ranging between 1–35 wt% and 3-carene ranging from 1–30 wt% (Table 1), making 3-carene another interesting feedstock besides α-pinene and β-pinene.[9,21,22,25–32]

As shown in Scheme 1, different pathways towards polymers based on turpentine have been developed.[7,9,21,25,30–34] Using different chemical transformations, usually oxidations towards the ketones, the lactams for those three terpenes are accessible *via* ring-expansion by Beckmann rearrangement.[30,34] Using anionic ring-opening polymerization (aROP) those lactams can be converted to the respective polyamides, which have been

Table 1 Distribution of the three main compounds found in different wood sources, adapted from references[22,26–29]

Compound	Composition (wt%)			
	USA	Indonesia	North. Europe	China
α-Pinene	40–70	73–87	55–70	40–70
β-Pinene	15–35	1–2	2–6	4–15
3-Carene	2–10	7–19	7–30	0–5

described thoroughly in recent years.[30,33–36] A similar pathway can be selected to generate the lactones, involving a Baeyer–Villiger oxidation of ketones, targeting polyester synthesis *via* catalytic ring-opening polymerization (cROP). However, compared to the lactams, the lactones are far from being described entirely, mainly due to difficulties regarding the Baeyer–Villiger oxidation as key step. While this transformation is known for α-pinene,[21,31] already limitations for β-pinene are reported. Here, the Baeyer–Villiger-oxidation involves very long reaction times, suffers from low yields and the obtained lactones are susceptible to cleavage by water or alcohols.[37] Direct utilization of β-pinene based lactones as monomers maintaining the bicyclic terpene structure are not reported so far, only after multi-step transformation of the carbon skeleton it could successfully be transformed to polyesters.[25] Another pathway exploiting the terpenes reactivity for monomer synthesis is the reductive ozonolysis of the terpene double bond to the diol, as reported for α-pinene by Syrén *et al.*, using it as bifunctional monomer for polycondensation with different dicarboxylic acids.[31] However, there remains a gap, as none of these pathways have been applied to 3-carene, which can, in principle, undergo the same transformations as α-pinene. The main difference of those molecules as starting material is the 4-membered ring in the terpenes bicyclic structure for α-pinene and β-pinene, compared to a 3-membered ring for 3-carene. Herein, we close this gap by accessing (co)polyesters based on the lactone and the diol originating from 3-carene *via* catalytic ring-opening polymerization and polycondensation, yielding materials with varying thermal properties.

Results and discussion

For converting 3-carene to monomers, two different pathways are employed. For the synthesis of lactones, the terpene structure of 3-carene is converted to a terpenoid in a two-step oxidation sequence. By applying a procedure by Suzuki *et al.*, 3-carene is converted to 4-iso-caranol by hydroboration with borane in tetrahydrofuran and subsequently oxidized to 4-iso-caranon with an ether-chromic acid procedure (Scheme 2, steps (a) and (b)).[38] For the ring-expansion *via* Baeyer–Villiger oxidation, different procedures have been investigated, but a solvent-free oxidation with *m*CPBA reported by Lochynski *et al.* (Scheme 2, step (c)) has shown the best results.[39] This reaction yielded two regioisomeric and stereoregular lactones, ε-carene-lactone (εCarL) and α-carenelactone (αCarL) in a 2 : 1 ratio. Using column chromatography, the lactones were separated yielding three different fractions, pure αCarL and εCarL and a 60 : 40 mixture of εCarL and αCarL. Overall, the synthesis route still suffers from the use of toxic chemicals and overall moderate yields, especially in the Baeyer–Villiger oxidation. Additionally, while all other reactions could be performed on a multi-gram scale, the Baeyer–Villiger oxidation itself is limited to the presented scale due to side products, heat transfer and separation issues. To address these issues, different monomer synthesis approaches should be investigated. Nevertheless, monomer grade lactones could be isolated. For the synthesis of 3-carene diol (3CarDiol) *via* reductive ozonolysis (Scheme 2, step (d)), a procedure by Tolstikov *et al.* for α-pinene was utilized, yielding the cyclopropane derivative which is used for polycondensation.[40]

The polyester synthesis *via* ring-opening polymerization is tested for αCarL and εCarL separately and the mixture of both monomers using four catalytic systems under different conditions (Scheme 2, right pathway). As catalysts tin(ɪɪ) 2-ethyl-hexanoate (Sn(Oct)$_2$), titanium iso-propoxide (Ti(O^{i}Pr)$_4$), a CH-bond activated 2-methoxyethylamino-bis(phenolate) yttrium catalyst [(ONOO)^{tBu}Y(*sym*-col)(thf)] and a salan type indium *tert*-butoxide [(ONNO)^{tBu}In(O^{t}Bu)] were tested. Polymerizing εCarL with Ti(O^{i}Pr)$_4$ in 200 : 1 ratio, bulk conditions and
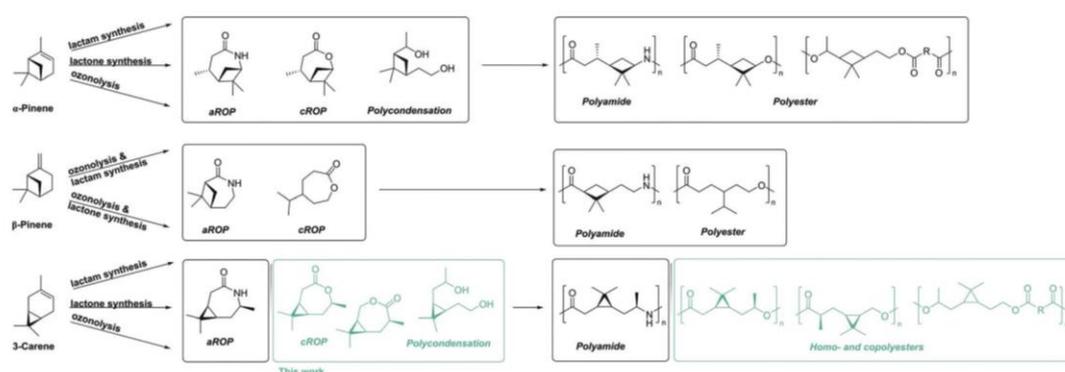
Scheme 1 Pathways from three major terpenes found in wood, α-pinene, β-pinene and 3-carene towards different (co)polyesters *via* catalytic ring-opening polymerization (cROP) or polycondensation and polyamides *via* anionic ring-opening polymerization (aROP).[9,20,21,23,28–32]
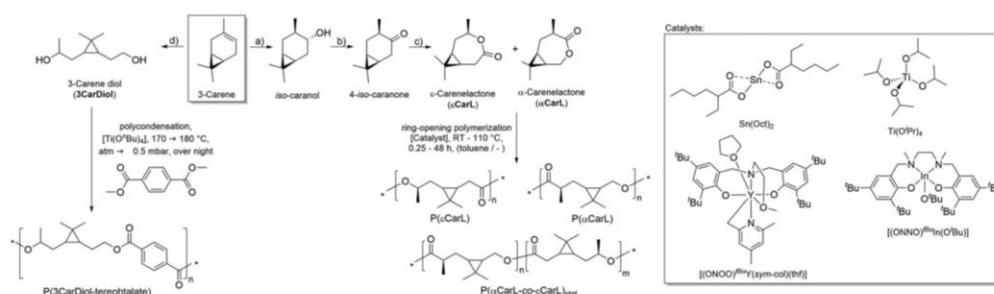
Scheme 2 Synthesis of regioisomeric lactones ε-carenelactone and α-carenelactone *via* hydroboration (a, 94% yield), chromic-etherate oxidation (b, 51% yield) and Baeyer–Villiger oxidation (c, ∑20% yield) for subsequent ring-opening polymerization to P(εCarL), P(αCarL) and P(αCarL-*co*-εCarL)$_{stat}$ using different organometallic catalysts (right pathway) and diol synthesis *via* reductive ozonolysis (d, 61% yield) for polycondensation with dimethyl terephthalate to P(3CarDiol-DMT) (left pathway).[28,36–38]

110 °C were chosen as reaction conditions, yielding a polyester with moderate dispersity ($Đ$ = 1.30, Fig. S18†) and an average molecular weight of 5.1 kg mol^{-1} (Table 2, entry 1). Switching to Sn(Oct)$_2$ in toluene at 110 °C, molecular weights from 3.8–6.1 kg mol^{-1} with moderate dispersity ($Đ$ = 1.23–1.28, Fig. S19 and S20†) were obtained, initiated by residual water (Fig. S37†). However, decreasing the monomer : catalyst ratio from 200 : 1 to 50 : 1 led to increase in molecular weight (Table 2, entries 2 and 3). For both catalysts, full conversion of the monomer was reached, yet high reaction temperatures were required, leading to a higher possibility of side reactions. Switching from those catalysts to more sophisticated metal complexes for ROP, the reaction temperature could be decreased to room temperature. Using a robust indium salan alkoxide catalyst that has shown very high activity in ROP for a range of cyclic esters,[41] full monomer conversion was reached at room temperature within few hours in toluene and dichloromethane in 200 : 1 and 50 : 1 ratios (Table 2, entries 4–6), achieving higher molecular weights ($M_{n,rel}$ = 10.9–12.2 kg mol^{-1}) with narrow dispersity ($Đ$ = 1.16–1.27). Unfortunately, all

polymers prepared with this catalyst suffer from a bimodal molecular weight distribution as observed in SEC (Fig. S21–S23†). To overcome this issue, a yttrium bis(phenolate) catalyst was employed. This catalyst is however not able to fully polymerize the monomer, showing a conversion limitation of 93% for a 100 : 1 ratio decreasing to 70% for a 200 : 1 ratio. While the polymers prepared with this catalyst maintain a monomodal and narrow molecular weight distribution ($Đ$ = 1.16, Fig. S24 and S25†), the overall molecular weight decreased to about 6.3–6.7 kg mol^{-1}, irrespective of the monomer : catalyst ratio (Table 2, entries 7 and 8). The polymerization proceeded *via* nucleophilic attack of the initiator, indicating catalytic polymerization (Fig. S38†).[42,43] Nevertheless, all catalysts were capable of polymerizing εCarL under the tested conditions, yielding defined P(εCarL) for the first time (Fig. 1, left). Shifting to αCarL, the same set of catalysts was applied, however, polymerization with the yttrium and the indium complex failed, most likely due to residual water content of the monomer. While εCarL could be dried over calcium hydride for one week, αCarL showed decomposition after one day,

Table 2 Ring-opening homo- and copolymerization of regioisomeric lactones ε-carenelactone and α-carenelactone using organometallic catalysts

Entry	Monomer[a]	Catalyst	M : Cat[b] [mol : mol]	Solvent[c]	t_{Pol} [h]	T_{Pol} [°C]	X_M[d] [%]	$M_{n,theo}$[e] [kg mol^{-1}]	$M_{n,rel}$[f] [kg mol^{-1}]	$Đ$[f] [–]
1	ε-CarL	Ti(O^{i}Pr)$_4$	200 : 1	—	48	110	99	33.5	5.1	1.30
2	ε-CarL	Sn(Oct)$_2$	200 : 1	Toluene	48	110	99	33.2	3.8	1.28
3	ε-CarL	Sn(Oct)$_2$	50 : 1	Toluene	48	110	99	8.5	6.1	1.23
4	ε-CarL	[(ONNO)^{tBu}In(O^{t}Bu)]	200 : 1	Toluene	0.25	RT	99	33.9	11.5	1.18
5	ε-CarL	[(ONNO)^{tBu}In(O^{t}Bu)]	200 : 1	CH$_2$Cl$_2$	3	RT	99	33.7	10.9	1.16
6	ε-CarL	[(ONNO)^{tBu}In(O^{t}Bu)]	50 : 1	Toluene	2	RT	99	8.6	12.2	1.27
7	ε-CarL	[(ONOO)^{tBu}Y(*sym*-col)(thf)]	200 : 1	Toluene	8	RT	70	23.6	6.3	1.16
8	ε-CarL	[(ONOO)^{tBu}Y(*sym*-col)(thf)]	100 : 1	Toluene	3	RT	93	15.7	6.7	1.16
9	α-CarL	Ti(O^{i}Pr)$_4$	200 : 1	—	48	110	99	33.6	3.5	1.25
10	α-CarL	Sn(Oct)$_2$	200 : 1	Toluene	48	110	66	22.2	3.2	1.15
11	α-CarL	Sn(Oct)$_2$	50 : 1	Toluene	48	110	99	8.4	4.5	1.25
12	α/ε-CarL	Ti(O^{i}Pr)$_4$	200 : 1	—	48	110	90	30.3	5.8	1.23
13	α/ε-CarL	Sn(Oct)$_2$	200 : 1	Toluene	28	110	99	33.6	7.3	1.22

[a] ε-Carenelactone dried over CaH$_2$ for 7 days, α-carenelactone and mixture composed of 60 : 40 ε-CarL : α-CarL dried over CaH$_2$ for 1 day. [b] Monomer-catalyst ratio as weighed, 1.19 mmol of monomer. [c] Reactions performed in bulk or in 0.5 mL of solvent. [d] Conversion of monomer calculated from aliquot ^{1}H NMR (detailed calculation see ESI, Fig. S11 and S12†). [e] Theoretical molecular weight $M_{n,theo}$ = [M : Cat] × X_M × 168.19 g mol^{-1}. [f] Relative molecular weight and polydispersity measured *via* SEC in THF at 30 °C relative to polystyrene.
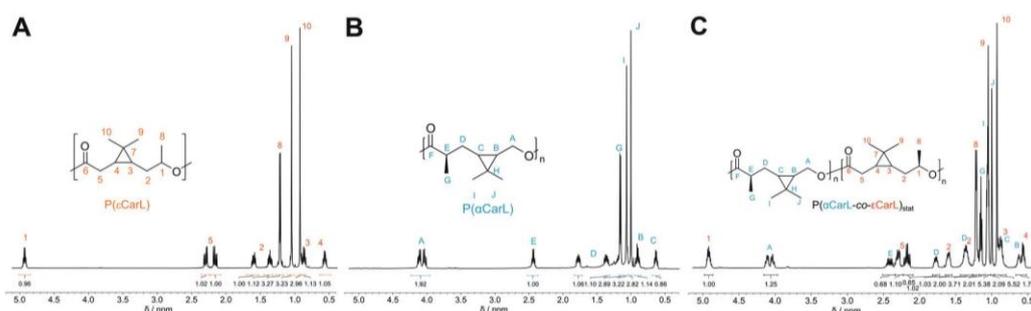
Fig. 1 ^{1}H NMR spectra (500 MHz, CDCl$_3$) of (A) P(εCarL) (Table 2, entry 1), (B) P(αCarL) (Table 2, entry 11) and (C) P(αCarL-*co*-εCarL)$_{\text{stat}}$ (Table 2, entry 13).

leading to shorter drying times. Nevertheless, the more robust catalysts Sn(Oct)$_2$ and Ti(O^{i}Pr)$_4$ were capable of polymerizing αCarL (Table 2, entries 9–11). Under bulk conditions, full conversion was reached in a 200 : 1 ratio but only shorter-chain polymers ($M_{\text{n,rel}}$ = 3.5 kg mol^{-1}, $Đ$ = 1.25, Fig. S26†) could be obtained. Switching to Sn(Oct)$_2$ in toluene, the conversion was limited to 66% for a 200 : 1 ratio, yielding the same short-chain polymers ($M_{\text{n,rel}}$ = 3.2 kg mol^{-1}, $Đ$ = 1.15, Fig. S27†). Lowering the monomer : catalyst ratio to 50 : 1, full conversion could be reached again yet the molecular weight is still limited to about 4.5 kg mol^{-1}, however with moderate dispersity ($Đ$ = 1.25, Fig. S28†). Overall, αCarl was successfully polymerized to defined P(αCarL) as well (Fig. 1, middle). Additionally the mixed fraction containing εCarL and αCarL in a 60 : 40 ratio obtained from column chromatography was dried and polymerized using Ti(O^{i}Pr)$_4$ (in bulk) and Sn(Oct)$_2$ (in solution) (Table 2, entries 12 and 13), obtaining defined copolyesters with moderate molecular weights and narrow dispersities ($M_{\text{n,rel}}$ = 5.8–7.3 kg mol^{-1}; $Đ$ = 1.22–1.23, Fig. S29 and S30†) (Fig. 1, right). Polymerization with the indium and the yttrium catalysts failed due to the shortened drying times of αCarL. Compared to the pure homopolymers, the copolyesters exhibits similar molecular weights and dispersities, indicating a successful copolymerization. SEC revealed a monomodal distribution, further supporting successful copolymerization of αCarL and εCarL. To investigate the copolymers architecture, ^{13}C NMR spectroscopy is applied, revealing four different signals in the carbonyl region (ESI, Fig. S15 and S16†). Two of those four signals correspond to the carbonyls from αCarL/αCarL and εCarL/εCarL linkages as observed in the homopolymers P(αCarL) and P(εCarL). The two additional signals result from the additional linkages combining αCarL/εCarL and εCarL/αCarL, verifying the formation of a statistical copolymer (ESI, Fig. S17†). Summarizing, the regioisomeric lactones αCarL and εCarL as well as a mixture of both monomers could successfully be polymerized to (co)polyesters with moderate molecular weight and mostly narrow dispersity using various catalyst systems.

To further explore the capability of 3-carene to serve as a valuable monomer starting material, the prepared 3-carene diol is used in a polycondensation with dimethyl terephthalate

(DMT) as model compound. DMT was chosen as the resulting polyesters can be directly compared to widely applied poly (ethylene terephthalate) in terms of its thermal properties. Yet, this approach is by no means limited to DMT as dicarboxylic acid and bio-based diacids such as itaconic acid or maleic acid could be utilized.[31] For the polycondensation 1 mol% titanium tetra-*n*-butoxide Ti(O^{n}Bu)$_4$ was employed as catalyst. A pre-condensation of a 2 : 1 mixture of 3CarDiol and DMT without solvent was heated to 170 °C until no more methanol evolution is observed (usually about 6 h) under ambient pressure, forming oligomeric precursor esters. Then the pressure is decreased to 0.5 mbar and the mixture is heated to 180 °C over night. When the first heating step is conducted slowly, a polyester with a molecular weight of 6.4 kg mol^{-1} and a dispersity of 1.5 was obtained (Fig. 2). Changing to rapid heating increased the molecular weight to 12.8 kg mol^{-1}, however, the dispersity increased as well to 2.0 as expected for this kind of polymerization (ESI, Table S1, Fig. S32 and S33†). For the observed limitation of the molecular weight, two main reasons can be distinguished. For such polycondensations with non-volatile compounds, perfect stoichiometry of dicarboxylic acid to diol must be achieved to obtain high molecular weights. However, only small deviations already lead to a drastic
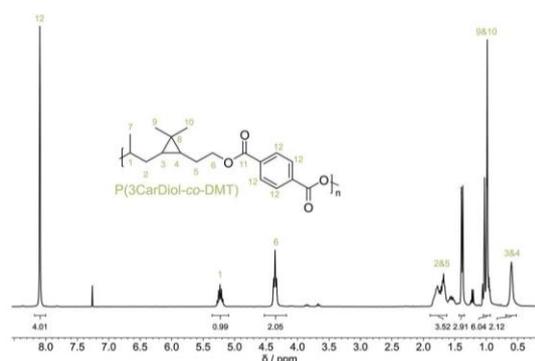
Fig. 2 ^{1}H NMR spectrum (400 MHz, CDCl$_3$) of P(3CarDiol-*co*-DMT) (ESI, Table S1,† entry 1).
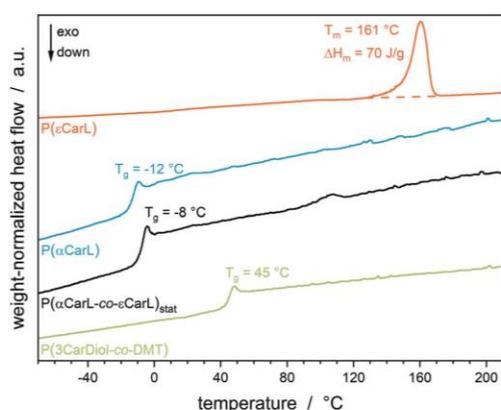
Fig. 3 Differential scanning calorimetry of P(εCarL) (Table 1, entry 1), P(αCarL) (Table 1, entry 9), P(αCarL-*co*-εCarL)$_{stat}$ (Table 1, entry 12) and P(3CarDiol-*co*-DMT) (Table S2,† entry 1).

decrease in the obtainable molecular weights, which might have occurred under the tested conditions. As an additional reason, elimination of the secondary alcohol might occur during heating, leaving an unreactive chain-end. Nevertheless, our polycondensation protocol delivered the polyesters P(3CarDiol-*co*-DMT) with satisfying molecular weight and dispersity.

As such polyesters are commonly found in the engineering plastics area, favourable thermal properties such as high decomposition temperature or high melting points are desired. Therefore, P(εCarL), P(αCarL), P(αCarL-*co*-εCarL)$_{stat}$ and P(3CarDiol-*co*-DMT) are subject to thermogravimetric analysis (ESI, Fig. S36†) and differential scanning calorimetry (Fig. 3). Regarding decomposition temperature, P(αCarL) shows the lowest $T_{5\%}$ with only 188 °C, which can most likely be attributed to the overall lower molecular weight of the polymer. Overall, the differences in the decomposition onset is mostly influenced by the overall polymer chain length and their structural differences.[31] This value is already increased for P(εCarL) with a $T_{5\%}$ of 237 °C, surpassed by the copolymer P(αCarL-*co*-εCarL)$_{stat}$ with 251 °C followed by P(3CarDiol-*co*-DMT) with a $T_{5\%}$ of 312 °C. Overall, the decomposition temperatures are in range of reported similar structures, however do not exhibit remarkably thermal stability.[31] In DSC analysis, both P(αCarL) and P(αCarL-*co*-εCarL)$_{stat}$ show amorphous behaviour with glass transition temperatures of −12 °C and −8 °C, whereas the copolymer of 3CarDiol with DMT shows a T_g of 45 °C. Contrary to our observation for P(αCarL), P(εCarL) is a semi-crystalline polyester with a high melting point of 161 °C (melting enthalpy $\Delta H_m = 70$ J g^{-1}) and no observable glass transition temperature. This polymer performs very similar in terms of thermal transitions to a α-pinene based polymer reported by Syren *et al.* (Scheme 1, top).[31] Powder X-Ray diffraction of P(εCarL) revealed a crystalline fraction of the polymer of 33% (Fig. S34 and S35†). While the semi-crystallinity of those polymers might result either from their stereoregularity

originating from the use of stereoregular monomers, the quite rigid 3- and 4-membered ring within the polyesters backbone, or both, it remains unclear, why P(αCarL) remains amorphous. Possible reasons might be the overall lower molecular weight of the polymer or the different connectivity of the methyl group and the 3-membered ring on the polymer backbone. Overall, the (co)polymers based on 3-carene exhibit both amorphous and semi-crystalline properties, making 3-carene an interesting feedstock material for polyester synthesis.

Experimental

General experimental

4-Iso-caranol,[38] 4-iso-caranone,[30,38] α-carenelactone,[39] ε-carenelactone[39] and 3-carene diol[40] were synthesized according to literature known procedures with slight modification, detailed synthesis procedures and analytics see ESI.† The catalysts Sn(Oct)$_2$, Ti(O^{i}Pr)$_4$ and Ti(O^{n}Bu)$_4$ were purchased by Sigma-Aldrich and distilled prior to use, [(ONOO)^{tBu}Y(*sym*-col)(thf)][31,44] and [(ONNO)^{tBu}In(O^{t}Bu)][41] were prepared according to literature procedures. Monomer batches of αCarL were dried over CaH$_2$ for one day prior to filtration, monomer batches of εCarL were dried for one week prior to filtration, 3CarDiol was used as is from synthesis and after distillation. Additional details on measurement protocols and further characterization of polymers see the ESI.†

Ring-opening polymerization

For the ring-opening polymerization in bulk conditions, 200 mg (1.19 mmol) of the lactone (mixture) are weighed into a crimp vial, the corresponding amount of Ti(O^{i}Pr)$_4$ is added and the sealed vial is heated to 110 °C for 48 hours. For solution polymerizations, 200 mg (1.19 mmol) of the lactone (mixture) are dissolved in 0.5 mL of dry toluene and the respective amount of catalyst (Sn(Oct)$_2$, [(ONOO)^{tBu}Y(*sym*-col) (thf)] or [(ONOO)^{tBu}In(O^{t}Bu)]) are added. The mixture is then stirred at 110 °C (Sn(Oct)$_2$) or room temperature for the indicated time. After polymerization an aliquot for conversion determination is withdrawn and quenched in 0.5 mL wet chloroform-d$_1$ before the mixture is precipitated in 40 mL methanol or water. The residue is dried *in vacuo* at 60 °C over night and analysed using ^{1}H-/^{13}C-NMR, SEC, TGA and DSC.

Polycondensation

For the polycondensation 6.0 g (35.0 mmol, 205 eq.) of 3CarDiol and 3.38 g (17.0 mmol, 100 eq.) dimethyl terephthalate together with 0.06 g (0.2 mmol, 1.0 eq.) Ti(O^{n}Bu)$_4$ are placed in a 100 mL flask. The mixture is stirred with a KPG stirrer and placed in a preheated oil bath with 170 °C under ambient pressure. Once no more methanol is evolving, usually about 6 hours, the pressure is lowered to 0.5 mbar and the temperature is increased to 180 °C over night. The resulting polymer is dissolved in dichloromethane and precipitated from cold methanol two-fold before drying *in vacuo* at 60 °C over night. The polyester was subjected to ^{1}H-/^{13}C-NMR, SEC, TGA and DSC.

Conclusions

This work highlights the opportunities of using renewable, turpentine oil-based terpene 3-carene as base feedstock for polyester synthesis. While the monomer synthesis still relies on the use of toxic chemicals and established protocols, the resulting polyesters are interesting structures making optimization, *e.g.* by use of efficient heterogeneous catalysts for the Baeyer–Villiger oxidation, of this synthesis route compelling.[45] Using different catalysts, εCarL, αCarL and a mixture of both were successfully polymerized for the first time, yielding amorphous and semi-crystalline, high-melting polyesters. To further elucidate the limitations in molecular weight, kinetic measurements and end-group analysis might provide useful insight into the polymerization behaviour. Additionally, the copolymerization should be investigated with regard to copolymerization parameters, possibly facilitating the synthesis of copolyesters with tuneable thermal properties based on a single feedstock. Using P(αCarL) as amorphous middle block and P(εCarL) as semi-crystalline outer blocks *via* sequential copolymerization, advanced structures like thermoplastic elastomers become thinkable.[43] Additionally, another pathway of utilizing 3-carene as base feedstock for polycondensations has been presented, further broadening the applicability of this terpene as monomer source.

Author contributions

M. Kränzlein: conceptualization, funding acquisition, writing – original draft, visualization, data curation, formal analysis; S. Pongratz: writing – review & editing, visualization, data curation, formal analysis; J. Bruckmoser: writing – review & editing, formal analysis; B. Bratić: writing – review & editing, data curation; J. M. Breitsameter: conceptualization, writing – review & editing, visualization, formal analysis; B. Rieger: funding acquisition, supervision, project administration, resources, writing – review & editing.

Conflicts of interest

There are no conflicts to declare.

Acknowledgements

Notes and references

1 M. A. Hillmyer, The promise of plastics from plants, *Science*, 2017, **358**, 868–870.

2 S. Walker and R. Rothman, Life cycle assessment of biobased and fossil-based plastic: A review, *J. Cleaner Prod.*, 2020, **261**, 121158.

3 A. Llevot, P.-K. Dannecker, M. von Czapiewski, L. C. Over, Z. Söyler and M. A. R. Meier, Renewability is not Enough: Recent Advances in the Sustainable Synthesis of Biomass-Derived Monomers and Polymers, *Chemistry*, 2016, **22**, 11510–11521.

4 R. T. Mathers, How well can renewable resources mimic commodity monomers and polymers?, *J. Polym. Sci., Part A: Polym. Chem.*, 2012, **50**, 1–15.

5 K. Satoh, Controlled/living polymerization of renewable vinyl monomers into bio-based polymers, *Polym. J.*, 2015, **47**, 527–536.

6 F. H. Isikgor and C. R. Becer, Lignocellulosic biomass, *Polym. Chem.*, 2015, **6**, 4497–4559.

7 Y. Jiang and K. Loos, Enzymatic Synthesis of Biobased Polyesters and Polyamides, *Polymers*, 2016, **8**, 243.

8 H. J. Kim, Y. Reddi, C. J. Cramer, M. A. Hillmyer and C. J. Ellison, Readily Degradable Aromatic Polyesters from Salicylic Acid, *ACS Macro Lett.*, 2020, **9**, 96–102.

9 F. Della Monica and A. W. Kleij, From terpenes to sustainable and functional polymers, *Polym. Chem.*, 2020, **11**, 5109–5127.

10 P. A. Wilbon, F. Chu and C. Tang, Progress in renewable polymers from natural terpenes, terpenoids, and rosin, *Macromol. Rapid Commun.*, 2013, **34**, 8–37.

11 L. Al-Shok, D. M. Haddleton and F. Adams, *Progress in Catalytic Ring-Opening Polymerization of Biobased Lactones*, Springer, Berlin, Heidelberg, 2022, 1–71.

12 F. Pion, P.-H. Ducrot and F. Allais, Renewable Alternating Aliphatic-Aromatic Copolyesters Derived from Biobased Ferulic Acid, Diols, and Diacids: Sustainable Polymers with Tunable Thermal Properties, *Macromol. Chem. Phys.*, 2014, **215**, 431–439.

13 T. Iwata, Biodegradable and bio-based polymers: future prospects of eco-friendly plastics, *Angew. Chem., Int. Ed.*, 2015, **54**, 3210–3215.

14 M. N. Balgacem and A. Gandini, *Monomers, polymers and composites from renewable resources*, Elsevier, Amsterdam, 2008.

15 D. Zhang, M. A. Hillmyer and W. B. Tolman, Catalytic polymerization of a cyclic ester derived from a "cool" natural precursor, *Biomacromolecules*, 2005, **6**, 2091–2095.

16 J. R. Lowe, M. T. Martello, W. B. Tolman and M. A. Hillmyer, Functional biorenewable polyesters from carvone-derived lactones, *Polym. Chem.*, 2011, **2**, 702–708.

17 M. J.-L. Tschan, E. Brulé, P. Haquette and C. M. Thomas, Synthesis of biodegradable polymers from renewable resources, *Polym. Chem.*, 2012, **3**, 836–851.

18 A. L. Holmberg, K. H. Reno, R. P. Wool and T. H. Epps, Biobased building blocks for the rational design of renewable block polymers, *Soft Matter*, 2014, **10**, 7405–7424.

19 C. R. Álvarez-Chávez, S. Edwards, R. Moure-Eraso and K. Geiser, Sustainability of bio-based plastics: general comparative analysis and recommendations for improvement, *J. Cleaner Prod.*, 2012, **23**, 47–56.

20 Y. Nakagawa, M. Tamura and K. Tomishige, Recent development of production technology of diesel- and jet-fuel-range hydrocarbons from inedible biomass, *Fuel Process. Technol.*, 2019, **193**, 404–422.

21 A. Stamm, A. Biundo, B. Schmidt, J. Brücher, S. Lundmark, P. Olsén, L. Fogelström, E. Malmström, U. T. Bornscheuer and P.-O. Syrén, A Retro-biosynthesis-Based Route to Generate Pinene-Derived Polyesters, *ChemBioChem*, 2019, **20**, 1664–1671.

22 D. García, F. Bustamante, A. L. Villa, M. Lapuerta and E. Alarcón, Oxyfunctionalization of Turpentine for Fuel Applications, *Energy Fuels*, 2020, **34**, 579–586.

23 H. Miyaji, K. Satoh and M. Kamigaito, Bio-Based Polyketones by Selective Ring-Opening Radical Polymerization of α-Pinene-Derived Pinocarvone, *Angew. Chem., Int. Ed.*, 2016, **55**, 1372–1376.

24 C. M. Byrne, S. D. Allen, E. B. Lobkovsky and G. W. Coates, Alternating copolymerization of limonene oxide and carbon dioxide, *J. Am. Chem. Soc.*, 2004, **126**, 11404–11405.

25 H. C. Quilter, M. Hutchby, M. G. Davidson and M. D. Jones, Polymerisation of a terpene-derived lactone, *Polym. Chem.*, 2017, **8**, 833–837.

26 R. Alén, in *Industrial biorefineries and white biotechnology*, ed. A. Pandey, Elsevier Science, Amsterdam, 2015, pp. 91–126.

27 B. Halmbom and R. Alén, *Biorefining of forest resources. Extraction and utilisation of non-structural wood and bark components*, 2011.

28 *Industrial biorefineries and white biotechnology*, ed. A. Pandey, Elsevier Science, Amsterdam, 2015.

29 A. Sukarno, E. Hardiyanto, S. Marsoem and M. Na'iem, Oleoresin Production, Turpentine Yield and Components of Pinus Merkusii from Various Indonesian Provenances, *J. Trop. For. Sci.*, 2015, 136–141.

30 P. N. Stockmann, D. L. Pastoetter, M. Woelbing, C. Falcke, M. Winnacker, H. Strittmatter and V. Sieber, New Bio-Polyamides from Terpenes: α-Pinene and (+)-3-Carene as Valuable Resources for Lactam Production, *Macromol. Rapid Commun.*, 2019, **40**, e1800903.

31 A. Stamm, J. Öhlin, C. Mosbech, P. Olsén, B. Guo, E. Söderberg, A. Biundo, L. Fogelström, S. Bhattacharyya, U. T. Bornscheuer, E. Malmström and P.-O. Syrén, Pinene-Based Oxidative Synthetic Toolbox for Scalable Polyester Synthesis, *JACS Au*, 2021, **1**, 1949–1960.

32 A. Stamm, M. Tengdelius, B. Schmidt, J. Engström, P. O. Syrén, L. Fogelström and E. Malmström, Chemo-enzymatic pathways toward pinene-based renewable materials, *Green Chem.*, 2019, **21**, 2720–2731.

33 P. N. Stockmann, D. van Opdenbosch, A. Poethig, D. L. Pastoetter, M. Hoehenberger, S. Lessig, J. Raab, M. Woelbing, C. Falcke, M. Winnacker, C. Zollfrank, H. Strittmatter and V. Sieber, Biobased chiral semi-crystalline or amorphous high-performance polyamides and their scalable stereoselective synthesis, *Nat. Commun.*, 2020, **11**, 509.

34 M. Winnacker, J. Sag, A. Tischner and B. Rieger, Sustainable, Stereoregular, and Optically Active Polyamides via Cationic Polymerization of ε-Lactams Derived from the Terpene β-Pinene, *Macromol. Rapid Commun.*, 2017, **38**, 1600787.

35 M. Winnacker, Pinenes, *Angew. Chem., Int. Ed.*, 2018, **57**, 14362–14371.

36 M. Winnacker, D. H. Lamparelli, C. Capacchione, H. H. Güngör, L. Stieglitz, K. S. Rodewald, M. Schmidt and T. F. Gronauer, Sustainable Polyesteramides and Copolyamides: Insights into the Copolymerization Behavior of Terpene–Based Lactams, *Macromol. Chem. Phys.*, 2020, **221**, 2000110.

37 A. F. Thomas and F. Rey, The Baeyer-Villiger Reaction of Pinanones (Bicyclo[3.1.1]heptanones), *Tetrahedron*, 1992, 1927–1942.

38 H. C. Brown and A. Suzuki, Hydroboration of Terpenes. IV. Hydroboration of (+)-3-Carene ([UNK] 3 -Carene). Configuration Assignments for the 4-Caranols and 4-Caranones. An Unusual Stability of 4-Isocaranone with a cis Relationship of the Methyl and gem -Dimethyl Groups, *J. Am. Chem. Soc.*, 1967, **89**, 1933–1941.

39 E. Wincza and S. Lochynski, Chemical and microbiological oxidation of (–)-cis-carane-4-one leading to chiral compounds and evaluation of their antifeedant activity, *ARKIVOC*, 2012, **2012**, 196–203.

40 G. Y. Ishmuratov, V. A. Vydrina, K. S. Denisova, M. P. Yakovleva, R. R. Gazetdinov, E. M. Vyrypaev and A. G. Tolstikov, Synthesis from (–)-α-Pinene of an Optically Active Macrocyclic Diesterdihydrazide with 2,6-Pyridinedicarboxylic and Adipic Acid Moities, *Chem. Nat. Compd.*, 2017, **53**, 63–65.

41 J. Bruckmoser, D. Henschel, S. Vagin and B. Rieger, Combining high activity with broad monomer scope: indium salan catalysts in the ring-opening polymerization of various cyclic esters, *Catal. Sci. Technol.*, 2022, **12**, 3295–3302.

42 M. Kränzlein, T. M. Pehl, F. Adams and B. Rieger, Uniting Group-Transfer and Ring-Opening Polymerization−Block Copolymers from Functional Michael-Type Monomers and Lactones, *Macromolecules*, 2021, 10860–10869.

43 F. Adams, T. Pehl, M. Kränzlein, S. A. Kernbichl, J.-J. Kang, C. M. Papadakis and B. Rieger, (Co)polymerization of (-)-Menthide and β-Butyrolactone with Yttrium-bis(phenolates), *Polym. Chem.*, 2020, 4426–4437.

44 F. Adams, M. R. Machat, P. T. Altenbuchner, J. Ehrmaier, A. Pöthig, T. N. V. Karsili and B. Rieger, Toolbox of Nonmetallocene Lanthanides, *Inorg. Chem.*, 2017, **56**, 9754–9764.

45 K. Yakabi, T. Mathieux, K. Milne, E. M. López-Vidal, A. Buchard and C. Hammond, Continuous Production of Biorenewable, Polymer-Grade Lactone Monomers through Sn-β-Catalyzed Baeyer-Villiger Oxidation with H$_2$O$_2$, *ChemSusChem*, 2017, **10**, 3652–3659.

7.   Copolymers from *Michael*-type monomers and lactones

Uniting Group-Transfer and Ring-Opening Polymerization – Block Copolymers from Functional Michael-Type Monomers and Lactones

7.1.   Bibliographic data

Title: "Uniting Group-Transfer and Ring-Opening Polymerization – Block Copolymers from Functional Michael-Type Monomers and Lactones"

Status: Article, Publication Date: 29.11.2021

Journal: Macromolecules

Publisher: American Chemical Society (ACS)

DOI: 10.1021/acs.macromol.1c01692

Authors: Moritz Kränzlein, Thomas M. Pehl, Friederike Adams and Bernhard Rieger[‡]

7.2.   Abstract graphic (TOC)
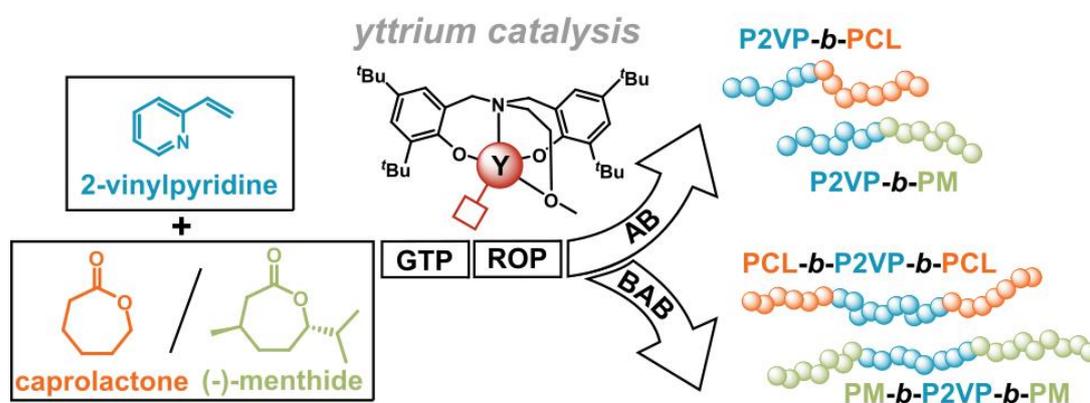
Figure 32: Table of content graphic for the manuscript titled "Uniting Group-Transfer and Ring-Opening Polymerization – Block Copolymers from Functional Michael-Type Monomers and Lactones".

7.3. Content

The last method discussed herein is the copolymerization of *Michael*-type monomers and lactones *via* group-transfer and subsequent ring-opening polymerization. While this approach has so far received only little attention, it could offer the possibility to generate block copolymers possessing a high degree of functionality as introduced from *Michael* monomers coupled with degradability offered by polyesters. Gaining access to such structures *via* catalytic methods and using a sequential addition approach would provide a highly tunable and adaptable polymerization technique capable of producing highly functional copolymers with little synthetic effort. So far, some catalytic approaches towards copolymers from methacrylates and lactones are known, yet only little characterization of the material properties and almost no mechanistic elucidation has been performed. Herein, a catalytic pathway towards copolymers from 2-vinylpyridine with either ε-caprolactone as classic lactone or (-)-menthide as new biobased monomer as second block is introduced. This way, novel AB- and BAB-type di- and triblock copolymer structures could be prepared. To gain a deeper understanding of the catalytic mechanism behind this sequential copolymerization, kinetic investigations are performed, revealing a living-type polymerization for both GTP and ROP. In an intermediate step, the catalyst-stabilized chain-end from GTP is capable of attacking and ring-opening the first lactone unit, successfully initiating a subsequent ROP. Changing the monomer addition sequence and adding the lactone first inhibited the formation of copolymers, emphasizing that as for GTP, also GTP-*co*-ROP is sensitive towards monomer coordination strength. The prepared polymer materials are investigated regarding their thermal transitions, revealing microphase separation and show a pH-dependent micellization in aqueous media. By adapting the feed ratios of the monomers, the presented catalytic pathway allows tuning of the copolymers molecular weight and composition, leading to tunable material properties regarding parameters like glass transition temperature or micelle size. Ultimately, such materials could possibly be used for advanced applications like drug delivery or coatings, benefiting from the responsiveness of the functional GTP-block paired with the possible susceptibility towards hydrolytic degradation offered by the ROP-based polyester block.

7.4.   Manuscript

Uniting Group-Transfer and Ring-Opening Polymerization—Block Copolymers from Functional Michael-Type Monomers and Lactones

Moritz Kränzlein, Thomas M. Pehl, Friederike Adams,* and Bernhard Rieger*

ACCESS | 📊 Metrics & More | 📰 Article Recommendations | 🆘 Supporting Information

ABSTRACT: Herein, the consecutive group-transfer polymerization (GTP) of the Michael-type monomer 2-vinylpyridine (2VP) and ring-opening polymerization (ROP) of ε-caprolactone (CL) or (−)-menthide (M) using a monometallic and a bimetallic 2-methoxaminethylamino-bis(phenolate) yttrium catalyst for the synthesis of AB- and BAB-type block copolymers (P2VP-*b*-PCL and P2VP-*b*-PM) are reported. Using the more demanding (−)-menthide, further insights into the catalytic nature of this combinatorial polymerization approach were gained using a kinetic copolymerization approach. These investigations revealed a living-type polymerization, for the initial GTP sequence as well as the subsequent ROP. To show the influence of the coordination strength of the monomers to the metal center, the addition sequence is alternated, uncovering a lower coordination strength of Michael-type monomer 2VP to the metal than that of lactones. Quenching of the active propagating chain end during ROP chain growth showed a coordination—insertion mechanism for the polymerization of CL and M initiated by an acyl-oxygen cleavage of lactones by the active P2VP chain. The AB- and BAB-type block copolymers of P2VP with PCL or PM showed the formation of precisely defined micelles in an acidic medium, and thermal transitions of the copolymers were shown to be microphase separation-influenced.
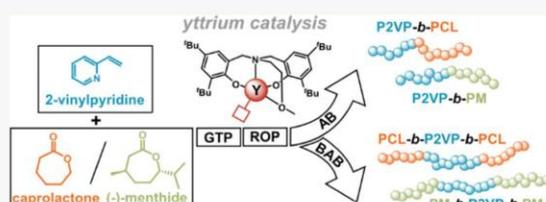
INTRODUCTION

Since the initial discovery of the rare-earth metal-mediated group-transfer polymerization (REM-GTP) by Yasuda et al. in 1992, a plethora of different monomers for this polymerization type has successfully been established.[1−4] Based on these monomers, different functional polymers have been synthesized, addressing areas such as radical-containing polymers,[5] optical polymers,[6] polymer−drug conjugates,[7,8] or pH- and temperature-responsive materials.[3,9−12] Furthermore, the topic of (co)polymer architectures has been addressed thoroughly, combining different functional Michael-type monomers to form even more sophisticated copolymers, utilizing the living nature of REM-GTP.[3,4,9,10] In general, block copolymers are accessible by REM-GTP via sequential addition of the monomers, in a row of increasing coordination strength to the metal center. Statistical copolymers can only be generated using monomers with the same coordinating motif and varying pendant groups, for example, differently substituted alkyl vinyl phosphonates or methacrylates.[3,12−15] Overall, in REM-GTP, the experimentally determined coordination of the monomer to the metal center increases in the following order: 2-vinylpyridine (2VP) < 2-*iso*-propenyl-2-oxazoline < alkyl methacrylates < bis(alkyl) acrylamides < alkyl vinyl phosphonates.[14,16]

Especially, symmetric yttrium 2-methoxyethylamino-bis-(phenolate) complexes emerged as a versatile catalyst class for both homo- and block copolymerizations. The copolymerization of different Michael-type monomers toward multifunctional polymers, for example, poly(2-vinylpyridine)-*b*-poly(dialkyl vinyl phosphonate) (P2VP-*b*-PDEVP), has been investigated in matters of dual-responsive drug-delivery (thermal and pH) systems utilizing micellization in aqueous media. In this context, a bimetallic complex has been designed via double C−H bond activation of 2,3,5,6-tetramethylpyrazine (TMPy) to generate BAB-type triblock copolymers.[9,11,17]

While catalysts **1−3** have been applied for the (co)-polymerization of various Michael-type monomers (Scheme 1),[9−11,17,18] Carpentier et al. established the 2-methoxamine-thylamino-bis(phenolate) yttrium structure featuring a set of different initiators as an efficient catalyst for the ring-opening polymerization (ROP) of (*rac*)-lactide and β-butyrolactone (BBL).[18−21] In this context, Rieger et al. showed that catalysts **2** and **3** are highly active in ring-opening (co)polymerization of BBL and terpene-based (−)-menthide (M), facilitating AB- and BAB-type block copolymers.[22] Combining the plethora of functional 1,4-Michael-type monomers with renewable polyesters, functional and mostly unknown copolymer combinations can be created. The initial proof of concept has been

Scheme 1. Different 2-Methoxyethylamino-bis(phenolate) Yttrium Catalysts for Homo- and Block Copolymerizations of Michael-Type Monomers and Lactones[9,11,17]

$[(ONOO)^{tBu}Y(CH_2TMS)(thf)]$
1

$[(ONOO)^{tBu}Y(sym\text{-}col)(thf)]$
2

$[((ONOO)^{tBu}Y(thf))_2(TMPy)]$
3
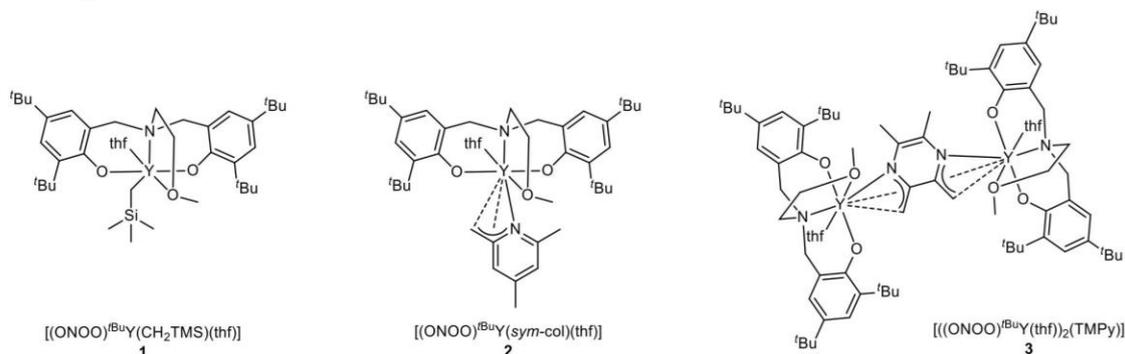
Scheme 2. AB and BAB Block Copolymerization of 2VP with CL ($R_1 = R_2 = H$) or M ($R_1 = Me$, $R_2 = {}^iPr$) with Monometallic Bis(phenolate) Yttrium Catalyst 2 and Bimetallic Bis(phenolate) Yttrium Catalyst 3

AB block copolymer:

P2VP-*b*-PCL $R_1 = R_2 = H$
P2VP-*b*-PM $R_1 = Me$, $R_2 = {}^iPr$

BAB triblock copolymer:

Ini =

PCL-*b*-P2VP-*b*-PCL $R_1 = R_2 = H$
PM-*b*-P2VP-*b*-PM $R_1 = Me$, $R_2 = {}^iPr$
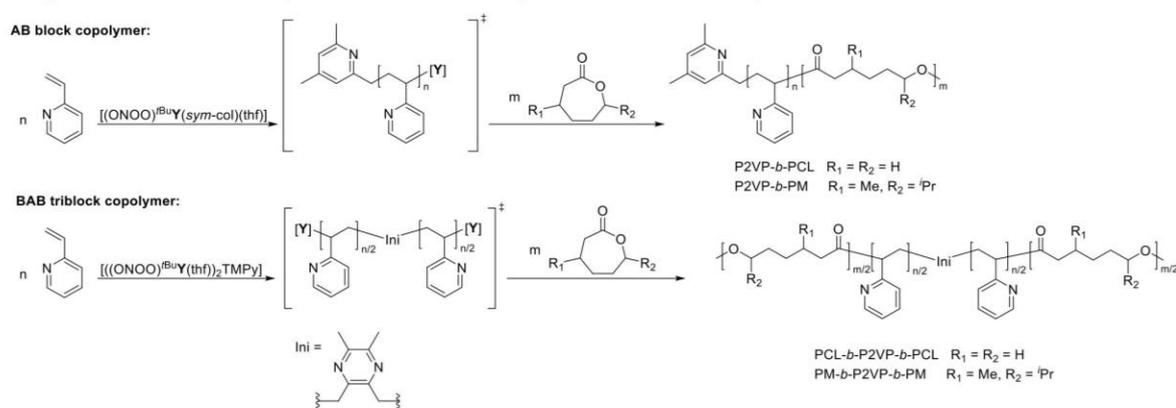
performed by Yasuda et al. in 1995, copolymerizing methyl methacrylate (MMA) with β-methylpropiolactone, δ-valerolactone (VL), and ε-caprolactone (CL); however, no further investigations beside first polymerization experiments were conducted by this group.[2] An approach adapting Yasuda et al. was performed by Kostakis et al. using $Cp_2ZrMe_2/B(C_6F_5)_3$, yielding the block copolymers MMA-*b*-CL and MMA-*b*-VL.[23] Further attempts of MMA copolymerization with lactones were made by Chiellini et al. and Kowalczuk et al., leading to imprecisely formed copolymers with broad polydispersities.[24,25] In a very recent approach, Mehrkhodavandi et al. facilitated the copolymerization of MMA with *rac*-lactide and CL using a single-site indium complex showing the high interest in this kind of materials.[26] An attempt for copolymerizing the Michael-type monomer 2VP with the lactone BBL using catalyst 1 by Rieger et al. failed, limiting the available scope of Michael-type monomers to MMA and some lactones.[2,17,23,26]

Overall, catalytic copolymerization of Michael-type systems and lactones would ultimately yield a novel class of functional block copolymers, which lead to the motivation of gaining deeper insights into this combination of monomers using rare-earth metal catalysis. Herein, the preparation of AB- and BAB-type block copolymers from the Michael-type monomer 2VP with lactones CL and (−)-menthide using yttrium bis(phenolate) catalysts 2 and 3 is reported. It is shown that

the active chain end of P2VP itself can successfully initiate the polymerization of lactones. Kinetic investigations underline living-type catalytic copolymerization mechanisms for both monomers and via end-group analysis. Additionally, the mechanism of the second reaction step is elucidated. Differently composed block copolymers were prepared via simple monomer feed variation and characterized regarding their solution properties, showing a pH-dependent micellization. Both types of block copolymers are additionally characterized regarding their thermal properties, revealing microphase separation for both the semicrystalline P2VP-*b*-PCL block copolymer and the fully amorphous P2VP-*b*-PM.

■ BLOCK COPOLYMERIZATION OF 2VP WITH CL

The copolymerization of 2VP with CL was conducted in a sequential addition of the monomers utilizing the living nature of the REM-GTP of 2VP and the ROP of CL. If the P2VP active chain end itself can initiate CL polymerization, a block copolymer is formed. Using the monometallic yttrium bis(phenolate) catalyst 2, AB diblock copolymers were synthesized. Switching to the bimetallic yttrium catalyst 3, BAB triblock copolymers were obtained (Scheme 2). Different block copolymers with regard to varying block lengths and block ratios were prepared. The corresponding characterization results are listed in Table 1; additional information on the

Table 1. Characterization of Block Copolymers from 2VP and CL Synthesized with the Monometallic Yttrium Catalyst 2 (Diblock Copolymers AB[X]) and the Bimetallic Yttrium Catalyst 3 (Triblock Copolymers BAB[X])

entry[a]	feed [Y]/[2VP]/[CL]	repeating unit and ratio[b] n_{2VP}/m_{CL} (mol %/mol %)	$M_{n,abs,A}$[c] [kg/mol]	$Đ_A$[c] [-]	$M_{n,NMR,AB}$[d] [kg/mol]	$Đ_{AB}$[e] [-]
AB[1]	1/100/100	120:200 (40:60)	12.1	1.03	34.7	1.61
AB[2]	1/200/200	270:250 (50:50)	28.8	1.08	57.7	1.46
AB[3]	1/400/400	700:6000 (10:90)	72.8	1.04	757	1.65
AB[4]	1/300/100	560:200 (75:25)	59.2	1.07	81.8	1.41
AB[5]	1/100/300	130:470 (20:80)	13.7	1.03	67.7	2.10
AB[6]	1/200/200[f]		18.0	3.57		
AB[7]	1/200/200[g]	340:330 (50:50)	36.1	1.06	73.7	1.27
A[1]	1/200/0	340:0 (100:0)	35.3	1.03		
B[1]	1/0/200	n.d. (0:100)[h]	70.0[h]	1.93		
BAB[1]	2/100/100	120:100 (55:45)	12.1	1.05	23.0	1.35
BAB[2]	2/200/200	230:210 (50:50)	24.1	1.11	47.6	1.34
BAB[3]	2/400/400	540:620 (45:55)	56.9	1.08	128	1.47
BAB[4]	2/300/100	730:230 (75:25)	77.3	1.12	104	1.66
BAB[5]	2/100/300	130:600 (20:80)	14.1	1.04	82.9	1.30

[a]AB[X] polymers using monometallic catalyst 2, BAB[X] polymers using bimetallic catalyst 3, catalyst/monomer ratios, 13.5 µmol catalyst, RT, conversions, solvents, and reaction times for each experiment, see the Supporting Information. [b]Absolute number of repeating units from absolute SEC analysis and composition/ratio determined via integration of P2VP aromatic signals vs CL signals in ^{1}H NMR spectra. [c]Absolute molecular weight determination and polydispersity of the P2VP block via the aliquot method via SEC in DMF (40 °C, with 25 mmol/L LiBr, triple detection, dn/dc = 0.149 mL/g). [d]Calculated molecular weight of the block copolymer via ^{1}H NMR spectra of AB block copolymers and $M_{n,abs,A}$ of block A. [e]Polydispersity of the block copolymer as determined via RI detection of SEC in DMF (40 °C, 25 mmol/L LiBr added, PMMA standards). [f]Thf as a solvent. [g]Toluene as a solvent. [h]Relative molecular weight of the PCL homopolymer in thf relative to polystyrene.

reaction conditions can be found in the Supporting Information.

To elucidate the potential of this system, AB diblock and BAB triblock copolymers have been synthesized using catalysts 2 and 3 with regard to the overall copolymer chain length with the fixed 2VP/CL ratio (AB[1]–AB[3]/BAB[1]–BAB[3]), varied block ratios (AB[4]–AB[5]/BAB[4]–BAB[5]), and reaction solvent (AB[8]–AB[9]). Additionally, P2VP (A[1]) and PCL (B[1]) homopolymers have been synthesized for comparison. Varying the overall copolymer chain length with a fixed 2VP/CL molar ratio of 1:1, monomer feeds with respect to the catalyst of 1:100:100 (AB[1]/BAB[1]), 1:200:200 (AB[2]/BAB[2]), and 1:400:400 (AB[3]/BAB[3]) have been tested. For low catalyst-to-monomer ratios, the equimolar feed composition is consistent with the molar ratio of the copolymer blocks. Additionally, for AB[2] and BAB[2] (1:200:200), approximately double the molecular weight as for AB[1] and BAB[1] (1:100:100) is observed and all polymers show moderate polydispersities. While the first block A always exhibits very narrow polydispersity, it is broadened significantly upon copolymerization of block B. This happens most likely due to termination reactions and intermolecular transesterification of the PCL block showing that ROP is less-controlled than GTP. In general, the used monomer feed ratios can be observed in the obtained polymers, while the overall degree of polymerization is higher than the given feed ratio due to the initiator efficiencies being below 100% (I = 47–98%, decreasing with higher 2VP to catalyst loading) as already reported in the literature.[9,11] For higher monomer-to-catalyst ratios in AB[3] and BAB[3] (1:400:400), the AB system reaches a limitation, showing a discrepancy between monomer feed and copolymer composition. The limitation of the AB[3] system might be explained by intermolecular transesterification and side reactions or a low initiator efficiency or the P2VP macroinitiator due to a catalyst overload or trace impurities in CL when using a high amount of CL. For BAB[3], the polymer composition still matches the monomer feed; however, BAB[3] shows about 3 times the molar mass of BAB[2]. In similarity to

AB[3], it seems that a decrease in initiator efficiency caused by deactivation processes leads to an increase in the catalyst-to-monomer ratio. For adapting the monomer ratios in the resulting polymers, the feed composition has been varied ranging from 2VP/CL = 20:80 up to 2VP/CL = 75:25 while using the same overall catalyst-to-monomer ratio of approximately 1:400 (AB[4/5] and BAB[4/5]). For those polymers, feed ratios are consistent with the obtained polymer compositions and the copolymers show narrow-to-moderate polydispersity. Additionally, the polydispersities from BAB triblock copolymers using catalyst 3 are comparably lower than those of the AB diblock copolymers using catalyst 2, which might be explained by a lower 2VP/yttrium center ratio in the bimetallic system.

Investigation into the capability of the active P2VP chain to initiate ROP resulted in consumption of the CL monomer as determined via vanishing of the monomer signals in aliquot ^{1}H NMRs. The successful formation of block copolymers was verified via comparison of the SEC traces from an aliquot taken after 2VP polymerization in block A to the SEC traces of the AB polymer and additionally via DOSY-NMR measurements. A clear shift of molar mass toward higher molar masses can be observed between block A and AB polymers (Supporting Information, Figures S2 and S8) indicating an increase in the molecular weight of the final polymer, as well as a general broadening of the polydispersity ($Đ_A$ = 1.11 to $Đ_{AB}$ = 2.10). DOSY-NMR was used to distinguish between copolymer and homopolymer byproducts via their diffusion coefficient (Supporting Information, Figures S3 and S9). In the DOSY-NMR spectrum of AB[2], the signals of P2VP and PCL appear at the same diffusion coefficient (D = 2.6 × 10^{−7} cm[2]/s) and no polymer signals with other diffusion coefficients can be observed, hinting selective formation of the block copolymer. The combination of SEC and DOSY-NMR successfully verifies block copolymerization for 2VP and CL. This behavior is observed for all AB- and BAB-type block copolymers, exclusively yielding the desired copolymers. Within the chosen

Table 2. Characterization of Block Copolymers from 2VP and M Synthesized with the Monometallic Yttrium Catalyst 2 (Diblock Copolymers AB^X) and the Bimetallic Yttrium Catalyst 3 (Triblock Copolymers BAB^X)

entry	feed[a] [Y]/[2VP]/[M]	repeating unit and ratio[b] n_{2VP}/m_M (mol %/mol %)	X_M[c] [%]	$M_{n,abs,A}$[d] [kg/mol]	$Đ_A$[d] [-]	$M_{n,NMR,AB}$[e] [kg/mol]	$Đ_{AB}$[f] [-]
AB^8	1/100/100	190:60 (75:25)	62	19.5	1.01	28.6	1.22
AB^9	1/200/200	280:120 (75:25)	65	29.5	1.02	50.0	1.14
AB^{10}	1/400/400	880:30 (95:5)	4	92.0	1.02	96.8	1.25
AB^{11}	1/100/300	190:60 (75:25)	30	20.4	1.02	30.8	1.13
AB^{12}	1/300/100	520:80 (85:15)	65	55.0	1.03	67.7	1.17
BAB^6	2/100/100	170:90 (60:40)	78	17.9	1.04	33.0	1.21
BAB^7	2/200/200	290:140 (65:35)	83	29.2	1.05	53.6	1.21
BAB^8	2/400/400	570:250 (70:30)	80	59.5	1.04	102	1.29
BAB^9	2/100/300	170:240 (40:60)	80	17.4	1.04	58.9	1.37
BAB^{10}	1/300/100	450:70 (85:15)	70	47.4	1.07	59.3	1.22

[a]AB^X polymers using monometallic catalyst 2, BAB^X polymers using bimetallic catalyst 3, catalyst/monomer ratios, 6.75 μmol catalyst, 2VP homopolymerization at RT, M copolymerization at 70 °C, conversions, solvents, and reaction times for each experiment, see the Supporting Information. [b]Composition determined via integration of P2VP aromatic signals vs M signals in ^{1}H NMR. [c]Conversion determined from aliquot ^{1}H NMR. [d]Absolute molecular weight determination and polydispersity of the P2VP block via the aliquot method before M addition via SEC in DMF (40 °C, 25 mmol/L LiBr added, triple detection, dn/dc = 0.149 mL/g). [e]Calculated molecular weight of the block copolymer via ^{1}H NMR spectra of AB block copolymers and $M_{n,abs,A}$ of block A. [f]Polydispersity of the block copolymer as determined via RI detection of SEC in DMF (40 °C, 25 mmol/L LiBr added, PMMA standards).

reaction times, the conversion of 2VP is between 85 and 99% and the conversion of CL is higher than 96%. The polymerization of CL usually proceeds in a very fast manner with gelation of the reaction mixture within seconds to few minutes after CL addition to the reaction mixture.

To investigate the influence of coordination strength of the monomers to the metal center on the obtained block copolymers, the addition sequence is switched, utilizing CL as the first block followed by 2VP addition. This procedure resulted in the exclusive formation of the PCL homopolymer with no observable conversion of 2VP. Additionally, a 50:50 mixture of 2VP/CL is prepared and added to the catalyst solution, again resulting in selective polymerization of solely PCL. This behavior is consistent with previous work focusing on REM-GTP block copolymerization of different Michael-type monomers, revealing monomer-metal coordination strength as a decisive parameter for successful copolymerization.[3,12−16] This concept can be adapted for copolymerization of Michael-type monomers and lactones with a stronger coordination of CL to the metal center compared to 2VP, revealing the addition sequence as a crucial factor for GTP-co-ROP-type copolymerizations as well.

To investigate the influence of the reaction solvent, AB^8 was prepared using tetrahydrofuran and AB^9 using toluene instead of dichloromethane. For thf, during homopolymerization of 2VP, a competitive coordination of thf and 2VP took place decreasing the turnover frequency (TOF) and increasing the polydispersity hindering successful block copolymerization.[27] A similar behavior is expected for pyridine, and a complete inhibition of 2VP polymerization was already observed in the literature,[28] while polar protic solvents are not applicable due to incompatibility with the yttrium complex. Using toluene, P2VP slightly precipitates over the course of the reaction; however, upon the addition of CL, the polymer is fully dissolved again, facilitating controlled copolymerization with narrow polydispersity of the observed polymer (AB^9). Overall, the copolymerization of 2VP and CL to AB di- and BAB triblock copolymers via simple sequential addition of the monomers yields defined polymers, featuring projectable chain length and tunable block composition.

■ BLOCK COPOLYMERIZATION OF 2VP WITH (−)-MENTHIDE

The copolymerization of 2VP with (−)-menthide is performed in similarity to the reaction of 2VP with CL (Scheme 2); however, as the copolymerization of (−)-menthide is reported to be more active at elevated temperatures, the reaction conditions were adapted. The temperature of the copolymerization was set to 70 °C to increase the catalyst activity and thus the solvent is switched to toluene to facilitate higher reaction temperatures. As for P2VP-b-PCL, P2VP-b-PM AB- and BAB-type block copolymers are synthesized using catalysts 2 and 3, again preparing different block copolymers with regard to varying block lengths and block ratios. The corresponding characterization results are listed in Table 2; additional information on the reaction conditions can be found in the Supporting Information.

As for the copolymerization of 2VP with CL, the block copolymer formation of 2VP with M has been verified by comparing the SEC traces of P2VP block A to the copolymer AB, showing a shift in retention time and broadening of the polydispersity (Supporting Information, Figures S13 and S15). Additionally, DOSY-NMR was used as further copolymerization proof (Supporting Information, Figures S14 and S16). As for P2VP-b-PCL copolymers, in the copolymerization of 2VP with M exclusively, the desired AB and BAB block copolymers were formed. Within the chosen reaction times, the conversion of 2VP was between 91 and 99% and the conversion of M was between 4 and 65% for the AB systems and between 70 and 83% for the BAB systems. Overall, the (−)-menthide conversion drops drastically with increased yttrium/menthide ratio (from X_M = 62% for 1:100:100 down to X_M = 4% for 1:400:400) for the AB systems, while this limitation could not be observed in any kind for the BAB systems with constant (−)-menthide conversion between 70 and 80%. Conversions and initiator efficiencies of both catalysts were within the expected range reported in the literature.[9,11]

Both AB- and BAB-type copolymers were varied regarding overall chain length with a fixed 2VP/M feed ratio of 50:50 (1:100:100 AB^8/BAB^6, 1:200:200 AB^9/BAB^7, and 1:400:400 AB^{10}/BAB^8), and the 2VP/M feed ratio was varied (AB$^{11/12}$ and BAB$^{9/10}$). Due to the decreasing (−)-menthide conversion
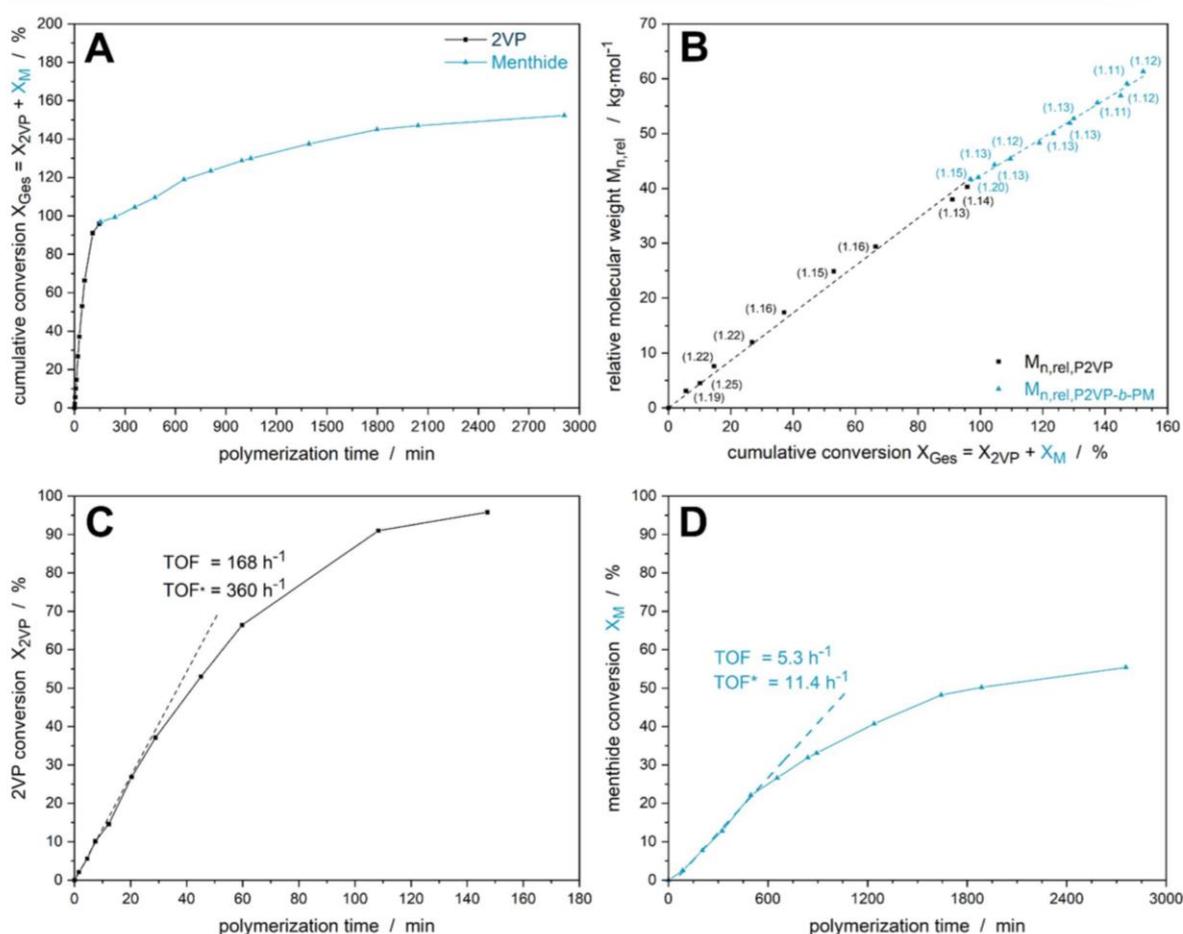
Figure 1. (A) Cumulative conversion of 2VP (black) and M (blue) over time in the AB block copolymerization with **2** ([Y]/[2VP]/[M] = 1/200/200); (B) relative molecular weight increase over cumulative conversion for both monomers, polydispersity in parenthesis; (C) close-up of conversion vs time plot for block A 2VP polymerization and TOF-fitting; and (D) zoom-in on conversion vs time for copolymerization of M onto the P2VP block and TOF-fitting.

with higher loadings, all P2VP-b-PM AB block copolymers with 50:50 feed ratios are biased toward higher 2VP content. This effect increases with an overall catalyst-to-monomer ratio (AB[8] 1:100:100 2VP/M = 75:25 down to AB[10] 1:400:400 2VP/M = 95:5), yet the overall polymer block length was increased and a narrow polydispersity was maintained ($Đ_{AB}$ < 1.25). For the BAB-type copolymers, the same behavior was observed, yet due to higher M conversions, the polymers were less-distorted toward high 2VP content and more consistent in their 2VP/M ratio with 60:40 (BAB[6]; 1:100:100) to 70:30 (BAB[8], 1:400:400). Furthermore, the molecular weight of the polymers is increasing in a linear fashion with increasing feed ratios while maintaining moderate polydispersities, analogously to the P2VP-b-PCL system.

Varying the feed ratio, the AB system with a lower 2VP ratio (AB[11]; 1:100:300) showed a much higher 2VP/M ratio than expected, due to strongly decreasing (−)-menthide conversion with a yttrium/menthide ratio of 1:300 (X_M = 30%), whereas AB[10] (1:300:100) with higher 2VP feed yields the expected copolymer. For the BAB systems, the 2VP/M ratio in the copolymer BAB[10] with a higher 2VP feed (1:300:100) is in

good agreement to the AB system. Due to higher conversions using catalyst **3**, BAB[9] with an increased (−)-menthide feed (1:100:300) is the only copolymer obtained in which the PM block is longer than the P2VP block (molar ratio of 2VP/M = 40:60). All P2VP-b-PM polymers maintain moderate polydispersities ($Đ_{AB}$ < 1.37). Overall, the P2VP-b-PM copolymer composition and polymer size can be tuned by varying the monomer feed; however, due to the incomplete conversion of M, there is a bigger discrepancy between calculated and obtained molar masses than for the P2VP-b-PCL system. However, the use of (−)-menthide as the second block in the copolymerization with the Michael-type monomer 2VP highlights the possibility of applying novel biobased monomers in this type of copolymerization, further broadening the scope of accessible monomers.

■ KINETIC INVESTIGATION OF THE COPOLYMERIZATION

To determine the catalytic parameters of the copolymerization of Michael-type monomers with lactones, reaction kinetics regarding monomer conversion over time and molecular

Scheme 3. Acyl-Oxygen Cleavage during Initiation of the First Lactone during Transfer from GTP to ROP via Nucleophilic Attack of the Metal-Stabilized Aza Enolate Macroinitiator after Complete P2VP Propagation Generating an Alcoholate Chain End
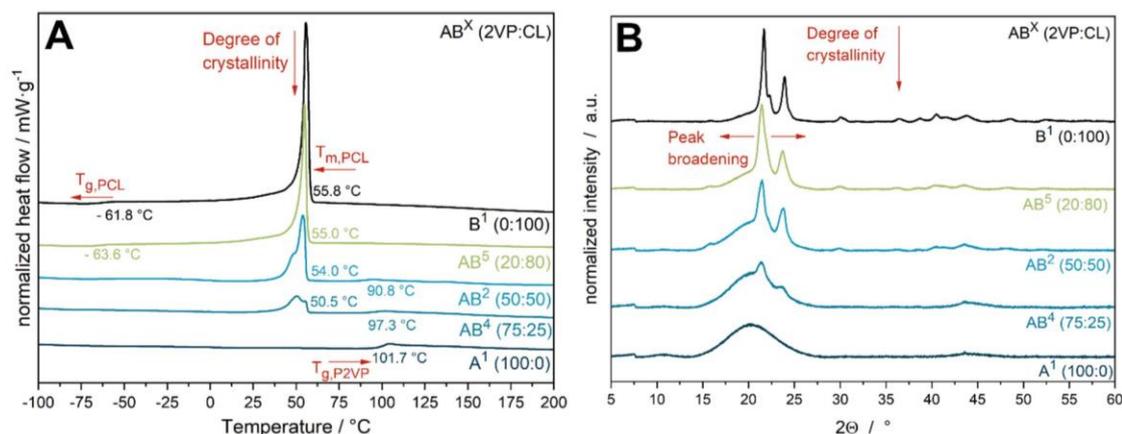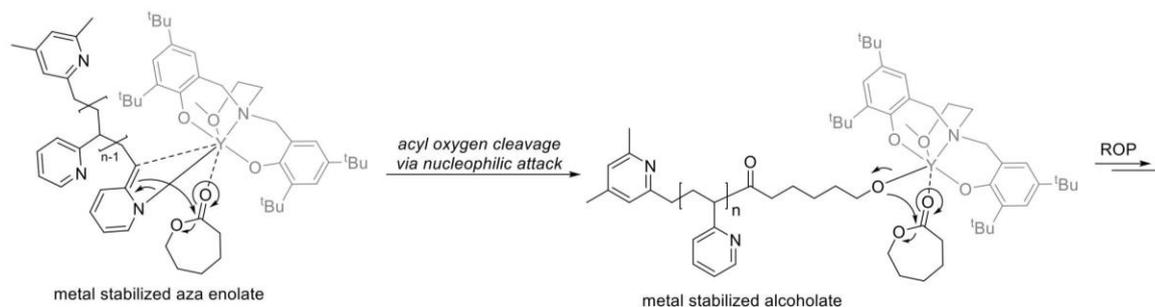
Figure 2. (A) DSC and (B) pXRD of different P2VP-*b*-PCL AB block copolymers with varying 2VP/CL composition (Table 1, entries 2, 4, 5, 8, and 9).

weight increase were determined. Since the polymerization of CL as the second block achieves full conversion within a few minutes, the sterically more demanding M was selected as it is reported that **2** polymerizes this monomer in a controlled but slower fashion.[22]

Kinetic monitoring of the copolymerization revealed a linear increase in the relative molecular weight for P2VP (Figure 1B, black graph) with increasing conversions, maintaining narrow molecular weight distribution ($Đ_A$ < 1.25, narrowing with increasing conversion) over the course of the reaction. The same behavior can be observed for the formation of the second block from (−)-menthide, where the relative molecular weight increases linearly as well, however, with a decreased activity (Figure 1B, blue graph) maintaining narrow polydispersity ($Đ_{AB}$ < 1.13). This indicates a controlled, living-type polymerization for both copolymer blocks, in which the coordinated, active P2VP chain end acts as a macroinitiator for the subsequent ROP.

To further study the activity, TOFs for 2VP homopolymerization and chain extension using M with catalyst **2** were determined. While the homopolymerization of 2VP proceeded relatively fast (X_{2VP} = 97% in 2.5 h, TOF = 168 h^{-1}; initiator efficiency normalized TOF* = TOF/I = 360 h^{-1}), the chain extension with (−)-menthide using the active P2VP chain as an initiator is comparably slow (X_M = 55% in 46 h, TOF = 5.3 h^{-1}, initiator efficiency normalized TOF* = TOF/I = 11.4 h^{-1})

and reaches a conversion plateau at 60%. These behaviors are in good accordance with data reported in the literature for the homopolymerizations of 2VP or M with **2**.[11,22] The results derived from the kinetic investigation of the P2VP-*b*-PM copolymerization indicates a catalytic copolymerization of both the Michael-type monomer via a REM-GTP mechanism and subsequent metal-catalyzed ROP of (−)-menthide.

As the ring-opening of the lactone by the active chain end of the P2VP polymer can proceed either via alkyl-oxygen cleavage or acyl-oxygen cleavage depending on the initiating system (Supporting Information, Figure S19), the propagating chain end of the polymerization was scavenged using chlorodiphenylphosphine oxide P(OPh)$_2$OCl as an end-capping agent, a technique introduced by Penczek et al.[29−31] If the copolymerization proceeds via acyl-oxygen cleavage, the propagating alkoxide chain end forms a phosphorus ester with P-(OPh)$_2$OCl. Contrary carboxylate chain ends obtained via alkyl-oxygen cleavage would result in the formation of a mixed carbon−phosphorus anhydride, which subsequently decomposes to the carbon−carbon anhydride and a pyrophosphate. Both species can be distinguished using ^{31}P NMR spectroscopy.[29−32] The P-capping experiment was conducted for both copolymerizations P2VP-*b*-PCL and P2VP-*b*-PM (Supporting Information, Figure S20). These ^{31}P NMR experiments revealed the formation of a phosphorus species at δ = −18 ppm and the absence of any pyrophosphate signal ($\delta \approx$ −25

ppm) in consistency with the formation of an alkoxide chain end. Mechanistically, the metal-stabilized aza enolate formed during P2VP propagation acts as a nucleophile in the ring-opening, generating an alcoholate chain end which propagates the subsequent ROP (Scheme 3). A similar reactivity was observed in a previous study investigating ring-opening of lactones using lithium enolates, generating alcoholate species as well.[33] The observed alcoholate-mediated propagation highlights a selective ring-opening of CL and M via acyl-oxygen cleavage [Figure S19, pathway (I)] and thus a coordination−insertion mechanism of the copolymerization.[22,29−32]

Additionally, ESI-MS analysis of P2VP-b-PCL oligomers (Supporting Information, Figure S21) prepared using catalyst 3 revealed a nucleophilic transfer of the TMPy unit of the catalyst onto the polymer chain during initiation as already observed for initiation of GTP and BBL/(−)-menthide ring-opening homopolymerizations, respectively.[11,22] In the ESI-MS graph, signals corresponding to TMPy/$[2VP]_n$/CL oligomers with one to five CL repeating units were observed, proving a connection of 2VP to CL and a chain growth of CL units. Overall, the mechanistic investigation of the copolymerization and the chain-end determination indicate a successful initiation of ROP using an active P2VP chain as a macroinitiator via metal-catalyzed ROP.

■ THERMAL TRANSITION BEHAVIOR

As the composition of the block copolymers can be tuned via the monomer feed, the prepared polymers with varying molar ratios of 2VP to CL or M were analyzed regarding their phase transition behavior and macroscopic structure using differential scanning calorimetry (DSC) and powder X-ray diffraction (pXRD). While the monomer combination of 2VP with CL unites two polymers with amorphous (2VP, Figure 2, A[1]) and semicrystalline (PCL, Figure 2, B[1]) phases, 2VP with M combines two fully amorphous polymers (PM, Supporting Information, Figures S17 and S18).

A semicrystalline PCL (B[1]) homopolymer exhibits a glass transition (T_g) at −62 °C and a melting transition (T_m) at 56 °C, whereas the amorphous P2VP (A[1]) only shows a T_g at 102 °C. With decreasing molar fraction of PCL in the AB block copolymers, the T_g of the CL block decreases to −64 °C in the 50:50 copolymer AB[2], and for further reduced molar fractions (75:25, AB[4]), the T_g of the CL block becomes unobservable. For the CL melting transitions of the P2VP-b-PCL copolymers, both the overall integral as well as the melting point itself decreased with a higher P2VP fraction to a minimum T_m of 50 °C (P2VP/PCL = 75:25, AB[4]), most likely due to an overall shrinking of the crystalline domain sizes as indicated in the pXRD. The glass transition of P2VP starts to become observable at 50% molar fraction of P2VP or higher (AB[2]) and the T_g continuously increased with increasing P2VP content. The diminishing of the sharp T_m signal of PCL and the appearance of a second signal can be attributed to a decrease in the overall degree of crystallinity as well as the crystallite size of the PCL as the P2VP blocks might disturb the crystallization pattern; the decreasing T_g of PCL further supports this assumption. As the reflex positions do not change, no other crystalline phases were formed while the overall crystallize size is decreasing as indicated by the peak broadening. The behavior of both DSC and pXRD suggests a partly microphase-separated copolymer system, in which the P2VP block and the PCL block are immiscible. In the

literature, phase behavior of polystyrene-b-polycaprolactone block copolymers is reported, undergoing microphase separation with a phase inversion dependent on the styrene/caprolactone ratio (between 33:67 and 44:57 styrene to caprolactone).[34] As the thermal behavior of this system is very similar to the one obtained for the herein reported P2VP-b-PCL system, a similar microphase separation is indicated by the observed thermal transitions. For BAB-type triblock copolymers of 2VP and CL, the same observations can be made in the DSC and pXRD (Supporting Information; Figures S10 and S11), however, less-pronounced due to the triblock BAB nature of the block copolymers.

For the combination of 2VP with M, the copolymers exhibit two separated glass transition temperatures, one in the range of −26 to −32 °C, lower than the T_g of pure amorphous PM (−23 °C), and one in the range of 94−102 °C, not significantly altered from the T_g of pure P2VP (Supporting Information, Figures S17 and S18). For both (−)-menthide-based AB- and BAB-type copolymers, the same behavior can be observed, indicating again a microphase separation-influenced copolymer morphology. As both blocks exhibit only amorphous domains, pXRD is not feasible in this case. Overall, the phase-transition behavior of these block copolymers is significantly changed compared to the homopolymers, making the class of poly(Michael-type monomers)-co-poly(esters) an interesting class of materials.

■ TUNING SOLUTION BEHAVIOR OF BLOCK COPOLYMERS

Utilizing the pH-dependent solubility of P2VP, the solution properties of the prepared di- and triblock copolymers P2VP-b-PCL and P2VP-b-PM were investigated using dynamic light scattering (DLS). While P2VP (A[1]) turned fully soluble below a pH of 4.5, the initially insoluble P2VP-b-PCL (AB[2]) started to form a stable, turbid solution, indicating micellization of the block copolymer due to protonation of the pyridine unit to a soluble poly(pyridinium) block, while the PCL block B remains insoluble.[10]

To compare the influence of the polymer composition on the micellization behavior, DLS measurements of different polymers at a fixed pH value of 3 were conducted (Figure 3). By variation of the overall polymer length with a fixed 2VP/CL
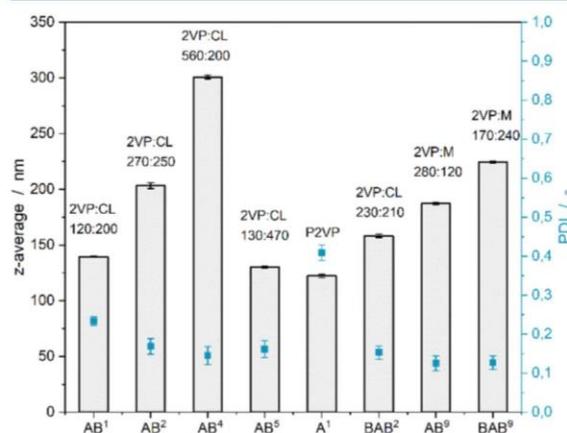
Figure 3. z-Average micelle size (left axis, black) and size dispersity (right axis, blue) of different block copolymer samples.

ratio of 50:50 (AB[1] 120/200; AB[2] 270/250), micelles with an adjustable diameter can be prepared. Copolymer AB[2] ($M_{n,NMR,AB}$ = 34.7 kg/mol) has an approximately 1.6-times higher molecular weight than the smaller copolymer AB[1] ($M_{n,NMR,AB}$ = 34.7 kg/mol) and forms about 1.5-times bigger micelles (AB[2] d_{Avg} = 203 nm; AB[1] d_{Avg} = 140 nm), making the overall micelle size tunable with the molecular weight of the copolymer. Comparing different compositions, the polymer with the highest P2VP content AB[4] (560/200; $M_{n,NMR,AB}$ = 81.8 kg/mol) shows the largest micelles with d_{Avg} = 301 nm, while the micelle size is shrinking with decreasing 2VP content from AB[2] (d_{Avg} = 203 nm) to AB[5] featuring the lowest 2VP/CL ratio (130/470; $M_{n,NMR,AB}$ = 67.7 kg/mol) and thus the smallest micelle diameter of 130 nm. For the pure homopolymer A[1], differently sized structures can be observed in the range of 1−10 and 100−100 nm, corresponding to fully dissolved P2VP chains as random coils. Comparing diblock copolymer AB[2] to triblock copolymer BAB[2] with the same 2VP/CL ratio, the triblock copolymer has a slightly smaller micelle diameter of 160 nm, mainly influenced by molecular weight ($M_{n,NMR,AB}$ = 47.6 kg/mol) rather than composition. Switching to (−)-menthide as block B, again precisely defined micelles were formed for both AB- and BAB-type block copolymers. AB[9] with higher 2VP/M-content (280/120; $M_{n,NMR,AB}$ = 50.0 kg/mol) forms micelles with d_{Avg} = 187 nm, whereas BAB[9] with a higher 2VP/M-ratio and approximately the same size (170/240; $M_{n,NMR,AB}$ = 58.9 kg/mol) forms slightly larger micelles with d_{Avg} = 225 nm. However, for those two copolymers, the parameters for tuning the micelle size are harder to control due to the incomplete (−)-menthide conversion during synthesis. Overall, all block copolymers form precisely defined micelles with good-to-moderate dispersities and possess high tunability regarding micelle size based on the herein-reported catalytic copolymer synthesis approach.[35−37] For example, the polycationic pyridinium block might be used for gene or nucleic acid delivery via complexation of genes or targeting distinct sizes, for example, between 100 and 200 nm. While the micellization of pH-responsive P2VP-based block copolymers[9,10,38,39] and PCL-based block copolymers[40−42] as well as the combination of P2VP and PCL[43−45] are known in the literature, those block copolymers are usually prepared by (living) anionic polymerization instead of applying catalytic techniques. Especially, the susceptibility of such copolymers toward ester bond cleavage by hydrolysis or enzymatic degradation makes these systems interesting tools for drug-delivery applications.[46−50] The presented novel preparation of such copolymers via yttrium catalysis is a facile tool not only for precisely tuning the micelle properties but also to offer the advantage of end-group functionalization for drug conjugation or imaging.[7,27,51,52]

■ CONCLUSIONS

Two GTP- and ROP-active 2-methoxyethylamino-bis-(phenolate)yttrium catalysts [(ONOO)^{tBu}Y(*sym*-col)(thf)] **2** and [((ONOO)^{tBu}Y(thf))$_2$(TMPy)] **3** have successfully been applied for the copolymerization of Michael-type monomer 2VP with CL or (−)-menthide. Different AB- and BAB-type block copolymers were synthesized with regard to the overall chain length and monomer ratios. All synthesized polymers maintained acceptable polydispersities, and block formation was verified using SEC, ESI-MS, and DOSY-NMR analyses. Copolymerization kinetics of 2VP with lactones were successfully determined via utilization of the sterically more demanding (−)-menthide, revealing a living, catalytic copolymerization. End-capping and subsequent ^{31}P NMR analysis revealed a coordination−insertion mechanism via acyl-oxygen cleavage for both lactones, indicating a coordination−insertion mechanism.

Applying the block copolymerization of 2VP with CL or M, materials undergoing microphase separation were obtained, which was shown using DSC and pXRD analyses. The P2VP-*b*-PCL system showed microphase separation while maintaining the semicrystalline character of the PCL block, whereas P2VP-*b*-PM is a fully amorphous system yet retaining microphase separation. Both materials could further be investigated using small-angle X-ray scattering or regarding their mechanical properties.

For the obtained block copolymers, pH-dependent micellization for both P2VP-*b*-PCL and P2VP-*b*-PM in acidic media could be observed. The micelle sizes correlated to catalytic copolymerization parameters which are adjustable during the polymer synthesis. This enabled targeted tuning of precisely defined micelles by the novel catalytic block copolymerization of Michael-type monomers and lactones for diverse applications.

The presented system is an advance from state-of-the-art GTP-*co*-ROP polymers, as the scope of Michael-type monomers is extended to 2VP as a functional block, and additionally, biobased lactone (−)-menthide was applied as the ROP block. The catalytic copolymerization was characterized with regard to its kinetic behavior for the first time. Overall, the combination of group-transfer polymerization and ROPs grants access to a novel class of functional copolymers comprising a stimuli-responsive block and a potentially hydrolysable polyester block. By adjusting the feed ratios, the overall chain length and the block ratios can be tuned, directly targeting physical properties such as phase behavior or micellization. Adapting the herein-reported methods for the synthesis of block copolymers from GTP and ROP, other monomers such as dimethyl acrylamide or diethyl vinyl phosphonates could be copolymerized with various lactones such as (*rac*)-lactide, giving access to a novel class of functional, tunable materials.

■ ASSOCIATED CONTENT

ⓢ Supporting Information

The Supporting Information is available free of charge at https://pubs.acs.org/doi/10.1021/acs.macromol.1c01692.

> General experimental details, block copolymerization results, mechanistic detail visualization, P-capping procedure, ESI-MS measurements, full SEC characterization, additional ^{1}H-/DOSY-NMR spectra and SEC traces, and DSC and pXRD measurements (PDF)

■ AUTHOR INFORMATION

Corresponding Authors

    Friederike Adams − *Institute of Polymer Chemistry, University of Stuttgart, 70569 Stuttgart, Germany; Faculty of Science, Eberhard Karls University of Tübingen, 72076 Tübingen, Germany*; Email: friederike.adams@ipoc.uni-stuttgart.de

    Bernhard Rieger − *WACKER-Chair of Macromolecular Chemistry, Catalysis Research Center, Department of Chemistry, Technical University of Munich, 85748 Garching,*

Germany; ⊙ orcid.org/0000-0002-0023-884X;
Email: rieger@tum.de

Authors

Moritz Kränzlein − *WACKER-Chair of Macromolecular Chemistry, Catalysis Research Center, Department of Chemistry, Technical University of Munich, 85748 Garching, Germany*

Thomas M. Pehl − *WACKER-Chair of Macromolecular Chemistry, Catalysis Research Center, Department of Chemistry, Technical University of Munich, 85748 Garching, Germany*

Complete contact information is available at:
https://pubs.acs.org/10.1021/acs.macromol.1c01692

Author Contributions

The manuscript was written through contributions of all authors. All authors have given approval to the final version of the manuscript.

Notes

The authors declare no competing financial interest.

ACKNOWLEDGMENTS

ABBREVIATIONS

GTP, group-transfer polymerization; ROP, ring-opening polymerization; 2VP/P2VP, 2-vinylpyridine/poly(2-vinylpyridine); CL/PCL, ε-caprolactone/poly(ε-caprolactone); M/PM, (−)-menthide/poly((−)-menthide); REM-GTP, rare-earth metal-mediated group-transfer polymerization; TMPy, 2,3,5,6-tetramethylpyrazine; *sym*-col, 2,4,6-trimethylpyridine/*sym*-collidine; (ONOO)^{tBu}, 6,6′-(((2-methoxyethyl)-azane-diyl)-bis(methylene))-bis(2,4-di-*tert*-butylphenolate); BBL, β-butyrolactone; VL, δ-valerolactone; MMA, methyl methacrylate; thf, tetrahydrofuran; TOF, turnover frequency; pXRD, powder X-ray diffraction

REFERENCES

(1) Yasuda, H.; Yamamoto, H.; Yokota, K.; Miyake, S.; Nakamura, A. Synthesis of monodispersed high molecular weight polymers and isolation of an organolanthanide(III) intermediate coordinated by a penultimate poly(MMA) unit. *J. Am. Chem. Soc.* **1992**, *114*, 4908−4910.

(2) Yasuda, H.; Ihara, E. Rare earth metal initiated polymerizations of polar and nonpolar monomers to give high molecular weight polymers with extremely narrow molecular weight distribution. *Macromol. Chem. Phys.* **1995**, *196*, 2417−2441.

(3) Adams, F.; Pahl, P.; Rieger, B. Metal-Catalyzed Group-Transfer Polymerization: A Versatile Tool for Tailor-Made Functional (Co)-Polymers. *Chemistry* **2018**, *24*, 509−518.

(4) Chen, E. Y.-X. Coordination polymerization of polar vinyl monomers by single-site metal catalysts. *Chem. Rev.* **2009**, *109*, 5157−5214.

(5) Pehl, T. M.; Adams, F.; Kränzlein, M.; Rieger, B. Expanding the Scope of Organic Radical Polymers to Polyvinylphosphonates Synthesized via Rare-Earth Metal-Mediated Group-Transfer Polymerization. *Macromolecules* **2021**, *54*, 4089−4100.

(6) Miyake, G. M.; Chen, E. Y.-X. Metallocene-Mediated Asymmetric Coordination Polymerization of Polar Vinyl Monomers to Optically Active, Stereoregular Polymers. *Macromolecules* **2008**, *41*, 3405−3416.

(7) Schwarzenböck, C.; Schaffer, A.; Nößner, E.; Nelson, P. J.; Huss, R.; Rieger, B. Fluorescent Polyvinylphosphonate Bioconjugates for Selective Cellular Delivery. *Chemistry* **2018**, *24*, 2584−2587.

(8) Schwarzenböck, C.; Schaffer, A.; Pahl, P.; Nelson, P. J.; Huss, R.; Rieger, B. Precise synthesis of thermoresponsive polyvinylphospho-nate-biomolecule conjugates via thiol−ene click chemistry. *Polym. Chem.* **2018**, *9*, 284−290.

(9) Altenbuchner, P. T.; Werz, P. D. L.; Schöppner, P.; Adams, F.; Kronast, A.; Schwarzenböck, C.; Pöthig, A.; Jandl, C.; Haslbeck, M.; Rieger, B. Next Generation Multiresponsive Nanocarriers for Targeted Drug Delivery to Cancer Cells. *Chemistry* **2016**, *22*, 14576−14584.

(10) Adams, F.; Altenbuchner, P. T.; Werz, P. D. L.; Rieger, B. Multiresponsive micellar block copolymers from 2-vinylpyridine and dialkylvinylphosphonates with a tunable lower critical solution temperature. *RSC Adv.* **2016**, *6*, 78750−78754.

(11) Adams, F.; Machat, M. R.; Altenbuchner, P. T.; Ehrmaier, J.; Pöthig, A.; Karsili, T. N. V.; Rieger, B. Toolbox of Nonmetallocene Lanthanides: Multifunctional Catalysts in Group-Transfer Polymerization. *Inorg. Chem.* **2017**, *56*, 9754−9764.

(12) Zhang, N.; Salzinger, S.; Rieger, B. Poly(vinylphosphonate)s with Widely Tunable LCST: A Promising Alternative to Conventional Thermoresponsive Polymers. *Macromolecules* **2012**, *45*, 9751−9758.

(13) Zhang, N.; Salzinger, S.; Soller, B. S.; Rieger, B. Rare earth metal-mediated group-transfer polymerization: From defined polymer microstructures to high-precision nano-scaled objects. *J. Am. Chem. Soc.* **2013**, *135*, 8810−8813.

(14) Mariott, W. R.; Chen, E. Y.-X. Mechanism and Scope of Stereospecific, Coordinative-Anionic Polymerization of Acrylamides by Chiral Zirconocenium Ester and Amide Enolates. *Macromolecules* **2005**, *38*, 6822−6832.

(15) Rodriguez-Delgado, A.; Mariott, W. R.; Chen, E. Y.-X. Living and Syndioselective Polymerization of Methacrylates by Constrained Geometry Titanium Alkyl and Enolate Complexes. *Macromolecules* **2004**, *37*, 3092−3100.

(16) Salzinger, S.; Rieger, B. Rare Earth metal-mediated group transfer polymerization of vinylphosphonates. *Macromol. Rapid Commun.* **2012**, *33*, 1327−1345.

(17) Altenbuchner, P. T.; Soller, B. S.; Kissling, S.; Bachmann, T.; Kronast, A.; Vagin, S. I.; Rieger, B. Versatile 2-Methoxyethylaminobis-(phenolate)yttrium Catalysts: Catalytic Precision Polymerization of Polar Monomers via Rare Earth Metal-Mediated Group Transfer Polymerization. *Macromolecules* **2014**, *47*, 7742−7749.

(18) Cai, C.-X.; Toupet, L.; Lehmann, C. W.; Carpentier, J.-F. Synthesis, structure and reactivity of new yttrium bis(dimethylsilyl)-amido and bis(trimethylsilyl)methyl complexes of a tetradentate bis(phenoxide) ligand. *J. Organomet. Chem.* **2003**, *683*, 131−136.

(19) Amgoune, A.; Thomas, C. M.; Carpentier, J.-F. Yttrium Complexes as Catalysts for Living and Immortal Polymerization of Lactide to Highly Heterotactic PLA. *Macromol. Rapid Commun.* **2007**, *28*, 693−697.

(20) Amgoune, A.; Thomas, C. M.; Ilinca, S.; Roisnel, T.; Carpentier, J.-F. Highly active, productive, and syndiospecific yttrium initiators for the polymerization of racemic beta-butyrolactone. *Angew. Chem., Int. Ed.* **2006**, *45*, 2782−2784.

(21) Ajellal, N.; Bouyahyi, M.; Amgoune, A.; Thomas, C. M.; Bondon, A.; Pillin, I.; Grohens, Y.; Carpentier, J.-F. Syndiotactic-Enriched Poly(3-hydroxybutyrate)s via Stereoselective Ring-Opening Polymerization of Racemic β-Butyrolactone with Discrete Yttrium Catalysts. *Macromolecules* **2009**, *42*, 987−993.

(22) Adams, F.; Pehl, T. M.; Kränzlein, M.; Kernbichl, S. A.; Kang, J.-J.; Papadakis, C. M.; Rieger, B. (Co)polymerization of (-)-Menthide and β-Butyrolactone with Yttrium-bis(phenolates):Tuning Material Properties of Sustainable Polyesters. *Polym. Chem.* **2020**, *11*, 4426−4437.

(23) Kostakis, K.; Mourmouris, S.; Karanikolopoulos, G.; Pitsikalis, M.; Hadjichristidis, N. Ring-opening polymerization of lactones using zirconocene catalytic systems:Block copolymerization with methyl methacrylate. *J. Polym. Sci., Part A: Polym. Chem.* **2007**, *45*, 3524−3537.

(24) Solaro, R.; Cantoni, G.; Chiellini, E. Polymerisability of different lactones and methyl methacrylate in the presence of various organoaluminum catalysts. *Eur. Polym. J.* **1997**, *33*, 205−211.

(25) Arslan, H. l.; Hazer, B.; Kowalczuk, M. Synthesis and characterization of poly[(R, S)-3-hydroxybutyrate] telechelics and their use in the synthesis of poly(methyl methacrylate)-b- poly(3-hydroxybutyrate) block copolymers. *J. Appl. Polym. Sci.* **2002**, *85*, 965−973.

(26) Jung, H.-J.; Yu, I.; Nyamayaro, K.; Mehrkhodavandi, P. Indium-Catalyzed Block Copolymerization of Lactide and Methyl Methacrylate by Sequential Addition. *ACS Catal.* **2020**, *10*, 6488−6496.

(27) Pehl, T. M.; Kränzlein, M.; Adams, F.; Schaffer, A.; Rieger, B. C−H Bond Activation of Silyl-Substituted Pyridines with Bis-(Phenolate)Yttrium Catalysts as a Facile Tool towards Hydroxyl-Terminated Michael-Type Polymers. *Catalysts* **2020**, *10*, 448.

(28) Kronast, A.; Reiter, D.; Altenbuchner, P. T.; Vagin, S. I.; Rieger, B. 2-Methoxyethylamino-bis(phenolate)yttrium Catalysts for the Synthesis of Highly Isotactic Poly(2-vinylpyridine) by Rare-Earth Metal-Mediated Group Transfer Polymerization. *Macromolecules* **2016**, *49*, 6260−6267.

(29) Sosnowski, S.; Duda, A.; Słomkowski, S.; Penczek, S. Determination of the structure of active centers in the anionic polymerization by 31P NMR, introducing a P-containing end group. *Makromol. Chem., Rapid Commun.* **1984**, *5*, 551−557.

(30) Penczek, S.; Brzezinska, K. Determination of structure and concentration of growing species in ionic polymerizations:The 31P NMR method. *Macromol. Symp.* **1994**, *85*, 45−64.

(31) Basko, M.; Nyk, A.; Klosinski, P.; Libiszowski, J.; Kubisa, P.; Penczek, S. Studies of structures and concentration of active species in vinyl anionic polymerization by phosphorus end-capping. *Polym. Bull.* **1991**, *26*, 63−70.

(32) Brulé, E.; Guérineau, V.; Vermaut, P.; Prima, F.; Balogh, J.; Maron, L.; Slawin, A. M. Z.; Nolan, S. P.; Thomas, C. M. Polymerization of cyclic esters using N-heterocyclic carbene carboxylate catalysts. *Polym. Chem.* **2013**, *4*, 2414.

(33) Lanners, S.; Khiri, N.; Solladié, G.; Hanquet, G. Ring-opening of lactones with enolate nucleophiles: a simple access to functionalised β-ketoesters, β,δ-diketoesters and β-ketosulfoxides. *Tetrahedron Lett.* **2005**, *46*, 619−622.

(34) Heuschen, J.; Jérôme, R.; Teyssié, P. Polycaprolactone-based block copolymers. II. Morphology and crystallization of copolymers of styrene or butadiene and ε-caprolactone. *J. Polym. Sci., Part B: Polym. Phys.* **1989**, *27*, 523−544.

(35) Aied, A.; Greiser, U.; Pandit, A.; Wang, W. Polymer gene delivery: overcoming the obstacles. *Drug discovery today* **2013**, *18*, 1090−1098.

(36) Ganta, S.; Devalapally, H.; Shahiwala, A.; Amiji, M. A review of stimuli-responsive nanocarriers for drug and gene delivery. *J. Controlled Release* **2008**, *126*, 187−204.

(37) Hartl, N.; Adams, F.; Costabile, G.; Isert, L.; Döblinger, M.; Xiao, X.; Liu, R.; Merkel, O. M. The Impact of Nylon-3 Copolymer Composition on the Efficiency of siRNA Delivery to Glioblastoma Cells. *Nanomaterials* **2019**, *9*, 986.

(38) Atanase, L. I.; Riess, G. Micellization of pH-stimulable poly(2-vinylpyridine)-b-poly(ethylene oxide) copolymers and their complexation with anionic surfactants. *J. Colloid Interface Sci.* **2013**, *395*, 190−197.

(39) Iurciuc-Tincu, C.-E.; Cretan, M. S.; Purcar, V.; Popa, M.; Daraba, O. M.; Atanase, L. I.; Ochiuz, L. Drug Delivery System Based on pH-Sensitive Biocompatible Poly(2-vinyl pyridine)-b-poly-(ethylene oxide) Nanomicelles Loaded with Curcumin and 5-Fluorouracil. *Polymers* **2020**, *12*, 1450.

(40) Cho, H.; Indig, G. L.; Weichert, J.; Shin, H.-C.; Kwon, G. S. In vivo cancer imaging by poly(ethylene glycol)-b-poly(ε-caprolactone) micelles containing a near-infrared probe. *Nanomedicine* **2012**, *8*, 228−236.

(41) Allen, C. Polycaprolactone−b-poly(ethylene oxide) copolymer micelles as a delivery vehicle for dihydrotestosterone. *J. Controlled Release* **2000**, *63*, 275−286.

(42) Hu, Y.; Zhang, L.; Cao, Y.; Ge, H.; Jiang, X.; Yang, C. Degradation behavior of poly(epsilon-caprolactone)-b-poly(ethylene glycol)-b-poly(epsilon-caprolactone) micelles in aqueous solution. *Biomacromolecules* **2004**, *5*, 1756−1762.

(43) Hameed, N.; Guo, Q. Nanostructure and hydrogen bonding in interpolyelectrolyte complexes of poly(ε-caprolactone)-block-poly(2-vinyl pyridine) and poly(acrylic acid). *Polymer* **2008**, *49*, 5268−5275.

(44) van Butsele, K.; Cajot, S.; van Vlierberghe, S.; Dubruel, P.; Passirani, C.; Benoit, J.-P.; Jérôme, R.; Jérôme, C. pH-Responsive Flower-Type Micelles Formed by a Biotinylated Poly(2-vinyl-pyridine)- block -poly(ethylene oxide)- block -poly(ε-caprolactone) Triblock Copolymer. *Adv. Funct. Mater.* **2009**, *19*, 1416−1425.

(45) Su, M.; Huang, H.; Ma, X.; Wang, Q.; Su, Z. Poly(2-vinylpyridine)-block -Poly(ε-caprolactone) single crystals in micellar solution. *Macromol. Rapid Commun.* **2013**, *34*, 1067−1071.

(46) Ali, S. A. M.; Zhong, S.-P.; Doherty, P. J.; Williams, D. F. Mechanisms of polymer degradation in implantable devices. *Biomaterials* **1993**, *14*, 648−656.

(47) Brückmann, N. E.; Kögel, S.; Hamacher, A.; Kassack, M. U.; Kunz, P. C. Fluorescent Polylactides with Rhenium(bisimine) Cores for Tumour Diagnostics. *Eur. J. Inorg. Chem.* **2010**, *2010*, 5063−5068.

(48) Gomes, M. E.; Azevedo, H. S.; Moreira, A. R.; Ellä, V.; Kellomäki, M.; Reis, R. L. Starch-poly(epsilon-caprolactone) and starch-poly(lactic acid) fibre-mesh scaffolds for bone tissue engineering applications: structure, mechanical properties and degradation behaviour. *J. Tissue Eng. Regener. Med.* **2008**, *2*, 243−252.

(49) Huang, M.-H.; Li, S.; Hutmacher, D. W.; Coudane, J.; Vert, M. Degradation characteristics of poly(ε-caprolactone)-based copolymers and blends. *J. Appl. Polym. Sci.* **2006**, *102*, 1681−1687.

(50) Sánchez-González, S.; Diban, N.; Urtiaga, A. Hydrolytic Degradation and Mechanical Stability of Poly(ε-Caprolactone)/Reduced Graphene Oxide Membranes as Scaffolds for In Vitro Neural Tissue Regeneration. *Membranes* **2018**, *8*, 12.

(51) Adams, F.; Pschenitza, M.; Rieger, B. Yttrium-Catalyzed Synthesis of Bipyridine-Functionalized AB-Block Copolymers:Micellar Support for Photocatalytic Active Rhenium-Complexes. *ChemCatChem* **2018**, *10*, 4309−4316.

(52) Schaffer, A.; Kränzlein, M.; Rieger, B. Synthesis and Application of Functional Group-Bearing Pyridyl-Based Initiators in Rare Earth Metal-Mediated Group Transfer Polymerization. *Macromolecules* **2020**, *53*, 4345−4354.

8.   Summary

Throughout this thesis, different modification points in the context of group-transfer and ring-opening polymerization have been addressed. With respect to functional end-groups, four different 2,6-dimethylpyridine based initiators have been synthesized, bearing a *tert*-butyl-dimethyl silyl protected alcohol, a bis(*tert*-butyl-dimethyl silyl) protected catechol, a trimethyl silyl protected alkyne and an unprotected azide. The silyl protected alcohol has successfully been used in the C-H bond activation and subsequent isolation of a versatile bis(phenolate) yttrium catalyst. This catalyst has been used for the polymerization of diethyl vinylphosphonate and 2-vinylpyridine in a highly controlled way. A thorough end-group analysis revealed covalent attachment of the initiator to the polymers and using different deprotection protocols, the desired hydroxyl end-group could be reobtained. In a similar approach, the silyl protected catechol and the silyl protected alkyne have been used for an *in-situ* C-H bond activation of an yttrium cyclopentadienyl precursor, again attaching the desired moieties to the prepared poly(vinylphosphonates). The same deprotection protocols cleaved the silyl protecting groups, giving access to catechols or alkynes as end-groups. Due to the reactivity of the azide, C-H bond activation of the respective yttrium compounds failed, while the respective reaction using a lutetium cyclopentadienyl catalyst showed the formation of the desired catalyst. Again, the functional group could successfully be transferred to poly(diethyl vinylphosphonates). By means of these initiators, the scope of applicable end-groups for GTP-based polymers has been extended to alcohols, catechols, alkynes and azides.

Regarding the sidechain modifications, a controlled *Lewis* pair polymerization of 4-vinyl-4'-methyl-2,2'-bipyridine using tri-*iso*-butyl aluminum and trimethyl phosphine has been established, giving access to a poly(vinyl bipyridine) prepared *via* a precise, catalytic polymerization technique. To these well-defined poly(vinyl bipyridines), photocatalytically active rhenium complexes and ruthenium complexes as photosensitizers were attached, generating a new class of polymeric photocatalysts. These photocatalysts have been characterized extensively and were successfully used for the photocatalytic reduction of CO_2. By tethering these complexes to the poly(vinyl bipyridine) macroligand and thus forcing them into spatial proximity, the catalyst stability and activity could be increased drastically compared to the mononuclear systems.

To further broaden the monomer scope applicable for ring-opening polymerization, 3-carene has been chemically converted into different monomers while retaining its characteristic 3-membered ring from the basic carbon framework. By means of a reductive ozonolysis, a 3-carene based diol could be synthesized, which was used in a polycondensation reaction with dimethyl terephthalate as comonomer. The prepared polyester is amorphous with a glass transition temperature of about 45 °C. Using different oxidative transformations and a *Baeyer-*

Villiger oxidation for a ring-extension, two different regioisomeric lactones, α- and ε-carene lactone, could be prepared. Both monomers could be converted into the respective homo- and copolymers by catalytic ring-opening polymerization using different metalorganic catalysts. While the homopolymer from α-carene lactone as well as the statistical copolymer of both lactones exhibit semi-crystalline properties with glass transition temperatures around -10 °C, the homopolymer from ε-carene lactone is semi-crystalline with a melting point of 161 °C. By introducing these new monomers, the scope of biobased monomers for polyester synthesis has been broadened.

The last modification point addressed throughout this thesis is the copolymerization of *Michael*-type monomers and lactones *via* sequential copolymerization. Using a monometallic and a bimetallic yttrium bis(phenolate) catalyst, different AB- and BAB- di- and triblock copolymers from 2-vinylpyridine and ε-caprolactone or (-)-menthide have been prepared. By means of this catalytic copolymerization, copolymers with tunable molecular weights and compositions, all exhibiting narrow to moderate polydispersities, could be synthesized. Changing the addition order to lactone ROP first led to the formation of homopolymers only, revealing the monomer coordination strength to be a decisive parameter in the copolymerization of *Michael*-type monomers and lactones as well. By means of catalytic investigations, a living-type polymerization has been found for both the group-transfer polymerization step as well as the for the subsequent ring-opening polymerization step. The thermal transition behavior of the semicrystalline P2VP-*b*-PCL and the amorphous P2VP-*b*-PM have been investigated, revealing microphase separation of the two polymer blocks. In aqueous media, the pH-dependent formation of micelles below a pH of 4 could be observed. By means of tuning the copolymers chain length, composition or block structure, micelle size and thermal properties could be modified.

Summarizing, four different modification points of group-transfer and ring-opening based (co)polymers have successfully been addressed. In the context of GTP, different functional initiators were prepared and introduced to the polymers as well as a sidechain modification of a poly(vinyl bipyridine) with rhenium and ruthenium complexes could be realized. For ROP, a novel monomer has been introduced, giving access to a semicrystalline, high melting polyester. And with respect to both GTP and ROP, copolymerization of two different monomer classes using yttrium catalysis has successfully been realized, giving access to novel, highly interesting materials.

9.   Outlook

With the herein successfully introduced pathways, polymers from GTP and ROP can be modified with respect to their different functionalities. With special focus on the end-group modification, the scope of available end-groups for GTP polymers has been broadened by alcohols, catechols, alkynes and azides. Together with the already reported double bonds,[294] bipyridines,[82] multifunctional pyridines,[85] amines and thiols,[88] most of the functional groups used for modifications is now reported. These functional groups can be introduced to the polymers and used based on the desired application, encompassing for example polymer-drug conjugates, various labelling techniques, or the mentioned surface-based applications. By using the *in-situ* approach with the yttrium cyclopentadienyl catalyst, versatile GTP catalysts can be prepared and used for a variety of different monomers, including the different alkyl vinylphosphonates, vinylpyridines or IPOx as highly functional monomers. When switching to the isolated complexes based on the yttrium bis(phenolate) mainframe, the same functional groups could possibly be introduced to even more monomers, including DMAA and lactones in general, severely broadening the applicability of these functional groups. Using this technique, a versatile toolbox of functional end-groups could be introduced to GTP- and ROP-based polymers, rendering it a useful synthetic method for polymer chemists.
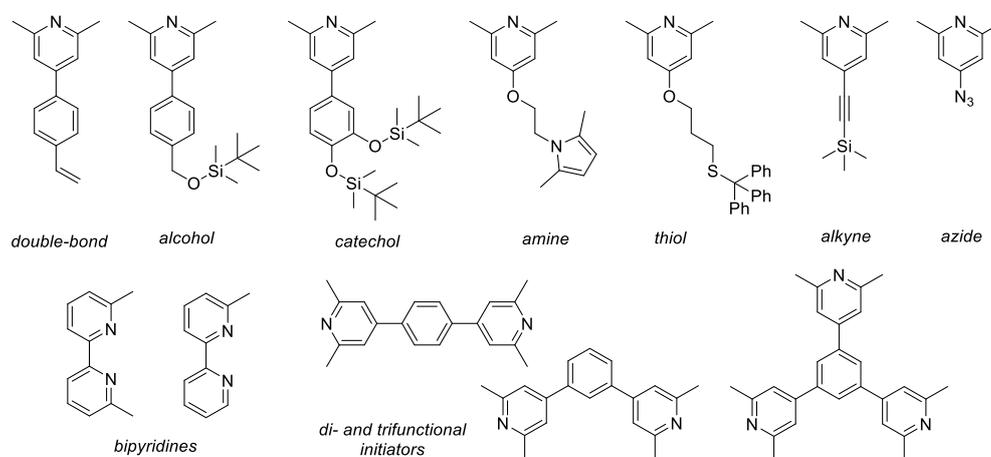
Figure 33: Scope of available functionalized α-methylpyridines for C-H bond activation of yttrium complexes.[82,85,88,294]

Regarding the sidechain modification of the prepared poly(vinyl bipyridines), a catalytical, precise method of polymerizing 4-vinyl-4'-methyl-2,2'-bipyridine is now accessible by means of *Lewis* pair polymerization. The prepared polymers possess narrow polydispersity and the absolute molecular weight of PVBpy can now be determined, thus making them highly defined macroligands for the use of polymer-metal complex compounds. While the herein presented example used these defined polymers for the synthesis of polymeric photocatalysts, this approach is by no means limited to such metal complexes. Bipyridine-based metal complexes

can be found in a variety of different applications, like for example biomedical imaging, DNA binding, electrocatalysis or organic light-emitting diodes.[331–334] Depending on the desired properties, precisely defined PVBpy could be used as macroligand for such complexes, allowing for different applications, like e.g. for use as biologically active, UV-triggered scaffold materials in implants.
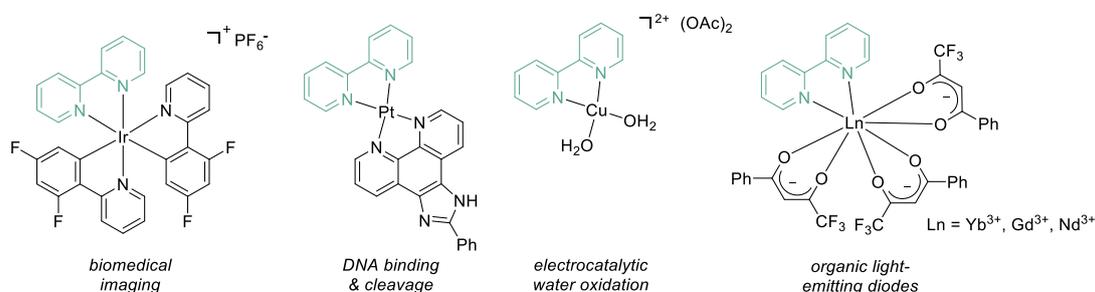
Figure 34: Various bipyridine-based metal complexes for different applications.[331–334]

By polymerizing ε-carene lactone as novel monomer, a semi-crystalline polyester based on turpentine oil is now accessible, while polymerization of α-carene lactone yields an amorphous polyester with a low glass transition temperature. The herein presented synthesis pathway from 3-carene as feedstock involving dual oxidation to the alcohol and subsequently the ketone with a *Baeyer-Villiger* oxidation as key step without rearrangement of the basic carbon skeleton allowed incorporation of the cyclic 3-membered ring structure of 3-carene into the polymer main chain. A similar pathway could be used for β-pinene, possibly allowing incorporation of the 4-membered ring into the polymer main chain. Apart from the investigated statistic copolymers of αCarL and εCarL, additional copolymers from those monomers in combination with each other or other lactones can be prepared. Further, those two monomers could be utilized for more advanced applications like biobased thermoplastic elastomers, where PεCarL serves as hard, semi-crystalline block while PαCarL could be used as soft, amorphous block. Overall, both lactones are interesting, biobased building blocks suited for further investigation.
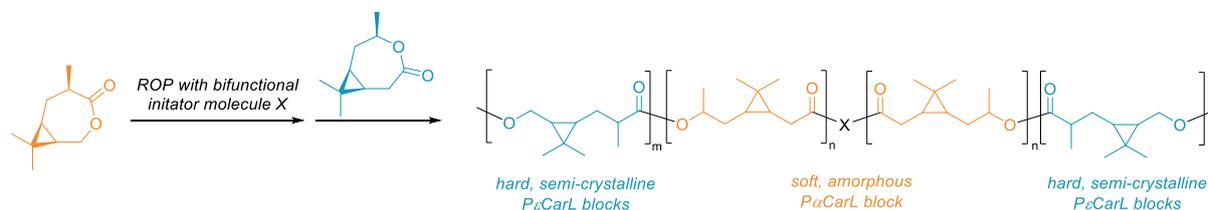
Figure 35: Possible thermoplastic elastomer from BAB-type block copolymers of αCarL and εCarL.

The last synthetic tool for polymer modifications, the copolymerization of *Michael*-type monomers and lactones, bear the potential to produce a variety of new materials with tailor-made properties. Those materials combine the high functionality and tunability of the *Michael*-monomer block with degradability of the polyester block, making them interesting candidates

for advanced applications like drug-delivery. The use of catalysis for such copolymers allows precise tuning of the molecular weight and thus hydrodynamic size of these polymers, all while maintaining a narrow polydispersity and the possibility of influencing the copolymer architecture. Furthermore, a broad variety of different monomers for both the group-transfer polymerization as well as the ring-opening polymerization-based blocks are available, which so far have not been copolymerized, including the alkyl vinylphosphonates or acrylamides on the one hand side and various other lactones on the other hand. Another way of introducing more advanced functionality to this class of copolymers could be to utilized allyl-group containing monomers like diallyl vinylphosphonate, diallyl acrylamide or dihydrocarvide for post-polymerization modifications.
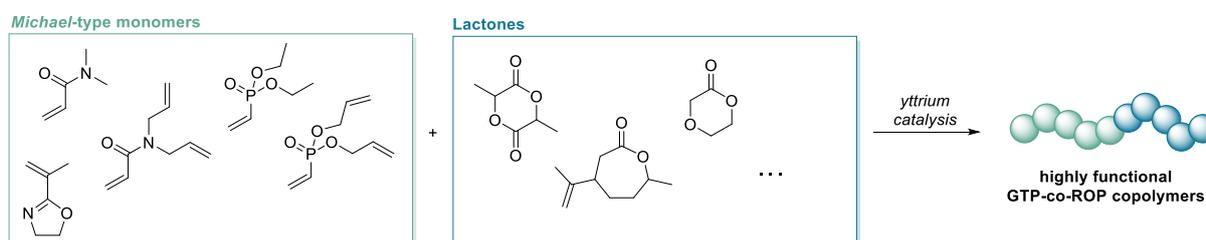
Figure 36: Scope of promising monomers for block copolymerization of *Michael*-type monomers and lactones.

Overall, within this thesis different ways of introducing functionality to group-transfer and ring-opening polymerization have successfully been addressed. All those modifications, while tested and presented in isolated examples, comprise promising tools for the synthesis of advanced polymer materials, fit for use in different applications. These methods and findings address the three main center points of modern polymer chemistry, (**1**) new properties and applications, (**2**) new synthesis methods and (**3**) sustainability.[3]

10. Literature

(1) Staudinger, H. Über Polymerisation. *Ber. dtsch. Chem. Ges. A/B* **1920**, *53* (6), 1073–1085.

(2) Frey, H.; Johann, T. Celebrating 100 years of "polymer science": Hermann Staudinger's 1920 manifesto. *Polym. Chem.* **2020**, *11* (1), 8–14.

(3) Abd-El-Aziz, A. S.; Antonietti, M.; Barner-Kowollik, C.; Binder, W. H.; Böker, A.; Boyer, C.; Buchmeiser, M. R.; Cheng, S. Z. D.; D'Agosto, F.; Floudas, G.; Frey, H.; Galli, G.; Genzer, J.; Hartmann, L.; Hoogenboom, R.; Ishizone, T.; Kaplan, D. L.; Leclerc, M.; Lendlein, A.; Liu, B.; Long, T. E.; Ludwigs, S.; Lutz, J.-F.; Matyjaszewski, K.; Meier, M. A. R.; Müllen, K.; Müllner, M.; Rieger, B.; Russell, T. P.; Savin, D. A.; Schlüter, A. D.; Schubert, U. S.; Seiffert, S.; Severing, K.; Soares, J. B. P.; Staffilani, M.; Sumerlin, B. S.; Sun, Y.; Tang, B. Z.; Tang, C.; Théato, P.; Tirelli, N.; Tsui, O. K. C.; Unterlass, M. M.; Vana, P.; Voit, B.; Vyazovkin, S.; Weder, C.; Wiesner, U.; Wong, W.-Y.; Wu, C.; Yagci, Y.; Yuan, J.; Zhang, G. The Next 100 Years of Polymer Science. *Macromol. Chem. Phys.* **2020**, *221* (16), 2000216.

(4) Webster, O. W.; Hertler, W. R.; Sogah, D. Y.; Farnham, W. B.; Rajan Babu, T. V. Group-transfer polymerization. 1. A new concept for addition polymerization with organosilicon initiators. *J. Am. Chem. Soc.* **1983**, *105* (17), 5706–5708.

(5) Webster, O. W. The discovery and commercialization of group transfer polymerization. *J. Polym. Sci. A Polym. Chem.* **2000**, *38* (16), 2855–2860.

(6) Salzinger, S.; Rieger, B. Rare Earth metal-mediated group transfer polymerization of vinylphosphonates. *Macromol. Rapid Commun.* **2012**, *33* (16), 1327–1345.

(7) Adams, F.; Pahl, P.; Rieger, B. Metal-Catalyzed Group-Transfer Polymerization:A Versatile Tool for Tailor-Made Functional (Co)Polymers. *Chemistry* **2018**, *24* (3), 509–518.

(8) Quirk, R. P.; Ren, J. Mechanistic studies of group transfer polymerization. Silyl group exchange studies. *Macromolecules* **1992**, *25* (24), 6612–6620.

(9) Mueller, A. H. E. Kinetic Discrimination between Various Mechanisms in Group-Transfer Polymerization. *Macromolecules* **1994**, *27* (7), 1685–1690.

(10) Chen, E. Y.-X. Coordination polymerization of polar vinyl monomers by single-site metal catalysts. *Chemical reviews* **2009**, *109* (11), 5157–5214.

(11) Yasuda, H.; Yamamoto, H.; Yokota, K.; Miyake, S.; Nakamura, A. Synthesis of monodispersed high molecular weight polymers and isolation of an organolanthanide(III) intermediate coordinated by a penultimate poly(MMA) unit. *J. Am. Chem. Soc.* **1992**, *114* (12), 4908–4910.

(12) Collins, S.; Ward, D. G. Group-transfer polymerization using cationic zirconocene compounds. *J. Am. Chem. Soc.* **1992**, *114* (13), 5460–5462.

(13) Zhang, Y.; Miyake, G. M.; Chen, E. Y.-X. Alane-based classical and frustrated *Lewis* pairs in polymer synthesis: Rapid polymerization of MMA and naturally renewable methylene butyrolactones into high-molecular-weight polymers. *Angew. Chem. Int. Ed.* **2010**, *49* (52), 10158–10162.

(14) Hong, M.; Chen, J.; Chen, E. Y.-X. Polymerization of Polar Monomers Mediated by Main-Group *Lewis* Acid-Base Pairs. *Chem. Rev.* **2018**, *118* (20), 10551–10616.

(15) Knaus, M. G. M.; Giuman, M. M.; Pöthig, A.; Rieger, B. End of Frustration: Catalytic Precision Polymerization with Highly Interacting *Lewis* Pairs. *J. Am. Chem. Soc.* **2016**, *138* (24), 7776–7781.

(16) Soller, B. S.; Salzinger, S.; Rieger, B. Rare Earth Metal-Mediated Precision Polymerization of Vinylphosphonates and Conjugated Nitrogen-Containing Vinyl Monomers. *Chem. Rev.* **2016**, *116* (4), 1993–2022.

(17) Zhang, N.; Salzinger, S.; Soller, B. S.; Rieger, B. Rare earth metal-mediated group-transfer polymerization: From defined polymer microstructures to high-precision nano-scaled objects. *J. Am. Chem. Soc.* **2013**, *135* (24), 8810–8813.

(18) Takenaka, Y.; Abe, H. Group-Transfer Polymerization of Various Crotonates Using Organic Acid Catalysts. *Macromolecules* **2019**, *52* (11), 4052–4058.

(19) Imada, M.; Takenaka, Y.; Tsuge, T.; Abe, H. Copolymers incorporated with β-substituted acrylate synthesized by organo-catalyzed group-transfer polymerization. *Polym. J.* **2021**, *53* (9), 989–999.

(20) Miyake, G. M.; Chen, E. Y.-X. Metallocene-Mediated Asymmetric Coordination Polymerization of Polar Vinyl Monomers to Optically Active, Stereoregular Polymers. *Macromolecules* **2008**, *41* (10), 3405–3416.

(21) Salzinger, S.; Soller, B. S.; Plikhta, A.; Seemann, U. B.; Herdtweck, E.; Rieger, B. Mechanistic studies on initiation and propagation of rare earth metal-mediated group transfer polymerization of vinylphosphonates. *J. Am. Chem. Soc.* **2013**, *135* (35), 13030–13040.

(22) Yasuda, H.; Ihara, E. Rare earth metal initiated polymerizations of polar and nonpolar monomers to give high molecular weight polymers with extremely narrow molecular weight distribution. *Macromol. Chem. Phys.* **1995**, *196* (8), 2417–2441.

(23) Yasuda, H.; Ihara, E.; Nitto, Y.; Kakehi, T.; Morimoto, M.; Nodono, M. Organo Rare Earth Metal Initiated Living Polymerizations of Polar and Nonpolar Monomers. In *Functional Polymers*; Patil, A. O., Schulz, D. N., Novak, B. M., Eds.; ACS Symposium Series; American Chemical Society, **1998**; pp 149–162.

(24) Xu, T.; Liu, J.; Lu, X.-B. Highly Active Half-Metallocene Yttrium Catalysts for Living and Chemoselective Polymerization of Allyl Methacrylate. *Macromolecules* **2015**, *48* (20), 7428–7434.

(25) Pugh, C.; Percec, V. Synthesis and group transfer polymerization and copolymerization of *p*-vinylbenzyl methacrylate. *Polymer Bulletin* **1985**, *14* (2), 109–116.

(26) Ihara, E.; Morimoto, M.; Yasuda, H. Living Polymerizations and Copolymerizations of Alkyl Acrylates by the Unique Catalysis of Rare Earth Metal Complexes. *Macromolecules* **1995**, *28* (23), 7886–7892.

(27) Jia, Q.; Yan, Z.-C.; Li, Y.; Liu, J.; Ding, Y.; Liu, Y.; Li, J.; Chen, Y. Synthesis of well-defined di- and triblock acrylic copolymers consisting of hard poly(dicyclopentanyl acrylate) and soft poly(alkyl acrylate) segments by organocatalyzed group transfer polymerization and their glass transition behavior. *Polym. Chem.* **2021**, *12* (23), 3427–3440.

(28) Chen, Y.; Kakuchi, T. Organocatalyzed Group Transfer Polymerization. *Chem. Rec.* **2016**, *16* (4), 2161–2183.

(29) Kaneko, H.; Nagae, H.; Tsurugi, H.; Mashima, K. End-functionalized polymerization of 2-vinylpyridine through initial C-H bond activation of N-heteroaromatics and internal alkynes by yttrium ene-diamido complexes. *J. Am. Chem. Soc.* **2011**, *133* (49), 19626–19629.

(30) He, J.; Zhang, Y.; Chen, E. Synthesis of Pyridine- and 2-Oxazoline-Functionalized Vinyl Polymers by Alane-Based Frustrated *Lewis* Pairs. *Synlett* **2014**, *25* (11), 1534–1538.

(31) Su, Y.; Zhao, Y.; Zhang, H.; Luo, Y.; Xu, X. Rare-Earth Aryloxide/Ylide-Functionalized Phosphine Frustrated *Lewis* Pairs for the Polymerization of 4-Vinylpyridine and Its Derivatives. *Macromolecules* **2021**, *54* (17), 7724–7731.

(32) Thomas M. Pehl; Moritz Kränzlein; Friederike Adams; Andreas Schaffer and Bernhard Rieger. C–H Bond Activation of Silyl-Substituted Pyridines with Bis(Phenolate)Yttrium Catalysts as a Facile Tool towards Hydroxyl-Terminated Michael-Type Polymers. *Catalysts* **2020**, *10* (4), 448.

(33) Zhang, N.; Salzinger, S.; Rieger, B. Poly(vinylphosphonate)s with Widely Tunable LCST: A Promising Alternative to Conventional Thermoresponsive Polymers. *Macromolecules* **2012**, *45* (24), 9751–9758.

(34) Schwarzenböck, C.; Nelson, P. J.; Huss, R.; Rieger, B. Synthesis of next generation dual-responsive cross-linked nanoparticles and their application to anti-cancer drug delivery. *Nanoscale* **2018**, *10* (34), 16062–16068.

(35) Pehl, T. M.; Adams, F.; Kränzlein, M.; Rieger, B. Expanding the Scope of Organic Radical Polymers to Polyvinylphosphonates Synthesized via Rare-Earth Metal-Mediated Group-Transfer Polymerization. *Macromolecules* **2021**, *54* (9), 4089–4100.

(36) Imada, M.; Takenaka, Y.; Hatanaka, H.; Tsuge, T.; Abe, H. Unique acrylic resins with aromatic side chains by homopolymerization of cinnamic monomers. *Commun. Chem.* **2019**, *2* (1), 6855.

(37) McGraw, M.; Chen, E. Y.-X. Catalytic *Lewis* Pair Polymerization of Renewable Methyl Crotonate to High-Molecular-Weight Polymers. *ACS Catal.* **2018**, *8* (10), 9877–9887.

(38) Clarke, R. W.; McGraw, M. L.; Gowda, R. R.; Chen, E. Y.-X. *Lewis* Pair Polymerization of Renewable Indenone to Erythro-Ditactic High-T_g Polymers with an Upcycling Avenue. *Macromolecules* **2020**, *53* (2), 640–648.

(39) Chen, X.; Caporaso, L.; Cavallo, L.; Chen, E. Y.-X. Stereoselectivity in metallocene-catalyzed coordination polymerization of renewable methylene butyrolactones: From stereo-random to stereo-perfect polymers. *J. Am. Chem. Soc.* **2012**, *134* (17), 7278–7281.

(40) Kikuchi, S.; Chen, Y.; Kitano, K.; Takada, K.; Satoh, T.; Kakuchi, T. Organic acids as efficient catalysts for group transfer polymerization of N,N-disubstituted acrylamide with silyl ketene acetal: Polymerization mechanism and synthesis of diblock copolymers. *Polym. Chem.* **2015**, *6* (38), 6845–6856.

(41) McGraw, M. L.; Chen, E. Y.-X. Borane/silane frustrated *Lewis* pairs for polymerization of β-substituted Michael acceptors. *Tetrahedron* **2019**, *75* (11), 1475–1480.

(42) Adams, F.; Altenbuchner, P. T.; Werz, P. D. L.; Rieger, B. Multiresponsive micellar block copolymers from 2-vinylpyridine and dialkylvinylphosphonates with a tunable lower critical solution temperature. *RSC Adv.* **2016**, *6* (82), 78750–78754.

(43) Kränzlein, M.; Pehl, T. M.; Adams, F.; Rieger, B. Uniting Group-Transfer and Ring-Opening Polymerization—Block Copolymers from Functional Michael-Type Monomers and Lactones. *Macromolecules* **2021**, 54 (23), 10860–10869.

(44) Altenbuchner, P. T.; Werz, P. D. L.; Schöppner, P.; Adams, F.; Kronast, A.; Schwarzenböck, C.; Pöthig, A.; Jandl, C.; Haslbeck, M.; Rieger, B. Next Generation Multiresponsive Nanocarriers for Targeted Drug Delivery to Cancer Cells. *Chemistry* **2016**, *22* (41), 14576–14584.

(45) Maier, A. S.; Thomas, C.; Kränzlein, M.; Pehl, T. M.; Rieger, B. Macromolecular Rhenium–Ruthenium Complexes for Photocatalytic CO$_2$ Conversion: From Catalytic *Lewis* Pair Polymerization to Well-Defined Poly(vinyl bipyridine)–Metal Complexes. *Macromolecules* **2022**, *55* (16), 7039-7048.

(46) Halama, K.; Schaffer, A.; Rieger, B. Allyl group-containing polyvinylphosphonates as a flexible platform for the selective introduction of functional groups via polymer-analogous transformations. *RSC Adv.* **2021**, *11* (61), 38555–38564.

(47) Lanzinger, D.; Salzinger, S.; Soller, B. S.; Rieger, B. Poly(vinylphosphonate)s as Macromolecular Flame Retardants for Polycarbonate. *Ind. Eng. Chem. Res.* **2015**, *54* (6), 1703–1712.

(48) Wenisch, S. E.; Schaffer, A.; Rieger, B. Effect of Hofmeister Salts on the LCST of Poly(diethyl vinylphosphonate) and Poly(2-vinylpyridine-block-diethyl vinylphosphonate). *Macromol. Chem. Phys.* **2022**, *223*, 2200063.

(49) Yan, C.; Liu, Z.-X.; Xu, T.-Q. Regioselective, stereoselective, and living polymerization of divinyl pyridine monomers using rare earth catalysts. *Polym. Chem.* **2020**, *11* (12), 2044–2052.

(50) McGraw, M. L.; Clarke, R. W.; Chen, E. Y.-X. Compounded Sequence Control in Polymerization of One-Pot Mixtures of Highly Reactive Acrylates by Differentiating *Lewis* Pairs. *J. Am. Chem. Soc.* **2020**, *142* (13), 5969–5973.

(51) Altenbuchner, P. T.; Soller, B. S.; Kissling, S.; Bachmann, T.; Kronast, A.; Vagin, S. I.; Rieger, B. Versatile 2-Methoxyethylaminobis(phenolate)yttrium Catalysts:Catalytic Precision Polymerization of Polar Monomers via Rare Earth Metal-Mediated Group Transfer Polymerization. *Macromolecules* **2014**, *47* (22), 7742–7749.

(52) Cai, C.-X.; Toupet, L.; Lehmann, C. W.; Carpentier, J.-F. Synthesis, structure and reactivity of new yttrium bis(dimethylsilyl)amido and bis(trimethylsilyl)methyl complexes of a tetradentate bis(phenoxide) ligand. *J. Organomet. Chem.* **2003**, *683* (1), 131–136.

(53) Webster, O. W. Group Transfer Polymerization: A Critical Review of Its Mechanism and Comparison with Other Methods for Controlled Polymerization of Acrylic Monomers. In *New Synthetic Methods*; Advances in Polymer Science; Springer Berlin Heidelberg, 2004; pp 1–34.

(54) Fuchise, K.; Chen, Y.; Satoh, T.; Kakuchi, T. Recent progress in organocatalytic group transfer polymerization. *Polym. Chem.* **2013**, *4* (16), 4278.

(55) Welch, G. C.; San Juan, R. R.; Masuda, J. D.; Stephan, D. W. Reversible, metal-free hydrogen activation. *Science* **2006**, *314* (5802), 1124–1126.

(56) Geier, S. J.; Stephan, D. W. Lutidine/B(C6F5)3: at the boundary of classical and frustrated *Lewis* pair reactivity. *J. Am. Chem. Soc.* **2009**, *131* (10), 3476–3477.

(57) McGraw, M. L.; Chen, E. Y.-X. *Lewis* Pair Polymerization: Perspective on a Ten-Year Journey. *Macromolecules* **2020**, *53* (15), 6102–6122.

(58) Watson, I. C.; Zhou, Y.; Ferguson, M. J.; Kränzlein, M.; Rieger, B.; Rivard, E. Trialkylaluminum N-Heterocyclic Olefin (NHO) Adducts as Catalysts for the Polymerization of Michael-Type Monomers. *Z. Anorg. Allg. Chem.* **2020**, *127*, 1136.

(59) Weger, M.; Grötsch, R. K.; Knaus, M. G.; Giuman, M. M.; Mayer, D. C.; Altmann, P. J.; Mossou, E.; Dittrich, B.; Pöthig, A.; Rieger, B. Non-Innocent Methylene Linker in Bridged *Lewis* Pair Initiators. *Angew. Chem. Int. Ed.***2019**, *58* (29), 9797–9801.

(60) Xu, T.; Chen, E. Y.-X. Probing site cooperativity of frustrated phosphine/borane *Lewis* pairs by a polymerization study. *J. Am. Chem. Soc.* **2014**, *136* (5), 1774–1777.

(61) Ute, K.; Tarao, T.; Hatada, K. Group Transfer Polymerization of Methyl Crotonate. *Polym. J.* **1997**, *29* (11), 957–958.

(62) Ute, K.; Tarao, T.; Kitayama, T. Enhanced Stereocontrol in Disyndiotactic-specific Group Transfer Polymerization of Methyl Crotonate—Stereochemical Evidence of Group Transfer. *Polym. J.* **2005**, *37* (8), 578–583.

(63) Mariott, W. R.; Chen, E. Y.-X. Stereospecific, Coordination Polymerization of Acrylamides by Chiral ansa -Metallocenium Alkyl and Ester Enolate Cations. *Macromolecules* **2004**, *37* (13), 4741–4743.

(64) Rodriguez-Delgado, A.; Mariott, W. R.; Chen, E. Y.-X. Living and Syndioselective Polymerization of Methacrylates by Constrained Geometry Titanium Alkyl and Enolate Complexes. *Macromolecules* **2004**, *37* (9), 3092–3100.

(65) Ning, Y.; Chen, E. Y.-X. Metallocene-catalyzed polymerization of methacrylates to highly syndiotactic polymers at high temperatures. *J. Am. Chem. Soc.* **2008**, *130* (8), 2463–2465.

(66) Bolig, A. D.; Chen, E. Y.-X. *ansa*-Zirconocene ester enolates: synthesis, structure, reaction with organo-*Lewis* acids, and application to polymerization of methacrylates. *J. Am. Chem. Soc.* **2004**, *126* (15), 4897–4906.

(67) Salzinger, S.; Seemann, U. B.; Plikhta, A.; Rieger, B. Poly(vinylphosphonate)s Synthesized by Trivalent Cyclopentadienyl Lanthanide-Induced Group Transfer Polymerization. *Macromolecules* **2011**, *44* (15), 5920–5927.

(68) Soller, B. S.; Salzinger, S.; Jandl, C.; Pöthig, A.; Rieger, B. C–H Bond Activation by σ-bond Metathesis as a Versatile Route toward Highly Efficient Initiators for the Catalytic Precision Polymerization of Polar Monomers. *Organometallics* **2014**, *34* (11), 2703–2706.

(69) Weger, M.; Pahl, P.; Schmidt, F.; Soller, B. S.; Altmann, P. J.; Pöthig, A.; Gemmecker, G.; Eisenreich, W.; Rieger, B. Isospecific Group-Transfer Polymerization of Diethyl Vinylphosphonate and Multidimensional NMR Analysis of the Polymer Microstructure. *Macromolecules* **2019**, *52* (18), 7073–7080.

(70) Adams, F.; Machat, M. R.; Altenbuchner, P. T.; Ehrmaier, J.; Pöthig, A.; Karsili, T. N. V.; Rieger, B. Toolbox of Nonmetallocene Lanthanides:Multifunctional Catalysts in Group-Transfer Polymerization. *Inorg. Chem.* **2017**, *56* (16), 9754–9764.

(71) Cui, C.; Shafir, A.; Reeder, C. L.; Arnold, J. Highly Isospecific Polymerization of Methyl Methacrylate with a Bis(pyrrolylaldiminato)samarium Hydrocarbyl Complex. *Organometallics* **2003**, *22* (17), 3357–3359.

(72) Xu, T.-Q.; Yang, G.-W.; Lu, X.-B. Highly Isotactic and High-Molecular-Weight Poly(2-vinylpyridine) by Coordination Polymerization with Yttrium Bis(phenolate) Ether Catalysts. *ACS Catal.* **2016**, *6* (8), 4907–4913.

(73) Yao, Y.; Luo, Y.; Chen, J.; Zhang, Z.; Zhang, Y.; Shen, Q. Synthesis and characterization of bis(guanidinate)lanthanide diisopropylamido complexes. *J. Organomet. Chem.* **2003**, *679* (2), 229–237.

(74) Altenbuchner, P. T.; Adams, F.; Kronast, A.; Herdtweck, E.; Pöthig, A.; Rieger, B. Stereospecific catalytic precision polymerization of 2-vinylpyridine via rare earth metal-mediated group transfer polymerization with 2-methoxyethylamino-bis(phenolate)-yttrium complexes. *Polym. Chem.* **2015**, *6* (38), 6796–6801.

(75) Waterman, R. σ-Bond Metathesis: A 30-Year Retrospective. *Organometallics* **2013**, *32* (24), 7249–7263.

(76) Arndtsen, B. A.; Bergman, R. G.; Mobley, T. A.; Peterson, T. H. Selective Intermolecular Carbon-Hydrogen Bond Activation by Synthetic Metal Complexes in Homogeneous Solution. *Acc. Chem. Res.* **2002**, *28* (3), 154–162.

(77) Labinger, J. A.; Bercaw, J. E. Understanding and exploiting C-H bond activation. *Nature* **2002**, *417* (6888), 507–514.

(78) Watson, P. L. Facile C–H activation by lutetium–methyl and lutetium–hydride complexes. *J. Chem. Soc., Chem. Commun.* **1983** (6), 276–277.

(79) Watson, P. L. Methane exchange reactions of lanthanide and early-transition-metal methyl complexes. *J. Am. Chem. Soc.* **1983**, *105* (21), 6491–6493.

(80) Evans, W. J.; Davis, B. L.; Champagne, T. M.; Ziller, J. W. C-H bond activation through steric crowding of normally inert ligands in the sterically crowded gadolinium and yttrium $(C_5Me_5)_3M$ complexes. *PNAS* **2006**, *103* (34), 12678–12683.

(81) Goldberg, K. I.; Goldman, A. S., Eds. *Activation and Functionalization of C—H Bonds*; ACS Symposium Series 885; American Chemical Society: Washington, DC, **2004**.

(82) Adams, F.; Pschenitza, M.; Rieger, B. Yttrium-Catalyzed Synthesis of Bipyridine-Functionalized AB-Block Copolymers: Micellar Support for Photocatalytic Active Rhenium-Complexes. *ChemCatChem* **2018**, *10* (19), 4309–4316.

(83) Duchateau, R.; Brussee, E. A. C.; Meetsma, A.; Teuben, J. H. Synthesis and Reactivity of Bis(alkoxysilylamido)yttrium η-2-Pyridyl and η 2-α-Picolyl Compounds. *Organometallics* **1997**, *16* (25), 5506–5516.

(84) Duchateau, R.; van Wee, C. T.; Teuben, J. H. Insertion and C−H Bond Activation of Unsaturated Substrates by Bis(benzamidinato)yttrium Alkyl, $[PhC(NSiMe_3)_2]_2YR$ (R = CH_2 Ph·THF, $CH(SiMe_3)_2$), and Hydrido, $\{[PhC(NSiMe_3)_2]_2Y(\mu\text{-}H)\}_2$, Compounds. *Organometallics* **1996**, *15* (9), 2291–2302.

(85) Pahl, P.; Schwarzenböck, C.; Herz, F. A. D.; Soller, B. S.; Jandl, C.; Rieger, B. Core-First Synthesis of Three-Armed Star-Shaped Polymers by Rare Earth Metal-Mediated Group Transfer Polymerization. *Macromolecules* **2017**, *50* (17), 6569–6576.

(86) Schwarzenböck, C.; Schaffer, A.; Pahl, P.; Nelson, P. J.; Huss, R.; Rieger, B. Precise synthesis of thermoresponsive polyvinylphosphonate-biomolecule conjugates via thiol–ene click chemistry. *Polym. Chem.* **2018**, *9* (3), 284–290.

(87) Schaffer, A.; Kränzlein, M.; Rieger, B. Precise Synthesis of Poly(dimethylsiloxane) Copolymers through C–H Bond-Activated Macroinitiators via Yttrium-Mediated Group Transfer Polymerization and Ring-Opening Polymerization. *Macromolecules* **2020**, *53* (19), 8382–8392.

(88) Schaffer, A.; Kränzlein, M.; Rieger, B. Synthesis and Application of Functional Group-Bearing Pyridyl-Based Initiators in Rare Earth Metal-Mediated Group Transfer Polymerization. *Macromolecules* **2020**, 53 (11), 4345–4354.

(89) Adams, F.; Pehl, T.; Kränzlein, M.; Kernbichl, S. A.; Kang, J.-J.; Papadakis, C. M.; Rieger, B. (Co)polymerization of (-)-Menthide and β-Butyrolactone with Yttrium-bis(phenolates):Tuning Material Properties of Sustainable Polyesters. *Polym. Chem.* **2020**, *27* (11), 4426–4437.

(90) Soller, B. S.; Zhang, N.; Rieger, B. Catalytic Precision Polymerization: Rare Earth Metal-Mediated Synthesis of Homopolymers, Block Copolymers, and Polymer Brushes. *Macromol. Chem. Phys.* **2014**, *215* (20), 1946–1962.

(91) Altenbuchner, P. T.; Kronast, A.; Kissling, S.; Vagin, S. I.; Herdtweck, E.; Pöthig, A.; Deglmann, P.; Loos, R.; Rieger, B. Mechanistic Investigations of the Stereoselective Rare Earth Metal-Mediated Ring-Opening Polymerization of β-Butyrolactone. *Chemistry* **2015**, *21* (39), 13609–13617.

(92) Kronast, A.; Reiter, D.; Altenbuchner, P. T.; Vagin, S. I.; Rieger, B. 2-Methoxyethylamino-bis(phenolate)yttrium Catalysts for the Synthesis of Highly Isotactic Poly(2-vinylpyridine) by Rare-Earth Metal-Mediated Group Transfer Polymerization. *Macromolecules* **2016**, *49* (17), 6260–6267.

(93) Pudasaini, B. Yttrium Catalyzed Dialkyl Vinyl Phosphonate Polymerization: Mechanistic Insights on the Precision Polymerization from DFT. *Organometallics* **2019**, *38* (5), 1091–1098.

(94) Soller, B. S.; Sun, Q.; Salzinger, S.; Jandl, C.; Pöthig, A.; Rieger, B. Ligand Induced Steric Crowding in Rare Earth Metal-Mediated Group Transfer Polymerization of Vinylphosphonates: Does Enthalpy Matter? *Macromolecules* **2016**, *49* (5), 1582–1589.

(95) Boffa, L. S.; Novak, B. M. Bimetallic Samarium (III) Initiators for the Living Polymerization of Methacrylates and Lactones. A New Route into Telechelic, Triblock, and" Link-Functionalized" Polymers. *Macromolecules* **1994**, *27* (23), 6993–6995.

(96) Adams, F.; Rieger, B. From Michael-type systems to biobased lactones: Designing novel polymer microstructures with modified bis(phenolate)lanthanides; Universitätsbibliothek der TU München, 2019.

(97) Mariott, W. R.; Chen, E. Y.-X. Mechanism and Scope of Stereospecific, Coordinative-Anionic Polymerization of Acrylamides by Chiral Zirconocenium Ester and Amide Enolates. *Macromolecules* **2005**, *38* (16), 6822–6832.

(98) Tomasi, S.; Weiss, H.; Ziegler, T. Group Transfer Polymerizations of Acrylates Catalyzed by Mononuclear Early d-Block and f-Block Metallocenes: A DFT Study. *Organometallics* **2006**, *25* (15), 3619–3630.

(99) Schaffer, A.; Weger, M.; Rieger, B. From lanthanide-mediated, high-precision group transfer polymerization of Michael-type monomers, to intelligent, functional materials. *Europ. Polym. J.* **2020**, *122*, 109385.

(100) Hsu, J.-C.; Chen, Y.; Kakuchi, T.; Chen, W.-C. Synthesis of Linear and Star-Shaped Poly[4-(diphenylamino)benzyl methacrylate]s by Group Transfer Polymerization and Their Electrical Memory Device Applications. *Macromolecules* **2011**, *44* (13), 5168–5177.

(101) Seemann, U. B.; Dengler, J. E.; Rieger, B. High-molecular-weight poly(vinylphosphonate)s by single-component living polymerization initiated by rare-earth-metal complexes. *Angew. Chem. Int. Ed.* **2010**, *49* (20), 3489–3491.

(102) Li, Y.; Ward, D. G.; Reddy, S. S.; Collins, S. Polymerization of Methyl Methacrylate Using Zirconocene Initiators:Polymerization Mechanisms and Applications. *Macromolecules* **1997**, *30* (7), 1875–1883.

(103) Rodriguez-Delgado, A.; Chen, E. Y.-X. Mechanistic Studies of Stereospecific Polymerization of Methacrylates Using a Cationic, Chiral *ansa*-Zirconocene Ester Enolate. *Macromolecules* **2005**, *38* (7), 2587–2594.

(104) Nguyen, H.; Jarvis, A. P.; Lesley, M. J. G.; Kelly, W. M.; Reddy, S. S.; Taylor, N. J.; Collins, S. Isotactic Polymerization of Methyl Methacrylate Using a Prochiral, Zirconium Enolate Initiator. *Macromolecules* **2000**, *33* (5), 1508–1510.

(105) Collins, S.; Ward, D. G.; Suddaby, K. H. Group-Transfer Polymerization Using Metallocene Catalysts: Propagation Mechanisms and Control of Polymer Stereochemistry. *Macromolecules* **1994**, *27* (24), 7222–7224.

(106) Rodriguez-Delgado, A.; Mariott, W. R.; Chen, E. Y.-X. Synthesis and MMA polymerization of chiral *ansa*-zirconocene ester enolate complexes with C$_2$- and C$_s$-ligation. *J. Organomet. Chem.* **2006**, *691* (16), 3490–3497.

(107) Becker, G.; Wurm, F. R. Functional biodegradable polymers via ring-opening polymerization of monomers without protective groups. *Chem. Soc. Rev.* **2018**, *47* (20), 7739–7782.

(108) Nuyken, O.; Pask, S. Ring-Opening Polymerization—An Introductory Review. *Polymers* **2013**, *5* (2), 361–403.

(109) Upitak, K.; Thomas, C. M. One-Pot Catalysis: A Privileged Approach for Sustainable Polymers? *Acc. Chem. Res.* **2022**, *55* (16), 2168-2179.

(110) Della Monica, F.; Kleij, A. W. From terpenes to sustainable and functional polymers. *Polym. Chem.* **2020**, *11* (32), 5109–5127.

(111) Jérôme, C.; Lecomte, P. Recent advances in the synthesis of aliphatic polyesters by ring-opening polymerization. *Adv. Drug. Deliv. Rev.* **2008**, *60* (9), 1056–1076.

(112) Abe, A.; Albertsson, A.-C.; Cantow, H.-J.; Dušek, K.; Edwards, S.; Höcker, H.; Joanny, J.-F.; Kausch, H.-H.; Lee, K.-S.; McGrath, J. E.; Monnerie, L.; Stupp, S. I.; Suter, U. W.; Wegner, G.; Young, R. J., Eds. *Degradable Aliphatic Polyesters*; Advances in Polymer Science, Vol. 157; Springer, **2002**.

(113) Olsén, P.; Odelius, K.; Albertsson, A.-C. Thermodynamic Presynthetic Considerations for Ring-Opening Polymerization. *Biomacromolecules* **2016**, *17* (3), 699–709.

(114) Al-Shok, L.; Haddleton, D. M.; Adams, F. Progress in Catalytic Ring-Opening Polymerization of Biobased Lactones. In ; Advances in Polymer Science; Springer Berlin Heidelberg, 2022.

(115) Tang, X.; Chen, E. Y.-X. Chemical synthesis of perfectly isotactic and high melting bacterial poly(3-hydroxybutyrate) from bio-sourced racemic cyclic diolide. *Nat. Commun.* **2018**, *9* (1), 2345.

(116) Bruckmoser, J.; Henschel, D.; Vagin, S.; Rieger, B. Combining high activity with broad monomer scope: indium salan catalysts in the ring-opening polymerization of various cyclic esters. *Catal. Sci. Technol.* **2022**, *12* (10), 3295–3302.

(117) Chen, T.; Qin, Z.; Qi, Y.; Deng, T.; Ge, X.; Wang, J.; Hou, X. Degradable polymers from ring-opening polymerization of α-angelica lactone, a five-membered unsaturated lactone. *Polym. Chem.* **2011**, *2* (5), 1190–1194.

(118) Isikgor, F. H.; Becer, C. R. Lignocellulosic biomass: A sustainable platform for the production of bio-based chemicals and polymers. *Polym. Chem.* **2015**, *6* (25), 4497–4559.

(119) Kim, H. J.; Reddi, Y.; Cramer, C. J.; Hillmyer, M. A.; Ellison, C. J. Readily Degradable Aromatic Polyesters from Salicylic Acid. *ACS Macro Lett.* **2020**, *9* (1), 96–102.

(120) Llevot, A.; Dannecker, P.-K.; Czapiewski, M. von; Over, L. C.; Söyler, Z.; Meier, M. A. R. Renewability is not Enough: Recent Advances in the Sustainable Synthesis of Biomass-Derived Monomers and Polymers. *Chemistry* **2016**, *22* (33), 11510–11521.

(121) Mathers, R. T. How well can renewable resources mimic commodity monomers and polymers? *J. Polym. Sci. A Polym. Chem.* **2012**, *50* (1), 1–15.

(122) Wilbon, P. A.; Chu, F.; Tang, C. Progress in renewable polymers from natural terpenes, terpenoids, and rosin. *Macromol. Rapid Commun.* **2013**, *34* (1), 8–37.

(123) Pion, F.; Ducrot, P.-H.; Allais, F. Renewable Alternating Aliphatic-Aromatic Copolyesters Derived from Biobased Ferulic Acid, Diols, and Diacids: Sustainable Polymers with Tunable Thermal Properties. *Macromol. Chem. Phys.* **2014**, *215* (5), 431–439.

(124) Nsengiyumva, O.; Miller, S. A. Synthesis, characterization, and water-degradation of biorenewable polyesters derived from natural camphoric acid. *Green Chem.* **2019**, *21* (5), 973–978.

(125) Holmberg, A. L.; Reno, K. H.; Wool, R. P.; Epps, T. H. Biobased building blocks for the rational design of renewable block polymers. *Soft matter* **2014**, *10* (38), 7405–7424.

(126) Álvarez-Chávez, C. R.; Edwards, S.; Moure-Eraso, R.; Geiser, K. Sustainability of bio-based plastics: general comparative analysis and recommendations for improvement. *J. Clean. Prod.* **2012**, *23* (1), 47–56.

(127) Nakagawa, Y.; Tamura, M.; Tomishige, K. Recent development of production technology of diesel- and jet-fuel-range hydrocarbons from inedible biomass. *Fuel. Process. Technol.* **2019**, *193*, 404–422.

(128) Stamm, A.; Biundo, A.; Schmidt, B.; Brücher, J.; Lundmark, S.; Olsén, P.; Fogelström, L.; Malmström, E.; Bornscheuer, U. T.; Syrén, P.-O. A Retro-biosynthesis-Based Route to Generate Pinene-Derived Polyesters. *Chembiochem* **2019**, *20* (13), 1664–1671.

(129) Hillmyer, M. A. The promise of plastics from plants. *Science* **2017**, *358* (6365), 868–870.

(130) Quilter, H. C.; Hutchby, M.; Davidson, M. G.; Jones, M. D. Polymerisation of a terpene-derived lactone: A bio-based alternative to ε-caprolactone. *Polym. Chem.* **2017**, *8* (5), 833–837.

(131) García, D.; Bustamante, F.; Villa, A. L.; Lapuerta, M.; Alarcón, E. Oxyfunctionalization of Turpentine for Fuel Applications. *Energy Fuels* **2020**, *34* (1), 579–586.

(132) Kukhta, N. A.; Vasilenko, I. V.; Kostjuk, S. V. Room temperature cationic polymerization of β-pinene using modified AlCl$_3$ catalyst: toward sustainable plastics from renewable biomass resources. *Green Chem.* **2011**, *13* (9), 2362.

(133) Lu, J.; Kamigaito, M.; Sawamoto, M.; Higashimura, T.; Deng, Y.-X. Cationic polymerization of β-pinene with the AlCl$_3$/SbCl$_3$ binary catalyst: Comparison with α-pinene polymerization. *J. Appl. Polym. Sci.* **1996**, *61* (6), 1011–1016.

(134) Miyaji, H.; Satoh, K.; Kamigaito, M. Bio-Based Polyketones by Selective Ring-Opening Radical Polymerization of α-Pinene-Derived Pinocarvone. *Angew. Chem. Int. Ed.* **2016**, *55* (4), 1372–1376.

(135) Satoh, K. Controlled/living polymerization of renewable vinyl monomers into bio-based polymers. *Polym. J.* **2015**, *47* (8), 527–536.

(136) Sessini, V.; Palenzuela, M.; Damián, J.; Mosquera, M. E.G. Bio-based polyether from limonene oxide catalytic ROP as green polymeric plasticizer for PLA. *Polymer* **2020**, *210*, 123003.

(137) Hauenstein, O.; Reiter, M.; Agarwal, S.; Rieger, B.; Greiner, A. Bio-based polycarbonate from limonene oxide and CO$_2$ with high molecular weight, excellent thermal resistance, hardness and transparency. *Green Chem.* **2016**, *18* (3), 760–770.

(138) Wambach, A.; Agarwal, S.; Greiner, A. Synthesis of Biobased Polycarbonate by Copolymerization of Menth-2-ene Oxide and CO$_2$ with Exceptional Thermal Stability. *ACS Sustainable Chem. Eng.* **2020**, *8* (39), 14690–14693.

(139) Stamm, A.; Öhlin, J.; Mosbech, C.; Olsén, P.; Guo, B.; Söderberg, E.; Biundo, A.; Fogelström, L.; Bhattacharyya, S.; Bornscheuer, U. T.; Malmström, E.; Syrén, P.-O. Pinene-Based Oxidative Synthetic Toolbox for Scalable Polyester Synthesis. *JACS Au* **2021**, *1* (11), 1949–1960.

(140) Thomsett, M. R.; Moore, J. C.; Buchard, A.; Stockman, R. A.; Howdle, S. M. New renewably-sourced polyesters from limonene-derived monomers. *Green Chem.* **2019**, *21* (1), 149–156.

(141) Peña Carrodeguas, L.; Martín, C.; Kleij, A. W. Semiaromatic Polyesters Derived from Renewable Terpene Oxides with High Glass Transitions. *Macromolecules* **2017**, *50* (14), 5337–5345.

(142) Van Zee, N. J.; Coates, G. W. Alternating Copolymerization of Propylene Oxide with Biorenewable Terpene-Based Cyclic Anhydrides: A Sustainable Route to Aliphatic Polyesters with High Glass Transition Temperatures. *Angew. Chem.* **2015**, *127* (9), 2703–2706.

(143) Zhang, D.; Hillmyer, M. A.; Tolman, W. B. Catalytic polymerization of a cyclic ester derived from a "cool" natural precursor. *Biomacromolecules* **2005**, *6* (4), 2091–2095.

(144) Lowe, J. R.; Martello, M. T.; Tolman, W. B.; Hillmyer, M. A. Functional biorenewable polyesters from carvone-derived lactones. *Polym. Chem.* **2011**, *2* (3), 702–708.

(145) Hillmyer, M. A.; Tolman, W. B. Aliphatic polyester block polymers:Renewable, degradable, and sustainable. *Acc. Chem. Res.* **2014**, *47* (8), 2390–2396.

(146) Wanamaker, C. L.; O'Leary, L. E.; Lynd, N. A.; Hillmyer, M. A.; Tolman, W. B. Renewable-resource thermoplastic elastomers based on polylactide and polymenthide. *Biomacromolecules* **2007**, *8* (11), 3634–3640.

(147) Lowe, J. R.; Tolman, W. B.; Hillmyer, M. A. Oxidized dihydrocarvone as a renewable multifunctional monomer for the synthesis of shape memory polyesters. *Biomacromolecules* **2009**, *10* (7), 2003–2008.

(148) Baeyer, A.; Villiger, V. Einwirkung des Caro'schen Reagens auf Ketone. *Ber. Dtsch. Chem. Ges.* **1899**, *32* (3), 3625–3633.

(149) Crudden, C. M.; Chen, A. C.; Calhoun, L. A. A Demonstration of the Primary Stereoelectronic Effect in the Baeyer–Villiger Oxidation of α-Fluorocyclohexanones. *Angew. Chem.* **2000**, *112* (16), 2973–2977.

(150) Brink, G.-J. ten; Arends, I. W. C. E.; Sheldon, R. A. The Baeyer-Villiger reaction: new developments toward greener procedures. *Chem. Rev.* **2004**, *104* (9), 4105–4124.

(151) Criegee, R.; Schnorrenberg, W.; Becke, J. Zur Konstitution von Ketonperoxyden. *Justus Liebigs Ann. Chem.* **1949**, *565* (1), 7–21.

(152) Doering, W. v. E.; Dorfman, E. Mechanism of the Peracid Ketone—Ester Conversion. Analysis of Organic Compounds for Oxygen-18 1. *J. Am. Chem. Soc.* **1953**, *75* (22), 5595–5598.

(153) Renz, M.; Meunier, B. 100 Years of Baeyer–Villiger Oxidations. *Eur. J. Org. Chem.* **1999**, *1999* (4), 737–750.

(154) Bertolini, V.; Appiani, R.; Pallavicini, M.; Bolchi, C. Green Oxidation of Ketones to Lactones with Oxone in Water. *J. Org. Chem.* **2021**, *86* (21), 15712–15716.

(155) Doig, S. D.; Avenell, P. J.; Bird, P. A.; Gallati, P.; Lander, K. S.; Lye, G. J.; Wohlgemuth, R.; Woodley, J. M. Reactor operation and scale-up of whole cell Baeyer-Villiger catalyzed lactone synthesis. *Biotechnol. Prog.* **2002**, *18* (5), 1039–1046.

(156) Delgove, M. A. F.; Fürst, M. J. L. J.; Fraaije, M. W.; Bernaerts, K. V.; Wildeman, S. M. A. de. Exploring the Substrate Scope of Baeyer-Villiger Monooxygenases with Branched Lactones as Entry towards Polyesters. *Chembiochem* **2018**, *19* (4), 354–360.

(157) Uyanik, M.; Ishihara, K. Baeyer–Villiger Oxidation Using Hydrogen Peroxide. *ACS Catal.* **2013**, *3* (4), 513–520.

(158) Yakabi, K.; Mathieux, T.; Milne, K.; López-Vidal, E. M.; Buchard, A.; Hammond, C. Continuous Production of Biorenewable, Polymer-Grade Lactone Monomers through Sn-β-Catalyzed Baeyer-Villiger Oxidation with H$_2$O$_2$. *ChemSusChem* **2017**, *10* (18), 3652–3659.

(159) Corma, A.; Navarro, M.-a. T.; Nemeth, L.; Renz, M. Sn-MCM-41—a heterogeneous selective catalyst for the Baeyer–Villiger oxidation with hydrogen peroxide. *Chem. Commun.* **2001** (21), 2190–2191.

(160) Corma, A.; Navarro, M. T.; Renz, M. *Lewis* acidic Sn(IV) centers—grafted onto MCM-41—as catalytic sites for the Baeyer–Villiger oxidation with hydrogen peroxide. *J. Catal.* **2003**, *219* (1), 242–246.

(161) Hoe, G. X. de; Zumstein, M. T.; Tiegs, B. J.; Brutman, J. P.; McNeill, K.; Sander, M.; Coates, G. W.; Hillmyer, M. A. Sustainable Polyester Elastomers from Lactones: Synthesis, Properties, and Enzymatic Hydrolyzability. *J. Am. Chem. Soc.* **2018**, *140* (3), 963–973.

(162) Gurusamy-Thangavelu, S. A.; Emond, S. J.; Kulshrestha, A.; Hillmyer, M. A.; Macosko, C. W.; Tolman, W. B.; Hoye, T. R. Polyurethanes based on renewable polyols from bioderived lactones. *Polym. Chem.* **2012**, *3* (10), 2941.

(163) Wanamaker, C. L.; Tolman, W. B.; Hillmyer, M. A. Poly(D-lactide)-Poly(menthide)-Poly(D-lactide) Triblock Copolymers as Crystal Nucleating Agents for Poly(L-lactide). *Macromol. Symp.* **2009**, *283-284* (1), 130–138.

(164) Wanamaker, C. L.; Tolman, W. B.; Hillmyer, M. A. Hydrolytic degradation behavior of a renewable thermoplastic elastomer. *Biomacromolecules* **2009**, *10* (2), 443–448.

(165) Ding, K.; John, A.; Shin, J.; Lee, Y.; Quinn, T.; Tolman, W. B.; Hillmyer, M. A. High-Performance Pressure-Sensitive Adhesives from Renewable Triblock Copolymers. *Biomacromolecules* **2015**, *16* (8), 2537–2539.

(166) Knight, S. C.; Schaller, C. P.; Tolman, W. B.; Hillmyer, M. A. Renewable carvone-based polyols for use in polyurethane thermosets. *RSC Adv.* **2013**, *3* (43), 20399.

(167) Carpentier, J.-F. Discrete Metal Catalysts for Stereoselective Ring-Opening Polymerization of Chiral Racemic β-Lactones. *Macromol. Rapid Commun.***2010**, *31* (19), 1696–1705.

(168) Albertsson, A.-C.; Varma, I. K. Recent developments in ring opening polymerization of lactones for biomedical applications. *Biomacromolecules* **2003**, *4* (6), 1466–1486.

(169) Carpentier, J.-F. Rare-Earth Complexes Supported by Tripodal Tetradentate Bis(phenolate) Ligands: A Privileged Class of Catalysts for Ring-Opening Polymerization of Cyclic Esters. *Organometallics* **2015**, *34* (17), 4175–4189.

(170) Thomas, C. M. Stereocontrolled ring-opening polymerization of cyclic esters:Synthesis of new polyester microstructures. *Chem. Soc. Rev.* **2010**, *39* (1), 165–173.

(171) Hamitou, A.; Ouhadi, T.; Jerome, R.; Teyssié, P. Soluble bimetallic μ-oxoalkoxides. VII. Characteristics and mechanism of ring-opening polymerization of lactones. *J. Polym. Sci. Polym. Chem. Ed.* **1977**, *15* (4), 865–873.

(172) Rieger, B., Ed. *Synthetic biodegradable polymers*; Advances in Polymer Science, Vol. 245; Springer, **2012**.

(173) Simic, V.; Spassky, N.; Hubert-Pfalzgraf, L. G. Ring-Opening Polymerization of D,L-Lactide Using Rare-Earth µ-Oxo Isopropoxides as Initiator Systems. *Macromolecules* **1997**, *30* (23), 7338–7340.

(174) Spassky, N.; Simic, V.; Montaudo, M. S.; Hubert-Pfalzgraf, L. G. Inter- and intramolecular ester exchange reactions in the ring-opening polymerization of (D,L)-lactide using lanthanide alkoxide initiators. *Macromol. Chem. Phys.* **2000**, *201* (17), 2432–2440.

(175) Stevels, W. M.; Ankoné, M. J. K.; Dijkstra, P. J.; Feijen, J. Kinetics and Mechanism of l - Lactide Polymerization Using Two Different Yttrium Alkoxides as Initiators. *Macromolecules* **1996**, *29* (19), 6132–6138.

(176) Stevels, W. M.; Ankoné, M. J. K.; Dijkstra, P. J.; Feijen, J. Well defined block copolymers of ε-caprolactone and L-lactide using $Y_5(\mu\text{-O})(OiPr)_{13}$ as an initiator. *Macromol. Chem. Phys.* **1995**, *196* (4), 1153–1161.

(177) Martin, E.; Dubois, P.; Jérôme R. "In Situ" Formation of Yttrium Alkoxides: A Versatile and Efficient Catalyst for the ROP of *ε*-Caprolactone. *Macromolecules* **2003**, *36* (16), 5934–5941.

(178) Save, M.; Schappacher, M.; Soum, A. Controlled Ring-Opening Polymerization of Lactones and Lactides Initiated by Lanthanum Isopropoxide, 1. General Aspects and Kinetics. *Macromol. Chem. Phys.* **2002**, *203* (5-6), 889–899.

(179) Tortosa, K.; Hamaide, T.; Boisson, C.; Spitz, R. Homogeneous and Heterogeneous Polymerization of -Caprolactone by Neodymium Alkoxides Prepared In Situ. *Macromol. Chem. Phys.* **2010**, *202*, 1156–1160.

(180) Arnold, P. L.; Buffet, J.-C.; Blaudeck, R. P.; Sujecki, S.; Blake, A. J.; Wilson, C. C 3 - Symmetric Lanthanide Tris(alkoxide) Complexes Formed by Preferential Complexation and Their Stereoselective Polymerization of rac-Lactide. *Angew. Chem.* **2008**, *120* (32), 6122–6125.

(181) Evans, W. J.; Katsumata, H. Polymerization of ε-Caprolactone by Divalent Samarium Complexes. *Macromolecules* **1994**, *27* (8), 2330–2332.

(182) Yamashita, M.; Takemoto, Y.; Ihara, E.; Yasuda, H. Organolanthanide-Initiated Living Polymerizations of ε-Caprolactone, δ-Valerolactone, and β-Propiolactone. *Macromolecules* **1996**, *29* (5), 1798–1806.

(183) Amgoune, A.; Thomas, C. M.; Ilinca, S.; Roisnel, T.; Carpentier, J.-F. Highly active, productive, and syndiospecific yttrium initiators for the polymerization of racemic β-butyrolactone. *Angew. Chem. Int. Ed.* **2006**, *45* (17), 2782–2784.

(184) Amgoune, A.; Thomas, C. M.; Carpentier, J.-F. Yttrium Complexes as Catalysts for Living and Immortal Polymerization of Lactide to Highly Heterotactic PLA. *Macromol. Rapid Commun.* **2007**, *28* (6), 693–697.

(185) Ajellal, N.; Bouyahyi, M.; Amgoune, A.; Thomas, C. M.; Bondon, A.; Pillin, I.; Grohens, Y.; Carpentier, J.-F. Syndiotactic-Enriched Poly(3-hydroxybutyrate)s via Stereoselective Ring-Opening Polymerization of Racemic β-Butyrolactone with Discrete Yttrium Catalysts. *Macromolecules* **2009**, *42* (4), 987–993.

(186) Aspinall, H. C.; Bacsa, J.; Beckingham, O. D.; Eden, E. G. B.; Greeves, N.; Hobbs, M. D.; Potjewyd, F.; Schmidtmann, M.; Thomas, C. D. Adding the right (or left) twist to tris-chelate complexes-coordination chemistry of chiral oxazolylphenolates with M^{3+} ions (M = Al or lanthanide). *Dalton Trans.* **2014**, *43* (3), 1434–1442.

(187) Heck, R.; Schulz, E.; Collin, J.; Carpentier, J.-F. Group 3 metal complexes based on a chiral tetradentate diamine-diamide ligand: Synthesis and use in polymerization of (d,l)-lactide and intramolecular alkene hydroamination catalysis. *J. Mol. Catal. A Chem.* **2007**, *268* (1-2), 163–168.

(188) Nie, K.; Fang, L.; Yao, Y.; Zhang, Y.; Shen, Q.; Wang, Y. Synthesis and characterization of amine-bridged bis(phenolate)lanthanide alkoxides and their application in the controlled polymerization of rac-lactide and rac-β-butyrolactone. *Inorg. Chem.* **2012**, *51* (20), 11133–11143.

(189) Pappalardo, D.; Bruno, M.; Lamberti, M.; Pellecchia, C. Ring-Opening Polymerization of Racemic β-Butyrolactone Promoted by Salan- and Salen-Type Yttrium Amido Complexes. *Macromol. Chem. Phys.* **2013**, *214* (17), 1965–1972.

(190) Zhuo, Z.; Zhang, C.; Luo, Y.; Wang, Y.; Yao, Y.; Yuan, D.; Cui, D. Stereo-selectivity switchable ROP of *rac*-β-butyrolactone initiated by salan-ligated rare-earth metal amide complexes: The key role of the substituents on ligand frameworks. *Chem. Commun.* **2018**, *54* (85), 11998–12001.

(191) Zeng, T.; Qian, Q.; Zhao, B.; Yuan, D.; Yao, Y.; Shen, Q. Synthesis and characterization of rare-earth metal guanidinates stabilized by amine-bridged bis(phenolate) ligands and their application in the controlled polymerization of *rac*-lactide and *rac*-β-butyrolactone. *RSC Adv.* **2015**, *5* (65), 53161–53171.

(192) Ajellal, N.; Durieux, G.; Delevoye, L.; Tricot, G.; Dujardin, C.; Thomas, C. M.; Gauvin, R. M. Polymerization of racemic beta-butyrolactone using supported catalysts: A simple access to isotactic polymers. *Chem. Commun.* **2010**, *46* (7), 1032–1034.

(193) Klitzke, J. S.; Roisnel, T.; Kirillov, E.; Casagrande, O. d. L.; Carpentier, J.-F. Yttrium– and Aluminum–Bis(phenolate)pyridine Complexes:Catalysts and Model Compounds of the Intermediates for the Stereoselective Ring-Opening Polymerization of Racemic Lactide and β-Butyrolactone. *Organometallics* **2013**, *33* (1), 309–321.

(194) Kerr, R. W. F.; Ewing, P. M. D. A.; Raman, S. K.; Smith, A. D.; Williams, C. K.; Arnold, P. L. Ultrarapid Cerium(III)–NHC Catalysts for High Molar Mass Cyclic Polylactide. *ACS Catal.* **2021**, *11* (3), 1563–1569.

(195) Zintl, M.; Molnar, F.; Urban, T.; Bernhart, V.; Preishuber-Pflügl, P.; Rieger, B. Variably isotactic poly(hydroxybutyrate) from racemic β-butyrolactone:Microstructure control by achiral chromium(III) salophen complexes. *Angew. Chem. Int. Ed.* **2008**, *47* (18), 3458–3460.

(196) Vagin, S.; Winnacker, M.; Kronast, A.; Altenbuchner, P. T.; Deglmann, P.; Sinkel, C.; Loos, R.; Rieger, B. New Insights into the Ring-Opening Polymerization of β-Butyrolactone Catalyzed by Chromium(III) Salphen Complexes. *ChemCatChem* **2015**, *7* (23), 3963–3971.

(197) Hayakawa, M.; Mitani, M.; Yamada, T.; Mukaiyama, T. Living ring-opening polymerization of lactones using cationic zirconocene complex catalysts. *Macromol. Chem. Phys.* **1997** (198), 1305–1317.

(198) Ning, Y.; Zhang, Y.; Rodriguez-Delgado, A.; Chen, E. Y.-X. Neutral Metallocene Ester Enolate and Non-Metallocene Alkoxy Complexes of Zirconium for Catalytic Ring-Opening Polymerization of Cyclic Esters. *Organometallics* **2008**, *27* (21), 5632–5640.

(199) Santoro, O.; Zhang, X.; Redshaw, C. Synthesis of Biodegradable Polymers: A Review on the Use of *Schiff*-Base Metal Complexes as Catalysts for the Ring Opening Polymerization (ROP) of Cyclic Esters. *Catalysts* **2020**, *10* (7), 800.

(200) Chamberlain, B. M.; Cheng, M.; Moore, D. R.; Ovitt, T. M.; Lobkovsky, E. B.; Coates, G. W. Polymerization of lactide with zinc and magnesium β-diiminate complexes: Stereocontrol and mechanism. *J. Am. Chem. Soc.* **2001**, *123* (14), 3229–3238.

(201) Rieth, L. R.; Moore, D. R.; Lobkovsky, E. B.; Coates, G. W. Single-site β-diiminate zinc catalysts for the ring-opening polymerization of *β*-butyrolactone and β-valerolactone to poly(3-hydroxyalkanoates). *J. Am. Chem. Soc.* **2002**, *124* (51), 15239–15248.

(202) Silvernail, C. M.; Yao, L. J.; Hill, L. M. R.; Hillmyer, M. A.; Tolman, W. B. Structural and mechanistic studies of bis(phenolato)amine zinc(II) catalysts for the polymerization of ε-caprolactone. *Inorg. Chem.* **2007**, *46* (16), 6565–6574.

(203) Williams, C. K.; Breyfogle, L. E.; Choi, S. K.; Nam, W.; Young, V. G.; Hillmyer, M. A.; Tolman, W. B. A highly active zinc catalyst for the controlled polymerization of lactide. *J. Am. Chem. Soc.* **2003**, *125* (37), 11350–11359.

(204) Williams, C. K.; Brooks, N. R.; Hillmyer, M. A.; Tolman, W. B. Metalloenzyme inspired dizinc catalyst for the polymerization of lactide. *Chem. Commun.* **2002** (18), 2132–2133.

(205) Cheng, M.; Attygalle, A. B.; Lobkovsky, E. B.; Coates, G. W. Single-Site Catalysts for Ring-Opening Polymerization: Synthesis of Heterotactic Poly(lactic acid) from *rac*-Lactide. *J. Am. Chem. Soc.* **1999**, *121* (49), 11583–11584.

(206) Penczek, S.; Pretula, J.; Slomkowski, S. Ring-opening polymerization. *CTI* **2021**, *3* (2), 33–57.

(207) Dagorne, S.; Normand, M.; Kirillov, E.; Carpentier, J.-F. Gallium and indium complexes for ring-opening polymerization of cyclic ethers, esters and carbonates. *Coord. Chem. Rev.* **2013**, *257* (11-12), 1869–1886.

(208) Normand, M.; Dorcet, V.; Kirillov, E.; Carpentier, J.-F. {Phenoxy-imine}aluminum versus -indium Complexes for the Immortal ROP of Lactide: Different Stereocontrol, Different Mechanisms. *Organometallics* **2013**, *32* (6), 1694–1709.

(209) Jianming, R.; Anguo, X.; Hongwei, W.; Hailin, Y. Review – recent development of ring-opening polymerization of cyclic esters using aluminum complexes. *Des. Monomers Polym.* **2014**, *17* (4), 345–355.

(210) Jung, H.-J.; Cho, Y.; Kim, D.; Mehrkhodavandi, P. Cationic aluminum, gallium, and indium complexes in catalysis. *Catal. Sci. Technol.* **2021**, *11* (1), 62–91.

(211) Wei, Y.; Wang, S.; Zhou, S. Aluminum alkyl complexes: synthesis, structure, and application in ROP of cyclic esters. *Dalton Trans.* **2016**, *45* (11), 4471–4485.

(212) MacDonald, J. P.; Shaver, M. P. Aluminum Salen and Salan Polymerization Catalysts: From Monomer Scope to Macrostructure Control. In *Green Polymer Chemistry: Biobased Materials and Biocatalysis*; Cheng, H. N., Gross, R. A., Smith, P. B., Eds.; ACS Symposium Series; American Chemical Society, **2015**; pp 147–167.

(213) Ovitt, T. M.; Coates, G. W. Stereochemistry of lactide polymerization with chiral catalysts: New opportunities for stereocontrol using polymer exchange mechanisms. *J. Am. Chem. Soc.* **2002**, *124* (7), 1316–1326.

(214) Cross, E. D.; Allan, L. E. N.; Decken, A.; Shaver, M. P. Aluminum salen and salan complexes in the ring-opening polymerization of cyclic esters:Controlled immortal and copolymerization of *rac*-β-butyrolactone and *rac*-lactide. *J. Polym. Sci. A Polym. Chem.* **2013**, *51* (5), 1137–1146.

(215) Hormnirun, P.; Marshall, E. L.; Gibson, V. C.; Pugh, R. I.; White, A. J. P. Study of ligand substituent effects on the rate and stereoselectivity of lactide polymerization using aluminum salen-type initiators. *PNAS* **2006**, *103* (42), 15343–15348.

(216) Hormnirun, P.; Marshall, E. L.; Gibson, V. C.; White, A. J. P.; Williams, D. J. Remarkable stereocontrol in the polymerization of racemic lactide using aluminum initiators supported by tetradentate aminophenoxide ligands. *J. Am. Chem. Soc.* **2004**, *126* (9), 2688–2689.

(217) Woodman, T. J.; Schormann, M.; Hughes, D. L.; Bochmann, M. Sterically Hindered Lanthanide Allyl Complexes and Their Use as Single-Component Catalysts for the Polymerization of Methyl Methacrylate and ε-Caprolactone. *Organometallics* **2004**, *23* (12), 2972–2979.

(218) Darensbourg, D. J.; Karroonnirun, O. Stereoselective Ring-Opening Polymerization of rac -Lactides Catalyzed by Chiral and Achiral Aluminum Half-Salen Complexes. *Organometallics* **2010**, *29* (21), 5627–5634.

(219) Tabthong, S.; Nanok, T.; Sumrit, P.; Kongsaeree, P.; Prabpai, S.; Chuawong, P.; Hormnirun, P. Bis(pyrrolidene) *Schiff* Base Aluminum Complexes as Isoselective-Biased Initiators for the Controlled Ring-Opening Polymerization of *rac*-Lactide: Experimental and Theoretical Studies. *Macromolecules* **2015**, *48* (19), 6846–6861.

(220) Douglas, A. F.; Patrick, B. O.; Mehrkhodavandi, P. A highly active chiral indium catalyst for living lactide polymerization. *Angew. Chem. Int. Ed.* **2008**, *47* (12), 2290–2293.

(221) Xu, C.; Yu, I.; Mehrkhodavandi, P. Highly controlled immortal polymerization of β-butyrolactone by a dinuclear indium catalyst. *Chem. Commun.* **2012**, *48* (54), 6806–6808.

(222) Goonesinghe, C.; Roshandel, H.; Diaz, C.; Jung, H.-J.; Nyamayaro, K.; Ezhova, M.; Mehrkhodavandi, P. Cationic indium catalysts for ring opening polymerization: Tuning reactivity with hemilabile ligands. *Chem. Sci.* **2020**, *48*, 233.

(223) Spassky, N.; Wisniewski, M.; Pluta, C.; Le Borgne, A. Highly stereoelective polymerization of rac-(D,L)-lactide with a chiral *Schiff*'s base/aluminium alkoxide initiator. *Macromol. Chem. Phys.* **1996**, *197* (9), 2627–2637.

(224) Ajellal, N.; Carpentier, J.-F.; Guillaume, C.; Guillaume, S. M.; Helou, M.; Poirier, V.; Sarazin, Y.; Trifonov, A. A. Bridging the gap in catalysis via multidisciplinary approaches. *Dalton Trans.* **2010**, *39* (36), 8354.

(225) Inoue, S. Immortal polymerization: The outset, development, and application. *J. Polym. Sci. A Polym. Chem.* **2000**, *38* (16), 2861–2871.

(226) O'Keefe, B. J.; Hillmyer, M. A.; Tolman, W. B. Polymerization of lactide and related cyclic esters by discrete metal complexes. *J. Chem. Soc., Dalton Trans.* **2001**, *15*, 2215–2224.

(227) Asano, S.; Aida, T.; Inoue, S. 'Immortal' polymerization. Polymerization of epoxide catalysed by an aluminium porphyrin–alcohol system. *J. Chem. Soc., Chem. Commun.* **1985**, *17*, 1148–1149.

(228) Mecerreyes, D.; Jérôme, R.; Dubois, P. Novel Macromolecular Architectures Based on Aliphatic Polyesters: Relevance of the "Coordination-Insertion" Ring-Opening Polymerization. In *Macromolecular Architectures*; Hilborn, J. G., Dubois, P., Hawker, C. J., Hedrick, J. L., Hilborn, J. G., Jérôme, R., Kiefer, J., Labadie, J. W., Mecerreyes, D., Volksen, W., Eds.; Advances in Polymer Science; Springer Berlin Heidelberg, **1999**; pp 1–59.

(229) Dechy-Cabaret, O.; Martin-Vaca, B.; Bourissou, D. Controlled ring-opening polymerization of lactide and glycolide. *Chem. Rev.* **2004**, *104* (12), 6147–6176.

(230) Li, H.; Shakaroun, R. M.; Guillaume, S. M.; Carpentier, J.-F. Recent Advances in Metal-Mediated Stereoselective Ring-Opening Polymerization of Functional Cyclic Esters towards Well-Defined Poly(hydroxy acid)s: From Stereoselectivity to Sequence-Control. *Chemistry* **2020**, *26* (1), 128–138.

(231) Delgove, M. A. F.; Wróblewska, A. A.; Stouten, J.; van Slagmaat, C. A. M. R.; Noordijk, J.; Wildeman, S. M. A. de; Bernaerts, K. V. Organocatalyzed ring opening polymerization of regio-isomeric lactones: reactivity and thermodynamics considerations. *Polym. Chem.* **2020**, *11* (21), 3573–3584.

(232) Csihony, S.; Culkin, D. A.; Sentman, A. C.; Dove, A. P.; Waymouth, R. M.; Hedrick, J. L. Single-component catalyst/initiators for the organocatalytic ring-opening polymerization of lactide. *J. Am. Chem. Soc.* **2005**, *127* (25), 9079–9084.

(233) Tang, J.; Chen, E. Y.-X. Increasing complexity in organopolymerization of multifunctional γ-butyrolactones. *Europ. Polym. J.* **2017**, *95*, 678–692.

(234) Kamber, N. E.; Jeong, W.; Waymouth, R. M.; Pratt, R. C.; Lohmeijer, B. G. G.; Hedrick, J. L. Organocatalytic ring-opening polymerization. *Chem. Rev.* **2007**, *107* (12), 5813–5840.

(235) Zhao, W.; Cui, D.; Liu, X.; Chen, X. Facile Synthesis of Hydroxyl-Ended, Highly Stereoregular, Star-Shaped Poly(lactide) from Immortal ROP of *rac*-Lactide and Kinetics Study. *Macromolecules* **2010**, *43* (16), 6678–6684. D

(236) Wang, L.; Poirier, V.; Ghiotto, F.; Bochmann, M.; Cannon, R. D.; Carpentier, J.-F.; Sarazin, Y. Kinetic Analysis of the Immortal Ring-Opening Polymerization of Cyclic Esters: A Case Study with Tin(II) Catalysts. *Macromolecules* **2014**, *47* (8), 2574–2584.

(237) Ajellal, N.; Lyubov, D. M.; Sinenkov, M. A.; Fukin, G. K.; Cherkasov, A. V.; Thomas, C. M.; Carpentier, J.-F.; Trifonov, A. A. Bis(guanidinate) alkoxide complexes of lanthanides:Synthesis, structures and use in immortal and stereoselective ring-opening polymerization of cyclic esters. *Chemistry* **2008**, *14* (18), 5440–5448.

(238) Nomura, N.; Taira, A.; Nakase, A.; Tomioka, T.; Okada, M. Ring-opening polymerization of lactones by rare-earth metal triflates and by their reusable system in ionic liquids. *Tetrahedron* **2007**, *63* (35), 8478–8484.

(239) Wang, Y.; Kunioka, M. Ring-Opening Polymerization of Cyclic Monomers with Aluminum Triflate. *Macromol. Symp.* **2005**, *224* (1), 193–206.

(240) Duda, A.; Kowalski, A. Thermodynamics and Kinetics of Ring-Opening Polymerization. In *Handbook of Ring-Opening Polymerization*; Dubois, P., Coulembier, O., Raquez, J.-M., Eds.; Wiley-VCH Verlag GmbH & Co. KGaA, **2009**; 1–51.

(241) Jung, H.-J.; Yu, I.; Nyamayaro, K.; Mehrkhodavandi, P. Indium-Catalyzed Block Copolymerization of Lactide and Methyl Methacrylate by Sequential Addition. *ACS Catal.* **2020**, *10* (11), 6488–6496.

(242) Schappacher, M.; Fur, N.; Guillaume, S. M. Poly(methyl methacrylate)−Poly(caprolactone) AB and ABA Block Copolymers by Combined Ring-Opening Polymerization and Atom Transfer Radical Polymerization. *Macromolecules* **2007**, *40* (25), 8887–8896.

(243) Song, J.; Xu, J.; Pispas, S.; Zhang, G. One-pot synthesis of poly(l-lactide)-b-poly(methyl methacrylate) block copolymers. *RSC Adv.* **2015**, *5* (48), 38243–38247.

(244) Wang, W.-W.; Ren, W.-Y.; Jiang, L.; Dan, Y. Synthesis and characterization of AB-type copolymers poly(L-lactide)-block-poly(methyl methacrylate) via a convenient route combining ROP and ATRP from a dual initiator. *J. Appl. Polym. Sci.* **2010**, 2379-2388.

(245) Kryuchkov, M. A.; Detrembleur, C.; Bazuin, C. G. Linear amphiphilic diblock copolymers of lactide and 2-dimethylaminoethyl methacrylate using bifunctional-initiator and one-pot approaches. *Polymer* **2014**, *55* (10), 2316–2324.

(246) Wolf, F. F.; Friedemann, N.; Frey, H. Poly(lactide)- block -Poly(HEMA) Block Copolymers: An Orthogonal One-Pot Combination of ROP and ATRP, Using a Bifunctional Initiator. *Macromolecules* **2009**, *42* (15), 5622–5628.

(247) Kang, H. U.; Yu, Y. C.; Shin, S. J.; Youk, J. H. One-step synthesis of block copolymers using a hydroxyl-functionalized trithiocarbonate RAFT agent as a dual initiator for RAFT polymerization and ROP. *J. Polym. Sci. A Polym. Chem.* **2013**, *51* (4), 774–779.

(248) Yildirim, I.; Sungur, P.; Crecelius-Vitz, A. C.; Yildirim, T.; Kalden, D.; Hoeppener, S.; Westerhausen, M.; Weber, C.; Schubert, U. S. One-pot synthesis of PLA-b-PHEA via sequential ROP and RAFT polymerizations. *Polym. Chem.* **2017**, *8* (39), 6086–6098.

(249) Themistou, E.; Battaglia, G.; Armes, S. P. Facile synthesis of thiol-functionalized amphiphilic polylactide–methacrylic diblock copolymers. *Polym. Chem.* **2014**, *5* (4), 1405–1417.

(250) Chiellini, E.; Solaro, R. Biodegradable Polymeric Materials. *Adv. Mater.* **1996**, *8* (4), 305–313.

(251) Solaro, R.; Cantoni, G.; Chiellini, E. Polymerisability of different lactones and methyl methacrylate in the presence of various organoaluminum catalysts. *Europ. Polym. J.* **1997** (33, 2), 205–211.

(252) Kostakis, K.; Mourmouris, S.; Karanikolopoulos, G.; Pitsikalis, M.; Hadjichristidis, N. Ring-opening polymerization of lactones using zirconocene catalytic systems:Block copolymerization with methyl methacrylate. *J. Polym. Sci. A Polym. Chem.* **2007**, *45* (16), 3524–3537.

(253) Liu, M.; Wang, B.; Pan, L.; Liu, X.-H.; Li, Y.-s. Sequentially bridging anionic addition and ring-opening polymerization by cooperative organocatalysis: well-defined block copolymers from methacrylates and cyclic esters. *Polym. Chem.* **2022**, *13* (23), 3451–3459.

(254) Pasparakis, G.; Tsitsilianis, C. LCST polymers: Thermoresponsive nanostructured assemblies towards bioapplications. *Polymer* **2020**, *211*, 123146.

(255) Islam, M. R.; Lu, Z.; Li, X.; Sarker, A. K.; Hu, L.; Choi, P.; Li, X.; Hakobyan, N.; Serpe, M. J. Responsive polymers for analytical applications: a review. *Anal. Chim. Acta* **2013**, *789*, 17–32.

(256) Crespy, D.; Rossi, R. M. Temperature-responsive polymers with LCST in the physiological range and their applications in textiles. *Polym. Int.* **2007**, *56* (12), 1461–1468.

(257) Gibson, M. I.; O'Reilly, R. K. To aggregate, or not to aggregate? considerations in the design and application of polymeric thermally-responsive nanoparticles. *Chem. Soc. Rev.* **2013**, *42* (17), 7204–7213.

(258) Dai, S.; Ravi, P.; Tam, K. C. pH-Responsive polymers: synthesis, properties and applications. *Soft matter* **2008**, *4* (3), 435–449.

(259) Kocak, G.; Tuncer, C.; Bütün, V. pH-Responsive polymers. *Polym. Chem.* **2017**, *8* (1), 144–176.

(260) Schmaljohann, D. Thermo- and pH-responsive polymers in drug delivery. *Adv. Drug. Deliv. Rev.* **2006**, *58* (15), 1655–1670.

(261) Reyes-Ortega, F. pH-responsive polymers: properties, synthesis and applications. In *Smart Polymers and their Applications*; Elsevier, **2014**; pp 45–92.

(262) Bazban-Shotorbani, S.; Hasani-Sadrabadi, M. M.; Karkhaneh, A.; Serpooshan, V.; Jacob, K. I.; Moshaverinia, A.; Mahmoudi, M. Revisiting structure-property relationship of pH-responsive polymers for drug delivery applications. *J. Control. Release* **2017**, *253*, 46–63.

(263) Tang, H.; Zhao, W.; Yu, J.; Li, Y.; Zhao, C. Recent Development of pH-Responsive Polymers for Cancer Nanomedicine. *Molecules* **2018**, *24* (1).

(264) Gasa, J. V.; Weiss, R. A.; Shaw, M. T. Ionic crosslinking of ionomer polymer electrolyte membranes using barium cations. *J. Membr. Sci.* **2007**, *304* (1-2), 173–180.

(265) Kerres, J. A. Development of ionomer membranes for fuel cells. *J. Membr. Sci.* **2001**, *185* (1), 3–27.

(266) Persigehl, P.; Jordan, R.; Nuyken, O. Functionalization of Amphiphilic Poly(2-oxazoline) Block Copolymers: A Novel Class of Macroligands for Micellar Catalysis. *Macromolecules* **2000**, *33* (19), 6977–6981.

(267) Rivas, B. Water-soluble polymer–metal ion interactions. *Progr. Polym. Sci.* **2003**, *28* (2), 173–208.

(268) Wang, B.; Wasielewski, M. R. Design and Synthesis of Metal Ion-Recognition-Induced Conjugated Polymers: An Approach to Metal Ion Sensory Materials. *J. Am. Chem. Soc.* **1997**, *119* (1), 12–21.

(269) Wu, X.; Fraser, C. L. Architectural Diversity via Metal Template-Assisted Polymer Synthesis: A Macroligand Chelation Approach to Linear and Star-Shaped Polymeric Ruthenium Tris(bipyridine) Complexes. *Macromolecules* **2000**, *33* (11), 4053–4060.

(270) Zarka, M. T.; Bortenschlager, M.; Wurst, K.; Nuyken, O.; Weberskirch, R. Immobilization of a Rhodium Carbene Complex to an Amphiphilic Block Copolymer for Hydroformylation of 1-Octene under Aqueous Two-Phase Conditions. *Organometallics* **2004**, *23* (21), 4817–4820.

(271) Zhang, B.; Yao, L.; Liu, X.; Zhang, L.; Cheng, Z.; Zhu, X. Facilely Recyclable Cu(II) Macrocomplex with Thermoregulated Poly(ionic liquid) Macroligand: Serving as a Highly Efficient Atom Transfer Radical Polymerization Catalyst. *ACS Sustainable Chem. Eng.* **2016**, *4* (12), 7066–7073.

(272) Zhang, L.; Brostowitz, N. R.; Cavicchi, K. A.; Weiss, R. A. Perspective: Ionomer Research and Applications. *Macromol. React. Eng.* **2014**, *8* (2), 81–99.

(273) Kumpfer, J. R.; Rowan, S. J. Thermo-, photo-, and chemo-responsive shape-memory properties from photo-cross-linked metallo-supramolecular polymers. *J. Am. Chem. Soc.* **2011**, *133* (32), 12866–12874.

(274) Marin, V.; Holder, E.; Hoogenboom, R.; Schubert, U. S. Functional ruthenium(II)- and iridium(III)-containing polymers for potential electro-optical applications. *Chem. Soc. Rev.* **2007**, *36* (4), 618–635.

(275) Elliott, C. M.; Baldy, C. J.; Nuwaysir, L. M.; Wilkins, C. L. Electrochemical polymerization of 4-methyl-4'-vinyl-2,2'-bipyridine-containing metal complexes: polymer structure and mechanism of formation. *Inorg. Chem.* **1990**, *29* (3), 389–392.

(276) Holder, E.; Marin, V.; Kozodaev, D.; Meier, M. A. R.; Lohmeijer, B. G. G.; Schubert, U. S. Iridium(III) Complexes with PEO and PS Polymer Macroligands and Light-Emitting Properties: Synthesis and Characterization. *Macromol. Chem. Phys.* **2005**, *206* (10), 989–997.

(277) Hoogenboom, R.; Schubert, U. S. The use of (metallo-)supramolecular initiators for living/controlled polymerization techniques. *Chem. Soc. Rev.* **2006**, *35* (7), 622–629.

(278) Pefkianakis, E. K.; Tzanetos, N. P.; Kallitsis, J. K. Synthesis and Characterization of a Novel Vinyl-2,2'-bipyridine Monomer and Its Homopolymeric/Copolymeric Metal Complexes. *Chem. Mater.* **2008**, *20* (19), 6254–6262.

(279) Schubert, U. S.; Eschbaumer, C. Macromolecules Containing Bipyridine and Terpyridine Metal Complexes: Towards Metallosupramolecular Polymers. *Angew. Chem. Int. Ed.* **2002**, *41* (16), 2892.

(280) Willenbacher, J.; Altintas, O.; Roesky, P. W.; Barner-Kowollik, C. Single-chain self-folding of synthetic polymers induced by metal-ligand complexation. *Macromol. Rapid Commun.* **2014**, *35* (1), 45–51.

(281) Zhou, G.; He, J.; Harruna, I. I. Synthesis and characterization of tris(2,2'-bipyridine)ruthenium-cored star-shaped polymers via RAFT polymerization. *J. Polym. Sci. A Polym. Chem.* **2007**, *45* (18), 4225–4239.

(282) Kaes, C.; Katz, A.; Hosseini, M. W. Bipyridine: the most widely used ligand. A review of molecules comprising at least two 2,2'-bipyridine units. *Chem. Rev.* **2000**, *100* (10), 3553–3590.

(283) Bajpai, A. K.; Shukla, S. K.; Bhanu, S.; Kankane, S. Responsive polymers in controlled drug delivery. *Progr. Polym. Sci.* **2008**, *33* (11), 1088–1118.

(284) Peppas, N. A.; Khare, A. R. Preparation, structure and diffusional behavior of hydrogels in controlled release. *Adv. Drug. Deliv. Rev.* **1993**, *11* (1-2), 1–35.

(285) Kumar, R.; Santa Chalarca, C. F.; Bockman, M. R.; van Bruggen, C.; Grimme, C. J.; Dalal, R. J.; Hanson, M. G.; Hexum, J. K.; Reineke, T. M. Polymeric Delivery of Therapeutic Nucleic Acids. *Chem. Rev.* **2021**, *121* (18), 11527–11652.

(286) Liechty, W. B.; Kryscio, D. R.; Slaughter, B. V.; Peppas, N. A. Polymers for drug delivery systems. *Annu. Rev. Chem. Biomol. Eng.* **2010**, *1*, 149–173.

(287) Mora-Huertas, C. E.; Fessi, H.; Elaissari, A. Polymer-based nanocapsules for drug delivery. *International journal of pharmaceutics* **2010**, *385* (1-2), 113–142.

(288) Qin, X.; Li, Y. Strategies To Design and Synthesize Polymer-Based Stimuli-Responsive Drug-Delivery Nanosystems. *Chembiochem* **2020**, *21* (9), 1236–1253.

(289) Qiu, L. Y.; Bae, Y. H. Polymer architecture and drug delivery. *Pharm. Res.* **2006**, *23* (1), 1–30.

(290) Wei, M.; Gao, Y.; Li, X.; Serpe, M. J. Stimuli-responsive polymers and their applications. *Polym. Chem.* **2017**, *8* (1), 127–143.

(291) Li, J.; Yao, S.; Wang, K.; Lu, Z.; Su, X.; Li, L.; Yuan, C.; Feng, J.; Yan, S.; Kong, B.; Song, K. Hypocrellin B-loaded, folate-conjugated polymeric micelle for intraperitoneal targeting of ovarian cancer in vitro and in vivo. *Cancer science* **2018**, *109* (6), 1958–1969.

(292) Haag, R.; Kratz, F. Polymere Therapeutika: Konzepte und Anwendungen. *Angew. Chem.* **2006**, *118* (8), 1218–1237.

(293) Ganta, S.; Devalapally, H.; Shahiwala, A.; Amiji, M. A review of stimuli-responsive nanocarriers for drug and gene delivery. *J. Control. Release* **2008**, *126* (3), 187–204.

(294) Schwarzenböck, C.; Schaffer, A.; Nößner, E.; Nelson, P. J.; Huss, R.; Rieger, B. Fluorescent Polyvinylphosphonate Bioconjugates for Selective Cellular Delivery. *Chemistry* **2018**, *24* (11), 2584–2587.

(295) Saurwein, A.; Schaffer, A.; Wieser, C.; Rieger, B. Synthesis, characterisation and functionalisation of BAB-type dual-responsive nanocarriers for targeted drug delivery: evolution of nanoparticles based on 2-vinylpyridine and diethyl vinylphosphonate. *RSC Adv.* **2021**, *11* (3), 1586–1594.

(296) Uhrich, K. E.; Cannizzaro, S. M.; Langer, R. S.; Shakesheff, K. M. Polymeric systems for controlled drug release. *Chem. Rev.* **1999**, *99* (11), 3181–3198.

(297) Edlund, U.; Albertsson, A.-C. Degradable Polymer Microspheres for Controlled Drug Delivery. In *Degradable Aliphatic Polyesters*; Abe, A., Albertsson, A.-C., Cantow, H.-J., Dušek, K., Edwards, S., Höcker, H., Joanny, J.-F., Kausch, H.-H., Lee, K.-S., McGrath, J. E., Monnerie, L., Stupp, S. I., Suter, U. W., Wegner, G., Young, R. J., Eds.; Advances in Polymer Science, Vol. 157; Springer, **2002**; pp 67–112.

(298) Dailey, L. A.; Wittmar, M.; Kissel, T. The role of branched polyesters and their modifications in the development of modern drug delivery vehicles. *J. Control. Release* **2005**, *101* (1-3), 137–149.

(299) Hu, Y.; Zhang, L.; Cao, Y.; Ge, H.; Jiang, X.; Yang, C. Degradation behavior of poly(ε-caprolactone)-b-poly(ethylene glycol)-b-poly(ε-caprolactone) micelles in aqueous solution. *Biomacromolecules* **2004**, *5* (5), 1756–1762.

(300) Hiroaki, O.; Masaki, Y.; Toshiro, H.; Yayoi, I.; Shigeru, K.; Yasuaki, O.; Hajime, T. Drug delivery using biodegradable microspheres. *J. Control. Release* **1994**, *28* (1-3), 121–129.

(301) Washington, K. E.; Kularatne, R. N.; Karmegam, V.; Biewer, M. C.; Stefan, M. C. Recent advances in aliphatic polyesters for drug delivery applications. *Wiley Interdiscip. Rev.: Nanomed. Nanobiotechnology* **2017**, *9* (4).

(302) Tong, R.; Cheng, J. Drug-Initiated, Controlled Ring-Opening Polymerization for the Synthesis of Polymer-Drug Conjugates. *Macromolecules* **2012**, *45* (5), 2225–2232.

(303) Wu, I.-E.; Anggelia, M. R.; Lin, S.-Y.; Chen, C.-Y.; Chu, I.-M.; Lin, C.-H. Thermosensitive Polyester Hydrogel for Application of Immunosuppressive Drug Delivery System in Skin Allograft. *Gels* **2021**, *7* (4).

(304) Kissel, T.; Li, Y.; Unger, F. ABA-triblock copolymers from biodegradable polyester A-blocks and hydrophilic poly(ethylene oxide) B-blocks as a candidate for in situ forming hydrogel delivery systems for proteins. *Adv. Drug. Deliv. Rev.* **2002**, *54* (1), 99–134.

(305) Benner, N. L.; Near, K. E.; Bachmann, M. H.; Contag, C. H.; Waymouth, R. M.; Wender, P. A. Functional DNA Delivery Enabled by Lipid-Modified Charge-Altering Releasable Transporters (CARTs). *Biomacromolecules* **2018**, *19* (7), 2812–2824.

(306) Rickert, C. A.; Wittmann, B.; Fromme, R.; Lieleg, O. Highly Transparent Covalent Mucin Coatings Improve the Wettability and Tribology of Hydrophobic Contact Lenses. *ACS Appl. Mater. Interfaces* **2020**, *12* (25), 28024–28033.

(307) Song, J.; Lutz, T. M.; Lang, N.; Lieleg, O. Bioinspired Dopamine/Mucin Coatings Provide Lubricity, Wear Protection, and Cell-Repellent Properties for Medical Applications. *Adv. Healthc. Mater.* **2021**, *10* (4), e2000831.

(308) Lynge, M. E.; van der Westen, R.; Postma, A.; Städler, B. Polydopamine - a nature-inspired polymer coating for biomedical science. *Nanoscale* **2011**, *3* (12), 4916–4928.

(309) Sangermano, M.; Razza, N. Light induced grafting-from strategies as powerfull tool for surface modification. *Express Polym. Lett.* **2019**, *13* (2), 135–145.

(310) Li, D.; Zheng, Q.; Wang, Y.; Chen, H. Combining surface topography with polymer chemistry: exploring new interfacial biological phenomena. *Polym. Chem.* **2014**, *5* (1), 14–24.

(311) Edmondson, S.; Osborne, V. L.; Huck, W. T. S. Polymer brushes via surface-initiated polymerizations. *Chem. Soc. Rev.* **2004**, *33* (1), 14–22.

(312) Hansson, S.; Trouillet, V.; Tischer, T.; Goldmann, A. S.; Carlmark, A.; Barner-Kowollik, C.; Malmström, E. Grafting efficiency of synthetic polymers onto biomaterials: a comparative study of grafting-from versus grafting-to. *Biomacromolecules* **2013**, *14* (1), 64–74.

(313) Tang, Z.; Kang, H.; Shen, Z.; Guo, B.; Zhang, L.; Jia, D. Grafting of Polyester onto Graphene for Electrically and Thermally Conductive Composites. *Macromolecules* **2012**, *45* (8), 3444–3451.

(314) Lagarrigue, P.; Soulié, J.; Grossin, D.; Dupret-Bories, A.; Combes, C.; Darcos, V. Well-defined polyester-grafted silica nanoparticles for biomedical applications: Synthesis and quantitative characterization. *Polymer* **2020**, *211*, 123048.

(315) Barbey, R.; Lavanant, L.; Paripovic, D.; Schüwer, N.; Sugnaux, C.; Tugulu, S.; Klok, H.-A. Polymer brushes via surface-initiated controlled radical polymerization: synthesis, characterization, properties, and applications. *Chem. Rev.* **2009**, *109* (11), 5437–5527.

(316) Reese, C. J.; Boyes, S. G. New methods in polymer brush synthesis: Non-vinyl-based semiflexible and rigid-rod polymer brushes. *Progr. Polym. Sci.* **2021**, *114*, 101361.

(317) Zhang, N.; Salzinger, S.; Deubel, F.; Jordan, R.; Rieger, B. Surface-initiated group transfer polymerization mediated by rare earth metal catalysts. *J. Am. Chem. Soc.* **2012**, *134* (17), 7333–7336.

(318) Denk, A.; Kernbichl, S.; Schaffer, A.; Kränzlein, M.; Pehl, T.; Rieger, B. Heteronuclear, Monomer-Selective Zn/Y Catalyst Combines Copolymerization of Epoxides and CO_2 with Group-Transfer Polymerization of Michael-Type Monomers. *ACS Macro Lett.* **2020**, *9* (4), 571–575.

(319) Sumi, K.; Furue, M.; Nozakura, S.-I. Preparation and luminescence properties of tris(bipyridine) ruthenium(II)-containing vinyl polymers: $Ru(bpy)_2$(poly-6-vinyl-2,2'-bipyridine)Cl_2 and $Ru(bpy)_2$(poly-4-methyl-4'-vinyl-,2,2'-bipyridine)Cl_2. *J. Polym. Sci. Polym. Chem. Ed.* **1984**, *22* (12), 3779–3788.

(320) Pitt, C. G.; Bao, Y.; Seltzman, H. H. The synthesis of polymers containing the 2,2'-bipyridine ligand. *J. Polym. Sci. C Polym. Lett.* **1986**, *24* (1), 13–16.

(321) Kamata, R.; Kumagai, H.; Yamazaki, Y.; Sahara, G.; Ishitani, O. Photoelectrochemical CO_2 Reduction Using a Ru(II)-Re(I) Supramolecular Photocatalyst Connected to a Vinyl Polymer on a NiO Electrode. *ACS Appl. Mater. Interfaces* **2019**, *11* (6), 5632–5641.

(322) Gould, S.; Strouse, G. F.; Meyer, T. J.; Sullivan, B. P. Formation of thin polymeric films by electropolymerization. Reduction of metal complexes containing bromomethyl-substituted derivatives of 2,2'-bipyridine. *Inorg. Chem.* **1991**, *30* (14), 2942–2949.

(323) Arslan, H.; Hazer, B.; Kowalczuk, M. Synthesis and characterization of poly[(R,S)-3-hydroxybutyrate] telechelics and their use in the synthesis of poly(methyl methacrylate)-b-poly(3-hydroxybutyrate) block copolymers. *J. Appl. Polym. Sci.* **2002** (85), 965–973.

(324) Borchert, U.; Lipprandt, U.; Bilang, M.; Kimpfler, A.; Rank, A.; Peschka-Süss, R.; Schubert, R.; Lindner, P.; Förster, S. pH-induced release from P2VP-PEO block copolymer vesicles. *Langmuir* **2006**, *22* (13), 5843–5847.

(325) Chagneux, N.; Trimaille, T.; Rollet, M.; Beaudoin, E.; Gérard, P.; Bertin, D.; Gigmes, D. Synthesis of Poly(*n*-butyl acrylate)-b-poly(ε-caprolactone) through Combination of SG1 Nitroxide-Mediated Polymerization and Sn(Oct)$_2$ -Catalyzed Ring-Opening Polymerization: Study of Sequential and One-Step Approaches from a Dual Initiator. *Macromolecules* **2009**, *42* (24), 9435–9442.

(326) You, Y.; Hong, C.; Wang, W.; Lu, W.; Pan, C. Preparation and Characterization of Thermally Responsive and Biodegradable Block Copolymer Comprised of PNIPAAM and PLA by Combination of ROP and RAFT Methods. *Macromolecules* **2004**, *37* (26), 9761–9767.

(327) Saiz-Poseu, J.; Mancebo-Aracil, J.; Nador, F.; Busqué, F.; Ruiz-Molina, D. The Chemistry behind Catechol-Based Adhesion. *Angew. Chem. Int. Ed.* **2019**, *58* (3), 696–714.

(328) Winkelhaus, D.; Neumann, B.; Stammler, H.-G.; Mitzel, N. W. Intramolecular *Lewis* acid-base pairs based on 4-ethynyl-2,6-lutidine. *Dalton Trans.* **2012**, *41* (30), 9143–9150.

(329) Sawanishi, H.; Tajima, K.; Tsuchiya, T. Studies on diazepines. XXVI. Syntheses of 6H-1,4-diazepines and 1-acyl-1H-1,4-diazepines from 4-pyridyl azides. *Chem. Pharm. Bull.* **1987**, *35* (8), 3175–3181.

(330) Kränzlein, M.; Pongratz, S.; Bruckmoser, J.; Bratić, B.; Breitsameter, J. M.; Rieger, B. Polyester synthesis based on 3-carene as renewable feedstock. *Polym. Chem.* **2022** (13), 3726–3732.

(331) Shaikh, S.; Wang, Y.; ur Rehman, F.; Jiang, H.; Wang, X. Phosphorescent Ir (III) complexes as cellular staining agents for biomedical molecular imaging. *Coord. Chem. Rev.* **2020**, *416*, 213344.

(332) Coban, B.; Yildiz, U.; Sengul, A. Synthesis, characterization, and DNA binding of complexes Pt(bpy)(pip)[2+] and Pt(bpy)(hpip)[2+]. *J. Biol. Inorg. Chem.* **2013**, *18* (4), 461–471.

(333) Barnett, S. M.; Goldberg, K. I.; Mayer, J. M. A soluble copper-bipyridine water-oxidation electrocatalyst. *Nat. Chem.* **2012**, *4* (6), 498–502.

(334) Santos, H. P.; Gomes, E. S.; dos Santos, M. V.; D'Oliveira, K. A.; Cuin, A.; Martins, J. S.; Quirino, W. G.; Marques, L. F. Synthesis, structures and spectroscopy of three new lanthanide β-diketonate complexes with 4,4'-dimethyl-2,2'-bipyridine. Near-infrared electroluminescence of ytterbium(III) complex in OLED. *Inorg. Chim. Acta* **2019**, *484*, 60–68.

11. Appendix

11.1. List of Figures

_____

11.2. List of Schemes

_____

11.3. List of Tables

11.4. Supporting Information

11.4.1. Supporting Information for Chapter 4

Supplementary Materials

C-H Bond Activation of Silyl-substituted Pyridines with Bis(phenolate)yttrium Catalysts as a facile Tool towards Hydroxyl-terminated *Michael*-type Polymers

Thomas M. Pehl [1,†], Moritz Kränzlein [1,†], Friederike Adams [1,†], Andreas Schaffer [1] and Bernhard Rieger [1,*]

[1] WACKER-Chair for Macromolecular Chemistry, Catalysis Research Center, Department of Chemistry, Technical University Munich, Lichtenbergstr. 4, 85748 Garching b. München, Germany

* Correspondence: rieger@tum.de; Tel.: +49-89-289-13570

† These authors contributed equally to this work.

1. Catalyst characterization
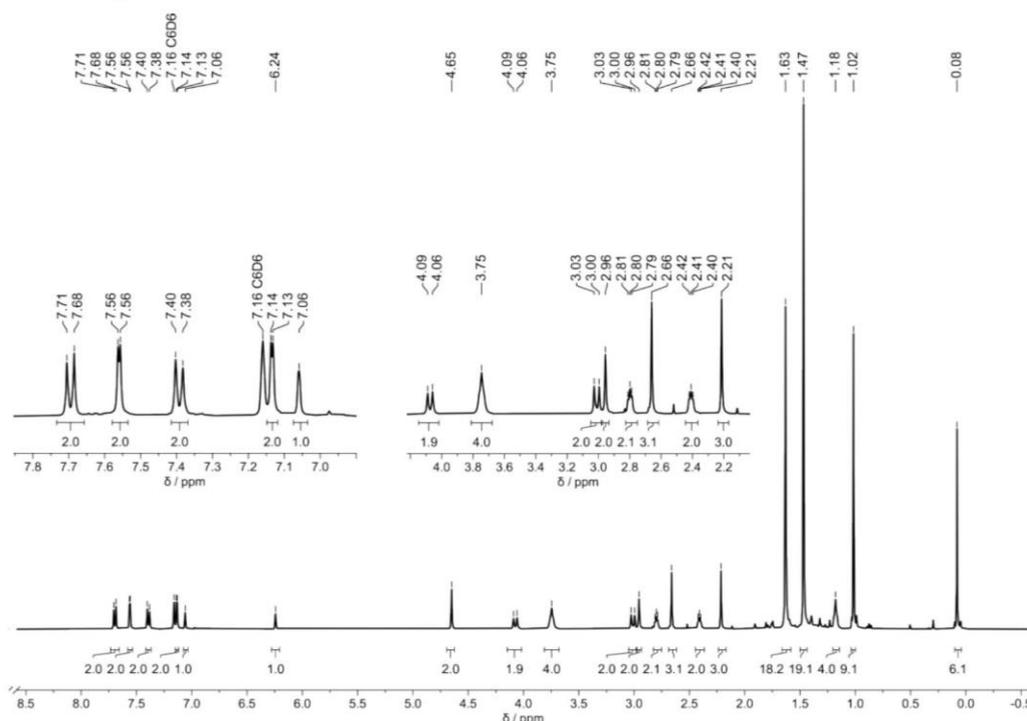
Figure S1: ^{1}H-NMR (400 MHz, C6D6, 300 K) of catalyst **4**.
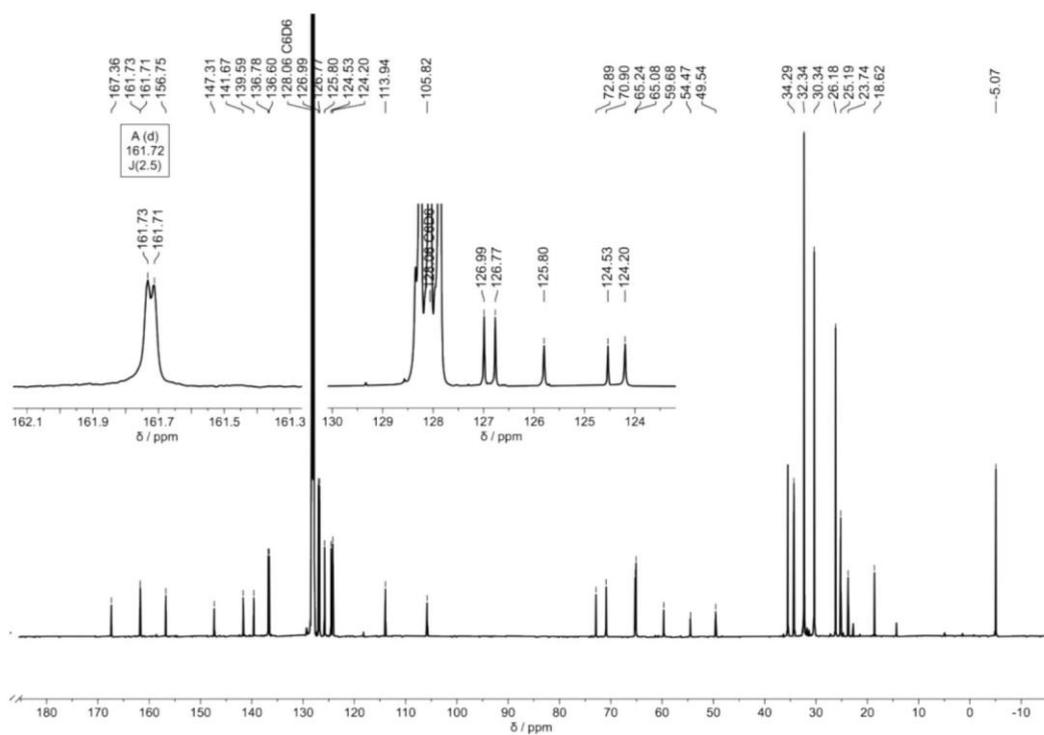
Figure S2: ^{13}C-NMR (125 MHz, C$_6$D$_6$, 300 K) of catalyst **4**.

Appendix

2. End-group analysis
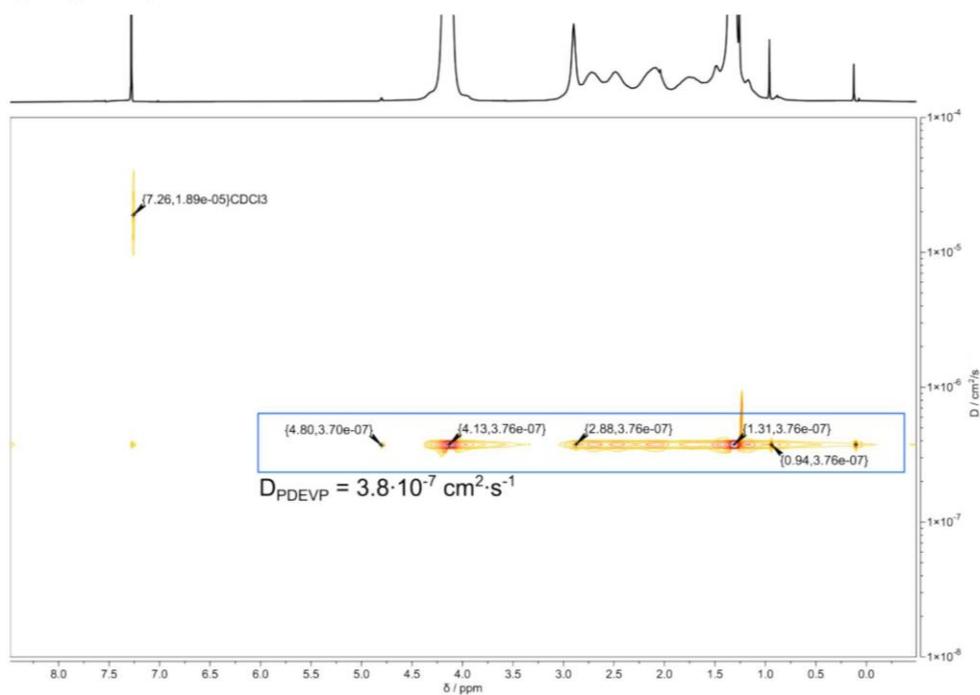
Figure S3: DOSY-NMR (CDCl₃, 400 MHz) of PDEVP (M_n = 43.4 kg mol⁻¹, Đ = 1.11).
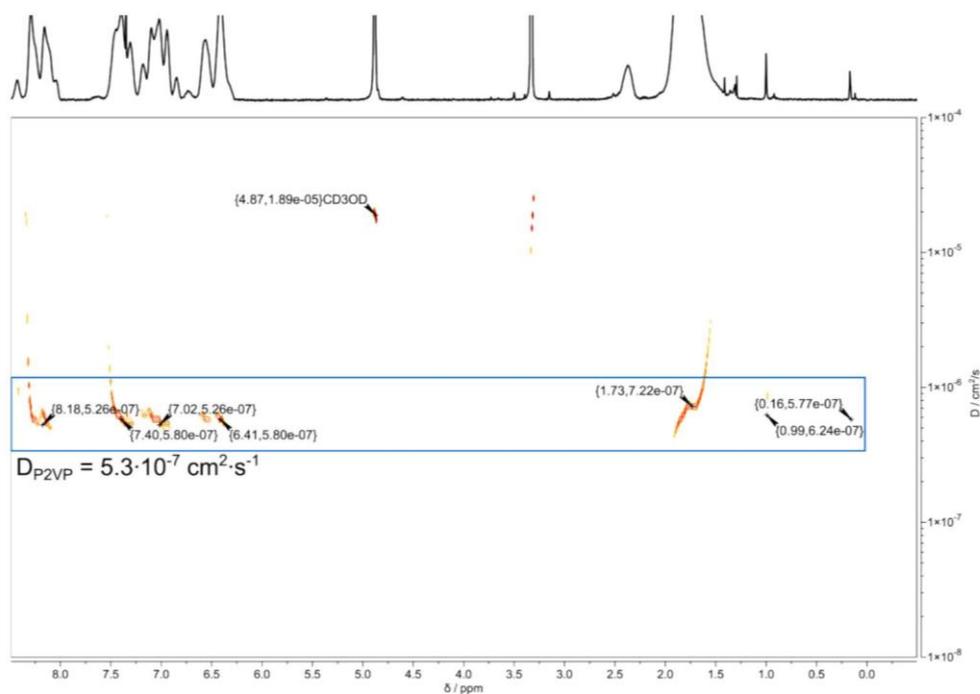
Figure S4: DOSY-NMR (MeOD, 400 MHz) of P2VP (M_n = 34.7 kg mol⁻¹, Đ = 1.07).

3. Characterization of PDEVP
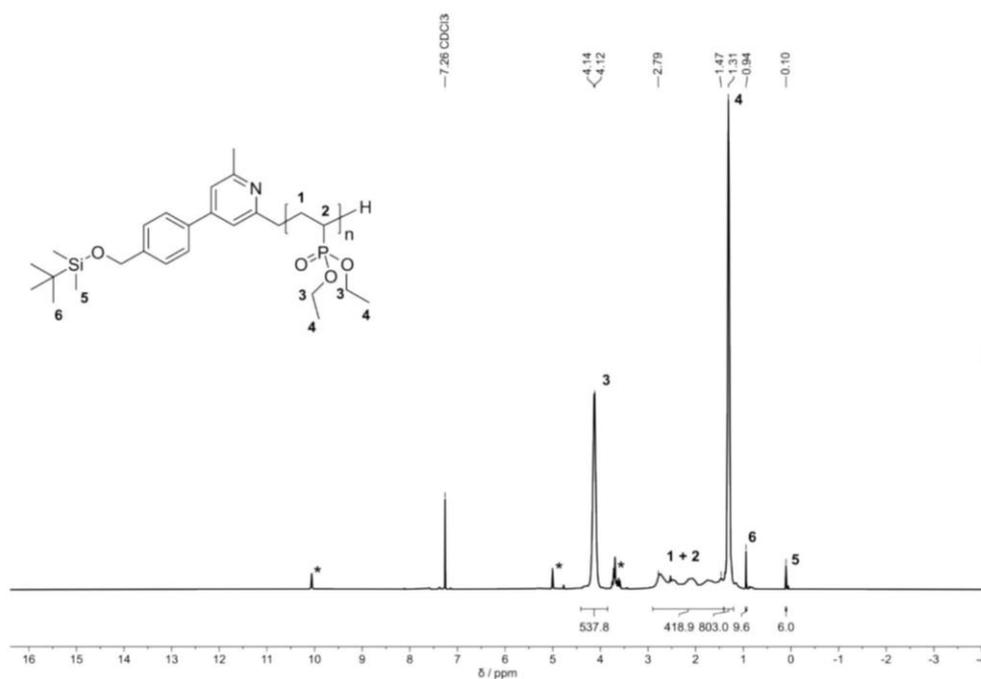
Figure S5: ^{1}H-NMR (CDCl$_3$, 400 MHz) of PDEVP produced with catalyst **4** (Table 2, entry 4, $M_{n,abs}$ = 16.6 kg/mol, $Đ$ = 1.04), impurities and artefacts are marked with *.
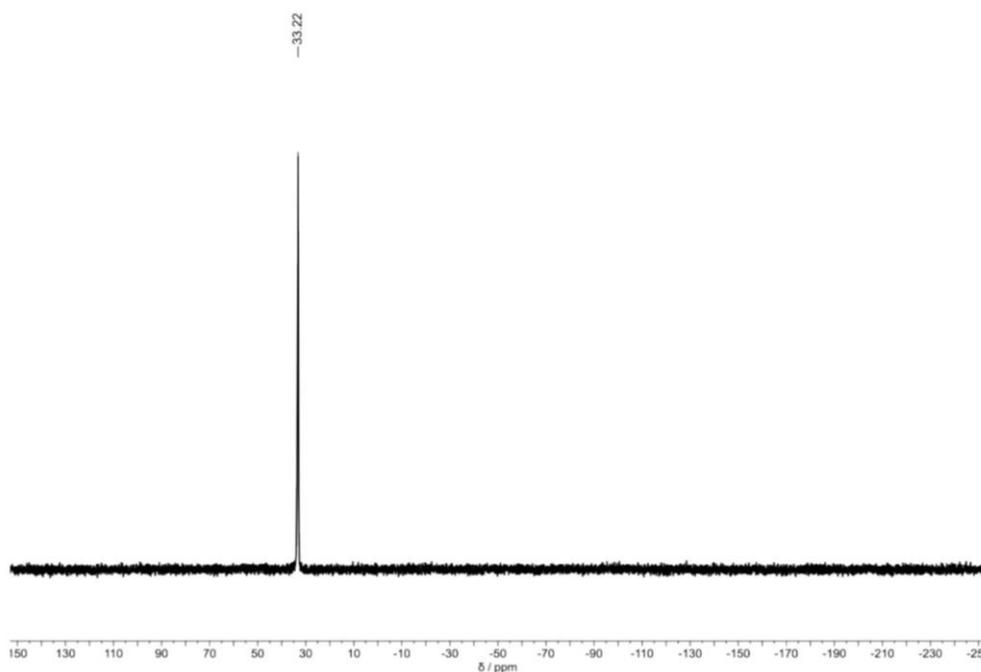
Figure S6: ^{31}P-NMR (CDCl$_3$, 162 MHz) of PDEVP produced with catalyst **4** (Table 2, entry 5, $M_{n,abs}$ = 104 kg/mol, $Đ$ = 1.33).

^{1}H-NMR (400 MHz, CDCl$_3$, 300 K): δ (ppm) = 0.10 (s, 6H, Si(CH$_3$)$_2$), 0.94 (s, 9H, Si(C(CH$_3$)$_3$)), 1.31 (m, 803H, P(OCH$_2$CH$_3$)), 1.47-2.79 (m, 419H, CH$_2$CHPOEt$_2$), 4.12-4.14 (m, 538H, P(OCH$_2$CH$_3$)$_2$).
^{31}P-NMR (125 MHz, CDCl$_3$, 300 K): δ (ppm) = 33.22 (P$_{side-chain}$).
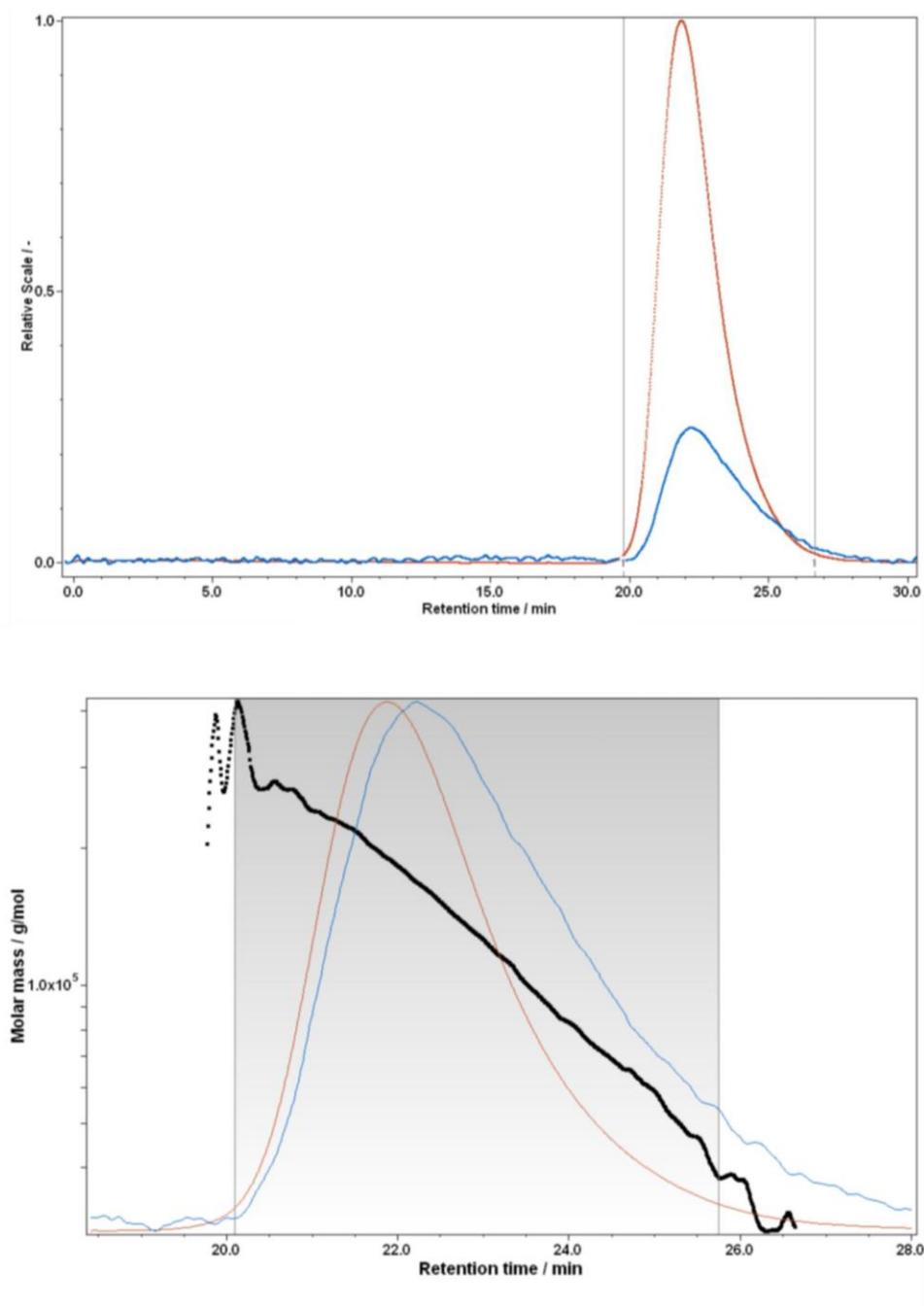
Figure S7: Representative SEC-MALS trace (top) and resulting fitting plot (bottom) for molecular weight determination of PDEVP produced with catalyst **4** (Table 2, entry 5, $M_{n,abs}$ = 104 kg/mol, $Đ$ = 1.33).

Appendix

4. Characterization of Poly(2-vinylpyridine)
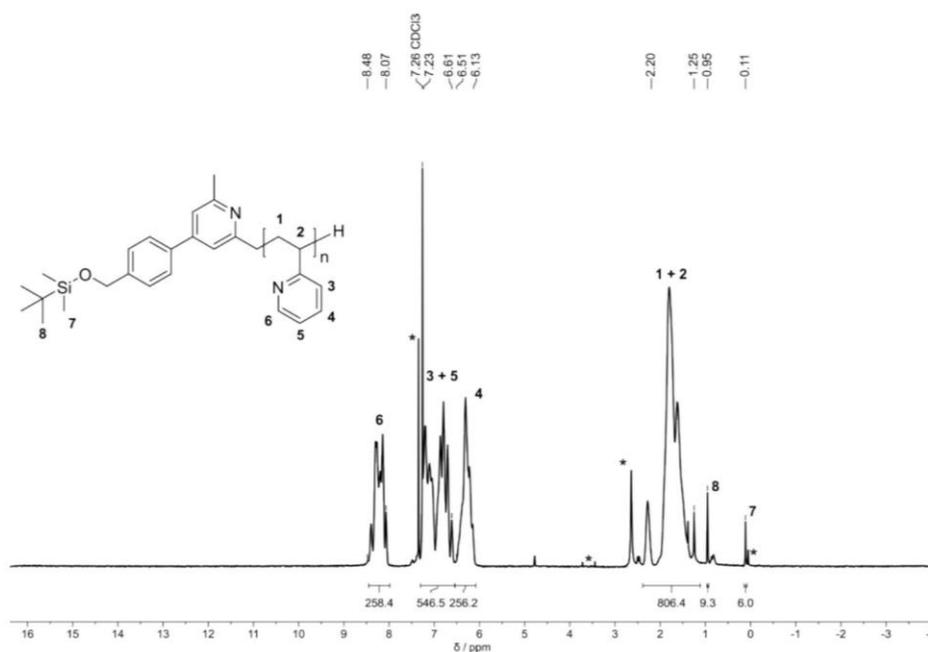
Figure S8: ^{1}H-NMR (CDCl₃, 400 MHz) of P2VP produced with catalyst **4** (Table 3, entry 1, $M_{n,abs}$ = 25.0 kg/mol, *Đ* = 1.04), impurities and artefacts are marked with *.
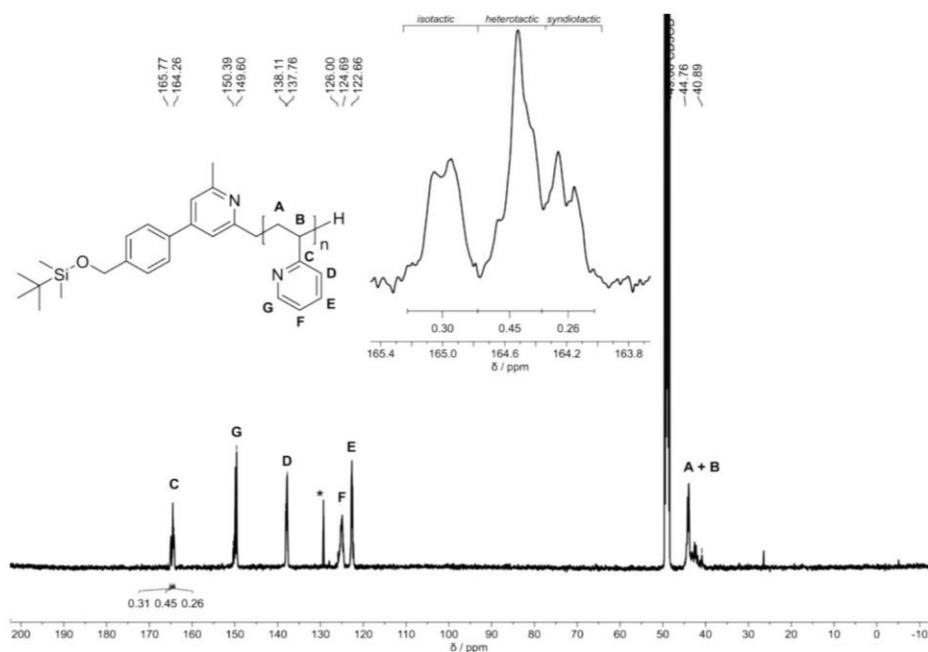
Figure S9: ^{13}C-NMR (MeOD, 500 MHz) of P2VP and section of the quaternary ^{13}C atom resonance of atactic P2VP produced with catalyst **4**, resonance assignment and microstructure determination according to Ref. [1], impurities and artefacts are marked with *.

^{1}H-NMR (400 MHz, CDCl₃, 300 K): δ (ppm) = 0.11 (s, 6H, Si(CH₃)₂), 0.95 (s, 9H, Si(C(CH₃)₃)), 1.25-2.20 (m, 806H, C*H₂*C*H*Ar), 6.13-6.50 (m, 256H, H$_{Ar}$), 6.51-7.23 (m, 456H, 2H$_{Ar}$), 8.07-8.48 (m, 258H, H$_{Ar}$).

Appendix

[13]**C-NMR** (100 MHz, CDCl$_3$, 300 K): δ (ppm) = 40.9-44.8 (carbon-backbone), 122.7-123.0, 124.7-126.0, 137.8-138.1, 159.6-150.4, 164.3-165.8.
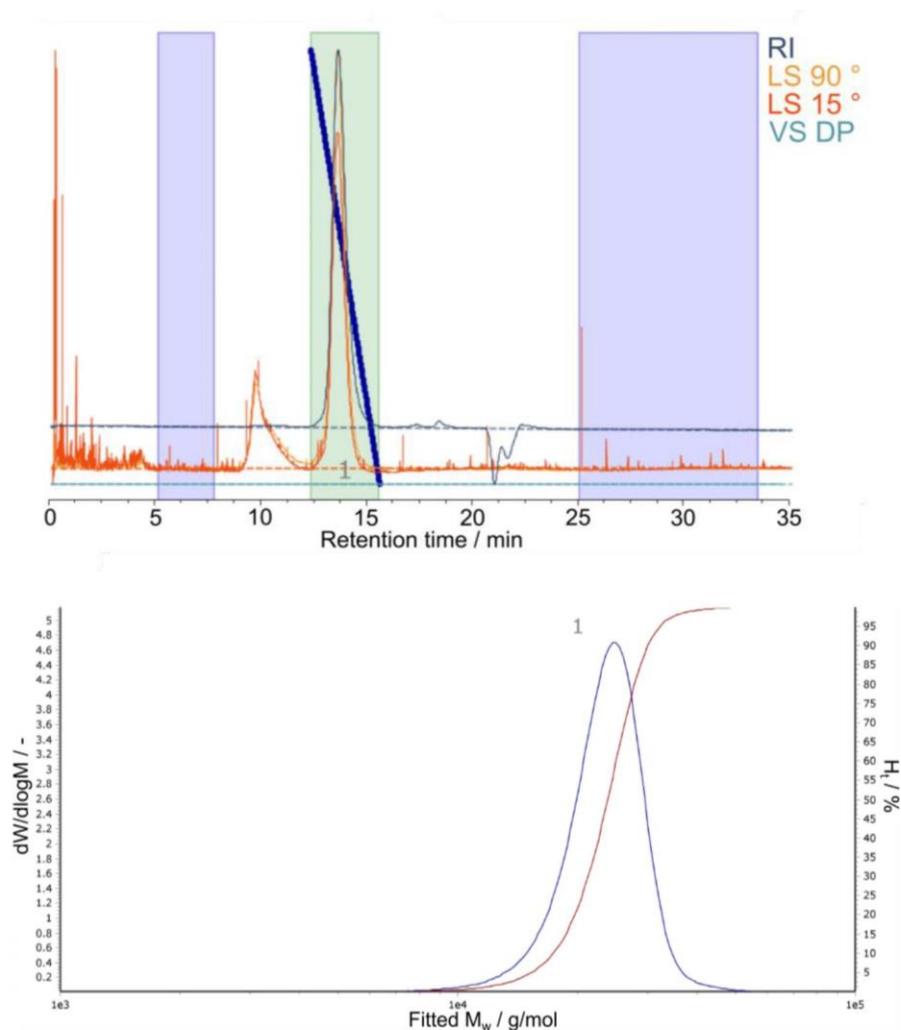
Figure S10: Representative SEC-trace (top) and distribution plot of molecular weight determination (bottom) of P2VP produced with catalyst **4** (Table 3, entry 3, $M_{n,abs}$ = 22.6 kg/mol, *Đ* = 1.06). Signals in the light scattering detectors (orange, red) with retention time below 10 min are not detectable via RI (dark blue), therefore signals do not belong to polymeric material.

5. Deprotection results
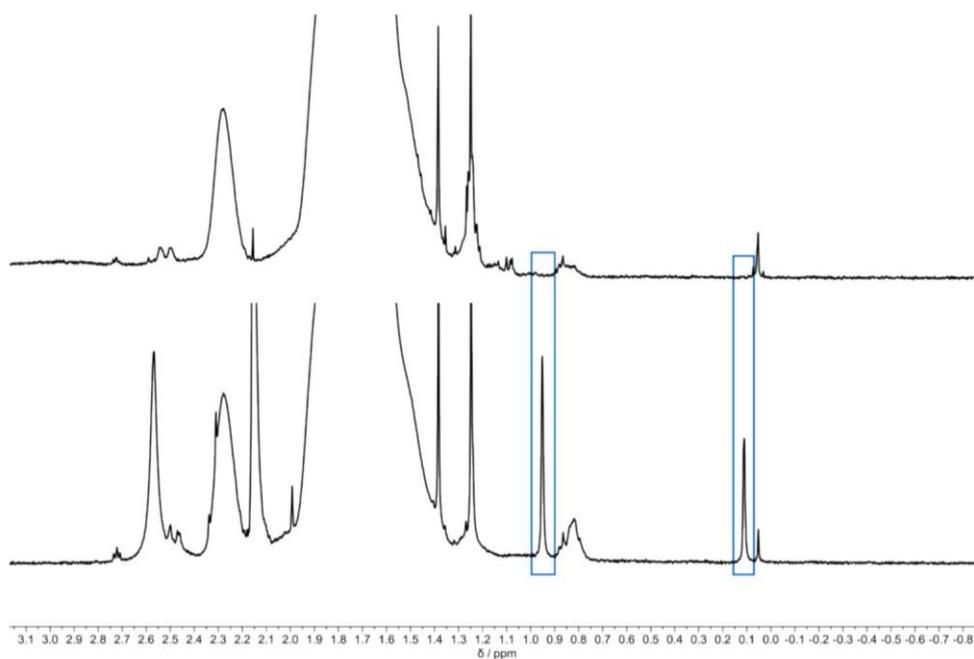
Figure S11: Representative comparison of ^{1}H-NMR spectra (silyl range, $\delta = -0.5 - 3.0$ ppm) of protected (bottom) and deprotected (top) P2VP (Table 4, entry 2) with close-up of the silyl region (TBDMS signals marked blue).
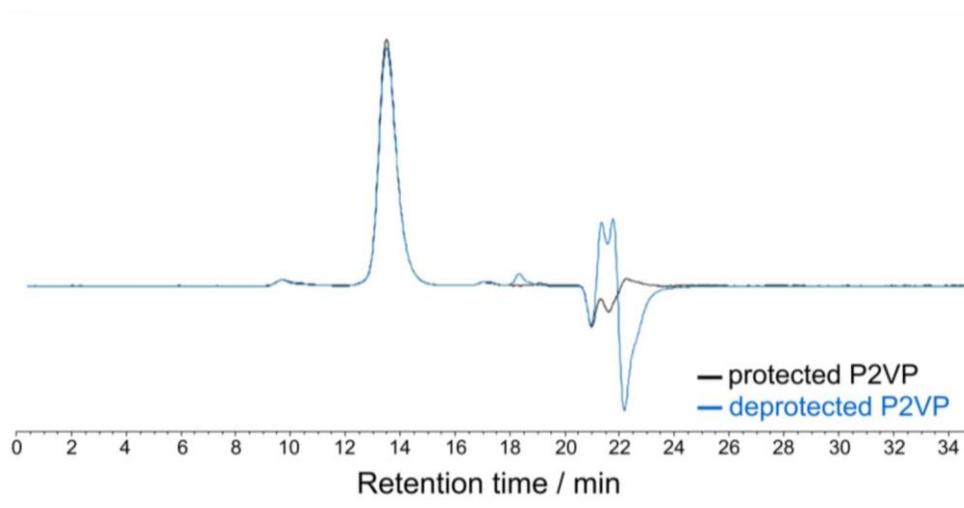
Figure S12: Overlay of SEC RI traces of P2VP protected and deprotected (Table 4, entry 2) (protected black, deprotected blue).

Appendix
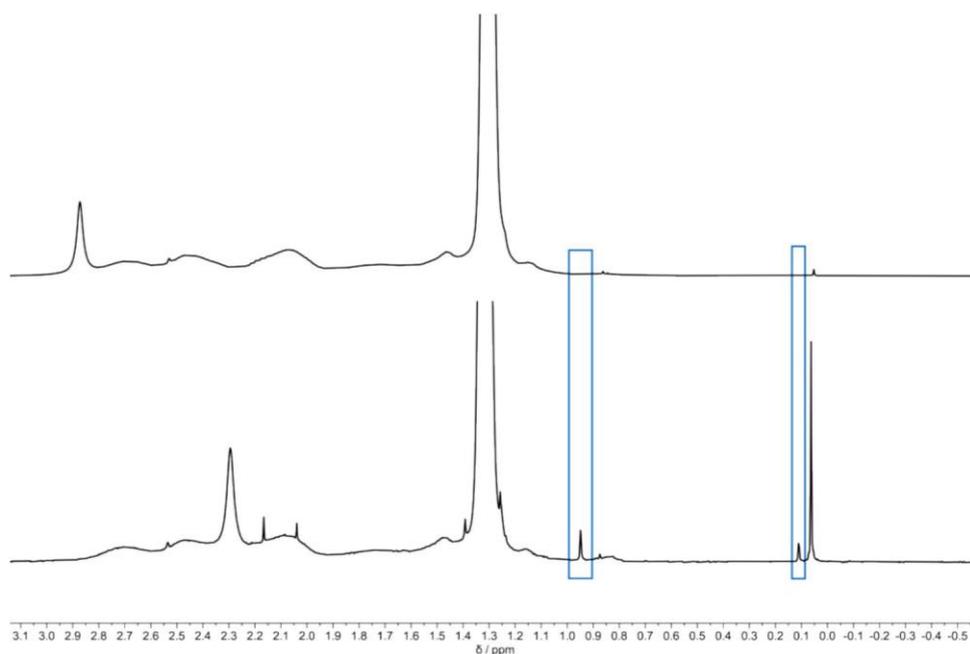
Figure S13: Representative comparison of ¹H-NMRs (silyl range, δ = -0.5 – 3.0 ppm) of protected (bottom) and unprotected (top) PDEVP (Table 4, entry 1) with close-up of the silyl region (TBDMS signals marked blue).
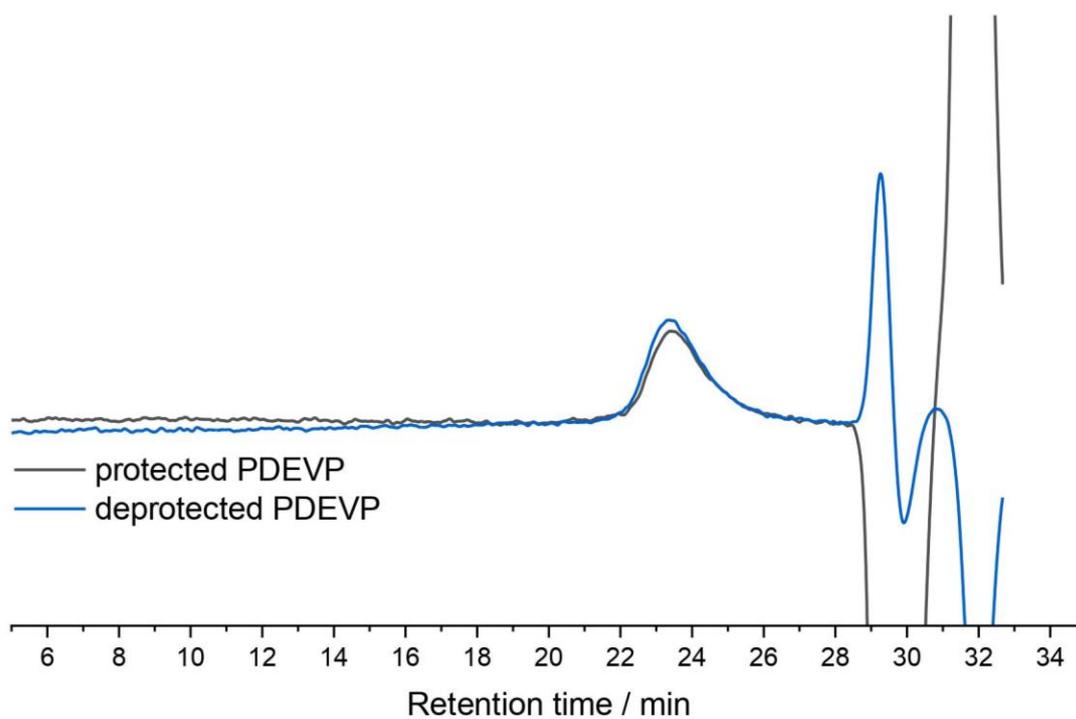
Figure S14: Overlay of SEC-MALS RI traces of PDEVP (Table 4, entry 1) protected and deprotected (protected black, deprotected blue).

6.　　Synthesis procedures

4-(4'-hydroxymethyl)benzyl)-2,6-dimethylpyridine [2]

1
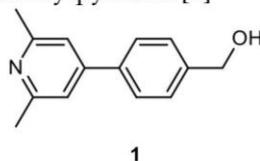
2.95 g (19.4 mmol, 1.1 eq.) 4-(hydroxymethyl)phenyl boronic acid are suspended in 120 mL ethanol and 2.48 g (17.5 mmol, 1.0 eq.) 4-chloro-2,6-dimethylpyridine in 150 mL toluene are added. To this suspension, a saturated sodium hydrogen carbonate solution (120 mL, 1.14M, 136 mmol, 7.7 eq.) is added and the two-phase mixture is degassed while stirring by applying 20 cycles of inert gas and vacuum until boiling is observed. Under argon overpressure, 4 mol% Pd(PPh$_3$)$_4$ catalyst (0.82 g, 0.71 mmol, 0.04 eq.) are added before heating to 80 °C for 72 hours. After cooling to room temperature, black catalyst residue is removed via filtration and the phases are separated. The aqueous phase is extracted with 2×80 mL ethyl acetate and 1×100 mL chloroform, the organic phases are combined and dried over MgSO$_4$. The solvent is removed *in vacuo* before purifying the crude product by column chromatography (alumina *Bronkhorst* activity grade 1, CHCl$_3$:MeOH = 95:5) giving 4-(4'-hydroxymethylbenzyl)-2,6-dimethlypyridine) **1** as fine, white powder (1.84 g, 8.6 mmol, 49 %).

^{1}H-NMR (400 MHz, CDCl$_3$, 300 K): δ (ppm) = 2.58 (s, 6H, CH$_3$), 4.76 (s, 2H, C*H$_2$*OH), 7.17 (s, 2H, H$_{Ar,Py}$), 7.46 (d, $^3J_{H,H}$ = 8.24 Hz, 2H, H$_{Ar,Benzyl}$), 7.61 (d, $^3J_{H,H}$ = 8.42 Hz, 2H, H$_{Ar,Benzyl}$).

^{13}C-NMR (100 MHz, CDCl$_3$, 300 K): δ (ppm) = 24.5, 64.6, 118.5, 127.2, 127.5, 137.8, 142.1, 149.0, 158.2.

DC: R_f = 0.47 (chloroform:methanol = 95:5) [fluorescence staining]

ESI-MS: 214.29 m/z [M+H$^+$].

EA:　calc:　　C 78.84, H 7.09, N 6.57, O 7.50.

　　　found:　C 78.33, H 7.08, N 6.52.

4-(4'-(((*tert*-butyldimethylsilyl)oxy)methyl)phenyl)-2,6-dimethylpyridine [2]

2
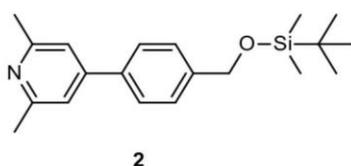
2.00 g (9.4 mmol, 1.0 eq.) unprotected pyridine **1** and 0.70 g (10.3 mmol, 1.1 eq.) imidazole are dissolved in 100 mL dry chloroform. 1.55 g (10.3 mmol, 1.1 eq.) *tert*-butyl-dimethylsilyl chloride are dissolved in 3 mL dry chloroform and are added to the alcohol mixture. The reaction solution is heated to 70 °C for 72 hours before removing the solvent *in vacuo*. 200 mL half-saturated sodium hydrogen carbonate solution (200 mL, 0.57m, 114 mmol, 12.1 eq.) are added to the crude product and the two-phase mixture is stirred for 30 min. The phases are separated and the aqueous phase is extracted with 3×150 mL benzene. The organic phases are combined and dried over MgSO$_4$. The solvent is removed, yielding 4-(4'-(((*tert*-butyldimethylsilyl)oxy)methyl)phenyl)-2,6-dimethylpyridine **2** as a yellow, viscous liquid (3.00 g, 9.2 mmol, 98 %).

^{1}H-NMR (400 MHz, C$_6$D$_6$, 300 K): δ (ppm) = 0.10 (s, 6H, Si(CH$_3$)$_2$), 1.03 (s, 9H, ^{t}Bu), 2.52 (s, 6H, CH$_3$), 4.66 (s, 2H, C*H$_2$*OH), 6.97 (s, 2H, H$_{Ar,Py}$), 7.36 (d, $^3J_{H,H}$ = 8.06 Hz, 2H, H$_{Ar,Benzyl}$), 7.41 (d, $^3J_{H,H}$ = 8.33 Hz, 2H, H$_{Ar,Benzyl}$).

^{13}C-NMR (100 MHz, C$_6$D$_6$, 300 K): δ (ppm) = -5.1, 18.6, 24.7, 26.1, 64.9, 118.2, 126.9, 127.3, 138.1, 142.4, 148.7, 158.6.

^{29}Si-NMR (80 MHz, C$_6$D$_6$, 300 K): δ (ppm) = 20.04.

ESI-MS: 329.0 m/z [M+H$^+$].

EA:　calc:　　C 73.34, H 8.92, N 4.28, O 4.88, Si 8.57.

　　　found:　C 73.38, H 9.14, N 4.48.

7. References

1. Altenbuchner, P.T.; Adams, F.; Kronast, A.; Herdtweck, E.; Pöthig, A.; Rieger, B. Stereospecific catalytic precision polymerization of 2-vinylpyridine via rare earth metal-mediated group transfer polymerization with 2-methoxyethylamino-bis(phenolate)- yttrium complexes. *Polym. Chem.*, **2015**, *6*, 6796–6801.
2. Schaffer, A; Kränzlein, M.; Rieger, B. Synthesis and Application of Functional Group-Bearing Pyridyl-based Initiators to Rare-Earth Metal-Mediated Group-Transfer Polymerization. *Macromolecules* under review.

Synthesis procedures for the initiators in the addendum Chapter 4.4

4-Iodo-2,6-dimethylpyridine[86], 4-trimethylsilylacetylene-2,6-dimethylpyridine[328], 4-azido-2,6-dimethylpyridine[329], $Cp_2Y(CH_2TMS)(thf)$[21] and $Cp_2Lu(CH_2TMS)(thf)$[21] have been prepared according to literature procedures.

4-(3,4-dimethoxy-phenyl)-2,6-dimethylpyridine
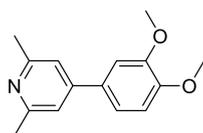
7.13 g (39.0 mmol, 1.1 eq.) (3,4-dimethoxyphenyl)boronic acid are suspended in 240 mL ethanol and 5.06 g (35.7 mmol, 1.0 eq.) 4-chloro-2,6-dimethylpyridine, 300 mL toluene and 240 mL 1.14M sodium bicarbonate solution are added. The mixture is degassed by applying 20 cycles of argon-vacuum prior to addition of 1.40 g (1.21 mmol, 0.03 eq.) tetrakis(triphenylphosphine)palladium(0). The solution is stirred for 72 hours at 80 °C. Afterwards, the catalyst is removed by filtration and 200 mL of water and 300 mL diethyl ether are added. The phases are separated, and the aqueous phase is extracted with 300 mL diethyl ether and 300 mL dichloromethane. The combined organic phases are dried over sodium sulfate and the solvent is removed in vacuo. The crude product is recrystallized from diethyl ether, yielding 7.80 g (32.1 mmol, 91 %) 4-(3,4-dimethoxy-phenyl)-2,6-dimethylpyridine.

¹H-NMR (400MHz, CDCl₃): δ (ppm) = 7.32 (dd, $^4J_{H,H}$ = 8.25 Hz, $^3J_{H,H}$ = 2.19 Hz), 7.26 (s, 2H), 7.23 (d, 3JH,H = 2.13 Hz), 7.07 (d, $^4J_{H,H}$ = 8.25 Hz), 4.08 (s, 3H), 4.05 (s, 3H), 2.70 (s, 6H).

_____

4-(3,4-dihydroxyphenyl)-2,6-dimethylpyridine
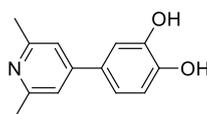
3.01 g (12.4 mmol, 1.0 eq.) 4-(3,4-dimethoxy-phenyl)-2,6-dimethylpyridine are dissolved in 30 mL 40 vol% HBr$_{(aq)}$ (15.0 mmol, 1.2 eq.) and the mixture is stirred at 140 °C for 48 hours. After cooling the mixture to room temperature, potassium bicarbonate solution is added until a neutral pH is reached, and the solution is extracted with dichloromethane. The organic phase is dried with magnesium sulfate and the solvent is removed in vacuo. 1.73 g (8.03 mmol, 65 %) of 4-(3,4-dihydroxyphenyl)-2,6-dimethylpyridine are isolated as yellow powder.

^{1}H-NMR (400MHz, CDCl$_3$): δ (ppm) = 9.34 (s, 1H, OH), 9.09 (s, 1H, OH), 7.23 (s, 2H), 7.14 (d, $^4J_{H,H}$ = 2.23 Hz), 7.07 (dd, $^3J_{H,H}$ = 8.20 Hz, $^4J_{H,H}$ = 2.23 Hz), 6.84 (d, $^3J_{H,H}$ = 8.21 Hz), 2.45 (s, 6H).

4-(3,4-di(tert-butyl-dimethylsilyl)oxy)-phenyl)-2,6-dimethylpyridine
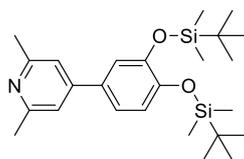
0.5 g (2.32 mmol, 1.0 eq.) 4-(3,4-dihydroxyphenyl)-2,6-dimethylpyridine are suspended in 100 mL dry tetrahydrofuran. 214 mg (5.35 mmol, 2.3 eq.) 60 wt% sodium hydride are added, and the suspension is stirred for 0.5 hours at room temperature. Afterwards, 780 mg (5.17 mmol, 2.2 eq.) *tert*-butyl-dimethylsilyl chloride are added and the mixture is stirred for 18 hours at room temperature. The solution is filtered and the solvent is removed in vacuo. The product if purified by column chromatography (R$_f$ = 0.5, pure diethyl ether), yielding 440 mg (0.99 mmol, 44 %) of pure 4-(3,4-di(tert-butyl-dimethylsilyl)oxy)-phenyl)-2,6-dimethylpyridine as a white powder.

GC-MS: t$_R$ = 15.9 min; m/z = 443.3 [M]$^+$, 386.2 [M-*t*Bu]$^+$.

TLC: R$_f$ = 0.50 (pure diethyl ether on silica, UV-detection).

^{1}H-NMR (400MHz, CDCl$_3$): δ (ppm) = 7.09 (d, 4H,), 6.90 (d, $^3J_{H,H}$ = 8.95 Hz), 2.58 (s, 6H), 1.01 (d, $^3J_{H,H}$ = 6.11 Hz, 18H), 0.23 (s, 12H).

11.4.2. Supporting Information for Chapter 5

Macromolecular rhenium-ruthenium complexes for photocatalytic CO_2 conversion – from catalytic Lewis pair polymerization to well-defined poly(vinyl bipyridine)-metal complexes

Anton S. Maier[‡], Christopher Thomas[‡], Moritz Kränzlein[‡], Thomas M. Pehl and Bernhard Rieger[*]

WACKER-Chair of Macromolecular Chemistry, Department of Chemistry, Technical University of Munich, Lichtenbergstr. 4, 85748 Garching (Germany)

[‡] These authors contributed equally.

Corresponding Authors

[*] rieger@tum.de

1

TABLE OF CONTENTS

1. GENERAL EXPERIMENTAL

All air and moisture sensitive compounds were prepared using standard *Schlenk* techniques with argon (99.996 vol.-%) from *Westfalen* as inert gas.

Unless otherwise stated, all chemicals were purchased from *Sigma-Aldrich*, *ABCR GmbH* or *TCI Chemicals* and used without further purification.

The monomers for the polymerization were purified and dried by column chromatography followed by twofold sublimation and subsequently stored under argon atmosphere. Dry solvents were obtained from an *MBraun* MB-SPS-800 solvent purification system or by drying over activated alumina and stored over activated 3 Å molecular sieve. Solvents for polymerizations and for the Lewis acid and base stock solutions were degassed by three consecutive freeze-pump-thaw cycles. Deuterated solvents were purchased from *Sigma-Aldrich* and dried over activated 3 Å molecular sieve.

As stationary phase in column chromatography, Silica 60 (*Acros Organics*, 0.060-0.200 mm) and aluminum oxide (*Sigma-Aldrich*, activated, neutral, *Brockmann* activity I), respectively, were used. Thin layer chromatography (TLC) was done on silica coated polyester plates (Macherey-Nagel, Silica 60) or aluminum oxide coated polyester plates (Macherey-Nagel, ALOX N/UV$_{254}$) with subsequent detection in UV light ($\lambda = 254$ nm).

Elemental analysis (EA). All elemental analysis were performed by the Laboratory for Microanalysis at the Institute of Inorganic Chemistry at the Technical University of Munich.

Electrospray ionization mass spectrometry (ESI-MS). ESI-MS spectra were recorded on a *Varian* ESI-MS 500 spectrometer in positive ionization mode (70 eV). The samples were

3

dissolved in acetonitrile or methanol and filtered prior to the measurements. The recorded spectra were analyzed using the *MS Data Review* software. **Differential scanning calorimetry (DSC).** DSC measurements were recorded on a DSC Q2000 from *TA Instruments* in *exo down* mode. The temperature program consisted of three consecutive heating and cooling cycles with a continuous heating ramp of 10 K/min between 0 °C and 200 °C and a sample mass of roughly 8 mg. The measurement data were analyzed using the *TA Universal Analysis* software. **Thermogravimetric analysis (TGA).** Thermogravimetric analysis was recorded on a Q5000 SA from *TA Instruments*. Roughly 1 mg of the polymer sample was applied in a tared platinum crucible and heated to 1000 °C under inert gas with a continuous heating ramp of 10 K/min. The measurement data were analyzed using the *TA Universal Analysis* software. **Micro gas chromatography (Micro-GC).** The gas phase composition in the reaction flask headspace during the photocatalytic reactions was analyzed with a *Varian* Micro 490-GC, equipped with a CO_x 1m heated column at 80 °C column temperature, 140 kPa column pressure, auto detector sensitivity, 5 s sampling time and 300 s run time using helium (99.999 vol.-%) as a carrier gas. The parameters were chosen to ensure a complete and quantitative separation of potential hydrogen, nitrogen/air, CO, methane, and CO_2 in the sample. **Refractive index increment determination (dn/dc).** For dn/dc determination, a *WGE Dr. Bures* dn/dc-2010 from PSS equipped with a 620 nm light source was used. Calibration is done using different potassium chloride in water; dn/dc measurements were performed in DMF with 25 mmol/L LiBr at 30 °C with 9 different polymer concentrations. For calculation details, see Figure S2. **Infrared spectroscopy (FT-IR).** The IR-spectra were recorded on a Vertex-70 FT-IR spectrometer from *Bruker* at room temperature. **Size-exclusion chromatography (SEC).** Average absolute molecular weights and polydispersities of the polymers were determined *via* size-exclusion chromatography (SEC) with sample concentrations in the range of 2-5 mg mL^{-1}.

4

The measurements of PVBpy were performed on an *Agilent* PL-GPC 50 (Santa Clara, CA, USA) with an integrated RI unit, two light scattering detectors (15° and 90°) and a differential pressure viscosimeter with two *Agilent* PolarGel M columns at 30 °C. As the eluent, *N,N*-dimethylformamide + 25 mmol/L LiBr was used. Absolute molecular weights and polydispersities of PVBpy were determined using the experimentally determined value for dn/dc of 0.190 mL g^{-1}. **Nuclear magnetic resonance spectroscopy (NMR).** ^{1}H-NMR- and ^{13}C-NMR spectra, as well as 2D-NMR-experiments of small molecules, polymers and metal complexes were recorded on a *Bruker Ascend* 400 MHz NMR-spectrometer at 400 MHz (^{1}H) and 101 MHz (^{13}C), respectively. All chemical shifts are given in parts per million (ppm) and referenced to the residual proton signal of the respective solvent (CDCl$_3$: δ = 7.26 ppm, DMSO-d$_6$: δ = 2.50 ppm). The NMR spectra were analyzed using the *MestReNova* software. Signal multiplicities are abbreviated as following: s - singlet, d - dublet, dd – dublet of dublets, m – multiplet, q - quartet, t – triplet. **Lyophilization.** The polymer samples subject to freeze-drying were dissolved in benzene and frozen under constant rotation in liquid nitrogen. For lyophilization, a VaCo 5-II-D from *Zirbus technology GmbH* was applied and the pressure adjusted to 2 mbar with a condenser temperature of -90 °C. **Microwave reactions.** The microwave reactions were conducted in a reactor from CEM with a focused microwave beam. The syntheses were conducted at 50 W, a temperature of 125 °C and dynamic power supply. **Photoluminescence spectroscopy (PL).** Emission spectra were recorded on an *Edinburgh Instruments* FS5 spectrofluorometer with a 150 W CW ozone-free xenon arc lamp, Czerny-Turner design monochromators and a R928P photomultiplier emission detector. Spectra were measured from 400 nm to 900 nm with 5 nm scan slit width, and a resolution of 1 nm at 25 °C. The samples were dissolved in *N,N*-dimethylformamide and analyzed in a QS 10×10 mm quartz glass cuvette from *Hellma GmbH & Co. KG*. **UV/Vis spectroscopy (UV/Vis).**

5

UV/Vis spectra were recorded on a *PerkinElmer, Inc.* Lambda 365 UV/Vis spectrophotometer in an UV quartz cuvette (40 mm x 10 mm x 2 mm). Spectra were measured from 250 nm to 950 nm with a spectral bandwidth (SBW) of 1 nm and a scan rate of 300 nm/min at 25 °C. The samples were dissolved in *N,N*-dimethylformamide and analyzed in a QS 10×10 mm quartz glass cuvette from *Hellma GmbH & Co. KG*. A base line correction with the pure solvent was performed prior to sample measurements. **Inductively coupled plasma mass spectrometry (ICP-MS).** To accurately quantify the Re and Ru amount loaded onto the polymers, ICP-MS for rhenium and ruthenium, respectively was conducted on a *Perkin Elmer* Nexlon 350D ICP-MS instrument. The respective samples were immersed in concentrated 7.5 mL nitric acid and 2.5 mL H_2O_2 30% (v/v) and treated in the microwave at 150 °C for 5 min. Subsequently, the microwave-digested samples were diluted 1/200 with Millipore Milli-Q® water. The extra pure solvents were checked for possible analyte contaminations before measurement. ^{104}Ru and ^{187}Re were used as target masses for the analytes and ^{103}Rh as an internal standard. Analyte quantification was carried out in standard mode with correction equation to avoid polyatomic interferences. Detection limit for Ru was 0.13 µg L^{-1} and 0.05 µg L^{-1} for Re. External calibration was performed in the range of 0 µg L^{-1} to 100 µg L^{-1}. Each sample was measured with five measurement replicates, a dwell time per 50 ms and an integration time of 750 ms. The Ru and Re concentrations were blank corrected *via* measurement of blank samples. **Gas-Phase infrared spectroscopy (IR)** has been measured on a *Thermo Fisher Scientific Nicolet 380 FT-IR* in transmittance mode with a resolution of 0.5 (0.241 cm^{-1}) in the range of 4000-400 cm^{-1} and 128 scans.

6

2. SYNTHESIS PROCEDURES

4-Hydroxyethyl-4-methyl-2,2'-bipyridine

$C_{12}H_{12}N_2$
M = 184.24 g/mol

$C_{13}H_{14}N_2O$
M = 214.27 g/mol

1. *n*-BuLi, DIPA, 0 °C → rt, 2 h
2. Paraformaldehyde, rt, 21 h
(THF)
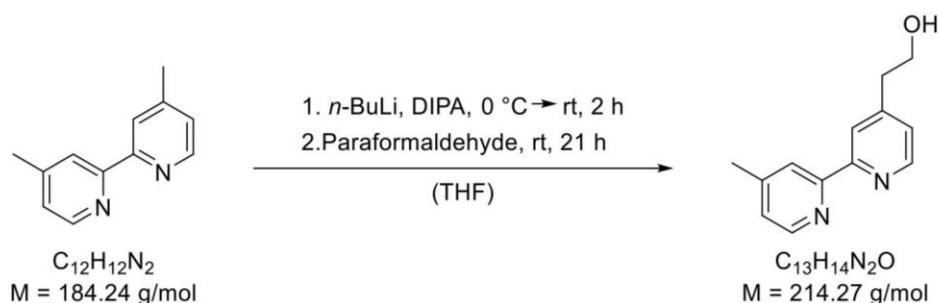
The synthesis of 4-hydroxyethyl-4'-methyl-2,2'-bipyridine was adapted from a literature-known procedure.[1] In an oven-dried Schlenk flask, 8.58 mL di-*iso*-propylamine (6.15 g, 60.8 mmol, 1.60 eq.) was dissolved in 50 mL of dry THF and cooled to 0 °C. To the resulting solution, 24.3 mL *n*-butyl lithium (2.5 M in hexanes, 60.8 mmol, 1.60 eq.) were added slowly and the reaction mixture was stirred at room temperature for one hour. To the previous solution, a solution of 7.00 g 4,4'-dimethyl-2,2'-bipyridil (38.0 mmol, 1.00 eq.) in 200 mL dry THF was transferred using a canula. The reaction mixture was stirred for two hours at room temperature and 4.56 g paraformaldehyde (152 mmol, 4.00 eq.) were added before stirring another 21 hours at room temperature. The reaction was quenched upon addition of 50 mL cold water and the mixture was extracted with diethyl ether (5 × 100 mL). The combined organic phases were dried over anhydrous Na_2SO_4, and the solvent was removed under reduced pressure to yield a brownish oil. The crude product was purified *via* column chromatography (Al_2O_3; CH_2Cl_2/MeOH = 50/1) to yield 4.57 g 4-hydroxyethyl-4'-methyl-2,2'-bipyridine (21.3 mmol, 56%) as a yellow oil.

7
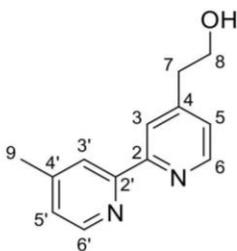
¹H-NMR (400 MHz, CDCl₃): δ (ppm) = 8.58 (d, ^3J = 5.0 Hz, 1 H, C-6-H), 8.52 (d, ^3J = 4.9 Hz, 1 H, C-6'-H), 8.27 (s, 1 H, C-3-H), 8.22 (s, 1 H, C-3'-H), 7.19 (dd, ^3J = 5.0 Hz, $^4J_{H,H}$ = 1.7 Hz, 1 H, C-5-H), 7.15 - 7.08 (m, 1 H, C-5'-H), 3.96 (q, ^3J = 6.2 Hz, 2 H, C-8-H), 2.95 (t, ^3J = 6.5 Hz, 2 H, C-7-H), 2.44 (s, 3 H, C-9-H).

TLC: R_f = 0.22 (CH₂Cl₂/MeOH = 50/1) [UV]

ESI-MS (solvent: MeCN) m/z: 214.9 ([M+H]⁺).

8

4-Vinyl-4'-methyl-2,2'-bipyridine (VBpy)

$C_{13}H_{14}N_2O$
M = 214.27 g/mol

KO*t*Bu, *p*-TsCl, rt, 14.5 h

(THF)

$C_{13}H_{12}N_2$
M = 196.25 g/mol
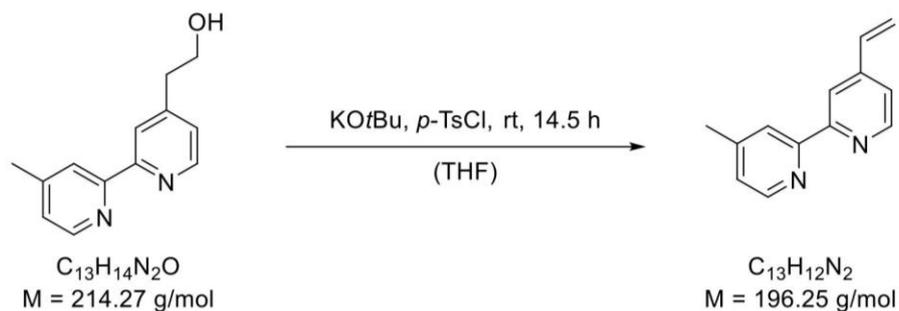
The synthesis of 4-vinyl-4'-methyl-2,2'-bipyridine was adapted from a literature-known procedure.[2] To a solution of 2.00 g 4-hydroxyethyl-4'-methyl-2,2'-bipyridine (9.33 mmol, 1.00 eq.) in 40 mL dry THF, 2.62 g potassium *tert*-butoxide (23.3 mmol, 2.50 eq.) were added at -10 °C. Subsequently, a solution of 2.67 g *p*-toluene sulfonyl chloride (14.0 mmol, 1.50 eq.) in 40 mL dry THF was added to the reaction mixture dropwise at -10 °C. The reaction mixture was stirred at -10 °C for another hour and at room temperature for additional 16 hours. The reaction was quenched by addition of 25 mL of a half saturated $NaHCO_3$ solution and the mixture extracted with diethyl ether (5 × 100 mL). The combined organic phases were dried over anhydrous Na_2SO_4, and the solvent was removed under reduced pressure to yield a yellowish solid. The crude product was purified *via* column chromatography (SiO_2; P/Et_2O/NEt_3 = 6/4/0.4) followed by twofold sublimation (80 °C, $2 \cdot 10^{-2}$ mbar) to yield 1.34 g 4-vinyl-4'-methyl-2,2'-bipyridine (6.81 mmol, 73%) as a white, crystalline solid.

9
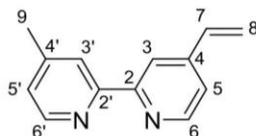
¹H-NMR (400 MHz, CDCl₃): δ (ppm) = 8.63 (d, ^3J = 5.1 Hz, 1 H, C-6-H), 8.56 (d, ^3J = 5.1 Hz, 1 H, C-6'-H), 8.44 (s, 1 H, C-3-H), 8.27 (s, 1 H, C-3'-H), 7.31 (dd, ^3J = 5.1 Hz, ^4J = 1.7 Hz, 1 H, C-5-H), 7.17 (dd, ^3J = 5.1 Hz, ^4J = 1.6 Hz, 1 H, C-5'-H), 6.77 (dd, ^3J = 17.6 Hz, ^3J = 10.9 Hz, 1 H, C-7-H), 6.11 (d, ^3J = 17.6 Hz, 1 H, C-8-H), 5.54 (d, ^3J = 10.9 Hz, 1 H, C-8-H), 2.46 (s, 3 H, C-9-H).

¹³C-NMR (101 MHz, CDCl₃): δ 156.67 (C-2), 155.83 (C-2'), 149.53 (C-6), 148.98 (C-6'), 148.48 (C-4'), 146.03 (C-4), 135.08 (C-7), 124.96 (C-5'), 122.22 (C-3'), 120.79 (C-5), 119.05 (C-8), 118.67 (C-3), 21.35 (C-9).

TLC: R_f = 0.35 (P/Et₂O/NEt₃ = 6/4/0.4) [UV]

ESI-MS (solvent: MeCN) m/z: 196.6 ([M+H]⁺).

Elemental analysis of C₁₃H₁₂N₂ (196.1): Calculated (%): **C** 79.56, **H** 6.16, **N** 14.27.

Found (%): **C** 79.44, **H** 6.16, **N** 14.27.
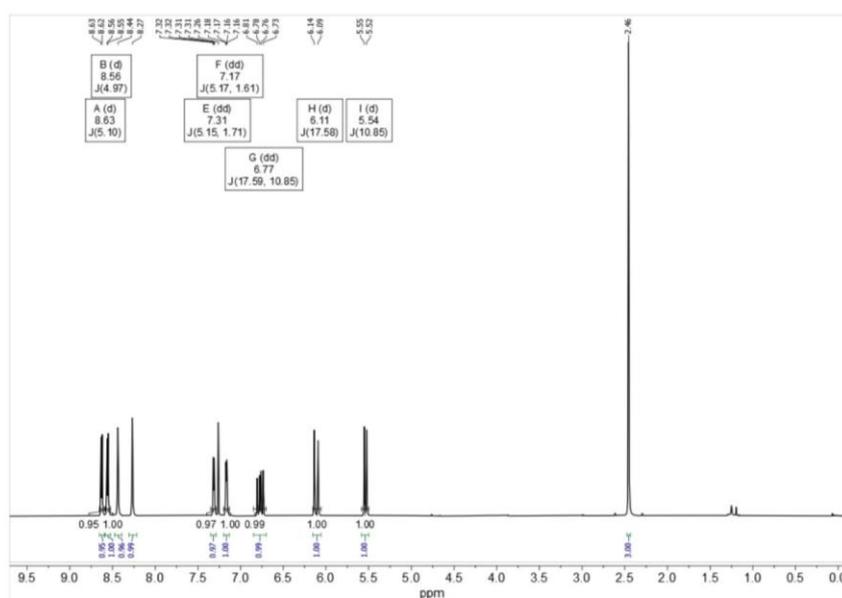
Figure S1: ¹H-NMR (400 MHz, CDCl₃, 300K) of the monomer 4-vinyl-4'-methyl-2,2'-bipyridine.

Synthesis of ruthenium precursor complex Ru(dmb)₂Cl₂

LiCl, microwave reaction, dynamic power supply,
50 W, 125 °C, 2 h

(DMF)

C₈H₁₂Cl₂Ru
M = 280.16 g/mol

C₂₄H₂₄Cl₂N₄Ru
M = 540.45 g/mol
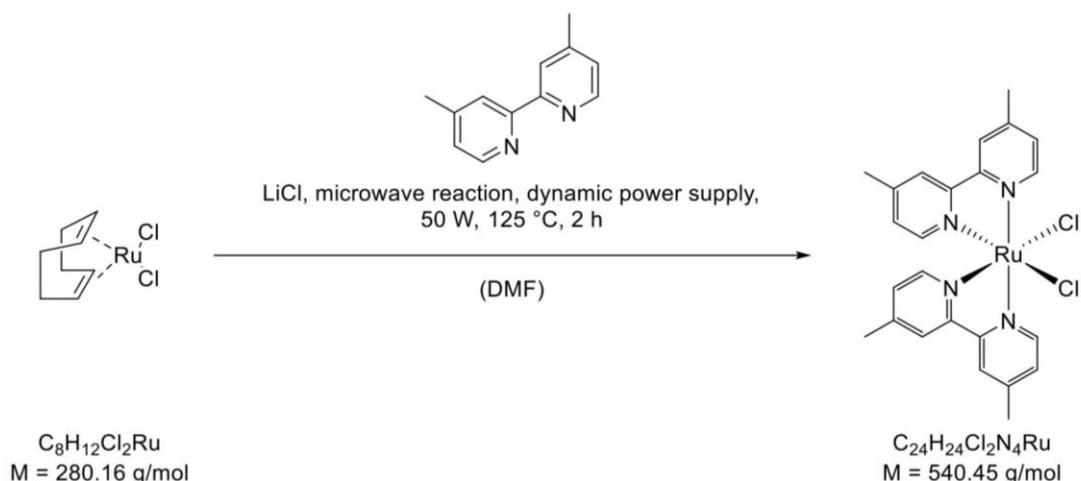
The synthesis of Ru(dmb)₂Cl₂ was adapted from a literature-known procedure.[3] Under inert gas atmosphere, 76.1 mg Ru(cod)Cl₂ (27.2 μmol, 1.00 eq.) and 98.9 mg lithium chloride (2.33 mmol, 8.59 eq.) are weighed into an oven-dried microwave vessel. Further, 100 mg 4,4-dimethyl-2,2'-bipyridine (54.3 μmol, 2.00 eq.) were added, the reactants suspended in 20 mL of dry *N,N*-dimethylformamide and heated in a closed vessel setup in a microwave reactor (125 °C, 50 W, dynamic mode) for two hours. After cooling to room temperature, the reaction mixture was filtered through a syringe filter and the solvent removed under reduced pressure. The residue was suspended in water, filtered over a fine frit (Por. 4) and washed with 100 mL of a 9/1 solution of water and acetonitrile. The crude product was eluted from the frit with chloroform and the solvent removed under reduced pressure. Recrystallisation of the crude product in acetonitrile (15 mL) yielded 60.5 mg Ru(dmb)₂Cl₂ (11.2 μmol, 41%) as a black powder.

ESI-MS (Solvent: MeCN) m/z: 541.5 ([M+H]$^+$). The ESI-MS spectrum exhibited the expected isotope distribution.

UV/Vis (DMF): λ_{max} (nm) = 567, 384.

Synthesis of the electron donor 1,3-dimethyl-2-phenyl-2,3-dihydro-1*H*-benzo[*d*]imidazole (BIH)
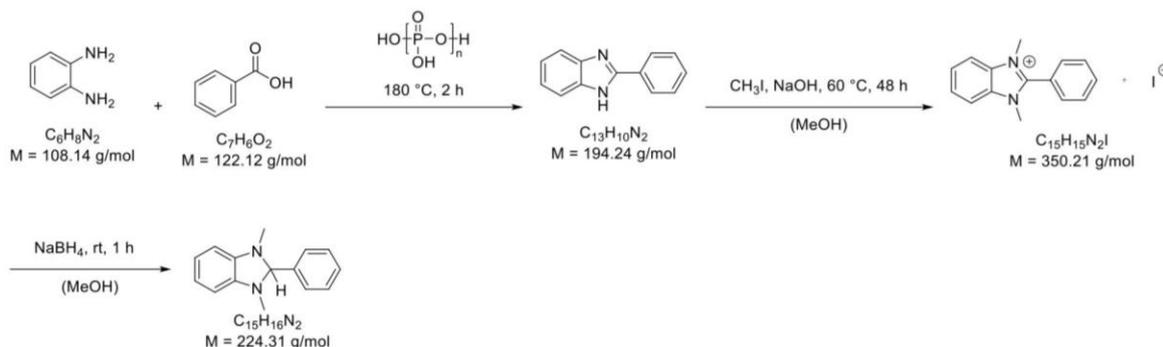
The synthesis of 2-phenyl-1*H*-benzo[*d*]imidazole was adapted from a literature-known procedure.[4] In a round bottom flask 6.14 g of benzoic acid (50.3 mmol, 1.00 eq.), 5.44 g *o*-phenylenediamine (50.3 mmol, 1.00 eq.) and 21.0 g polyphosphoric acid were heated to 180 °C for two hours. After slowly cooling to room temperature, the acid was neutralized by addition of 100 mL of ammonia solution (6wt% in water) and the crude product filtered off using a frit. The crude product was washed with ammonia solution (6wt% in water) until the blue colour disappeared and then dried in vacuo, yielding 9.77 g 2-phenyl-1*H*-benzo[*d*]imidazole (50.3 mmol, quant.) as a pink solid.

^{1}H-NMR (400 MHz, CDCl$_3$): δ (ppm) = 8.11 - 8.03 (m, 2 H, C-H$_{Ar}$), 7.70 - 7.62 (m, 2 H, C-H$_{Ar}$), 7.52 - 7.46 (m, 3 H, C-H$_{Ar}$), 7.31 - 7.26 (m, 2 H, C-H$_{Ar}$).

The synthesis of 1,3-dimethyl-2-phenyl-1*H*-benzo[*d*]imidazole-3-ium iodide was adapted from a literature-known procedure.[5] In a round bottom flask, 9.77 g 2-phenyl-1*H*-benzo[*d*]imidazole (50.3 mmol, 1.00 eq.) and 2.01 g sodium hydroxide (50.3 mmol, 1.00 eq.) were dissolved in 50 mL of dry methanol. Under vigorous stirring, 11.4 mL methyl iodide (26.0 g, 183 mmol, 3.60 eq.) were added dropwise and the solution heated to 60 °C for 48 hours. After cooling to room

temperature, the solvent was removed under reduced pressure and the residue dissolved in 320 mL of a hot ethanol/water mixture (EtOH/H$_2$O = 5/1). Subsequently, three spatula tips of activated charcoal were suspended in this solution and after 30 minutes removed via filtration over Celite®. Finally the solvent was removed under reduced pressure and the crude product recrystallized from ethanol (250 mL). Drying of the product in vacuo yielded 8.19 g 1,3-dimethyl-2-phenyl-1*H*-benzo[*d*]imidazole-3-ium iodide (23.4 mmol, 46%) as a yellow solid.

¹H-NMR (400 MHz, DMSO-d$_6$): δ (ppm) = 8.18 - 8.09 (m, 2 H, C-H$_{Ar}$), 7.96 - 7.88 (m, 2 H, C-H$_{Ar}$), 7.87 - 7.74 (m, 5 H, C-H$_{Ar}$), 3.90 (s, 6 H, N-CH$_3$).

The synthesis of 1,3-dimethyl-2-phenyl-2,3-dihydro-1*H*-benzo[*d*]imidazole was adapted from a literature-known procedure.[5] Under inert gas atmosphere, 8.19 g 1,3-dimethyl-2-phenyl-1*H*-benzo[*d*]imidazole-3-ium iodide (23.4 mmol, 1.00 eq.) were dissolved in 300 mL of dry methanol and 4.00 g sodium borohydride (106 mmol, 4.50 eq.) slowly added. The reaction mixture was stirred for one hour at room temperature and the solvent then removed under reduced pressure. The crude product was purified via twofold recrystallization from an ethanol/water mixture (EtOH/H$_2$O = 2/1, 200 mL). The product was dried in vacuo to yield 5.24 g of 1,3-dimethyl-2-phenyl-2,3-dihydro-1*H*-benzo[*d*]imidazole (23.4 mmol, quant.) as yellow, crystalline needles.

¹H-NMR (400 MHz, DMSO-d$_6$): δ (ppm) = 7.58 – 7.40 (m, 5 H, C-2-*Ph*), 6.62 (m, 2 H, C-H$_{Ar}$), 6.45 (m, 2 H, C-H$_{Ar}$), 4.87 (s, 1 H, C-2-H), 2.48 (s, 6 H, N-CH$_3$).

13

3. POLYMERIZATION RESULTS

3.1 POLYMERIZATION PROCEDURE

The calculated amount of Lewis acid was dissolved in 0.5 mL dry toluene. Subsequently, a solution of 1.02 mmol of the monomer in 1.5 mL dry toluene was added to the mixture. The polymerization was started by addition of the Lewis base and the conversion of the monomer was monitored via ^{1}H-NMR by periodically removing aliquots (0.1 mL of the reaction mixture + 0.4 mL of undried CDCl$_3$). When no further conversion could be detected in the NMR, the reaction was quenched by addition of 0.5 mL undried CDCl$_3$ and the polymer was precipitated in pentane. After decanting of the supernatant, the residual polymer was dissolved in benzene and freeze-dried to yield the pure polymer as a white solid.

3.2 POLYMER SYNTHESIS RESULTS FOR METAL LOADING

Table S1: Characterization of PVBpy1-3 prepared with the Lewis pair Al(i-Bu)$_3$/PMe$_3$.

Polymer	[VBpy]/[LA]/[LB][a] [eq.]/[eq.]/[eq.]	t_R [b] [h]	X_{VBpy} [c] [%]	$M_{n,theo}$ [d] [kg/mol]	$M_{n,abs}$ [e] [kg/mol]	Đ [e] [-]	I.E. [f] [%]
PVBpy 1	100/2/1	17	85	16.7	33.8	1.36	50
PVBpy 2	100/2/1	17	80	15.7	23.3	1.48	68
PVBpy 3	100/2/1	17	92	18.0	36.7	1.66	49

[a] Desired reactant ratio; [b] 1.02 mmol monomer in 2 mL toluene, room temperature, Lewis-acid and monomer were pre-mixed and the polymerization was started by addition of Lewis-base; [c] determination of conversion via aliquot-^{1}H-NMR; [d] theoretical molecular weight determined via $M_{n,theo} = X_{VBpy} \times M_{VBpy} \times$ [VBpy]/[LA]/[LB] assuming full initiator efficiency; [e] absolute molecular weight and polydispersity determined using SEC with triple detection in DMF with added LiBr (25 mmol/L) at 30 °C using the experimentally determined dn/dc = 0.190 mL g^{-1}; [f] initiator efficiency I.E. = $M_{n,theo}/M_{n,abs} \times$ 100%.

14
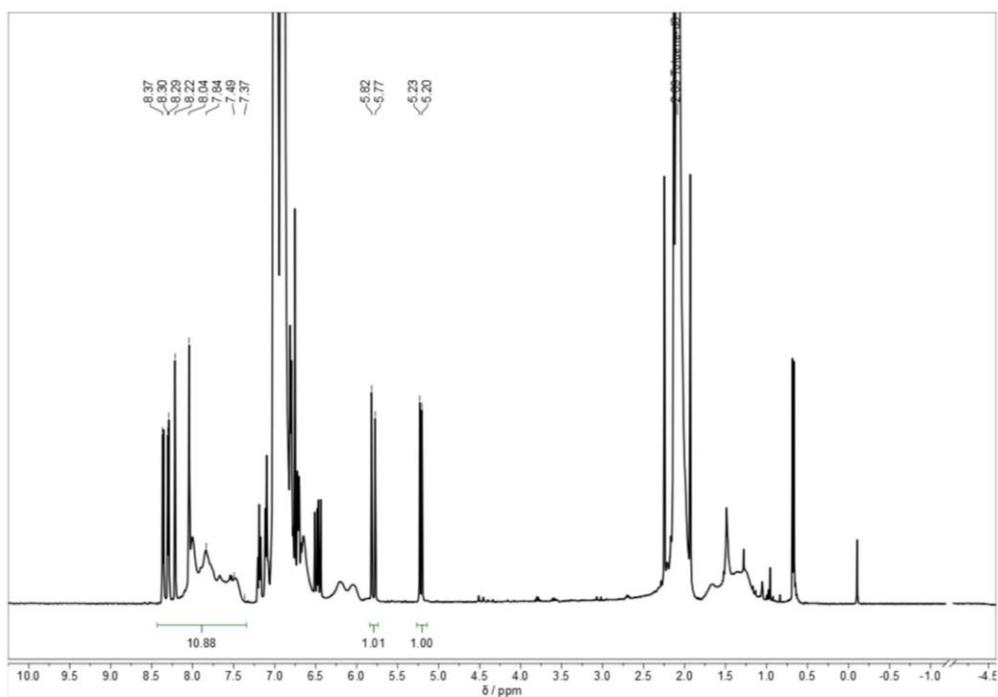
Figure S2: Aliquot-^{1}H-NMR (400 MHz, CDCl$_3$, 300K) for polymerization determination via integration of the signals between 7.37-8.37 ppm I$_{Pol}$ versus vinyl signals from 5.20-5.23 I$_V$ set to one with conversion X = (I$_{Pol}$ - 4)/I$_{Pol}$ x 100%.
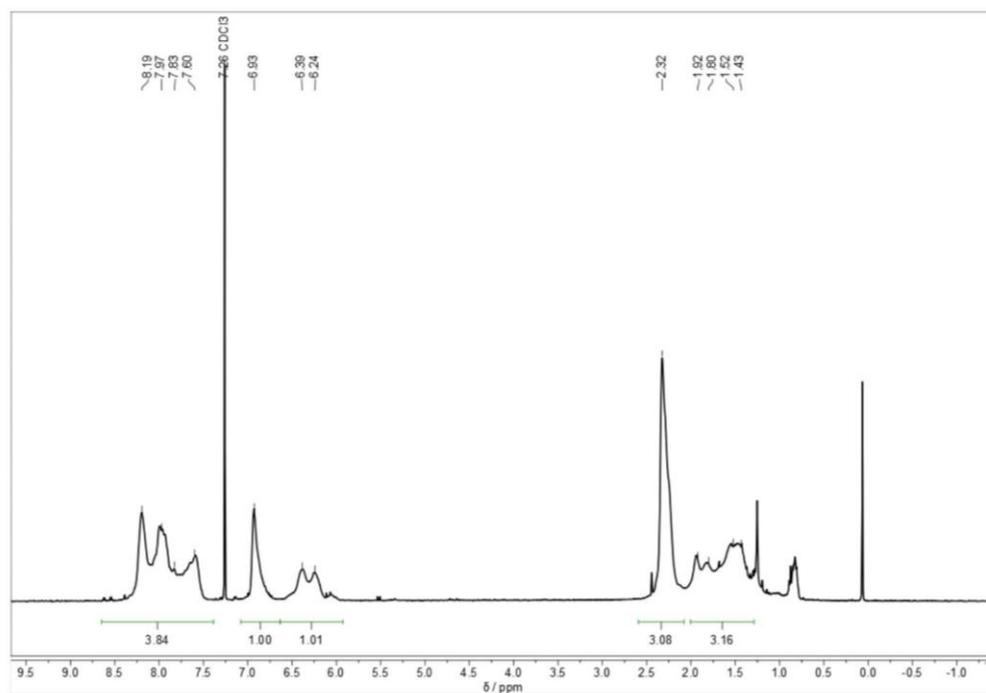
Figure S3: ^{1}H-NMR (400 MHz, CDCl$_3$, 300 K) of PVBpy (Table 1, entry 2).

15
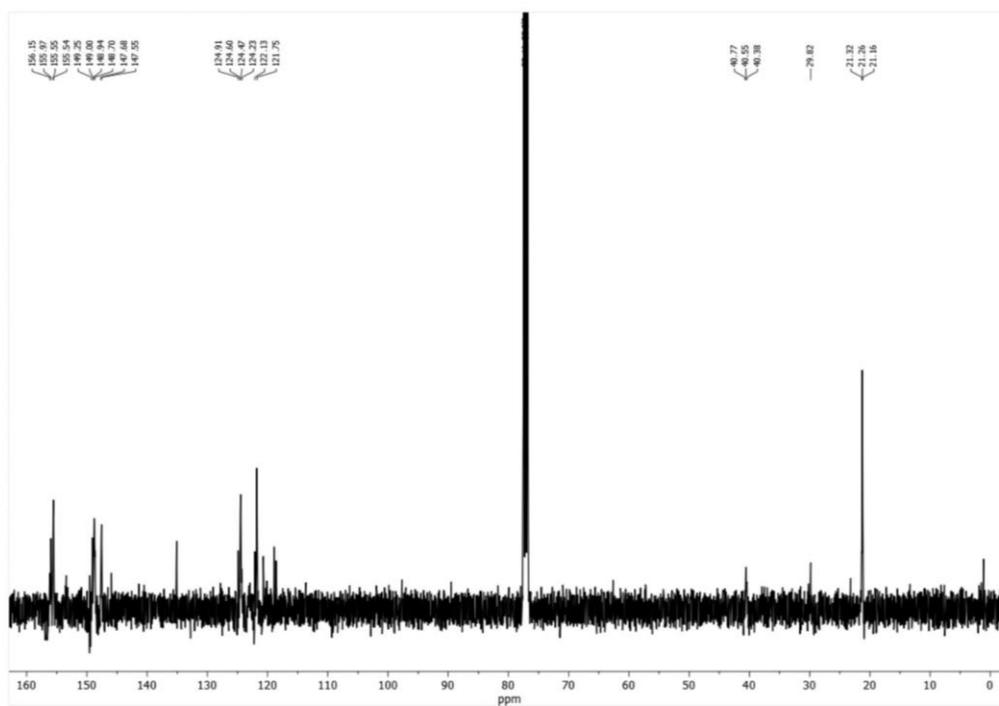
Figure S4: ^{13}C-NMR (101 MHz, CDCl$_3$, 300 K) of PVBpy (Table 1, entry 8).

3.3 SIZE-EXCLUSION CHROMATOGRAPHY DATA
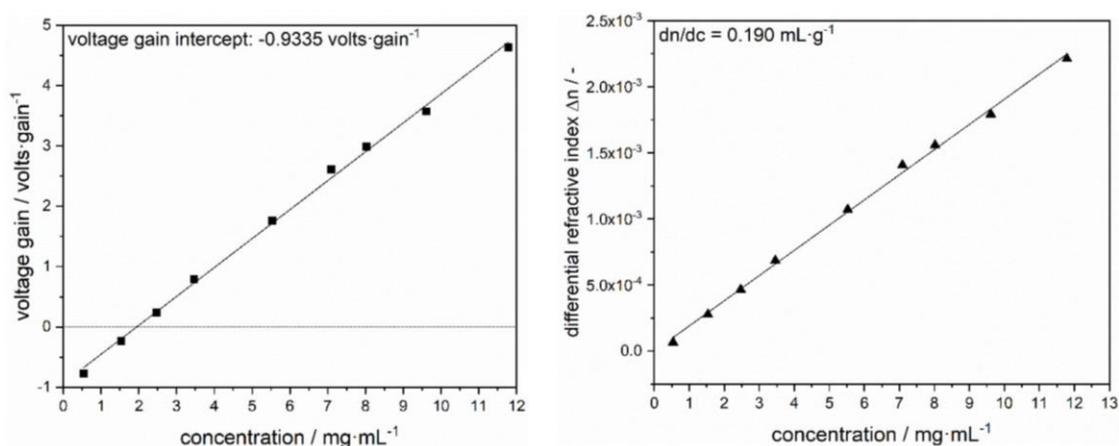
Figure S5: Voltage gain-concentration plot (left) and calculated differential refractive index-concentration plot (right) for the dn/dc determination using 9 different concentrations in the range of 0.5 to 12 mg/mL of the same PVBpy sample. The differential refractive index is calculated by the difference between each voltage gain at a certain concentration and the extrapolated voltage gain intercept at zero concentration multiplied by the detector constant from calibration. The dn/dc is the slope of the linear fit in the differential refractive index-concentration plot.
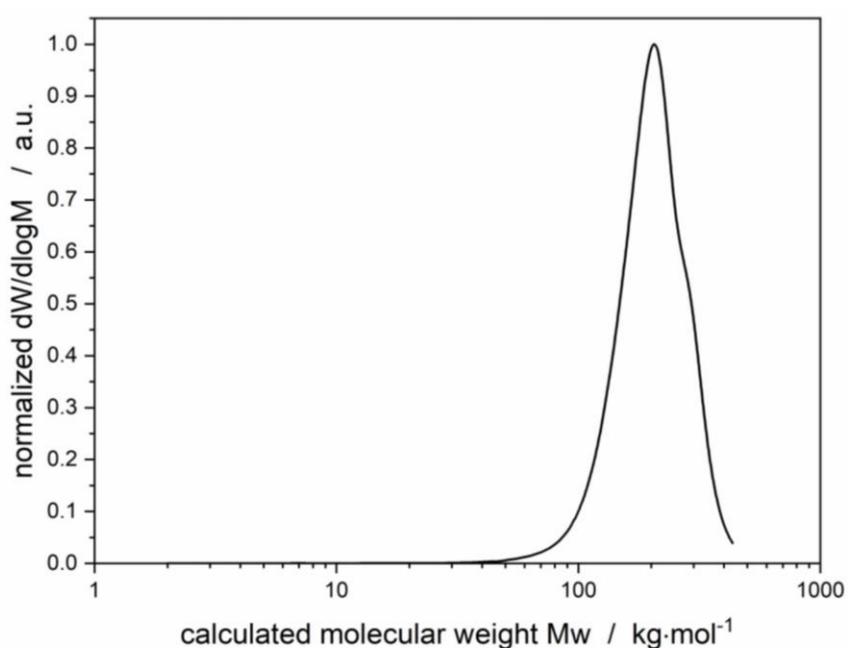
Figure S6: Molecular weight distribution of PVBpy (Table 1, entry 1) determined via SEC (DMF + 25 mmol/L LiBr, 30 °C, triple detection).

17
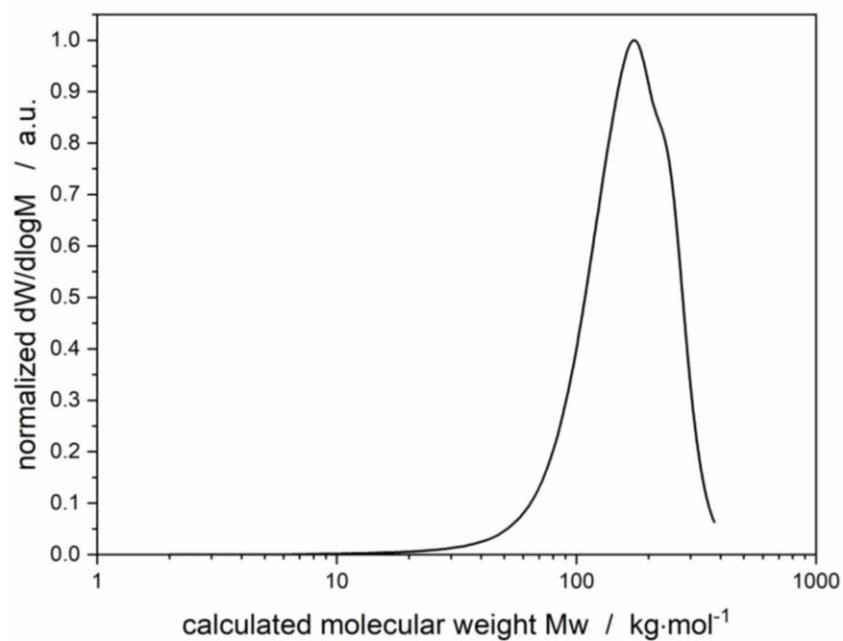
Figure S7: Molecular weight distribution of PVBpy (Table 1, entry 2) determined via SEC (DMF + 25 mmol/L LiBr, 30 °C, triple detection).
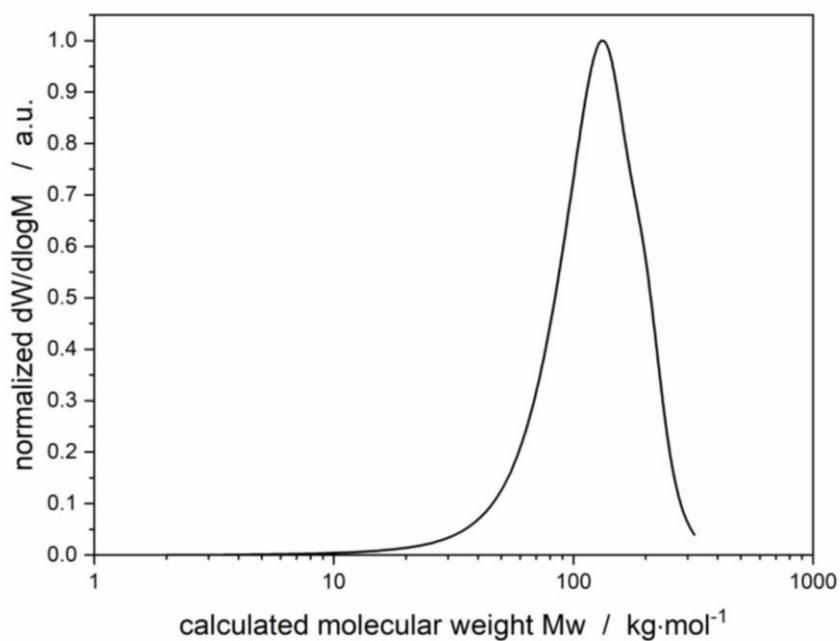
Figure S8: Molecular weight distribution of PVBpy (Table 1, entry 3) determined via SEC (DMF + 25 mmol/L LiBr, 30 °C, triple detection).

18
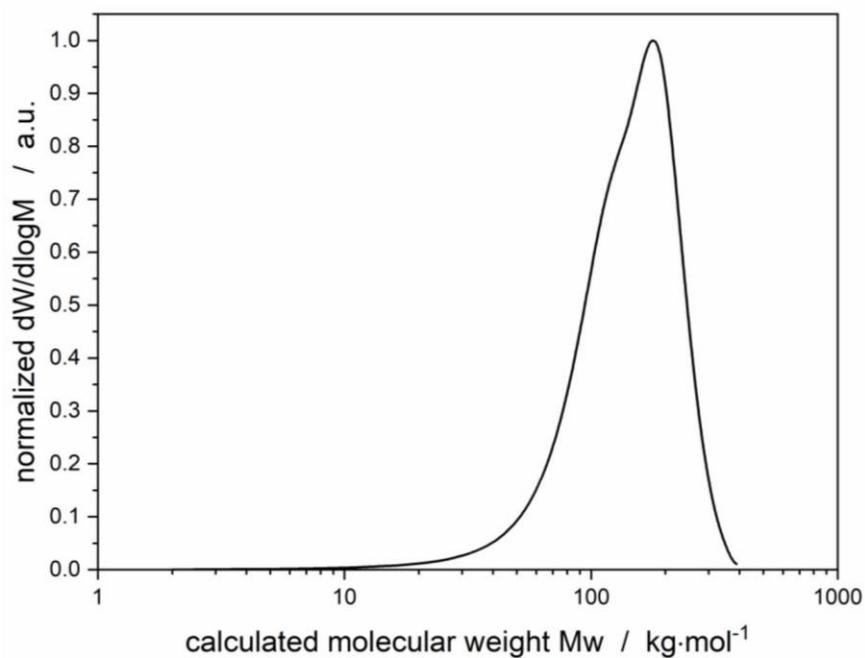
Figure S9: Molecular weight distribution of PVBpy (Table 1, entry 4) determined via SEC (DMF + 25 mmol/L LiBr, 30 °C, triple detection).
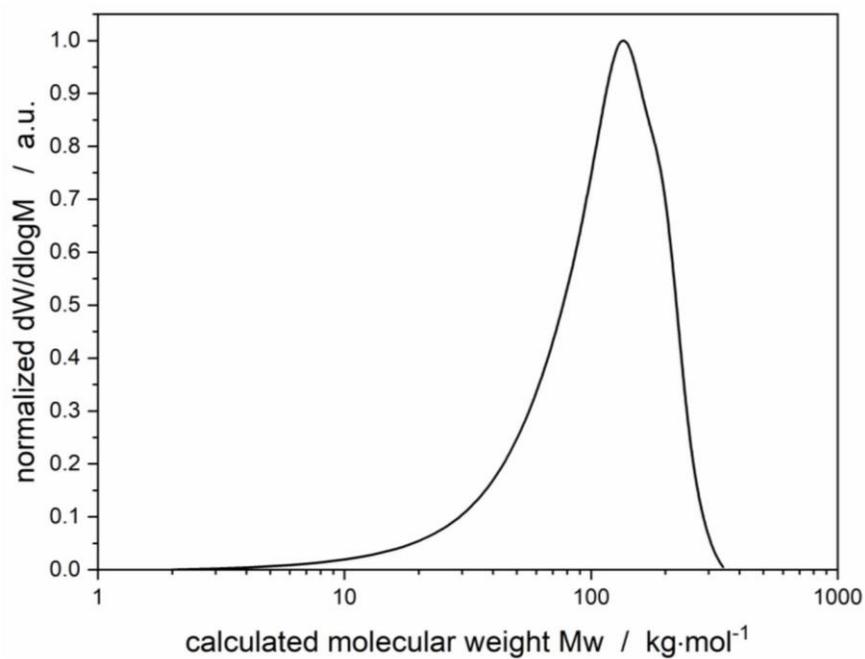
Figure S10: Molecular weight distribution of PVBpy (Table 1, entry 5) determined via SEC (DMF + 25 mmol/L LiBr, 30 °C, triple detection).

19
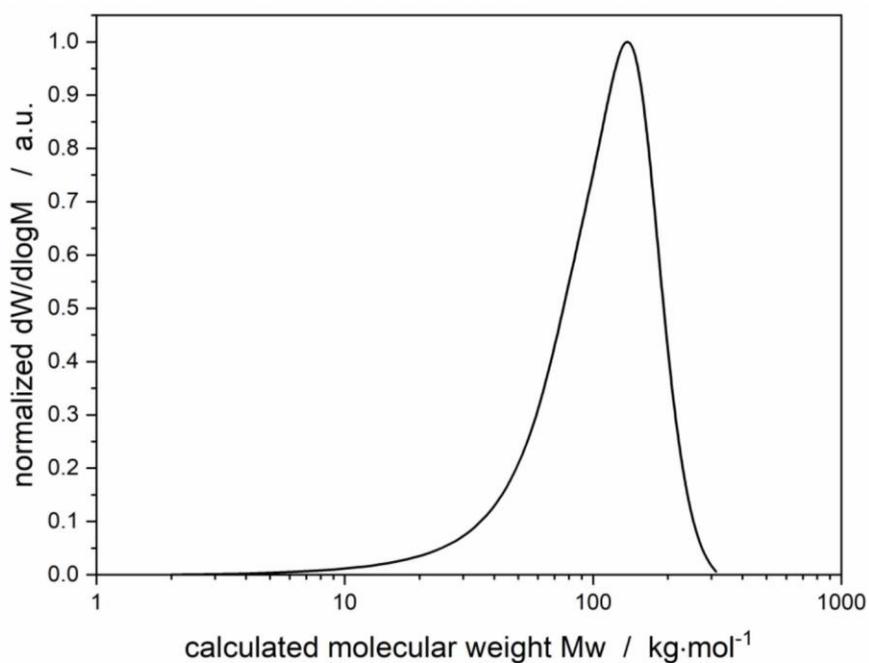
Figure S11: Molecular weight distribution of PVBpy (Table 1, entry 6) determined via SEC (DMF + 25 mmol/L LiBr, 30 °C, triple detection).
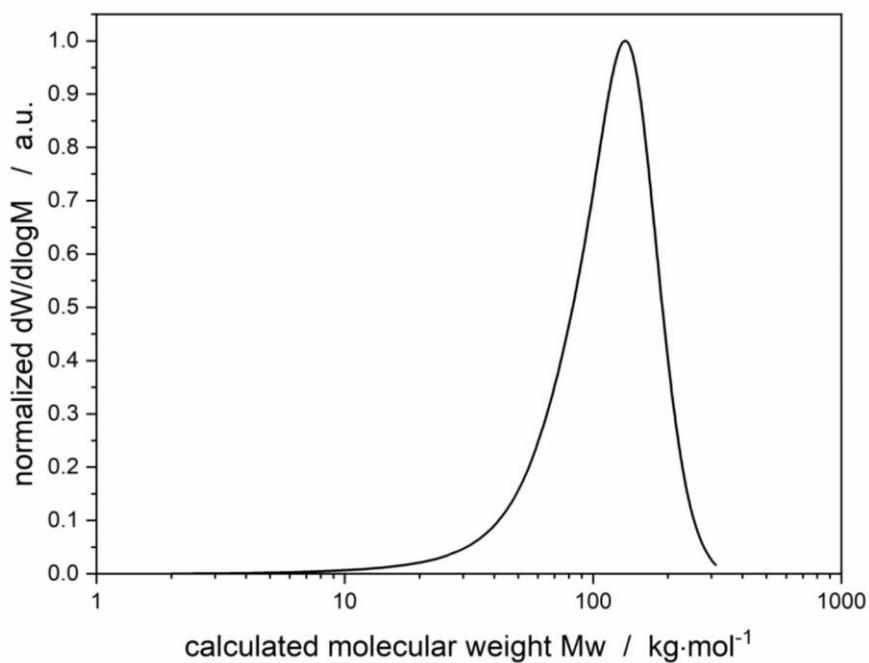
Figure S12: Molecular weight distribution of PVBpy (Table 1, entry 7) determined via SEC (DMF + 25 mmol/L LiBr, 30 °C, triple detection).

20
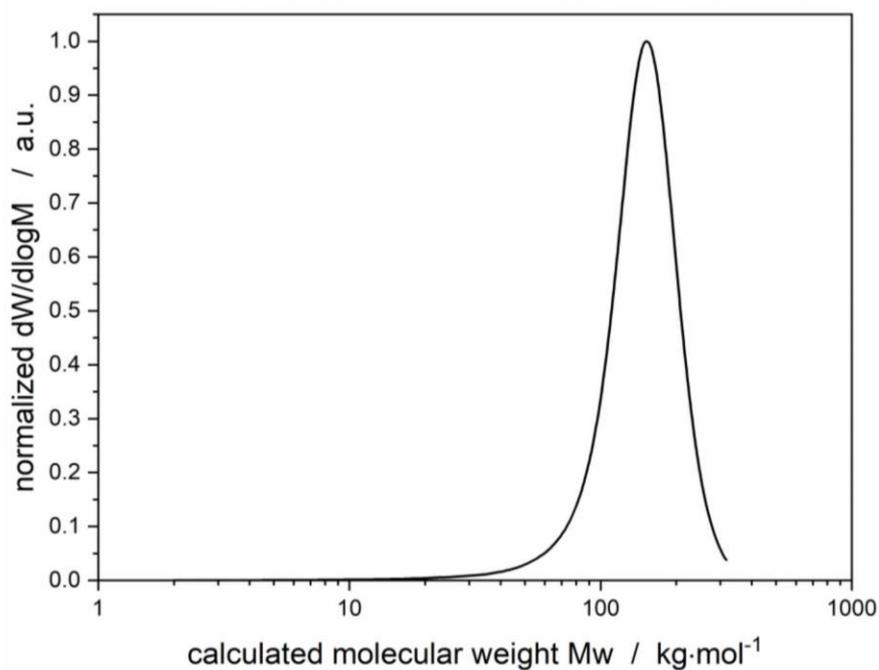
Figure S13: Molecular weight distribution of PVBpy (Table 1, entry 8) determined via SEC (DMF + 25 mmol/L LiBr, 30 °C, triple detection).
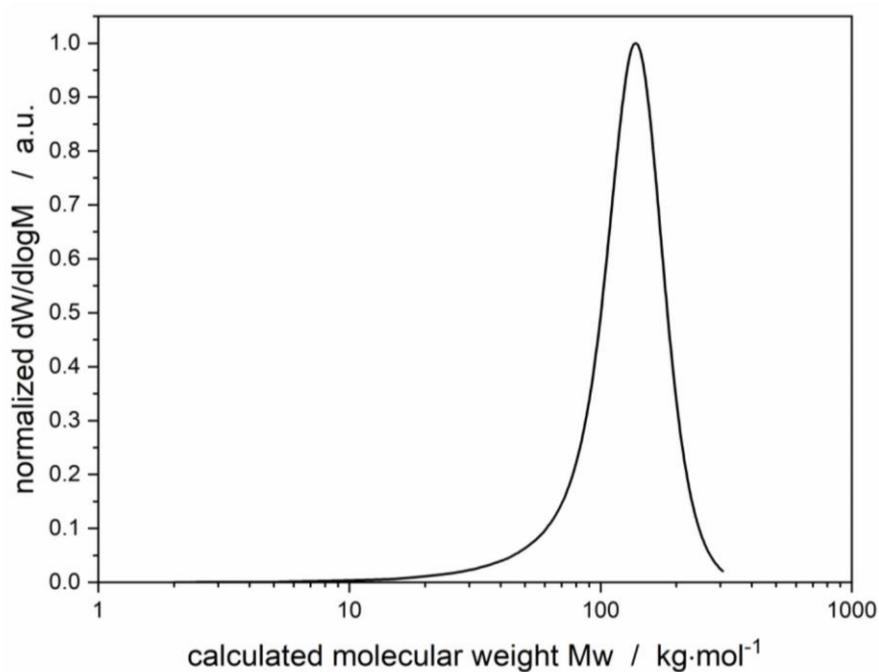
Figure S14: Molecular weight distribution of PVBpy (Table 1, entry 9) determined via SEC (DMF + 25 mmol/L LiBr, 30 °C, triple detection).

21
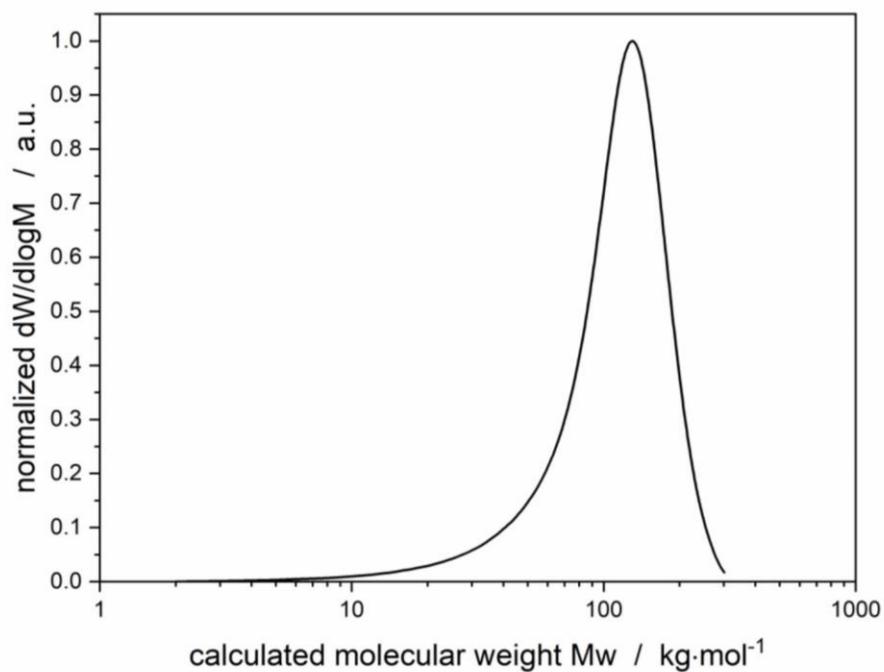
Figure S15: Molecular weight distribution of PVBpy (Table 1, entry 10) determined via SEC (DMF + 25 mmol/L LiBr, 30 °C, triple detection).
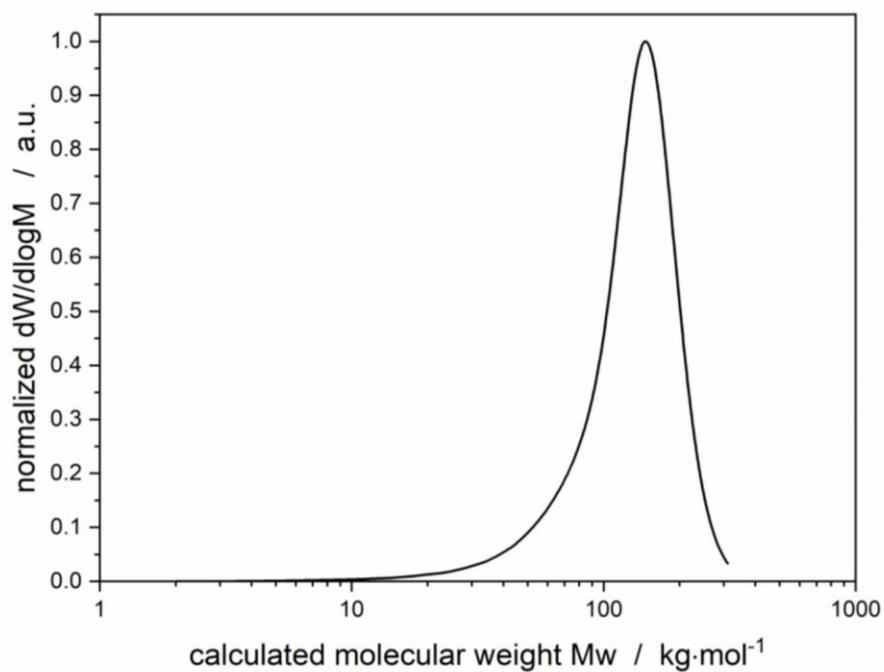
Figure S16: Molecular weight distribution of PVBpy (Table 1, entry 11) determined via SEC (DMF + 25 mmol/L LiBr, 30 °C, triple detection).

22
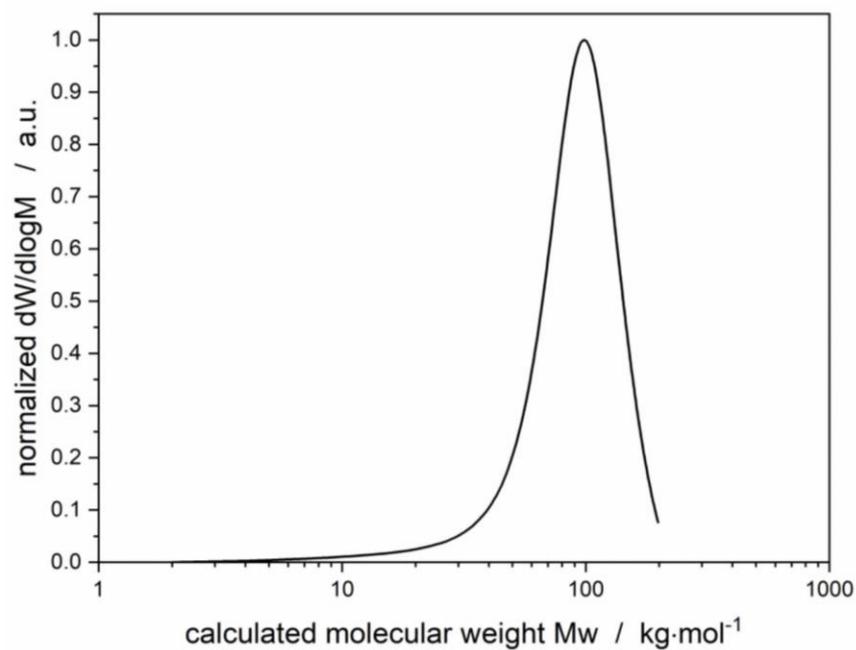
Figure S17: Molecular weight distribution of PVBpy1 (Table S1, entry 1) determined via SEC (DMF + 25 mmol/L LiBr, 30 °C, triple detection).
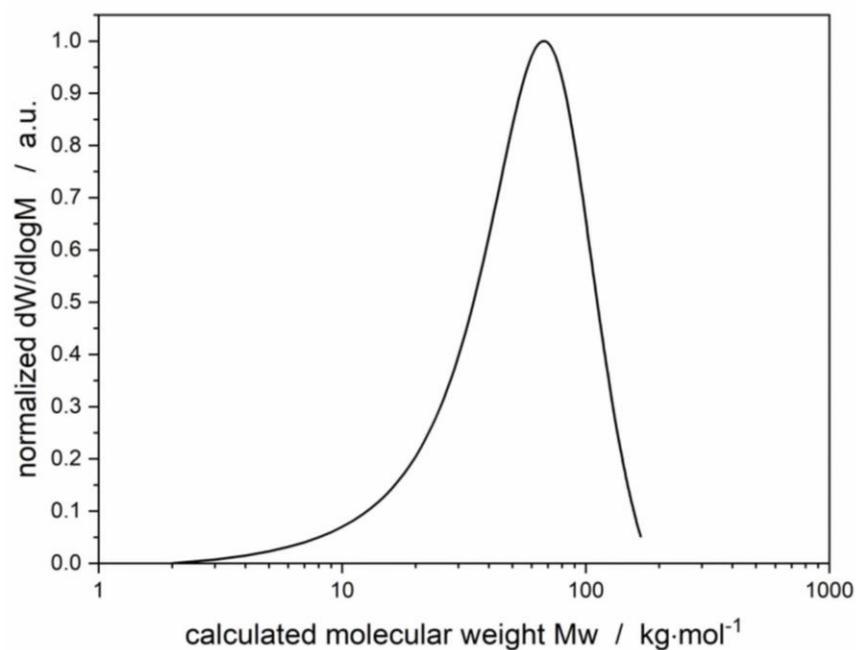
Figure S18: Molecular weight distribution of PVBpy2 (Table S1, entry 2) determined via SEC (DMF + 25 mmol/L LiBr, 30 °C, triple detection).

23
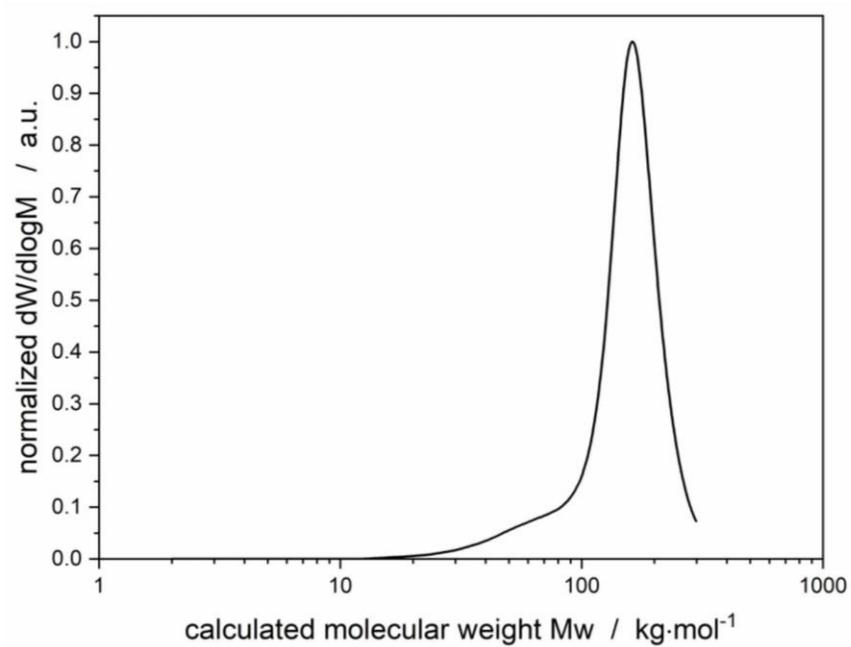
Figure S19: Molecular weight distribution of PVBpy3 (Table S1, entry 3) determined via SEC (DMF + 25 mmol/L LiBr, 30 °C, triple detection).

3.4 ADDITIONAL POLYMER ANALYTICS
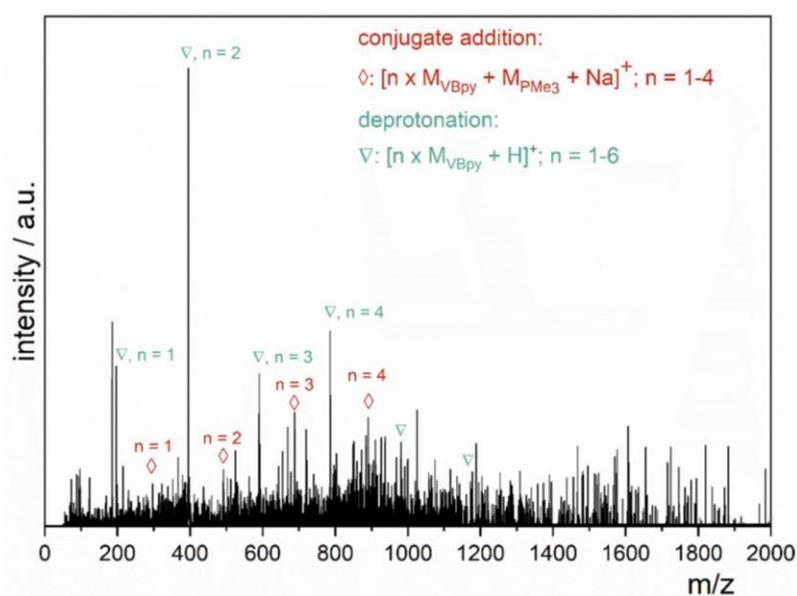
Figure S20: ESI-MS of PVBpy oligomers prepared with the Lewis pair Al(i-Bu)$_3$/PMe$_3$ in acetonitrile, positive ionization; assignments of series to phosphine-terminated oligomers (red) from conjugate addition initiation and olefin-terminated oligomers (green) from deprotonation initiation.
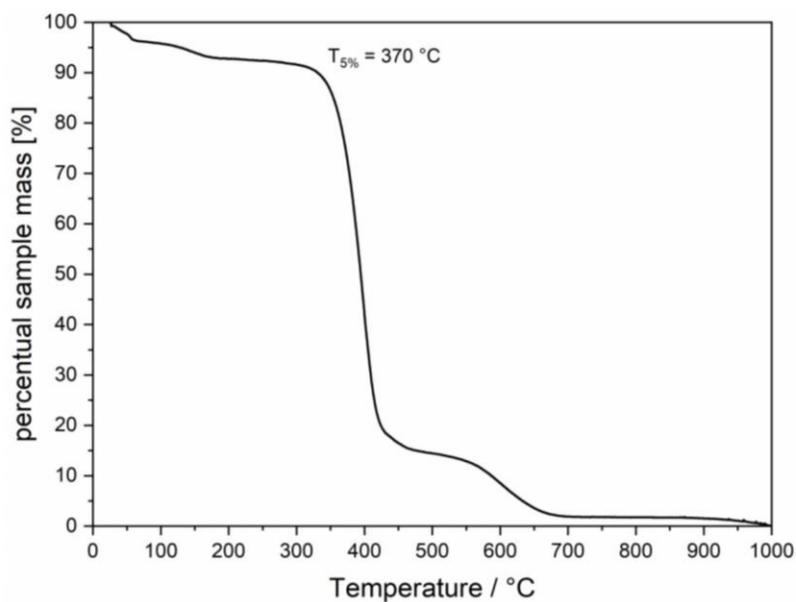
Figure S21: TGA measurement of PVBpy (Table 1, entry 7) from 23 to 1000 °C under argon atmosphere.

25
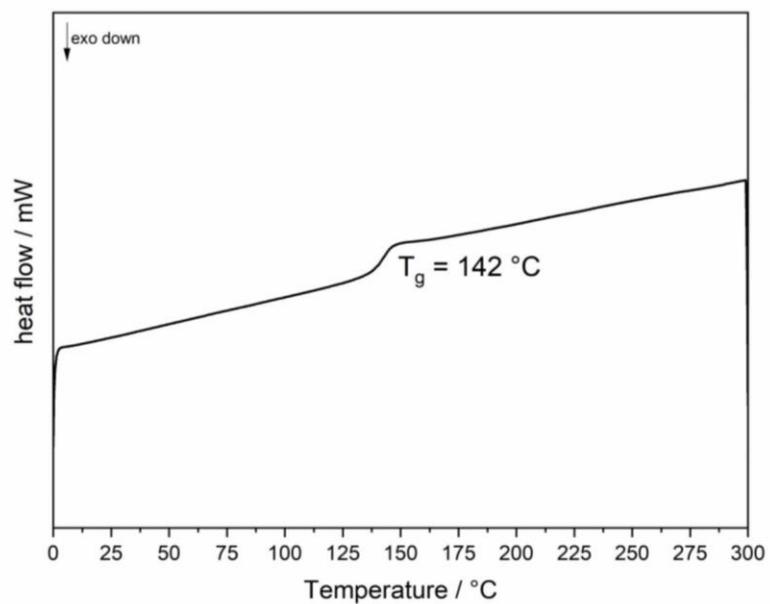
Figure S22: DSC measurement of PVBpy (Table 1, entry 9) in the range of 0 to 300 °C measured in exo down mode.

26

4. PHOTOCATALYSIS

4.1 METAL LOADING OF POLYMERS

Rhenium loading
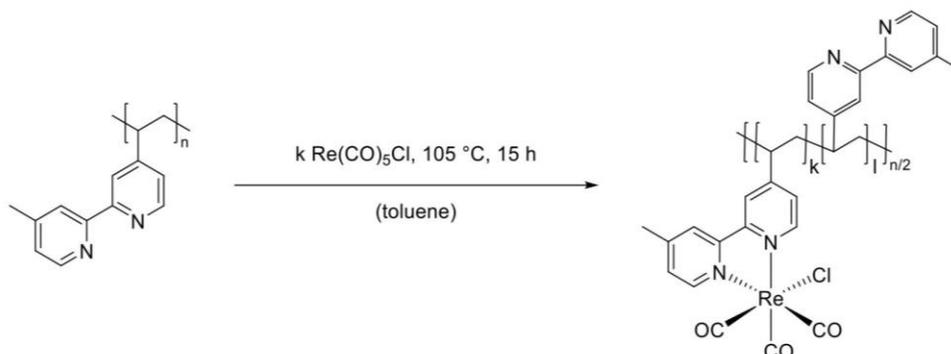
The synthesis of Re loaded PVBpy was adapted from the literature-known procedure for the synthesis of mononuclear Re complexes with bipyridine ligands.[6] The polymer was dissolved in dry toluene in an oven-dried pressure Schlenk flask and the Re precursor $Re(CO)_5Cl$ added. Subsequently, the Schlenk flask was sealed, and the reaction mixture heated to 105 °C overnight. After cooling to room temperature, the solvent was removed under reduced pressure and the polymer dried in vacuo.

IR: v (cm^{-1}) = 2014 (v (C=O), s), 1872 (v (C=O), s), 1608 (v (C=C/C=N), m), 1487 (v (C=C/C=N), m), 1423 (v (C=C/C=N), m), 1029 (v (CH$_x$), m), 907 (v (CH$_x$), m), 830 (v (CH$_x$), m).

PL (DMF): λ_{max} (nm) = 614.

UV/Vis (DMF): λ_{max} (nm) = 372, 290.

27

Ru loading of Re loaded polymers
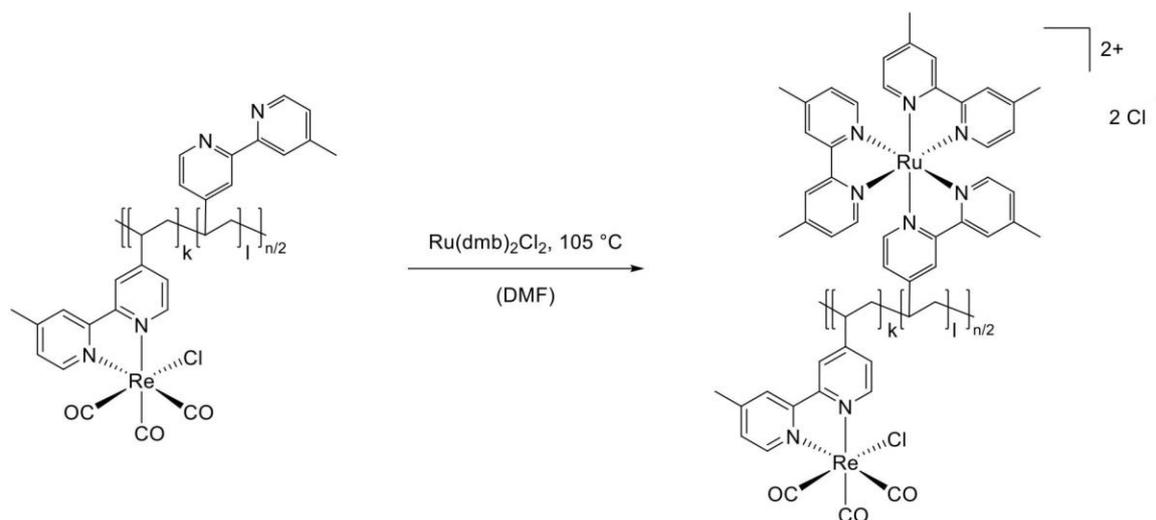
In a pressure Schlenk flask, the Re loaded polymer was dissolved in 5 mL of dry *N,N*-dimethylformamide and a solution of the respective amount of Ru(dmb)$_2$Cl$_2$ (1.10 eq. with regard to free bipyridine coordination sites) in 15 mL *N,N*-dimethylformamide added. The Schlenk flask was sealed, and the reaction mixture heated to 105 °C overnight. After cooling to room temperature, the solvent was removed under reduced pressure, the residue dissolved in methanol and precipitated from an aqueous NH$_4$PF$_6$ solution. For purification, the precipitates were washed with methanol and dried in vacuo. For the UV/Vis investigation PVBpy^{Ru} was prepared according to the same procedure with unloaded polymer instead of a rhenium-loaded polymer.

PL (DMF): λ_{max} = 640 nm.

UV/Vis (DMF): λ_{max} (nm) = 464, 371, 290.

28

4.2 CHARACTERIZATION OF PHOTOCATALYSTS
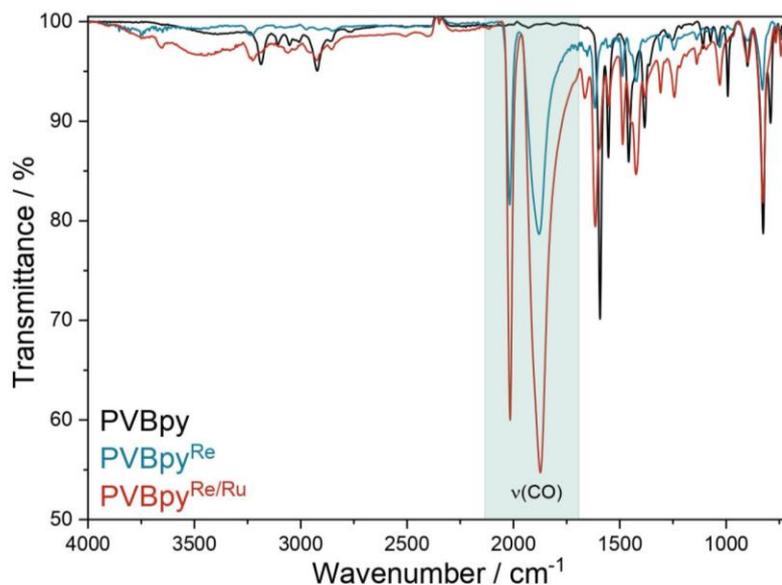
Figure S23: FT-IR spectra of unloaded PVBpy (black), PVBpy after loading with Re(CO)₅Cl precursor (blue) and PVBpy after loading with Re(CO)₅Cl precursor and Ru(dmb)₂Cl₂ precursor (red). The characteristic Re-CO signals, inphase a`(1) (v = 2015 cm^{-1}), antisymmetric a`` (v = 1908 cm^{-1}), and out of-phase symmetric a`(2) (v = 1873 cm^{-1}) of PVBpy^{Re} and PVBpy$^{Re/Ru}$ are marked. The IR band at 1616 cm^{-1} can be assigned to the stretching of the bipyridine ligands.[7]
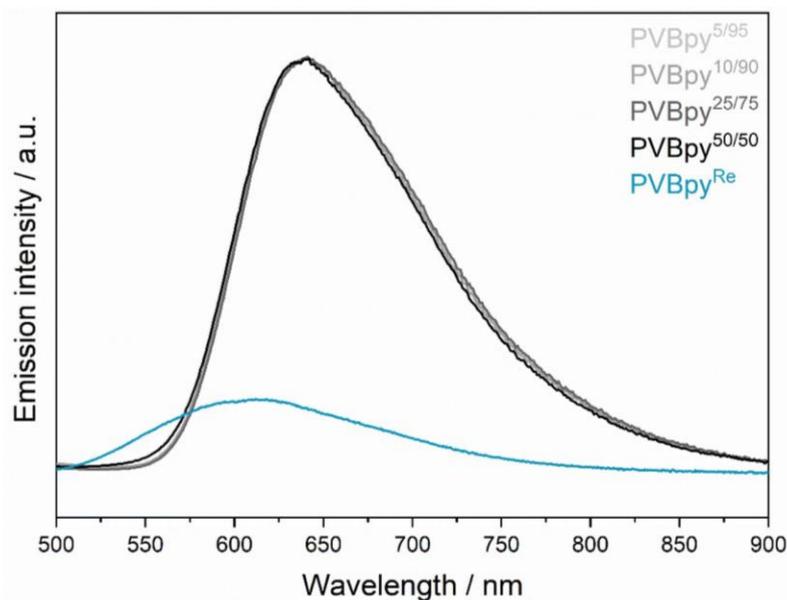
Figure S24: Photoluminescence spectra of **PVBpy$^{5/95}$**, **PVBpy$^{10/90}$**, **PVBpy$^{25/75}$**, **PVBpy$^{50/50}$** and **PVBpy^{Re}** upon irradiation at λ = 365 nm.

Table S2: ICP-MS measurement values for Re and Ru in various polymer samples, the resulting catalyst/photosensitizer ratios immobilized ($R_{Re/Ru}$) and the calculated catalyst (Re) loading on the respective polymer.

Sample	Re mass (m) [µg]	Ru mass (m) [µg]	Sample mass (m) [mg]	Re [µmol/mg_polymer]	Ru [µmol/mg_polymer]	$R_{Re/Ru, calc}$	Catalyst loading [nmol_Re/ mg_polymer]
PVBpy$^{5/95}$	26.9	66.0	1.70	0.094	0.384	0.25	478
PVBpy$^{10/90}$	66.0	44.6	1.50	0.236	0.294	0.80	530
PVBpy$^{25/75}$	164	52.1	1.53	0.575	0.336	1.70	912
PVBpy$^{50/50}$	234	27.0	1.31	0.959	0.204	4.70	1163

$$n\left(Re_{per\ mg\ polymer}\right)=\frac{m_{Re}}{M_{Re}}\cdot\frac{1}{m_{sample}}=\frac{26.9\ \mu g}{186.207\ \frac{g}{mol}}\cdot\frac{1}{1.70\ mg_{polymer}}=0.094\ \frac{\mu mol}{mg_{polymer}} \quad (1)$$

$$n\left(Ru_{per\ mg\ polymer}\right)=\frac{m_{Ru}}{M_{Ru}}\cdot\frac{1}{m_{sample}}=\frac{66.0\ \mu g}{101.070\ \frac{g}{mol}}\cdot\frac{1}{1.70\ mg_{polymer}}=0.384\ \frac{\mu mol}{mg_{polymer}} \quad (2)$$

$$R_{P(VBpy),calc}=\frac{n\left(Re_{per\ mg\ polymer}\right)}{n\left(Ru_{per\ mg\ polymer}\right)}=\frac{0.094\ \frac{\mu mol}{mg_{polymer}}}{0.384\ \frac{\mu mol}{mg_{polymer}}}=0.25 \quad (3)$$

The percentage ratio of Re loaded, Ru loaded and unloaded vinyl bipyridines in the polymer chain was calculated using the following formulas. The amounts of metal centers required for this calculation were determined by ICP-MS (see above) and corrected to one milligram of polymer. For this reason, all masses and amounts of substances given here are based on one milligram of polymer. The abbreviations Re and Ru stand for the corresponding units Re(VBpy)(CO)₃Cl and

30

Ru(dmb)$_2$(VBpy)(PF$_6$)$_2$, respectively. With equation 11, the percentage ratio of Re loaded und Ru loaded vinyl bipyridines can be calculated in analogy. An exemplary calculation is provided below for PVBpy$^{5/95}$ with full measurement data.

$$m_{Re}[\mu g]= n_{Re}[\mu mol] \cdot M_{Re} \left[\frac{\mu g}{\mu mol} \right] \tag{4}$$

$$m_{Re(PVBpy^{5/95})}[\mu g]= 94.33 \cdot 10^{-3} \ \mu mol \cdot 502.01 \frac{\mu g}{\mu mol} = 47.36 \ \mu g \tag{5}$$

$$m_{Ru}[\mu g]= n_{Ru}[\mu mol] \cdot M_{Ru} \left[\frac{\mu g}{\mu mol} \right] \tag{6}$$

$$m_{Ru(PVBpy^{5/95})}[\mu g]= 384.01 \cdot 10^{-3} \ \mu mol \cdot 956.13 \frac{\mu g}{\mu mol} = 367.16 \ \mu g \tag{7}$$

$$m_{VBpy(PVBpy^{5/95})}[\mu g]=m_{PVBpy^{5/95}} [\mu g]-m_{Re} [\mu g]-m_{Re} [\mu g] \tag{8}$$

$$m_{VBpy(PVBpy^{5/95})}[\mu g]=1000 \ \mu g-47.36 \ \mu g-367.16 \ \mu g=585.48 \ \mu g \tag{9}$$

$$n_{VBpy}[\mu mol]=\frac{m_{VBpy}[\mu g]}{M_{VBpy} \left[\frac{\mu g}{\mu mol} \right]} = \frac{585.48 \ \mu g}{196.10 \frac{\mu g}{\mu mol}} =2.99 \ \mu mol \tag{10}$$

$$X_{unoccupied \ VBpy} \ [\%]= \frac{n_{VBpy}[nmol]}{n_{VBpy}[nmol]+n_{Re}[nmol]+n_{Ru}[nmol]} = \frac{2990 \ nmol}{2990 \ nmol+94.33 \ nmol+384.01 \ nmol} =86.2\% \tag{11}$$

31

4.3 PHOTOCATALYTIC RESULTS

To avoid any light-induced deactivation processes, all photocatalytic experiments were conducted in a darkened room and respective reaction flasks were protected from visible light irradiation by wrapping them in aluminum foil outside of the irradiation times. The photocatalytic experiments were performed in Schlenk tubes with known total volume, with a constant volume of catalyst solution of 11 mL. Prior to the photocatalysis, the calculated amount of respective catalyst is weighed-in, dissolved in N,N-dimethylformamide and transferred to the Schlenk tube. Subsequently, the electron donor 1,3-dimethyl-2-phenyl-2,3-dihydro-1H-benzo[d]imidazole (BIH), as well as the base triethanolamine (TEOA) are added. The reaction mixture is then saturated with CO_2 (4.5) for ten minutes by bubbling the gas into the stirred solution under exclusion of visible light irradiation. Finally, the reaction flask is pressurized with CO_2 to an overpressure of 1.45 bar and sealed with a septum. For the photocatalytic experiments, the prepared samples are placed in front of a green LED ($\lambda = 520 \pm 30$ nm) and the gas phase composition in the reaction flask headspace is analyzed via Micro-GC in regular time intervals.

Photocatalysis turnover number (TON) calculations. The turnover numbers for the photocatalytic CO_2 reduction experiments were calculated from the exact molar catalyst amounts in each experiment. The catalyst amount was obtained through multiplying the $\mu mol/mg_{polymer}$ values from ICP-MS analysis (Table S2) with the weigh-in. The Micro-GC measurements yielded area% results for each of the gasses present in the headspace of the reaction flasks. For carbon monoxide, those values were converted to vol%, volume, and moles utilizing the total gas phase volume of the reaction vessel. An exemplary TON calculation for PVBpy$^{5/95}$ with full measurement data is provided below. The TOF was derived from the slope between the first two GC measurements.

32

Note: The headspace volume $V_{headspace}$ is obtained by subtracting the solvent volume (11 mL in this case) from the total volume of the reaction flask, which was predetermined by filling the vessel with water. The pressure p includes the applied CO_2 overpressure for a total pressure of 1.45 bar and solvated CO in DMF is neglected in this calculation.

$$n_{Re}[\mu mol] = n_{Re}\left[\frac{\mu mol}{mg_{polymer}}\right] \cdot m_{sample}[mg] = 0.094\ \frac{\mu mol}{mg_{polymer}} \cdot 2.33\ mg = 0.22\ \mu mol \tag{12}$$

$$Vol\%_{CO} = Area\%_{CO} \cdot 1.195 = 12.64\% \cdot 1.195 = 15.10\% \tag{13}$$

$$V_{CO,gas}[mL] = \frac{Vol\%_{CO}}{100} \cdot V_{headspace}[mL] = \frac{15.10\%}{100} \cdot 149.1\ mL = 22.51\ mL \tag{14}$$

$$n_{CO,gas}[mmol] = \frac{p \cdot V_{CO}}{R \cdot T} = \frac{1.45 \cdot 10^5\ Pa \cdot 22.51\ mL}{8.314\ \frac{J}{mol \cdot K} \cdot 293.15\ K} = 1.34\ mmol \tag{15}$$

$$TON_{CO} = \frac{n_{CO,total}[mmol]}{n_{Re}[\mu mol]} = \frac{1.34\ mmol}{0.22\ \mu mol} = 6088 \tag{16}$$

$$TOF_{CO,\ t(1)} = \frac{n_{CO,t(1)}[mmol]}{n_{Re}[\mu mol] * time\ interval\ (1)\ [h]} = \frac{0.27\ mmol}{0.22\ \mu mol * 18.5\ h} = 66\ h^{-1} \tag{17}$$

33

Table S3: TOFs and TONs of the Re/Ru loaded polymers in CO_2-saturated (15 min) DMF solution with BIH ([BIH]/[Re] = 10000) and TEOA (1.7 M). Irradiation was performed at λ = 520 nm. The calculation of the TON was performed according to the equations 12-16. The TOF was derived from the slope between the first two GC measurements. In-depth analysis of the gas phase composition after irradiation with an RGD (reduction gas detector) revealed traces of hydrogen evolution.

Catalyst	Rhenium concentration [μM]	Irradiation time [h]	TOF [h⁻¹]	TON [-]
PVBpy[10/90]	20.0	280	38	898
PVBpy[25/75]	20.0	260	6.9	724
PVBpy[50/50]	20.0	335	4.2	927
PVBpy[5/95]	20.0	713	66	5650
PVBpy[5/95]	1.25	160	42	677
PVBpy[5/95]	2.50	91	51	1176
PVBpy[5/95]	5.00	91	42	990
PVBpy[5/95]	10.0	234	46	1704
PVBpy[5/95]	30.0	503	52	5493
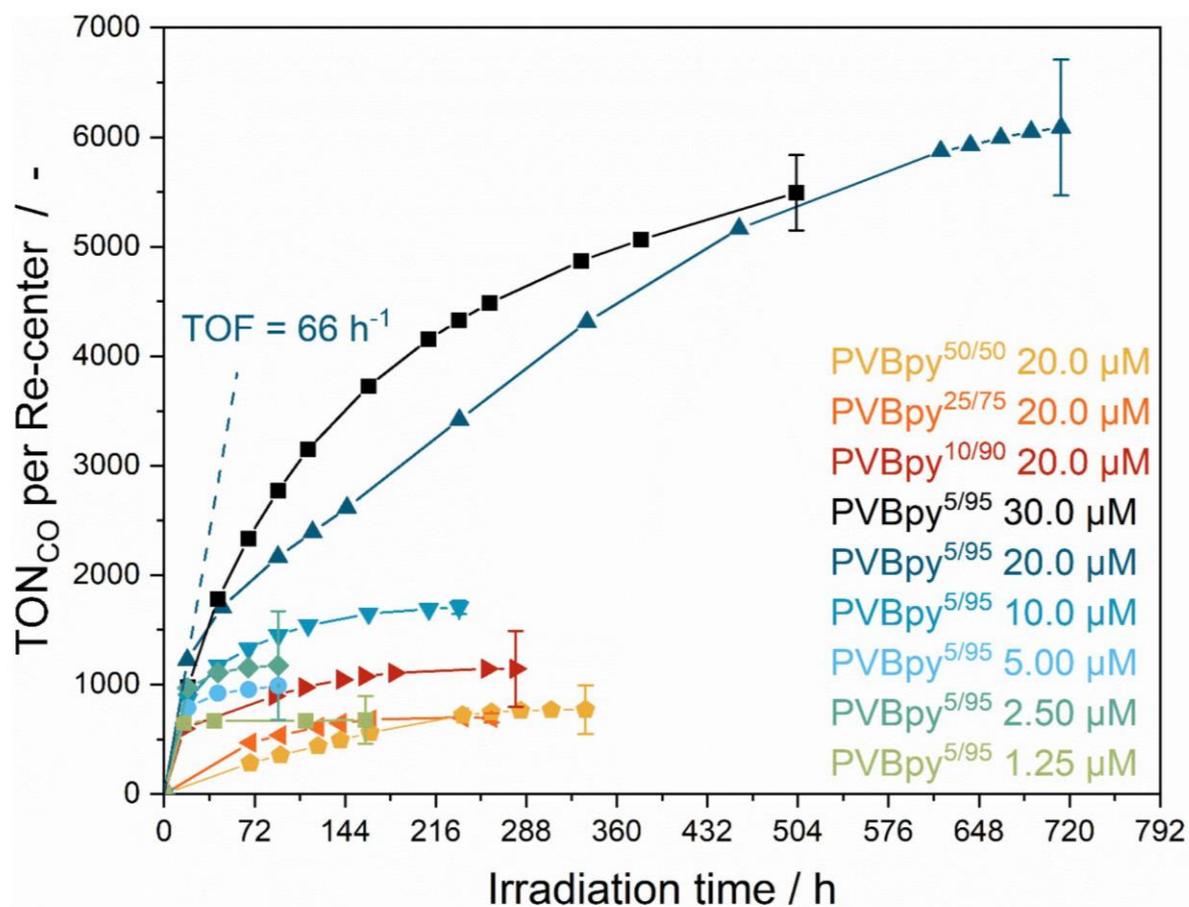
Figure S25: Turnover numbers of different macromolecular photocatalysts with varying rhenium concentrations in the photocatalytic reduction of CO_2. The catalyst-containing, CO_2-saturated (15 min) DMF solution with BIH ([BIH]/[Re] = 10000) and TEOA (1.72 M) was irradiated at $\lambda = 520$ nm.

35

Table S4: TOFs and TONs of the control experiments for the Re/Ru loaded polymers and suiting combinations in CO_2-saturated (15 min) DMF solution with BIH ([BIH]/[Re] = 10000) and TEOA (1.7 M). Irradiation was performed at λ = 520 nm. The calculation of the TON was performed according to the equations 12-16. The TOF was derived from the slope between the first two GC measurements. Deviations from the standard experiment are denoted under condition variation.

Catalyst / Combination	Rhenium concentration [μM]	Condition variation	Irradiation time [h]	TOF [h⁻¹]	TON [-]
PVBpy^{Ru}	-	no rhenium	74	0.3 [a]	21 [a]
PVBpy^{Re}	20.0 [b]	no ruthenium	74	0.4	30
PVBpy^{Ru} + PVBpy^{Re}	20.0 [b]	mixed catalysts	188	7.3	1365
PVBpy$^{25/75}$	20.0	no light	2	0	0
PVBpy$^{50/50}$	20.0	no BIH	3	-	-
-	-	no catalyst	3	0	0
PVBpy$^{50/50}$	20.0	no CO_2 overpressure	16	-	traces of CO (via FID)
PVBpy$^{5/95}$	10.0	$^{13}CO_2$ for IR-experiment	150	n. d. [c]	n. d. [c]

[a] related to ruthenium concentration assuming quantitative loading; [b] assuming quantitative rhenium loading; [c] not determined.
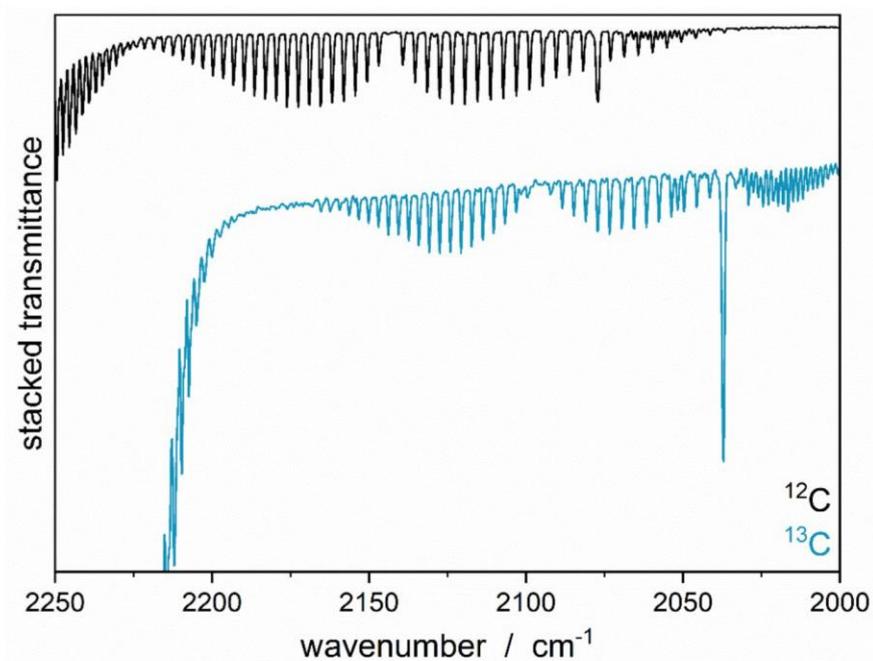
Figure S26: Gas-phase IR of the headspace taken after 150 h of irradiation time from $^{12}C/^{13}C$ CO_2 reduction isotope labelling control experiment with PVBpy5/95 under standard conditions.

37

REFERENCES

(1) Lu, Z.; Ladrak, T.; Roubeau, O.; van der Toorn, J.; Teat, S. J.; Massera, C.; Gamez, P.; Reedijk, J. Selective, catalytic aerobic oxidation of alcohols using $CuBr^2$ and bifunctional triazine-based ligands containing both a bipyridine and a TEMPO group. *Dalton Trans.* **2009** (18), 3559–3570. DOI: 10.1039/b820554j.

(2) Abruna, H. D.; Breikss, A. I.; Collum, D. B. Improved synthesis of 4-vinyl-4'-methyl-2,2'-bipyridine. *Inorg. Chem.* **1985**, *24* (7), 987–988. DOI: 10.1021/ic00201a003.

(3) Meister, S.; Reithmeier, R. O.; Ogrodnik, A.; Rieger, B. Bridging Efficiency within Multinuclear Homogeneous Catalysts in the Photocatalytic Reduction of Carbon Dioxide. *ChemCatChem* **2015**, *7* (21), 3562–3569. DOI: 10.1002/cctc.201500674.

(4) Jiang, S.; Tian, X.-J.; Feng, S.-Y.; Li, J.-S.; Li, Z.-W.; Lu, C.-H.; Li, C.-J.; Liu, W.-D. Visible-Light Photoredox Catalyzed Double C-H Functionalization: Radical Cascade Cyclization of Ethers with Benzimidazole-Based Cyanamides. *Org. Let.* **2021**, *23* (3), 692–696. DOI: 10.1021/acs.orglett.0c03853.

(5) Lee, I.-S. H.; Jeoung, E. H.; Kreevoy, M. M. Marcus Theory of a Parallel Effect on α for Hydride Transfer Reaction between NAD + Analogues. *J. Am. Chem. Soc.* **1997**, *119* (11), 2722–2728. DOI: 10.1021/ja963768l.

(6) Smieja, J. M.; Kubiak, C. P. Re(bipy-tBu)(CO)$_3$Cl-improved catalytic activity for reduction of carbon dioxide: IR-spectroelectrochemical and mechanistic studies. *Inorg. Chem.* **2010**, *49* (20), 9283–9289. DOI: 10.1021/ic1008363.

(7) Bian, Z.-Y.; Wang, H.; Fu, W.-F.; Li, L.; Ding, A.-Z. Two bifunctional RuII/ReI photocatalysts for CO_2 reduction: A spectroscopic, photocatalytic, and computational study. *Polyhedron* **2012**, *32* (1), 78–85. DOI: 10.1016/j.poly.2011.08.037.

38

11.4.3. Supporting Information for Chapter 6

Polyester synthesis based on 3-carene as renewable feedstock

Supporting Information

Moritz Kränzlein⸸, Stefanie Pongratz⸸, Jonas Bruckmoser, Brigita Bratić, Jonas Martin Breitsameter and Bernhard Rieger*

WACKER-Chair of Macromolecular Chemistry, Catalysis Research Centre, Department of Chemistry, Technical University of Munich, Lichtenbergstr. 4, 85748 Garching (Germany)

⸸ These authors contributed equally.

Corresponding Authors:

* rieger@tum.de

TABLE OF CONTENTS

1

1. GENERAL EXPERIMENTAL

All reactions and polymerizations involving air- and moisture-sensitive compounds were performed in a MBraun LabMaster120 glovebox filled with 4.6 argon purchased from Westfalen or using standard Schlenk techniques. Chemicals were purchased from Sigma-Aldrich, ABCR or TCI Europe and used without purification unless stated otherwise. Solvents were dried using an MBraun SPS-800 or by filtration over activated aluminium oxide and stored over 3 Å molecular sieve.

Nuclear magnetic resonance (NMR) spectra (^{1}H/^{13}C/2D-experiments) were recorded on a Bruker AV-400HD or a Brucker AV-500CR as indicated. The NMR spectroscopical shifts δ are reported in ppm relative to the residual carbon or proton signal of the deuterated solvent. CDCl$_3$ was purchased from Deutero and dried over 3 Å molecular sieve prior to use. Spectra interpretation was performed using MestreNova software.

Size-exclusion chromatography (SEC) was performed on a PL-GPC50 plus from Polymer Laboratories with THF (with 222 mg/L 3,5-di-*tert*-butyl-4-hydroxytoluol as stabilizing agent) as eluent at 30 °C. Size separation was done using two Polargel Mixed-C columns by Agilent Technologies with a polymer sample concentration of 2.0-3.0 mg/L. Molecular weight and polydispersity is measured via single RI-detection and reported against polystyrene standards.

Gas-chromatography mass spectrometry (GC-MS) measurements were performed on an Agilent GC-7890B equipped with a MSD 59771 mass detector, a 7693 automatic liquid sampler and a G4513A autoinjector. Sample separation is done using a HP-5MS UI column (30 m length, 0.25 mm diameter, 0.25 μm film) in a temperature range of 60-300 °C followed by mass spectrometry using full scan method in a mass range of 40-500 au. Samples are prepared by dissolving 1 mg/mL in HPLC grade dichloromethane prior to measurement.

Attenuated total reflection infrared spectroscopy (ATR-IR) spectra were recorded on a Bruker Vertex 70v ATR-IR spectrometer at room temperature under argon as inert gas.

Thermogravimetric analysis (TGA) is performed from 2 mg samples on a TGA Q5000 by TA Instruments. Samples are heated from room temperature to 1000 °C with a heat rate of 10 K/min under argon. Analysis of mass loss and determination of $T_{5\%}$ is done using TA Analysis software.

Differential scanning calorimetry (DSC) was measured using a DSC Q2000 by TA instruments in exo-down mode. Sample size is about 6 mg in non-hermetic aluminum pans in the range of -100 °C to 250 °C depending on the sample. Analysis is performed using TA Analysis.

Powder X-Ray diffractometry (pXRD) was performed using a PANalytical Empyrean diffractometer with a PANalytical PIXcel 1D detector in Bragg-Brentano geometry. Cu K$_\alpha$ radiation with a voltage of 45 kV (40 mA intensity) with λ_1 = 1.5406 Å / λ_2 = 1.5444 Å [I_1/I_2 = 0.5] was used for measurements in the 2θ of 5-60 ° (step size 0.01 °, measurement time 7 h). The obtained data was analysed using HighScore software, Cu K$_\alpha$ is stripped using the *Rachinger* method and the amorphous background is determined using the *Sonneveld* and *Visser* method with a granularity of 15 and a bending factor of 8 for the subsequent peak fit. The calculation of crystallinity fraction in the region of $5 - 27$ ° is done by a peak deconvolution using OriginPro 2020 with 2 peaks for the amorphous backscattering of the polymer and 8 peaks for the crystalline diffraction peaks. The degree of crystallinity X$_C$ is obtained by peak integration and the areas of the amorphous parts AA and crystalline parts AC via X$_C$ = A$_C$ / (A$_C$ + A$_A$).[4]

Electron-Spray Ionization Mass Spectrometry (ESI-MS) was measured on a Thermo Fisher Scientific Exactive Plus in negative mode in HPLC acetronitrile directly from the reaction mixture without purification. Oligomers were prepared using a 1:5 ratio of catalyst to monomer with the conditions reported in the manuscript.

2. MONOMER SYNTHESIS

2.1 Hydroboration of 3-carene[1]

136.24 g/mol   154.14 g/mol
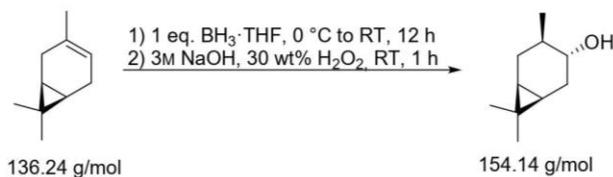
Under inert conditions 260 mL 1M borane in tetrahydrofuran (260 mmol, 1.0 eq.) were cooled to 0 °C. Via addition funnel 37.0 g (272 mmol, 1.0 eq.) 3-carene dissolved in 100 mL tetrahydrofuran were added dropwise to the stirred borane solution. The mixture is stirred at 0 °C for one hour and additional 12 hours at room temperature. Subsequently, 40 mL water and 40 mL tetrahydrofuran are added, the mixture is stirred for additional two hours and 40 mL of a 3M aqueous sodium hydroxide solution are added. To complete the reaction, 40 mL 30 wt% $H_2O_{2(aq)}$ were added dropwise, keeping the temperature below 40 °C. The mixture is stirred for an additional hour before extracting with diethyl ether (3×300 mL). The combined organic phases are washed with water (3×200 mL) and brine (2×200 mL) before drying over magnesium sulphate. The solvent was removed in vacuo resulting in 40.1 g of crude 4-*iso*-caranol. Distillation under reduced pressure using a Vigreux column ($bp_{5\,mbar}$ = 76 °C) yielded 38.6 g (250 mmol, 92 %) 4-*iso*-caranol as colourless oil.

¹H-NMR spectrum (400 MHz, CDCl₃, 300 K): δ (ppm) = 3.06 (td, $^3J_{H,H}$ = 9.8, 6.6 Hz, 1H), 2.08 (dd, $^3J_{H,H}$ = 14.1, 6.6 Hz, 1H), 2.02-1.89 (m, 1H), 1.65-1.48 (m, 1H), 1.30-1.15 (m, 1H), 0.97 (s, 3H), 0.92 (s, 3H), 0.90 (s, 3H), 0.85-0.75 (m, 1H), 0.74-0.64 (m, 2H).

¹³C-NMR spectrum (125 MHz, CDCl₃, 300 K): δ (ppm) = 74.8, 36.5, 30.5, 29.0, 28.6, 22.0, 20.3, 17.9, 17.8 16.1.

GC-MS: t_R = 8.13 min, m/z = 154.1 (M⁺), 136.1 ([M-OH]⁺).

3
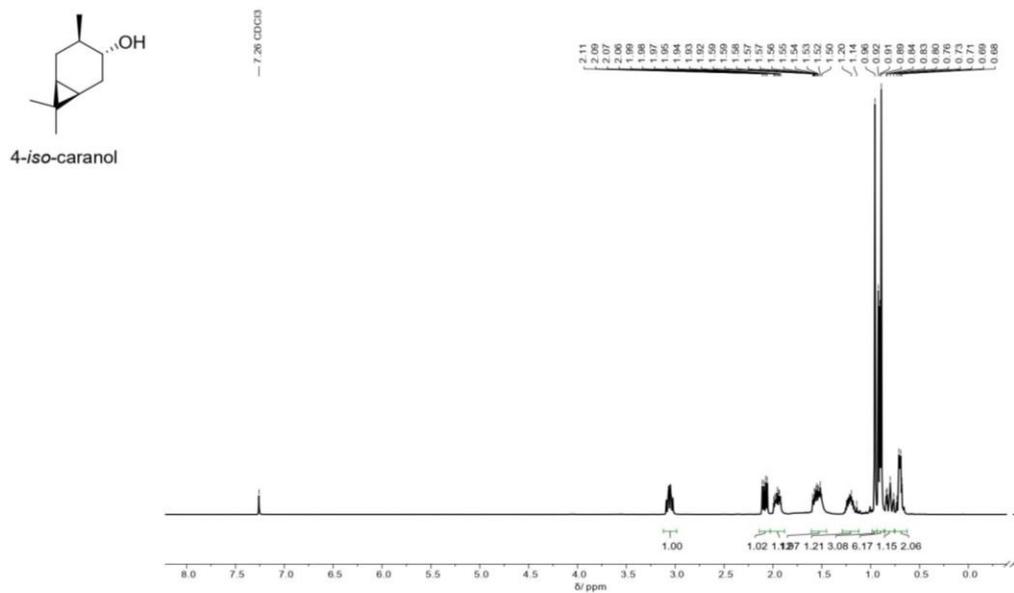
Figure S1: ¹H-NMR spectrum (400 MHz, CDCl₃, 300K) of 4-*iso*-caranol.
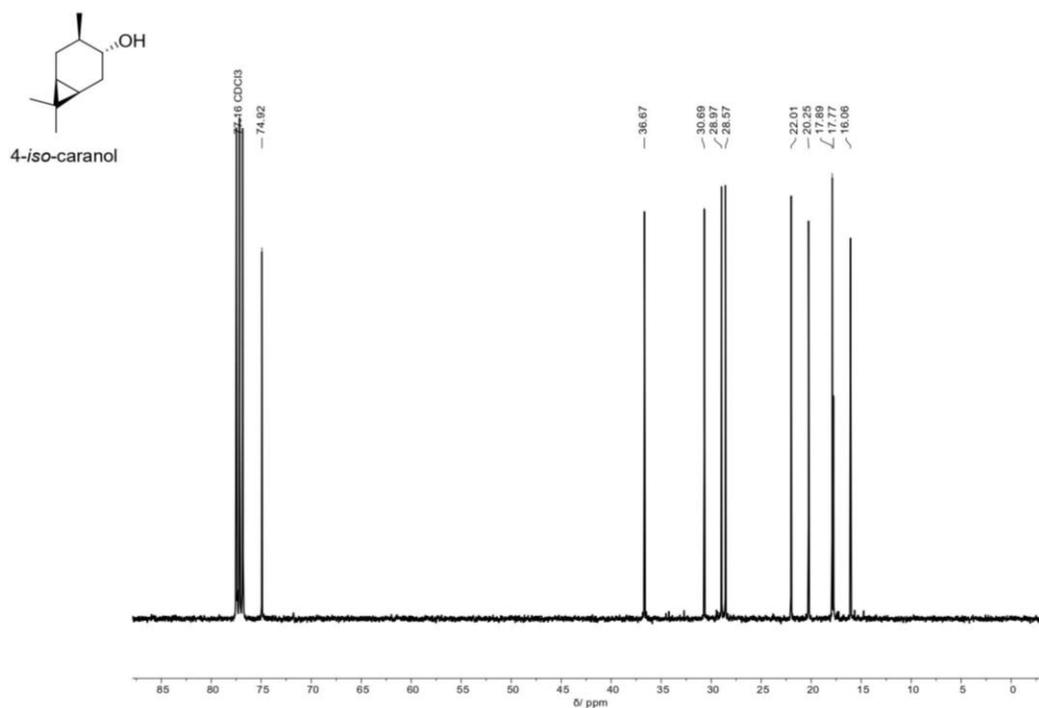
Figure S2: ¹³C-NMR spectrum (125 MHz, CDCl₃, 300K) of 4-*iso*-caranol.

2.2 Oxidation of 4-*iso*-caranol[1]

154.14 g/mol

152.14 g/mol
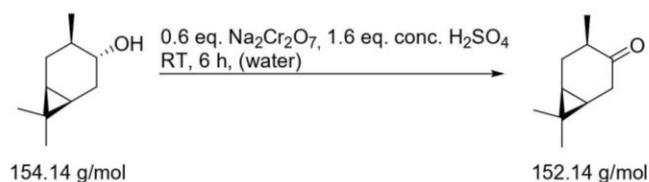
For the oxidation of 4-*iso*-caranol to 4-*iso*-caranone, a chromic acid solution was prepared by adding 8.5 mL (15.6 g, 159 mmol, 1.6 eq.) concentrated sulfuric acid to 16.12 g (54 mmol, 0.6 eq.) sodium dichromate and 90 mL water were added for dilution. 15.0 g (97 mmol, 1.0 eq.) 4-*iso*-caranol were diluted in 50 mL diethyl ether and the chromic acid solution was added to the alcohol over 2 hours at room temperature. After complete addition, the remaining suspension is stirred for additional 4 hours at room temperature before separating the phases and extracting the aqueous phase with diethyl ether (2×50 mL). The combined organic phases were washed with water (2×60 mL) and brine (2×60 mL) before drying over magnesium sulphate. Afterwards the solvent was removed in vacuo and the crude product was purified via column chromatography (silica, *p*-anisaldehyde staining, hexanes/ethyl acetate = 1:20), yielding 7.65 g (50 mmol, 51%) 4-*iso*-caranone as colorless oil.

^{1}H-NMR spectrum (400 MHz, CDCl$_3$, 300 K): δ (ppm) = 2.51 (dd, $^3J_{H,H}$ = 18.0, 8.4 Hz, 1H), 2.41-2.33 (m, 1H), 2.32-2.20 (m, 2H), 1.32-1.15 (m, 1H), 1.12-1.05 (m, 1H), 1.00 (s, 3H), 1.01-0.95 (m, 1H), 0.94 (d, $^3J_{H,H}$ = 6.4 Hz, 3H), 0.80 (s, 3H).

^{13}C-NMR spectrum (125 MHz, CDCl$_3$, 300 K): δ (ppm) = 216.8, 42.1, 36.9, 29.9, 28.0, 22.9, 20.5, 19.6, 15.0, 14.2.

GC-MS: t_R = 8.15 min, m/z = 152.1 (M$^+$), 136.1 ([M-Me]$^+$).
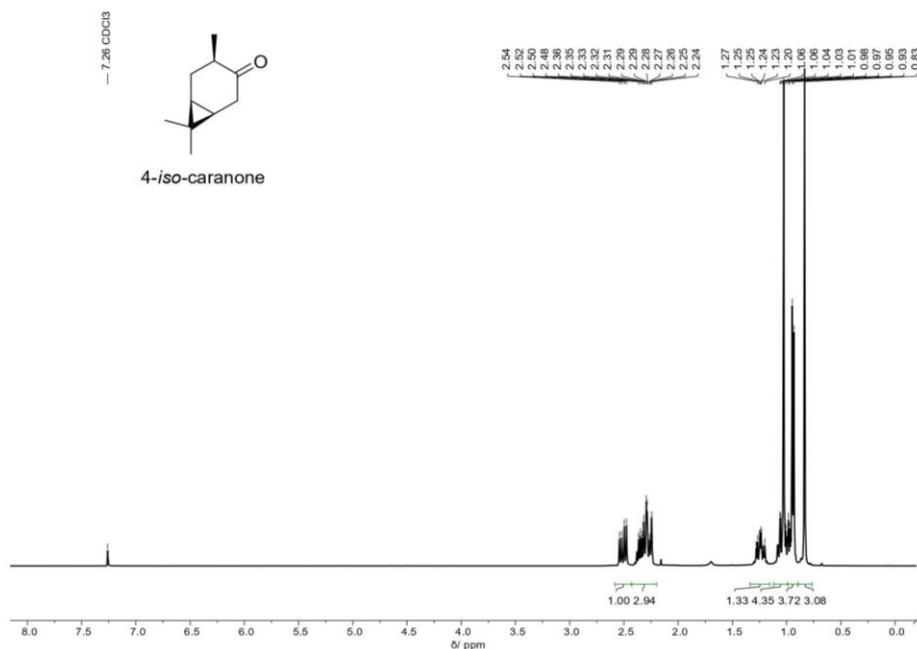
Figure S3: ^{1}H-NMR spectrum (400 MHz, CDCl$_3$, 300K) of 4-*iso*-caranone.

5
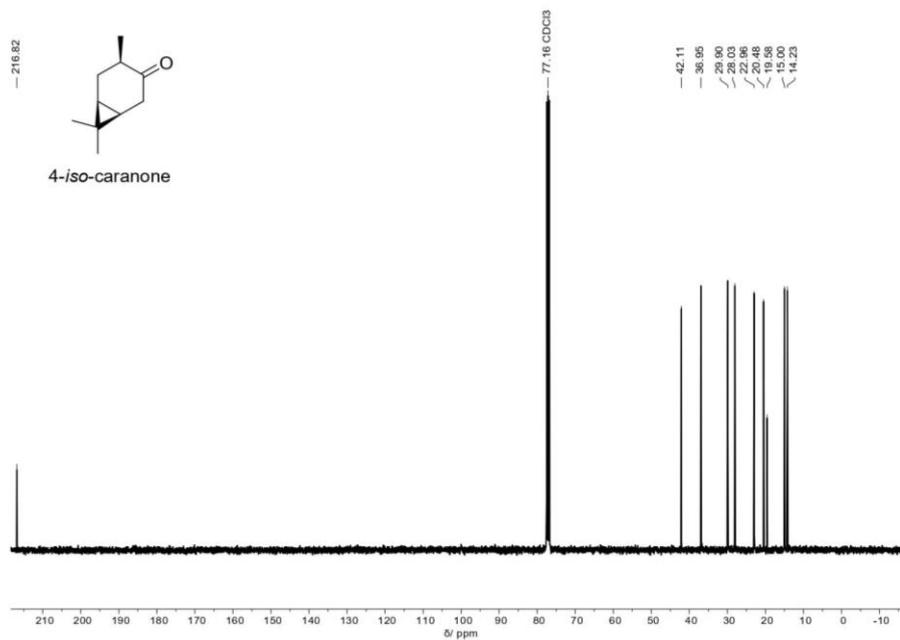
Figure S4: ^{13}C-NMR spectrum (125 MHz, CDCl$_3$, 300K) of 4-*iso*-caranone.

6

2.3 Baeyer-Villiger Oxidation of 4-*iso*-caranone[2]

1.5 eq. *m*CPBA, RT, 6h, (-)

152.14 g/mol   168.12 g/mol
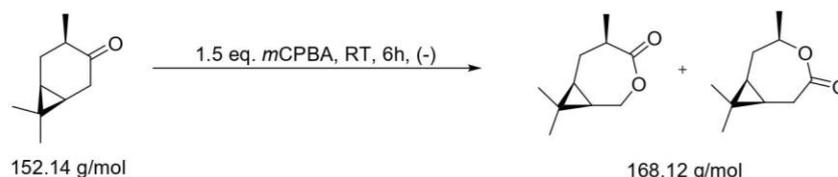
For the lactone synthesis, 3.0 g (20.0 mmol, 1.0 eq.) 4-*iso*-caranone were put in a 50 mL flask with stirring bar and 5.03 g (29.0 mmol, 1.5 eq.) *meta*-chloroperbenzoic acid were added without solvent and a reflux condenser was attached. After stirring at room temperature for 6 hours, the mixture is diluted with 20 mL dichloromethane, 11.1 g (80 mmol, 4.0 eq.) potassium carbonate were added to remove residual *m*CPBA and 4-chlorobenzoic acid and the solution was filtered off. After solvent removal the crude product was dissolved in 40 mL diethyl ether and the organic phase was washed with saturated sodium sulfite solution (3×40 mL), water (2×40 mL) and brine (2x40 mL) and dried with magnesium sulphate. The solvent was removed to yield 1.66 g crude product. GC-MS analysis revealed a conversion of 65 % with regard to used 4-*iso*-caranone. Separation via column chromatography (silica, hexane/diethyl ether = 1:3, CAM staining) yielded 0.23 g α-carenelactone (0.8 mmol, 4 %) as yellow oil, 0.31 g ε-carenelactone (1.7 mmol, 8 %) as white crystals and a mixture of both lactones (0.31 g, 2.0 mmol, 10 %, αCarL:εCarL = 40:60). Non-converted 4-*iso*-caranone was isolated as separate fraction and reused for the BVO.

α-carenelactone:
^{1}H-NMR spectrum (400 MHz, CDCl$_3$, 300 K): δ (ppm) = 4.45 (dd, $^3J_{H,H}$ = 13.1 Hz, $^2J_{H,H}$ = 3.7 Hz, 1H, OC*H*HCH), 4.30 (dd, $^3J_{H,H}$ = 13.1 Hz, $^2J_{H,H}$ = 3.7 Hz, 1H, OCH*H*CH), 3.00-2.84 (m, 1H, Me-C*H*-CH$_2$), 1.99-1.87 (m, 1H, Me-CH-CH*H*), 1.58-1.45 (m, 1H, Me-CH-C*H*H), 1.27 (d, $^3J_{H,H}$ = 7.1 Hz, 3H, Me), 1.10 (s, 3H, *gem*-Me), 1.05 (s, 3H, *gem*-Me), 1.04-0.98 (m, 2H, CH$_{cyclopropane}$).
^{13}C-NMR spectrum (101 MHz, CDCl$_3$, 300 K): δ (ppm) = 177.3 (CO), 66.3 (CH2), 41.3 (CH), 27.4 (*gem*-CH$_3$), 27.4 (CH$_2$), 25.4 (CH), 24.9 (CH), 20.2 (C$_{quart}$), 19.7 (CH$_3$), 15.3 (*gem*-CH$_3$).
GC-MS: t_R = 10.2 min, m/z = 168.1 (M$^+$), 153.2 ((M-Me)$^+$).
ATR-IR: ṽ = 3440 cm^{-1}, 2940 cm^{-1}, 2866 cm^{-1}, 1722 cm^{-1}, 1470 cm^{-1}, 1286 cm^{-1}, 1276 cm^{-1}, 1193 cm^{-1}.

ε-carenelactone:
^{1}H-NMR spectrum (400 MHz, CDCl$_3$, 300 K): δ (ppm) = 4.68-4.55 (m, 1H, O-CH-Me), 3.16 (dd, $^3J_{H,H}$ = 15.6 Hz, $^2J_{H,H}$ = 4.3 Hz, 1H, OCC*H*H) 2.96 (dd, $^3J_{H,H}$ = 15.6 Hz, $^2J_{H,H}$ = 4.3 Hz, OCCH*H*), 2.11 (dd, $^3J_{H,H}$ = 16.3, 10.0 Hz, 1H, CH$_2$), 1.78 (td, $^3J_{H,H}$ = 15.9, 10.2, $^2J_{H,H}$ = 5.1 Hz, 1H, CH$_2$), 1.30 (d, $^3J_{H,H}$ = 6.4 Hz, 3H, Me), 1.05 (s, 3H, *gem*-Me), 1.03 (s, 3H, *gem*-Me), 0.95-0.83 (m, 1H, C*H*$_{cyclopropane}$), 0.78-0.68 (m, 1H, C*H*$_{cyclopropane}$).

^{13}C-NMR spectrum (101 MHz, CDCl$_3$, 300 K): δ (ppm) = 173.3 (CO), 77.06 (CH), 33.2 (CH$_2$), 30.8 (CH$_2$), 29.2 (CH$_3$), 22.2 (CH, CH$_3$), 20.9 (CH), 18.6 (C$_{quart}$), 15.0 (CH$_3$).
GC-MS: t_R = 10.2 min, m/z = 168.1 (M$^+$), 153.2 ((M-Me)$^+$).
ATR-IR: ṽ = 3440 cm^{-1}, 2940 cm^{-1}, 2866 cm^{-1}, 1722 cm^{-1}, 1470 cm^{-1}, 1286 cm^{-1}, 1276 cm^{-1}, 1193 cm^{-1}.
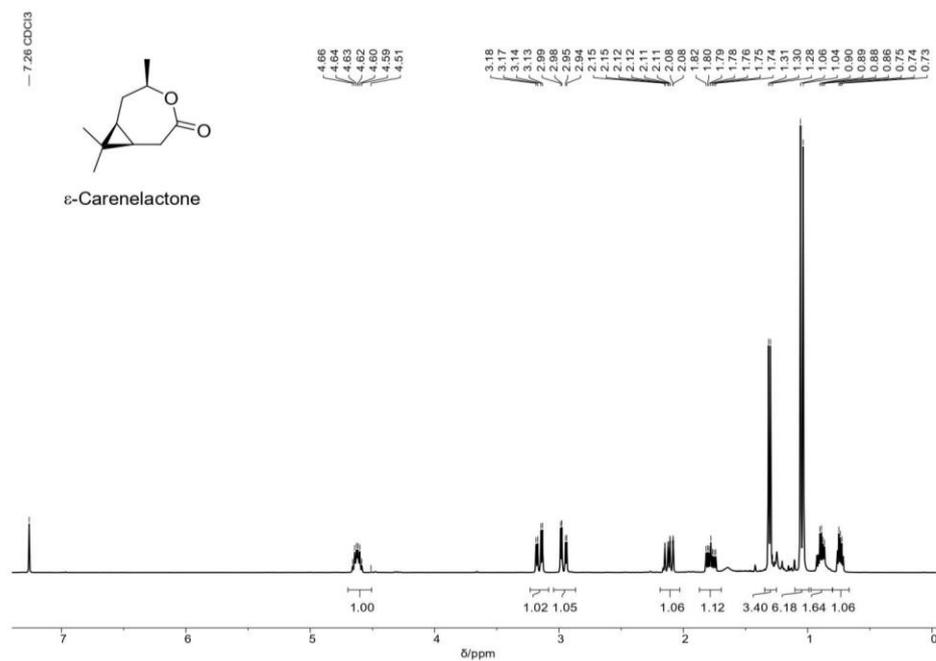
Figure S5: ^{1}H-NMR spectrum (400 MHz, CDCl$_3$, 300K) of ε-carenelactone.
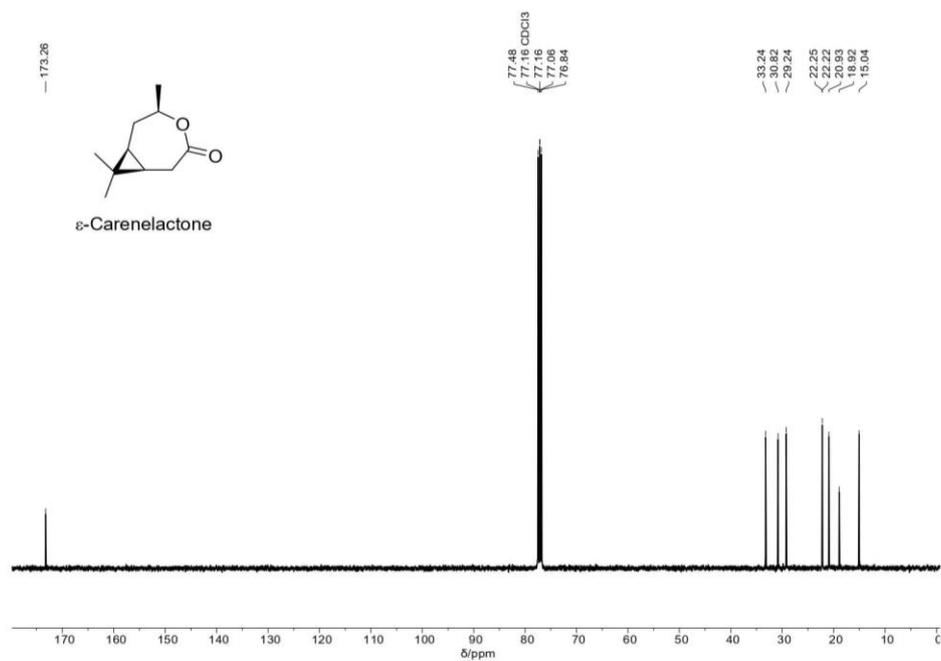
Figure S6: ^{13}C-NMR spectrum (400 MHz, CDCl$_3$, 300K) of ε-carenelactone.

8
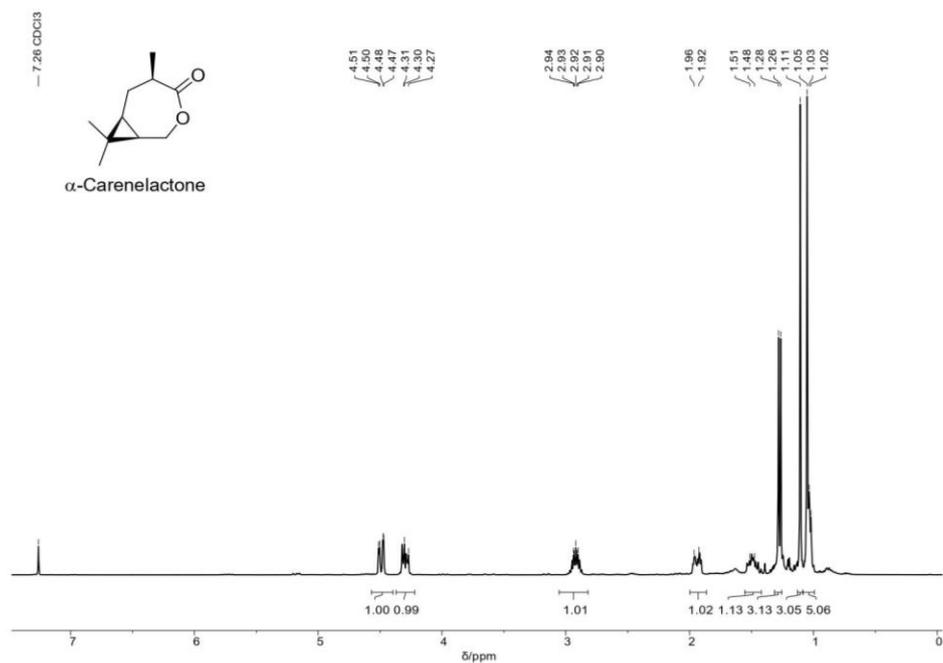
Figure S7: ^{1}H-NMR spectrum (400 MHz, CDCl$_3$, 300K) of α-carenelactone.
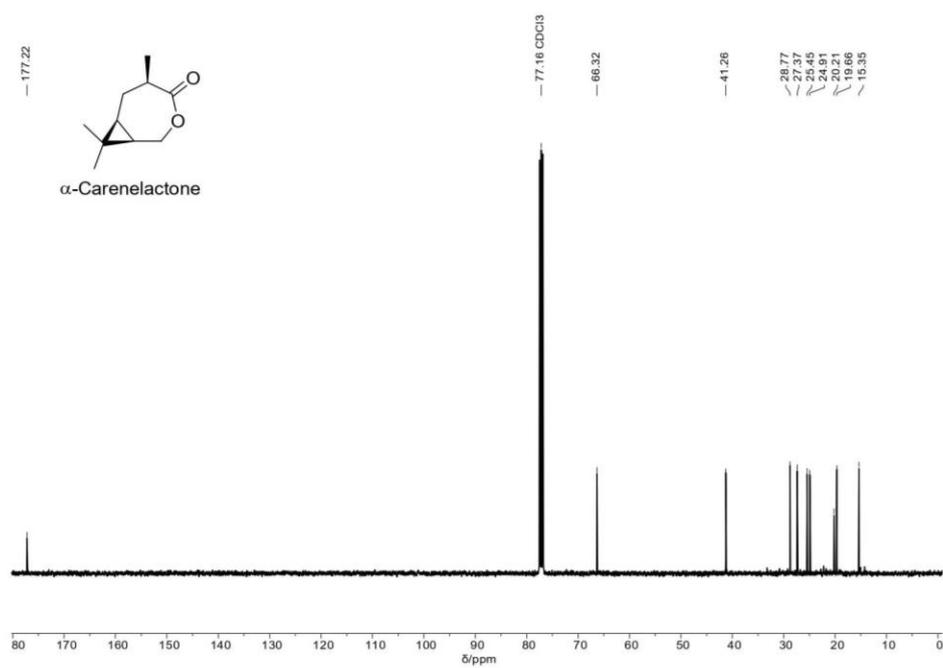
Figure S8: ^{13}C-NMR spectrum (125 MHz, CDCl$_3$, 300K) of α-carenelactone.

9

2.4 Reductive ozonolysis of 3-carene[3]

154.14 g/mol → 172.15 g/mol

1) O_3, -78 °C, 4 h, (MeOH:DCM = 1:1)
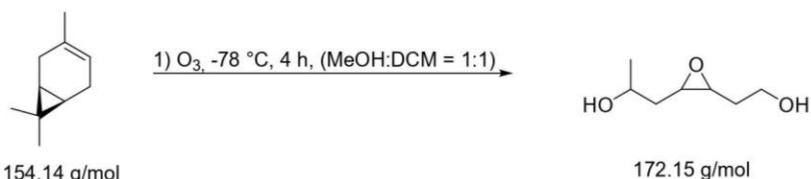
25.5 g (187 mmol, 1.0 eq.) 3-carene were dissolved in a 50:50 vol% mixture of dichloromethane and methanol, the reaction flask was cooled to -78 °C and a steady flow of ozone was bubbled through the mixture until a blue color occurred (approx. 4 h). To remove excess of ozone, the flask was purged with argon for 30 min. Subsequently, 7.5 g (198 mmol, 1.1 eq.) sodium borohydride were added stepwise, and the mixture was allowed to warm to room temperature overnight. 20 mL water and 20 mL 1M hydrochloric acid were added and a pH of 1 was adjusted. The reaction mixture was extracted with ethyl acetate (2×80 mL). Afterwards the organic phase was washed with water (2×200 mL) and brine (2×200 mL) before drying over magnesium sulphate. After solvent removal in vacuo, the crude product was distilled under reduced pressure (b_p = 150 °C, 7 mbar) to yield 19.8 g (115 mmol, 61 %) 3-carene diol as colorless oil.

^{1}H-NMR spectrum (400 MHz, CDCl$_3$, 300 K): δ (ppm) = 3.97-3.81 (m, 1H, CH$_2$CHMe), 3.79-3.58 (m, 2H, CH$_2$OH), 1.67-1.48 (m, 2H, CH$_2$), 1.47-1.31 (m, 2H, CH$_2$), 1.27-1.19 (m, 3H, Me), 1.07 (d, $^3J_{H,H}$ = 3.1 Hz, gem-Me), 0.94 (d, $^3J_{H,H}$ = 12.9 Hz, 3H, gem-Me), 0.63-0.50 (m, 2H, CH$_{cyclopropane}$).

^{13}C-NMR spectrum (101 MHz, CDCl$_3$, 300 K): δ (ppm) = 70.0, 68.4, 63.6, 63.5, 33.9, 33.8, 29.3, 28.0, 27.7, 23.7, 23.1, 16.8, 16.2, 15.4.

GC-MS: t_R = 9.86 min, m/z = 172.1 (M$^+$), 125.1 ((M-Me-2×OH)$^+$)
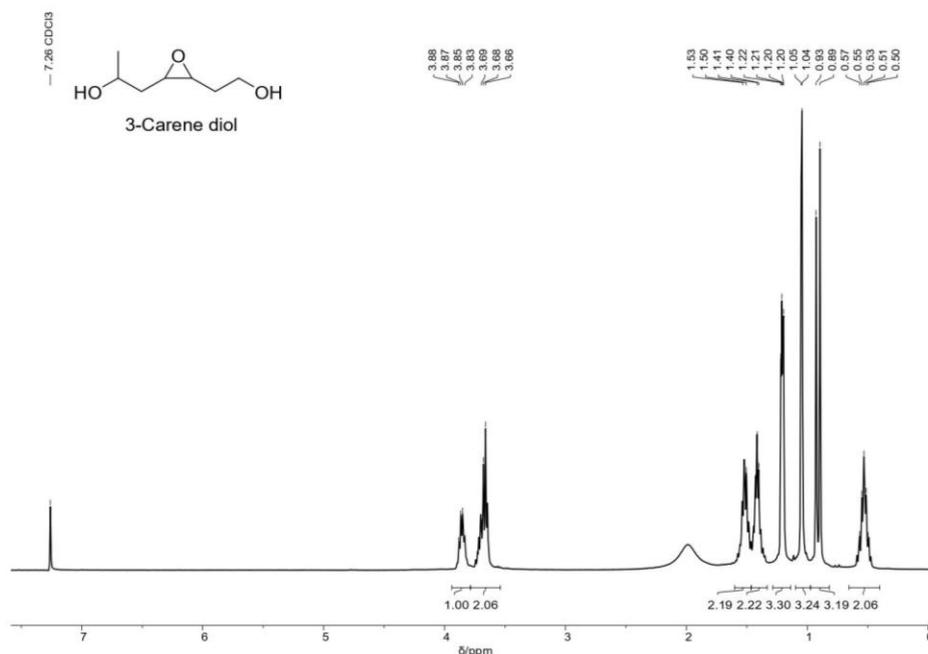
Figure S9: ^{1}H-NMR spectrum (400 MHz, CDCl$_3$, 300K) of 3-carene diol.

10
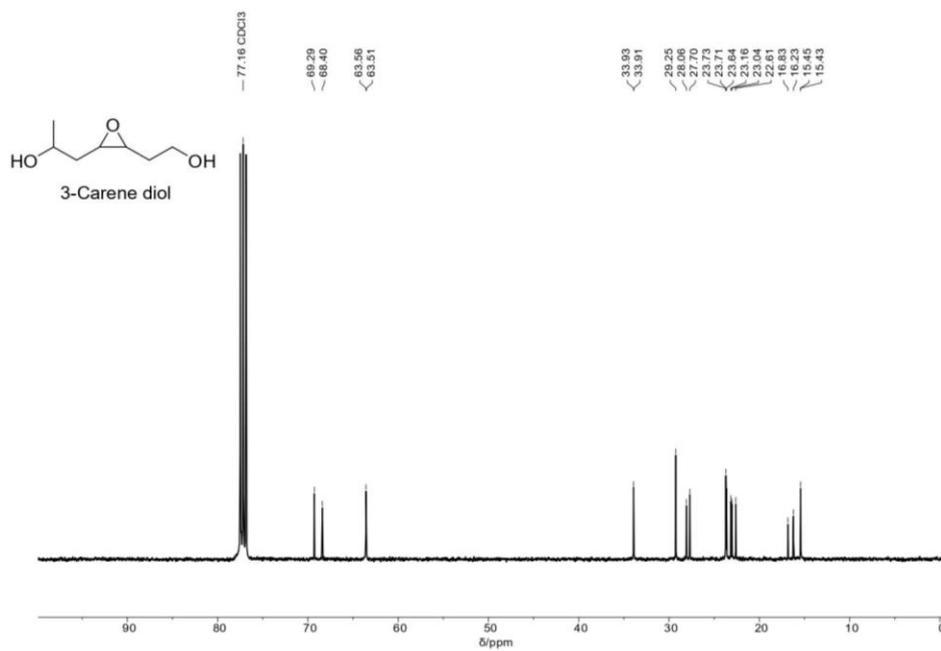
Figure S10: ^{13}C-NMR spectrum (125 MHz, CDCl$_3$, 300K) of 3-carene diol.

11

3. RING-OPENING POLYMERIZATION OF CARENLACTONES

3.1 Polymerization conversion determination
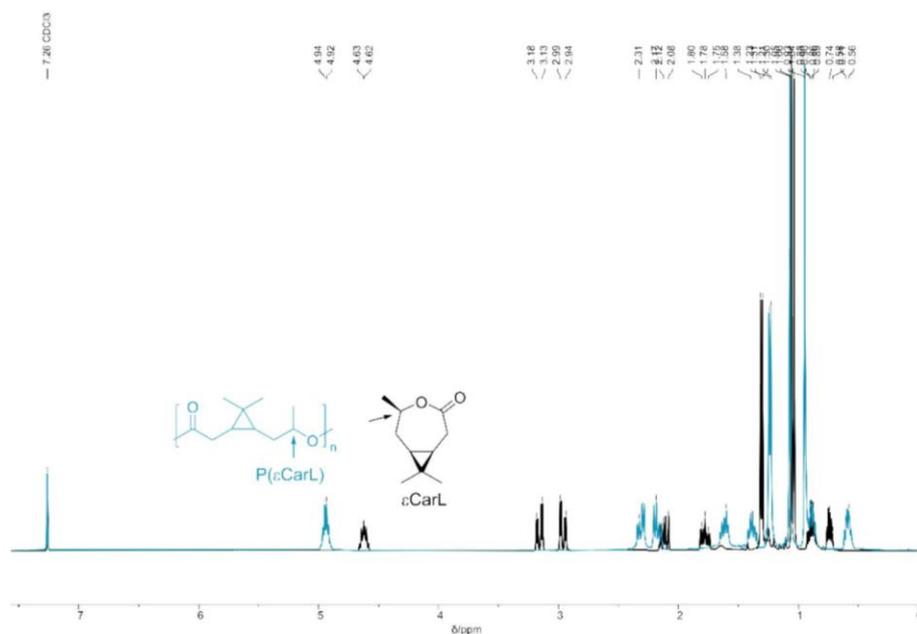
Figure S11: Conversion determination for the polymerization of εCarL (black) to P(εCarL) (blue) via integration of the methine proton as indicated by the arrow with $X = I_{Polymer}/(I_{Monomer}+I_{Polymer})$.
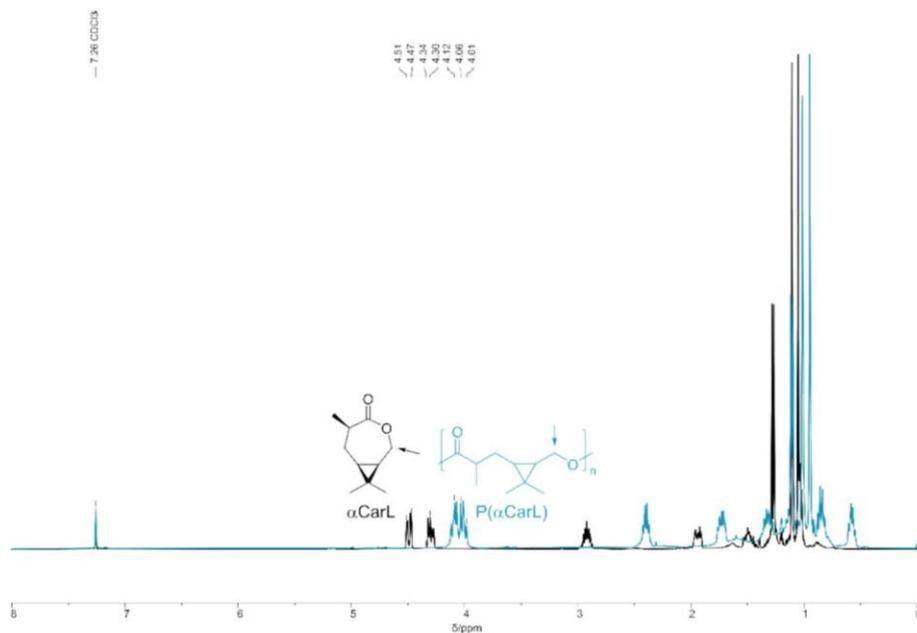
Figure S12: Conversion determination for the polymerization of αCarL (black) to P(αCarL) (blue) via integration of the CH_2-group in α-position to the main chain ester oxygen as indicated by the arrow with $X = I_{Polymer}/(I_{Monomer}+I_{Polymer})$.

12

3.2 Additional ^{13}C-NMR spectra
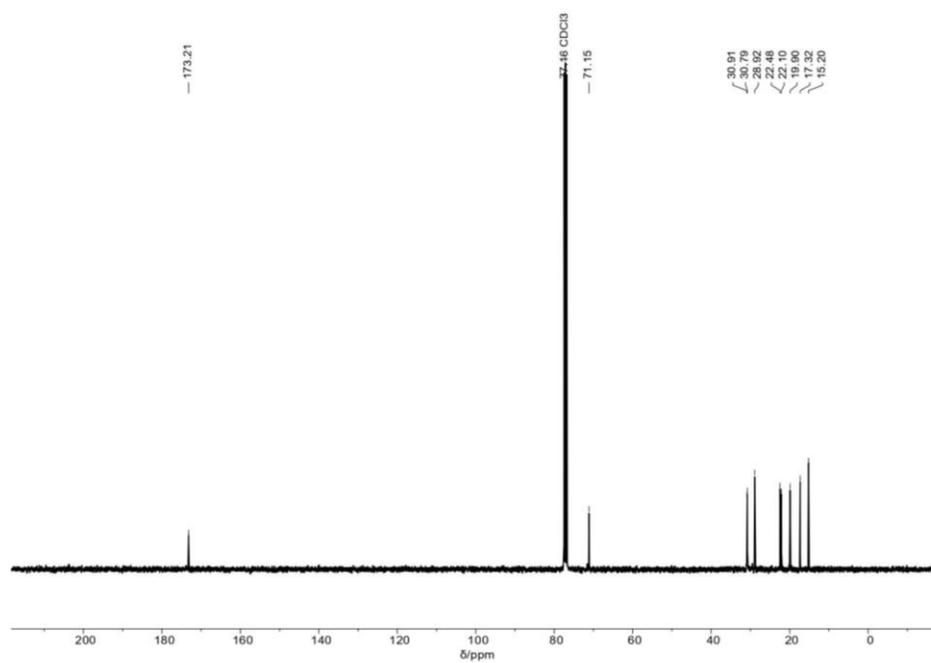
Figure S13: ^{13}C-NMR spectrum (125 MHz, CDCl$_3$, 300K) of P(εCarL).
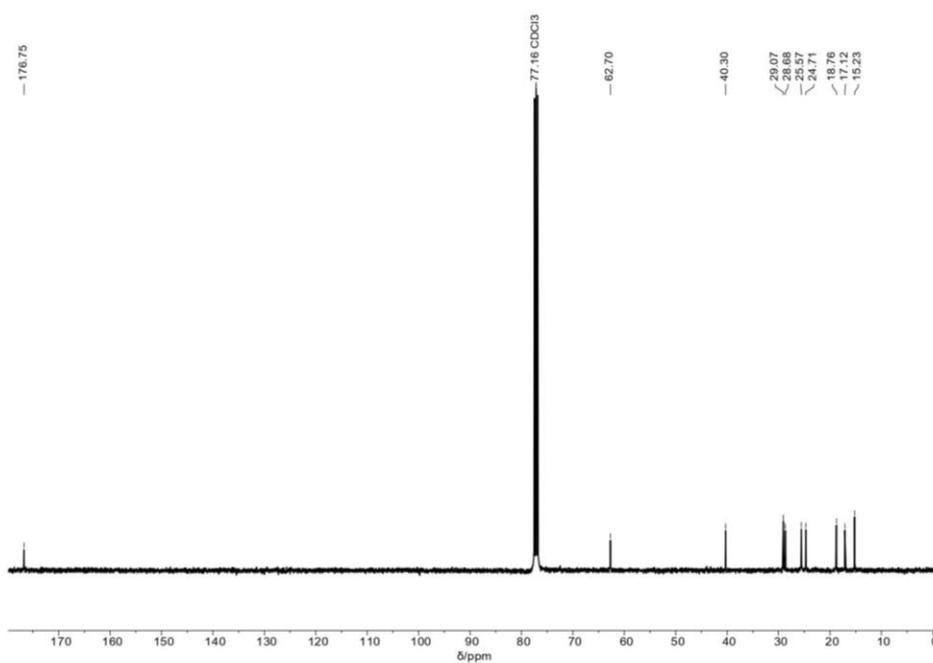
Figure S14: ^{13}C-NMR spectrum (125 MHz, CDCl$_3$, 300K) of P(αCarL).

13

3.3 Copolymer linkage analysis of P(αCarL-co-εCarL)$_{stat}$
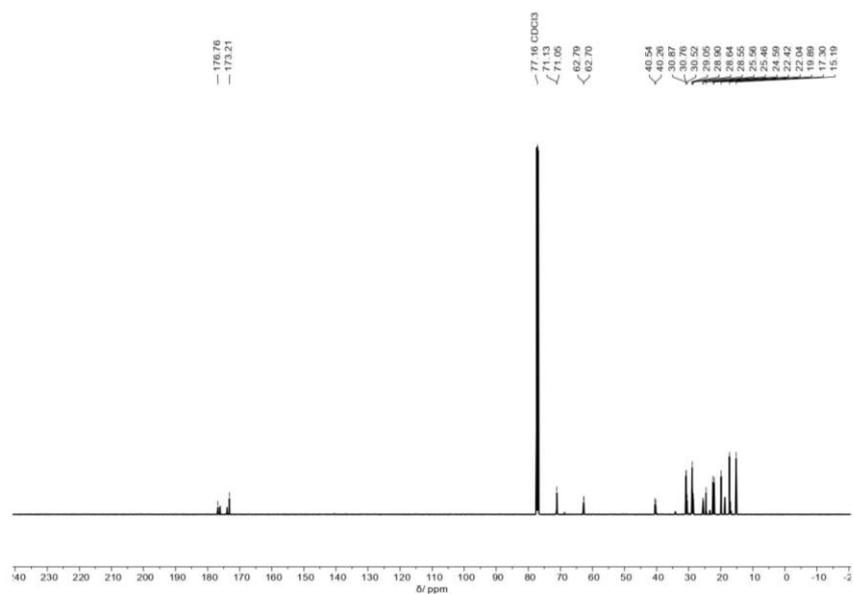
Figure S15: ^{13}C-NMR spectrum (125 MHz, CDCl$_3$, 300K) of P(αCarL-co-εCarL)$_{stat}$.
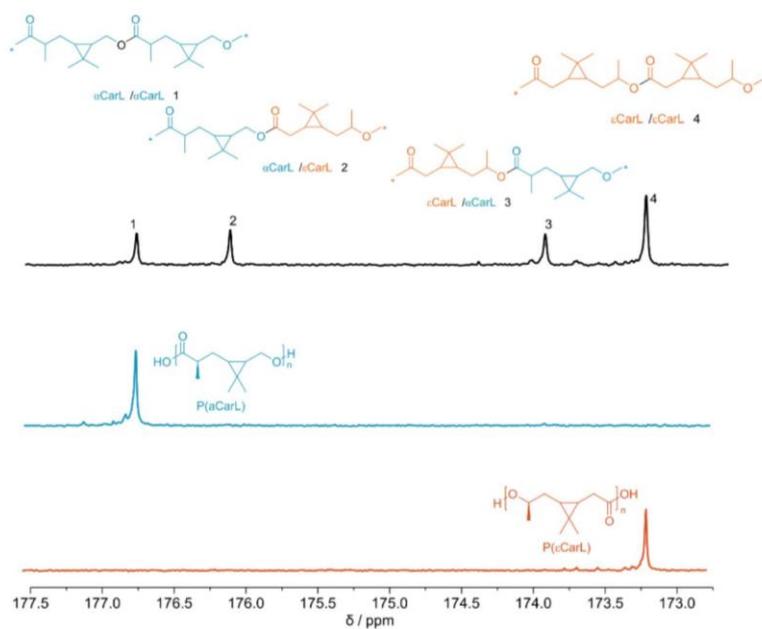
Figure S16: Close-up of the carbonyl region in the ^{13}C-NMR spectra (125 MHz, CDCl$_3$, 300 K) of P(εCarL) (orange, bottom), P(αCarL) (blue, middle) and P(αCarL-co-εCarL)$_{stat}$ (black, top) with the four different observable linkages of εCarL and αCarL.

14
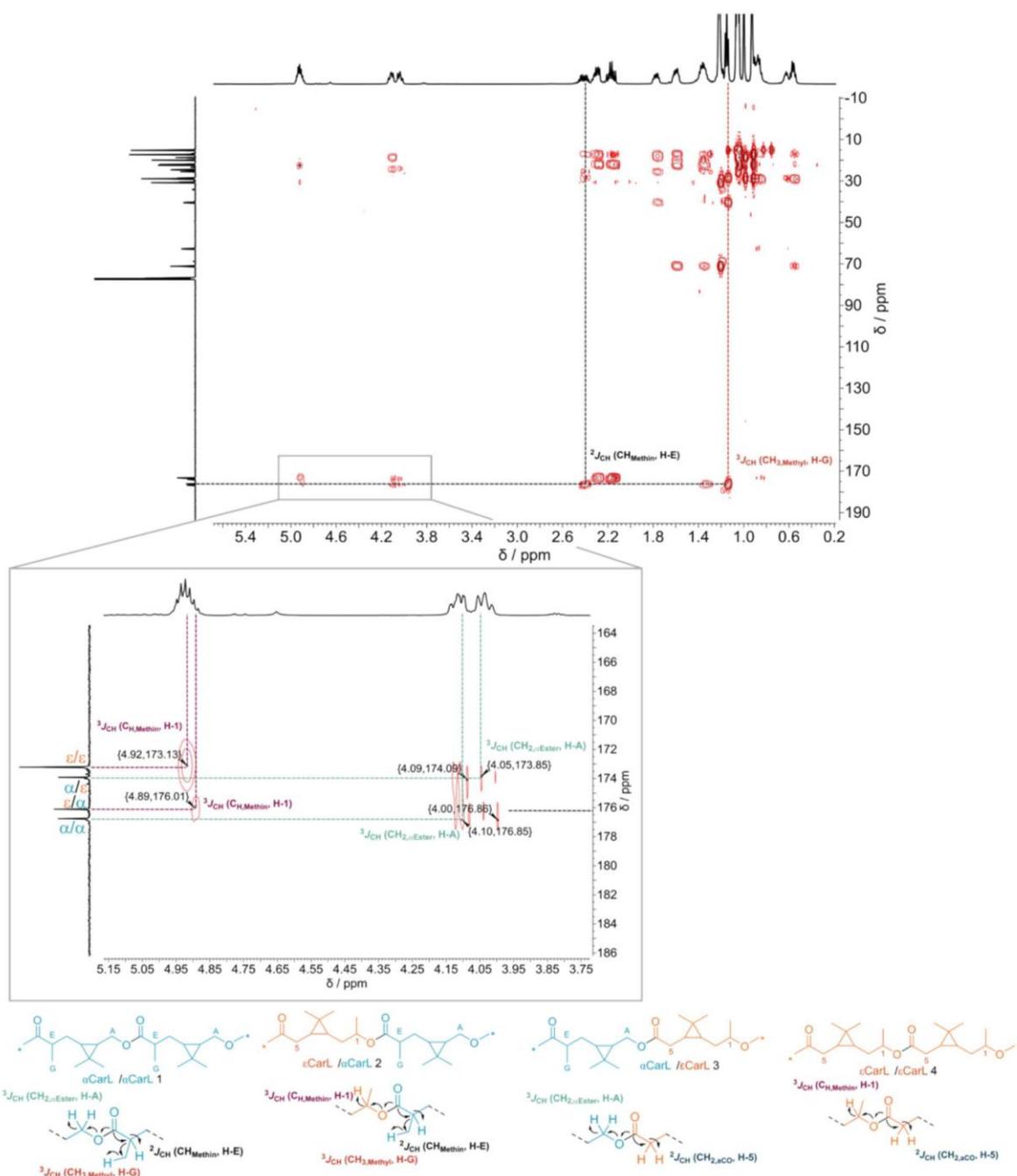
Figure S17: ^{1}H-^{13}C-HMBC (500 MHz, CDCl$_3$, 300K) peak assignment of the different carbonyl signals in the copolyesters P P(αCarL-co-ϵCarL)$_{stat}$.

3.4 SEC characterization of ROP polymers (Table 1)
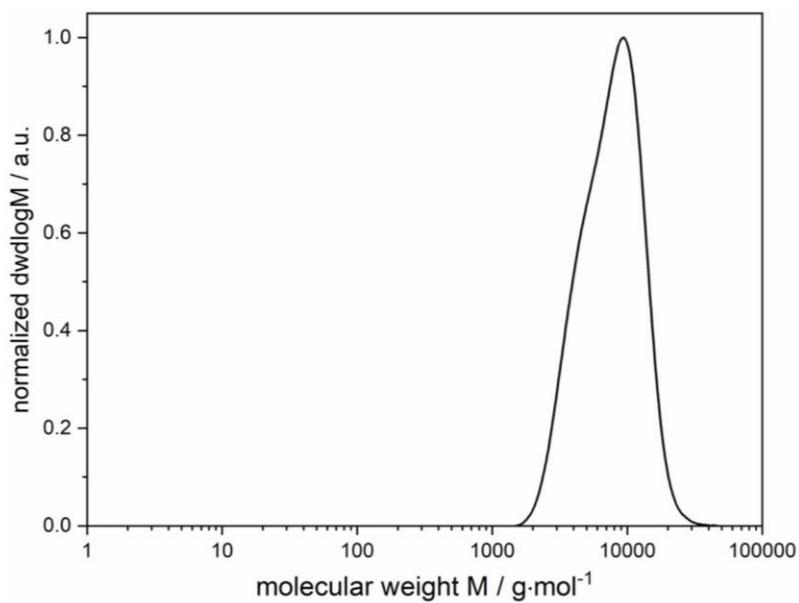
Figure S18: Molecular weight distribution of P(εCarL) (Table 2, entry 1) determined via SEC in THF at 30 °C using RI detection.
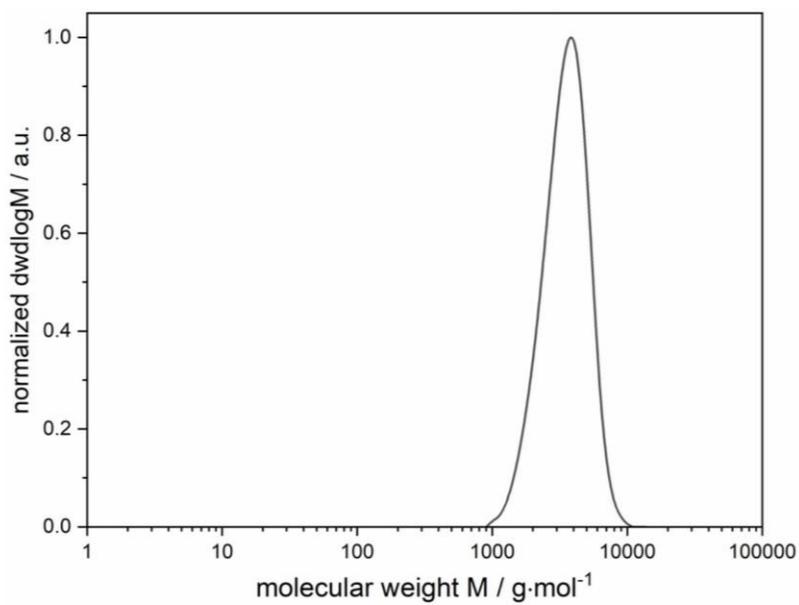

Figure S19: Molecular weight distribution of P(εCarL) (Table 2, entry 2) determined via SEC in THF at 30 °C using RI detection.

16
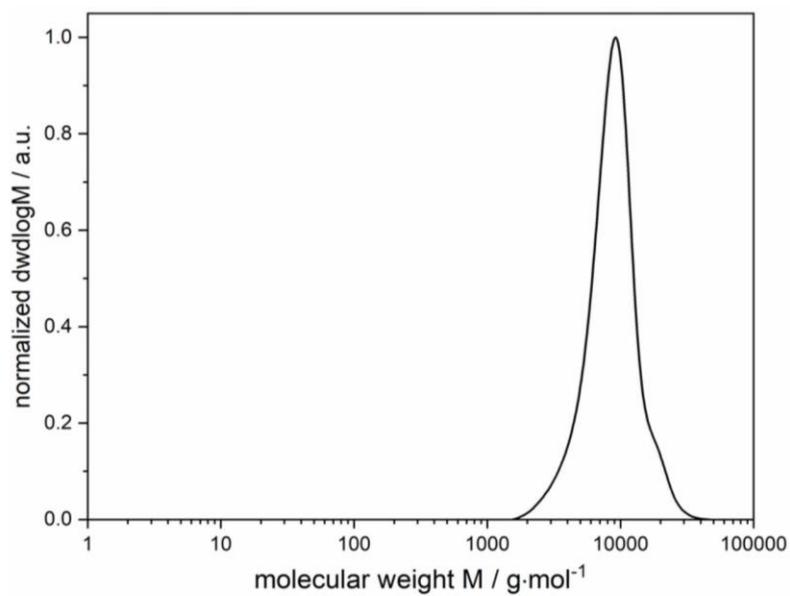
Figure S20: Molecular weight distribution of P(εCarL) (Table 2, entry 3) determined via SEC in THF at 30 °C using RI detection.
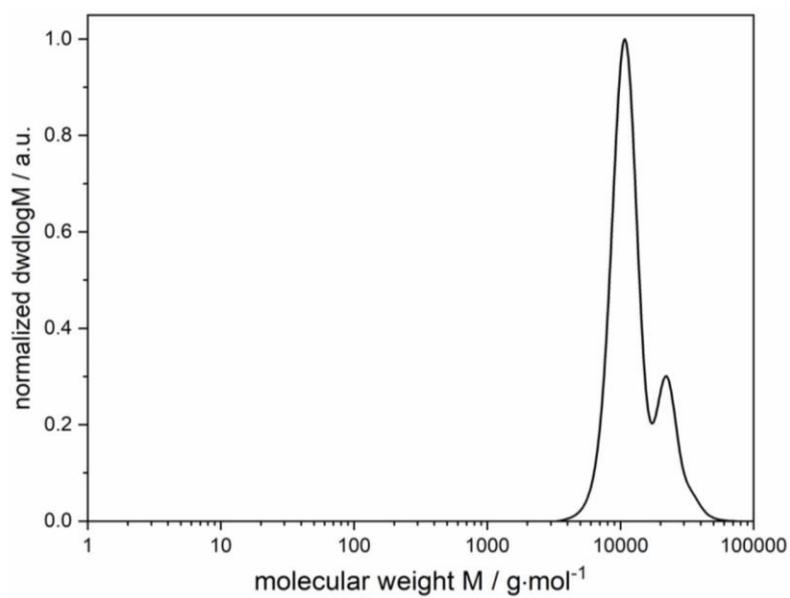
Figure S21: Molecular weight distribution of P(εCarL) (Table 2, entry 4) determined via SEC in THF at 30 °C using RI detection.

17
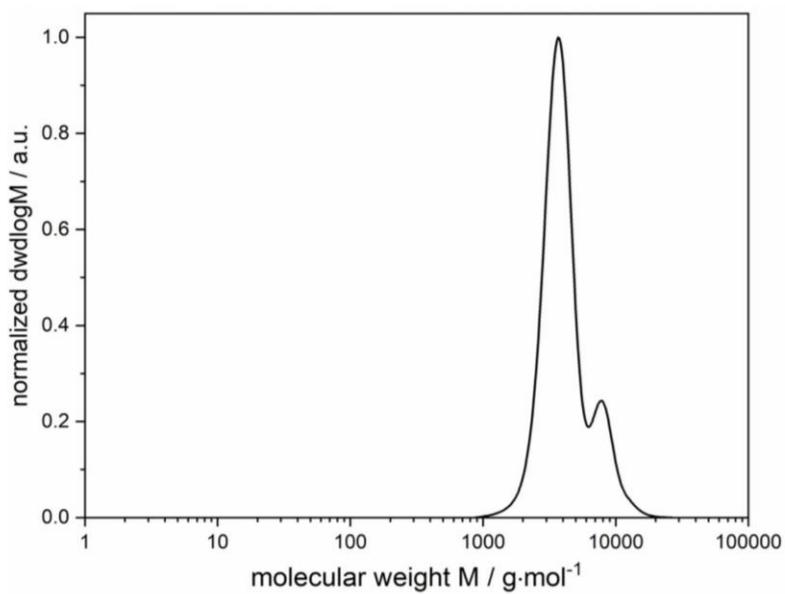
Figure S 22: Molecular weight distribution of P(εCarL) (Table 2, entry 5) determined via SEC in THF at 30 °C using RI detection.
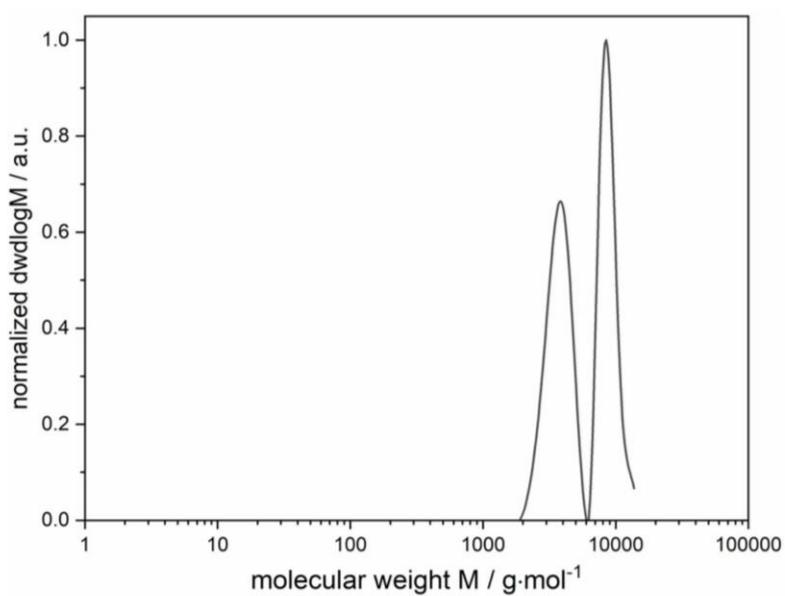
Figure S 23: Molecular weight distribution of P(εCarL) (Table 2, entry 6) determined via SEC in THF at 30 °C using RI detection.

18
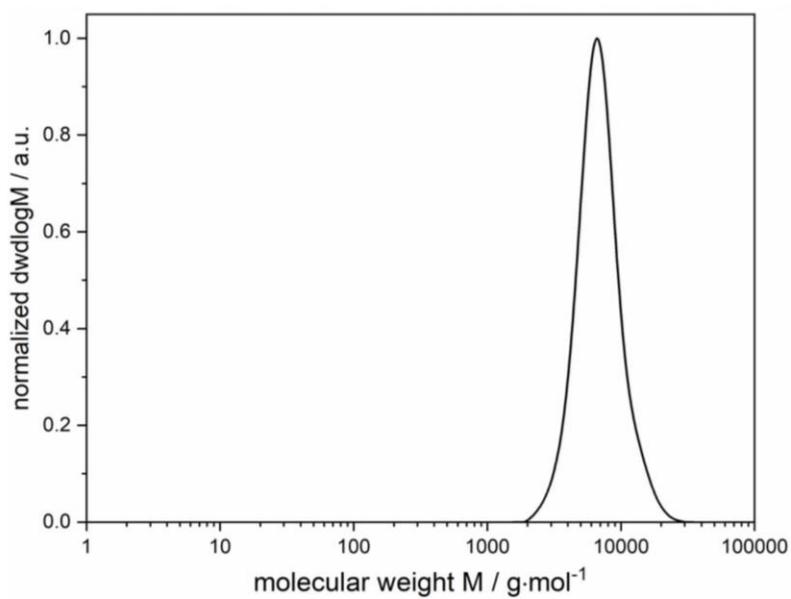
Figure S24: Molecular weight distribution of P(εCarL) (Table 2, entry 7) determined via SEC in THF at 30 °C using RI detection.
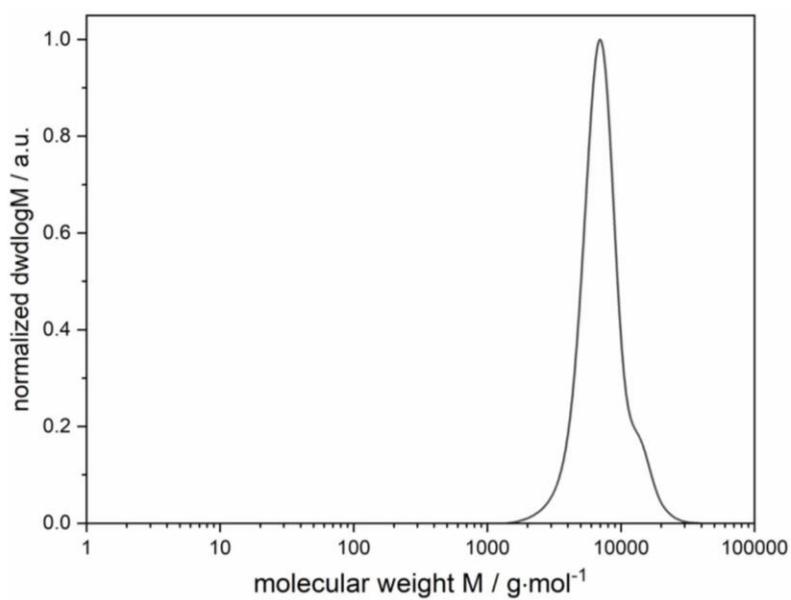
Figure S25: Molecular weight distribution of P(εCarL) (Table 2, entry 8) determined via SEC in THF at 30 °C using RI detection.

19
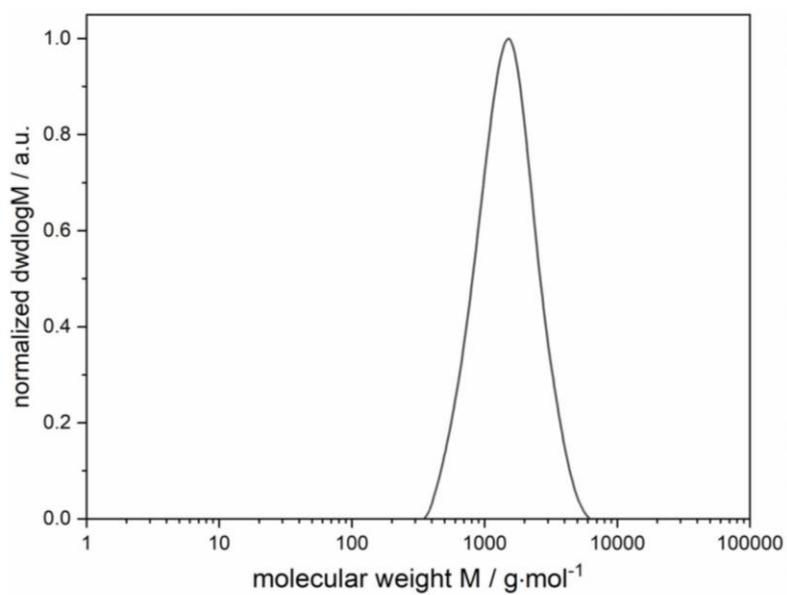
Figure S26: Molecular weight distribution of P(αCarL) (Table 2, entry 9) determined via SEC in THF at 30 °C using RI detection.
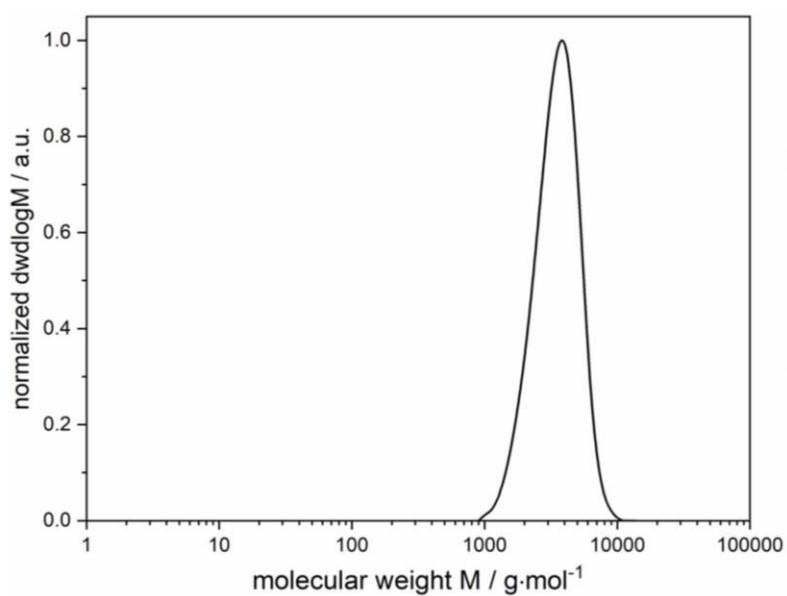
Figure S27: Molecular weight distribution of P(αCarL) (Table 2, entry 10) determined via SEC in THF at 30 °C using RI detection.

20
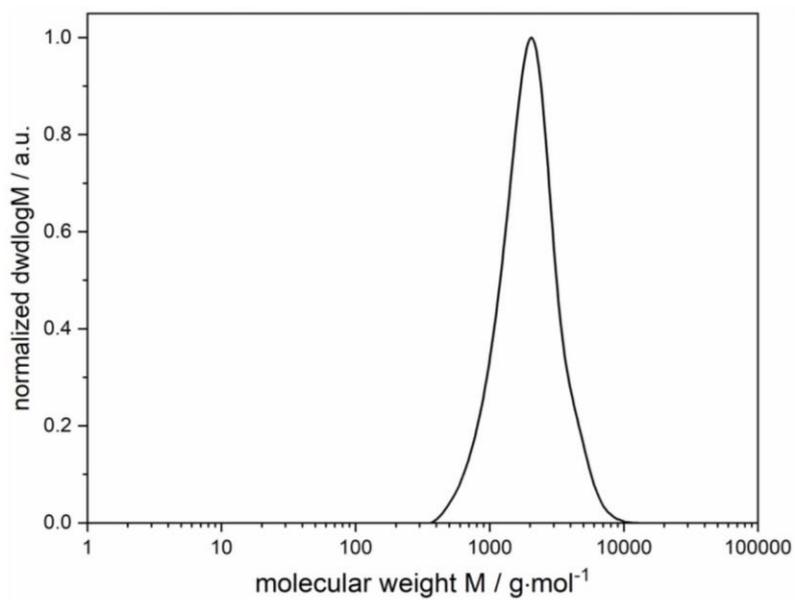
Figure S28: Molecular weight distribution of P(αCarL) (Table 2, entry 11) determined via SEC in THF at 30 °C using RI detection.
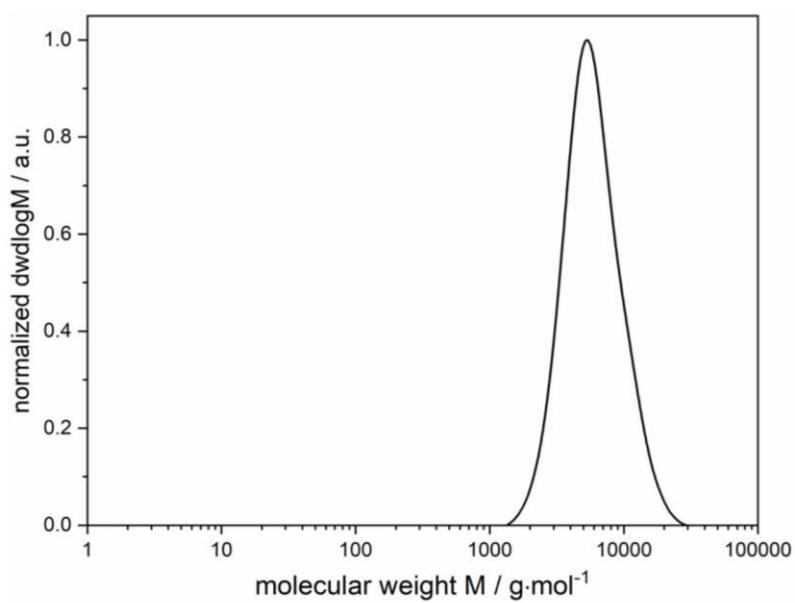
Figure S29: Molecular weight distribution of P(αCarL-*co*-εCarL)$_{stat}$ (Table 2, entry 12) determined via SEC in THF at 30 °C using RI detection.

21
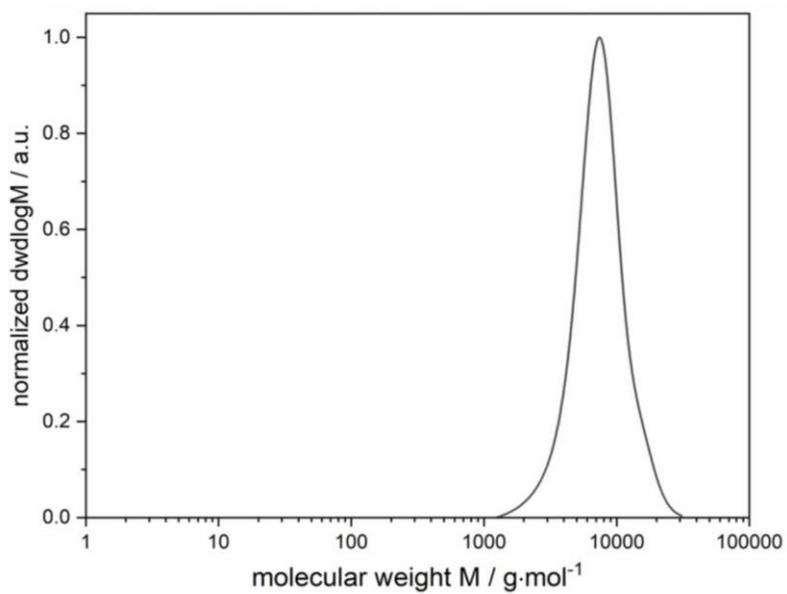
Figure S30: Molecular weight distribution of P(αCarL-*co*-εCarL)stat (Table 2, entry 13) determined via SEC in THF at 30 °C using RI detection.

4. POLYCONDENSATION OF 3-CARENE DIOL

Table S1: Reaction parameters and molecular weights for the polycondensation of 3-carene diol with DMT.

| Entry | [3CarDiol]:[DMT]:[Cat][a] | Precondensation | | Polycondensation | | Method [b] | $M_{n,rel}$ [c] | Đ [c] |
	[mol]:[mol]:[mol]	p_1 [mbar]	T_1 [°C]	p_2 [mbar]	T_2 [°C]		[kg/mol]	[-]
1	200:100:1	1013	170	0.5	180	slow	6.4	1.5
2	200:100:1	1013	170	0.5	180	fast	12.8	2.0

[a] ratio of 3-carene diol to dimethyl terephthalate to catalyst titanium tetra-n-butanolate as weighed, 35 mmol of 3-carene diol; [b] heating method with heating to T_1 over time (slow) versus sudden increase in temperature (fast), [c] relative molecular weight and polydispersity measured in THF at 30 °C relative to polystyrene.
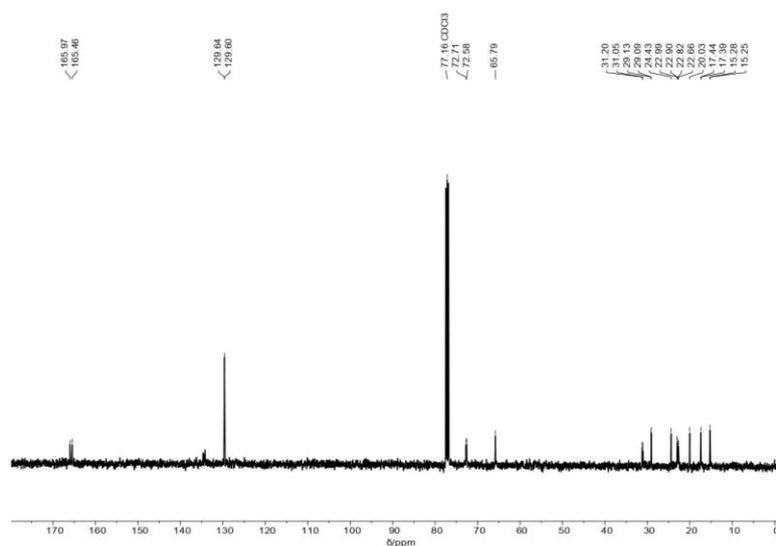
Figure S31: ^{13}C-NMR spectrum (125 MHz, CDCl$_3$, 300K) of P(3CarDiol-co-DMT).
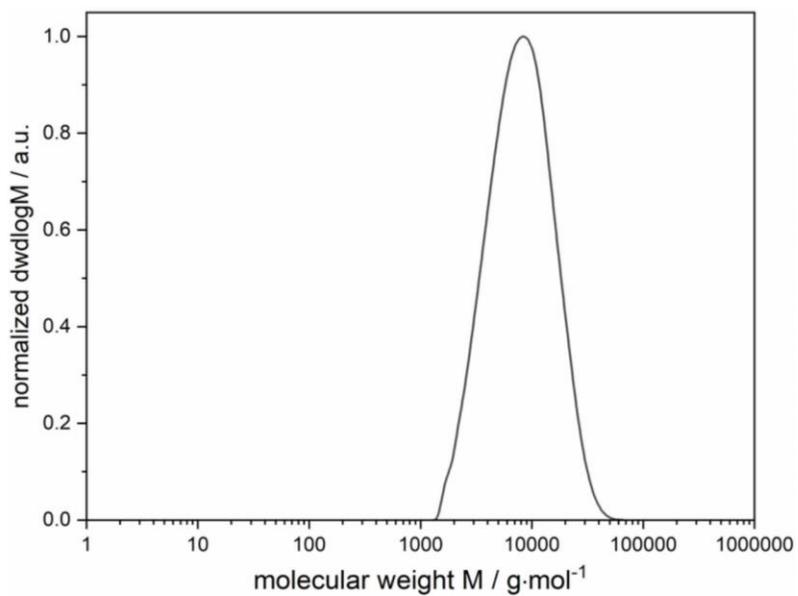
Figure S32: Molecular weight distribution of P(3CarDiol-*co*-DMT) (Table S1, entry 1) determined via SEC in THF at 30 °C using RI detection.
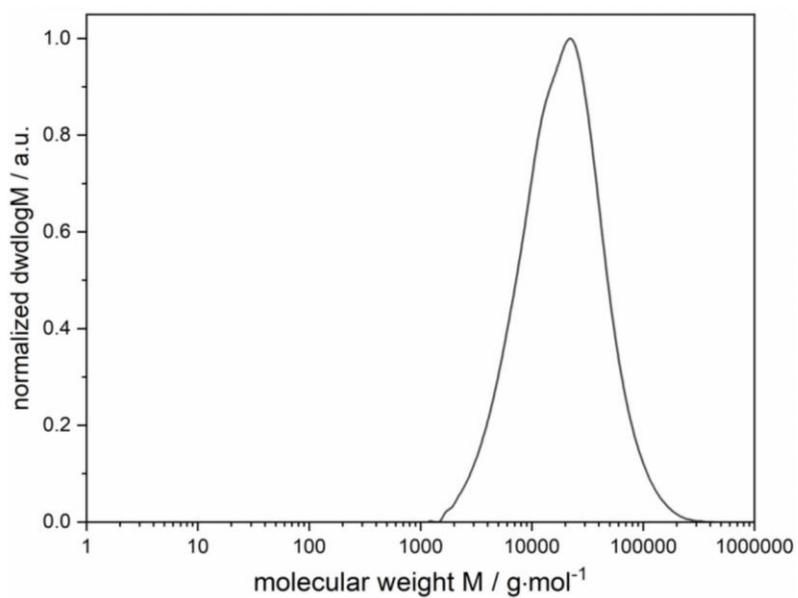
Figure S33: Molecular weight distribution of P(3CarDiol-*co*-DMT) (Table S1, entry 2) determined via SEC in THF at 30 °C using RI detection.

24

5. ADDITIONAL ANALYSIS
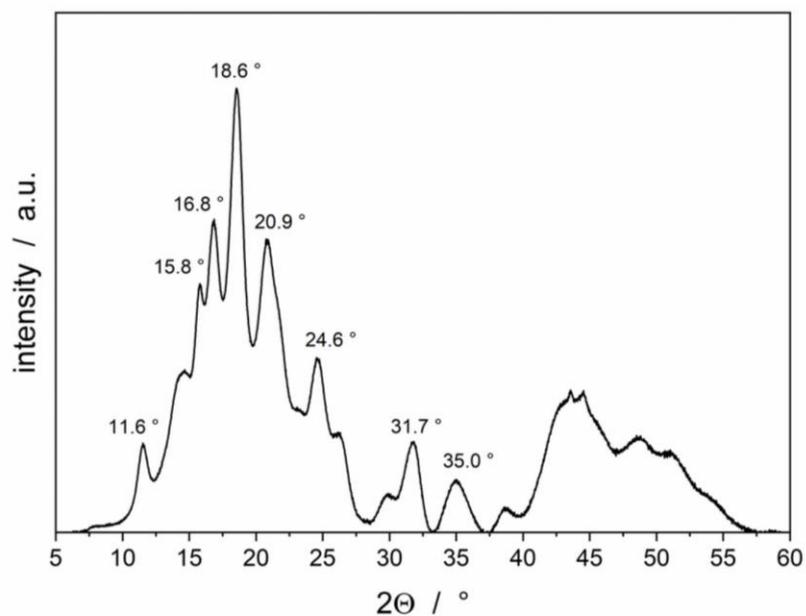
Figure S34: Powder X-Ray diffractogram of P(εCarL) (Table 2, entry 7).
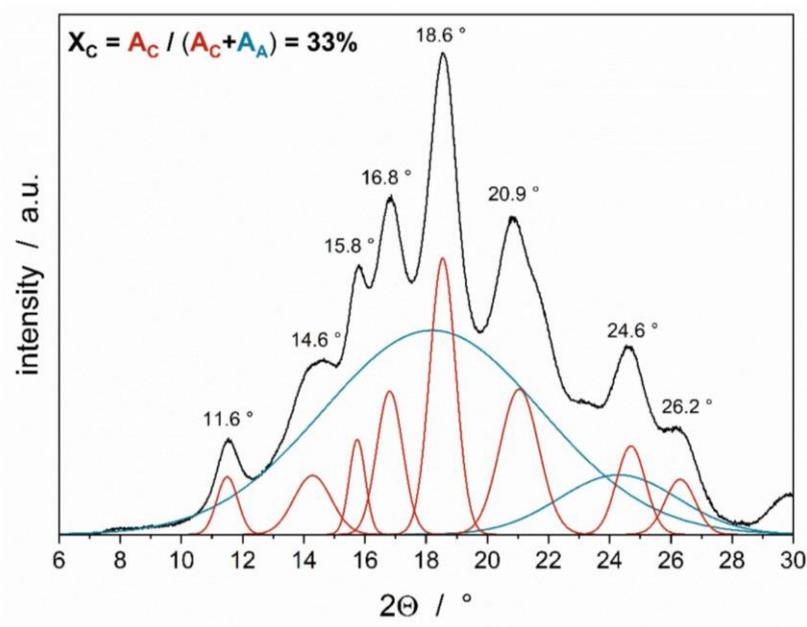
Figure S35: Peak deconvolution in the peak area between 7 – 28 ° (amorphous background blue, crystalline peaks red) for calculation of crystalline fraction X_C via area integration of the amorphous parts A_A and the crystalline parts A_C.[4]

25
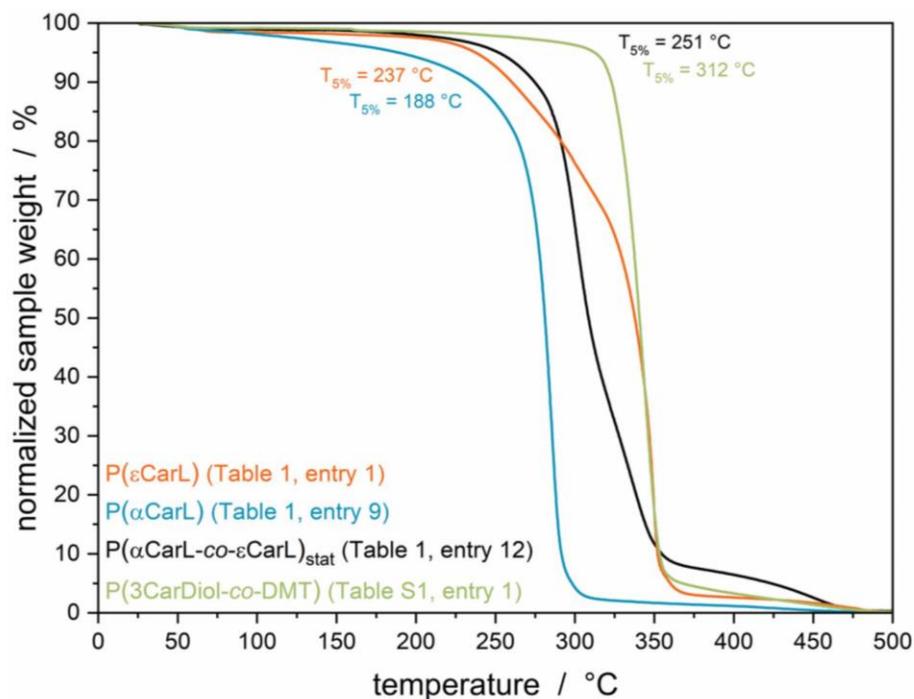
Figure S36: Thermogravimetric analysis of P(εCarL) (orange), P(αCarL) (blue), P(αCarL-*co*-εCarL)$_{stat}$ (black) and P(3CarDiol-*co*-DMT) (green).

∇ m/z = [M_{H_2O} + n x $M_{\varepsilon CarL}$ + Na]$^+$
$\Diamond$ m/z = [M_{H_2O} + n x $M_{\varepsilon CarL}$ - 18 + Na]$^+$
$\Diamond$ m/z = [n x $M_{\varepsilon CarL}$ + Na]$^+_{cyclic}$
$*$ m/z = [M_{H_2O} + (n-1) x $M_{\varepsilon CarL}$ - 46 + H]$^+$
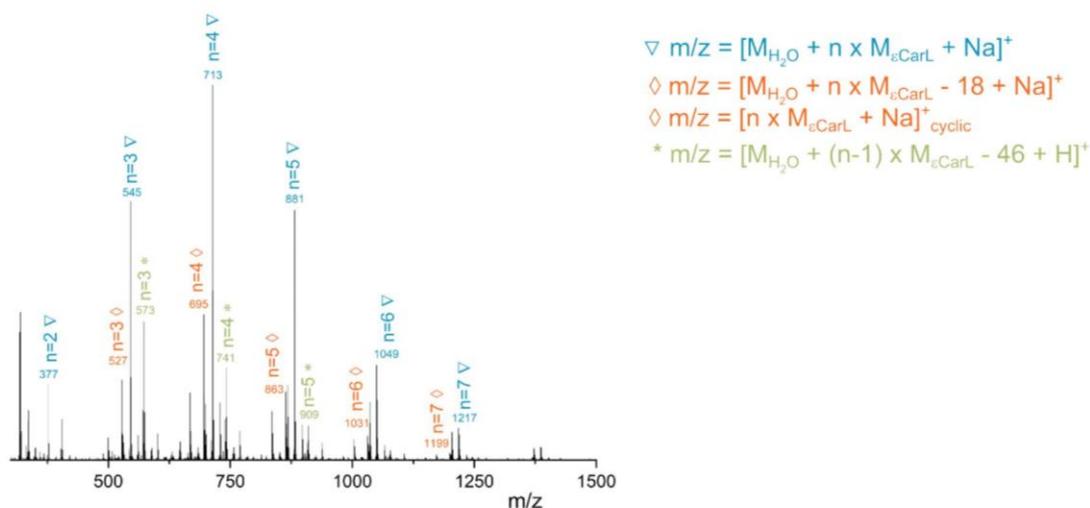
Figure S37: ESI-MS of P(εCarL) oligomers prepared with tin 2-ethylhexanoate SnOct$_2$ (M:Cat = 5:1, toluene, 110 °C, 20 min) and peak assignment.

26
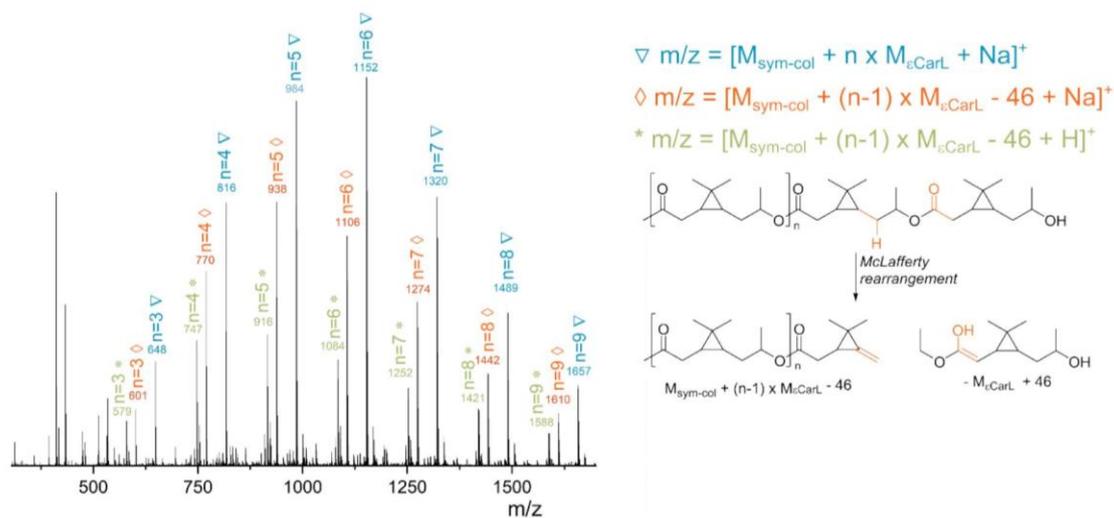
Figure S38: ESI-MS of P(εCarL) oligomers prepared with 2-methoxyethylamino-bisphenolate yttrium catalyst [(ONOO)^{tBu}Y(sym-col)(thf)] (M:Cat = 5:1, toluene, rt, 10 min) and peak assignment.

6. REFERENCES

- 232 -

1   H. C. Brown and A. Suzuki, Hydroboration of Terpenes. IV. Hydroboration of (+)-3-Carene ([UNK] 3 - Carene). Configuration Assignments for the 4-Caranols and 4-Caranones. An Unusual Stability of 4-Isocaranone with a cis Relationship of the Methyl and gem -Dimethyl Groups, *J. Am. Chem. Soc.*, 1967, **89**, 1933–1941.

2   E. Wincza and S. Lochynski, Chemical and microbiological oxidation of (−)-cis-carane-4-one leading to chiral compounds and evaluation of their antifeedant activity, *Arkivoc*, 2012, **2012**, 196–203.

3   G. Y. Ishmuratov, V. A. Vydrina, K. S. Denisova, M. P. Yakovleva, R. R. Gazetdinov, E. M. Vyrypaev and A. G. Tolstikov, Synthesis from (−)-α-Pinene of an Optically Active Macrocyclic Diesterdihydrazide with 2,6-Pyridinedicarboxylic and Adipic Acid Moities, *Chem. Nat. Compd.*, 2017, **53**, 63–65.

4   M. Doumeng, L. Makhlouf, F. Berthet, O. Marsan, K. Delbé, J. Denape and F. Chabert, A comparative study of the crystallinity of polyetheretherketone by using density, DSC, XRD, and Raman spectroscopy techniques, *Polym. Test.*, 2021, **93**, 106878.

Uniting group-transfer and ring-opening polymerization – block copolymers from functional Michael-type monomers and lactones

Moritz Kränzlein[⊥], Thomas M. Pehl[⊥], Friederike Adams[§,~,] and Bernhard Rieger[⊥,*]*

[⊥] WACKER-Chair of Macromolecular Chemistry, Catalysis Research Center, Department of Chemistry, Technical University of Munich, Lichtenbergstr. 4, 85748 Garching (Germany)

[§] Chair of Structure & Properties of Polymeric Materials, Institute of Polymer Chemistry, University of Stuttgart, Pfaffenwaldring 55, 70569 Stuttgart (Germany)

[~] Faculty of Science, Eberhard Karl University of Tübingen, Auf der Morgenstelle 8, 72076 Tübingen (Germany)

Corresponding Authors

* friederike.adams@ipoc.uni-stuttgart.de; rieger@tum.de

1

TABLE OF CONTENTS

1. GENERAL EXPERIMENTAL

All reactions and polymerizations with moisture and air-sensitive reactants were carried out in a MBraun LabMaster120 glovebox filled with argon 4.6 from Westfalen or using standard Schlenk techniques. All glassware was heat-dried prior to use. All chemicals were purchased from Sigma-Aldrich, ABCR, or TCI Europe and used without further purification unless otherwise stated. Dichloromethane, tetrahydrofuran, toluene, and pentane were dried using an MBraun SPS-800 solvent purification system and stored over 3 Å molecular sieve. 2-Vinylpyridine and ε-caprolactone were dried over CaH_2 for several days and distilled prior to use. (-)-Menthide was crystallized from a concentrated solution in dried toluene and was purified via two-fold sublimation for drying and purification. The symmetric 2-methoxyethylaminobisphenol ligand[1], catalyst precursors $Y(CH_2TMS)_3(thf)_2$[2] and $[(ONOO)^{tBu}Y(CH_2TMS)(thf)]$[3], catalysts $[(ONOO)^{tBu}Y(sym\text{-}col)(thf)]$[4] and $[((ONOO)^{tBu}Y(thf))_2(TMPy)]$[5] as well as (-)-menthide[6,7] were prepared according to literature procedures.

NMR spectra were recorded on a Bruker AV-400HD spectrometer. ^{1}H (400 MHz), ^{13}C (125 MHz) and ^{31}P (162 MHz). NMR spectroscopical shifts δ were reported in ppm relative to the residual proton or carbon signal of the deuterated solvent. Deuterated solvents ($CDCl_3$, benzene-d_6) were purchased from Sigma-Aldrich or Deutero and dried over 3 Å molecular sieves prior to use. DOSY NMR spectra (RT, 16 scans) were transformed with MestreNova software using the Bayesian DOSY Transform with a resolution factor of 5.00 and 5 repetitions, adapting the minimum and maximum according to the sample and with 128 points in diffusion dimension. Molecular weights and polydispersity of the polymers were determined by triple detection using two-angle light scattering at 15 ° and 90 ° coupled with a viscometer and a refractive index detector in N,N-dimethylformamide with 25 mmol/L LiBr as eluent at 30 °C on a Agilent GPC50 equipped

3

with two Agilent PolarGel-M columns; for absolute molecular weight (triple detection) determination of pure P2VP aliquots and homopolymers, the refractive index increment of P2VP (dn/dc = 0.149 mL/g)[8] was used. For relative molecular weight (single detection) determination, poly(methyl methacrylate) calibration standards were used. Lyophilization was performed on a VaCO 5-II-D at a pressure of 2 mbar and -90 °C condenser temperature from either 1,4-dioxane or benzene. Elemental analysis was performed by the Laboratory of Microanalytics at the Institute of Inorganic Chemistry at the Technical University of Munich, Department of Chemistry, Catalysis Research Center. Dynamic light scattering was performed using a Malvern Zetasizer Nano ZS in Millipore water with adjusted pH values (prepared by addition of 0.1 M HCl) and a polymer concentration of 0.5 mg/mL, each sample is filtered using a 0.45 μm PTFE syringe filter. Each sample was measured three times with 12 measurement points and the micelle diameter was averaged. Dynamic scanning calorimetry (DSC) was performed on a DSC Q2000 from TA instruments in exo-down mode with a heat rate of 10 K/min in a temperature range of -150 – 240 °C with 2 – 10 mg sample. Three cycles were recorded and the transition temperatures were determined from the third cycle (heating, cooling, heating) using TA Universal Analysis. Powder X-Ray diffraction measurements were performed on a *PANalytical Empyrean* diffractometer in Bragg-Brentano geometry equipped with a *PANalytical PIXcel 1D* detector. For the measurements, Cu K$_\alpha$ radiation with a voltage of 45 kV and an intensity of 40 mA is used with λ_1 = 1.5406 Å and λ_1 = 1.5444 Å (I$_1$/I$_2$ = 0.5) in the range of 5 ° to 60 ° (2Θ). Obtained data was processed using *TopSpin* Software by *Malvern Panalytical*, stripping Cu K$_\alpha$ using *Rachingers* method and background determination was done using the *Sonneveld* and *Visser* method. The data is normalized for comparison reasons. Electrospray Ionization Mass Spectrometry (ESI-MS) was

4

measured using a Thermo Fisher Scientific Exactive Plus Orbitrap in positive mode in HPLC acetonitrile straight from the reaction mixture without quenching.

2. GENERAL COPOLYMERIZATION PROCEDURE

For the copolymerization of 2VP and CL, 13.5 µmol catalyst **2** or **3** were dissolved in 4 mL dichloromethane. 2VP was added and the polymerization was stirred at room temperature for 60 – 90 min. 0.1 mL as aliquot was removed from the mixture and quenched by addition of 0.3 mL wet CDCl$_3$. The respective amount of CL relative to 2VP was added immediately and the polymerization was stirred for additional 60 min. Afterwards, another 0.1 mL aliquot was withdrawn and quenched with wet CDCl$_3$ before adding 0.5 mL ethanol to the polymerization mixture quenching the reaction. The polymer was precipitated from 50 mL pentane, centrifuged, the solution was decanted off and the residual polymer was freeze-dried from 1,4-dioxane or benzene. The aliquots were subjected to ^{1}H-NMR spectroscopy to determine the conversions of 2VP and CL and SEC analysis to determine the absolute molecular weight and polydispersity of the P2VP block as well as the relative molecular weight and the polydispersity of the copolymer.

For the copolymerization of 2VP and M, 6.75 µmol catalyst **2** or **3** were dissolved in 2 mL toluene. 2VP was added and the polymerization was stirred at room temperature for 90 – 120 min. 0.1 mL as aliquot was removed from the mixture and quenched by addition of 0.3 mL wet CDCl$_3$. The respective amount of M relative to 2VP was added immediately and the polymerization was stirred for additional 48 hours. Afterwards, another 0.1 mL aliquot was withdrawn and quenched with wet CDCl$_3$ before adding 0.5 mL ethanol to the polymerization mixture quenching the reaction. The polymer was precipitated from 50 mL pentane, centrifuged, the solution was decanted off and the residual polymer is dried at 60 °C under vacuum overnight. The aliquots were subject to ^{1}H-NMR spectroscopy to determine the conversions of 2VP and M and SEC analysis to determine the

5

absolute molecular weight and polydispersity of the P2VP block as well as the relative molecular weight and the polydispersity of the copolymer.

Slight variation from the given general procedure and exact reaction parameters can be found in Table S1 and S2.

3. ACTIVITY MEASUREMENTS

20.5 µmol of catalyst **2** was dissolved in 6 mL toluene and the polymerization was started by addition of 4.07 mmol 2VP while stirring at room temperature. In regular intervals, aliquots of 0.1 mL were removed, quenched by addition of wet $CDCl_3$ and subject to ^{1}H-NMR and SEC analysis revealing the corresponding conversion, molecular weight, and polydispersity. After the polymerization of 2VP was completed, remaining amount of reaction solution was determined by weighing. The polymerization mixture was heated to 70 °C and an equimolar amount of (-)-menthide (2.53 mmol) was added. Again, in regular intervals 0.1 mL aliquots were withdrawn and subjected to ^{1}H-NMR and SEC analysis. Turnover frequencies TOF $[h^{-1}]$ for both polymerizations were determined as steepest slope of conversion over time. The normalized turnover frequency for the P2VP block was determined using $TOF^* = TOF/I.E.$ with initiator efficiency $I.E. = M_{n,theo}/M_{n,abs}$ and $M_{n,abs}$ from the last P2VP aliquot. For the PM block, the calculated theoretical molecular weight using the initiator efficiency from block A and assuming 100% initiation efficiency of the P2VP macroinitiator in the (-)-menthide copolymerization is in good correspondence to the actual number of repeating units observed via NMR spectroscopy. In this case the normalized turnover frequency for M copolymerization corresponds to $TOF^* = TOF$.

6

4. BLOCK COPOLYMERIZATION OF 2VP WITH CL

Table S1: Block copolymerization conditions for 2VP-CL copolymerization synthesized with the monometallic yttrium catalyst **2** (diblock copolymers AB^X) and the bimetallic yttrium catalyst **3** (triblock copolymers BAB^X).

Entry [a]	Feed [Y]/[2VP]/[CL]	Solvent	V_R [b] [mL]	$t_{R,2VP}$ [min]	X_{2VP} [c] [%]	$M_{n,theo,2VP}$ [d] [kg/mol]	I.E. [e] [%]	$t_{R,CL}$ [min]	X_{CL} [f] [%]
AB^1	1/100/100	CH$_2$Cl$_2$	3	60	96	7.7	63	60	98
AB^2	1/200/200	CH$_2$Cl$_2$	3.5	60	96	21.2	74	60	98
AB^3	1/400/400	CH$_2$Cl$_2$	7	120	87	78.8	48	60	97
AB^4	1/300/100	CH$_2$Cl$_2$	4	60	85	27.7	47	60	96
AB^5	1/100/300	CH$_2$Cl$_2$	4	60	84	7.5	55	90	98
AB^6	1/200/200	thf	4	90	19	3.8	21	60	96
AB^7	1/200/200	toluene	4	75	83	20.6	57	60	99
A^1	1/200/0	CH$_2$Cl$_2$	4	60	95	21.2	60	-	-
B^1	1/0/200	CH$_2$Cl$_2$	4	-	-	-	-	20	98
BAB^1	2/100/100	CH$_2$Cl$_2$	4	60	99	11.8	98	60	97
BAB^2	2/200/200	CH$_2$Cl$_2$	4	60	99	20.3	84	60	98
BAB^3	2/400/400	CH$_2$Cl$_2$	7	75	93	39.3	69	60	98
BAB^4	2/300/100	CH$_2$Cl$_2$	4	120	99	45.9	59	60	97
BAB^5	2/100/300	CH$_2$Cl$_2$	4	75	99	9.3	66	60	98

[a] AB^X polymers using monometallic catalyst **2**, BAB^X polymers using bimetallic catalyst **3**, catalyst-monomer ratios, 13.5 μmol catalyst, RT, [b] reaction volume for copolymerization, [c] conversion of 2-vinylpyridine determined via aliquot-^{1}H-NMR [d] theoretical molecular weight $M_{n,theo} = (M_{2VP} \times [2VP]/[Y] \times X_{2VP})$, [e] initiator efficiency determined via I.E. $= M_{n,theo,2VP}/M_{n,abs,2VP}$, [f] caprolactone conversion determined via aliquot-^{1}H-NMR integration of the CH$_2$-group in α-position of the ester.

7
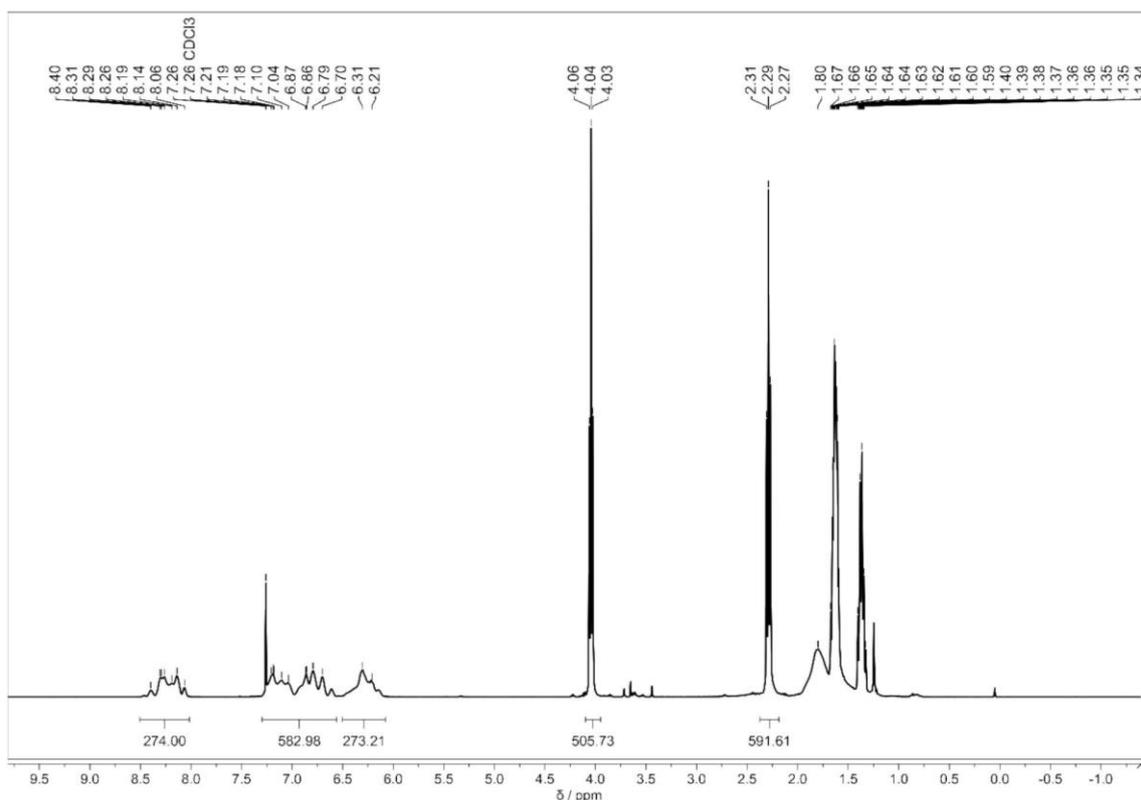
Figure S1: Exemplary ^{1}H-NMR spectrum in CDCl$_3$ from P2VP-*b*-PCL (AB^1, $M_{n,NMR,AB}$ = 57.7 kg/mol, 2VP:CL = 50:50, Đ = 1.46, Table 1, entry 1).

For the calculation of the molecular ratios of 2VP to CL in the copolymer, the integral I$_{2VP}$ (δ = 8.06 – 8.40 ppm) of the proton signal in α-position of the nitrogen atom in the 2VP ring and the integral of the CH$_2$-group signal adjacent to the ester unit I$_{CL}$ (δ = 4.04 ppm) were determined. The ratio of 2VP to CL was then calculated as %$_{2VP}$ = I$_{2VP}$/(I$_{2VP}$+0.5·I$_{CL}$), this method is applicable for both AB and BAB type copolymers. Accordingly, the ratio of CL to 2VP is calculated as %$_{CL}$ = 0.5·I$_{CL}$/(I$_{2VP}$+0.5·I$_{CL}$). The absolute molecular weight of the copolymer is calculated from absolute SEC of the P2VP aliquot and the P2VP:PCL ratio derived from the ^{1}H-NMR spectrum.

8
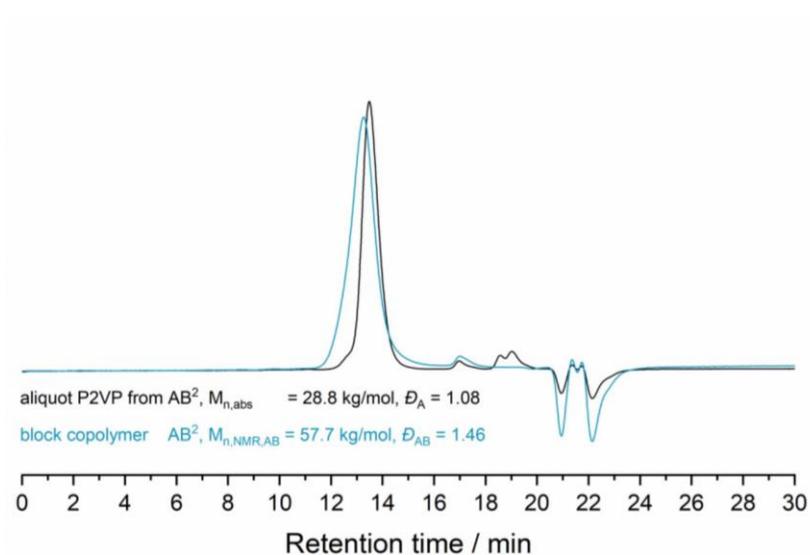
Figure S2: SEC traces from P2VP aliquot (black) and isolated P2VP-*b*-PCL AB diblock copolymer (blue) for AB^2 (Table 1, entry 2).
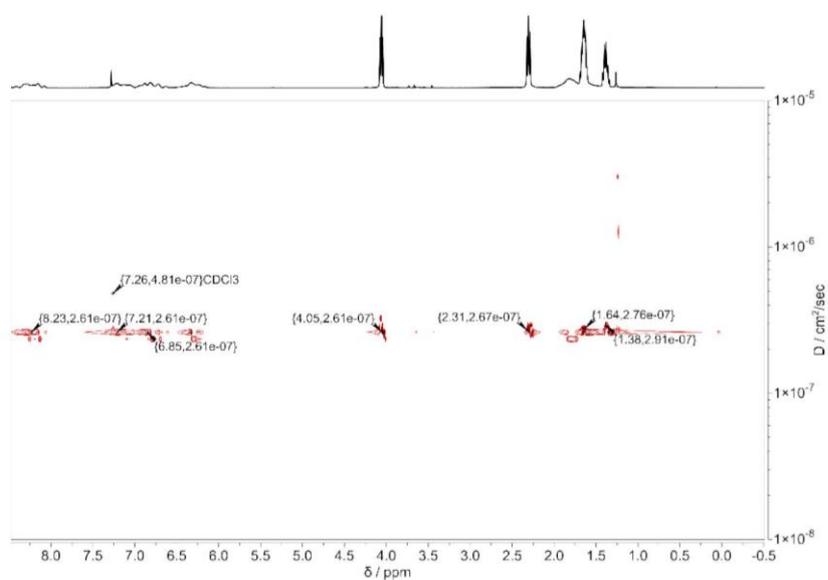
Figure S3: DOSY-NMR in CDCl$_3$ (bottom) for AB^2 (Table 1, entry 2).

9
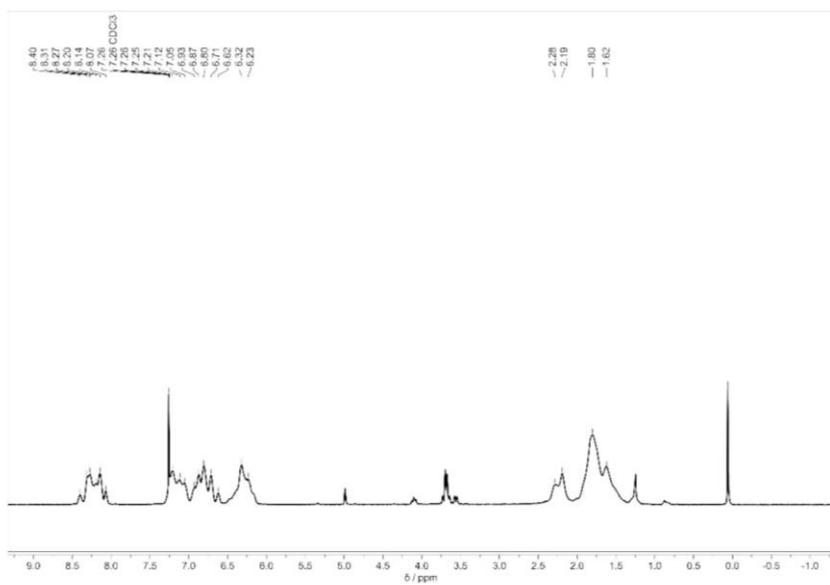
Figure S4: ¹H-NMR spectrum in CDCl₃ of P2VP homopolymer A¹ (Table 1, entry 8).
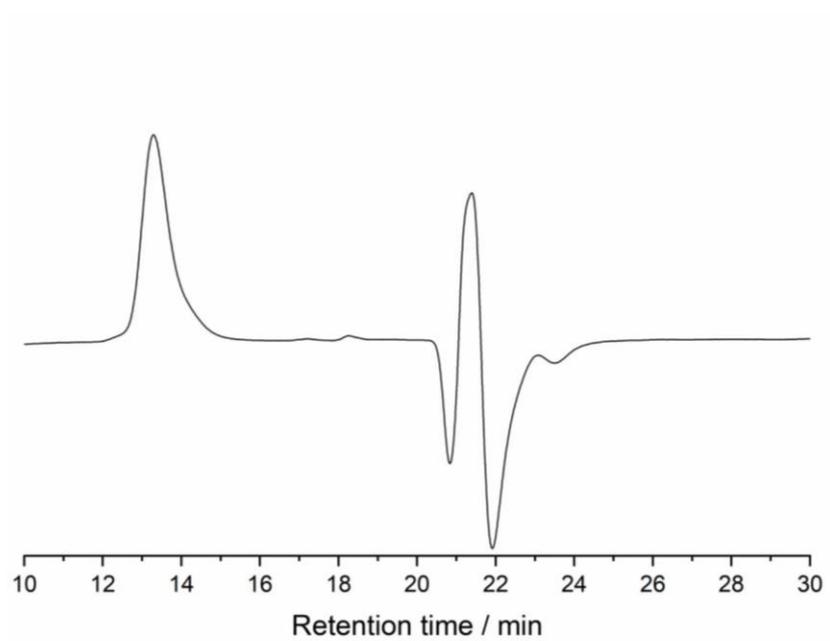
Figure S5: SEC trace of P2VP homopolymer A¹ (Table 1, entry 8).

10
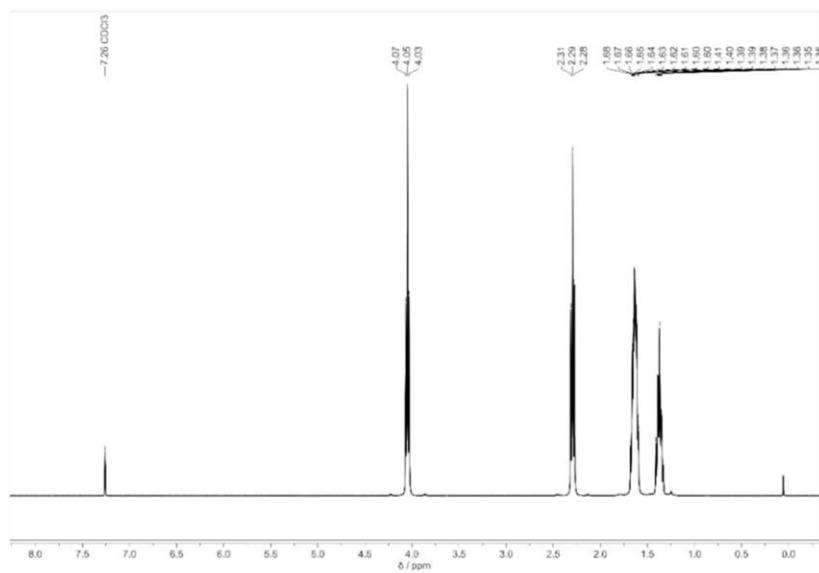
Figure S6: ^{1}H-NMR spectrum in CDCl$_3$ of PCL homopolymer B[1] (Table 1, entry 9).
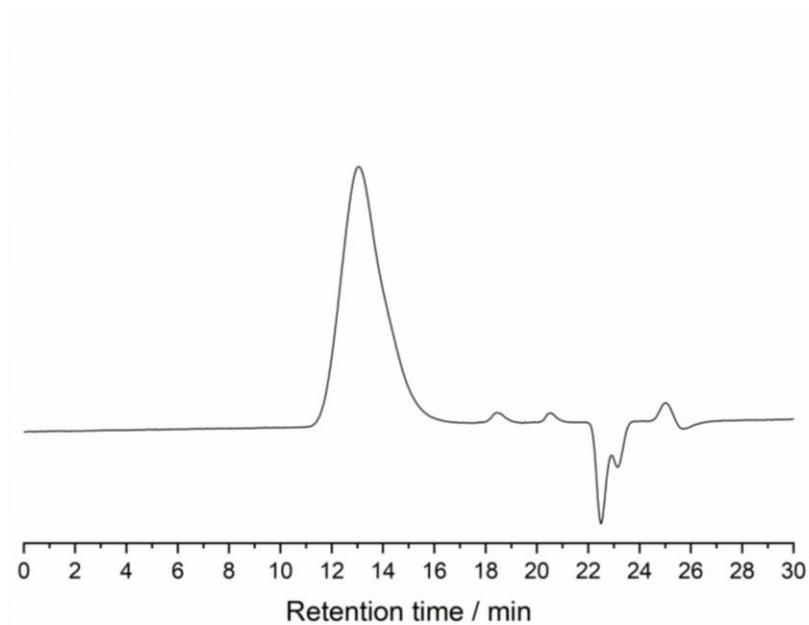
Figure S7: SEC trace of PCL homopolymer B[1] (Table 1, entry 9).

11
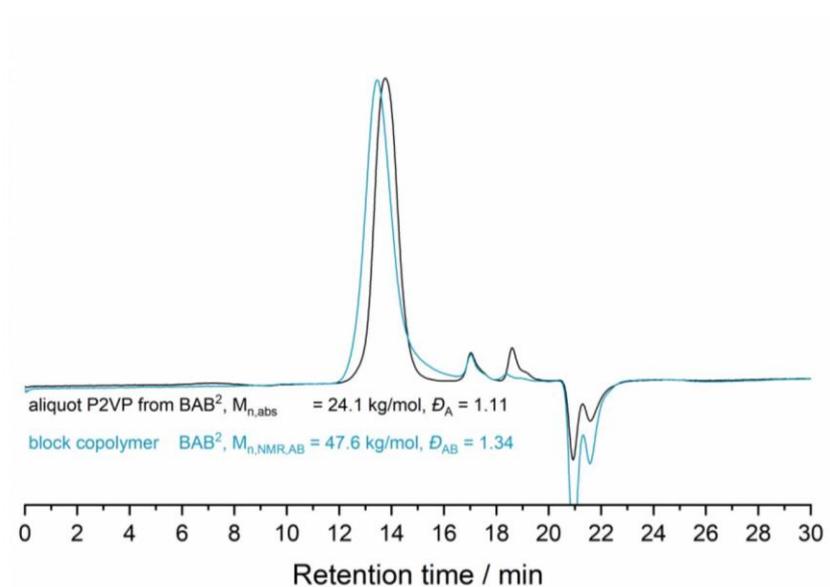
Figure S8: SEC traces of P2VP aliquot (black) and isolated P2VP-*b*-PCL triblock copolymer BAB^2 (blue) (Table 1, entry 10).
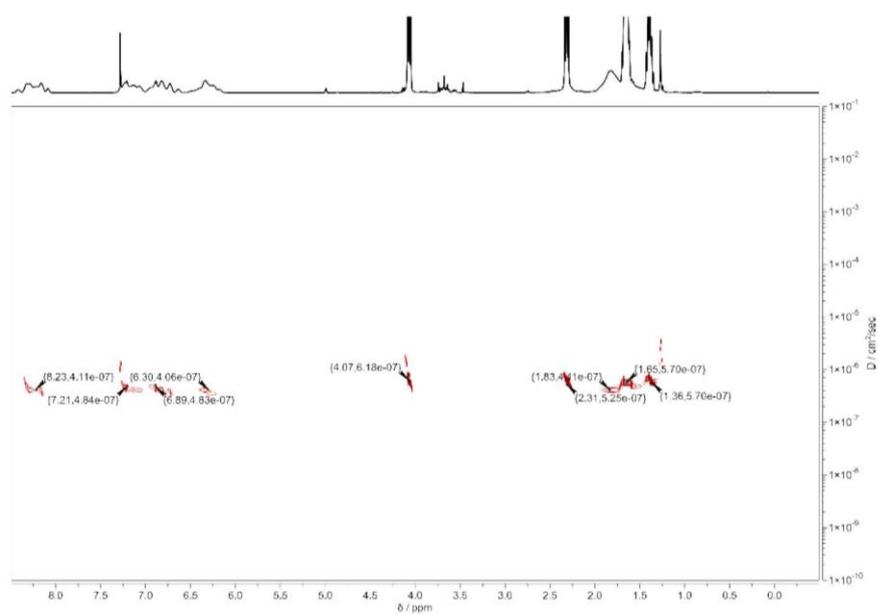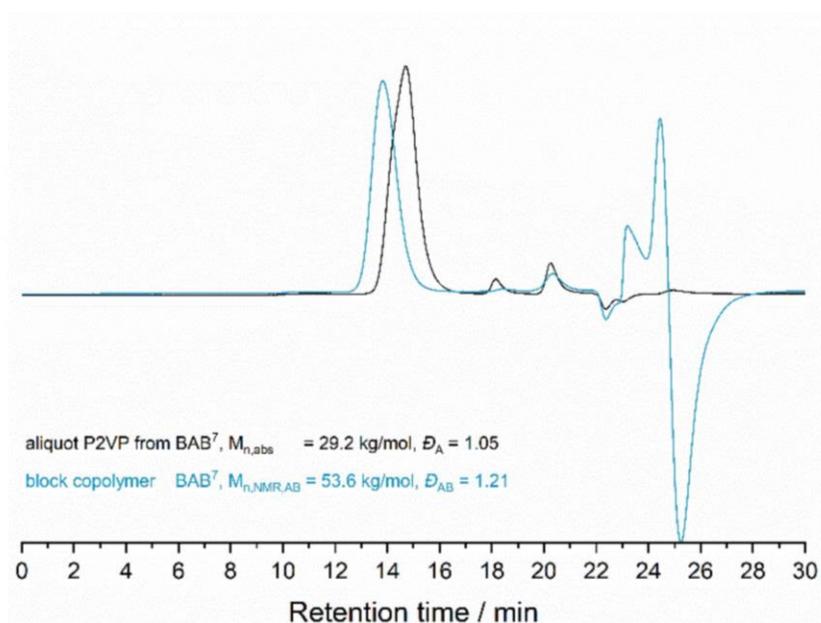

Figure S9: DOSY-NMR spectrum in CDCl$_3$ (bottom) of BAB^2 (Table 1, entry 10).

12
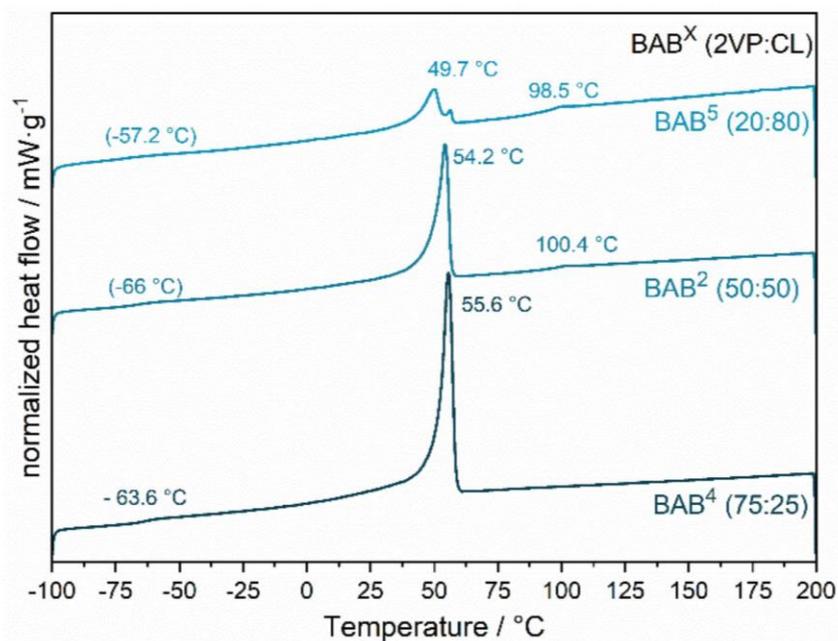
Figure S10: DSC measurements for triblock copolymers BAB[2], BAB[4] and BAB[5] (Table 1, entries 10, 13, 14).
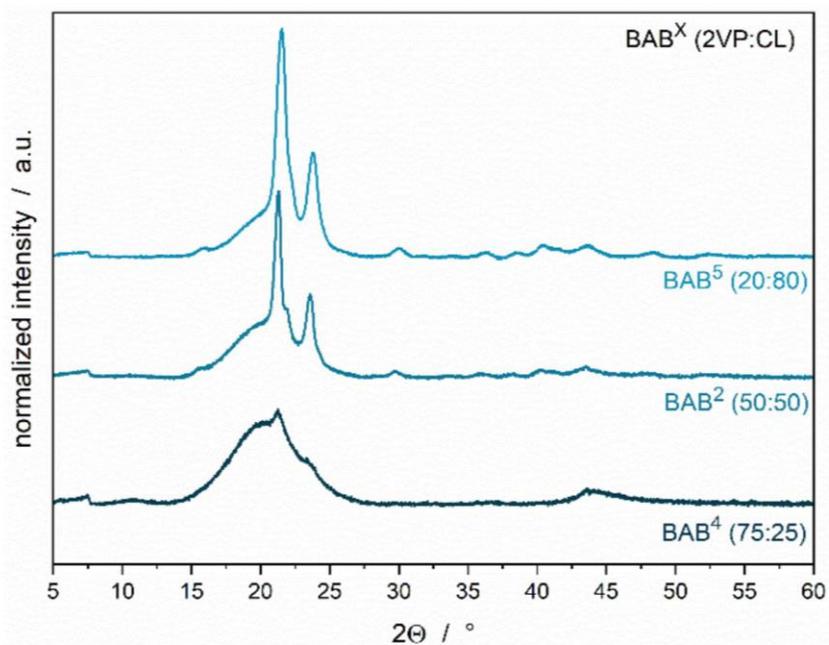
Figure S11: pXRD measurements for triblock copolymers BAB[2], BAB[4] and BAB[5] (Table 1, entries 10, 13, 14).

13

5. BLOCK COPOLYMERIZATION OF 2VP WITH M

Table S2: Block copolymerization conditions for 2VP-M copolymerization synthesized with the monometallic yttrium catalyst **2** (diblock copolymers AB^X) and the bimetallic yttrium catalyst **3** (triblock copolymers BAB^X).

Entry [a]	Feed [Y]/[2VP]/[CL]	Solvent	V_R [b] [mL]	$t_{R,2VP}$ [min]	X_{2VP} [c] [%]	$M_{n,theo,2VP}$ [d] [kg/mol]	I.E. [e] [%]	$t_{R,M}$ [h]	X_M [f] [%]
AB^8	1/100/100	toluene	2	90	93	9.8	51	48	62
AB^9	1/200/200	toluene	2	90	95	17.0	58	48	65
AB^{10}	1/400/400	toluene	1.5 [g]	120	94	46.1	50	48	4
AB^{11}	1/100/300	toluene	2	90	95	14.2	70	48	30
AB^{12}	1/300/100	toluene	2	90	91	31.5	57	48	65
BAB^6	2/100/100	toluene	2	90	99	13.1	76	48	78
BAB^7	2/200/200	toluene	2	90	99	24.0	82	48	83
BAB^8	2/400/400	toluene	1.5 [g]	90	99	42.3	71	48	80
BAB^9	2/100/300	toluene	2	90	98	13.1	73	48	80
BAB^{10}	1/300/100	toluene	2	90	99	33.8	71	48	70

[a] AB^X polymers using monometallic catalyst **2**, BAB^X polymers using bimetallic catalyst **3**, catalyst-monomer ratios, 6.75 µmol catalyst, [b] reaction volume for copolymerization, [c] conversion of 2-vinylpyridine determined via aliquot-^{1}H-NMR [d] theoretical molecular weight $M_{n,theo} = (M_{2VP} \times [2VP]/[Y] \times X_{2VP})$, [e] initiator efficiency determined via I.E. $= M_{n,theo,2VP}/M_{n,abs,2VP}$, [f] menthide conversion determined via aliquot-^{1}H-NMR integration of the methine protons, [g] 0.75-fold experiment.

14

- 246 -
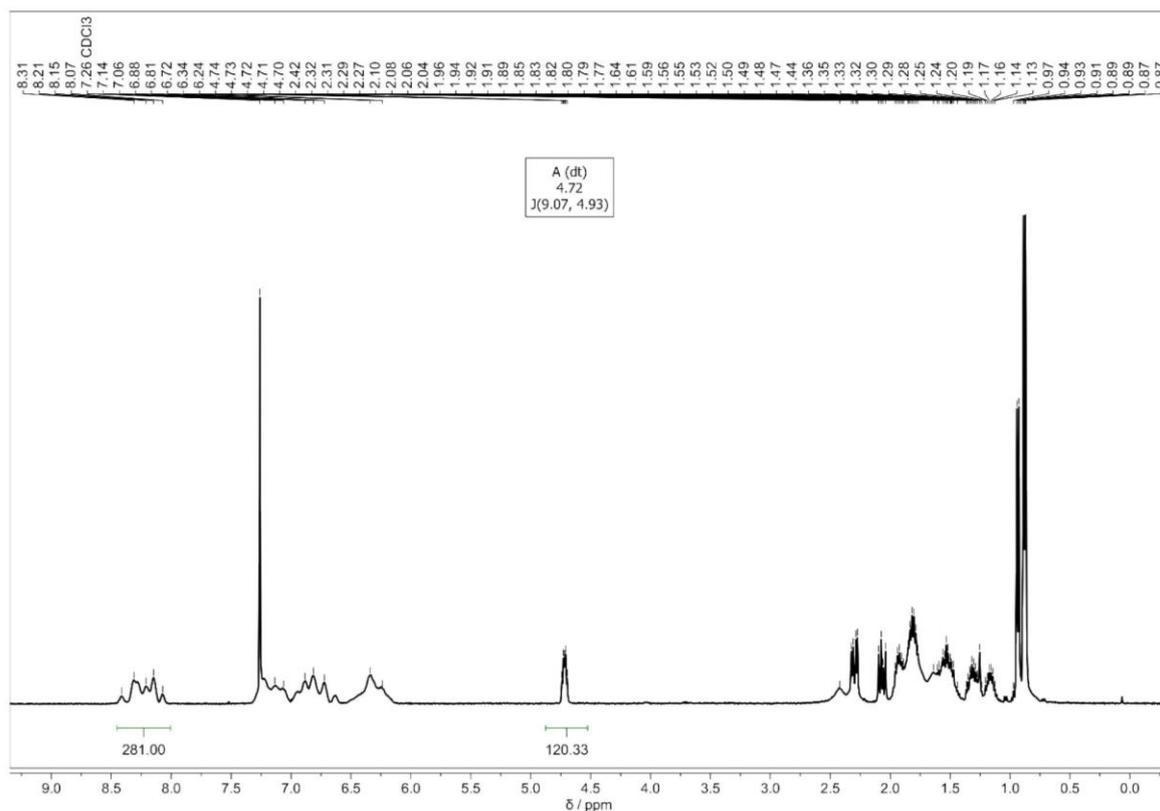
Figure S12: Exemplary ^{1}H-NMR spectrum in CDCl$_3$ from P2VP-*b*-PM AB[9] (M$_{n,NMR,AB}$ = 50.0 kg/mol, Đ$_{AB}$ = 1.14, 2VP:M = 75:25, Table 2, entry 2).

For the calculation of the molecular ratios of 2VP to M in the copolymer, the integral I$_{2VP}$ (δ = 8.06 – 8.40 ppm) of the proton signal in α-position of the nitrogen atom in the 2VP ring and the integral of the CH-group signal adjacent to the ester unit I$_M$ (δ = 4.04 ppm) were determined. The ratio of 2VP to M is then calculated as %$_{2VP}$ = I$_{2VP}$/(I$_{2VP}$+I$_M$), this method is applicable for both AB and BAB type copolymers. Accordingly, the ratio of M to 2VP is calculated as %$_M$ = I$_M$/(I$_{2VP}$+I$_M$) The absolute molecular weight of the copolymer is calculated from absolute SEC of the P2VP aliquot and the P2VP:PM ratio derived from the ^{1}H-NMR spectrum.
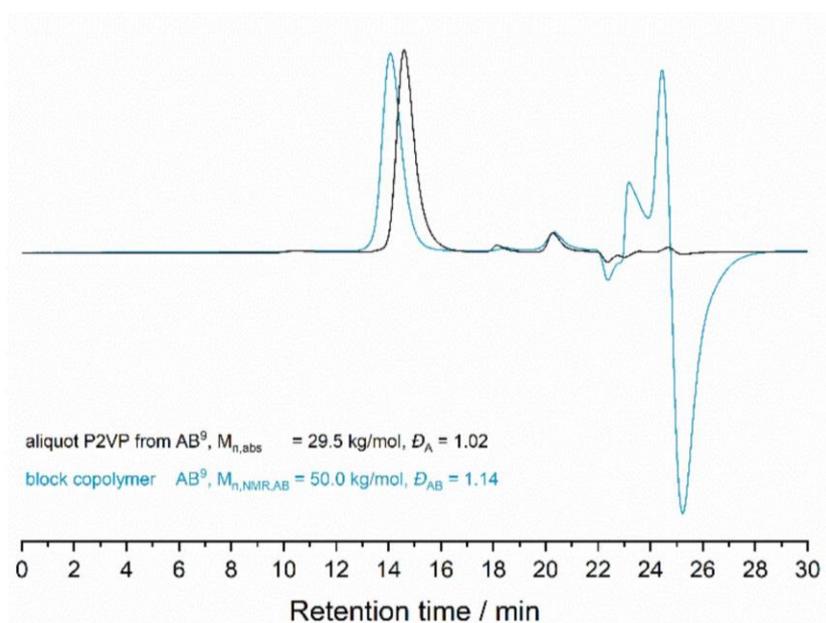
Figure S13: SEC traces of from P2VP aliquot (black) and isolated P2VP-*b*-PM diblock copolymer

AB[9] (blue) (Table 2, entry 2).
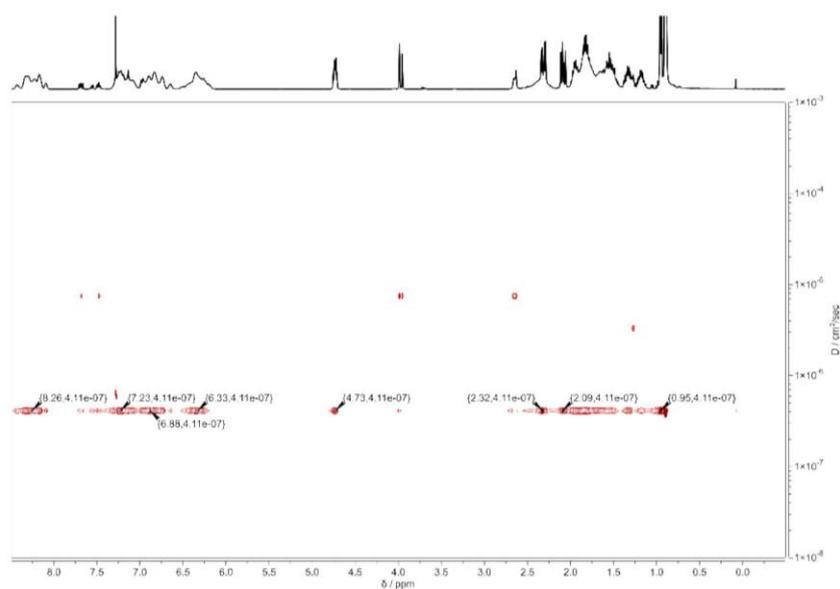
Figure S14: DOSY-NMR spectrum in CDCl$_3$ (bottom) of AB[9] (Table 2, entry 2).

16

Figure S15: SEC traces of from P2VP aliquot (black) and isolated P2VP-*b*-PM triblock copolymer

BAB[7] (blue) (Table 2, entry 7).
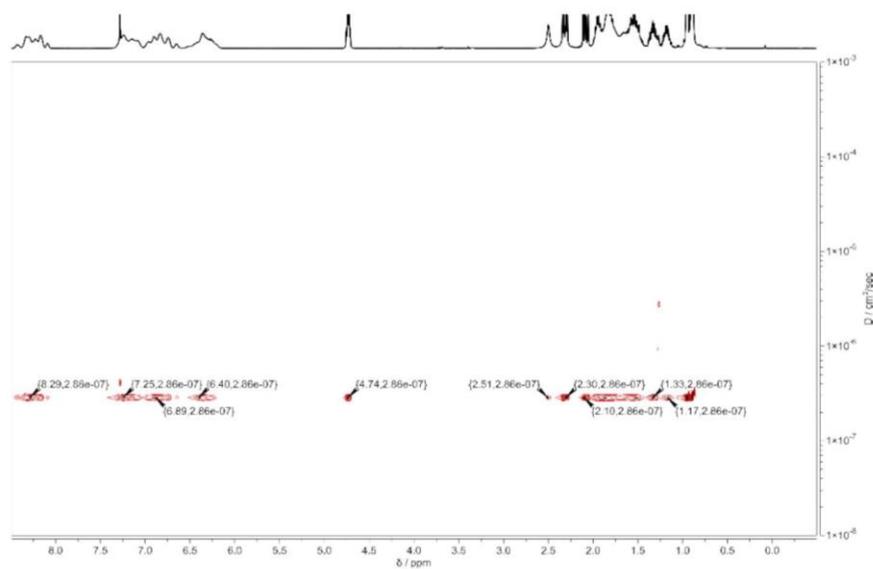
Figure S16: DOSY-NMR spectrum in CDCl$_3$ (bottom) of BAB[7] (Table 2, entry 7).

17
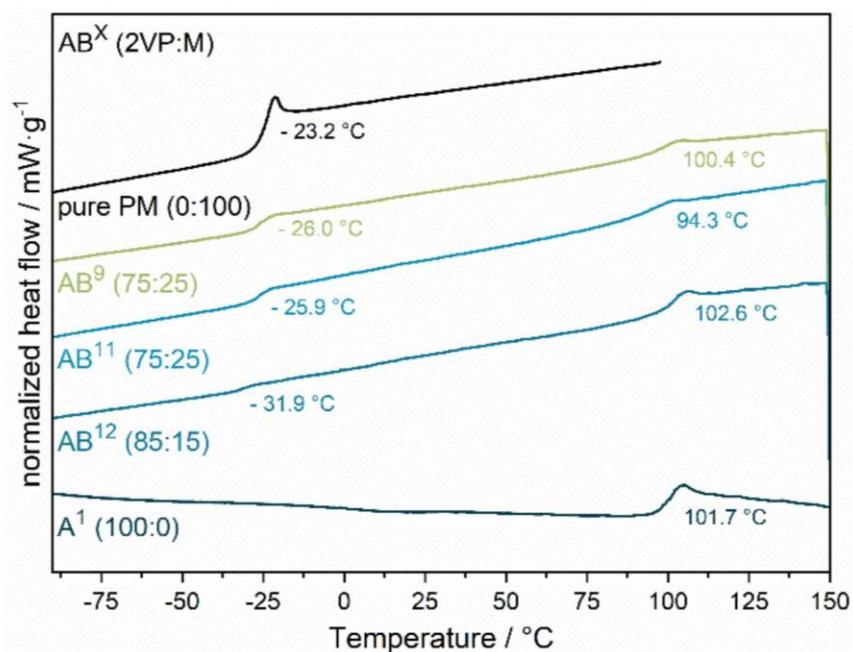
Figure S17: DSC measurements of AB block copolymers AB[9], AB[11], AB[12] and A[1] (Table 2, entries 2, 4 and 5; Table 1, entry 1).
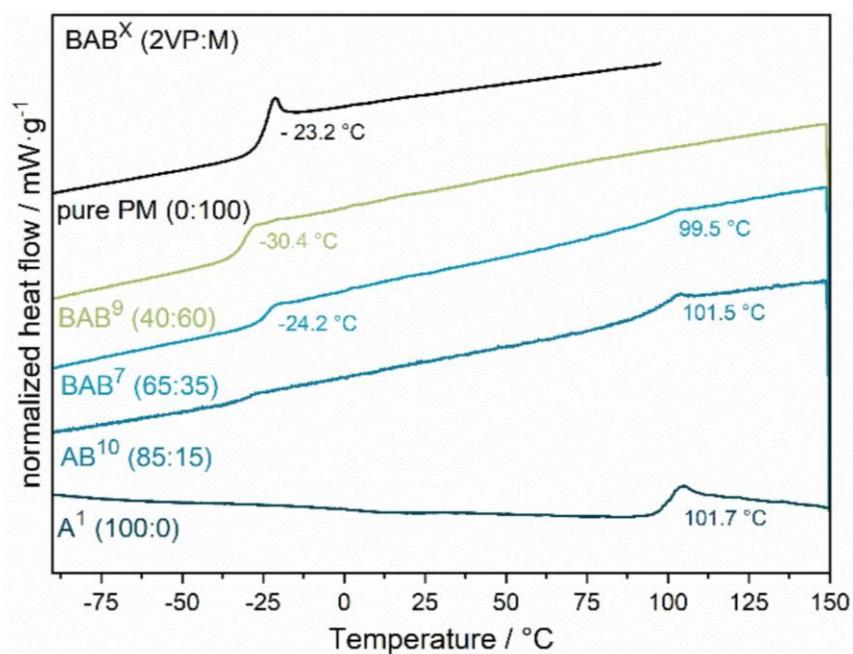
Figure S18: DSC measurements of BAB block copolymers BAB[7], BAB[9] and BAB[10] and A[1] (Table 2, entries 7, 9 and 10; Table 1, entry 1).

18

6. ADDITIONAL MECHANISTIC DETAILS
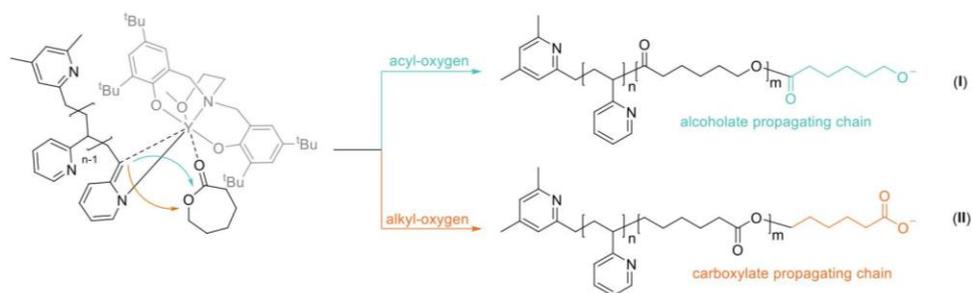
Figure S19: Initiation pathways of lactone ring-opening by a stabilized aza enolate as active initiator of the P2VP chain coordinated to complex **2** via (I) acyl-oxygen cleavage with alkoxide chain-end or (II) alkyl-oxygen cleavage with a carboxylate chain-end.[9–11]

19

7. ^{31}P-NMR END-CAPPING

For the phosphorus end-capping experiment, 7.4 µmol of catalyst **2** were dissolved in 1 mL C$_6$D$_6$ and 20-40 eq. of 2VP were added. The reaction mixture was stirred for 40 min before an equimolar amount of the respective lactone was added. For CL, the reaction mixture was stirred for an additional minute before an excess of chlorodiphenylphosphine oxide was added and the mixture was stirred over night at 70 °C. For M, the reaction mixture was stirred for additional 180 min at 70 °C before an excess of chlorodiphenylphosphine oxide was added and the mixture was stirred over night at 70 °C. From each experiment, ^{31}P-NMR was measured, and the chemical shifts were assigned to the formed corresponding phosphorus species.

20
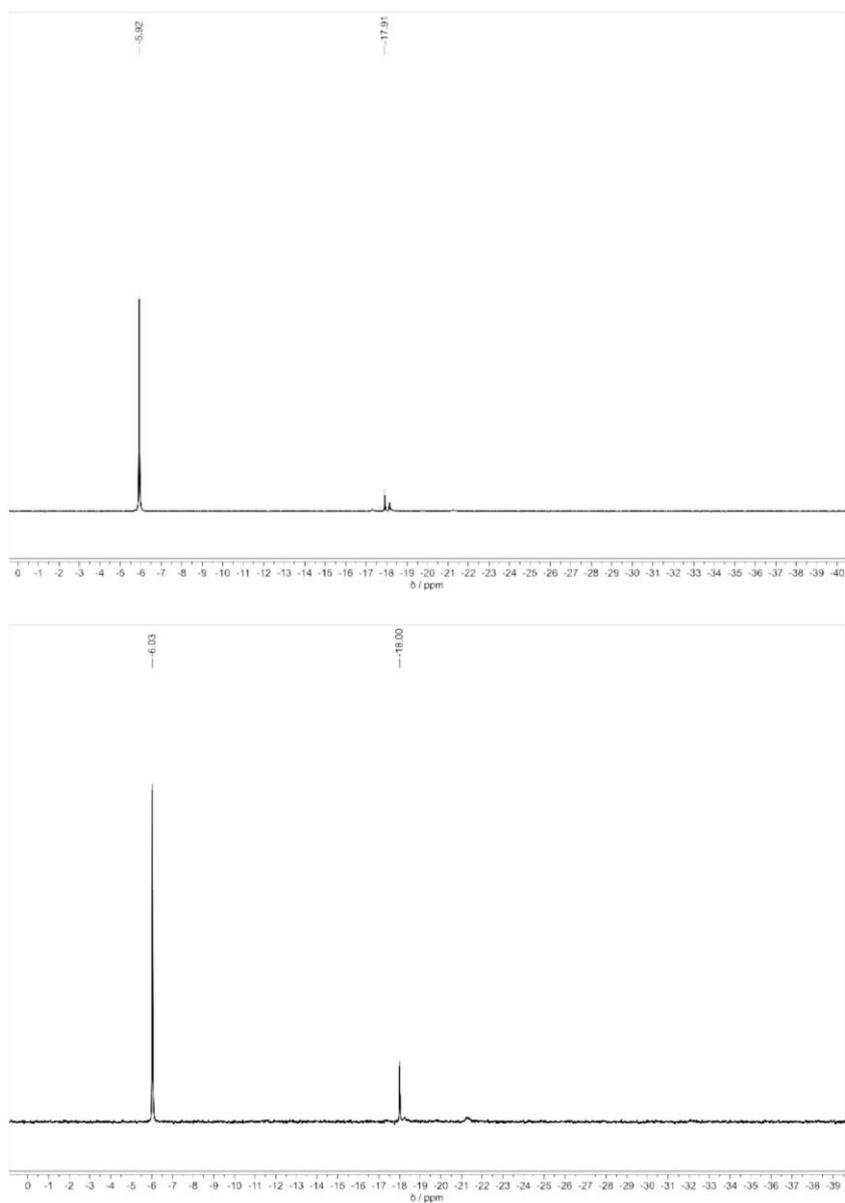
Figure S20: ^{31}P-NMR spectra in C_6D_6 from phosphorus end-capping experiments of P2VP-*b*-PCL (top) and P2VP-*b*-PM (bottom).

21

8. ESI-MS MEASUREMENTS OF COPOLYMERS

For obtaining oligomers for ESI-MS analysis, 27.0 µmol of catalyst **2** were dissolved in 0.6 mL dichloromethane and 135 µmol (5 eq.) 2VP in 0.5 mL dichloromethane were added. The reaction mixture was stirred for 30 min before 54 µmol (2 eq.) CL in 0.5 mL dichloromethane were added. After additional 10 min of reaction time, the resulting solution was diluted in acetonitrile (concentration of 100 µg analyte per 1 mL solvent) and ESI-MS (positive ionization) was measured.

Peak assignment

Δ: [TMPy + CL + n x 2VP - 18] + Na⁺
◊: [TMPy + 3 x CL + m x 2VP - 18] + Na⁺
or [TMPy + CL + (m+2) x 2VP] + Na⁺
○: [TMPy + 4 x CL + p x 2VP - 18] + Na⁺
or [TMPy + 2 x CL + (p+2) x 2VP] + Na⁺
∫: [TMPy + 5 x CL + q x 2VP - 18] + Na⁺
or [TMPy + 3 x CL + (q+2) x 2VP] + Na⁺

$: [TMPy + 4 x CL + r x 2VP - 18 - H + Na] + Na⁺
or [TMPy + 2 x CL + (r+2) x 2VP - H + Na] + Na⁺
□: [TMPy + 5 x CL + s x 2VP - 18 - H + Na] + Na⁺
or [TMPy + 3 x CL + (s+2) x 2VP - 18 - H + Na] + Na⁺
√: [TMPy + 2 x CL + t x 2VP - 2 x 18] + Na⁺
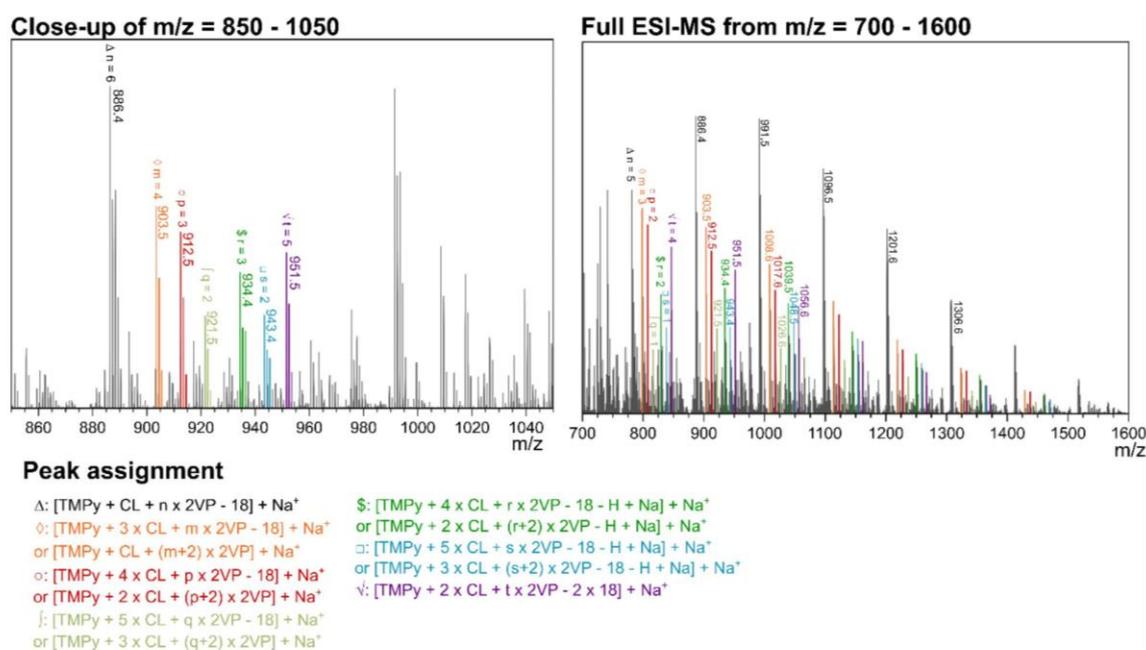
Figure S21: ESI-MS analysis and peak assignment for P2VP-*b*-PCL oligomers prepared with catalyst **3**.

22

9. FULL SEC-CHARACTERIZATION OF P2VP-*B*-PCL AB-BLOCK COPOLYMERS
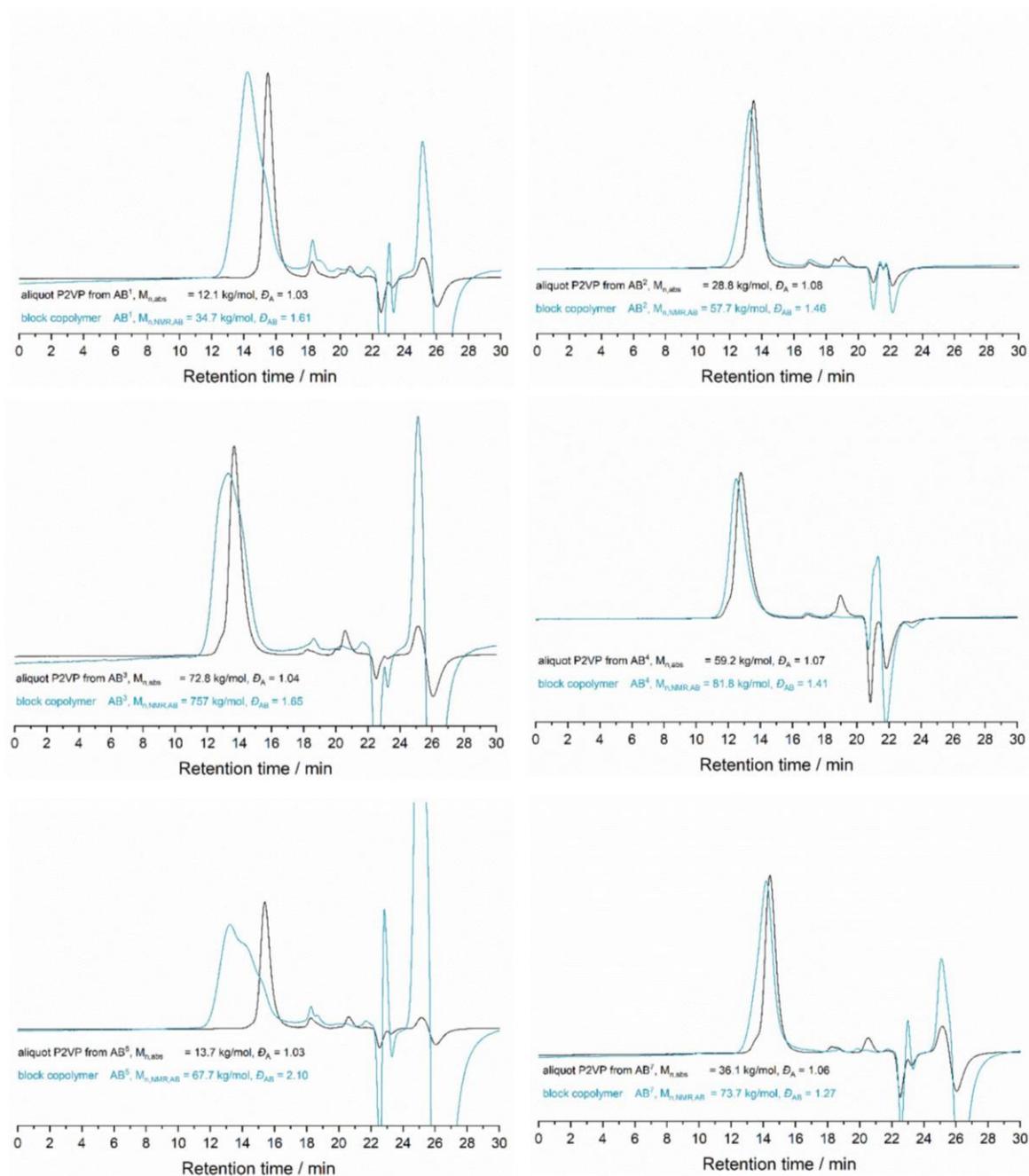
Figure S22: Additional stacked SEC traces of P2VP aliquot (black) and isolated P2VP-*b*-PCL diblock copolymers (blue) AB[1], AB[2], AB[3], AB[4], AB[5] and AB[7] (Table 1, entries 1-5, 7).

23

10. FULL SEC-CHARACTERIZATION OF P2VP-B-PCL BAB-BLOCK COPOLYMERS
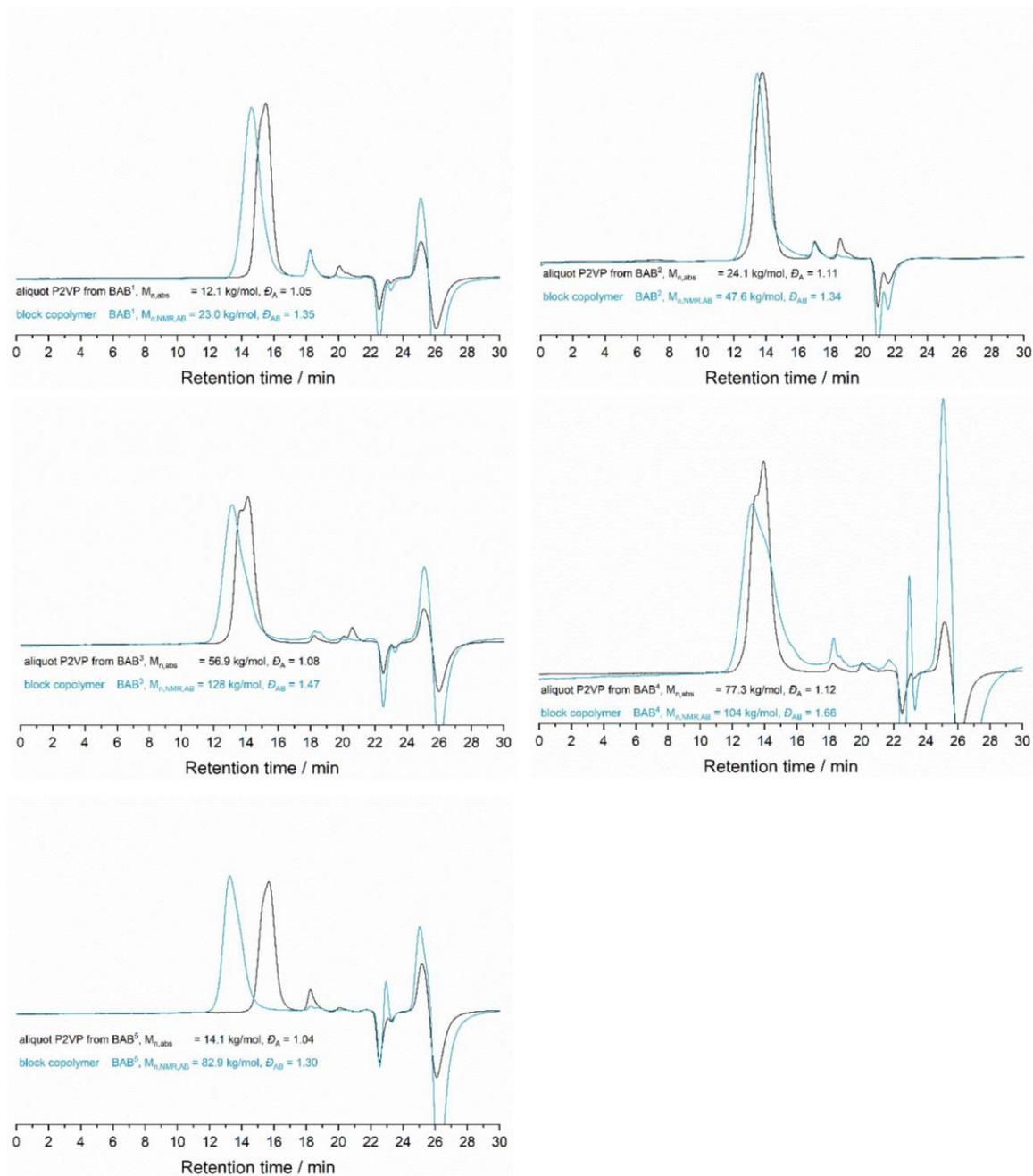
Figure S23: Additional stacked SEC traces of P2VP aliquot (black) and isolated P2VP-*b*-PCL triblock copolymers (blue) BAB[1], BAB[2], BAB[3], BAB[4] and BAB[5] (Table 1, entries 10-14).

24

11. FULL SEC-CHARACTERIZATION OF P2VP-*B*-PM AB-BLOCK COPOLYMERS
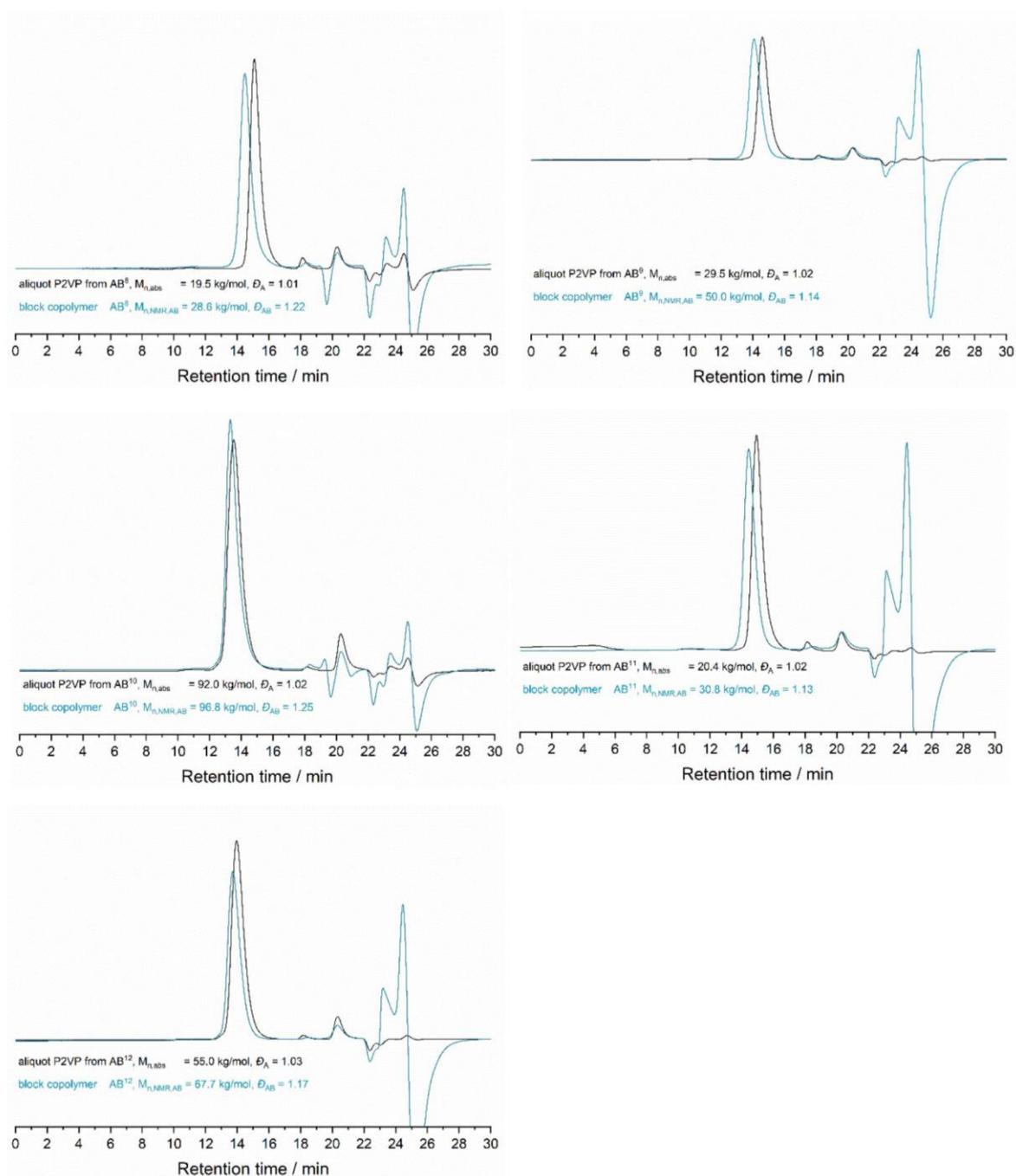
Figure S24: Additional stacked SEC traces of P2VP aliquot (black) and isolated P2VP-*b*-PM diblock copolymers (blue) AB[8], AB[9], AB[10], AB[11] and AB[12] (Table 2, entries 1-5).

25

12. FULL SEC-CHARACTERIZATION OF P2VP-*B*-PM BAB-BLOCK COPOLYMERS
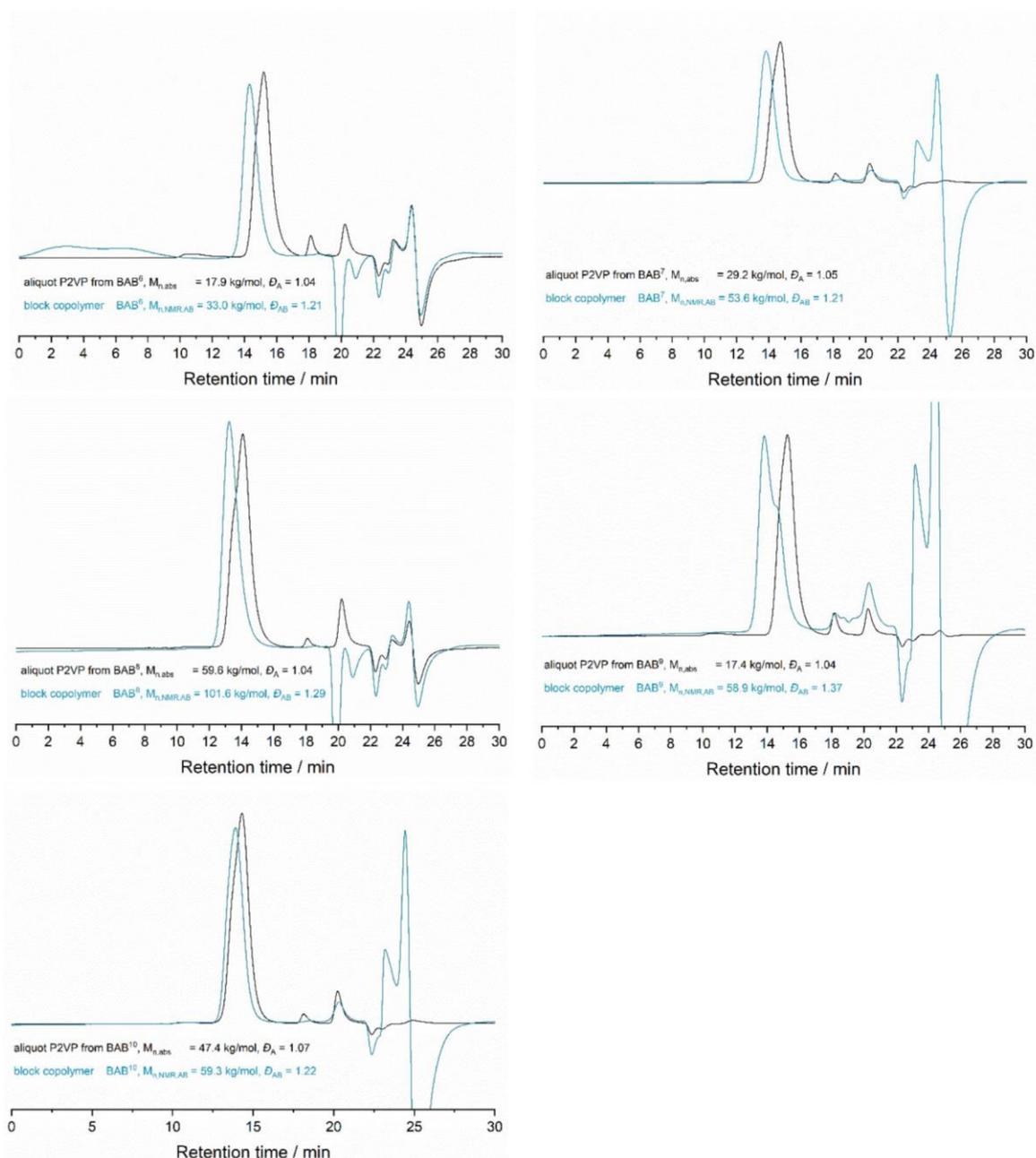
Figure S25: Additional stacked SEC traces of P2VP aliquot (black) and isolated P2VP-*b*-PM triblock copolymers (blue) BAB[6], BAB[7], BAB[8], BAB[9] and BAB[10] (Table 2, entries 6-10).

26

REFERENCES

(1) Tshuva, E. Y.; Groysman, S.; Goldberg, I.; Kol, M.; Goldschmidt, Z. [ONXO]-Type Amine Bis(phenolate) Zirconium and Hafnium Complexes as Extremely Active 1-Hexene Polymerization Catalysts. *Organometallics* **2002**, *21* (4), 662–670. DOI: 10.1021/om010493w.

(2) Hultzsch, K. C.; Voth, P.; Beckerle, K.; Spaniol, T. P.; Okuda, J. Single-Component Polymerization Catalysts for Ethylene and Styrene: Synthesis, Characterization, and Reactivity of Alkyl and Hydrido Yttrium Complexes Containing a Linked Amido–Cyclopentadienyl Ligand. *Organometallics* **2000**, *19* (3), 228–243. DOI: 10.1021/om990583p.

(3) Adams, F.; Altenbuchner, P. T.; Werz, P. D. L.; Rieger, B. Multiresponsive micellar block copolymers from 2-vinylpyridine and dialkylvinylphosphonates with a tunable lower critical solution temperature. *RSC Adv.* **2016**, *6* (82), 78750–78754. DOI: 10.1039/C6RA17160E.

(4) Adams, F.; Machat, M. R.; Altenbuchner, P. T.; Ehrmaier, J.; Pöthig, A.; Karsili, T. N. V.; Rieger, B. Toolbox of Nonmetallocene Lanthanides:Multifunctional Catalysts in Group-Transfer Polymerization. *Inorg. Chem.* **2017**, *56* (16), 9754–9764. DOI: 10.1021/acs.inorgchem.7b01261.

(5) Altenbuchner, P. T.; Werz, P. D. L.; Schöppner, P.; Adams, F.; Kronast, A.; Schwarzenböck, C.; Pöthig, A.; Jandl, C.; Haslbeck, M.; Rieger, B. Next Generation Multiresponsive Nanocarriers for Targeted Drug Delivery to Cancer Cells. *Chemistry* **2016**, *22* (41), 14576–14584. DOI: 10.1002/chem.201601822.

(6) Shin, J.; Martello, M. T.; Shrestha, M.; Wissinger, J. E.; Tolman, W. B.; Hillmyer, M. A. Pressure-Sensitive Adhesives from Renewable Triblock Copolymers. *Macromolecules* **2011**, *44* (1), 87–94. DOI: 10.1021/ma102216d.

27

(7) Zhang, D.; Hillmyer, M. A.; Tolman, W. B. Catalytic polymerization of a cyclic ester derived from a "cool" natural precursor. *Biomacromolecules* **2005**, *6* (4), 2091–2095. DOI: 10.1021/bm050076t.

(8) Adams, F.; Pschenitza, M.; Rieger, B. Yttrium-Catalyzed Synthesis of Bipyridine-Functionalized AB-Block Copolymers: Micellar Support for Photocatalytic Active Rhenium-Complexes. *ChemCatChem* **2018**, *10* (19), 4309–4316. DOI: 10.1002/cctc.201801009.

(9) Guillaume, S. M.; Carpentier, J.-F. Recent advances in metallo/organo-catalyzed immortal ring-opening polymerization of cyclic carbonates. *Catal. Sci. Technol.* **2012**, *2* (5), 898. DOI: 10.1039/c2cy00507g.

(10) Albertsson, A.-C.; Varma, I. K. Recent developments in ring opening polymerization of lactones for biomedical applications. *Biomacromolecules* **2003**, *4* (6), 1466–1486. DOI: 10.1021/bm034247a.

(11) Carpentier, J.-F. Discrete Metal Catalysts for Stereoselective Ring-Opening Polymerization of Chiral Racemic β-Lactones. *Macromol. Rapid Commun.* **2010**, *31* (19), 1696–1705. DOI: 10.1002/marc.201000114.

11.4.5. Reprint permissions for copyrighted material

The contents for Chapter 4 and the corresponding supporting information in Chapter 11.4.1 for the manuscript titled "C-H Bond Activation of Silyl-Substituted Pyridines with Bis(Phenolate)Yttrium Catalysts as Facile Tool towards Hydroxyl-Terminated Michael-Type Polymers" has been published as Open Access under the terms and conditions of the Creative Commons Attribution CC BY 4.0. The authors possess the copyright of the reprinted material, manuscript and supporting information have been reprinted from ref. [32].

The contents for Chapter 5 and the corresponding supporting information in Chapter 11.4.2 for the manuscript titled "Macromolecular Rhenium−Ruthenium Complexes for Photocatalytic CO_2 Conversion: From Catalytic Lewis Pair Polymerization to Well-Defined Poly(vinyl bipyridine)−Metal Complexes" have been reprinted with permission from ref. [45] Copyright 2022 American Chemical Society.

_____

The contents for Chapter 6 and the corresponding supporting information in Chapter 11.4.3 for the manuscript titled "Polyester synthesis based on 3-carene as renewable feedstock" has been published as been reproduced from Ref. [330] with permission from the Royal Society of Chemistry.

The contents for Chapter 7 and the corresponding supporting information in Chapter 11.4.4 for the manuscript titled "Uniting Group-Transfer and Ring-Opening Polymerization–Block Copolymers from Functional Michael-Type Monomers and Lactones" have been reprinted with permission from ref. [43] Copyright 2021 American Chemical Society.

Copyright permissions for Figure 19 (ref. [7]) and Figure 21 (ref. [317]):

JOHN WILEY AND SONS LICENSE
TERMS AND CONDITIONS

Jan 04, 2023

This Agreement between Technical University of Munich -- Moritz Kränzlein ("You") and John Wiley and Sons ("John Wiley and Sons") consists of your license details and the terms and conditions provided by John Wiley and Sons and Copyright Clearance Center.

License Number	5462902693
License date	Jan 04, 2023
Licensed Content Publisher	John Wiley and Sons
Licensed Content Publication	Chemistry - A European Journal
Licensed Content Title	Metal-Catalyzed Group-Transfer Polymerization: A Versatile Tool for Tailor-Made Functional (Co)Polymers
Licensed Content Author	Bernhard Rieger, Philipp Pahl, Friederike Adams
Licensed Content Date	Nov 23, 2017
Licensed Content Volume	24
Licensed Content Issue	3
Licensed Content Pages	10
Type of use	Dissertation/Thesis

Requestor type	University/Academic
Format	Print and electronic
Portion	Figure/table
Number of figures/tables	1
Will you be translating?	No
Title	Functional (Co)Polymers from Group-Transfer and Ring-Opening Polymerization – Monomers, Catalysis, Applications
Institution name	Technical University of Munich
Expected presentation date	Jan 2023
Portions	Figure 6
Requestor Location	Technical University of Munich Lichtenbergstraße 4 Garching, 85747 Germany Attn: Technical University of Munich
Publisher Tax ID	EU826007151
Total	0.00 EUR
Terms and Conditions	

TERMS AND CONDITIONS

This copyrighted material is owned by or exclusively licensed to John Wiley & Sons, Inc. or

Appendix

one of its group companies (each a "Wiley Company") or handled on behalf of a society with which a Wiley Company has exclusive publishing rights in relation to a particular work (collectively "WILEY"). By clicking "accept" in connection with completing this licensing transaction, you agree that the following terms and conditions apply to this transaction (along with the billing and payment terms and conditions established by the Copyright Clearance Center Inc., ("CCC's Billing and Payment terms and conditions"), at the time that you opened your RightsLink account (these are available at any time at http://myaccount.copyright.com).

Terms and Conditions

- The materials you have requested permission to reproduce or reuse (the "Wiley Materials") are protected by copyright.

- You are hereby granted a personal, non-exclusive, non-sub licensable (on a stand-alone basis), non-transferable, worldwide, limited license to reproduce the Wiley Materials for the purpose specified in the licensing process. This license, and any **CONTENT (PDF or image file) purchased as part of your order, is for a one-time use only and limited to any maximum distribution number specified in the license. The first instance of republication or reuse granted by this license must be completed within two years of the date of the grant of this license (although copies prepared before the end date may be distributed thereafter).** The Wiley Materials shall not be used in any other manner or for any other purpose, beyond what is granted in the license. Permission is granted subject to an appropriate acknowledgement given to the author, title of the material/book/journal and the publisher. You shall also duplicate the copyright notice that appears in the Wiley publication in your use of the Wiley Material. Permission is also granted on the understanding that nowhere in the text is a previously published source acknowledged for all or part of this Wiley Material. Any third party content is expressly excluded from this permission.

- With respect to the Wiley Materials, all rights are reserved. Except as expressly granted by the terms of the license, no part of the Wiley Materials may be copied, modified, adapted (except for minor reformatting required by the new Publication), translated, reproduced, transferred or distributed, in any form or by any means, and no derivative works may be made based on the Wiley Materials without the prior permission of the respective copyright owner.**For STM Signatory Publishers clearing permission under the terms of the STM Permissions Guidelines only, the terms of the license are extended to include subsequent editions and for editions in other languages, provided such editions are for the work as a whole in situ and does not involve the separate exploitation of the permitted figures or extracts,** You may not alter, remove or suppress in any manner any copyright, trademark or other notices displayed by the Wiley Materials. You may not license, rent, sell, loan, lease, pledge, offer as security, transfer or assign the Wiley Materials on a stand-alone basis, or any of the rights granted to you hereunder to any other person.

- The Wiley Materials and all of the intellectual property rights therein shall at all times remain the exclusive property of John Wiley & Sons Inc, the Wiley Companies, or their respective licensors, and your interest therein is only that of having possession of and the right to reproduce the Wiley Materials pursuant to Section 2 herein during the continuance of this Agreement. You agree that you own no right, title or interest in or

---

to the Wiley Materials or any of the intellectual property rights therein. You shall have no rights hereunder other than the license as provided for above in Section 2. No right, license or interest to any trademark, trade name, service mark or other branding ("Marks") of WILEY or its licensors is granted hereunder, and you agree that you shall not assert any such right, license or interest with respect thereto

- NEITHER WILEY NOR ITS LICENSORS MAKES ANY WARRANTY OR REPRESENTATION OF ANY KIND TO YOU OR ANY THIRD PARTY, EXPRESS, IMPLIED OR STATUTORY, WITH RESPECT TO THE MATERIALS OR THE ACCURACY OF ANY INFORMATION CONTAINED IN THE MATERIALS, INCLUDING, WITHOUT LIMITATION, ANY IMPLIED WARRANTY OF MERCHANTABILITY, ACCURACY, SATISFACTORY QUALITY, FITNESS FOR A PARTICULAR PURPOSE, USABILITY, INTEGRATION OR NON-INFRINGEMENT AND ALL SUCH WARRANTIES ARE HEREBY EXCLUDED BY WILEY AND ITS LICENSORS AND WAIVED BY YOU.

- WILEY shall have the right to terminate this Agreement immediately upon breach of this Agreement by you.

- You shall indemnify, defend and hold harmless WILEY, its Licensors and their respective directors, officers, agents and employees, from and against any actual or threatened claims, demands, causes of action or proceedings arising from any breach of this Agreement by you.

- IN NO EVENT SHALL WILEY OR ITS LICENSORS BE LIABLE TO YOU OR ANY OTHER PARTY OR ANY OTHER PERSON OR ENTITY FOR ANY SPECIAL, CONSEQUENTIAL, INCIDENTAL, INDIRECT, EXEMPLARY OR PUNITIVE DAMAGES, HOWEVER CAUSED, ARISING OUT OF OR IN CONNECTION WITH THE DOWNLOADING, PROVISIONING, VIEWING OR USE OF THE MATERIALS REGARDLESS OF THE FORM OF ACTION, WHETHER FOR BREACH OF CONTRACT, BREACH OF WARRANTY, TORT, NEGLIGENCE, INFRINGEMENT OR OTHERWISE (INCLUDING, WITHOUT LIMITATION, DAMAGES BASED ON LOSS OF PROFITS, DATA, FILES, USE, BUSINESS OPPORTUNITY OR CLAIMS OF THIRD PARTIES), AND WHETHER OR NOT THE PARTY HAS BEEN ADVISED OF THE POSSIBILITY OF SUCH DAMAGES. THIS LIMITATION SHALL APPLY NOTWITHSTANDING ANY FAILURE OF ESSENTIAL PURPOSE OF ANY LIMITED REMEDY PROVIDED HEREIN.

- Should any provision of this Agreement be held by a court of competent jurisdiction to be illegal, invalid, or unenforceable, that provision shall be deemed amended to achieve as nearly as possible the same economic effect as the original provision, and the legality, validity and enforceability of the remaining provisions of this Agreement shall not be affected or impaired thereby.

- The failure of either party to enforce any term or condition of this Agreement shall not constitute a waiver of either party's right to enforce each and every term and condition of this Agreement. No breach under this agreement shall be deemed waived or excused by either party unless such waiver or consent is in writing signed by the party granting such waiver or consent. The waiver by or consent of a party to a breach of

- 264 -

Appendix

any provision of this Agreement shall not operate or be construed as a waiver of or consent to any other or subsequent breach by such other party.

- This Agreement may not be assigned (including by operation of law or otherwise) by you without WILEY's prior written consent.

- Any fee required for this permission shall be non-refundable after thirty (30) days from receipt by the CCC.

- These terms and conditions together with CCC's Billing and Payment terms and conditions (which are incorporated herein) form the entire agreement between you and WILEY concerning this licensing transaction and (in the absence of fraud) supersedes all prior agreements and representations of the parties, oral or written. This Agreement may not be amended except in writing signed by both parties. This Agreement shall be binding upon and inure to the benefit of the parties' successors, legal representatives, and authorized assigns.

- In the event of any conflict between your obligations established by these terms and conditions and those established by CCC's Billing and Payment terms and conditions, these terms and conditions shall prevail.

- WILEY expressly reserves all rights not specifically granted in the combination of (i) the license details provided by you and accepted in the course of this licensing transaction, (ii) these terms and conditions and (iii) CCC's Billing and Payment terms and conditions.

- This Agreement will be void if the Type of Use, Format, Circulation, or Requestor Type was misrepresented during the licensing process.

- This Agreement shall be governed by and construed in accordance with the laws of the State of New York, USA, without regards to such state's conflict of law rules. Any legal action, suit or proceeding arising out of or relating to these Terms and Conditions or the breach thereof shall be instituted in a court of competent jurisdiction in New York County in the State of New York in the United States of America and each party hereby consents and submits to the personal jurisdiction of such court, waives any objection to venue in such court and consents to service of process by registered or certified mail, return receipt requested, at the last known address of such party.

WILEY OPEN ACCESS TERMS AND CONDITIONS

Wiley Publishes Open Access Articles in fully Open Access Journals and in Subscription journals offering Online Open. Although most of the fully Open Access journals publish open access articles under the terms of the Creative Commons Attribution (CC BY) License only, the subscription journals and a few of the Open Access Journals offer a choice of Creative Commons Licenses. The license type is clearly identified on the article.

The Creative Commons Attribution License

The Creative Commons Attribution License (CC-BY) allows users to copy, distribute and transmit an article, adapt the article and make commercial use of the article. The CC-BY

---

license permits commercial and non-

Creative Commons Attribution Non-Commercial License

The Creative Commons Attribution Non-Commercial (CC-BY-NC)License permits use, distribution and reproduction in any medium, provided the original work is properly cited and is not used for commercial purposes.(see below)

Creative Commons Attribution-Non-Commercial-NoDerivs License

The Creative Commons Attribution Non-Commercial-NoDerivs License (CC-BY-NC-ND) permits use, distribution and reproduction in any medium, provided the original work is properly cited, is not used for commercial purposes and no modifications or adaptations are made. (see below)

Use by commercial "for-profit" organizations

Use of Wiley Open Access articles for commercial, promotional, or marketing purposes requires further explicit permission from Wiley and will be subject to a fee.

Further details can be found on Wiley Online Library http://olabout.wiley.com/WileyCDA /Section/id-410895.html

Other Terms and Conditions:

v1.10 Last updated September 2015

Questions? customercare@copyright.com or +1-855-239-3415 (toll free in the US) or +1-978-646-2777.

- 265 -

11.5. Statutory Declaration

Ich, Moritz Kränzlein, erkläre an Eides statt, dass ich die bei der promotionsführenden Einrichtung

TUM School of Natural Sciences / TUM Graduate School

der TUM zur Promotionsprüfung vorgelegte Arbeit mit dem Titel:

Functional (Co)Polymers from Group-Transfer and Ring-Opening Polymerization – Monomers, Catalysis, Applications

unter der Anleitung und Betreuung durch: Prof. Dr. Dr. h. c. Bernhard Rieger_____

ohne sonstige Hilfe erstellt und bei der Abfassung nur die gemäß § 7 Abs. 6 und 7 angegebenen Hilfsmittel benutzt habe.

☒ Ich habe keine Organisation eingeschaltet, die gegen Entgelt Betreuer*innen für die Anfertigung von Dissertationen sucht, oder die mir obliegenden Pflichten hinsichtlich der Prüfungsleistungen für mich ganz oder teilweise erledigt.

☒ Ich habe die Dissertation in dieser oder ähnlicher Form in keinem anderen Prüfungsverfahren als Prüfungsleistung vorgelegt.

☒ Teile der Dissertation wurden in Macromolecules (ACS), RSC Polymer Chemistry (RSC) und Polymers (MDPI) veröffentlicht.

☒ Ich habe den angestrebten Doktorgrad noch nicht erworben und bin nicht in einem früheren Promotionsverfahren für den angestrebten Doktorgrad endgültig gescheitert.

☐ Ich habe bereits am _____ bei der promotionsführenden Einrichtung _____ der Hochschule _____ unter Vorlage einer Dissertation mit dem Thema _____

die Zulassung zur Promotion beantragt mit dem Ergebnis:

_____

☒ Ich habe keine Kenntnis über ein strafrechtliches Ermittlungsverfahren in Bezug auf wissenschaftsbezogene Straftaten gegen mich oder eine rechtskräftige strafrechtliche Verurteilung mit Wissenschaftsbezug.

Die öffentlich zugängliche Promotionsordnung sowie die Richtlinien zur Sicherung guter wissenschaftlicher Praxis und für den Umgang mit wissenschaftlichem Fehlverhalten der TUM sind mir bekannt, insbesondere habe ich die Bedeutung von § 27 PromO (Nichtigkeit der Promotion) und § 28 PromO (Entzug des Doktorgrades) zur Kenntnis genommen. Ich bin mir der Konsequenzen einer falschen Eidesstattlichen Erklärung bewusst.

Mit der Aufnahme meiner personenbezogenen Daten in die Alumni-Datei bei der TUM bin ich

☒ einverstanden,   ☐ nicht einverstanden.

München, 11.01.2023